UNIVERSITY OF CALIFORNIA, SAN DIEGO

Platinum and Palladium Isocyanides as Platforms on which to Study Metal/Lewis Acid Cooperativity and Ligand-based Redox-Noninnocence

A dissertation submitted in partial satisfaction of the
requirements for the degree of Doctor of Philosophy

in

Chemistry

by

Brandon Richard Barnett

Committee in charge:

Professor Joshua S. Figueroa, Chair
Professor Richard A. Firtel
Professor Arnold L. Rheingold
Professor Yitzhak Tor
Professor William C. Trogler

The Dissertation of Brandon Richard Barnett is approved, and it is acceptable in quality and form for publication on microfilm and electronically:

_____

_____

_____

_____

_____

Chair

University of California, San Diego

2016

DEDICATION

For my parents, Rick and Kandi.

EPIGRAPH

Ego sum, ego existo; certum est. Quandiu autem? Nempe quandiu cogito; nam forte etiam fieri posset, si cessarem ab omni cogitatione, ut illico totus esse desinerem.

I am, I exist – that is certain; but for how long do I exist? For as long as I think;
for it might perhaps happen, if I totally ceased thinking,
that I would at the same time completely
cease to be.

René Descartes, Meditations on First Philosophy

Trans. Laurence J. LaFleur

TABLE OF CONTENTS

Signature Page……... iii

Dedication……...iv

Epigraph……...v

Table of Contents……vi

List of Figures……ix

List of Schemes……..xv

List of Tables……...xvii

Acknowledgements……xx

Vita……xxvii

Abstract of the Dissertation……xxix

Chapter 1 Synthesis of a Mononuclear Binary Isocyanide Complex of Platinum(0).....1

1.1. Group 10 metal carbonyls……1
1.2. Group 10 metal isocyanides……..3
1.3. Synthesis and electronic structure of a two-coordinate Pt(0) isocyanide…….5
1.4. Concluding remarks and outlook……13
1.5. Synthetic procedures and characterization data……..13
1.6. Details of DFT computational studies……17
1.7. Details of crystallographic structure determinations……..27
1.8. Acknowledgements……28
1.9. References……...29

Chapter 2 Cooperative Transition Metal/Lewis Acid Activation of Small Molecules by a Bidentate (boryl)iminomethane Complex: A Significant Metal-Borane Interaction Fostered by a Small Bite Angle LZ Chelate……..34

2.1. Introduction……34
2.2. Synthesis and electronic structure of a singly-buttressed platinum-borane adduct accessed by hydroboration of a coordinated isocyanide……35
2.3. Oxidative addition reactivity of Pt(κ^2-*N,B*-^{Cy2}BIM)(CNAr^{Dipp2})……41
2.4. Oxidative insertion reactivity of Pt(κ^2-*N,B*-^{Cy2}BIM)(CNAr^{Dipp2})……...54
2.5. Concluding remarks……67
2.6. Synthetic procedures and characterization data……..69
2.7. Details of DFT computational studies……92

2.8. CSD search results……..98
2.9. Details of crystallographic structure determinations……100
2.10. Acknowledgements……108
2.11. References……..108

Chapter 3 Frustrated Lewis Pair Behavior of Monomeric (boryl)iminomethanes Accessed from Isocyanide 1,1-hydroboration……114
3.1. Introduction……..114
3.2. Frustrated Lewis Pair reactivity of ^{Cy2}BIM……..116
3.3. Synthesis of a (boryl)iminomethane bearing a tethered organic backbone and examination of its FLP reactivity……123
3.4. Synthesis of a (boryl)iminomethane bearing a borane unit of weak Lewis acidity……..128
3.5. Concluding remarks……..130
3.6. Synthetic procedures and characterization data……131
3.7. Details of DFT computational studies……..141
3.8. Details of crystallographic structure determinations……160
3.9. Acknowledgements……..165
3.10. References……..165

Chapter 4 Metal-only Lewis Pairs Between Group 10 Metals and Tl(I) or Ag(I): Insights into the Electronic Consequences of Z-type Ligand Binding……..169
4.1. Introduction……...169
4.2. Synthesis and spectroscopic features of Metal-only Lewis Pairs containing a Tl(I) Lewis acidic center……..172
4.3. Synthesis and spectroscopic features of Metal-only Lewis Pairs containing a Ag(I) Lewis acidic center……182
4.4. Rationalization of observed solvent binding *trans* to Ag…..……186
4.5. Concluding remarks……..190
4.6. Synthetic procedures and characterization data……192
4.7. CSD search results……198
4.8. Details of crystallographic structure determinations……201
4.9. Acknowledgements……...207
4.10. References……...207

Chapter 5 Monomeric Chini-Type Triplatinum Clusters Featuring Dianionic and Radical Anionic π*-Systems……..214
5.1. Introduction……..214
5.2. Synthesis and characterization of the clusters $[Pt_3(\mu\text{-}CO)_3(CNAr^{Dipp2})_3]^{n-}$ (n = 0, 1, 2)……..216
5.3. Electronic structure insights via Density Functional Theory (DFT) calculations revealing ligand-based redox-noninnocence……...223
5.4. Metal-based reactivity of $K_2[Pt_3(\mu\text{-}CO)_3(CNAr^{Dipp2})_3]$ with electrophiles...227
5.5. Synthesis of the neutral tripalladium cluster $Pd_3(\mu\text{-}CO)_3(CNAr^{Dipp2})_3$, its electrochemical behavior, and attempted chemical reductions……231

5.6. Concluding remarks……..234
5.7. Synthetic procedures and characterization data……235
5.8. X-band EPR procedures and measurements……244
5.9. Details of DFT computational studies……..244
5.10. Details of crystallographic structure determinations……..260
5.11. Acknowledgements……265
5.12. References……...265

Chapter 6 Solution Dynamics of Redox-Noninnocent Nitrosoarene Ligands: Mapping the Electronic Criteria for the Formation of Persistent Metal-Coordinated Nitroxide Radicals……..270
6.1. Introduction……...270
6.2. Solution dynamics of $Pd(\kappa^1\text{-}N\text{-}PhNO)_2(CNAr^{Dipp2})_2$: Identification of an equilibrium between a κ^1-bis-nitroxide and an η^2-metalloxaziridine complex……273
6.3. Formation of solution-phase behavior of Pd bis-nitroxide diradicals featuring mono-substituted aryl groups……...281
6.4. Origin of the solution-phase persistence of *para*-cyano and *para*-formyl bis-arylnitroxide radical complexes……...292
6.5. Concluding remarks……..298
6.6. Synthetic procedures and characterization data……299
6.7. Details of DFT computational studies……..315
6.8. Details of crystallographic structure determinations……321
6.9. Acknowledgements……...330
6.10. References……...330

LIST OF FIGURES

Figure 1.1. Molecular structure of *cis*-$PtCl_2(CNAr^{Dipp2})_2$ • 2 CH_2Cl_2 (***cis*-1** • 2 CH_2Cl_2).....6

Figure 1.2. Molecular structure of *trans*-$PtCl_2(CNAr^{Dipp2})_2$ • C_6H_5F • 2 MeCN (***trans*-1** • C_6H_5F • 2 MeCN)……7

Figure 1.3. Molecular structure of $Pt(CNAr^{Dipp2})_2$ • THF (**2** • THF)……..9

Figure 1.4. ^1H NMR spectrum (300.0 MHz, C_cD_6, 20 ˚C) of a 1:1 mixture of $Pt(CNAr^{Dipp2})_2$ (**2**) and $CNAr^{Dipp2}$……..11

Figure 1.5. Calculated 5*d* orbital manifold of $Pt(CNAr^{Dipp2})_2$ (**2**)……12

Figure 1.6. Optimized molecular structure of *cis*-$PtCl_2(CNPh)_2$……..19

Figure 1.7. Optimized molecular structure of *trans*-$PtCl_2(CNPh)_2$……..20

Figure 1.8. Optimized molecular structure of $Pt(CNAr^{Dipp2})_2$……..26

Figure 2.1. Synthesis (top) and molecular structure (bottom) of Pt(κ^2-*N,B*-^{Cy2}BIM)($CNAr^{Dipp2}$) • 0.5 C_5H_{12} (**1** • 0.5 C_5H_{12})……...37

Figure 2.2. Localized molecular orbital from NBO calculations showing the dative bonding interaction between the platinum center and borane unit in the model complex Pt(κ^2-*N,B*-^{Me2}BIM)(CNMe)……...37

Figure 2.3. Molecular structure of ^{Cy2}BIM→BCl_3 • 2 C_5H_{12} (**3** • 2 C_5H_{12})……..39

Figure 2.4. Molecular structure of *trans*-PtI_2(κ^1-*N*-^{Cy2}BIM)($CNAr^{Dipp2}$) • 1.5 C_6H_6 (**4** • 1.5 C_6H_6)……43

Figure 2.5. Molecular structure of PtH(μ^2-H)(κ^1-*N*-^{Cy2}BIM)($CNAr^{Dipp2}$) • Et_2O (**5** • Et_2O)……..44

Figure 2.6. Molecular structure of PtH(μ-OH)(κ^1-*N*-^{Cy2}BIM)($CNAr^{Dipp2}$) • 0.5 Et_2O (**7** • 0.5 Et_2O)……47

Figure 2.7. Molecular structure of borinic acid **8**……48

Figure 2.8. Molecular structure of PtH(μ-OMe)(κ^1-*N*-^{Cy2}BIM)($CNAr^{Dipp2}$) (**9**)……..49

Figure 2.9. Molecular structure of PtH(μ-NH(*p*-$NO_2C_6H_4$))(κ^1-*N*-^{Cy2}BIM)($CNAr^{Dipp2}$) (**10**)……50

Figure 2.10. Molecular structure of PtH(η^2-*C,C*-κ^1-*N*-PhCC-^{Cy2}BIM)(CNAr^{Dipp2}) • 1.5 Et_2O (**11** • 1.5 Et_2O)……...50

Figure 2.11. Molecular structure of PtBr(μ-PBr_2)(^{Cy2}BIM)(CNAr^{Dipp2}) • 1.5 C_5H_{12} (**12** • 1.5 C_5H_{12})……...53

Figure 2.12. Molecular structure of Pt(SbF_2)(μ-F)(^{Cy2}BIM)(CNAr^{Dipp2}) • MeCN (**13** • MeCN).....53

Figure 2.13. Molecular Structure of Pt(μ-Me_2CO)(^{Cy2}BIM)(CNAr^{Dipp2}) (**14**)…….55

Figure 2.14. Molecular Structure of Pt(μ-PhC(H)O)(^{Cy2}BIM)(CNAr^{Dipp2}) • 4.5 C_6H_{12} (**15** • 4.5 C_6H_{12})……56

Figure 2.15. Molecular Structure of **17** • 1.5 C_5H_{12}……..59

Figure 2.16. Molecular structure of Pt(μ-N_3Ad)(^{Cy2}BIM)(CNAr^{Dipp2}) • C_6H_6 (**18** • C_6H_6)……..61

Figure 2.17. Zoom-in of the Pt-bound Dipp ring in **18**, showing the dearomatization as evidenced by the long C_{ipso}-C_{ortho} bond lengths…….62

Figure 2.18. Molecular structure of **19** • 2 C_5H_{12}…….66

Figure 2.19. Zoom-in of the Pt-bound Dipp ring in **19**, showing the dearomatization as evidenced by the long C_{ipso}-C_{ortho} bond lengths…….67

Figure 2.20. Optimized molecular structure of Pt(κ^2-*N*-*B*-^{Me2}BIM)(CNMe)……...95

Figure 2.21. Optimized molecular structure of ^{Me2}BIM……98

Figure 2.22. Histogram showing CSD search results for B-O bond distances in four-coordinate borates……..99

Figure 2.23. Histogram showing CSD search results for Pt-F bond distances in platinum fluorides……...100

Figure 3.1. Synthesis (top) and molecular structure (bottom) of **2a**……...118

Figure 3.2. Molecular structure of **3** • 1.5 C_6H_6…….121

Figure 3.3. Molecular structure of **4**……..121

Figure 3.4. Molecular structure of (Cy)((CH_3)$_3$CC≡C)BCH(Cy)NHAr^{Dipp2} **(5)**……...122

Figure 3.5. Molecular structure of $^{9\text{-BBN}}$BIM•THF • 1.5 (C_6H_6) (**1b•THF** • 1.5 (C_6H_6))……124

Figure 3.6. Molecular structure of (9-BBN)CH_2N(9-BBN)Ar^{Dipp2} • C_5H_{12} (**6** • C_5H_{12})……...125

Figure 3.7. Molecular structure of **2b**……127

Figure 3.8. Molecular structure of **7**……...128

Figure 3.9. Synthesis (top) and molecular structure (bottom) of ^{Pin}BIM (**1c**)……..130

Figure 3.10. Optimized molecular structure of ^{Cy2}BIM (**1a**)……147

Figure 3.11. Optimized molecular structure of **2a**……149

Figure 3.12. Optimized molecular structure of **2a***……152

Figure 3.13. Optimized molecular structure of **1b•thf**……...155

Figure 3.14. Optimized molecular structure of **2b**……157

Figure 3.15. Optimized molecular structure of **2b***……160

Figure 4.1. Molecular structure of [TlPt($CNAr^{Dipp2}$)$_2$]OTf • 1.5 Et_2O (**1** • 1.5 Et_2O)….174

Figure 4.2. FTIR spectrum (υ(C≡N) region) of [TlPd($CNAr^{Dipp2}$)$_2$]OTf (**2**) showing the presence of Pd($CNAr^{Dipp2}$)$_2$……175

Figure 4.3. Molecular structure of [(Et_2O)TlPt($CNAr^{Dipp2}$)$_2$]BAr^F_4 (**3**(Et_2O))……..176

Figure 4.4. Molecular structure of [TlPt($CNAr^{Dipp2}$)$_2$]BAr^F_4 (**3**)……177

Figure 4.5. Molecular structure of [(η^6-C_7H_8)$_2$TlPd($CNAr^{Dipp2}$)$_2$]BAr^F_4 (**4**(Tol)$_2$)……177

Figure 4.6. Comparative Pd K-edge XANES spectra of Pd($CNAr^{Dipp2}$)$_2$ (red), [TlPd($CNAr^{Dipp2}$)$_2$]OTf (**2**, blue), and Pd(η^2-O_2)($CNAr^{Dipp2}$)$_2$ (black)……180

Figure 4.7. Comparative Ni K-edge XANES spectra of Ni($CNAr^{Mes2}$)$_3$ (red) and [TlNi($CNAr^{Mes2}$)$_3$]OTf (blue)……..181

Figure 4.8. Molecular structure of [AgPt($CNAr^{Dipp2}$)$_2$(THF)]OTf • 3 THF (**5**(THF) • 3 THF).....184

Figure 4.9. Molecular structure of [AgPt(CNAr^{Dipp2})$_2$(η^1-C_6H_6)]OTf • 3 C_6H_6 (**5**(C_6H_6) • 3 C_6H_6)……184

Figure 4.10. Molecular structure of [AgPd(CNAr^{Dipp2})$_2$(η^1-C_7H_8)]OTf • C_7H_8 (**6**(C_7H_8) • C_7H_8).....185

Figure 4.11. Molecular orbital diagram for a transition metal (**M**) bound to a σ-acceptor fragment (**Z**), showing how the LUMO of the resulting adduct can be stabilized with respect to the acceptor-free complex……..188

Figure 4.12. Molecular structure of {[Ag_2Pt(CNAr^{Dipp2})$_2$(η^1-C_6H_6)]$_2$(μ-OTf)$_2$}(OTf)$_2$ • 2 C_6H_6 (**7** • 2 C_6H_6)……190

Figure 4.13. CSD search results for complexes containing Pt-O_{Ether} bonds……..199

Figure 4.14. CSD search results for complexes containing Pd-O_{Ether} bonds……..199

Figure 4.15. CSD search results for complexes containing Pt-Ag bonding interactions……...200

Figure 4.16. CSD search results for complexes containing Pd-Ag bonding interactions……...200

Figure 5.1. Molecular structure of Pt_3(μ-CO)$_3$(CNAr^{Dipp2})$_3$·C_5H_{12} (**1**·C_5H_{12})……217

Figure 5.2. Cyclic voltammogram of **1** showing two reversible redox events……...218

Figure 5.3. Molecular structure of K_2(DME)$_3$[Pt_3(μ-CO)$_3$(CNAr^{Dipp2})$_3$]·2DME (K_2(DME)$_3$[**1**]·2 DME)……220

Figure 5.4. Molecular structure of K(THF)$_4$[Pt_3(μ-CO)$_3$(CNAr^{Dipp2})$_3$]·2THF (K(THF)$_4$[**1**]·2(THF))……..222

Figure 5.5. Experimental (black) and simulated (red) solid-state X-band EPR spectrum of K(THF)$_4$[Pt_3(μ-CO)$_3$(CNAr^{Dipp2})$_3$] recorded at 294 K……223

Figure 5.6. DFT Calculated HOMOs of [**1***]$^{2-}$ (A), [Pt_3(CO)$_6$)]$^{2-}$ (B), and [Pt_3(μ-CO)$_3$(PMe_3)$_3$]$^{2-}$ (C). BP86/def2-TZVP/ZORA……226

Figure 5.7. (A) DFT calculated metal-based a_2''-symmetric valence orbitals of [**1***]$^{2-}$, which is HOMO–19 and is calculated to lie 4.40 eV below the HOMO. (B) DFT calculated metal-based a_2''-symmetric valence orbitals of [Pt_3(CO)$_6$]$^{2-}$, which is HOMO–10 and is calculated to lie 4.40 eV below the HOMO……226

Figure 5.8. Molecular structure of $K[Pt_3(\mu^3\text{-}SnPh_3)(\mu\text{-}CO)_3(CNAr^{Dipp2})_3]\cdot 4(C_5H_{12})$ (**2**·4(C_5H_{12}))…….229

Figure 5.9. Molecular structure of $K(Et_2O)[Pt_3(SiEt_3)(\mu\text{-}CO)_3(CNAr^{Dipp2})_3]$ (**3**)……..229

Figure 5.10. Molecular structure of $K(Et_2O)_2[Pt_3(\mu^3\text{-}AuPPh_3)(\mu\text{-}CO)_3(CNAr^{Dipp2})_3]\cdot 2(Et_2O)$ (**4**·2(Et_2O))……..230

Figure 5.11. Molecular structure of $Pt_3(\mu^3\text{-}AuPPh_3)_2(\mu\text{-}CO)_3(CNAr^{Dipp2})_3\cdot 3Et_2O$ (**5**·3 Et_2O)……231

Figure 5.12. Molecular structure of $Pd_3(\mu\text{-}CO)_3(CNAr^{Dipp2})_3 \bullet Et_2O$ (**6** • Et_2O)……233

Figure 5.13. Cyclic voltammogram of complex **6**……..234

Figure 5.14. Optimized molecular structure of $Pt_3(\mu\text{-}CO)_3(CNAr^{Ph2})_3$ (**1***)……..252

Figure 5.15. Optimized molecular structure of $[Pt_3(\mu\text{-}CO)_3(CNAr^{Ph2})_3]^{\bullet-}$ ($[\mathbf{1}^*]^-$)……..255

Figure 5.16. Optimized molecular structure of $[Pt_3(\mu\text{-}CO)_3(CNAr^{Ph2})_3]^{2-}$ ($[\mathbf{1}^*]^{2-}$)……258

Figure 5.17. Optimized molecular structure of $[Pt_3(CO)_6]^{2-}$……..259

Figure 5.18. Optimized molecular structure of $[Pt_3(\mu\text{-}CO)_3(PMe_3)_3]^{2-}$……..260

Figure 6.1. Solution FTIR spectrum (C_6D_6, 25 ºC, υ(C≡N) region) of a solution prepared from a crystalline sample of *trans*-$Pd(\kappa^1\text{-}N\text{-}PhNO)_2(CNAr^{Dipp2})_2$ (**1a**)……...275

Figure 6.2. Molecular structure of $Pd(\eta^2\text{-}N,O\text{-}PhNO)(CNAr^{Dipp2})_2$ (**2a**)……...276

Figure 6.3. Variable temperature FTIR spectra (υ(C≡N) region; CaF_2 windows) of toluene solutions prepared from crystalline samples of $Pd(\kappa^1\text{-}N\text{-}PhNO)_2(CNAr^{Dipp2})_2$ (**1a**)……...278

Figure 6.4. Molecular structure of $[Pd(\mu^2\text{:}\eta^{2\text{-}}N,O\text{-}\eta^1\text{-}N\text{-}PhNO)(CNAr^{Dipp2})]_3$ (**4**)…….280

Figure 6.5. Molecular structures of $Pd(\kappa^1\text{-}N\text{-}ArNO)_2(CNAr^{Dipp2})_2$ (**1b-c, e-j**)……..284

Figure 6.6. Molecular structures of $Pd(\eta^2\text{-}N,O\text{-}ArNO)(CNAr^{Dipp2})_2$ (**2b-e, g-h, j**)……286

Figure 6.7. Molecular structure of $Pd(\kappa^1\text{-}N\text{-}p\text{-}C(O)H\text{-}C_6H_4NO)_2(CNAr^{Dipp2})_2$ (**1k**)…..288

Figure 6.8. Molecular structure of $Pd(\kappa^1\text{-}N\text{-}p\text{-}CN\text{-}C_6H_4NO)_2(CNAr^{Dipp2})_2 \bullet 3\ Et_2O$ (**1l** • 3 Et_2O)……288

Figure 6.9. FTIR spectra (υ(C≡N) region) of THF solutions freshly prepared from crystalline samples of Pd(κ^1-*N*-*p*-C(O)H-$C_6H_4NO)_2(CNAr^{Dipp2})_2$ (**1k**, Top) and Pd(κ^1-*N*-*p*-CN-$C_6H_4NO)_2(CNAr^{Dipp2})_2$ (**1l**, bottom)……..289

Figure 6.10. FTIR spectra (υ(C≡N) region) of C_6D_6 solutions prepared as 0.013 M Pd(κ^1-*N*-*p*-C(O)H-$C_6H_4NO)_2(CNAr^{Dipp2})_2$ (**1k**, Top (includes inset of υ(C=O) region) or Pd(κ^1-*N*-*p*-CN-$C_6H_4NO)_2(CNAr^{Dipp2})_2$ (**1l**, bottom) and allowed to stir at 20 ºC for three days……..291

Figure 6.11. Spin density plots overlaid with Mulliken spin populations of the BS(1,1) solutions for the model complexes Pd(k^1-*N*-*p*-C(O)H-$C_6H_4NO)_2(CNPh)_2$ (top) and Pd(k^1-*N*-*p*-CN-$C_6H_4NO)_2(CNPh)_2$ (bottom). B3LYP, ZORA-def2-TZVP, α-spin in red, β-spin in yellow……...294

Figure 6.12. Variable temperature SQUID data (circles) and simulation (line) for Pd(κ^1-*N*-*p*-C(O)H-$C_6H_4NO)_2(CNAr^{Dipp2})_2$ (**1k**) and Pd(κ^1-*N*-*p*-CN-$C_6H_4NO)_2(CNAr^{Dipp2})_2$ (**1l**)……296

Figure 6.13. SQUID variable temperature magnetic data (circles) and simulation (line) for Pd(κ^1-*N*-*p*-$ClC_6H_4NO)_2(CNAr^{Dipp2})_2$ (**1g**)……..297

Figure 6.14. Optimized molecular structure of Pd(κ^1-*N*-*p*-COH-$C_6H_4NO)_2(CNPh)_2$…318

Figure 6.15. Optimized molecular structure of Pd(κ^1-*N*-*p*-CN-$C_6H_4NO)_2(CNPh)_2$…...321

LIST OF SCHEMES

Scheme 1.1. Synthesis of *cis/trans*-$PtCl_2(CNAr^{Dipp2})_2$ (***cis/trans*-1**) and reduction of the isomeric mixture to $Pt(CNAr^{Dipp2})_2$ (**2**)……6

Scheme 2.1. Synthesis of ^{Cy2}BIM (**2**) and its adduct with BCl_3 (**3**)……..39

Scheme 2.2. Potential mechanisms for the formation of **1**……41

Scheme 2.3. Oxidative addition reaction pinwheel for $Pt(\kappa^2$-*N,B*-^{Cy2}BIM)$(CNAr^{Dipp2})$ (**1**)……...42

Scheme 2.4. Frustrated Lewis Pair reactivity of ^{Cy2}BIM toward H_2, H_2O and CO_2…….45

Scheme 2.5. Metallaboration of acetone and benzaldehyde effected by **1**……55

Scheme 2.6. Reaction of **1** with CO_2 to yield **16**, which ostensibly proceeds via unobserved intermediate **A**……57

Scheme 2.7. Proposed mechanistic pathway leading to the formation of **17**……59

Scheme 2.8. Synthesis of $Pt(\mu$-$N_3Ad)(^{Cy2}BIM)(CNAr^{Dipp2})$ (**18**) and its thermal decomposition to give the carbodiimide ^{Dipp2}ArN=C=NAd and free ^{Cy2}BIM with presumed loss of Pt metal…….....61

Scheme 2.9. Reactivity of **1** with $DippN_3$, $TMSN_3$ and *p*-$TolN_3$……..66

Scheme 3.1. Regioisomers of monomeric (boryl)iminomethanes and head-to-tail dimerization of sterically unencumbered *syn-N,B* (boryl)iminomethanes to 1,3-diaza-2,4-diboretidines…….116

Scheme 3.2. Calculated enthalpies of reaction in the formation of **2a*** and **2a** from ^{Cy2}BIM (**1a**) and CO_2……...119

Scheme 3.3. Activation of MeCN, PhCN and *t*-BuCCH by ^{Cy2}BIM (**1a**)……..120

Scheme 3.4. Single- and double-hydroboration of $CNAr^{Dipp2}$ with 9-borabicyclo[3.3.1]nonane (9-BBN)…….124

Scheme 3.5. CO_2 activation and heterolytic H-O cleavage of water by **1b**·THF……..126

Scheme 3.6. Enthalpies of reaction in the formation of **2b*** and **2b** from $^{9\text{-BBN}}$BIM•THF (**1b•THF**) and CO_2……..127

Scheme 4.1. Synthesis of Tl(I)-containing MOLPs based off of the $M(CNAr^{Dipp2})_2$ (M = Pt, Pd) platform……173

Scheme 4.2. Synthesis of Ag-containing MOLPs based off of the $M(CNAr^{Dipp2})_2$ (M = Pt, Pd) platform……183

Scheme 5.1. Synthesis of $Pt_3(\mu\text{-}CO)_3(CNAr^{Dipp2})_3$ (**1**)……216

Scheme 5.2. Synthesis of the anionic cluster $K_2[Pt_3(\mu\text{-}CO)_3(CNAr^{Dipp2})_3]^{n-}$ (K_2[**1**]) via reduction of **1** and comproportionation to give the monoanionic radical $K[Pt_3(\mu\text{-}CO)_3(CNAr^{Dipp2})_3]^{n-}$ (K[**1**])……..219

Scheme 5.3. Reactivity pinwheel for K_2[**1**]……228

Scheme 5.4. Synthesis of $Pd_3(\mu\text{-}CO)_3(CNAr^{Dipp2})_3$ (**6**)……...232

Scheme 6.1. Reactivity of $Pd(CNAr^{Dipp2})_2$ with one and two equivalents of nitrosobenzene……275

Scheme 6.2. Equilibrium between bis-nitroxide diradical **1a** and metalloxaziridine **2a**……..277

Scheme 6.3. Proposed mechanism leading to the formation of azoxybenzene, $OCNAr^{Dipp2}$ (**3**), and $[Pd(\mu^2\text{:}\eta^{2\text{-}}N,O\text{-}\eta^1\text{-}N\text{-}PhNO)(CNAr^{Dipp2})]_3$ (**4**)……281

Scheme 6.4. Formation of **1b-l** and **2b-l** from $Pd(CNAr^{Dipp2})_2$ and monosubstituted nitrosoarenes……282

Scheme 6.5. Quinonoid resonance structure of nitrosoarenes bearing *para*-oriented electron releasing groups as exemplified by 4-(dimethylamino)nitrosobenzene……282

LIST OF TABLES

Table 1.1. Comparison of selected metrical parameters between crystallographically characterized $Pt(CNAr^{Dipp2})_2$ (**2**, "Crystal") and DFT optimized coordinates ("DFT")……..27

Table 1.2. Crystallographic data collection and refinement information……..28

Table 2.1. Comparative metrical parameters between $Pt(\kappa^2\text{-}N\text{-}B\text{-}^{Cy2}BIM)(CNAr^{Dipp2})$ (Exp. X-ray) and $Pt(\kappa^2\text{-}N\text{-}B\text{-}^{Me2}BIM)(CNMe)$ (calc'd)…….96

Table 2.2. Atomic and fragment charges (q) derived from the Natural Population Analysis calculations for $Pt(\kappa^2\text{-}N\text{-}B\text{-}^{Me2}BIM)(CNMe)$ and ^{Me2}BIM……..98

Table 2.3. Crystallographic data collection and refinement information……102

Table 2.4. Crystallographic data collection and refinement information……103

Table 2.5. Crystallographic data collection and refinement information……104

Table 2.6. Crystallographic data collection and refinement information……105

Table 2.7. Crystallographic data collection and refinement information……106

Table 2.8. Crystallographic data collection and refinement information……107

Table 3.1. Comparative metrical parameters between experimental (X-ray crystal structure) and calculated versions of **2a**……...150

Table 3.2. Listing of total bonding energies for reactants and products (including putative intermediate **2a***) in the formation of **2a** (BP86/TZ2P)……..152

Table 3.3. Comparative metrical parameters between the experimental (X-ray crystal structure) and calculated versions of **1b•thf**……155

Table 3.4. Comparative metrical parameters between the experimental (X-ray crystal structure) and calculated versions of **2b**……..158

Table 3.5. Listing of total bonding energies for reactants and products (including putative intermediate **2b***) in the formation of **2b** (BP86/TZ2P)……..160

Table 3.6. Crystallographic data collection and refinement information……162

Table 3.7. Crystallographic data collection and refinement information……163

Table 3.8. Crystallographic data collection and refinement information……164

Table 4.1. Selected bond distances (X-ray structure) of $Pt(CNAr^{Dipp2})_2$, $Pd(CNAr^{Dipp2})_2$, and their Tl-containing MOLPs……...179

Table 4.2. Selected bond distances (X-ray structure) in Ag-containing Metal-only Lewis pairs……..186

Table 4.3. Crystallographic data collection and refinement information……203

Table 4.4. Crystallographic data collection and refinement information……204

Table 4.5. Crystallographic data collection and refinement information……205

Table 4.6. Crystallographic data collection and refinement information……206

Table 5.1. Selected bond distances from the solid-state structures of complexes **1**, $K(THF)_4$[**1**], and $K_2(DME)_3$[**1**]……220

Table 5.2. Comparison of selected metrical parameters between crystallographically characterized $Pt_3(\mu\text{-}CO)_3(CNAr^{Dipp2})_3$ (**1**, "Crystal") and optimized coordinates of $Pt_3(\mu\text{-}CO)_3(CNAr^{Ph2})_3$ (**1***, "DFT")……...252

Table 5.3. Comparison of selected metrical parameters between crystallographically characterized $K(THF)_4[Pt_3(\mu\text{-}CO)_3(CNAr^{Dipp2})_3]$ ($K(THF)_4$[**1**], "Crystal") and optimized coordinates of $[Pt_3(\mu\text{-}CO)_3(CNAr^{Ph2})_3]^-$ ([**1***]$^-$, "DFT")…….255

Table 5.4. Comparison of selected metrical parameters between crystallographically characterized $K_2(DME)_3[Pt_3(\mu\text{-}CO)_3(CNAr^{Dipp2})_3]$ ($K_2(DME)_3$[**1**], "Crystal") and optimized coordinates of $[Pt_3(\mu\text{-}CO)_3(CNAr^{Ph2})_3]^{2-}$ ([**1***]$^{2-}$, "DFT")……..258

Table 5.5. Crystallographic data collection and refinement information……262

Table 5.6. Crystallographic data collection and refinement information……263

Table 5.7. Crystallographic data collection and refinement information……264

Table 6.1. Nitrosoarene N-O bond lengths and isocyanide stretching frequencies for complexes **1a-l** in the solid state……..284

Table 6.2. Nitrosoarene N-O bond lengths and isocyanide stretching frequencies for complexes **2a-l** in the solid state……..286

Table 6.3. Crystallographic data collection and refinement information……323

Table 6.4. Crystallographic data collection and refinement information……324

Table 6.5. Crystallographic data collection and refinement information……325

Table 6.6. Crystallographic data collection and refinement information……326

Table 6.7. Crystallographic data collection and refinement information……327

Table 6.8. Crystallographic data collection and refinement information……328

Table 6.9. Crystallographic data collection and refinement information……329

ACKNOWLEDGEMENTS

I've been told that the Acknowledgements section of the dissertation would be the most challenging one to write. This has proven accurate, if only because I composed the rest of this document using primarily three keys on my keyboard ("command", "c", "v"). Regardless, I undoubtedly feel more of a burden in composing this section than I do the remainder of the dissertation combined. Much like Joseph Grand from Albert Camus' The Plague, I feel as though I could work forever on any given sentence in the few paragraphs that follow without truly having done the efforts of the person(s) named therein justice. While it seems far more appropriate that these expressions of gratitude be formulated as a tear-jerking moving picture montage accompanied by a John Williams-composed overture, the written word will have to suffice as our medium.

I arrived at UCSD in 2011 having little intention of studying organometallic chemistry for the next X years. Despite this reluctance, it quickly became impossible to ignore the enthusiasm and brilliance exuded by Josh Figueroa. More than anything, I craved an environment composed of supremely motivated individuals that would push me to be better as a scientist, yet where I simultaneously would be given artistic freedom in my research. It is hard to fathom how anyone could have cultivated such an environment better than Josh has. Josh, I have long admired your innate ability to know when it's time to push someone for more, and when a little patience will eventually pay dividends. While you have without question been a phenomenal research mentor, I am perhaps even more grateful for the myriad of times when I sat in your office as you gave me *ad hoc* views into the behind the scenes world of academia. Although this is not the place in which to list many of the nuggets that I've taken from those conversations, I

have little doubt that they will prove invaluable no matter where life takes me in the future. Few people would describe graduate school as "fun," but I can unabashedly say that I've enjoyed the last five years, and that I've grown as both a scientist and a person. For this and so much more, I'll always be grateful.

No acknowledgements section would be complete without a shout-out to those who've had to put up with my (occasionally) affable and (typically) insufferable personality on a daily basis – my lab-mates. As alluded to above, before I arrived on the scene, Josh had assembled a team of highly-talented individuals who had begun the noble endeavor of Making Chemistry Great Again. Firstly, I must thank Dr. Liezel Labios, who put up with an over-eager first year student rolling into her glovebox and working on her chemistry, and yet was still willing to teach him invaluable lessons such as how to make PdL_2, how make sure you don't leave the water-cooler jug empty (this is done by replacing it), and how to air-saxophone the bejeezus out of that one George Michael song. Even if we had never talked, I am certain that I would have learned a ton just from working next to you. I could say the same about Dr. Treff Ditri. Although I know you won't believe me, I can't overstate how much I look up to you as a scientist and a person. Thanks for having my back when I didn't deserve it, and thanks for being a friend. I must thank the most ethical guy I know, Dr. Matt Millard, for the Dadaistic piece of art upon which I used to gaze as I approached our old office. Also, thanks for not killing ACar or Chuckles, even though they may have deserved it. I raise a delicious braised turkey leg and a glass of milk in your honor. My occasional reckless forays into computational chemistry owe their beginnings to Dr. Steve George, who for some reason was always willing to answer the ignorant questions of a clueless second-year grad student,

something for which I'm extremely grateful. I also have to thank Julia Stauber and Patrick Smith, both of whom were extremely talented and long-tenured undergrads in the group when I joined – thanks for being emblematic embodiments of the get-it-done mentality. As for Dr. Alex Carpenter (formerly "ACar," now "Twitch"), Charles "Chuckles" Mokhtarzadeh, and Doug Agnew – it seems only appropriate to mention you all together. In addition to being three of the best young scientists I know, I am fortunate to count each of you as a great friend. The days of ABCD witnessed a flurry of awesome chemistry, and I have no doubt in saying that I would have accomplished significantly less had I not had the privilege of working alongside of all three of you for the lion's share of my grad school tenure. From FBGS to Smell Yo D*ck, from Kotija's to green drink, and from the Porter's patio to New Orleans hotel rooms, we may have jumped the shark a few times, but it was one hell of a ride. As for the "younger" (quotation marks primarily for Kyle) group members, I really have enjoyed working (and drinking) with all of you. Each of you is extremely talented, and I look forward to seeing the amazing results you guys put out in the upcoming years. Kyle – make sure that your "-eines" are never in short supply and that your "-ynes" are always hydrometallated. Noah – that Justin Turner bobblehead has got to go. Joanne – give burritos another chance. They're like cats, only tastier. Myles – slow down on Untappd, you're embarrassing me. Mike – keep BIMsanity bitchin and don't fall to your death on the Ho Chi Min trail. Alejandra – Squash the bug and use your mitt, not your shin.

By any metric one could apply, UCSD Chemistry can boast having a world-class Inorganic department. As such, I've been able to interact with many other brilliant and motivated individuals who have each made important contributions to my research

efforts. First and foremost, I must thank those in my second home on campus – the X-ray Crystallography facility. I owe a huge thank you to Prof. Arnie Rheingold for letting me have essentially unabated access to one of the best academic small-molecule crystallography facilities on the planet. I am also indebted to Dr. Curtis Moore and Dr. Milan Gembicky, both of who have taught me a ton about crystallography. Thanks to the efforts of all three of you, this dissertation is at least twice as long as it would otherwise be. I have really valued the open-door policy that most faculty members in the department hold; accordingly, I'd like to thank Prof. William Trogler, Prof. Clifford Kubiak, Prof. Seth Cohen, Prof. Carlos Guerrero and Prof. Jeffrey Rinehart for enlightening and thought-provoking discussions. As has every synthetic chemist in the department, I've benefitted enormously from the NMR expertise of Dr. Anthony Mrse; however, despite many mutual brainstorming sessions, I still can't figure out why the Padres suck. Others to whom I owe thanks include Dr. Mohand Melaimi (cyclic voltammetry); Dr. Maria Angelella (EPR); Dr. Yongxuan Su (mass spectrometry); Dr. Matt Thompson (varous ROMP monomers); Dr. (Prof!) Charles Machan (UV-vis, Wing Wednesdays); Dr. John Walzer (car bar, enlightening discussions); Dr. Matt Del Bel (life-changing "loan" of dicyclohexylborane, general synthetic badassery).

Although I enjoy synthetic chemistry enough to do it for free, being able to eat is great. As such, I am immensely grateful to the National Science Foundation for a Graduate Research Fellowship, which funded me for my final three years in the program. I'd also like to thank UCSD and the U.S. Department of Education for a GAANN fellowship, which provided funding during my second year.

I also can't express enough thanks to my undergrad mentors and peers who were instrumental in my training and education prior to graduate school. I can count accepting Prof. Joe Fritsch's invitation to join his lab at Pepperdine after taking his Dark Arts class as one of the more important decisions I've made in my life. No one person was more instrumental in my decision to get a Ph.D. Joe – thanks for letting me be a part of Team Fritsch and for helping me hone the skills I needed to deliver huge projects really fast. I'd also like to thank my undergrad lab-mates and partners in Inorganic Wizardry Dr. (!) Courtney "Zort" Roberts (also goes by "Serena"), Nomaan "Noms" Rezayee and Kimberly Gerling. It was alongside these other members of the "First to Come, Last to Leave" gang that both my affinity for masochistic lab hours and disdain of column chromatography were fostered, days on which I only reflect on with the happiest of memories. Thanks also go out to Prof. Jane Ganske and Prof. Donna Nofziger-Plank, without whose efforts I might instead have a B.A. in Psychology, and to Prof. Dave Green who, when he wasn't busy starring in Dos Equis commercials, managed to fix whatever instrument we'd broken in the lab that week. Finally, I have to acknowledge Pepperdine Great Books Colloquium faculty Prof. Victoria Myers, Prof. Donald Marshall and Prof. Michael Gose. Taking the full two-year Colloquium was the second best decision I made as an undergraduate, and the communication skills and love of classic literature that I took from this series have contributed immensely to my personal and professional growth in countless ways. I can't thank you all enough for your enthusiasm and patience.

Without a doubt, no single person listed above has bore the brunt of my insanity more than the indomitable Jessie Peters (see also "J-Pizzle", "Peterpotamus"). She can

rightfully claim to be the only person who can put a smile on my face regardless of mood, and is without question one of the kindest and most caring humans that I know. Jessie, the fact that you managed to do more than merely tolerate me, and did so without resorting to binge drinking, testifies that you're a stronger person than I could ever hope to be. Thank you for being my best friend.

Lastly, I thank my family, who has often gotten me at my worst but has given me only their best in return. To my sister and brother-in-law Sara and James Mayne – I love you both and am immensely proud of what you've accomplished so far in life. Finally, I get to you, Mom and Dad, likely the only two who would still be reading this section anyway. Unfortunately, it is here that I really don't know what to say. I could write for days without stopping about how much you've done for me, yet ultimately whatever I penned would be insulting in its brevity. As such, I will say only this: If it weren't for your unconditional love, I'm pretty sure I know where I'd be today. That place is not here. Thank you.

Chapters 1 and 2: Parts of these chapters are adapted with permission from Barnett, B.R.; Moore, C.E.; Rheingold, A.L.; Figueroa, J. S. "Cooperative Transition Metal/Lewis Acid Bond-Activation Reactions by a Bidentate (Boryl)iminomethane Complex: A Significant Metal-Borane Interaction Promoted by a Small Bite-Angle LZ Chelate." *Journal of the American Chemical Society,* **2014**, *136*, 10262. Copyright 2014, American Chemical Society. The dissertation author is the first author of this paper.

Chapter 3: This chapter is adapted with permission from Barnett, B. R.; Moore, C. E.; Rheingold, A. L.; Figueroa, J. S. "Frustrated Lewis Pair Behavior of Monomeric

(boryl)iminomethanes Accessed from Isocyanide 1,1-hydroboration", *Chemical Communications*, **2015**, *51*, 541. Copyright 2015, Royal Society of Chemistry. The dissertation author is the first author of this paper.

Chapter 4: This chapter is adapted with permission from Barnett, B. R.; Moore, C. E.; Chandrasekaran, P; Sproules, S.; Rheingold, A. L.; DeBeer, S.; Figueroa, J. S. "Metal-only Lewis Pairs Between Group 10 Metals and Tl(I) or Ag(I): Insights into the Electronic Consequences of Z-type Ligand Binding", *Chemical Science,* **2015**, *6*, 7169. Copyright 2015, Royal Society of Chemistry. The dissertation author is the first author of this paper.

Chapter 5: This chapter is adapted with permission from Barnett, B.R.; Rheingold, A.L.; Figueroa, J.S. "Monomeric Chini-Type Triplatinum Clusters Featuring Dianionic and Radical Anionic π*-Systems," *Angewandte Chemie, International Edition*, **2016**, *55*, 9253. Copyright 2016 Wiley-VCH, Weinheim. The dissertation author is the first author of this paper.

Chapter 6: This chapter is adapted with permission from Barnett, B. R.; Labios, L. A.; Moore, C. E.; England, J.; Rheingold, A. L.; Wieghardt, K.; Figueroa, J.S. "Solution Dynamics of Redox Noninnocent Nitrosoarene Ligands: Mapping the Electronic Criteria for the Formation of Persistent Metal-Coordinated Nitroxide Radicals*"*, *Inorganic Chemistry*, **2015**, 54, 7110. Copyright 2015, American Chemical Society. The dissertation author is the first author of this paper.

VITA

2016 Ph.D. in Chemistry, University of California, San Diego

2013 M.S. in Chemistry, University of California, San Diego

2011 B.S. in Chemistry, Summa Cum Laude, Pepperdine University

PUBLICATIONS

Barnett, B. R.; Labios, L. A.; Stauber, J. M.; Moore, C. E.; Rheingold, A. L.; Figueroa, J. S. "Generation and Intermolecular Trapping of a Pd(0) Monoisocyanide: Synthetic and Mechanistic Interrogation of Catalytic Intermediates in Pd-Catalyzed Cross-Coupling." *Submitted*.

Barnett, B. R.; Rheingold, A. L.; Figueroa, J. S. "Monomeric Chini-Type Triplatinum Clusters Featuring Dianionic and Radical Anionic π*-Systems." *Angewandte Chemie, International Edition*, **2016**, *55*, 9253.

Smith, S. J.; Radford, R. J.; Subramanian, R. H.; Barnett, B. R.; Figueroa, J. S.; Tezcan, F. A. "Tunable helicity, stability and DNA-binding properties of short peptides with hybrid metal coordination motifs." *Chemical Science*, **2016**, *7*, 5453.

Barnett, B. R.; Moore, C. E.; Chandrasekaran, P.; Sproules, S.; Rheingold, A. L.; DeBeer, S.; Figueroa, J. S. "Metal-only Lewis pairs between group 10 metals and Tl(I) or Ag(I): insights into the electronic consequences of Z-type ligand binding." *Chemical Science*, **2015**, *6*, 7169.

Barnett, B. R.; Labios, L. A.; Moore, C. E.; England, J.; Rheingold, A. L.; Wieghardt, K.; Figueroa, J. S. "Solution Dynamics of Redox Noninnocent Nitrosoarene Ligands: Mapping the Electronic Criteria for the Formation of Persistent Metal-Coordinated Nitroxide Radicals." *Inorganic Chemistry*, **2015**, *54*, 7110.

Barnett, B. R.; Moore, C. E.; Rheingold, A. L.; Figueroa, J. S. "Frustrated Lewis pair behavior of monomeric (boryl)iminomethanes accessed from isocyanide 1,1-hydroboration." *Chemical Communications*, **2015**, *51*, 541.

Carpenter, A. E.; McNeece, A. J.; Barnett, B. R.; Estrada, A. L.; Mokhtarzadeh, C. C.; Moore, C. E.; Rheingold, A. L.; Perrin, C. L.; Figueroa, J. S. "Direct Observation of β-Chloride Elimination from an Isolable β-Chloroalkyl Complex of Square-Planar Nickel." *Journal of the American Chemical Society*, **2014**, *136*, 15481.

Barnett, B. R.; Moore, C. E.; Rheingold, A. L.; Figueroa, J. S. “Cooperative Transition Metal/Lewis Acid Bond-Activation Reactions by a Bidentate (Boryl)iminomethane Complex: A Significant Metal-Borane Interaction Promoted by a Small Bite-Angle LZ Chelate.” *Journal of the American Chemical Society*, **2014**, *136*, 10262.

Roberts, C. C.; Barnett, B. R.; Green, D. B.; Fritsch, J. M. “Synthesis and Structures of Tridentate Ketoiminate Zinc Complexes That Act As *L*-Lactide Ring-Opening Polymerization Catalysts.” *Organometallics*, **2012**, *31*, 4133.

Barnett, B. R.; Evans, A. L.; Roberts, C. C.; Fritsch, J. M. “Batch reactor kinetic studies on the reductive dechlorination of chlorinated ethylenes by *tetrakis*-(4-sulfonatophenyl)porphyrin cobalt.” *Chemosphere*, **2011**, *82*, 592.

ABSTRACT OF THE DISSERTATION

Platinum and Palladium Isocyanides as Platforms on which to Study Metal/Lewis Acid Cooperativity and Ligand-based Redox-Noninnocence

by

Brandon Richard Barnett

Doctor of Philosophy in Chemistry

University of California, San Diego, 2016

Prof. Joshua S. Figueroa, Chair

This dissertation describes various investigations into the reactivity and electronic structure of platinum and palladium complexes supported by *m*-terphenyl isocyanides. Use of these encumbering ligands facilitated the formation of two-coordinate $Pt(CNAr^{Dipp2})_2$, which serves an isolable mimic of the unstable carbonyl $Pt(CO)_2$. Importantly, $Pt(CNAr^{Dipp2})_2$, along with its palladium congener $Pd(CNAr^{Dipp2})_2$, represent

the only monomeric and zero-valent binary isocyanide complexes of these metals. These complexes can act as the Lewis basic component of Metal-only Lewis Pairs (MOLPs), binding thallium(I) and silver(I) via retrodative σ-bonds. Reactivity studies of $Pt(CNAr^{Dipp2})_2$ culminated in the discovery of a very rare singly-buttressed metal-borane adduct $Pt(\kappa^2\text{-}N,B\text{-}^{Cy2}BIM)(CNAr^{Dipp2})$, which is synthesized via hydroboration of a coordinated isocyanide ligand to form an ambiphilic (boryl)iminomethane (BIM) ligand. This complex exhibits rich reactivity with small molecules via metal/borane cooperation. It is shown to effect various E-H and E-X bond activations, as well as oxidative insertions of organoazides, organocarbonyls and organonitriles, most of which represent unprecedented reactivity modes for metal-borane adducts. Unligated ^{Cy2}BIM can also be synthesized upon hydroboration of $CNAr^{Dipp2}$ with dicyclohexylborane. It is shown to be monomeric in solution, allowing it to act as a highly competent Frustrated Lewis pair despite bearing a Lewis acid of only moderate acidity.

Two vignettes of ligand-based redox-noninnocence can be found in Chapters 5 and 6. The trinuclear dianion $K_2[Pt_3(\mu\text{-}CO)_3(CNAr^{Dipp2})_3]$ and radical anion $K(THF)_4[Pt_3(\mu\text{-}CO)_3(CNAr^{Dipp2})_3]$ were synthesized, notable as the all-carbonyl variants $[Pt_3(CO)_6]^{2-/1-}$ are unstable and have never been crystallographically characterized. Most importantly, it is shown that the highest occupied molecular orbital in these complexes is primarily CO/CNR π*, producing the first example of an ensemble of CO and isocyanide ligands exhibiting redox-noninnocence. Finally, solution dynamics of the palladium bis-nitroxide diradicals *trans*-$Pd(\kappa^1\text{-}N\text{-}ArNO)_2(CNAr^{Dipp2})_2$ were examined to gain insights into their stability and mode of decomposition. Judicious electronic modulation of the redox-active nitrosoarene ligands revealed that installation of *para*-formyl or *para*-cyano

substituents greatly increased the kinetic stability of the corresponding diradicals, signaling a potentially general strategy for the stabilization of inherently short-lived classical nitroxide spin adducts.

Chapter 1

Synthesis of a Mononuclear Binary Isocyanide Complex of Platinum(0)

1.1. Group 10 metal carbonyls

The study of carbonyl complexes of the Group 10 metals (Ni, Pd, Pt) can claim a rich historical legacy, given that both the first metal carbonyl complex (*cis*-$PtCl_2(CO)_2$, discovered by Schützenberger in 1868)[1] and the first binary carbonyl complex ($Ni(CO)_4$, synthesized by Mond in 1890)[2] are members of this family. Through the 20th and into the 21st century, the study of transition metal carbonyl complexes has retained its place as a central pursuit of organometallic chemistry.[3-8] As one of only two metal carbonyl complexes which can be prepared directly from the bulk metal and carbon monoxide (the other being $Fe(CO)_5$),[9,10] and despite its acute toxicity, the electronic structure and reaction chemistry of $Ni(CO)_4$ have been vigorously explored. Reduction results in CO evolution *en route* to formation of polynuclear nickelate clusters such as $[Ni_6(CO)_{12}]^{2-}$ and $[Ni_5(CO)_{12}]^{2-}$.[11-13] Ligand substitution chemistry with neutral, two-electron donor ligands yields complexes of the type $Ni(CO)_3L$. Importantly, kinetic and computational investigations reveal that substitution reactions proceed by a dissociative mechanism,[14-17] implicating the intermediacy of tri-coordinate $Ni(CO)_3$. While the unsaturated and highly reactive nature of $Ni(CO)_3$ obviates its isolation in the condensed phase, it can be accessed in cryogenic matrices by either photolysis of $Ni(CO)_4$[18] or carbonylation of atomic Ni.[19] Evaluation by IR spectroscopy indicates that $Ni(CO)_3$ adopts a trigonal planar D_{3h} coordination geometry, a finding that is corroborated by both Molecular

Orbital theory predictions[20] and Density Functional Theory calculations.[21] The mono- and di-carbonyls NiCO and $Ni(CO)_2$ can also be observed in gas matrices when dilute CO conditions are employed. Notably, despite previous investigations suggesting that two-coordinate $Ni(CO)_2$ is linear,[19] more recent work has conclusively demonstrated that it adopts a bent C_{2v}-symmetric structure.[21-23]

In somewhat startling contrast to the case of Ni, the neutral tetracarbonyls of the heavier members of Group 10 (Pd, Pt) are not isolable, an oddity which can largely be traced to the attenuated σ-donor and π-acid capabilities of CO toward Pd and Pt compared to Ni.[24] Indeed, the only binary mononuclear carbonyl complexes of these metals that have been isolated in the condensed phase are square planar $[Pt(CO)_4]^{2+}$ and $[Pd(CO)_4]^{2+}$, which have been generated in superacidic media.[25] Although the ability of platinum to form anionic binary carbonyl clusters is well-known,[8,26-29] not a single stable binary carbonyl cluster of palladium has been found.[30] Due to the lack of isolable mononuclear complexes of oxidation state zero, experimental investigations of $M(CO)_n$ (M = Pd, Pt; n = 1-4) have been confined to low temperature matrices, where they can be generated by carbonylation of metal atoms produced by either metal vapor or laser ablation methods.[31] As is the case for Ni, both IR spectroscopic and computational work indicate that the tetra- and tri-carbonyls of Pd and Pt adopt T_d and D_{3h} symmetry, respectively.[21,24,32] While matrix IR work supports a linear geometry for $Pd(CO)_2$ and $Pt(CO)_2$, this assignment is predicated on the inability to observe the symmetric carbonyl stretch, an endeavor which is complicated by band overlap in the region in which it would resonate.[21,24,33] Further, relativistic DFT calculations favor a bent C_{2v}-symmetric structure for both dicarbonyls.[21] The structural ambiguity surrounding $Pd(CO)_2$ and

$Pt(CO)_2$, coupled with the inherent inability to explore their reactivity profies, rendered the targeting of isolable condensed phase analogues a heuristic and worthwhile pursuit.

1.2. Group 10 metal isocyanides

As isolobal surrogates to CO, isocyanides (C≡N-R) are likewise ubiquitous ligands in organometallic chemistry. Although they are recognized to generally bear higher σ-donor/π-acid ratios compared to the carbonyl ligand,[34-36] the presence of orthogonal and degenerate π*-orbitals in both ligands renders isocyanides superior CO mimics to other strongly π-acidic ligands such as phosphites,[37] cyclic alkyl amino carbenes (CAACs)[38] and PF_3.[39,40] Importantly, isocyanides present the opportunity to modulate both the ligand electronic and steric profile through a judicious choice of the N-bound organic substitutent. Nevertheless, prior to our group's work, binary isocyanide complexes of low-valent metals invariably achieved coordinative saturation or aggregated to form cluster compounds. In the case of Ni, all previously known mononuclear complexes of this class were of the formulation $Ni(CNR)_4$.[41,42] While complexes formulated as $Ni(CNR)_2$ and $Pd(CNR)_2$ had been reported,[43,44] later studies showed that these complexes were in fact multinuclear.[45-49] The literature was similarly devoid of authenticated mononuclear binary isocyanide complexes of platinum(0).[41] Historically, platinum isocyanide chemistry had been dominated by complexes of the type *triangulo*-$Pt_3(\mu\text{-}CNR)_3(CNR)_3$,[50,51] with even higher nuclearity species occasionally seen.[52] It is indeed notable that, despite the larger steric profile of isocyanides compared to CO, no isocyano analogues to any of the unstable mononuclear Group 10 carbonyls had been found. This discrepancy signaled that significantly more imposing steric

profiles than those found in commonplace isocyanide ligands would be needed to kinetically stabilize unsaturated metal centers.

In order to address this void, our group has introduced a series of very encumbering isocyanides supported by an *m*-terphenyl unit.[36,53-55] The *m*-terphenyl group has seen extensive usage in coordination chemistry as both a σ-aryl ligand[56,57] and as an imposing ancillary group for amido,[58,59] imido[58,60] and carboxylate[61,62] functionalities. Although isolated reports of *m*-terphenyl isocyanides predate our work,[63,64] their structural chemistry and ability to foster coordinative unsaturation had not been explored. In our hands, these ligands have proven reliable workhorses for the synthesis of unsaturated complexes of mid- and late- transition metals.[53,65-71] In the case of Ni, the tris-isocyanide $Ni(CNAr^{Mes2})_3$ (Ar^{Mes2} = 2,6-(2,4,6-$Me_3C_6H_2)_2C_6H_3$) was synthesized by exploiting a novel Tl(I)-mediated coordination site protection strategy.[65] Use of the even larger *m*-terphenyl isocyanide $CNAr^{Dipp2}$ (Ar^{Dipp2} = 2,6-(2,6-*i*$PrC_6H_3)_2C_6H_3$) allowed for the protecting group-free synthesis of $Ni(CNAr^{Dipp2})_3$.[70] Both of these tris-isocyano species adopt rigorous D_{3h} symmetry and can be regarded as isostructural and isolobal to $Ni(CO)_3$. For Pd, access to the bis-isocyanide $Pd(CNAr^{Dipp2})_2$ yielded the first authentic example of a mononuclear isocyanide complex of Pd(0).[66] In the solid state, $Pd(CNAr^{Dipp2})_2$ deviates from a linear coordination geometry (C-Pd-C = 169.8(2)˚), while in solution the symmetric FTIR ν(C≡N) stretch is readily observed, potentially providing support for the bent geometry of $Pd(CO)_2$ predicted by DFT.[21] An intriguing counterpoint to two-coordinate Pd(0) complexes supported by encumbering and primarily σ-donating phosphines and N-heterocyclic carbenes (NHCs), $Pd(CNAr^{Dipp2})_2$ has been found to have

a rich reactivity profile.[66,72,73] These exciting discoveries inspired the pursuit of an unsaturated binary isocyanide complex of Pt(0).

1.3. Synthesis and electronic structure of a two-coordinate Pt(0) isocyanide

Our targeted synthetic route to a two- or three-coordinate isocyanide complex of Pt(0) involved isocyanide metalation to a divalent precursor followed by two-electron reduction, as this method had successfully yielded the palladium congener $Pd(CNAr^{Dipp2})_2$ in high yield.[66] Accordingly, addition of two equivalents of $CNAr^{Dipp2}$ to the common Pt(II) starting material $PtCl_2(\eta^4\text{-}1,5\text{-COD})$ (1,5-COD = 1,5-cyclooctadiene) in THF readily displaces the diolefin and yields $PtCl_2(CNAr^{Dipp2})_2$ (**1**) as a mixture of *cis*- and *trans*- isomers (Scheme 1.1). After removal of the THF solvent under reduced pressure, successive cycles of washing the residue in *n*-pentane and drying *in vacuo* were performed to facilitate complete removal of liberated 1,5-COD. Separation of the *cis*- and *trans*-isomers could be accomplished via extraction with acetonitrile, a solvent in which the *cis*-isomer is selectively soluble. Structural characterization of *cis*-$PtCl_2(CNAr^{Dipp2})_2$ (***cis*-1**) and *trans*-$PtCl_2(CNAr^{Dipp2})_2$ (***trans*-1**) via X-ray diffraction (Figures 1.1-2) reveals square planar coordination geometries as is typical for complexes of Pt(II). FTIR spectroscopic analysis shows that *cis*-$PtCl_2(CNAr^{Dipp2})_2$ (***cis*-1**) gives rise to two $\nu(C{\equiv}N)$ bands (2203 cm^{-1}, weak; 2172 cm^{-1}, strong), while only a single $\nu(C{\equiv}N)$ band (2192 cm^{-1}, very strong) is seen for *trans*-$PtCl_2(CNAr^{Dipp2})_2$ (***trans*-1**), as expected from basic symmetry considerations. The bands appear at higher energies compared to the $\nu(C{\equiv}N)$ stretch in unligated $CNAr^{Dipp2}$ (2118 cm^{-1}),[54] consistent with the isocyanide ligands acting primarily as σ-donors toward the Pt(II) center.

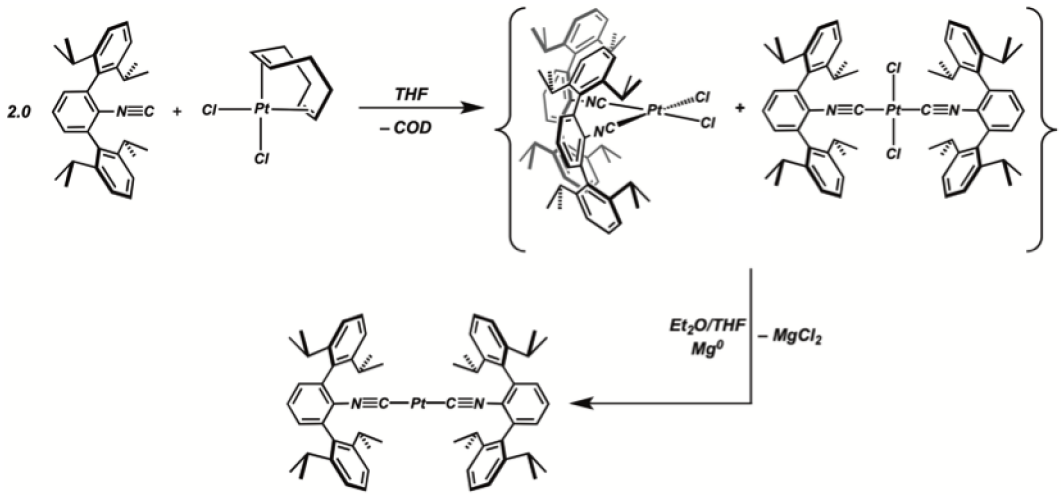

Scheme 1.1. Synthesis of *cis/trans*-$PtCl_2(CNAr^{Dipp2})_2$ (***cis/trans*-1**) and reduction of the isomeric mixture to $Pt(CNAr^{Dipp2})_2$ (**2**).

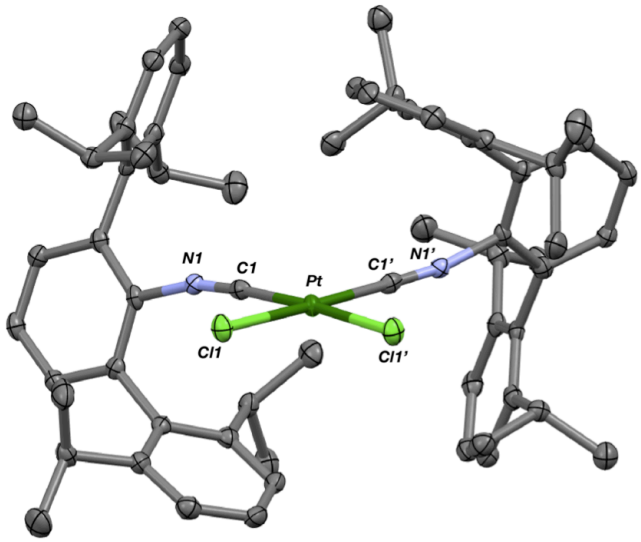

Figure 1.1. Molecular structure of *cis*-$PtCl_2(CNAr^{Dipp2})_2$ • 2 CH_2Cl_2 (***cis*-1** • 2 CH_2Cl_2). Co-crystallized molecules of dichloromethane have been omitted for clarity. Selected bond distances (Å): Pt-C1 = 1.923(4); Pt-Cl1 = 2.306(1).

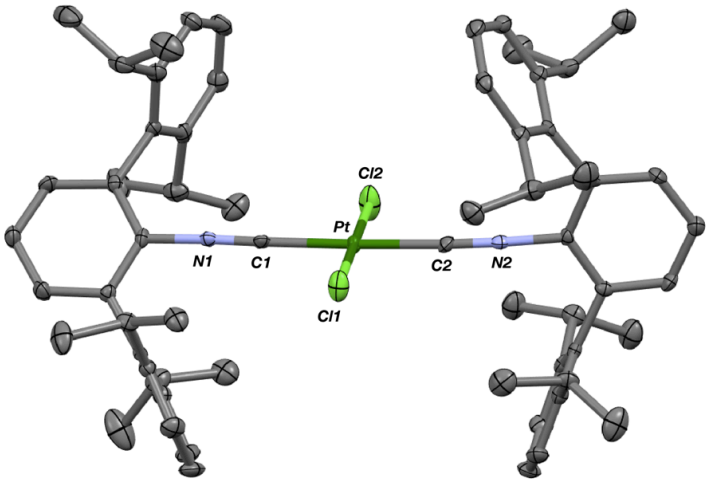

Figure 1.2. Molecular structure of *trans*-$PtCl_2(CNAr^{Dipp2})_2 \cdot C_6H_5F \cdot 2$ MeCN (***trans*-1** $\cdot C_6H_5F \cdot$ 2 MeCN). Co-crystallized molecules of fluorobenzene and acetonitrile have been omitted for clarity. Selected bond distances (Å): Pt-C1 = 1.961(4); Pt-C2 = 1.955(4); Pt-Cl1 = 2.299(1); Pt-Cl2 = 2.291(1).

The observation of a *trans* isomer of **1** was surprising. Despite the fact that addition of $CNAr^{Dipp2}$ to $PdCl_2$(1,5-COD) produced exclusively *trans*-$PdCl_2(CNAr^{Dipp2})_2$,[66] all previously characterized complexes of the formulation $PtCl_2(CNR)_2$ have displayed exclusively a *cis* geometry.[74] This signaled a thermodynamic preference for *cis* coordination geometries in $PtCl_2(CNR)_2$ complexes which might be partially overcome by kinetic effects induced by the sterically-imposing *m*-terphenyl isocyanides. Accordingly, Density Functional Theory calculations at the BP86 level for $PtCl_2(CNPh)_2$, which should present a nearly identical electronic profile as $PtCl_2(CNAr^{Dipp2})_2$,[36] show that the *cis* isomer lies 4.5 kcal/mol lower in energy than the corresponding *trans* isomer. Further, the amount of ***trans*-1** that is experimentally obtained is highly dependent on the concentration of $CNAr^{Dipp2}$ present in the reaction mixture. If the synthesis of **1** is performed by adding 2.0 equivalents of the isocyanide

ligand to $PtCl_2$(1,5-COD) in a single portion, the ***cis*-1**/***trans*-1** ratio is approximately 2:1 according to ^{1}H NMR. However, employing a slow addition of isocyanide to the reaction mixture over 2 hours has yielded ***cis*-1**/***trans*-1** ratios as high as 6:1. Extended stirring of reaction mixtures at room temperature does not alter the observed *cis/trans* ratio. Further, it should be noted that addition of exogenous $CNAr^{Dipp2}$ to isolated mixtures of ***cis*-1**/***trans*-1** does not result in enrichment of either isomer or in consumption of the unligated isocyanide. These observations indicate that ***trans*-1** is a kinetic product that is rendered isolable due to the steric pressures of the isocyanide ligands, which can be mitigated by orienting the ligands about Pt in a mutually *trans* disposition. Further, under the reaction conditions employed, *cis*/*trans* isomerization likely is not operative at all, and certainly does not occur through isocyanide association to transiently form a tris-isocyanide complex.

Reduction of either ***cis*-1** or ***trans*-1** with Mg metal proceeds to an identical product **2** (Scheme 1.1). The FTIR spectrum of **2** displays two ν(C≡N) bands (2065 cm^{-1}, strong; 2019 cm^{-1}, weak) which are shifted to lower energy compared to those in **1**, suggestive of reduction to the Pt(0) oxidation state. Structure determination on brilliant yellow single crystals grown from THF reveal **2** to be the two-coordinate binary isocyanide complex $Pt(CNAr^{Dipp2})_2$ (Figure 1.3). Consistent with the observation of two IR ν(C≡N) bands, the solid-state structure of **2** diverges from a rigorously linear coordination geometry (C1-Pt-C2 = 170.5˚). Similar deviations have been observed in the solid-state structure of other two-coordinate Pt(0) complexes, as well as in the nearly isostructural palladium complex $Pd(CNAr^{Dipp2})_2$ which also exhibits two ν(C≡N) bands of similar energies and intensities.[66] Due to the convergent reduction chemistry of ***cis*-1** and

***trans*-1**, a typical preparative procedure of **2** utilized crude, unseparated isomeric mixtures of **1**. Although the reduction of **1** to **2** with Mg metal initially proceeds smoothly, **2** can react further with Mg to yield dark brown/black solutions containing intractable mixtures. In order to mitigate unwanted over-reduction, the reaction mixtures were typically decanted from the residual Mg turnings when the reaction had reached approximately 95–98% completion according to ^{1}H NMR and IR. At this point, reaction mixtures were devoid of ***trans*-1**, with any remaining starting material being in the form of ***cis*-1**. Fortunately, **2** can be isolated in pure form after work-up via crystallization from THF layered with *n*-pentane at –35 ˚C, conditions under which ***cis*-1** does not precipitate from solution if it is present in only small amounts. This purification procedure allows for **2** to be isolated as an analytically pure bright yellow solid in overall yields consistently approaching 70%.

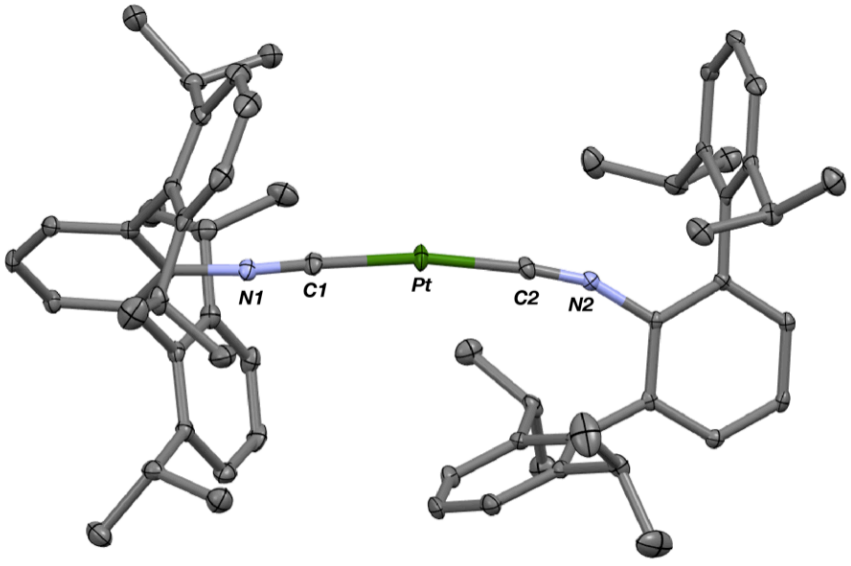

Figure 1.3. Molecular structure of $Pt(CNAr^{Dipp2})_2$ • THF (**2** • THF). Co-crystallized molecule of THF has been omitted for clarity. Selected bond distances (Å) and angles (˚): Pt-C1 = 1.904(3); Pt-C2 = 1.909(3); C1-N1 = 1.164(4); C2-N2 = 1.161(4); C1-Pt-C2 = 170.5(1).

Although the solid-state structure of $Pt(CNAr^{Dipp2})_2$ (**2**) is reminiscent of that seen for the Pd congener $Pd(CNAr^{Dipp2})_2$, moving down the periodic table to the heaviest member of Group 10 has noticeable ramifications for the kinetic lability of the metal-ligand bonds in **2**. For $Pd(CNAr^{Dipp2})_2$, our group has shown that addition of stoichiometric $CNAr^{Dipp2}$ in C_6D_6 or toluene-d_8 results in isocyanide exchange which remains rapid on the NMR timescale at temperatures as low as –80 ˚C.[66] Contrastingly, performing the analogous experiment with **2** and $CNAr^{Dipp2}$ at 20 ˚C produces sharp ^1H NMR spectra displaying the peaks for both species in a 1:1 ratio at the expected chemical shift values (Figure 1.4). Further, 2-D ^1H NMR EXSY experiments (20 ˚C) using these mixtures do not reveal chemical exchange between ligated and unligated $CNAr^{Dipp2}$, even when mixing times as long as 1 ms are employed. The apparently static nature of the metal-ligand bonds in **2** is consistent with the typical kinetic interness displayed by complexes of third-row metals when compared to their lighter counterparts.

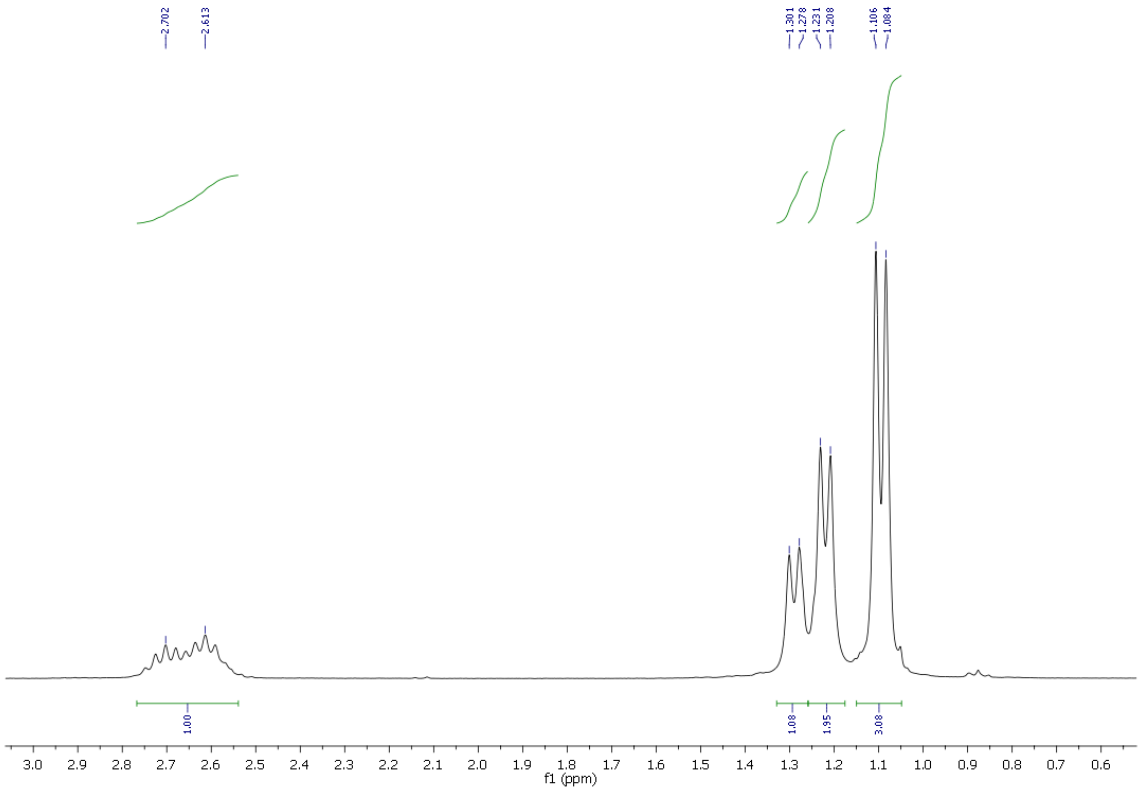

Figure 1.4. ^{1}H NMR spectrum (300.0 MHz, C_cD_6, 20 ˚C) of a 1:1 mixture of Pt(CNAr^{Dipp2})$_2$ (**2**) and CNAr^{Dipp2}. The septet at 2.61 ppm corresponds to **2**, while the septet at 2.70 ppm is attributable to CNAr^{Dipp2}. Note that the doublet centered at 1.10 ppm consists of overlapping doublets from these two compounds.

Density Functional Theory calculations were carried out on Pt(CNAr^{Dipp2})$_2$ (**2**) at the BP86 level of theory. The geometry-optimized structure of **2** agrees well with that seen in the solid state, with the exception of the C-Pt-C angle, which widens to near linearity (178.1˚, see Table 1.1). This suggests that the difference in energies with respect to C-Pt-C may be very small in the range of 170-180˚, with the larger degree of bending observed in the solid state due in part to crystallographic packing forces. While these values are substantially larger than those calculated by Andrews for Pt(CO)$_2$ (157.1˚, B3LYP level of theory), it should be kept in mind that the steric encumbrance of the *m*-terphenyl isocyanides may enforce a larger C-Pt-C angle than the thermodynamically-

predicted value for a complex of formulation $Pt(CNR)_2$. Further, the stronger π-acid character of CO relative to isocyanides may bias $Pt(CO)_2$ to adopt a more acute C-Pt-C angle so that backdonation from an otherwise orthogonal 5*d* orbital might be possible. The calculated 5*d* manifold of **2** is intuitive and contains of two nearly degenerate dπ orbitals, which are stabilized due to backbonding interactions (Figure 1.5). This set lies roughly 1 eV below a non-bonding s/d_{z2} hybrid and the doubly-degenerate non-bonding $d_{xy}/d_{x2\text{-}y2}$ set. This electronic landscape mirrors that calculated for $Pd(CNAr^{Dipp2})_2$.[66]

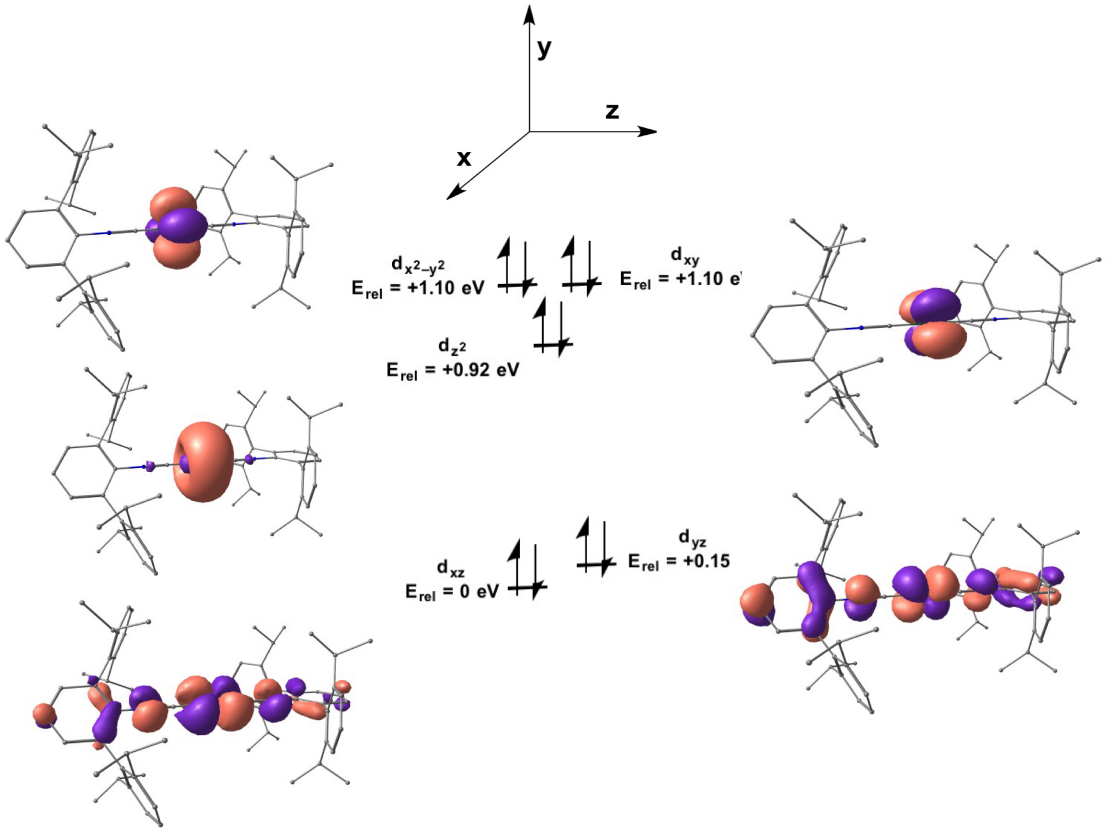

Figure 1.5. Calculated 5*d* orbital manifold of $Pt(CNAr^{Dipp2})_2$ (**2**). BP86/def2-TZVP/ZORA.

1.4. Concluding remarks and outlook

Reduction of $PtCl_2(CNAr^{Dipp2})_2$ (**1**) provides access to $Pt(CNAr^{Dipp2})_2$ (**2**), which is the first monomeric binary isocyanide complex of Pt(0) and the first two-coordinate Pt complex supported by a π-acidic ligand set. This complex represents the starting point for much of the work described in the remainder of this dissertation. Although the delineation of a broad reactivity profile for **2** is not emphasized here, intriguing synthetic transformations of **2** were uncovered that provided complexes which are the focus of Chapters 2 and 5. Further, the ability of **2** (as well as other zero-valent Group 10 *m*-terphenyl isocyanide complexes) to act as the Lewis basic component of Metal-only Lewis Pairs is the subject of Chapter 4.

1.5. Synthetic Procedures and Characterization Data

General considerations. All manipulations were carried out under an atmosphere of purified dinitrogen using standard Schlenk and glovebox techniques. Unless otherwise stated, reagent-grade starting materials were purchased from commercial sources and either used as received or purified by standard procedures.[75] Solvents were dried and deoxygenated according to standard procedures.[76] Benzene-d_6 (Cambridge Isotope Laboratories) was distilled from NaK alloy and stored over 4 Å molecular sieves under N_2 for at least 24 h prior to use. Celite 405 (Fisher Scientific) was dried under vacuum (24 h) at a temperature above 250 ˚C and stored in the glovebox prior to use. The *m*-terphenyl isocyanide $CNAr^{Dipp2}$ was prepared as previously reported.[54]

Solution ^1H and $^{13}C\{^1H\}$ NMR spectra were recorded on a Bruker Avance 300, a Varian Mercury 400, a Jeol ECA 500, or a Varian X-SENS 500 spectrometer. ^1H and

$^{13}C\{^{1}H\}$ chemical shifts are reported in ppm relative to $SiMe_4$ (^{1}H and ^{13}C $\delta = 0.0$ ppm) with reference to residual solvent resonances of 7.16 ppm (^{1}H) and 128.06 ppm (^{13}C) for C_6D_6. FTIR spectra were recorded on a Thermo-Nicolet iS10 FTIR spectrometer. Samples were prepared as C_6D_6 solutions injected into a ThermoFisher solution cell equipped with KBr windows. For solution FTIR spectra, solvent peaks were digitally subtracted from all spectra by comparison with an authentic spectrum obtained immediately prior to that of the sample. The following abbreviations were used for the intensities and characteristics of important IR absorption bands: vs = very strong, s = strong, m = medium, w = weak, vw = very weak; b = broad, vb = very broad, sh = shoulder. Combustion analyses were performed by Robertson Microlit Laboratories of Madison, NJ (USA).

Synthesis of $PtCl_2(CNAr^{Dipp2})_2$ (1, mixture of *cis- and trans- isomers*). To a THF solution of $PtCl_2$(1,5-COD) (COD = cyclooctadiene; 0.890 g, 2.37 mmol, 150 mL) was added a THF solution of $CNAr^{Dipp2}$ (2.06 g, 4.86 mmol, 2.05 equiv, 25 mL). The pale yellow solution was stirred for 36 h, whereupon all volatiles were removed under reduced pressure. ^{1}H NMR analysis of the resulting crude solid indicated a mixture of *cis*-$PtCl_2(CNAr^{Dipp2})_2$ and *trans*-$PtCl_2(CNAr^{Dipp2})_2$ in an approximately 3:1 ratio. The resulting solid was subjected to three cycles of slurrying in *n*-pentane (25 mL), stirring for 5 min, and drying *in vacuo* to facilitate the removal of liberated 1,5-COD. The solid was then extracted with acetonitrile (100 mL), filtered through Celite, and the filtrate was then dried *in vacuo* to afford exclusively *cis*-$PtCl_2(CNAr^{Dipp2})_2$ as a colorless solid. This solid is free of *trans*-$PtCl_2(CNAr^{Dipp2})_2$ as assayed by ^{1}H NMR spectroscopy. The pale yellow solid remaining on the Celite filter pad was dissolved in THF (20 mL) and then

dried *in vacuo*. Dissolution of this solid in 8 mL THF, followed by storage at –40 ˚C for 3 d yielded pale yellow crystals of *trans*-$PtCl_2(CNAr^{Dipp2})$, which were collected and dried *in vacuo*.

***cis*-$PtCl_2(CNAr^{Dipp2})_2$ (*cis*-1)**: Yield: 1.96 g, 1.76 mmol, 74%. Crystals of ***cis*-1** • 2 CH_2Cl_2 suitable for X-ray diffraction were grown via layering a CH_2Cl_2 solution with *n*-hexane and storing at –40 ˚C. ^{1}H NMR (499.8 MHz, C_6D_6, 20 ˚C): δ = 7.31 (t, 4H, *J* = 8 Hz, *p*-Dipp), 7.19 (d, 8H, *J* = 8 Hz, *m*-Dipp), 6.96 (d, 4H, *J* = 8 Hz, *m*-Ar), 6.89 (t, 2H, *J* = 8 Hz, *p*-Ar), 2.60 (septet, 8H, *J* = 7 Hz, C*H*$(CH_3)_2$), 1.20 (d, 24H, *J* = 7 Hz, CH(C*H*$_3)_2$), 1.05 (d, 24H, *J* = 7 Hz, CH(C*H*$_3)_2$) ppm. ^{13}C{^{1}H} NMR (125.7 MHz, C_6D_6, 20 ˚C): δ = 146.5, 139.6, 133.6, 130.8, 130.1, 129.4, 128.3, 127.2 (*C*≡N), 123.8, 31.3, 25.1, 24.2 ppm. FTIR (C_6D_6, KBr windows, 20 ˚C): ν(*C*≡N) = 2203 (w) and 2172 (s) cm^{-1}, also 2964, 2928, 2906, 2868, 1594, 1578, 1463, 1411, 1385, 1364, 1056, 794, 759 cm^{-1}. Anal. Calcd for $C_{62}H_{74}N_2Cl_2Pt$: C, 66.89; H, 6.70; N, 2.52. Found: C, 66.57; H, 6.62; N, 2.47.

***trans*-$PtCl_2(CNAr^{Dipp2})_2$ (*trans*-1)**: Yield: 0.25 g, 0.22 mmol, 9%. Crystals of ***trans*-1** • C_6H_5F • 2 MeCN suitable for X-ray diffraction were grown from an acetonitrile/fluorobenzene solution stored at –40 ˚C. ^{1}H NMR (499.8 MHz, C_6D_6, 20 ˚C): δ = 7.33 (t, 4H, *J* = 8 Hz, *p*-Dipp), 7.18 (d, 8H, *J* = 8 Hz, *m*-Dipp), 6.89 (d, 4H, *J* = 8 Hz, *m*-Ar), 6.84 (t, 2H, *J* = 8 Hz, *p*-Ar), 2.52 (septet, 8H, *J* = 7 Hz, C*H*$(CH_3)_2$), 1.34 (d, 24H, *J* = 7 Hz, CH(C*H*$_3)_2$), 1.03 (d, 24H, *J* = 7 Hz, CH(C*H*$_3)_2$) ppm. ^{13}C{^{1}H} NMR (125.7 MHz, C_6D_6, 20 ˚C): δ = 146.3, 140.6, 133.1, 132.6 (*C*≡N), 130.0, 129.9, 129.8, 126.2, 123.7, 31.5, 24.8, 24.1 ppm. FTIR (C_6D_6, KBr windows, 20 ˚C): ν(*C*≡N) = 2192 cm^{-1},

also 2962, 2929, 2906, 2865, 1615, 1598, 1577, 1455, 1414, 1386, 1360, 1054, 795, 756 cm^{-1}. Anal. Calc'd for $C_{62}H_{74}N_2Cl_2Pt$: C, 66.89; H, 6.70; N, 2.52. Found: C, 66.62; H, 6.62; N, 2.47.

Synthesis of $Pt(CNAr^{Dipp2})_2$ (2): To 40 mL of a 4:1 Et_2O/THF solution containing $PtCl_2(CNAr^{Dipp2})_2$ (3.30 g, 2.97 mmol, 3:1 mixture of *cis*- and *trans*-isomers) was added freshly activated Mg^0 turnings (0.36 g, 14.8 mmol, 5.0 equiv). The mixture was stirred for 7 h, during which time it became dark brown in color. The solution was decanted off from the residual Mg^0 turnings and all volatiles were then removed under reduced pressure. The resulting brown solid was subjected to three cycles of slurrying in *n*-pentane (25 mL), stirring for 5 min, and drying *in vacuo* so as to remove remaining THF. The residue was then extracted with Et_2O (200 mL), filtered through Celite, and dried *in vacuo*. The resulting solid was dissolved in 15 mL THF, layered with 5 mL *n*-pentane, and stored at –35 ˚C for 3 days to afford $Pt(CNAr^{Dipp2})_2$ as bright yellow crystals, which were collected, washed with 2 x 10 mL *n*-pentane, and dried *in vacuo*. Concentration of the mother liquor to 3 mL and storage at –40 ˚C for 4 weeks afforded a second crop of crystals, which were also collected and dried. Yield: 2.12 g, 2.03 mmol, 68%. ^{1}H NMR (399.9 MHz, C_6D_6, 20 ˚C): δ = 7.30 (t, 4H, *J* = 8 Hz, *p*-Dipp), 7.17 (d, 8H, *J* = 8 Hz, *m*-Dipp), 6.95-6.88 (m, 6H, *p*-Ar and *m*-Ar), 2.61 (septet, 8H, *J* = 7 Hz, C*H*$(CH_3)_2$), 1.22 (d, 24H, *J* = 7 Hz, CH(C*H*$_3)_2$), 1.09 (d, 24H, *J* = 7 Hz, CH(C*H*$_3)_2$) ppm. ^{13}C{^{1}H} NMR (100.6 MHz, C_6D_6, 20 ˚C): δ = 169.2 (*C*≡N), 146.5, 139.4, 134.7, 129.7, 129.5, 127.7, 123.4, 122.9, 31.4, 24.6, 24.3 ppm. FTIR (C_6D_6, KBr Windows, 20 ˚C): ν(C≡N) = 2065 (s), 2019 (w) cm^{-1}, also 2963, 2926, 2869, 1580, 1463, 1384, 1364, 1262,

1029, 796, 753 cm^{-1}. Anal. Calc'd for $C_{62}H_{74}N_2Pt$: C, 71.44; H, 7.16; N, 2.69. Found: C, 71.19; H, 7.25; N, 2.66.

1.6. Details of DFT computational studies

Density Functional Theory (DFT) calculations were carried out on $Pt(CNAr^{Dipp2})_2$ (**2**, full molecule), as well as for the model complexes *cis*- and *trans*-$PtCl_2(CNPh)_2$. Calculations were carried out using the ORCA program package.[77] Geometry optimizations and single-point calculations were performed using the BP86 pure density functional.[78-80] The all-electron Ahlrichs triple-zeta basis sets def2-TZVP (standard)[81] and def2-TZVP/J (auxiliary)[82] were used in all calculations. The resolution of identity (RI) approximation was employed.[83] Relativistic effects were included by use of the zeroth-order regular approximation (ZORA).[84-86] Crystallographic atomic coordinates were used as input for geometry optimizations where appropriate. Viewing of optimized structures and rendering of molecular orbitals was performed using the program *Chemcraft*.[87]

Input file for geometry optimization of *cis*-$PtCl_2(CNPh)_2$

```
%pal nprocs 8 end

! RKS Opt BP86 ZORA def2-TZVP def2-TZVP/J KeepDens NormalPrint TightSCF
Grid4 PrintMOs
%output
Print[ P_Basis ] 2
Print[ P_MOs ] 1
end

* xyz 0 1
Pt       9.68670322       7.03785899       5.12956294
Cl      11.21439845       5.37269928       5.67728883
N        7.35829829       8.80592157       4.17685266
C        8.30604453       8.22913689       4.57149942
C        6.15398419       9.31287056       3.71569826
C        5.87756751       9.28291506       2.32394374
```

C	4.64179572	9.78904579	1.90007107
H	4.42072503	9.78488628	0.83239088
C	3.70888803	10.29042681	2.80615992
H	2.75174311	10.67316969	2.44905142
C	4.00427146	10.30899131	4.16772585
H	3.28269510	10.70780041	4.88174379
C	5.22936248	9.83516210	4.65510773
H	16.12347212	10.65453089	5.36413007
C	14.16955653	9.79869296	5.59336818
H	16.65955478	10.60834314	7.79565627
Cl	8.14426770	5.38318993	4.59011522
C	15.39996726	10.26036820	6.07877167
N	12.03284632	8.78759693	6.07249072
C	11.07932644	8.21858948	5.68049755
C	13.24231890	9.28225681	6.53347737
C	13.52137926	9.24600609	7.92438178
C	14.76280012	9.73979035	8.34647884
H	14.98616133	9.73067812	9.41365448
C	15.69816214	10.23532462	7.43968228
H	6.58508221	8.88755688	1.61014065
H	5.45179634	9.87103819	5.71134448
H	13.94504908	9.83924481	4.53773948
H	12.81183279	8.85521237	8.63868150
*			

Optimized Cartesian coordinates of *cis*-$PtCl_2(CNPh)_2$

Pt	9.68935283616328	6.53088043845772	5.11381090330804
Cl	11.19205636755053	4.89268290402246	5.79518465742284
N	7.57634156605265	8.53423911586454	4.14399768042824
C	8.40206773600928	7.78712351213474	4.52544984814095
C	6.49100540882672	9.22211679194961	3.64159511601851
C	5.39432106989619	8.49778607637473	3.14472536575854
C	4.29969243577607	9.19446411060037	2.63767882324486
H	3.44561246642620	8.63765565975055	2.25067917388967
C	4.29260508294721	10.59299218659771	2.62346655129924
H	3.43133785066414	11.12982261058422	2.22454750033332
C	5.38955728164356	11.30318640150152	3.12044242818480
H	5.38639603206557	12.39365293425559	3.11024688930836
C	6.49456421412071	10.62543324563258	3.63215983777285
H	14.02627500727085	12.35406164647432	7.13558926129313
C	12.91185025833447	10.58941358421922	6.61530082648601
H	15.97131163783061	11.08399316454198	8.03425919411088
Cl	8.16761575550034	4.91754717753650	4.41433622250386
C	14.01800088647924	11.26359587969664	7.12934472733614
N	11.82188399689112	8.50215775493709	6.10610557345006
C	10.98949369520363	7.76740420815020	5.71565220938215
C	12.90862549665464	9.18605609578667	6.61061600578546
C	13.99957558115270	8.45805749554067	7.11460493468492
C	15.09548084664366	9.15126755457626	7.62382001427808
H	15.94540249280286	8.59176793201337	8.01606686679663
C	15.10934492977403	10.54970497176241	7.63348340991778
H	5.42047969409082	7.40850614217320	3.16495015160475
H	7.35757400796152	11.16381995211168	4.02306273808928

```
H    12.05339949008319     11.13102815090367      6.21893945917784
H    13.96882631518412      7.36888681184988      7.09759067999275
```

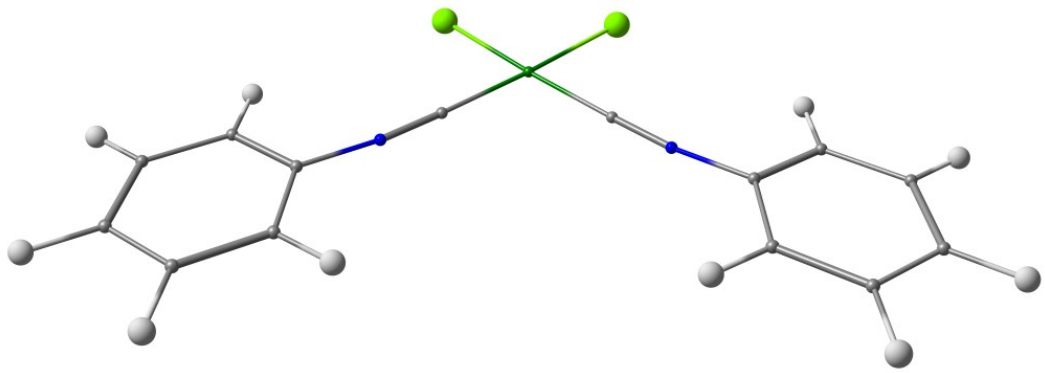

Figure 1.6. Optimized molecular structure of *cis*-$PtCl_2(CNPh)_2$.

Input file for geometry optimization of *trans*-$PtCl_2(CNPh)_2$

```
%pal nprocs 8 end

! RKS Opt BP86 ZORA def2-TZVP def2-TZVP/J KeepDens NormalPrint TightSCF
Grid4 PrintMOs
%output
Print[ P_Basis ] 2
Print[ P_MOs ] 1
end

* xyz 0 1
Pt      11.32281700      14.46745200       4.53145500
Cl       9.68464600      15.34345500       5.88527000
Cl      12.94713500      13.60089600       3.16841300
N       13.36333400      14.41255900       6.86987900
N        9.39989400      14.37094200       2.10213800
C       12.59527400      14.44779300       6.02417100
C       10.08329900      14.43400600       3.01891900
C       14.26838400      14.42124000       7.94281700
C       15.05491500      13.28940600       8.17004700
C       15.89224000      13.32336400       9.28057200
H       16.44019500      12.57195700       9.47534100
C       15.94149400      14.43528200      10.10406900
H       16.50022400      14.42813300      10.87289400
C       15.18728600      15.55128600       9.81704100
H       15.25962900      16.31494800      10.37572000
C       14.32379500      15.58396700       8.73043500
C        8.58411800      14.23766400       0.97042800
H        7.64520600      15.84260600      -1.67774700
C        7.02952600      13.96089800      -1.25745600
H        6.62009900      12.12259400      -0.48692300
H        6.50158100      13.85877000      -2.03994900
C        8.50715800      15.31383800       0.07688200
```

```
C        7.71601000      15.13817800      -1.04389400
C        7.88993900      13.04098000       0.80470400
C        7.10956500      12.92302200      -0.33486600
H       15.01743147      12.42910748       7.51821770
H       13.73153902      16.46010246       8.51130146
H        9.03581047      16.24046396       0.24508099
H        7.95388210      12.24073538       1.52714419
*
```

Optimized Cartesian coordinates of *trans*-$PtCl_2(CNPh)_2$

```
Pt   11.43251860147065     14.30228238087372      4.45628359764354
Cl   11.00159795549551     16.58741616307003      4.71613230552415
Cl   11.86406003471405     12.01716023084211      4.19706298104741
N    13.36804012454039     14.39465824239031      6.88154690121386
N    9.49626018895238     14.21007388539459      2.03168367073866
C    12.63757134384072     14.35936784820208      5.96444149803671
C    10.22741211525600     14.24518930739262      2.94826857062484
C    14.22844565004023     14.43667475740244      7.95813583090031
C    14.88130077066498     13.26247366602389      8.36557380809741
C    15.74872757507134     13.31627690443900      9.45452237168170
H    16.26001907869899     12.40892770538253      9.77753835344527
C    15.96361981509522     14.52208816955706     10.12936260498721
H    16.64410183489121     14.55548877192926     10.98086892337219
C    15.30742268327869     15.68512829400720      9.71416499612632
H    15.47422144346540     16.62615617849830     10.23926195356031
C    14.43601424452998     15.65320778835355      8.62754018373701
C    8.63880118457879     14.16940876770839      0.95269302698274
H    6.61255718073132     16.20022207300414     -0.86931894085590
C    6.90980545195552     14.08749683425622     -1.22362050969308
H    7.39957975280595     11.98372162349775     -1.33567944427736
H    6.23216810162565     14.05553327880603     -2.07757467415851
C    7.98694442966425     15.34417816082929      0.54537995613730
C    7.12278647990554     15.29228886846875     -0.54630450843569
C    8.43303244112034     12.95395047650329      0.28090337543444
C    7.56475853803933     12.92380244046233     -0.80828603005321
H    14.69960210827214     12.33356780187460      7.82579969565578
H    13.91456581563980     16.54753837542878      8.28790271793603
H    8.16705956854474     16.27230118063985      1.08697704210801
H    8.95343154711082     12.05906510476195      0.62084408248253
```

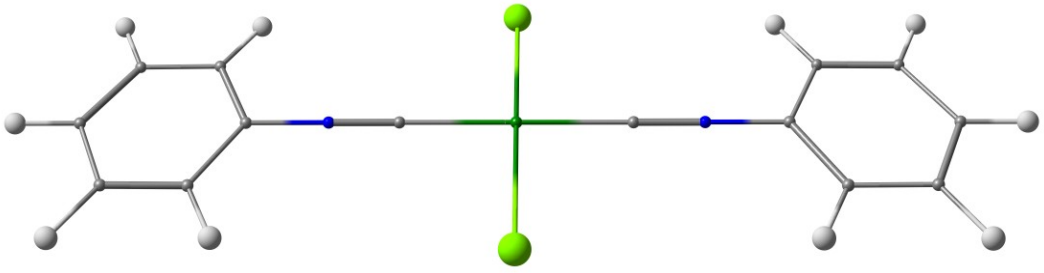

Figure 1.7. Optimized molecular structure of *trans*-$PtCl_2(CNPh)_2$.

Input file for geometry optimization of Pt(CNAr^{Dipp2})$_2$

```
%pal nprocs 8 end

! RKS Opt BP86 ZORA def2-TZVP def2-TZVP/J KeepDens NormalPrint TightSCF
Grid4 PrintMOs
%output
Print[ P_Basis ] 2
Print[ P_MOs ] 1
end

* xyz 0 1
H      13.81536400      11.47177800       7.16521900
H      14.18566600       9.98159600       6.84524800
H      13.48662200      10.86454500       5.75734600
H      16.74048900      11.31422600       2.61523000
H      16.34014200       9.49745100       1.22442300
H      14.19437400       8.70968900       0.91511700
H      15.72831800      15.87175500       6.03465500
H      15.89850800      13.77598100       6.98603500
H      15.74234800      10.69386400       5.25605800
H      15.08769200      16.10480100       3.83112000
H      17.36919100      11.55383700       6.73859100
H      16.64612900      10.28357100       7.30600600
H      16.25401700      11.70810700       7.82862600
H      14.41893100      13.44938800       1.54226100
H      15.66344300      15.98991900       1.57212500
H      15.35196800      15.16441100       0.27517500
H      16.42690200      14.64908300       1.29268300
H      12.48218800      14.52599600       2.30592500
H      12.91073900      15.14307600       0.93218200
H      13.21367300      15.91114300       2.26326200
H       9.71686700       7.42793500       3.13998300
H       8.34861800       8.40771400       1.57639100
H       9.13207500      10.10960700       0.23677900
H      12.37061600      11.61784200       0.43302800
H      10.89167800      10.51990000      -1.70011300
H      12.19666900      10.29013600      -1.46333400
H       9.70251300      12.29072200      -0.20904800
H      10.92718600      13.26393600      -0.31143900
H      10.42402900      12.78143200       1.09216800
H      13.05636200       8.41263700       3.90578000
H      11.29958700       8.71953600       5.43950800
H      12.21209500       7.50835300       5.84053900
H      10.81972900       7.25233000       5.16433300
H      11.86310800       5.94595900       3.23384100
H      13.19674200       6.07397000       4.04870100
H      13.14350800       6.54006200       2.55336900
H       2.70318000      13.32958300       1.83876700
H       1.51818200      13.82357500       3.77352600
H       2.53045900      13.63976400       5.84053900
H       6.84970000      15.10697000       8.37257700
H       6.73249100      13.29840100       9.79324800
H       5.67231500      11.36510200       9.15117300
H       3.67430000      10.95645100       6.24796900
```

H	5.76836700	10.32460000	5.42457700
H	4.95474800	9.04941100	5.83840600
H	6.09218000	9.59263900	6.77272100
H	4.41475900	9.59592100	8.60935500
H	3.24068200	9.18727000	7.65370800
H	3.13540800	10.49528200	8.51123100
H	5.55287400	15.20215800	5.04487700
H	4.12325200	16.39528800	6.44848400
H	5.11644900	17.38983700	5.75308000
H	5.34676900	16.96641500	7.24627900
H	7.68339000	16.30010000	6.52101100
H	7.39231700	16.55776400	5.00434800
H	7.87493200	15.14471700	5.48003800
H	5.88350400	10.07514300	-0.46929100
H	7.14355900	11.68184800	-1.54866000
H	7.31550800	13.80224000	-0.68900400
H	5.74775400	14.98552300	2.29952600
H	5.88756200	15.92919600	-0.35623400
H	5.56456600	16.83676300	0.88098700
H	4.55815000	15.71748500	0.44796000
H	8.07186000	14.73114200	2.24833000
H	7.69821700	16.23773600	2.02648400
H	8.12298900	15.34658100	0.80846000
H	3.95528900	10.57569900	2.49150800
H	5.81280300	8.65224800	1.54439400
H	4.89668000	8.46843700	2.80508000
H	6.05472300	9.52699200	2.82427800
H	2.75467800	10.20807700	0.53115200
H	2.91076800	8.84918900	1.29694900
H	3.81369600	9.15444600	0.05332900
C	11.35052300	12.07523700	3.79037800
C	7.58554400	12.54969900	4.11354800
C	13.52686900	11.15339100	2.91557700
C	15.04034200	12.86086500	3.99217300
C	15.87089000	11.01061000	2.48788200
C	15.63056900	9.91348700	1.65595700
C	14.33875200	9.44165100	1.47165400
C	13.25536900	10.04346800	2.10349000
C	15.16945200	15.25369000	4.19759400
C	14.91137000	14.13835100	3.40555900
C	14.80733500	11.65214300	3.12846400
C	15.54632300	15.11648900	5.52462100
C	15.65397300	13.85787500	6.09225000
C	15.39451500	12.70429700	5.33711800
C	15.48401200	11.31701600	5.96788700
C	14.11610100	10.86618700	6.48154800
C	16.53459400	11.20590900	7.06090900
C	14.50732400	14.33250200	1.95715600
C	15.58784700	15.10532900	1.20415800
C	13.15050600	15.04460500	1.85519200
C	11.85010400	9.56605200	1.93155900
C	11.36850200	8.53917200	2.77308300
C	10.04710500	8.11624200	2.60733800
C	9.22615500	8.70214000	1.66918300
C	9.69715700	9.72376800	0.86584200

C	11.00705700	10.18395200	0.98615100
C	11.49269500	11.33145800	0.10260400
C	11.66181600	10.86946900	-1.34814500
C	10.54866600	12.52737900	0.17534400
C	12.23931000	7.87942100	3.82386800
C	11.58246400	7.83658700	5.19313100
C	12.64802300	6.48098000	3.37313500
C	5.06751900	12.87563500	4.00369200
C	4.47481700	12.92946500	2.73276600
C	3.12802500	13.28313800	2.66578600
C	2.41137300	13.56870100	3.82941400
C	3.02539300	13.47318500	5.07111500
C	4.36397700	13.13264200	5.17969200
C	5.07295000	13.14002800	6.50095900
C	5.78042500	14.30279700	6.86530000
C	6.39310100	14.34054300	8.10742700
C	6.32937700	13.25080700	8.95577700
C	5.68064500	12.09542300	8.57629200
C	5.03576400	12.01172300	7.34696300
C	4.37784000	10.72225600	6.88705800
C	5.39191500	9.84045500	6.16349600
C	3.73171500	9.92579600	8.02103500
C	5.90039300	15.48821400	5.91647900
C	5.04033300	16.67100500	6.38491600
C	7.34539200	15.91278400	5.71169700
C	5.26593300	12.57169000	1.51495600
C	5.20467900	11.26056000	1.02881400
C	5.92136100	10.93987500	-0.12756200
C	6.68797100	11.90176500	-0.76793100
C	6.77933400	13.17531300	-0.26003000
C	6.07604500	13.54178600	0.89250600
C	6.19522900	14.95959300	1.42835100
C	5.48542600	15.95217200	0.51579300
C	7.65941900	15.35642800	1.64827800
C	4.42163000	10.17115100	1.73147000
C	5.38664900	9.10439100	2.27776800
C	3.37923100	9.53683900	0.81869900
N	12.44387000	11.79869900	3.51520200
N	6.42604600	12.62174600	4.07621800
Pt	9.49485100	12.40529200	4.07651700
H	11.98911043	11.24735168	-2.14418710

*

Optimized Cartesian coordinates of $Pt(CNAr^{Dipp2})_2$

H	13.24479869153030	12.00972736459368	8.03436023110470
H	13.40418422854720	10.27686234343460	7.69008749022059
H	12.33200535861797	11.29071252570423	6.69100811860016
H	16.74675240715133	11.93647876193738	3.39874363203736
H	17.25625505157000	9.88214452997704	2.08630383299142
H	15.39880431242045	8.45166196075980	1.24704695239172
H	13.78752570759672	16.17681086708412	6.16902175630002
H	14.06805849549647	14.00637804708309	7.32838465588733
H	14.49192571824694	10.73235739973335	5.53140785009596

H	13.83459788159628	16.27691215638864	3.69488662486479
H	16.66196169964302	11.64842667648615	6.34910619290338
H	15.93861386508570	10.54505404362534	7.54555223446115
H	15.85643793997195	12.30507296778690	7.78939089389224
H	14.27097453556948	13.25313529720145	1.50284479209818
H	15.41209061660860	16.08888702034143	1.80347788298805
H	15.45919149518666	15.09326656847259	0.33117063901203
H	16.36139732142742	14.58795160320928	1.78144038844849
H	12.01095836162529	14.33544899266617	1.68662730075612
H	12.91639950975527	14.88842181479532	0.25462896284387
H	12.78039406575057	15.93625537818569	1.67971094414630
H	10.94470818026947	6.02316057169974	2.41259989080201
H	9.99984645293709	6.41497097344573	0.15757463523180
H	10.78244356238759	8.33303363558771	-1.19996672983371
H	13.36911484587743	10.79375090338736	-0.01878994748916
H	12.70700079043762	9.11114313107264	-2.50142324426195
H	14.24297086270297	9.07870747753467	-1.60991965117349
H	10.73681631272720	10.61267947647085	-1.59711415075822
H	11.84193268649018	11.99975701579931	-1.53311009097561
H	10.95576590686867	11.49343085513901	-0.07160691360884
H	13.53027946221797	8.24740880728559	3.99565659354849
H	11.15340577558795	8.32544392170728	4.80299180838565
H	12.17778026096089	7.26601886615997	5.80523075347012
H	11.04201641581081	6.56053454245186	4.63903866031829
H	13.03753540681077	5.25568662870562	3.50668279711110
H	14.09786230665793	5.95243982144123	4.75253251596990
H	14.49028832559907	6.15818574258073	3.02736530947099
H	2.27080468029909	13.88117175075633	2.32940665905142
H	1.38018709263580	14.29201417426342	4.61829240686024
H	2.86581741055644	14.01553296705160	6.59719950296109
H	7.55487878852417	15.07170138174415	8.68205371009895
H	7.57928507750832	12.91848064511450	9.90478973986675
H	6.27531728225859	10.99281126425804	9.05273276922778
H	4.24895381391463	11.09529415862609	5.88829746832534
H	6.42381216659654	9.84253966284162	5.94770087248547
H	5.01953863206932	8.77843210378145	6.21594059494488
H	6.04350725194292	9.26124689890095	7.58194899655789
H	3.91632165573047	10.22945822227588	8.81684350720947
H	2.95441078117703	9.64693619635295	7.43891632147347
H	2.85547151177364	11.35296588490238	7.94127687416813
H	5.65621832111329	15.61960938016375	5.48328317221821
H	4.47765439125021	16.53026423442011	7.48441535449579
H	5.49096652347898	17.77254728753458	6.70860901633279
H	6.03440649647700	16.98601530112319	8.20785538695121
H	8.26151027445783	16.37139707677388	6.93183250526662
H	7.61426539776109	17.10907144419818	5.45370140964236
H	8.16125907943970	15.41319970122574	5.43990336281153
H	5.00644391599872	10.68327661116437	-0.75525427246041
H	5.90388803872743	12.57785955130494	-2.07399411075765
H	6.09764245001438	14.82281744328954	-1.04676974312848
H	5.15052259097805	15.56155036094143	2.51606311498411
H	4.65644033544996	16.71221654966855	-0.28870994653145
H	4.52638180824267	17.60458105630929	1.24387982927688
H	3.40109692297813	16.27073609219411	0.88795885417250
H	7.56976661997495	15.44881387336309	1.85436890350248

H	6.94749550094111	17.11878088906024	1.87621981368768
H	7.19107171608350	16.28101194999376	0.33165038090714
H	3.91124628706970	10.98285537495808	2.82878596719621
H	5.33722067583874	9.08342968024677	0.87650095942802
H	4.73666029026376	8.68460237770816	2.49780148970865
H	6.08272360840656	9.83586680357140	2.30157870380027
H	2.02278327574814	10.97393297449022	1.19775165923650
H	2.36876340119108	9.33369096383334	1.80003329618485
H	2.89845311705254	9.81699702645309	0.17343876410944
C	11.14324554561398	11.49854125214744	3.28060520857694
C	7.51414928456505	12.51687461032477	3.82300348580911
C	13.57658922081831	10.85317348583596	2.81941265526200
C	14.33867257168471	12.92456498245248	4.10161292590052
C	15.93642239976696	11.30641969814129	3.02931002375707
C	16.22043000267397	10.15500831566410	2.29360999831372
C	15.18057239660671	9.35229767943124	1.82271271946775
C	13.84173012162599	9.67753004697503	2.07196071855658
C	13.96933731254093	15.31751472150404	4.19811339620593
C	14.16392780915995	14.16013163113957	3.43233582113037
C	14.61716358975697	11.68254278167699	3.30941054436535
C	13.94135164963559	15.26492465305343	5.58918808026910
C	14.10111040347991	14.04325355566593	6.23788573130806
C	14.29745327792545	12.85854602137738	5.51554548531896
C	14.47018447886882	11.54574404742753	6.27278477451584
C	13.29237474887052	11.26727039280073	7.22400520637164
C	15.81046499963001	11.50921850403003	7.03072418228754
C	14.19270303358997	14.27196251360561	1.91164254312118
C	15.42942291297435	15.05374317299514	1.43048250779244
C	12.89842130078479	14.89178535512629	1.35474623503078
C	12.74202934274918	8.79743919991662	1.55743983730052
C	12.28847031366394	7.71055870515288	2.34411500612356
C	11.30240733497392	6.86551817377613	1.81740960035800
C	10.76802924365764	7.08347414438121	0.55011036033902
C	11.21133254948911	8.16196385653036	-0.21078783969321
C	12.19553775070189	9.03457491798228	0.27257204089398
C	12.64785262057735	10.20019645957965	-0.60065933232120
C	13.37745928997767	9.70732924529747	-1.86416477461827
C	11.47677278232961	11.12929496079171	-0.96769788622038
C	12.84525306507180	7.42625555417380	3.73533017477569
C	11.73869963911376	7.39575599239837	4.80469655347622
C	13.66668397454707	6.12375400837704	3.75471629611401
C	5.07341494358653	13.22009203138904	4.13679967339597
C	4.24726066701803	13.37277159256765	2.99451718828675
C	2.91750394514449	13.76019897138634	3.19959064547677
C	2.41979242974862	13.99017156135827	4.48280670918896
C	3.25126611892803	13.83539347816795	5.59269022217190
C	4.58941053634672	13.44893490533051	5.45000954868387
C	5.45987738863235	13.28767912536081	6.66022019405911
C	6.21549939140426	14.38781329975940	7.13396838291022
C	6.96860096969254	14.23136567156869	8.30525365881276
C	6.98571771492572	13.02185339995654	8.99469425089862
C	6.25053061045622	11.94165788696864	8.51357578394711
C	5.48265108366476	12.04900626076601	7.34623997269848
C	4.69477297141784	10.83644419404491	6.86070454376607
C	5.60071786078859	9.61206314292951	6.63788455825942

C	3.53754624821113	10.49929353811988	7.81938717837456
C	6.22415419857362	15.73477348141487	6.41893426620741
C	5.51367147890169	16.81657913745188	7.25326430711080
C	7.64818823991518	16.17792827476983	6.03901567891921
C	4.75655482220578	13.13819376977834	1.60364864271843
C	4.65916181180349	11.84856948658158	1.02717770647428
C	5.07689295416322	11.67240280423520	-0.29885704512534
C	5.58373267847556	12.73488106485506	-1.04237146469856
C	5.68940999301481	13.99616288286719	-0.46211151563967
C	5.28605843452246	14.22150296251362	0.86080930955066
C	5.42084688870439	15.62136115762317	1.45086653392942
C	4.44271327015197	16.60751898615328	0.78573375375203
C	6.86684617692085	16.14320667714445	1.37399533557984
C	4.10975371618818	10.65291981252049	1.79774700052242
C	5.12838129723305	9.50097952812404	1.87277757597329
C	2.77194030897433	10.16925909951627	1.20825774749334
N	12.27190169805026	11.20022957121081	3.07505220572845
N	6.38259005163358	12.83935895969062	3.96639592987583
Pt	9.32941866593366	11.99545346501149	3.58006561735411
H	13.73683189557678	10.55973985433664	-2.46029438306267

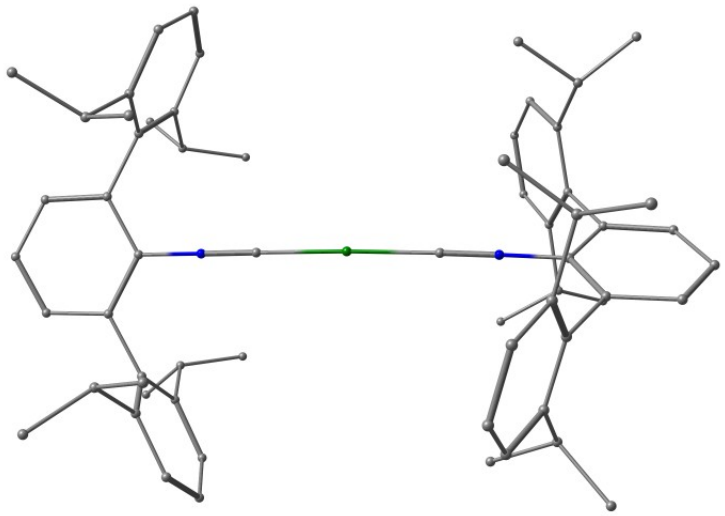

Figure 1.8. Optimized molecular structure of $Pt(CNAr^{Dipp2})_2$.

Table 1.1. Comparison of selected metrical parameters between crystallographically characterized $Pt(CNAr^{Dipp2})_2$ (**2**, "Crystal") and DFT optimized coordinates ("DFT").

Parameter	Mean d(Pt-C_{CNR}) (Å)	C1-Pt-C2 (°)
Crystal	1.906(2)	170.5(1)
DFT	1.904	178.1
% Difference	0.1%	4.4%

1.7. Details of crystallographic structure determinations

General considerations. Single crystal X-ray structure determinations were carried out at low temperature on Bruker Kappa Diffractometers equipped with a Mo radiation source and a Bruker APEX or APEX-II detector. All structures were solved via direct methods with SIR 2004[88] or SHELXS[89] and refined by full-matrix least-squares procedures utilizing SHELXL[89] within the OLEX2 small molecule structure solution and refinement software.[90] Crystallographic data collection and refinement information are listed in Table 1.2.

Table 1.2. Crystallographic data collection and refinement information.

Name	***cis*-1** • 2 CH_2Cl_2	***trans*-1** • (C_6H_5F, 2 C_2H_3N)	**2** • C_4H_8O
Formula	$PtC_{64}H_{78}N_2Cl_6$	$PtC_{72}H_{85}N_4Cl_2F$	$PtC_{66}H_{82}N_2OPt$
Crystal System	Monoclinic	Orthorhombic	Monoclinic
Space Group	*C2/c*	$Pna2_1$	$P2_1/n$
a, Å	23.427(3)	15.392(3)	16.2253(8)
b, Å	12.408(2)	25.532(5)	16.4117(8)
c, Å	22.030(3)	17.085(3)	21.4546(9)
α, deg	90	90	90
β, deg	111.479(5)	90	96.143(2)
γ, deg	90	90	90
V, $Å^3$	5959(1)	6714(2)	5680.2(5)
Z	4	4	4
Radiation (λ, Å)	Mo-Kα, 0.71073	Mo-Kα, 0.71073	Mo-Kα, 0.71073
ρ (calcd.), g/cm^3	1.430	1.278	1.303
μ, mm^{-1}	2.664	2.214	2.513
Temp, K	100	100	100
θ max, deg	26.413	26.791	26.000
data/parameters	6349 / 339	14148 / 739	11157 / 647
R_1	0.0397	0.0248	0.0283
wR_2	0.0791	0.0446	0.0612
GOF	1.120	1.002	1.047

1.8. Acknowledgements

The complexes ***cis*-1**, ***trans*-1** and **2** originally appeared in Barnett, B.R.; Moore, C.E.; Rheingold, A.L.; Figueroa, J. S. *Journal of the American Chemical Society,* **2014**, *136*, 10262. Copyright 2014, American Chemical Society. Permission to include published material in this dissertation has been obtained from all coauthors. The dissertation author is the first author of this paper.

1.9. References

(1) Schützenberger, P. *Bull. Soc. Chim. Fr.* **1868**, *10*, 188.

(2) Mond, L.; Langer, C.; Quincke, F. *J. Chem. Soc.* **1890**, *57*, 749.

(3) Abel, E. W.; Stone, F. G. A. *Q. Rev., Chem. Soc.* **1970**, *24*, 498.

(4) Collman, J. P. *Acc. Chem. Res.* **1975**, *8*, 342.

(5) Ellis, J. E., in *Advances in Organometallic Chemistry*, ed. F.G.A. Stone and R. West, Academic Press, **1990**, *31*, 1.

(6) Ellis, J. E. *Organometallics* **2003**, *22*, 3322.

(7) Behrens, H., in *Advances in Organometallic Chemistry*, ed. F.G.A. Stone and R. West, Academic Press, **1980**, *18*, 1.

(8) Chini, P. *J. Orgaonomet. Chem.* **1980**, *200*, 37.

(9) Mond, L.; Quincke, F. *J. Chem. Soc.* **1891**, *59*, 604.

(10) Mond, L.; Langer, C. *J. Chem. Soc.* **1891**, *59*, 1090.

(11) Calabrese, J. C.; Dahl, L. F.; Cavalieri, A.; Chini, P.; Longoni, G.; Martinengo, S. *J. Am. Chem. Soc.* **1974**, *96*, 2616.

(12) Longoni, G.; Chini, P.; Lower, L. D.; Dahl, L. F. *J. Am. Chem. Soc.* **1975**, *97*, 5034.

(13) Longoni, G.; Chini, P.; Cavalieri, A. *Inorg. Chem.* **1976**, *15*, 3025.

(14) Basolo, F.; Wojcicki, A. *J. Am. Chem. Soc.* **1961**, *83*, 520.

(15) Day, J. P.; Basolo, F.; Pearson, R. G.; Kangas, L. F.; Henry, P. M. *J. Am. Chem. Soc.* **1968**, *90*, 1925.

(16) Day, J. P.; Basolo, F.; Pearson, R. G. *J. Am. Chem. Soc.* **1968**, *90*, 6927.

(17) Carbó, J. J.; Bo, C.; Poblet, J. M.; Moretó, J. M. *Organometallics* **2000**, *19*, 3516.

(18) Rest, A. J.; Turner, J. J. *J. Chem. Soc., Chem. Commun.* **1969**, 1026.

(19) DeKock, R. L. *Inorg. Chem.* **1971**, *10*, 1205.

(20) Burdett, J. K. *Inorg. Chem.* **1975**, *14*, 375.

(21) Liang, B.; Zhou, M.; Andrews, L. *J. Phys. Chem. A* **2000**, *104*, 3905.

(22) Manceron, L.; Alikhani, M. E. *Chem. Phys.* **1999**, *244*, 215.

(23) Zhou, M.; Andrews, L. *J. Am. Chem. Soc.* **1998**, *120*, 11499.

(24) Kuendig, E. P.; McIntosh, D.; Moskovits, M.; Ozin, G. A. *J. Am. Chem. Soc.* **1973**, *95*, 7234.

(25) Willner, H.; Bodenbinder, M.; Bröchler, R.; Hwang, G.; Rettig, S. J.; Trotter, J.; Ahsen, von, B.; Westphal, U.; Jonas, V.; Thiel, W.; Aubke, F. *J. Am. Chem. Soc.* **2001**, *123*, 588.

(26) Calabrese, J. C.; Dahl, L. F.; Chini, P.; Longoni, G.; Martinengo, S. *J. Am. Chem. Soc.* **1974**, *96*, 2614.

(27) Longoni, G.; Chini, P. *J. Am. Chem. Soc.* **1976**, *98*, 7225.

(28) Bengtsson-Kloo, L.; Iapalucci, C. M.; Longoni, G.; Ulvenlund, S. *Inorg. Chem.* **1998**, *37*, 4335.

(29) Zacchini, S. *Eur. J. Inorg. Chem.* **2011**, 4125.

(30) Ciabatti, I.; Femoni, C.; Iapalucci, M. C.; Longoni, G.; Lovato, T.; Zacchini, S. *Inorg. Chem.* **2013**, *52*, 4384.

(31) Zhou, M.; Andrews, L.; Bauschlicher, C. W. *Chem. Rev.* **2001**, *101*, 1931.

(32) Kündig, E. P.; Moskovits, M.; Ozin, G. A. *Can. J. Chem.* **1972**, *50*, 3587.

(33) Manceron, L.; Tremblay, B.; Alikhani, M. E. *J. Phys. Chem. A* **2000**, *104*, 3750.

(34) Weber, L. *Angew. Chem., Int. Ed.* **1998**, *37*, 1515.

(35) Barybin, M. V.; Young, V. G.; Ellis, J. E. *J. Am. Chem. Soc.* **2000**, *122*, 4678.

(36) Carpenter, A. E.; Mokhtarzadeh, C. C.; Ripatti, D. S.; Havrylyuk, I.; Kamezawa, R.; Moore, C. E.; Rheingold, A. L.; Figueroa, J. S. *Inorg. Chem.* **2015**, *54*, 2936.

(37) Dias, P. B.; de Piedade, M. E. M.; Simões, J. A. M. *Coord. Chem. Rev.* **1994**, *135-136*, 737.

(38) Soleilhavoup, M.; Bertrand, G. *Acc. Chem. Res.* **2015**, *48*, 256.

(39) Kruck, T. *Angew. Chem., Int. Ed.* **1967**, *6*, 53.

(40) Xiao, S.; Trogler, W. C.; Ellis, D. E.; Berkovitch-Yellin, Z. *J. Am. Chem. Soc.* **1983**, *105*, 7033.

(41) Yamamoto, Y. *Coord. Chem. Rev.* **1980**, *32*, 193.

(42) Otsuka, S.; Yoshida, T.; Tatsuno, Y. *J. Am. Chem. Soc.* **1971**, *93*, 6462.

(43) Malatesta, L. *J. Chem. Soc.* **1955**, 3924.

(44) Otsuka, S.; Nakamura, A.; Tatsuno, Y. *J. Am. Chem. Soc.* **1969**, *91*, 6994.

(45) Day, V. W.; Day, R. O.; Kristoff, J. S.; Hirsekorn, F. J.; Muetterties, E. L. *J. Am. Chem. Soc.* **1975**, *97*, 2571.

(46) Thomas, M. G.; Pretzer, W. R.; Beier, B. F.; Hirsekorn, F. J.; Muetterties, E. L. *J. Am. Chem. Soc.* **1977**, *99*, 743.

(47) Christofides, A. *J. Organomet. Chem.* **1983**, *259*, 355.

(48) Yamamoto, Y.; Yamazaki, H. *J. Chem. Soc., Dalton Trans.* **1989**, 2161.

(49) Francis, C. G.; Khan, S. I.; Morton, P. R. *Inorg. Chem.* **1984**, *23*, 3680.

(50) Green, M.; Howard, J. A.; Spencer, J. L.; Stone, F. G. A. *J. Chem. Soc., Chem. Commun.* **1975**, 3.

(51) Green, M.; Howard, J. A. K.; Murray, M.; Spencer, J. L.; Stone, F. G. A. *J. Chem. Soc., Dalton Trans.* **1977**, 1509.

(52) Yamamoto, Y.; Aoki, K.; Yamazaki, H. *Chem. Lett.* **1979**, *4*, 391.

(53) Fox, B. J.; Sun, Q. Y.; DiPasquale, A. G.; Fox, A. R.; Rheingold, A. L.; Figueroa, J. S. *Inorg. Chem.* **2008**, *47*, 9010.

(54) Ditri, T. B.; Fox, B. J.; Moore, C. E.; Rheingold, A. L.; Figueroa, J. S. *Inorg. Chem.* **2009**, *48*, 8362.

(55) Ditri, T. B.; Carpenter, A. E.; Ripatti, D. S.; Moore, C. E.; Rheingold, A. L.; Figueroa, J. S. *Inorg. Chem.* **2013**, *52*, 13216.

(56) Twamley, B.; Haubrich, S. T.; Power, P. P. In *Advances in Organometallic*

Chemistry, ed. Hill, A.F., Academic Press, **1999**, *44*, 1.

(57) Clyburne, J. A. C.; McMullen, N. *Coord. Chem. Rev.* **2000**, *210*, 73.

(58) Gavenonis, J.; Tilley, T. D. *Organometallics* **2002**, *21*, 5549.

(59) Wright, R. J.; Steiner, J.; Beaini, S.; Power, P. P. *Inorg. Chim. Acta.* **2006**, *359*, 1939.

(60) Gavenonis, J.; Tilley, T. D. *Organometallics* **2004**, *23*, 31.

(61) Hagadorn, J. R.; Que, L.; Tolman, W. B.; Prisecaru, I.; Münck, E. *J. Am. Chem. Soc.* **1999**, *121*, 9760.

(62) Yoon, S.; Lippard, S. J. *J. Am. Chem. Soc.* **2005**, *127*, 8386.

(63) Tanabiki, M.; Tsuchiya, K.; Kumanomido, Y.; Matsubara, K.; Motoyama, Y.; Nagashima, H. *Organometallics* **2004**, *23*, 3976.

(64) Ito, H.; Kato, T.; Sawamura, M. *Chem. Lett.* **2006**, *35*, 1038.

(65) Fox, B. J.; Millard, M. D.; DiPasquale, A. G.; Rheingold, A. L.; Figueroa, J. S. *Angew. Chem., Int. Ed.* **2009**, *48*, 3473.

(66) Labios, L. A.; Millard, M. D.; Rheingold, A. L.; Figueroa, J. S. *J. Am. Chem. Soc.* **2009**, *131*, 11318.

(67) Stewart, M. A.; Moore, C. E.; Ditri, T. B.; Labios, L. A.; Rheingold, A. L.; Figueroa, J. S. *Chem. Commun.* **2011**, *47*, 406.

(68) Margulieux, G. W.; Weidemann, N.; Lacy, D. C.; Moore, C. E.; Rheingold, A. L.; Figueroa, J. S. *J. Am. Chem. Soc.* **2010**, *132*, 5033.

(69) Carpenter, A. E.; Margulieux, G. W.; Millard, M. D.; Moore, C. E.; Weidemann, N.; Rheingold, A. L.; Figueroa, J. S. *Angew. Chem., Int. Ed.* **2012**, *51*, 9412.

(70) Emerich, B. M.; Moore, C. E.; Fox, B. J.; Rheingold, A. L.; Figueroa, J. S. *Organometallics* **2011**, *30*, 2598.

(71) Agnew, D. W.; Moore, C. E.; Rheingold, A. L.; Figueroa, J. S. *Angew. Chem., Int. Ed.* **2015**, *54*, 12673.

(72) Tomson, N. C.; Labios, L. A.; Weyhermüller, T.; Figueroa, J. S.; Wieghardt, K. *Inorg. Chem.* **2011**, *50*, 5763.

(73) Barnett, B. R.; Labios, L. A.; Moore, C. E.; England, J.; Rheingold, A. L.; Wieghardt, K.; Figueroa, J. S. *Inorg. Chem.* **2015**, *54*, 7110.

(74) Cambridge Structural Database (CSD), version 5.37 (November **2015**).

(75) Armarego, W. L. F.; Chai, C. L. L. *Purification of Laboratory Chemicals*, 5th Ed.; Elsevier, **2003**.

(76) Pangborn, A. B.; Giardello, M. A.; Grubbs, R. H.; Rosen, R. K.; Timmers, F. J. *Organometallics*, **1996**, *15*, 1518.

(77) Neese, F. *Wiley Interdiscip. Rev.: Comput. Mol. Sci.* **2012**, *2*, 73.

(78) Becke, A. D. *Phys. Rev. A,* **1988**, *38*, 3098.

(79) Perdew, J. P. *Phys. Rev. B,* **1986**, *33*, 8822.

(80) Perdew, J. P. *Phys. Rev. B,* **1986**, *34*, 7406 (*Erratum*).

(81) Schaefer, A.; Horn, H.; Ahlrichs, R. *J. Chem. Phys.* **1992**, *97*, 2571.

(82) Weigent, F.; Ahlrichs, R. *Phys. Chem. Chem. Phys.* **2005**, *7*, 3297.

(83) Werner, H.-J.; Manby, F. R.; Knowles, P. J. *J. Chem. Phys.* **2003**, *118*, 8149.

(84) van Lenthe, E.; Baerents, E. J.; Snijders, J. G. *J. Chem. Phys.* **1993**, *99*, 4597.

(85) van Lenthe, A.; Snijders, J. G.; Baerents, E. J. *J. Chem. Phys.* **1996**, *105*, 6505.

(86) Pantazis, D. A.; Chen, X. Y.; Landis, C. R.; Neese, F. *J. Chem. Theory Comput.* **2008**, *4*, 908.

(87) *Chemcraft*. Zhurko, G. A.; Zhurko, D. A. 2014, www.chemcraftprog.com.

(88) Burla, M. C.; Caliandro, R.; Camalli, M.; Carrozzini, B.; Cascarano, G. L.; De Caro, L.; Giacovazzo, C.; Polidori, G.; Spagna, R. J. *J. Appl. Crystallogr.* **2005**, *38*, 381.

(89) Sheldrick, G. M.; *Acta Crystallogr. A.* **2008**, *64*, 112.

(90) Dolomanov, O. V.; Bourhis, L. J.; Gildea, R. J.; Howard, J. A. K.; Puschmann, H. *J. Appl. Cryst.* **2009**, *42*, 339.

Chapter 2

Cooperative Transition Metal/Lewis Acid Activation of Small Molecules by a Bidentane (boryl)iminomethane Complex: A Significant Metal-Borane Interaction Fostered by a Small Bite Angle LZ Chelate

2.1. Introduction

Transition metal-borane complexes ($L_nM \rightarrow BR_3$) featuring so-called reverse-dative σ-interactions have received increasing attention in coordination and small-molecule activation chemistry.[1-7] It is now established that coordination of a Lewis acidic borane center (Z-type ligands) can significantly modulate the electronic and geometric structure properties of a transition metal center in a manner distinct from traditional Lewis basic, two-electron donor ligands (L-type ligands).[4,8,9] Increasingly, reactivity profiles of metal-borane complexes with small molecule substrates have been uncovered that significantly diverge from those of either free boranes (BR_3) or transition metal fragments featuring only σ-donating, L-type ligands.[5,7] These studies have led to new catalytic processes that exploit the 'reverse polarity' of the metal-ligand interaction of the metal-borane unit,[10,11] and also the ability of coordinated boranes to function in a hemi-labile fashion to modulate the electronic structure of a metal center during multi-electron transformations of small molecules.[12-14]

Ligand design strategies that enable a significant primary interaction between a transition metal and a borane have relied on the presence of two or more L-type ligands to buttress the metal-to-borane σ-interaction (*i.e.* L_2Z or L_3Z).[1,4,5,7,15] The presence of

multiple two-electron donor groups within a borane ligand framework is typically necessary to overcome the inherently low coordinative ability of free borane molecules (BR_3). Indeed, transition-metal borane complexes that lack additional donor groups and are also devoid of any secondary coordinative interactions have yet to be fully authenticated.[16] In addition, ligand frameworks possessing only a single L-type buttress have thus far shown limited ability to foster a significant metal-to-borane interaction.[17,18] However, such bidentate LZ chelates are of interest for the development of isolable metal-borane complexes that offer increased coordinative unsaturation and flexibility toward incoming ligands and substrates. Accordingly, herein we report platinum complexes featuring a (boryl)iminomethane ($(R_2B)(H)C{=}NR$) ligand, which is accessed by the 1,1-hydroboration of a coordinated isocyanide ligand, that enables the formation of significant metal-borane interactions within a bidentate LZ chelate. We also demonstrate rich and cooperative reaction chemistry of the Pt-to-borane linkage with a host of small-molecule substrates. The ability of the (boryl)iminomethane ligand to provide a significant metal-borane interaction within a bidentate framework arises from a small bite angle between the Z-type borane and L-type imino nitrogen coordinating groups.

2.2. Synthesis and electronic structure of a singly-buttressed platinum-borane adduct accessed by hydroboration of a coordinated isocyanide.

Treatment of $Pt(CNAr^{Dipp2})_2$ (Ar^{Dipp2} = 2,6-(2,6-*i*$Pr_2C_6H_3)_2C_6H_3$) with dicyclohexylborane ($HBCy_2$) results in the clean formation of three-coordinate $Pt(\kappa^2$-*N,B*-^{Cy2}BIM)($CNAr^{Dipp2}$) (**1**), which features a chelating ambiphilic (boryl)iminomethane (BIM) moiety (Figure 2.1). Evidence for a Pt-B retrodative σ-interaction is provided by

the ^{11}B NMR spectrum of **1**, which displays a broad singlet at +18 ppm. For comparison, the free (boryl)iminomethane ^{Cy2}BIM (*vida infra*) displays a downfield-shifted ^{11}B resonance at +74 ppm, indicating an increase in the coordination number at boron upon ligation to Pt(0).[19] Further indication of a Pt-B interaction is found in the crystal structure of Pt(κ^2-*N,B*-^{Cy2}BIM)(CNAr^{Dipp2}) (**1**), which reveals a Pt-B distance of 2.314(6) A. This compares well to the Pt-BR_3 distances found in the four-coordinate Pt(0) metallaboratrane Pt[κ^4-TPB] (2.224(2) Å, TPB = (*o*-^{iPr2}PC$_6$H$_4$)$_3$B),[20] and is significantly shortened relative to the M-BR_3 distance in the only other structurally characterized borane-containing LZ chelates AuCl(*o*-^{iPr2}PC$_6$H$_4$BR$_2$) (2.90 Å, R = cyclohexyl; 2.66 Å, R_2 = fluorene).[17] The N1-Pt-B angle in **1** is of particular note, as this small bite angle enforces a short Pt-B interatomic separation upon coordination of the imine donor arm. For comparison, Pt[κ^4-TPB] features an average P-Pt-B bite angle of 85.7˚ and accordingly requires a three-donor buttress to stabilize a short Pt-B interaction.[20] Near-90˚ bite angles are also present in AuCl(*o*-^{iPr2}PC$_6$H$_4$BR$_2$), which possesses only a weak Au-B interaction according to ^{11}B NMR spectroscopy.[17] The presence of a significant reverse-dative σ-interaction in **1** is also indicated by NBO calculations on the model complex Pt(κ^2-*N,B*-^{Me2}BIM)(CNMe), which reveal a fully occupied bonding orbital that is 81% Pt and 19% B in parentage (Figure 2.2). Importantly, the boron contribution in this localized orbital is an admixture of both 2*s* and 2p_z orbital character, thereby indicating a rehybridization of the boron center from sp^2 to sp^3 upon interaction with the platinum center. This hybridization change also rationalizes the observed pyramidalization of the organic substituents around boron in the solid-state structure of **1** (Σ(C–B–C) = 348.4˚).

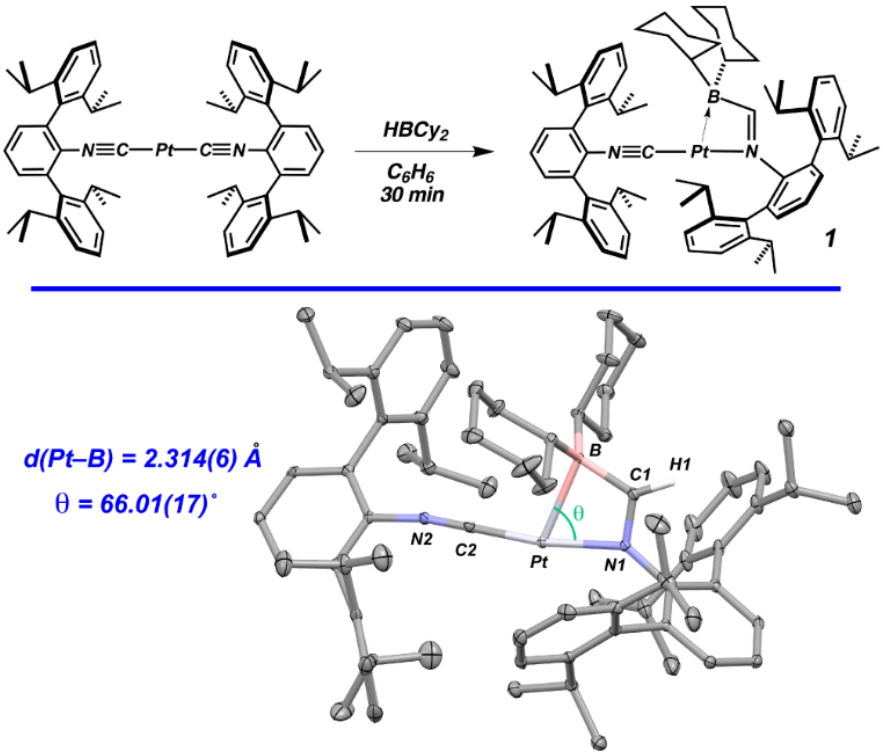

Figure 2.1. Synthesis (top) and molecular structure (bottom) of Pt(κ^2-*N,B*-^{Cy2}BIM)(CNAr^{Dipp2}) • 0.5 C_5H_{12} (**1** • 0.5 C_5H_{12}). Co-crystallized *n*-pentane has been omitted for clarity. Selected bond distances (Å) and angles (˚): Pt-B1 = 2.314(6). Pt-N1 = 2.077(2). Pt-C2 = 1.848(3). B1-C1 = 1.582(7). C1-N1 = 1.289(3). C2-N2 = 1.173(3). B1-Pt-N1 = 66.0(2). N1-C1-B1 = 113.1(3).

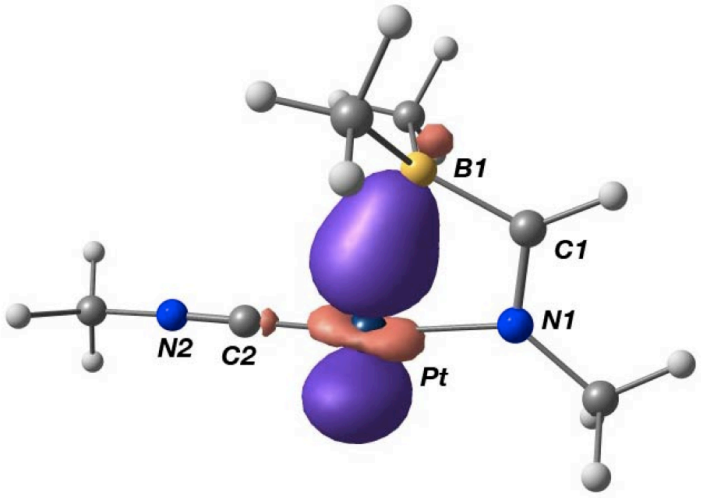

Figure 2.2. Localized molecular orbital from NBO calculations showing the dative bonding interaction between the platinum center and borane unit in the model complex Pt(κ^2-*N,B*-^{Me2}BIM)(CNMe).

It is important to note that the reaction between $Pt(CNAr^{Dipp2})_2$ and $HBCy_2$ is complete within 20 min at room temperature, with no observable intermediates seen when the reaction is followed by ^1H NMR. Furthermore, the unligated (boryl)iminomethane ^{Cy2}BIM (**2**) can be independently synthesized upon addition of dicyclohexylborane to the *m*-terphenyl isocyanide[21] $CNAr^{Dipp2}$ via a geminal hydroboration of the isocyano functionality (Scheme 2.1). Although isocyanide 1,1-hydroboration is to our knowledge unprecedented, the insertion of isocyanides into the boron-element bonds of a variety of boranes has been studied, and is typically thought to proceed via the formation of an isocyanide-borane Lewis pair.[22-26] Importantly, previous examples of isocyanide insertion into triorganoboranes typically have produced dimeric products.[22,25] In the case of ^{Cy2}BIM (**2**), the ^{11}B NMR resonance at +74 ppm unequivocally indicates the presence of a tricoordinate boron atom; presumably, the combined steric bulk of the *m*-terphenyl and cyclohexyl substituents work in tandem to preclude the formation of inter- or intra-molecular N-B interactions. Although attempts to grow crystals of ^{Cy2}BIM suitable for X-ray diffraction were unsuccessful, the corresponding BCl_3 adduct **3** was synthesized and structurally characterized, confirming the formation of an imine functionality, as well as *E*-stereochemistry about the C-N imine bond (Scheme 2.1 and Figure 2.3).

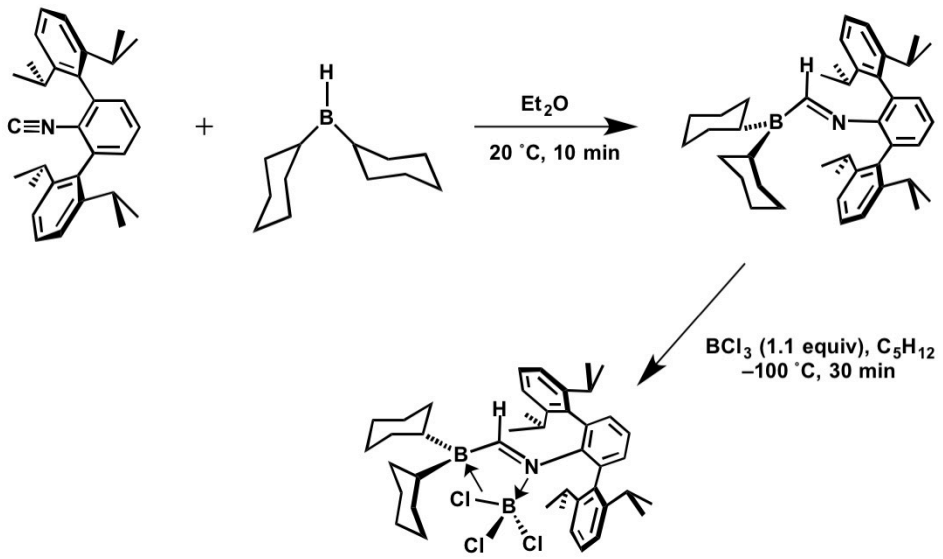

Scheme 2.1. Synthesis of ^{Cy2}BIM (**2**) and its adduct with BCl_3 (**3**).

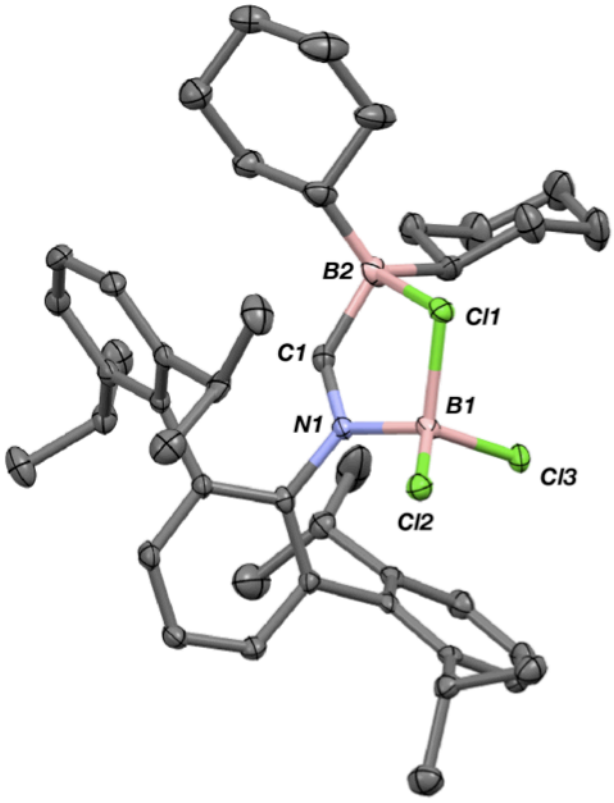

Figure 2.3. Molecular structure of ^{Cy2}BIM→BCl_3 • 2 C_5H_{12} (**3** • 2 C_5H_{12}). Co-crystallized molecules of *n*-pentane have been omitted for clarity. Selected bond distances (Å) and angles (˚): N1-B1 = 1.586(4). B1-Cl1 = 1.906(3). B1-Cl2 = 1.825(3). B1-Cl3 = 1.806(4). Cl1-B2 = 2.115(4). B2-C1 = 1.601(4). C1-N1 = 1.292(4). B1-Cl1-B2 = 92.9(2). N1-C1-B2 = 124.8(3).

Given the ability of $CNAr^{Dipp2}$ to readily undergo 1,1-hydroboration, it was initially postulated that the formation of Pt(κ^2-*N,B*-^{Cy2}BIM)($CNAr^{Dipp2}$) (**1**) might proceed via isocyanide dissociation from Pt($CNAr^{Dipp2}$)$_2$, hydroboration of $CNAr^{Dipp2}$ and ligation of incipient ^{Cy2}BIM to the Pt($CNAr^{Dipp2}$) fragment (Path A, Scheme 2.2). However, 2D EXSY ^{1}H NMR studies on C_6D_6 solutions (20 ˚C) containing equimolar Pt($CNAr^{Dipp2}$)$_2$/$CNAr^{Dipp2}$ failed to demonstrate the occurrence of isocyanide exchange, even when mixing times as long as 1 ms were employed. Given that the reaction between Pt($CNAr^{Dipp2}$)$_2$ and $HBCy_2$ is complete within 20 minutes at 20 ˚C, this observation seems to be inconsistent with the formation of **1** proceeding by the dissociative mechanism outlined above. Alternatively, two associative mechanisms have been considered, in which the reaction proceeds either via an oxidative addition-migratory insertion-reductive elimination pathway (Scheme 2.2 Path B) or via formation of a transient unsupported Pt-borane adduct which undergoes hydride insertion into a coordinated isocyanide (Scheme 2.2 Path C). Attempts to differentiate between Paths B and C have primarily focused on the independent synthesis of a complex of the formulation *cis*-PtH(BR_2)($CNAr^{Dipp2}$)$_2$ (*i.e.* the putative product of oxidative addition in Path B), all of which have thus far been unsuccessful. Further studies are currently underway to ascertain the mechanism by which **1** is formed.

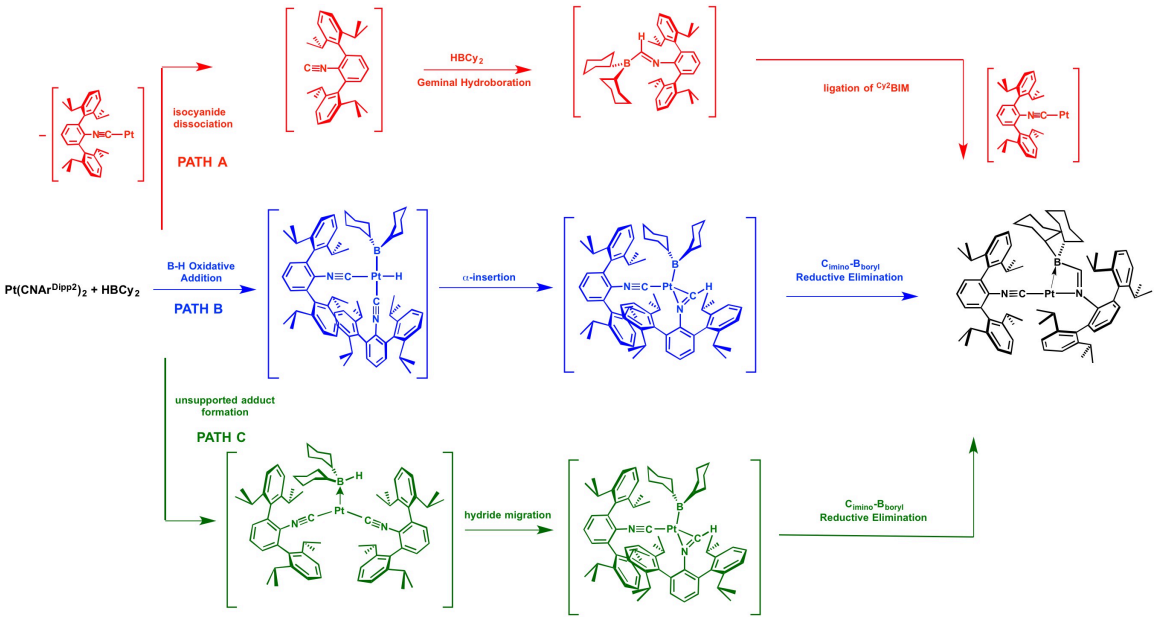

Scheme 2.2. Potential mechanisms for the formation of **1**.

2.3. Oxidative addition reactivity of Pt(κ^2-*N,B*-^{Cy2}BIM)(CNAr^{Dipp2}) (1)

The absence of multiple donor buttresses surrounding the platinum-boron unit, as well as the small bite angle and constrained metallocycle effected by ^{Cy2}BIM ligation, encourage a variety of substrates to add across this bond under ambient conditions (Scheme 2.3). Accordingly, addition of equimolar I_2 to a diethyl ether solution of Pt(κ^2-*N,B*-^{Cy2}BIM)(CNAr^{Dipp2}) (**1**) results in the precipitation of *trans*-PtI$_2$(κ^1-*N*-^{Cy2}BIM)(CNAr^{Dipp2}) (**4**). Examination of the crystal structure of **4** (Figure 2.4) reveals the eradication of the Pt-B bond, whereby the fourth coordination site at boron has been replaced by a weak interaction with an iodide ligand (d(B-I) = 2.555(6) Å). The ^{11}B NMR spectrum of **4** shows a singlet at +25 ppm that is still shifted significantly upfield from the peak seen for free ^{Cy2}BIM (+74 ppm), intimating donation into the empty *p* orbital of the borane unit. Further, the ^{1}H and ^{13}C{^{1}H} NMR spectra are consistent with

a C_s-symmetric structure in solution, suggesting that this interaction is static and that the borane functionality does not "jump" between the two iodide units. The ability of this borane unit to function as a pendant Lewis acid toward bases in the secondary coordination sphere likely accounts for a portion of the thermodynamic driving force allowing Pt(κ^2-*N,B*-^{Cy2}BIM)(CNAr^{Dipp2}) (**1**) to undergo oxidative addition despite the withdrawal of electron density from the platinum center effected by metal-to-ligand σ-donation.

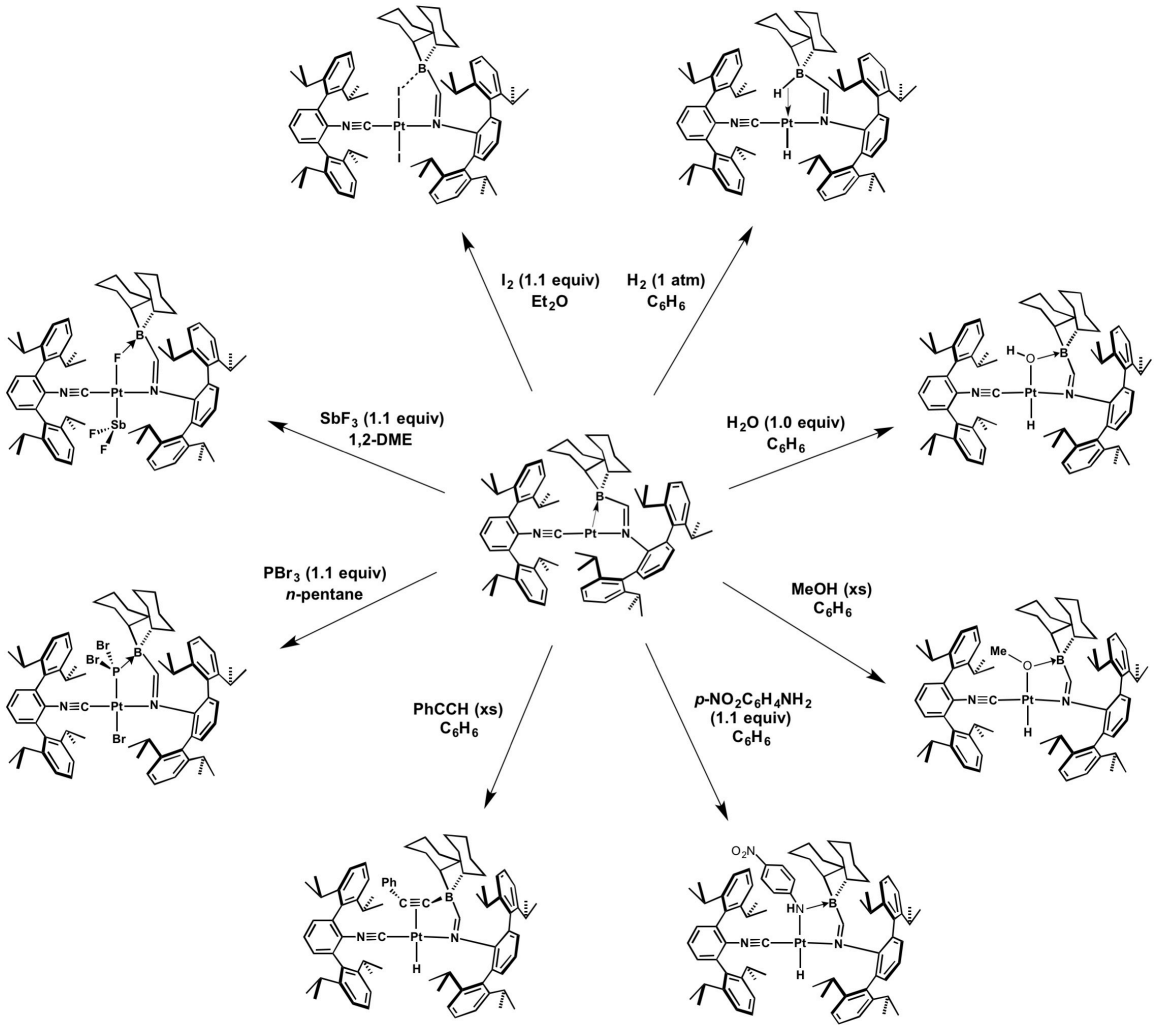

Scheme 2.3. Oxidative addition reaction pinwheel for Pt(κ^2-*N,B*-^{Cy2}BIM)(CNAr^{Dipp2}) (**1**).

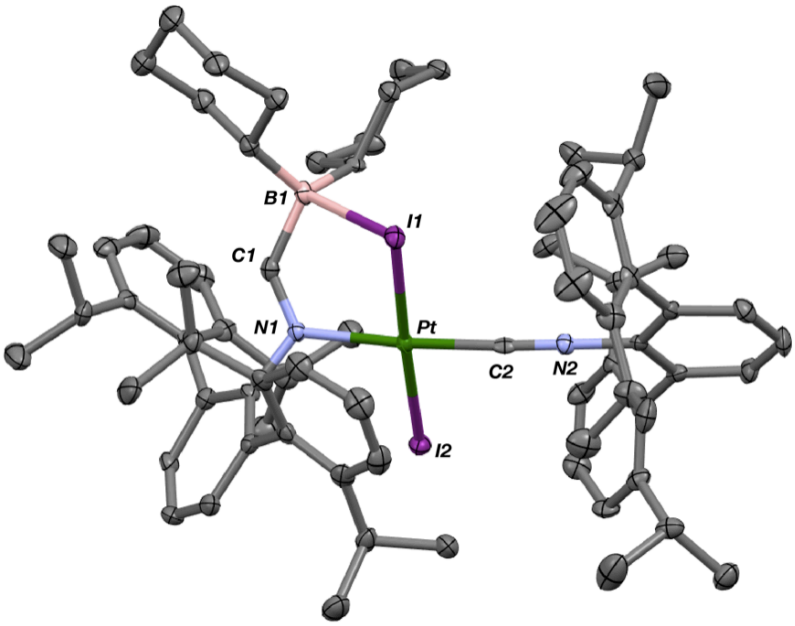

Figure 2.4. Molecular structure of *trans*-$PtI_2(\kappa^1$-*N*-^{Cy2}BIM)(CNAr^{Dipp2}) • 1.5 C_6H_6 (**4** • 1.5 C_6H_6). Co-crystallized molecules of benzene have been omitted for clarity. Selected bond distances (Å) and angles (˚): Pt-I1 = 2.5836(5). Pt-I2 = 2.5977(5). Pt-N1 = 2.082(4). Pt-C2 = 1.900(5). B1-I1 = 2.556(5). C1-N1 = 1.294(6). Pt-I1-B1 = 83.5(1). C1-N1-Pt = 119.0(3). N1-Pt-I2 = 95.3(1). I2-Pt-C2 = 86.2(1). C2-Pt-I1 = 92.0(1).

Exposure of a solution of Pt(κ^2-*N,B*-^{Cy2}BIM)(CNAr^{Dipp2}) (**1**) to 1 atm of H_2 gas provides access to the hydride-borohydride PtH(μ^2-H)(κ^1-*N*-^{Cy2}BIM)(CNAr^{Dipp2}) (**5**, Scheme 2.3**)**. The addition of H_2 addition across a metal-borane bond, currently limited to several examples,[10,11,27-29] has garnered interest as a potential technique for hydrogen atom storage.[7] In **5**, The borohydride H-atom appears as a broad doublet of doublets in the ^{1}H NMR spectrum, being coupled to the terminal hydride and aldimine protons, and also displays satellites due to coupling with ^{195}Pt (I = ½, abundance = 33.8 %), while the ^{11}B NMR resonance appears as a broad singlet at –7 ppm, indicative of a quaternized boron center.[19] Hydride-borohydride **5** is isolable in the solid state, and structural

characterization confirms the presence of a borohydride B-H σ-complex (Figure 2.5). The activation of dihydrogen by Pt(κ^2-*N,B*-^{Cy2}BIM)(CNAr^{Dipp2}) (**1**) is irreversible, as solutions of PtH(μ^2-H)(κ^1-*N*-^{Cy2}BIM)(CNAr^{Dipp2}) (**5**) stored under N_2 do not display any regeneration of starting material or decomposition. Further, preliminary screenings indicate a limited capacity for PtH(μ^2-H)(κ^1-*N*-^{Cy2}BIM)(CNAr^{Dipp2}) (**5**) to effect transfer hydrogenation, as heating benzene solutions of **5** and equimolar styrene to 65 ^{o}C for 6 days results in production of only trace ethylbenzene according to ^{1}H NMR and GC-MS (**5** decomposes at higher temperatures). We attribute these observations to the general kinetic inertness of the Pt(II) oxidation state, as opposed to related hydride-borohydride complexes of first-row transition metals that readily hydrogenate olefins under catalytic conditions.[10,11]

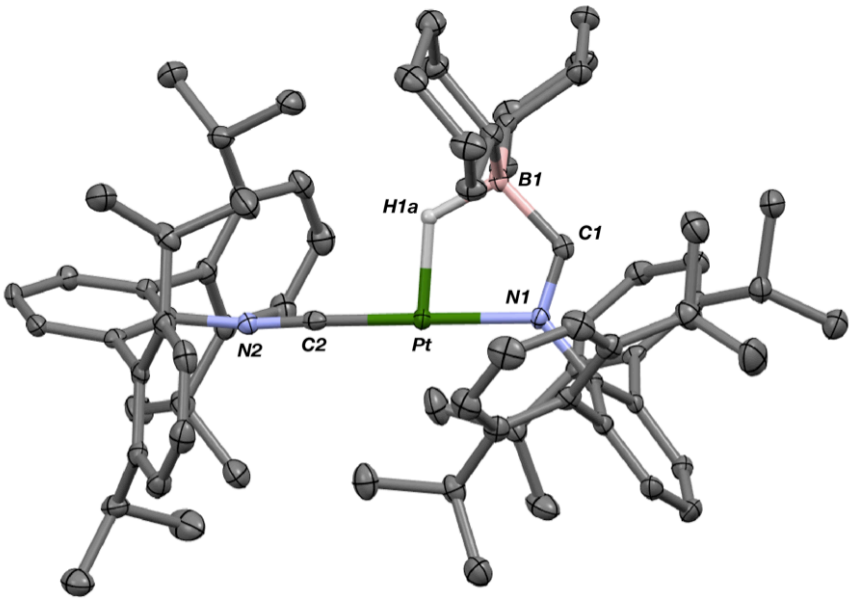

Figure 2.5. Molecular structure of PtH(μ^2-H)(κ^1-*N*-^{Cy2}BIM)(CNAr^{Dipp2}) • Et_2O (**5** • Et_2O). The terminal hydride ligand was not located in the electron difference map. Co-crystallized diethyl ether has been omitted for clarity. Selected bond distances (Å) and angles (˚): Pt-N1 = 2.055(2), Pt-C2 = 1.884(3), Pt-H1a = 1.77(3), B1-H1a = 1.38(3), C1-N1 = 1.290(4), Pt-H1a-B1 = 123(2), N1-Pt-H1a = 84.8(10), N1-C1-B1 = 118.4(3), C1-B1-H1a = 105(1).

The ambiphilicity of the free (boryl)iminomethane ^{Cy2}BIM (**2**), coupled with the indication from ^{11}B NMR that it contains a tricoordinate boron center, suggested that it might function as a Frustrated Lewis Pair.[30,31] Indeed, ^{Cy2}BIM is capable of dihydrogen activation at ambient temperatures. However, instead of the expected iminium borohydride zwitterion, what is instead observed is the product of internal imine hydrogenation, $(Cy)_2BCH_2NHAr^{Dipp2}$ (**6**), which was isolated and characterized by multinuclear NMR and high-resolution mass spectrometry (Scheme 2.4). The ability of intramolecular Frustrated Lewis Pairs to hydrogenate imines has been demonstrated by Stephan.[32,33] In the case of ^{Cy2}BIM, the putative iminium borohydride formed upon H_2 activation quickly rearranges to hydrogenated product upon formal hydride migration from boron to carbon.

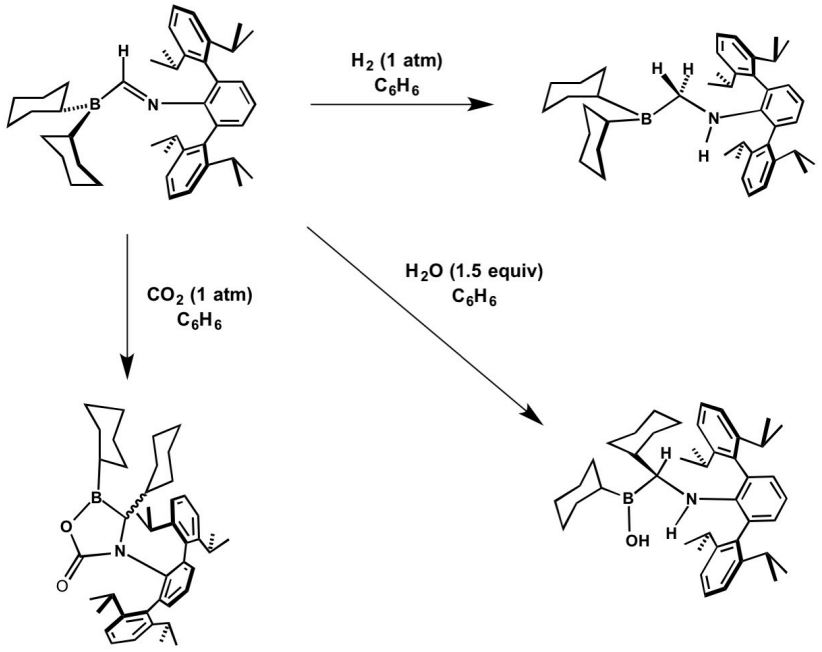

Scheme 2.4. Frustrated Lewis Pair reactivity of ^{Cy2}BIM toward H_2, H_2O and CO_2.

Interestingly, Pt(κ^2-*N,B*-^{Cy2}BIM)(CNAr^{Dipp2}) (**1**) also exhibits clean reactivity with water. Treatment of **1** with 1.0 equivalents of H_2O at 20 ˚C effects instantaneous conversion to the hydride-hydroxide PtH(μ-OH)(κ^1-*N*-^{Cy2}BIM)(CNAr^{Dipp2}) (**7**, Scheme 2.3), which is subsequently isolated by crystallization from diethyl ether. Structural characterization of PtH(μ-OH)(κ^1-*N*-^{Cy2}BIM)(CNAr^{Dipp2}) (**7**) reveals a *trans*-orientation of the hydride and hydroxide moieties, with the later engaged in a three-centered interaction involving the Pt, O, and B atoms (Figure 2.6). In this way, the activation of water by Pt(κ^2-*N,B*-^{Cy2}BIM)(CNAr^{Dipp2}) (**1**) parallels the heterolytic cleavage of H_2 by transition metal borane complexes, whereby a proton is delivered to the Lewis basic metal center while the borane assists in the ligation of the resultant conjugate base. In the case of **7**, the O-B bond length of 1.550(3) Å is quite long for a borate species bearing oxygen donors (see Figure 2.22), leading us to favor a transition metal hydroxide as opposed to a hydroxyborate description for **7**. The ^{11}B NMR resonance of **7** appears at +5 ppm, indicative of a quaternized boron center and legitimizing the presence of a hydroxide-borane interaction. While oxidative addition of water is a seemingly elementary process, examples of hydride hydroxide metal complexes derived from this transformation are rare,[34-37] as these metal-bound functional groups are often unstable toward further reactivity. The presence of Lewis acids in the secondary coordination sphere is one plausible strategy to hinder this unwanted reactivity, as their interaction with "hard" ligands such as hydroxide can protect against reactivity with exogenous electrophiles. In the case of **7**, prolonged heating results in only the production of Pt(CNAr^{Dipp2})$_2$ and the boronic acid (HO)(Cy)BCH(Cy)NHAr^{Dipp2} (**8**), the latter of which can be independently synthesized upon exposure of the (boryl)iminomethane ^{Cy2}BIM to

water (Scheme 2.4 and Figure 2.7). This transformation is accompanied by a 1,2-cyclohexyl shift from boron to the imine carbon atom, as well as proton transfer from oxygen to nitrogen. Along with the inertness displayed by $Pt(CNAr^{Dipp2})_2$ toward water under ambient conditions, the formation of **7** accentuates the ability of the platinum-borane interaction to modulate the reactivity of the resulting complex, enabling otherwise unattainable reactivity.

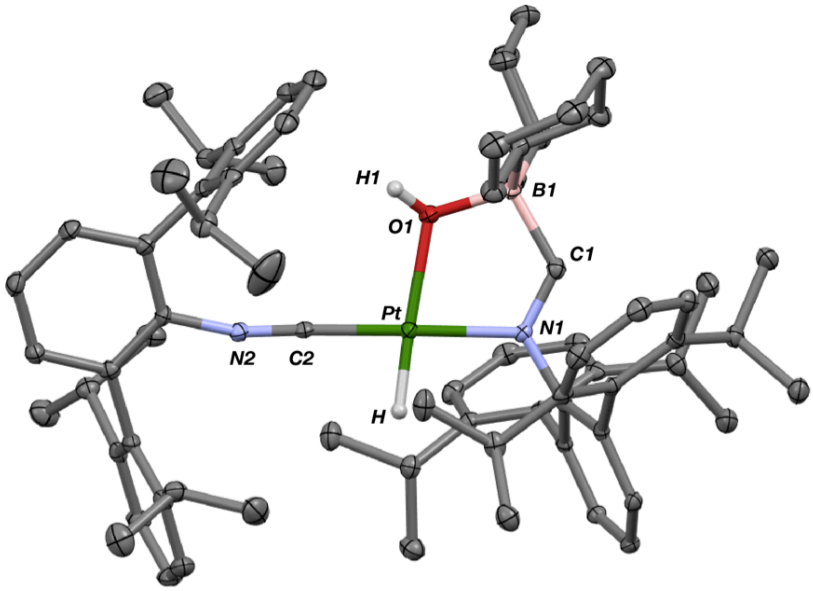

Figure 2.6. Molecular structure of $PtH(\mu\text{-}OH)(\kappa^1\text{-}N\text{-}^{Cy2}BIM)(CNAr^{Dipp2})$ • 0.5 Et_2O (**7** • 0.5 Et_2O). Selected bond distances (Å) and angles (˚): Pt-N1 = 2.051(2). Pt-C2 = 1.872(3). Pt-O1 = 2.124(2). Pt-H = 1.47(3). B1-O1 = 1.552(3). C1-N1 = 1.289(3). Pt-O1-B1 = 115.3(2). O1-B1-C1 = 102.2(2). B1-N1-C1 = 123.3(2).

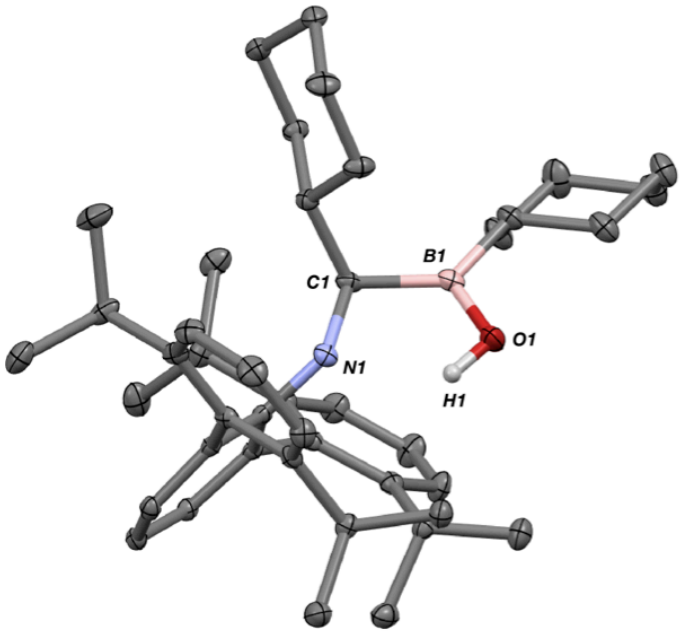

Figure 2.7. Molecular structure of borinic acid **8**. Selected bond distances (Å) and angles (˚): N1-C1 = 1.482(2). C1-B1 = 1.606(2). B1-O1 = 1.352(2). N1-C1-B1 = 107.4(1).

The activation of H-X bonds by the platinum-borane unit in **1** can also be realized for other protic substrates (Scheme 2.3). Treatment with methanol or *para*-nitroaniline results in formation of the corresponding platinum hydride-alkoxide PtH(μ-OMe)(κ^1-*N*-^{Cy2}BIM)(CNAr^{Dipp2}) (**9**, Figure 2.8) or hydride-anilide PtH(μ-NH(*p*-$NO_2C_6H_4$))(κ^1-*N*-^{Cy2}BIM)(CNAr^{Dipp2}) (**10**, Figure 2.9), respectively. Structural characterization of **9** and **10** reaveals that the methoxide and *p*-nitroanilide ligands bridge the Pt and B centers in a manner analogous to the hydroxide ligand in **7**. In contrast, the addition of phenylacetylene (HCCPh) to **1** provides the hydride complex PtH(η^2-*C,C*-κ^1-*N*-PhCC-^{Cy2}BIM)(CNAr^{Dipp2}) (**11**, Figure 2.10). Interestingly, the acetylide unit in **11** is σ-bound to the boron center, resulting in a four-coordinate borate center (^{11}B NMR δ = –10.6 ppm).

The acetylide is also bound in a η^2-fashion to the platinum center *trans* to the hydride ligand. Notably, this η^2-*C,C*-coordination mode is in direct contrast to the large number of σ-bound Pt(II) acetylides reported in the literature[38,39] and demonstrates how borane ligation to a transition metal not only facilitates substrate activation but also can significantly influence the structural and electronic properties of the resultant products.

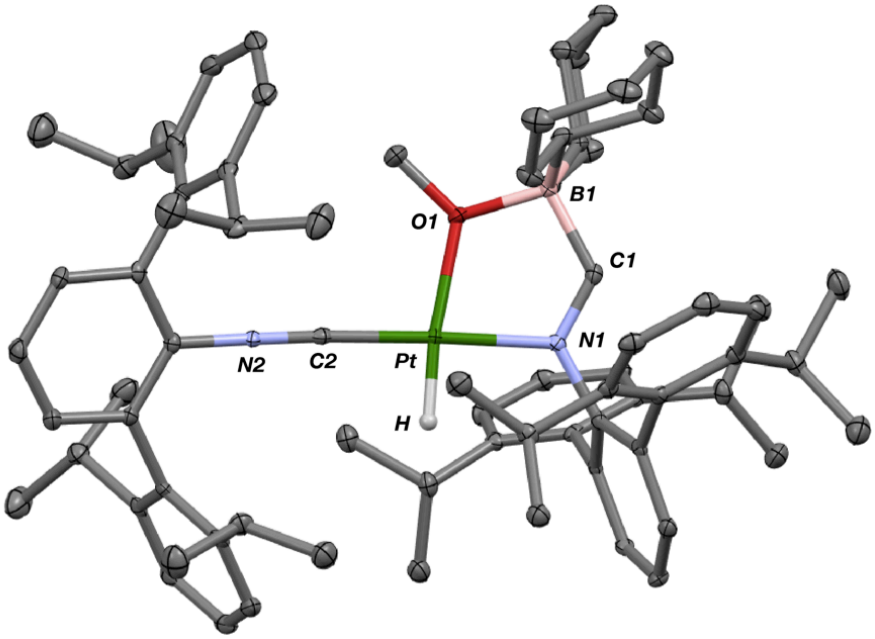

Figure 2.8. Molecular structure of PtH(μ-OMe)(κ^1-*N*-^{Cy2}BIM)(CNAr^{Dipp2}) (**9**). Selected bond distances (Å) and angles (˚): Pt-N1 = 2.053(4). Pt-C2 = 1.886(5). Pt-O1 = 2.121(3). Pt-H = 1.42(5). B1-O1 = 1.562(6). C1-N1 = 1.292(6). Pt-O1-B1 = 115.5(2). O1-B1-C1 = 101.3(4). B1-C1-N1 = 123.7(4). C1-N1-Pt = 116.0(3).

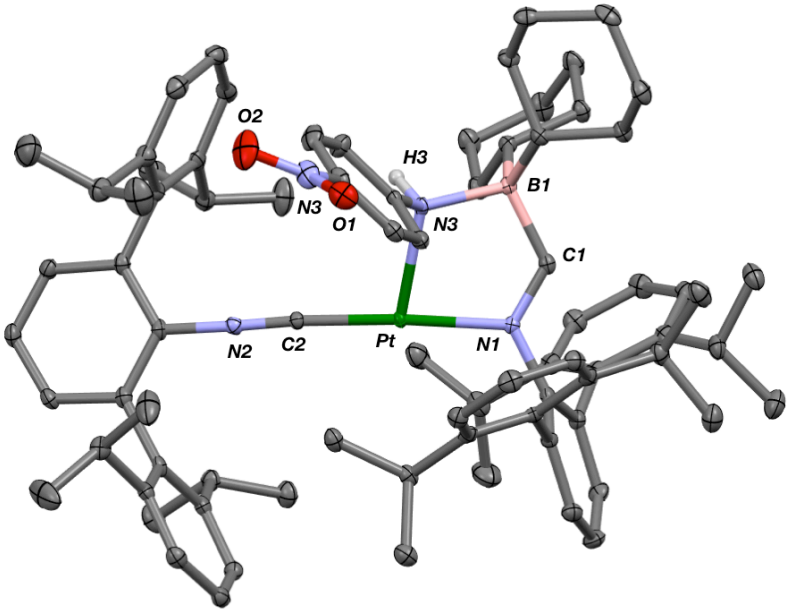

Figure 2.9. Molecular structure of PtH(μ-NH(*p*-$NO_2C_6H_4$))(κ^1-*N*-^{Cy2}BIM)(CNAr^{Dipp2}) (**10**). The terminal hydride ligand was not located in the electron difference map. Selected bond distances (Å) and angles (˚): Pt-N1 = 2.059(2). Pt-C2 = 1.896(2). Pt-N3 = 2.192(3). N3-B1 = 1.669(4). C1-N1 = 1.298(4). Pt-N3-B1 = 109.5(2). N1-Pt-N3 = 81.64(9). Pt-N1-C1 = 117.2(2). N1-C1-B1 = 123.6(2).

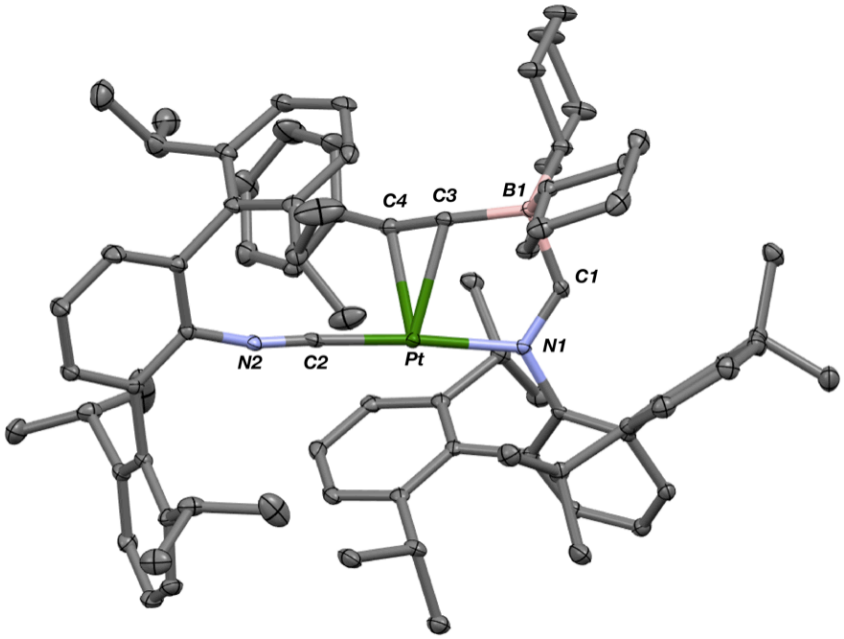

Figure 2.10. Molecular structure of PtH(η^2-*C,C*-κ^1-*N*-PhCC-^{Cy2}BIM)(CNAr^{Dipp2}) • 1.5 Et_2O (**11** • 1.5 Et_2O). The terminal hydride ligand was not located in the electron difference map. Selected bond distances (Å) and angles (˚): Pt-N1 = 2.090(3). Pt-C2 = 1.901(5). Pt-C3 = 2.315(4). Pt-C4 = 2.348(5). B1-C3 = 1.605(7). C3-C4 = 1.241(6). N1-Pt-C2 = 174.2(2). N1-C1-B1 = 125.6(4). C1-B1-C3 = 100.5(4). B1-C3-C4 = 157.4(5).

Finally, Pt(κ^2-*N,B*-^{Cy2}BIM)(CNAr^{Dipp2}) (**1**) is also competent for the oxidative addition of pnictogen halide bonds (Scheme 2.3). Treatment of **1** with PBr_3 yields the Pt(II) complex PtBr(μ-PBr_2)(^{Cy2}BIM)(CNAr^{Dipp2}) (**12**). Structure determination on crystals grown from *n*-pentane reveals that the dibromophosphido ligand bridges the Pt and B centers (Figure 2.11). Examples of heavier dihalophosphido (*i.e.* not difluorophosphido) analogues typically bridge multiple transition metal centers, although a few mononuclear complexes bearing dichlorophosphido ligands have been structurally authenticated.[40,41] The presence of two reactive P-Br bonds in **12** renders it a potential synthon in the pursuit of borane-stabilized platinum phosphinidines or phosphides. Accordingly, attempts to access such species by either halide abstraction or reduction are currently underway.

In addition, **1** can activate the antimony-fluoride bond in SbF_3, providing access to Pt(SbF_2)(μ-F)(^{Cy2}BIM)(CNAr^{Dipp2}) (**13**, Figure 2.12). In contrast to **12**, the dihalopnictinide ligand in **13** exists as a terminal entity, while the fluoride ligand bridges the Pt and B centers. The ^{19}F NMR spectrum of **13** shows two peaks integrating in a 2:1 ratio. The resonance assigned to the difluorostibyl ligand appears as a singlet at –133.8 ppm with satellites due to coupling with ^{195}Pt (J = 85 Hz). Interestingly, the Cambridge Structural Database[42] is devoid of other complexes bearing difluorostibyl ligands, although several other examples have been synthesized very recently by our group.[43] The bridging fluoride ligand gives rise to a ^{19}F NMR resonance at δ = –221.1 ppm. Although this chemical shift is comparable that that seen in other systems for a fluoride moiety bridging two Lewis acids,[44,45] further evaluation of the spectrum reveals a surprisingly

large coupling to the ^{195}Pt nucleus of 1.56 kHz. This value is substantially larger than has been observed in the limited number of known Pt(II) fluorides.[46-49] Examination of the solid state structure of **13** does not illuminate a reason for this large coupling constant, as the platinum-fluoride bond distance of 2.211(2) Å is somewhat elongated compared those seen in other platinum fluorides (Figure 2.23). Although the precise reason for this large coupling constant is not currently understood, we suspect that it may be connected to the very weak σ-donor properties of the difluorostibyl ligand as observed previously in our laboratory.[43] This supposition is corroborated by the relative $J_{Pt,F}$ values seen for *cis*-$PtF_2(PR_3)_2$ (R = Ph) and *trans*-$PtF_2(PR_3)_2$ (R = *i*Pr).[46] For the former complex, a rather small $J_{Pt,F}$ value of 108 Hz is observed, presumably due to the *trans* disposition that each fluoride bears with respect to a strongly-donating triphenylphosphine ligand. Contrastingly, the $J_{Pt,F}$ value observed for *trans*-$PtF_2(P(iPr)_3)_2$ is nearly an order of magnitude larger (974 Hz), presumably due to the fact that the two fluorides are *trans* to each other and therefore donate into the same Pt-based orbitals. Similarly, the $-SbF_2$ moiety should accordingly exert a very weak *trans* influence on the fluoride ligand, allowing for a strong interaction between the Pt and F centers with an attendant increase in $J_{Pt,F}$. Undoubtedly, this is also facilitated by the bridging nature of the fluoride ligand, which serves to attenuate its "hardness" and thereby promotes bonding with the soft Pt(II) center.

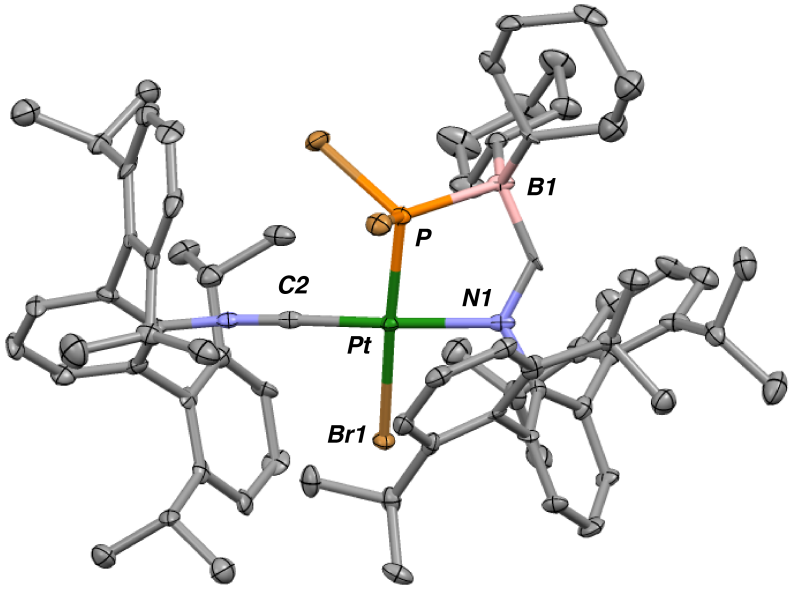

Figure 2.11. Molecular structure of PtBr(μ-PBr_2)(^{Cy2}BIM)($CNAr^{Dipp2}$) • 1.5 C_5H_{12} (**12** • 1.5 C_5H_{12}). Co-crystallized molecules of *n*-pentane were accounted for using SQUEEZE. The asymmetric unit contains two molecules of **12**. Not pictured is the second crystallographically independent molecule which contains disorder in the B-bound cyclohexyl groups. Selected bond distances (Å, reported as the mean values of the two independent molecules): Pt-Br1 = 2.4722(6); Pt-P = 2.214(1); P-B = 2.020(7)

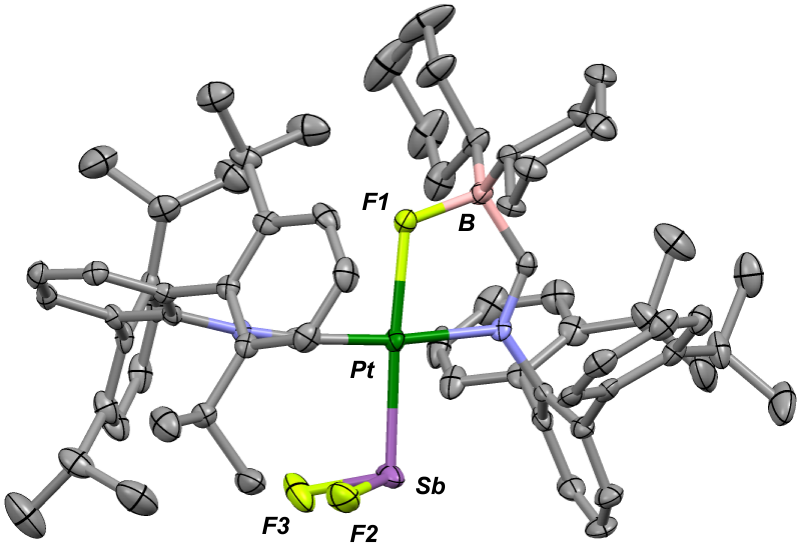

Figure 2.12. Molecular structure of Pt(SbF_2)(μ-F)(^{Cy2}BIM)($CNAr^{Dipp2}$) • MeCN (**13** • MeCN). Co-crystallized acetonitrile has been omitted for clarity. Selected bond distances (Å): Pt-Sb = 2.5220(3); Pt-F1 = 2.211(2); F1-B = 1.530(5).

2.4. Oxidative insertion reactivity of Pt(κ^2-*N,B*-^{Cy2}BIM)(CNAr^{Dipp2}) (1)

An unequivocal demonstration of metal-ligand cooperative substrate activation is found in the formation of bright red Pt(μ-Me$_2$CO)(^{Cy2}BIM)(CNAr^{Dipp2}) (**14**) or purple Pt(μ-Ph(H)CO)(^{Cy2}BIM)(CNAr^{Dipp2}) (**15**) upon addition of acetone or benzaldehyde to Pt(κ^2-*N,B*-^{Cy2}BIM)(CNAr^{Dipp2}) (**1**, Scheme 2.5). Structural characterization of **14** (Figure 2.13) and **15** (Figure 2.14) revealed an insertion of the carbonyl unit into the Pt-borane bond, the former of which is now best described as a single bond (d(C-O) ~ 1.40 Å). The reduction of the carbonyl functional group is concomitant with a 1,2-cyclohexyl shift and eradication of imine C-N π-bond, as well as formation of a π-type η^1-arene interaction between platinum and the *ipso* carbon of a flanking Dipp ring at the coordination site *trans* to the newly formed Pt-C σ-bond. The insertion of unsaturated substrates into metal-boryl bonds is well-known and is of great interest in metal-catalyzed hydroboration and diboration of unsaturated organics,[50-53] and the related insertion of an aldehyde into a copper-boryl bond has been illustrated by Sadighi.[53] Interestingly, the presence of a boron-bound α,β-unsaturated group in ^{Cy2}BIM allows for analogous insertion chemistry to be accessed in the metal-borane complex Pt(κ^2-*N,B*-^{Cy2}BIM)(CNAr^{Dipp2}) (**1**) via alkyl migration from boron to carbon and the transformation of the imino nitrogen to an anionic amido donor, obviating the buildup of electron density at boron. These metallaboration reactions highlight the remarkable capacity of the Pt(CNAr^{Dipp2}) and ^{Cy2}BIM fragments to work in concert toward the activation of unsaturated organic substrates.

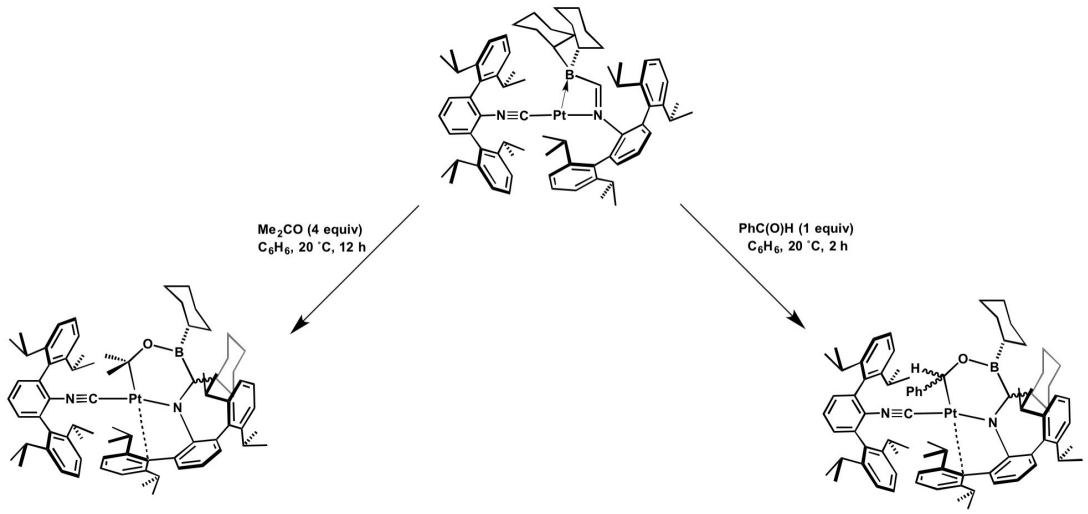

Scheme 2.5. Metallaboration of acetone and benzaldehyde effected by **1**.

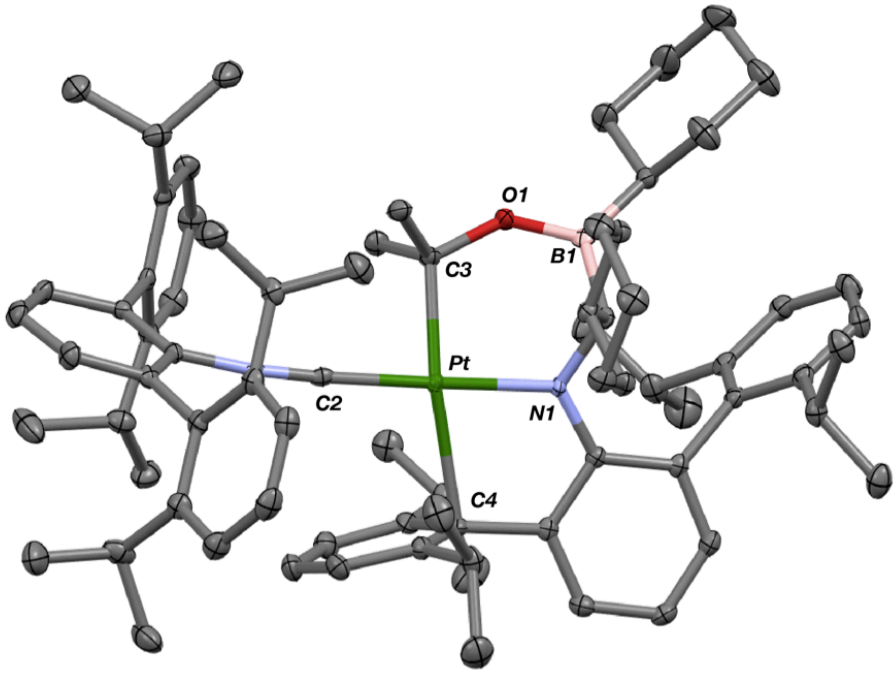

Figure 2.13. Molecular Structure of Pt(μ-Me_2CO)(^{Cy2}BIM)($CNAr^{Dipp2}$) (**14**). Selected bond distances (Å) and angles (°): Pt-N1 = 2.033(2) = Pt-C2: 1.907(3). Pt-C3 = 2.083(3). Pt-C4 = 2.430(3). C1-N1 = 1.487(3). C3-01 = 1.429(3). O1-B1 = 1.353(4). N1-Pt-C3 = 93.07(9). N1-Pt-C4 = 78.84(9). C2-Pt-C3 = 86.5(1). C2-Pt-C4: 103.5(1). Pt-C3-O1 = 115.8(2). C3-O1-B1 = 132.6(2).

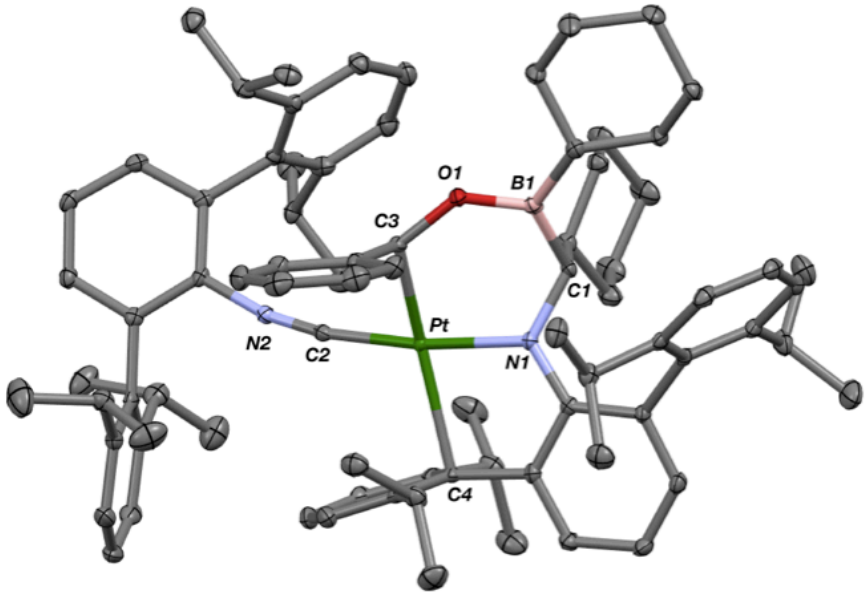

Figure 2.14. Molecular Structure of Pt(μ-PhC(H)O)(^{Cy2}BIM)(CNAr^{Dipp2}) • 4.5 C_6H_{12} (**15** • 4.5 C_6H_{12}). Co-crystallized molecules of cyclohexane have been omitted for clarity. Selected bond distances (Å) and angles (˚): Pt-N1 = 2.022(2). Pt-C2 = 1.910(2). Pt-C3 = 2.063(2). Pt-C4 = 2.413(2). C1-N1 = 1.488(2). O1-C3 = 1.419(2). B1-O1 = 1.356(3). N1-Pt-C3 = 93.31(7). N1-Pt-C4 = 79.43(6). C2-Pt-C3 = 83.54(8). C2-Pt-C4 = 107.46(7). Pt-C3-O1 = 118.6(1). C3-O1-B1 = 132.8(2).

Very recently, Bourissou and coworkers reported a singly-buttressed platinum alane adduct based off of the geminal phosphino alane ambiphile [Mes_2PC(=CHPh)Al*t*Bu_2] ("PAl", Mes = 2,4,6-$Me_3C_6H_2$).[54] Importantly, as noted for **1**, the presence of a rigid ligand topology that enforces a small bite angle between the ligand donor and acceptor sites effectively engenders a significant reverse-dative σ-interaction between the platinum center and the pendant Lewis acid. The authors demonstrate the ability of Pt(PAl)(PPh_3) to activate CO_2 via a 1,2-insertion reaction, and were able to structurally characterize the resulting adduct containing new Pt-C and Al-O bonds. This reaction was performed under 1 bar CO_2 at room temperature, and was reported to go to completion within 17 h. Prior to this work being published, we had investigated the

reactivity of **1** with CO_2. Placing a C_6D_6 solution of **1** in a J-Young NMR tube under 1 bar CO_2 results in slow depletion of **1** over the course of approximately 20 h at 20 ˚C as monitored by ^{1}H NMR spectroscopy. While this reaction almost certainly proceeds via the 1,2-insertion of CO_2 into the Pt-B linkage, the resulting adduct is unstable toward cyclization and dissociation from the platinum center. This yields the boralactone **16** (Scheme 2.6), which is also produced from the activation of CO_2 by free ^{Cy2}BIM.[55] The incipient Pt(CNAr^{Dipp2}) fragment disproportionates to yield Pt(CNAr^{Dipp2})$_2$ and metallic platinum. We believe that the inability to observe the product of CO_2 insertion into **1** can be attributed to the proclivity of the ^{Cy2}BIM ligand to undergo boron to carbon alkyl group migration. Insertion of CO_2 ostensibly yields intermediate **A**, which is structurally reminiscent of the products of ketone/aldehyde metallaboration **14** and **15**. However, this species is unstable toward C-N reductive elimination, liberating **16** and leaving behind the monoligated Pt(CNAr^{Dipp2}) fragment. Contrastingly, the PAl ligand utilizes a saturated triorganophosphine as its donor buttress that is unable to undergo reduction without the cleavage of a P-C bond.[54] This structural feature likely obviates analogous alkyl migration processes and contributes to the stability of the resultant CO_2 insertion product.

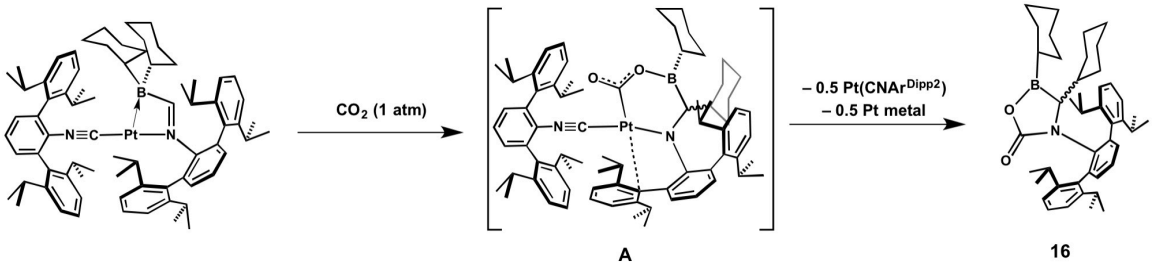

Scheme 2.6. Reaction of **1** with CO_2 to yield **16**, which ostensibly proceeds via unobserved intermediate **A**.

Insertion chemistry of substrates containing C-N multiple bonds can also be realized with **1**. Addition of excess acetonitrile to a benzene solution of **1** results in formation of the imine isocyanide Pt(0) complex **17** as ascertained by X-ray crystallography. The solid-state structure (Figure 2.15) reveals a Pt center that is rigorously two-coordinate and displays a linear geometry (C3-Pt-N1 = 176.1(2)˚) with no close contacts to either the flanking Dipp or cyclohexyl rings (shortest d(Pt-H) = 2.75 Å). Interestingly, of the small contingent of two-coordinate Pt(0) complexes in the Cambridge Structural Database,[42] **17** is the first to include a N-donor ligand. As seen for the ketone/aldehyde insertion products **14** and **15**, cyclohexyl group migration from boron to carbon is apparent, an event which is reflected by the downfield shifted ^{11}B NMR resonance (δ = +63.6 ppm) indicative of a three-coordinate boron center.[19] The formation of **17** is envisioned to proceed by 1,2-insertion of the nitrile functional group into the Pt-B linkage accompanied by cyclohexyl migration to carbon, furnishing an iminoacyl intermediate which can undergo C-N reductive elimination and coordination of the imine N center to platinum (Scheme 2.7). It should also be noted that unligated ^{Cy2}BIM readily activates acetonitrile to yield an exocyclic eneamine that is a tautomer of the Pt-bound imine fragment in **17**.[55] This tautomeric divergence provides circumstantial evidence that the formation of **17**, as well as the formation of **16** from **1** and CO_2, proceeds via 1,2-insertion into the Pt-B linkage followed by C-N reductive elimination rather than by dissociation of ^{Cy2}BIM and substrate activation via metal-free organic Frustrated Lewis Pair chemistry.

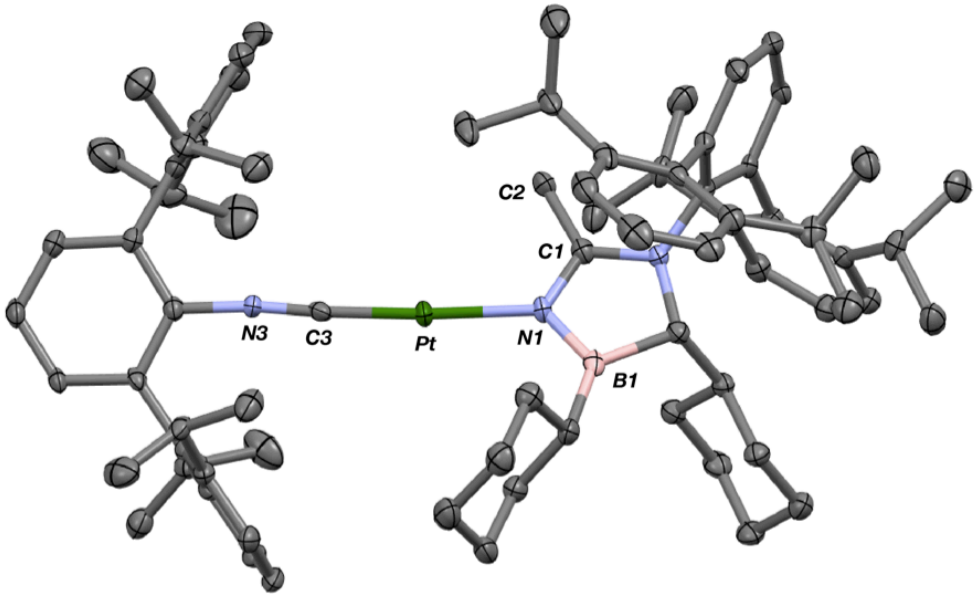

Figure 2.15. Molecular Structure of **17** • 1.5 C_5H_{12}. Co-crystallized molecules of *n*-pentane have been omitted for clarity. Selected bond distances (Å) and angles (°): Pt1-N1: 2.070(5). Pt1-C3: 1.812(6). N1-C1: 1.325(8). C1-C2: 1.503(9). C3-N3: 1.183(7). C3-Pt-N1: 176.1(2). C1-N1-B1: 108.6(5). N1-C1-C2: 120.7(5).

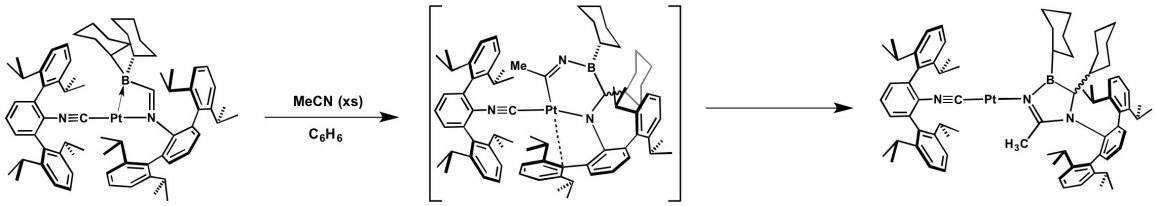

Scheme 2.7. Proposed mechanistic pathway leading to the formation of **17**.

Organoazides represent a canonical synthon for the formation of metal imido (M=NR) complexes.[56] Such a transformation typically proceeds via coordination of the azide group to the metal center followed by N_2 extrusion, with the latter step proceeding via either a unimolecular or bimolecular mechanism. While the intermediate organoazide adducts are often not observed, several have been isolated and structurally characterized.[57-66] Interestingly, we have found that reaction of 1-azidoadamantane (1.1

equiv) with Pt(κ^2-*N*-*B*-^{Cy2}BIM)(CNAr^{Dipp2}) (**1**) in *n*-pentane results in the precipitation of brown **18** over the course of 6 h. Analysis of this solid by ^{1}H NMR shows a highly magnetically desymmetrized environment and several upfield-shifted C_{aryl}-*H* resonances, both suggestive of boron-to-carbon cyclohexyl group migration and an interaction between one of the flanking Dipp rings and the Pt center. Structure determination on yellow crystals grown from a diethl ether/benzene solution shows **18** to be the product of Nγ insertion into the Pt-B linkage accompanied by boron to carbon cyclohexyl group migration (Scheme 2.8 and Figure 2.16). The Pt-bound azide group is best described as an anionic (boryl)diazenylamido donor in analogy to the diazenylimido functionalities typically derived from κ^1-*N*γ azide coordination to a transition metal center.[56] Consistent with this assignment are Pt-N2, N2-B, and N2-N3 distances consistent with single bonds (see Figure 2.16), as well as a short N3-N4 bond (1.247(3) Å) that compares well to the *bona fide* N=N double bond in *trans*-azobenzene (1.247(2) Å).[67] The coordination sphere around Pt is complimented by an *ipso* η^1-arene interaction with a flanking Dipp ring. While believed to be primarily π-type in nature, it should be noted that some degree of dearomatization is evident in the Pt-bound Dipp ring, with the C_{ipso}-C_{ortho} bond lengths being noticeably elongated (Figure 2.17) and the C_{ipso}-Ar bond vector (where Ar is the central aryl ring of the terphenyl system) being bent out of the plane by 23.3˚, findings suggestive of partial aryl-to-Pt charge transfer.[68] Similar structural distortions are apparent in the products of ketone and aldehyde metallaboration **14** and **15**, although to a lesser degree.

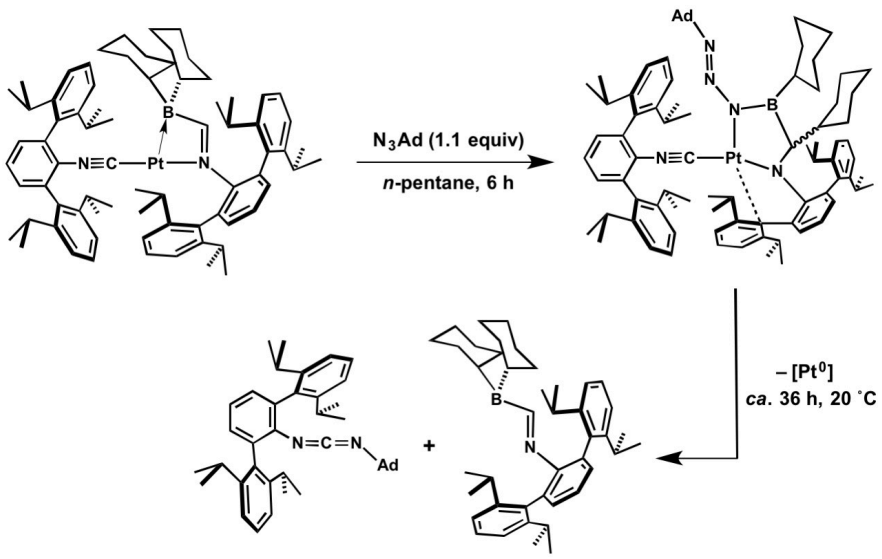

Scheme 2.8. Synthesis of Pt(μ-N_3Ad)(^{Cy2}BIM)(CNAr^{Dipp2}) (**18**) and its thermal decomposition to give the carbodiimide ^{Dipp2}ArN=C=NAd and free ^{Cy2}BIM with presumed loss of Pt metal.

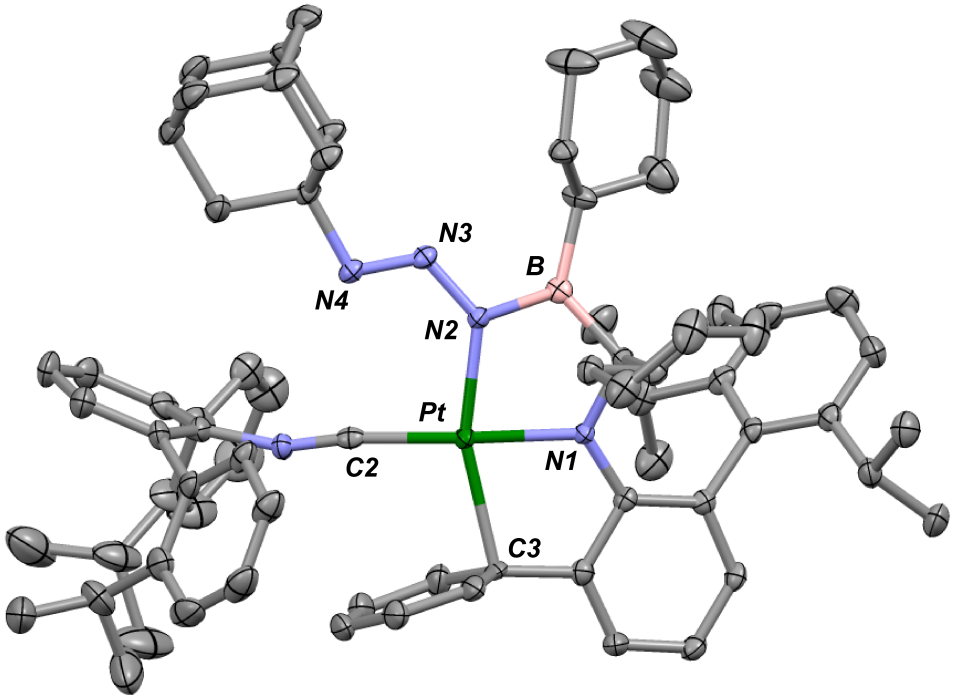

Figure 2.16. Molecular structure of Pt(μ-N_3Ad)(^{Cy2}BIM)(CNAr^{Dipp2}) • C_6H_6 (**18** • C_6H_6). Selected isopropyl groups, as well as the co-crystallized benzene molecule, have been omitted for clarity. Selected bond distances (Å) and angles (˚): Pt-N1 = 2.009(2); Pt-C2 = 1.920(3); Pt-C3 = 2.290(3); Pt-N2 = 2.031; N2-B = 1.435(4); N2-N3 = 1.366(3); N3-N4 = 1.247(3); B-N2-N3 = 112.6(2); N2-N3-N4 = 121.1(2).

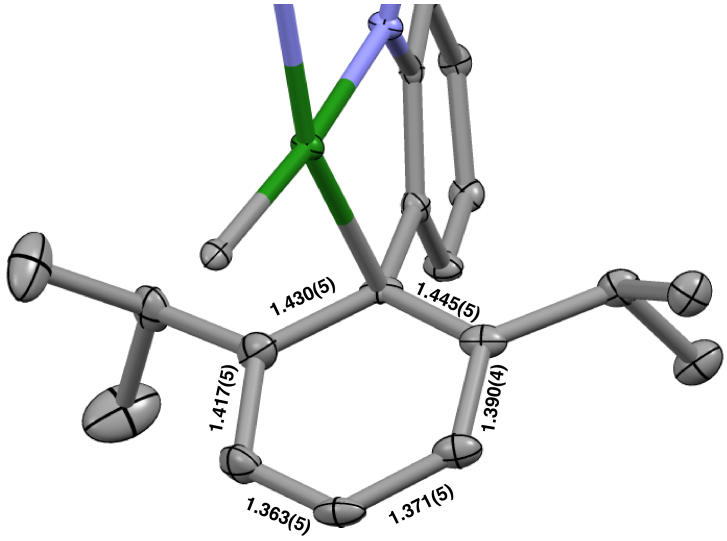

Figure 2.17. Zoom-in of the Pt-bound Dipp ring in **18**, showing the dearomatization as evidenced by the long C_{ipso}-C_{ortho} bond lengths. Selected atoms have been omitted for clarity.

The activation of 1-azidoadamantane by **1** is reminiscent of reactivity seen by Bergman for the early/late heterobimetallic complex [$Cp_2Zr(\mu$-N*t*Bu)IrCp*], which was shown to form the μ:κ^1-κ^1 adduct [$Cp_2Zr(\mu$-N*t*Bu)(μ-N_3Ph)IrCp*] upon insertion of the Nγ bond of phenylazide.[61] As frequently seen with other isolable transition metal adducts of organoazides, thermolysis of [$Cp_2Zr(\mu$-N*t*Bu)(μ-N_3Ph)IrCp*] resulted in evolution of N_2 and formation of a new imido ligand, yielding [$Cp_2Zr(\mu$-N*t*Bu)(μ-NPh)IrCp*]. In the case of **18**, simply stirring a C_6D_6 solution at room temperature is sufficient to effect the its complete exhaustion over *ca.* 36 h, producing the asymmetric carbodiimide AdN=C=NAr^{Dipp2} and free (boryl)iminomethane ^{Cy2}BIM (**2**) as the primary products as followed by ^{1}H NMR, with the Pt center presumably lost as Pt metal (Scheme 2.8). Although not isolated in pure form from these reaction mixtures, the carbodiimide AdN=C=NAr^{Dipp2} was identified by electrospray ionization-mass spectrometry (ESI-MS)

and by its diagnostic FTIR ν(N=C=N) stretching modes (2147 and 2088 cm^{-1}). The decomposition of **18** does not appear to be photochemically promoted, as irradiating C_6D_6 solutions of **18** (254 nm, Hg lamp) does not appreciably alter its rate of disappearance. The release of ^{Cy2}BIM is particularly surprising, as it demonstrates that reversible boron to carbon cyclohexyl migration can be achieved in this system. As described in a previous paper[55] and in Chapter 3 of this dissertation, cyclohexyl group migration provides over 18 kcal/mol of thermodynamic driving force in the capture of CO_2 by **2** to form the boralactone **16**. This had contributed to our assumption that alkyl migrations in ^{Cy2}BIM would continue to prove irreversible and deactivating. Accordingly, the ejection of **2** in the decomposition of **18** provides hope that interconversion between Pt-bound (boryl)iminomethane and reduced sp^3-C bridged boryl amido forms of this ligand might be realized.

The production of carbodiimide AdN=C=NAr^{Dipp2} suggested the potential intermediacy of a borane-stabilized imido or (boryl)alkylamido ligand. The proposition of a Lewis-acid-protected imido ligand particularly piqued our interest due to the known difficulties and dearth of examples of late metal complexes containing metal-ligand multiple bonds. Although efforts to circumvent the ramifications of the "oxo wall[69]" have largely focused on utilizing late metal complexes with trigonal coordination environments[66,70-74] or low coordination numbers,[75,76] the use of a tethered Lewis acid which could render the multiply-bonded species isolable yet still allow for its transfer to exogenous substrates would represent a novel approach in this regard. Indeed, late metal oxo and imido ligands commonly bridge multiple transition metal centers; however, the formation of two metal-ligand σ-bonds often endows these species with a kinetic stability

sufficient to preclude their exploitation in group transfer reactivity. In order to probe for a transient nitrene species in the decomposition of the azide complex **18**, trapping experiments were undertaken. Stirring **18** in C_6D_6 solutions containing 10 equivalents of cyclohexene (or, alternatively, in neat cyclohexene) does not provide any evidence of olefin aziridination. Alternatively, **18** in the presence of stoichiometric PMe_3 does not yield the phosphimine Me_3P=NAd, with the only species visible in the $^{31}P\{^1H\}$ NMR spectrum of these reaction mixtures containing one-bond coupling to ^{195}Pt, suggesting complexation of the phosphine ligand to unidentified platinum species. While the search for a transient imido/nitrene has thus far proven inconclusive, it should be noted that N-N bond cleavage does not necessarily precede N-$C_{isocyanide}$ bond formation in the production of carbodiimide. Indeed, examination of the solid-state structure of **18** reveals that the α-N atom (N4) resides in close proximity (*ca*. 2.8 Å) to the isocyanide carbon (C2), allowing one to envision the cascade of carbodiimide formation and cyclohexyl reversion to boron beginning with C-N bond formation, thereby obviating the formation of complexed or free nitrene species.

The reactivity of Pt(κ^2-*N*-*B*-^{Cy2}BIM)($CNAr^{Dipp2}$) (**1**) with other organoazides has also been examined (Scheme 2.9). Trimethylsilyl azide does not yield an observable azide adduct, instead producing the carbodiimide Me_3SiN=C=NAr^{Dipp2} as the principal product as determined by ^1H NMR and ESI-MS. Encumbered 2,6-diisopropylphenylazide ($DippN_3$) does not react with **1 (**1:1 mixture) at room temperature in benzene solution. However, heating a C_6D_6 solution of **1** with five equivalents of $DippN_3$ to 40 ˚C results in surprising formation of the hydride-borohydride PtH(μ^2-H)(κ^1-*N*-^{Cy2}BIM)($CNAr^{Dipp2}$) (**5**) as the primary –Ar^{Dipp2} containing species, presumably via dehydrogenation of $DippN_3$.

Although the Fe-mediated intramolecular dehydrogenation of an isopropyl group in an imido ligand derived from $DippN_3$ has recently been observed by Betley,[77] this reactivity was predicated on the iminyl character of the Fe-bound N center. Such open-shell species are unlikely in our system given the strong preference of platinum for closed-shell electronic configurations. While the fate of the $DippN_3$ fragment in this transformation is unknown, we discovered that the unencumbered aryl azide *p*-$MeC_6H_4N_3$ (*p*-$TolN_3$) undergoes smooth insertion reactivity with **1** to provide **19** (Scheme 2.9). Structural characterization of **19** by X-ray diffraction reveals a structure that is wholly analogous to that of **18**, including boron to carbon cyclohexyl migration and formation of a (boryl)diazenylamido ligand (Figure 2.18). As noted for **18**, dearomatization in the Pt-bound Dipp ring is evident in **19** (Figure 2.19). The Pt-C_{ipso} distance of 2.248(2) Å is contracted compared to that in **18** (2.290(3) Å), which also reflects an attendant increase in the degree to which the C_{ipso}-Ar bond vector (where Ar is the central aryl ring of the terphenyl system) has moved out of the plane of the Dipp ring (28.9˚ in **19** vs. 23.3˚ in **18**). These observations suggest that there may be an even greater degree of arene-to-Pt charge transfer in **19** compared to **18**.

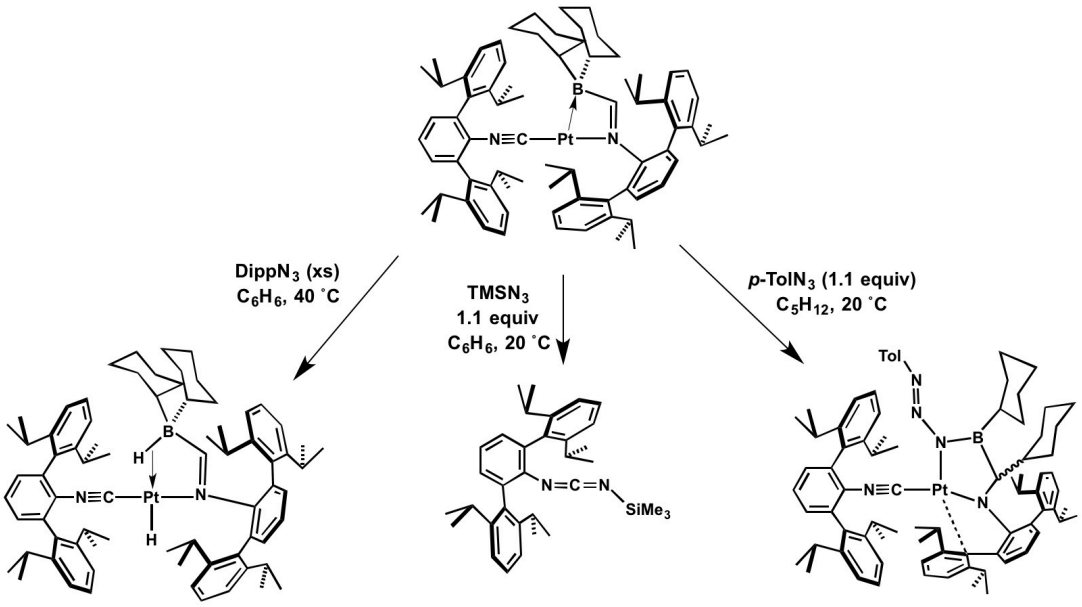

Scheme 2.9. Reactivity of **1** with $DippN_3$, $TMSN_3$ and *p*-$TolN_3$.

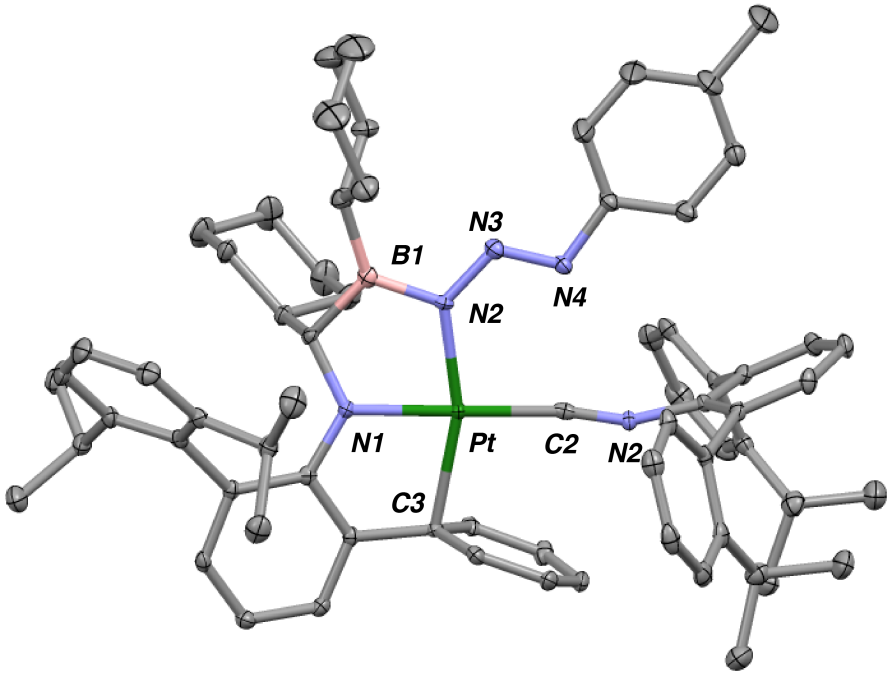

Figure 2.18. Molecular structure of **19** • 2 C_5H_{12}. Co-crystallized molecules of *n*-pentane and selected isopropyl groups have been omitted for clarity. Selected bond distances (Å) and angles (˚): Pt-N1 = 2.004(2); Pt-C2 = 1.909(3); Pt-C3 = 2.248(2); Pt-N2 = 2.032(2); N2-B1 = 1.438(3); N2-N3 = 1.353(3); N3-N4 = 1.261(3); B1-N2-N3 = 113.9(2); N2-N3-N4 = 118.6(2).

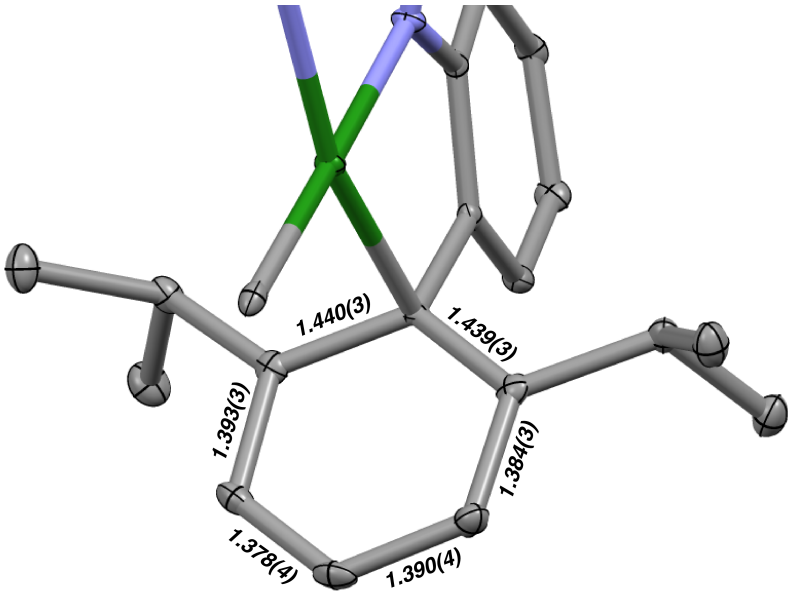

Figure 2.19. Zoom-in of the Pt-bound Dipp ring in **19**, showing the dearomatization as evidenced by the long C_{ipso}-C_{ortho} bond lengths. Selected atoms have been omitted for clarity.

2.5. Concluding remarks

In conclusion, the 1,1-hydroboration of a coordinated isocyanide ligand in $Pt(CNAr^{Dipp2})_2$ can be effected using $HBCy_2$ to afford the singly-buttressed platinum-borane complex $Pt(\kappa^2\text{-}N,B\text{-}^{Cy2}BIM)(CNAr^{Dipp2})$ (**1**). Although nearly all transition metal-borane adducts reported to date have utilized ligand scaffolds which employ multiple donor arms, the (boryl)iminomethane ligand in **1** is capable of fostering a significant reverse-dative platinum borane interaction as evidenced by ^{11}B NMR, X-ray diffraction and Density Functional Theory computational studies. The rigid topology of the (boryl)iminomethane framework whereby the donor and acceptor atoms are linked by a single sp^2-hybridized carbon atom engenders a small bite angle, which is likely responsible for the significant Pt-B interaction. Remarkably, the unligated

(boryl)iminomethane ^{Cy2}BIM (**2**) can be readily accessed via addition of $HBCy_2$ to the *m*-terphenylisocyanide $CNAr^{Dipp2}$, and is shown by ^{11}B NMR to possess a monomeric structure containing a tri-coordinated boron center. Importantly, while these examples of isocyanide 1,1-hydroboration are unprecedented in the literature, the resistance of ^{Cy2}BIM to undergo head-to-tail dimerization can be traced to the sterically imposing *m*-terphenyl and cyclohexyl substituents. The monomeric nature of **2** allows it to effect the heterolytic cleavge H_2 and H_2O under mild conditions in a Frustrated Lewis Pair-type manner. The absence of multiple donor buttresses in the platinum complex **1** allows it to undergo rich cooperative reactivity with a host of substrates. Oxidative addition of I_2, SbF_3, PBr_3 and various E-H bonds (E = H, N, O) has been demonstrated. In each case, one of the incipient Pt-bound X-ligands is seen to bridge the Pt and B centers. The flexibility of the BIM framework, which allows the borane center to act either as a Z-type σ-acceptor or as a pendant Lewis acid, can be exploited to effect both bond activation and subsequent stabilization of hard, π-donor ligands at a soft Pt(II) center. Oxidative insertion reactivity of **1** with acetone, benzaldehyde, acetonitrile and two different organoazides has also been demonstrated, each of which represents an unprecedented reactivity mode for transition metal-borane complexes. Each of these reactions is accompanied by boron-to-carbon cyclohexyl migration, thereby avoiding the buildup of formal negative charge at the boron center. Importantly, however, the release of free ^{Cy2}BIM in the thermal decomposition of 1-azidoadamantane adduct **18** shows that this process is not necessarily irreversible. Future work in this platinum (boryl)iminomethane system will focus on using the pendant borane as a protecting group for highly reactive ligands containing multiple bonds to Pt for applications in group transfer-type reactivity. Also envisioned is

the use of **1** as a catalyst for the hydrogenation, hydration or hydroamination of unsaturated organic species, which could exploit both the proclivity of **1** to heterolytically cleave E-H bonds and subsequently stabilize dihydride, hydride/hydroxide, or hydride/amide equivalents. Finally, the extension of (boryl)iminomethane chemistry to metals other than platinum represents a seminal goal. Although not described in this dissertation, extensive efforts to obtain BIM complexes of Ni, Pd and Au have been carried out, yet thus far proven fruitless. A principal hurdle in the pursuit of catalytic turnover using **1** has been the inertness of many of the resultant Pt(II) products. Indeed, kinetic stability of metal-ligand bonds is a hallmark of many Pt(II) species. We therefore believe it will be vital to delineate the exact mechanism whereby **1** is formed, as well as to understand why all efforts to ligate a pre-formed BIM to various transition metal fragments have so far been unsuccessful. In doing so, we hope that rational synthetic routes to (boryl)iminomethane complexes of many different transition metals might one day be realized.

2.6. Synthetic procedures and characterization data

General considerations. All manipulations were carried out under an atmosphere of purified dinitrogen using standard Schlenk and glovebox techniques. Unless otherwise stated, reagent-grade starting materials were purchased from commercial sources and either used as received or purified by standard procedures.[78] Solvents were dried and deoxygenated according to standard procedures.[79] Benzene-d_6 (Cambridge Isotope Laboratories) was distilled from NaK alloy and stored over 4 Å molecular sieves under N_2 for at least 24 h prior to use. Chloroform-*d* (Cambridge Isotope Laboratories) was

distilled from P_2O_5 and stored over 4 Å molecular sieves under N_2 for at least 24 h prior to use. Celite 405 (Fisher Scientific) was dried under vacuum (24 h) at a temperature above 250 ˚C and stored in the glovebox prior to use. KBr (FTIR grade from Aldrich) was stirred overnight in anhydrous THF, filtered and dried under vacuum at a temperature above 250 ˚C prior to use. The *m*-terphenyl isocyanide[21] $CNAr^{Dipp2}$ and the two-coordinate platinum complex[80] $Pt(CNAr^{Dipp2})_2$ were prepared as previously reported. Dicyclohexylborane ($HBCy_2$) was prepared according to a literature procedure.[81]

Solution ^1H, $^{13}C\{^1H\}$, ^{19}F, $^{31}P\{^1H\}$ and ^{11}B NMR spectra were recorded on a Bruker Avance 300, a Varian Mercury 400, a Jeol ECA 500, or a Varian X-SENS 500 spectrometer. ^1H and $^{13}C\{^1H\}$ chemical shifts are reported in ppm relative to $SiMe_4$ (^1H and ^{13}C $\delta = 0.0$ ppm) with reference to residual solvent resonances of 7.16 ppm (^1H) and 128.06 ppm (^{13}C) for C_6D_6, 7.26 (^1H) and 77.16 (^{13}C) for $CDCl_3$. ^{19}F NMR chemical shifts were referenced externally to a solution of neat trifluoroacetic acid ($\delta = -78.5$ ppm vs. $CFCl_3$. $^{31}P\{^1H\}$ chemical shifts were referenced externally to 85% H_3PO_4 ($\delta = 0.0$ ppm). ^{11}B NMR chemical shifts were referenced externally to a solution of phenylboronic acid in acetone-d_6 ($\delta = 29.0$ ppm vs. $BF_3{\cdot}Et_2O$). FTIR spectra were recorded on a Thermo-Nicolet iS10 FTIR spectrometer. Samples were prepared either as KBr pellets or as C_6D_6 solutions injected into a ThermoFisher solution cell equipped with KBr windows. For solution FTIR spectra, solvent peaks were digitally subtracted from all spectra by comparison with an authentic spectrum obtained immediately prior to that of the sample. The following abbreviations were used for the intensities and characteristics of important IR absorption bands: vs = very strong, s = strong, m = medium, w = weak, vw = very weak; b = broad, vb = very broad, sh = shoulder. High-resolution mass

spectrometry (HRMS) was performed using an Agilent 6230 ESI-TOFMS instrument running in positive ion mode. Combustion analyses were performed by Robertson Microlit Laboratories of Madison, NJ (USA) or Midwest Microlabs of Indianapolis, IN (USA).

Synthesis of Pt(κ^2-*N*-*B*-^{Cy2}BIM)(CNAr^{Dipp2}) (1). Benzene (6 mL) was added to solid Pt(CNAr^{Dipp2})$_2$ (0.210 g, 0.201 mmol) and HBCy$_2$ (0.039 g, 0.219 mmol, 1.1 equiv). The solution was stirred over the course of 30 min and gradually changed in color from yellow to light orange. All volatile materials were then removed *in vacuo*. The resulting orange residue was slurried in 2 mL of a 1:1 *n*-pentane/hexamethyldisiloxane (O(SiMe$_3$)$_2$) mixture and stirred for 10 min to produce a dark-colored mother liquor and a yellow solid. The mother liquor was decanted, and the resulting solid was then dissolved in *n*-pentane (15 mL), filtered through Celite, and dried under reduced pressure. Dissolution of the yellow residue in benzene (3 mL), followed by lyophilization provided Pt(κ^2-*N,B*-^{Cy2}BIM)(CNAr^{Dipp2}) of sufficient purity by ^{1}H and ^{11}B NMR for further studies. Yield: 0.186 g, 0.152 mmol, 76%. Storage of an *n*-pentane solution of Pt(κ^2-*N,B*-^{Cy2}BIM)(CNAr^{Dipp2}) at –40 ˚C provided analytically pure yellow crystals of **1** • 0.5 C$_5$H$_{12}$ suitable for X-ray diffraction. ^{1}H NMR (500.2 MHz, C$_6$D$_6$, 20 ˚C): δ = 8.35 (s, 1H, $J_{Pt,H}$ = 120 Hz, C$_{imine}$-*H*), 7.39 (t, 2H, *p*-Dipp, *J* = 8 Hz), 7.32 (t, 2H, *p*-Dipp, *J* = 8 Hz), 7.24 (d, 4H, *m*-Dipp, *J* = 8 Hz), 7.16 (d, 4H, *J* = 8 Hz, *m*-Dipp), 7.08 (d, 2H, *J* = 8 Hz, *m*-Ar), 6.94 (t, 1H, *J* = 8 Hz, *p*-Ar), 6.90 (t, 1H, *J* = 8 Hz, *p*-Ar), 6.81 (d, 2H, *J* = 8 Hz, *m*-Ar), 2.76 (septet, 4H, *J* = 7 Hz, C*H*(CH$_3$)$_2$), 2.72 (septet, 4H, *J* = 7 Hz, C*H*(CH$_3$)$_2$), 1.83-1.60 (m, 8H, Cy), 1.51-1.39 (m, 4H, Cy), 1.36 (d, 12H, *J* = 7 Hz, CH(C*H*$_3$)$_2$), 1.34 (d, 12H, *J* = 7 Hz, CH(C*H*$_3$)$_2$), 1.24 (m, 6H, Cy), 1.10 (d, 12H, *J* = 7 Hz, CH(C*H*$_3$)$_2$), 1.05 (d, 12H, *J* =

7 Hz, CH(CH_3)$_2$), 0.17 (m, 4H, Cy) ppm. ^{13}C{^{1}H} NMR (125.7 MHz, C_6D_6, 20 ˚C): δ = 214.5 (C_{imine}), 148.4, 146.7, 146.5, 143.9 (C≡N), 138.7, 136.6, 135.6, 134.6, 131.6, 130.9, 129.7, 129.6, 129.0, 126.6, 125.4, 123.6, 123.3, 32.4, 31.6, 31.4, 31.0, 29.2, 28.9, 27.7, 26.0, 24.6, 24.5, 23.9 ppm. *Note: The isocyanide (C≡N) resonance for this compound could not be conclusively assigned.* ^{11}B NMR (160.5 MHz, C_6D_6, 20 ˚C): δ = 18.6 (bs) ppm. FTIR (C_6D_6, KBr Windows, 20 ˚C): ν(C≡N) = 2094 (s) cm^{-1}, also 2963, 2926, 2868, 2847, 1461, 1446, 1414, 1385, 1361, 1056, 791, 756 cm^{-1}. Anal. Calc'd for $C_{74}H_{97}N_2BPt$: C, 72.82; H, 8.01; N, 2.30. Found: C, 71.44; H, 7.68; N, 2.18.

Synthesis of ^{Cy2}BIM (2). To a solid mixture of CNAr^{Dipp2} (0.182 g, 0.429 mmol) and $HBCy_2$ (0.079 mg, 0.444 mmol, 1.03 equiv) was added 5 mL of Et_2O. The resulting bright yellow solution was stirred for 10 min and then all volatile materials were removed under reduced pressure. The resulting yellow oil was dissolved in 3 mL *n*-pentane, filtered through Celite, and dried agian *in vacuo*. The oily residue produced was then subjected to four cycles of dissolution in *n*-pentane (3 mL) and drying *in vacuo* to afford ^{Cy2}BIM as a yellow solid. Yield: 0.235 g, 0.391 mmol, 90%. ^{1}H NMR (500.2 MHz, C_6D_6, 20 ˚C): δ = 8.35 (s, 1H, C_{imine}-H), 7.27 (t, 2H, J = 8 Hz, *p*-Dipp), 7.16 (d, 2H, J = 8 Hz, *m*-Ar), 7.15 (d, 4H, J = 8 Hz, *m*-Dipp), 7.05 (t, 1H, J = 8 Hz, *p*-Ar), 3.04 (septet, 4H, J = 7 Hz, CH(CH$_3$)$_2$), 1.68-1.61 (m, 8H, Cy), 1.32-1.26 (m, 4H, Cy), 1.27 (d, 12H, J = 7 Hz, CH(CH_3)$_2$), 1.16 (d, 12H, J = 7 Hz, CH(CH_3)$_2$), 1.16-1.11 (m, 6H, Cy), 0.76-0.69 (m, 4H, Cy) ppm. ^{13}C{^{1}H} NMR (125.8 MHz, C_6D_6, 20 ˚C): δ = 181.0 (C_{imine}), 153.2, 147.0, 137.5, 130.8, 130.2, 128.3, 123.6, 123.0, 36.1, 31.2, 22.8, 26.9, 26.1, 25.5, 23.3 ppm. ^{11}B NMR (160.5 MHz, C_6D_6, 20 ˚C): δ = 74.3 (bs) ppm. FTIR (C_6D_6, KBr Windows, 25 ˚C):

2961, 2923, 2851, 1614, 1578, 1452, 1413, 1382, 1363, 1058, 761 cm^{-1}. HRMS (ESI-TOF): *m/z* calc'd for $C_{43}H_{63}NOB$ $[M+H+H_2O]^+$: 619.5034 Found: 619.5035.

Synthesis of ^{Cy2}BIM→BCl_3 (3). An *n*-pentane solution of ^{Cy2}BIM (0.055 g, 0.092 mmol, 3 mL) was frozen in a glovebox cold well. Upon removal from the cold well, 0.100 mL of a hexane solution of BCl_3 (1.0 M, 0.100 mmol, 1.09 equiv) was added as the reaction mixture thawed. The solution was allowed to warm to room temperature over the course of 30 min, during which time it changed in color from bright yellow to colorless. All volatiles were then removed under reduced pressure. Dissolution of the resulting solid in *n*-pentane (1 mL) and storage at –40 ˚C for 2 days afforded colorless crystals, which were collected and dried *in vacuo*. Yield: 0.038 g, 0.053 mmol, 57%. ^{1}H NMR (499.8 MHz, C_6D_6, 20 ˚C): δ = 9.00 (s, 1H, C_{imine}-*H*), 7.29 (t, 2H, *J* = 8 Hz, *p*-Ar), 7.21 (d, 2H, *J* = 8 Hz, *m*-Ar), 7.11 (d, 2H, *J* = 8 Hz, *m*-Ar), 7.04 (d, 2H, *J* = 8 Hz, *m*-Ar), 6.92 (t, 1H, *J* = 8 Hz, *p*-Ar), 3.44 (septet, 2H, *J* = 7 Hz, C*H*$(CH_3)_2$), 2.42 (septet, 2H, *J* = 7 Hz, C*H*$(CH_3)_2$), 1.72-1.67 (m, 7H, Cy), 1.52-1.43 (m, 4H, Cy), 1.50 (d, 6H, *J* = 7 Hz, CH(C*H*$_3)_2$), 1.37-1.25 (m, 7H, Cy), 1.27 (d, 6H, *J* = 7 Hz, CH(C*H*$_3)_2$), 1.15 (d, 6H, *J* = 7 Hz, CH(C*H*$_3)_2$), 0.80 (d, 6H, *J* = 7 Hz, CH(C*H*$_3)_2$), 0.80-0.73 (m, 4H, Cy) ppm. ^{13}C{^{1}H} NMR (125.7 MHz, C_6D_6, 20 ˚C): δ = 213.6 (*C*$_{imine}$), 152.6, 148.6, 146.6, 141.7, 136.8, 136.7, 133.8, 130.4, 128.4, 127.5, 125.1, 122.7, 32.4, 31.4, 31.4, 31.3, 31.1, 28.6, 28.1, 27.4, 26.6, 25.4, 24.0, 22.1 ppm. ^{11}B NMR (160.5 MHz, C_6D_6, 20 ˚C): δ = 9.4 (bs, Cy_2(C)*B*Cl), –4.1 (s, N*B*Cl_3) ppm. FTIR (C_6D_6, KBr Windows, 25 ˚C): 2964, 2927, 2868, 2849, 1552, 1460, 1382, 1361, 1341, 1325, 1166, 1055, 852, 831, 775, 758, 739, 694 cm^{-1}. Anal. Calc'd for $C_{43}H_{60}NB_2Cl_3$: C, 71.84; H, 8.41; N, 1.95. Found: C, 72.57; H, 8.50; N, 1.87.

Synthesis of *trans*-$PtI_2(\kappa^1$-*N*-^{Cy2}BIM)($CNAr^{Dipp2}$) (4). To an Et_2O solution of $Pt(\kappa^2$-*N,B*-^{Cy2}BIM)($CNAr^{Dipp2}$) (0.100 g, 0.082 mmol, 3 mL) was added an Et_2O solution of I_2 (0.024 g, 0.095 mmol, 1.15 equiv, 2 mL). The reaction mixture was stirred for 2 h, during which time a light-colored precipitate was observed to form. The reaction mixture was then cooled to –40 ˚C to induce further precipitation. The supernatant was then decanted from a beige solid, which was washed with cold Et_2O (–40 ˚C, 5 mL) and dried *in vacuo* to afford *trans*-$PtI_2(\kappa^1$-*N*-^{Cy2}BIM)($CNAr^{Dipp2}$). Yield: 0.103 g, 0.070 mmol, 85%. Storage of a saturated C_6H_6 solution at of *trans*-$PtI_2(\kappa^1$-*N*-^{Cy2}BIM)($CNAr^{Dipp2}$) at room temperature over 2 d provided analytically pure crystals of **4** • 1.5 C_6H_6 which were suitable for X-ray diffraction. ^{1}H NMR (500.2 MHz, $CDCl_3$, 20 ˚C): δ = 9.09 (s, 1H, $J_{Pt,H}$ = 100 Hz, C_{imine}-*H*), 7.48 (t, 1H, *J* = 8 Hz, *p*-Ar), 7.35 (t, 2H, *J* = 8 Hz, *p*-Ar), 7.23-7.19 (m, 4H), 7.18 (d, 4H, *J* = 8 Hz, *m*-Ar), 7.14 (m, 3H), 7.11 (d, 2H, *J* = 8 Hz, *m*-Ar), 7.02 (d, 2H, *J* = 8 Hz, *m*-Ar), 3.89 (septet, 2H, *J* = 7 Hz, C*H*(CH_3)$_2$), 2.45 (septet, 4H, *J* = 7 Hz, C*H*(CH_3)$_2$), 2.05 (septet, 2H, *J* = 7 Hz, C*H*(CH_3)$_2$), 1.52-1.41 (m, 6H, Cy), 1.17 (d, 12H, *J* = 7 Hz, CH(C*H*$_3$)$_2$), 1.16 (d, 6H, *J* = 7 Hz, CH(C*H*$_3$)$_2$), 1.10 (d, 6H, *J* = 7 Hz, CH(C*H*$_3$)$_2$), 1.08 (d, 6H, *J* = 7 Hz, CH(C*H*$_3$)$_2$), 1.06 (d, 12H, *J* = 7 Hz, CH(C*H*$_3$)$_2$), 1.02-0.98 (m, 2H, Cy), 0.93-0.86 (m, 10H, Cy), 0.70 (d, 6H, *J* = 7 Hz, CH(C*H*$_3$)$_2$), 0.62 (m, 2H, Cy), 0.48-0.42 (m, 2H, Cy) ppm. ^{13}C{^{1}H} NMR (125.7 MHz, $CDCl_3$, 20 ˚C): δ = 213.4 (C_{imine}), 151.8, 147.8, 147.4, 146.3, 140.0, 135.7, 134.3, 134.1, 131.8, 130.8, 129.6, 129.0, 128.6, 128.5, 127.5, 124.8, 124.4, 123.6, 122.2, 110.4, 34.8, 32.5, 31.1, 30.8, 30.3, 29.9, 28.8, 28.4, 27.1, 26.5, 25.7, 24.7, 24.5, 22.4 ppm. *Note: The isocyanide (C≡N) resonance for this compound could not be conclusively assigned*. ^{11}B NMR (160.5 MHz,

$CDCl_3$, 20 ˚C): δ = 25.3 (bs) ppm. FTIR (C_6D_6, 20 ˚C): ν(C≡N) = 2180 cm^{-1}, also 2959, 2926, 2867, 2845, 1560, 1277, 1241, 1188, 1044, 1033, 753 cm^{-1}. Anal. Calc'd for $C_{74}H_{97}N_2BI_2Pt$: C, 60.29; H, 6.63; N, 1.90. Found: C, 60.03; H, 6.63; N, 1.84.

Synthesis of PtH(μ-H)(^{Cy2}BIM)(CNAr^{Dipp2}) (5). An ampoule was charged with a benzene solution of Pt(κ^2-*N,B*-^{Cy2}BIM)(CNAr^{Dipp2}) (0.100 g, 0.082 mmol, 5 mL). This solution was degassed and subsequently exposed to 1.0 atm of H_2 gas. The ampoule was sealed and stirred vigorously for 10 h, whereupon all volatiles were removed under reduced pressure. Dissolution of the resulting residue in 1 mL *n*-pentane and storage at –40 ˚C for 1 week resulted in the formation of colorless crystals, which were collected and dried *in vacuo*. Yield: 0.033 g, 0.027 mmol, 33%. ^{1}H NMR (300.0 MHz, C_6D_6, 20 ˚C): δ = 10.43 (d, 1H, $J_{H,H}$ = 10 Hz, $J_{Pt,H}$ = 75 Hz, C_{imine}-*H*), 7.41 (t, 2H, *J* = 8 Hz, *p*-Ar), 7.31 (t, 2H, *J* = 8 Hz, *p*-Ar), 7.25 (d, 2H, *J* = 8 Hz, *m*-Ar), 7.23 (d, 4H, *J* = 8 Hz, *m*-Ar), 7.11 (d, 2H, *J* = 8 Hz, *m*-Ar), 7.05 (d, 2H, *J* = 8 Hz, *m*-Ar), 6.92 (t, 1H, *J* = 8 Hz, *p*-Ar), 6.88-6.81 (m, 3H), 3.10 (septet, 2H, *J* = 7 Hz, C*H*(CH_3)$_2$), 2.62 (septet, 4H, *J* = 7 Hz, C*H*(CH_3)$_2$), 2.33 (septet, 2H, *J* = 7 Hz, C*H*(CH_3)$_2$), 1.90-1.72 (m, 10H, Cy), 1.51-1.30 (m, 4H, Cy), 1.31 (d, 12H, *J* = 7 Hz, CH(C*H*$_3$)$_2$), 1.27 (d, 6H, *J* = 7 Hz, CH(C*H*$_3$)$_2$), 1.22 (d, 6H, *J* = 7 Hz, CH(C*H*$_3$)$_2$), 1.09 (d, 12H, *J* = 7 Hz, CH(C*H*$_3$)$_2$), 1.06 (d, 6H, *J* = 7 Hz, CH(C*H*$_3$)$_2$), 0.95 (d, 6H, *J* = 7 Hz, CH(C*H*$_3$)$_2$), 0.90 (m, 2H, Cy), 0.59 (m, 4H, Cy), 0.01 (m, 2H, Cy), –2.34 (dd, 1H, $J_{H,H}$ = 25, 10 Hz, $J_{Pt,H}$ = 550 Hz, B-*H*-Pt), –15.00 (d, 1H, $J_{H,H}$ = 25 Hz, $J_{Pt,H}$ = 1420 Hz, Pt-*H*) ppm. ^{13}C{^{1}H} NMR (125.7 MHz, C_6D_6, 20 ˚C): δ = 219.8 (*C*$_{imine}$), 150.0, 147.3, 147.2, 146.3, 139.5, 136.2, 134.3, 133.7, 131.3, 130.2, 129.8, 129.3, 128.6, 128.4, 125.0, 123.7, 123.6, 123.2, 122.9, 32.5, 31.8, 31.6, 31.4, 31.2, 29.8, 29.6, 28.9,

27.7, 26.9, 26.5, 26.3, 25.1, 24.7, 24.5, 22.2 ppm. *Note: The isocyanide (C≡N) resonance for this compound could not be conclusively assigned.* ^{11}B NMR (160.5 MHz, C_6D_6, 20 ^{o}C): δ = –6.9 (bs) ppm. FTIR (C_6D_6, 20 ˚C): ν(C≡N) = 2154 cm^{-1}, also 2962, 2920, 2868, 2845, 1580, 1460, 1413, 1382, 1363, 1055, 791, 755 cm^{-1}. Anal. Calc'd for $PtC_{74}H_{99}N_2B$: C, 72.70; H, 8.16; N, 2.29. Found: C, 71.26, H, 8.11; N, 2.17.

Synthesis of $(Cy)_2BCH_2NHAr^{Dipp2}$ (6). A J-Young NMR tube was charged with a C_6D_6 solution containing ^{Cy2}BIM (0.050 g, 0.083 mmol, 0.8 mL). The solution was degassed and then exposed to H_2 gas (1 atm). The NMR tube was sealed and shaken intermittently over the course of 3 days, during which time it slowly changed in color from bright yellow to colorless. All volatiles were removed under reduced pressure. The resulting residue was extracted with *n*-pentane (3 mL), filtered through Celite, and dried *in vacuo*. This yielded a colorless residue that consists of pure $(Cy)_2BCH_2NHAr^{Dipp2}$ as assayed by ^{1}H and ^{11}B NMR. Yield: 0.035 g, 0.058 mmol, 66%. ^{1}H NMR (300.0 MHz, C_6D_6, 20 ˚C): δ = 7.33 (t, 2H, *J* = 8 Hz, *p*-Ar), 7.22-7.16 (m, 4H), 6.87 (t, 1H, *J* = 8 Hz, *p*-Ar), 3.80 (t, 1H, *J* = 5 Hz, N-*H*), 3.12 (septet, 4H, *J* = 7 Hz, C*H*$(CH_3)_2$), 2.69 (d, 2H, *J* = 5 Hz, B-C*H*$_2$-N), 1.70-1.62 (m, 8H, Cy), 1.27 (d, 12H, *J* = 7 Hz, CH(C*H*$_3)_2$), 1.15 (d, 12H, *J* = 7 Hz, CH(C*H*$_3)_2$), 1.15-1.02 (m, 10H, Cy), 0.86-0.73 (m, 4H, Cy) ppm. ^{13}C{^{1}H} NMR (125.7 MHz, C_6D_6, 20 ˚C): δ = 147.9, 146.4, 138.2, 130.6, 128.6, 127.2, 123.3, 117.7, 46.2, 33.6, 30.9, 27.7, 27.3, 26.8, 25.2, 23.5 ppm. ^{11}B NMR (96.2 MHz, C_6D_6, 20 ˚C): δ = 78.6 (bs) ppm. FTIR (C_6D_6, KBr Windows, 20 ˚C): ν(NH) = 3396 cm^{-1}, also 2962, 2920, 2865, 2847, 1496, 1460, 1432, 1400, 1382, 1361, 1140, 1057, 763 cm^{-1}. HRMS (ESI-TOF): *m/z* calc'd for $C_{43}H_{63}NB$ $[M+H]^+$: 604.5055. Found: 604.5058.

Synthesis of PtH(μ-OH)(^{Cy2}BIM)(CNAr^{Dipp2})$_2$ (7). A benzene solution of Pt(κ^2-*N,B*-^{Cy2}BIM)(CNAr^{Dipp2}) (0.060 g, 0.049 mmol, 1.5 mL) was loaded into a J-Young NMR tube and connected to a Schlenk line. To this was added 0.5 mL of a degassed, 0.17 M THF solution of deionized water (0.085 mmol, 1.7 equiv) via vacuum transfer. The resulting solution was shaken intermittently for 45 min and then all volatiles were removed under reduced pressure. The resulting pale-yellow residue which was dissolved in 0.5 mL *n*-pentane, shaken for 1 min, and dried *in vacuo*. The resulting solid was then dissolved in 1 mL of a 3:1 Et_2O/*n*-pentane mixture, filtered, and stored at –40 ˚C for 2 weeks to afford colorless crystals, which were washed with cold *n*-pentane (3 x 1 mL, –40 ˚C) and dried in vacuo. Yield: 0.015 g, 0.012 mmol, 25%. ^{1}H NMR (499.8 MHz, C_6D_6, 20 ˚C): δ = 8.43 (s, 1H, $J_{Pt,H}$ = 80 Hz, C_{imine}-*H*), 7.42 (t, 2H, *J* = 8 Hz, *p*-Ar), 7.29-7.19 (m, 10H), 7.11 (d, 2H, *J* = 8 Hz, *m*-Ar), 7.04 (d, 1H, *J* = 8 Hz, *m*-Ar) 6.88 (m, 3H), 3.29 (septet, 2H, *J* = 7 Hz, C*H*$(CH_3)_2$), 2.60 (septet, 4H, *J* = 7 Hz, C*H*$(CH_3)_2$), 2.36 (septet, 2H, *J* = 7 Hz, C*H*$(CH_3)_2$), 1.98-1.79 (m, 6H, Cy), 1.54 (m, 2H, Cy), 1.48-1.30 (m, 10H, Cy), 1.32 (d, 6H, *J* = 7 Hz, CH(C*H*$_3)_2$), 1.30 (d, 12H, *J* = 7 Hz, CH(C*H*$_3)_2$), 1.14 (d, 6H, *J* = 7 Hz, CH(C*H*$_3)_2$), 1.04 (d, 12H, *J* = 7 Hz, CH(C*H*$_3)_2$), 0.94 (d, 6H, *J* = 7 Hz, CH(C*H*$_3)_2$), 0.72 (m, 1H, Cy), 0.38 (m, 2H, Cy), 0.13 (m, 1H, Cy), –0.38 (s, 1H, O*H*), –21.93 (s, 1H, $J_{Pt,H}$ = 1410 Hz, Pt-*H*) ppm. ^{13}C{^{1}H} NMR (125.7 MHz, C_6D_6, 20 ˚C): δ = 222.4 (C_{imine}), 152.1, 147.4, 147.1, 146.8, 139.3, 136.4, 136.4, 134.6, 133.5, 132.7 (*C*≡N), 131.4, 130.1, 129.9, 129.2, 127.8, 127.7, 127.5, 124.6, 123.6, 123.3, 123.1, 31.9, 31.8, 31.4, 31.2, 30.3, 29.8, 29.6, 29.1, 28.2, 26.5, 26.4, 25.5, 24.6, 24.3, 22.2 ppm. ^{11}B NMR (160.5 MHz, C_6D_6, 20 ^{o}C): δ = 5.5 (bs) ppm. FTIR (C_6D_6, KBr Windows, 20 ˚C):

ν(C≡N) = 2151 cm^{-1}, ν(OH) = 3600 cm^{-1}, also 2962, 2919, 2866, 2842, 1551, 1458, 1447, 1412, 1383, 1363, 1278, 1250, 1183, 1036, 791, 757 cm^{-1}. Anal. Calc'd for $C_{74}H_{99}N_2OBPt$: C, 71.76; H, 8.06; N, 2.26. Found: C, 71.76; H, 8.32; N, 2.13.

Synthesis of (Cy)(OH)BCH(Cy)NHAr^{Dipp2} (8). To a benzene solution of ^{Cy2}BIM (0.110 g, 0.183 mmol, 3 mL) was added deionized water (0.005 mL, 0.278 mmol, 1.5 equiv) via microsyringe. The solution rapidly changed in color from bright yellow to colorless. After stirring for 15 minutes, all volatiles were removed *in vacuo*. Dissolution of the crude material in 1 mL *n*-pentane and storage at –40 ˚C for 1 week yielded (Cy)(OH)BCH(Cy)NHAr^{Dipp2} as colorless crystals. Yield: 0.028 g, 0.045 mmol, 25%. ^{1}H NMR (300.0 MHz, C_6D_6, 20 ˚C): δ = 7.29 (t, 2H, *J* = 8 Hz, *p*-Ar), 7.29 (t, 1H, *J* = 8 Hz, *p*-Ar), 7.22 (d, 2H, *J* = 8 Hz, *m*-Ar), 7.17 (d, 2H, *J* = 8 Hz, *m*-Ar), 7.08 (d, 2H, *J* = 8 Hz, *m*-Ar), 6.81 (t, 1H, *J* = 8 Hz, *p*-Ar), 3.72 (d, 1H, *J* = 8 Hz, N-*H*), 3.14 (septet, 2H, *J* = 7 Hz, C*H*$(CH_3)_2$), 3.04 (dd, 2H, *J* = 8, 3 Hz, B-C*H*-N), 2.94 (septet, 2H, *J* = 7 Hz, C*H*$(CH_3)_2$), 1.73-1.62 (m, 3H, Cy), 1.50-1.32 (m, 4H, Cy), 1.38 (d, 6H, *J* = 7 Hz, CH(C*H*$_3)_2$), 1.36 (d, 6H, *J* = 7 Hz, CH(C*H*$_3)_2$), 1.24-1.10 (m, 4H, Cy), 1.07 (d, 6H, *J* = 7 Hz, CH(C*H*$_3)_2$), 1.05 (d, 6H, *J* = 7 Hz, CH(C*H*$_3)_2$), 1.00-0.77 (m, 7H, Cy), 0.66 (m, 2H, Cy), 0.50 (m, 2H, Cy) ppm. ^{13}C{^{1}H} NMR (125.7 MHz, C_6D_6, 20 ˚C): δ = 147.8, 147.6, 145.7, 138.0, 132.4, 128.8, 127.6, 127.1, 123.7, 123.5, 117.4, 56.6, 41.6, 31.3, 31.1, 30.9, 30.1, 29.6, 28.3, 28.1, 27.9, 27.9, 27.4, 27.0, 26.8, 26.5, 26.1, 25.9, 23.1, 22.7 ppm. ^{11}B NMR (160.5 MHz, C_6D_6, 20 ˚C): δ = 51.6 (bs) ppm. FTIR (C_6D_6, KBr Windows, 20 ˚C): ν(OH) = 3361 cm^{-1}, also 2962, 2923, 2861, 2853, 1582, 1460, 1446, 1408, 1380, 1355, 1224, 1177, 1002, 788, 761 cm^{-1}. HRMS (ESI-TOF): *m/z* calc'd for $C_{43}H_{63}NOB$ $[M+H]^+$: 620.5005. Found: 620.5004.

Synthesis of PtH(μ-OMe)(^{Cy2}BIM)(CNAr^{Dipp2}) (9). To a benzene solution of Pt(κ^2-*N,B*-^{Cy2}BIM)(CNAr^{Dipp2}) (0.070 g, 0.057 mmol, 2 mL) was added methanol via microsyringe (0.010 mL, 0.250 mmol, 4.4 equiv). The solution was stirred for 30 min, and then all volatiles were removed under reduced pressure. Analysis of the crude solid material by ^{1}H NMR indicated a 4:1 mixture of PtH(μ-OMe)(^{Cy2}BIM)(CNAr^{Dipp2}) to PtH(μ-OH)(^{Cy2}BIM)(CNAr^{Dipp2})$_2$, presumably due to the presence of water within the methanol. Dissolution of the solid mixture in 1 mL Et_2O and storage at –40 ˚C for 1 week afforded 0.011 g of colorless crystals, which ^{1}H NMR indicates consist of a 85:15 mixture of PtH(μ-OMe)(^{Cy2}BIM)(CNAr^{Dipp2}) to PtH(μ-OH)(^{Cy2}BIM)(CNAr^{Dipp2})$_2$. A single crystal of PtH(μ-OMe)(^{Cy2}BIM)(CNAr^{Dipp2}) was manually separated from the bulk quantity of crystallized material and was used to perform single-crystal X-ray diffraction analysis. ^{1}H NMR (499.8 MHz, C_6D_6, 20 ˚C): δ = 8.44 (s, 1H, C_{imine}-*H*), 7.30-7.22 (m, 6H), 7.11 (m, 2H), 7.08 (d, 4H, *J* = 8 Hz, *m*-Ar), 7.04 (d, 2H, *J* = 8 Hz, *m*-Ar), 6.87-6.80 (m, 3H), 6.78 (t, 1H, *J* = 8 Hz, *p*-Ar), 3.41 (septet, 2H, *J* = 7 Hz, C*H*$(CH_3)_2$), 2.76 (s, 3H, O-C*H*$_3$), 2.57 (septet, 4H, *J* = 7 Hz, C*H*$(CH_3)_2$), 2.34 (septet, 2H, *J* = 7 Hz, C*H*$(CH_3)_2$), 1.91-1.83 (m, 4H, Cy), 1.75-1.72 (m, 2H, Cy), 1.59 (m, 2H, Cy), 1.50-1.30 (m, 4H, Cy), 1.25-1.19 (m 3H, Cy), 1.35 (d, 6H, *J* = 7 Hz, CH(C*H*$_3)_2$), 1.33 (d, 12H, *J* = 7 Hz, CH(C*H*$_3)_2$), 1.25 (d, 12H, *J* = 7 Hz, CH(C*H*$_3)_2$), 1.00 (d, 12H, *J* = 7 Hz, CH(C*H*$_3)_2$), 0.92 (d, 6H, *J* = 7 Hz, CH(C*H*$_3)_2$), 0.81 (m, 2H, Cy), 0.70 (m, 1H, Cy), 0.49 (m, 2H, Cy), 0.25 (m, 2H, Cy), –23.07 (s, 1H, $J_{Pt,H}$ = 1380 Hz, Pt-*H*) ppm. ^{13}C{^{1}H} NMR (125.7 MHz, C_6D_6, 20 ˚C): δ = 221.0 (C_{imine}), 151.9, 147.5, 147.2, 146.6, 139.2, 136.2, 134.8, 133.2, 131.3, 131.0, 129.7, 129.2, 128.3, 124.7, 123.6, 123.4, 123.0, 57.9, 32.1, 31.3, 31.1, 30.5,

30.2, 30.2, 30.1, 28.3, 26.4, 26.3, 25.8, 24.7, 24.3, 22.6 ppm. *Note: The isocyanide (C≡N) resonance for this compound could not be conclusively assigned.* ^{11}B NMR (160.5 MHz, C_6D_6, 20 ˚C): δ = 5.7 (bs) ppm. FTIR (C_6D_6, KBr Windows, 20 ˚C): ν(C≡N) = 2146 cm^{-1}, also 2962, 2917, 2867, 2840, 1460, 1443, 1413, 1382, 1360, 1177, 1052, 791, 758, 680 cm^{-1}. Due to the presence of PtH(μ-OH)(^{Cy2}BIM)($CNAr^{Dipp2}$)$_2$ in these samples, combustion analysis was not obtained for PtH(μ-OMe)(^{Cy2}BIM)($CNAr^{Dipp2}$).

Synthesis of PtH(μ-NH(*p*-$NO_2C_6H_4$)(^{Cy2}BIM)($CNAr^{Dipp2}$) (10). Benzene (3 mL) was added to a solid mixture of Pt(κ^2-*N,B*-^{Cy2}BIM)($CNAr^{Dipp2}$) (0.057 g, 0.047 mmol) and *para*-nitroaniline (0.007 g, 0.051 mmol, 1.08 equiv). The reaction mixture was stirred for 5 h and then all volatile materials were removed under reduced pressure. The resulting solid was dissolved in Et_2O (1.5 mL) and stored at –40 ˚C for 24 h to afford pale yellow crystals, which were collected and dried *in vacuo*. Yield: 0.031 g, 0.023 mmol, 49%. ^{1}H NMR (499.8 MHz, $CDCl_3$, 20 ˚C): δ = 8.99 (s, 1H, C_{imine}-*H*), 7.70 (bs, 1H), 7.58 (t, 1H, *J* = 8 Hz, *p*-Ar), 7.46 (t, 2H, *J* = 8 Hz, *p*-Ar), 7.40 (bs, 1H), 7.37-7.27 (m, 6H), 7.17 (t, 2H, *J* = 8 Hz, *p*-Ar), 7.13-7.07 (m, 5H), 7.01-6.96 (m, 2H), 5.66 (bs, 1H), 5.41 (bs, 1H), 3.29 (d, 1H, *J* = 2 Hz, N-*H*), 2.93 (septet, 1H, *J* = 7 Hz, C*H*(CH_3)$_2$), 2.87 (septet, 1H, *J* = 7 Hz, C*H*(CH_3)$_2$), 2.48 (septet, 2H, *J* = 7 Hz, C*H*(CH_3)$_2$), 2.45 (septet, 2H, *J* = 7 Hz, C*H*(CH_3)$_2$), 2.37 (septet, 1H, *J* = 7 Hz, C*H*(CH_3)$_2$), 2.34 (septet, 1H, *J* = 7 Hz, C*H*(CH_3)$_2$), 1.60-1.43 (m, 7H, Cy), 1.28 (d, 3H, *J* = 7 Hz, CH(C*H*$_3$)$_2$), 1.23 (d, 3H, *J* = 7 Hz, CH(C*H*$_3$)$_2$), 1.15 (d, 6H, *J* = 7 Hz, CH(C*H*$_3$)$_2$), 1.09 (d, 3H, *J* = 7 Hz, CH(C*H*$_3$)$_2$), 1.08 (d, 6H, *J* = 7 Hz, CH(C*H*$_3$)$_2$), 1.06 (d, 6H, *J* = 7 Hz, CH(C*H*$_3$)$_2$), 1.06 (d, 3H, *J* = 7 Hz, CH(C*H*$_3$)$_2$), 1.04 (d, 3H, *J* = 7 Hz, CH(C*H*$_3$)$_2$), 1.00 (d, 6H, *J* = 7 Hz,

CH(CH_3)$_2$), 0.97 (d, 3H, J = 7 Hz, CH(CH_3)$_2$), 0.94-0.82 (m, 5H, Cy), 0.80-0.68 (m, 4H, Cy), 0.80 (d, 3H, J = 7 Hz, CH(CH_3)$_2$), 0.64 (m, 1H, Cy), 0.55 (m, 1H, Cy), 0.50 (d, 3H, J = 7 Hz, CH(CH_3)$_2$), 0.44 (d, 1H, J = 13 Hz, Cy), 0.28 (m, 1H, Cy), 0.12 (m, 1H, Cy), 0.04 (m, 1H, Cy), –18.92 (d, 1H, $J_{H,H}$ = 2 Hz, $J_{Pt,H}$ = 1300 Hz, Pt-*H*) ppm. $^{13}C\{^1H\}$ NMR (125.7 MHz, $CDCl_3$, 20 ˚C): δ = 224.4 (C_{imine}), 157.2, 151.3, 147.7, 147.6, 147.0, 146.9, 146.7, 146.6, 140.6, 138.9, 137.1, 135.7, 134.7, 133.4, 132.1, 131.9, 131.8, 131.2, 129.5, 129.3, 129.2, 128.5, 127.4, 124.8, 124.6, 124.2, 123.8, 123.4, 123.4, 122.6, 120.6, 35.9, 32.9, 31.6, 31.4, 31.2, 31.2, 31.1, 31.1, 31.0, 30.8, 29.9, 29.8, 29.4, 29.0, 27.6, 27.4, 26.1, 25.5, 25.3, 25.1, 25.0, 24.8, 24.6, 24.3, 24.2, 24.2, 22.6, 22.4 ppm. *Note: The isocyanide (C≡N) resonance for this compound could not be conclusively assigned.* ^{11}B NMR (160.5 MHz, $CDCl_3$, 20 ˚C): δ = –0.8 (bs) ppm. FTIR (C_6D_6, KBr Windows, 20 ˚C): ν(C≡N) = 2144 cm^{-1}, ν(NH) 3398 cm^{-1}, also 2962, 2923, 2864, 2845, 1591, 1513, 1462, 1444, 1415, 1377, 1360, 1335, 1316, 1252, 1227, 1177, 1133, 1058, 758 cm^{-1}. Anal. Calc'd for $C_{80}H_{103}N_4BO_2Pt$: C, 70.72; H, 7.64; N, 4.12. Found: C, 70.08; H, 7.60; N, 4.05.

Synthesis of PtH(η^2-*C,C*-κ^1-*N*-PhCC-^{Cy2}BIM)(CNAr^{Dipp2}) (11). To a benzene solution of Pt(κ^2-*N,B*-^{Cy2}BIM)(CNAr^{Dipp2}) (0.075 g, 0.061 mmol, 2 mL) was added phenylacetylene (0.027 mL, 0.246 mmol, 4.0 equiv). The reaction mixture was stirred for 4 h, during which time it became dark red in color, and then all volatiles were removed *in vacuo*. Dissolution of the resulting residue in 1 mL Et_2O and storage at –40 ˚C for 1 week provided pink crystals, which were washed with three 1 mL portions of *n*-pentane and dried *in vacuo*. Yield: 0.013 g, 0.010 mmol, 16%. ^1H NMR (499.8 MHz, C_6D_6, 20 ˚C): δ = 9.66 (s, 1H, $J_{Pt,H}$ = 100 Hz, C_{imine}-*H*), 7.29 (t, 2H, J = 8 Hz, *p*-Ar), 7.28

(t, 2H, J = 8 Hz, *p*-Ar), 7.20 (d, 2H, J = 8 Hz, *m*-Ar), 7.12 (d, 4H, J = 8 Hz, *m*-Ar), 7.02-6.94 (m, 9H), 6.82 (t, 1H, J = 8 Hz, *p*-Ar), 6.78 (m, 3H), 2.95 (septet, 2H, J = 7 Hz, C*H*$(CH_3)_2$), 2.60 (septet, 2H, J = 7 Hz, C*H*$(CH_3)_2$), 2.52 (septet, 4H, J = 7 Hz, C*H*$(CH_3)_2$), 1.96 (m, 7H, Cy), 1.87 (m, 2H, Cy), 1.67 (m, 2H, Cy), 1.56-1.45 (m, 7H, Cy), 1.20 (d, 6H, J = 7 Hz, CH(C*H*$_3)_2$), 1.17 (d, 12H, J = 7 Hz, CH(C*H*$_3)_2$), 1.17 (d, 6H, J = 7 Hz, CH(C*H*$_3)_2$), 1.17-1.14 (m, 4H, Cy), 1.11 (d, 6H, J = 7 Hz, CH(C*H*$_3)_2$), 0.97 (d, 12H, J = 7 Hz, CH(C*H*$_3)_2$), 0.93 (d, 6H, J = 7 Hz, CH(C*H*$_3)_2$), –12.33 (s, 1H, $J_{Pt,H}$ = 1355 Hz, Pt-*H*) ppm. $^{13}C\{^1H\}$ NMR (125.7 MHz, C_6D_6, 20 ˚C): δ = 235.6 (C_{imine}), 152.6, 147.2, 147.1, 146.0, 139.4, 137.9, 134.5, 133.7, 133.0, 132.8, 131.2, 130.0, 129.0, 128.6, 128.2, 128.0, 127.5, 126.9, 125.1, 124.1, 123.9, 123.6, 123.3, 95.4, 32.8, 32.6, 31.5, 31.4, 31.4, 30.2, 30.2, 28.3, 26.1, 26.0, 24.5, 24.2, 22.6 ppm. *Note: The isocyanide (C≡N) resonance for this compound could not be conclusively assigned.* ^{11}B NMR (160.5 MHz, C_6D_6, 20 ˚C): δ = –10.6 (bs) ppm. FTIR (KBr pellet, 20 ˚C): ν(*C*≡N) = 2143 cm^{-1}, ν(*C*≡*C*) = 2206 cm^{-1}, also 2962, 2918, 2865, 2840, 2143, 1486, 1459, 1444, 1411, 1384, 1362, 1259, 1178, 1054, 819, 804, 793, 752, 689 cm^{-1}. Anal. Calc'd for $PtC_{82}H_{103}N_2B$: C, 74.46; H, 7.85; N, 2.12. Found: C, 74.21; H, 7.67, N, 1.91.

Synthesis of PtBr(μ-PBr_2)(^{Cy2}BIM)(CNAr^{Dipp2}) (12). To a *n*-pentane solution of Pt(κ^2-*N,B*-^{Cy2}BIM)(CNAr^{Dipp2}) (0.100 g, 0.082 mmol, 5 mL) was added PBr_3 (0.010 mL, 0.106 mmol, 1.3 equiv) via microsyringe. After stirring for 30 min, all volatiles were removed *in vacuo*. The resulting residue was extracted with 2 x 3 mL *n*-pentane to afford a pale yellow powder, which was collected and dried. Yield: 0.018 g, 0.012 mmol, 15%. Crystals of PtBr(μ-PBr_2)(^{Cy2}BIM)(CNAr^{Dipp2}) • 1.5 C_5H_{12} suitable for X-ray diffraction were grown from a *n*-pentane solution spiked with *ca.* 1 % benzene and stored at –35 ˚C.

^{1}H NMR (499.8 MHz, C_6D_6, 20 ˚C): δ = 8.46 (d, 1H, $J_{P,H}$ = 70 Hz, C_{imine}-*H*), 7.40 (d, 2H, *J* = 7 Hz, *m*-Ar), 7.31–7.23 (m, 4H, *m*- and *p*-Ar), 7.19–7.13 (m, 4H, *m*-Ar), 7.09 (d, 2H, *J* = 8 Hz, *m*-Ar), 6.91 (d, 2H, *J* = 8 Hz, *m*-Ar), 6.84 (t, 2H, *J* = 8 Hz, *p*-Ar), 4.22 (septet, 2H, *J* = 7 Hz, C*H*(CH_3)$_2$), 2.64 (septet, 4H, *J* = 7 Hz, C*H*(CH_3)$_2$), 2.43 (septet, 2H, *J* = 7 Hz, C*H*(CH_3)$_2$), 2.01 (br d, 2H, *J* = 8 Hz, -Cy), 1.82–1.79 (m, 6H, -Cy), 1.72 (d, 2H, *J* = 12 Hz, -Cy), 1.46 (d, 6H, *J* = 7 Hz, CH(C*H*$_3$)$_2$), 1.41 (d, 12H, *J* = 7 Hz, CH(C*H*$_3$)$_2$), 1.37 (d, 6H, *J* = 7 Hz, CH(C*H*$_3$)$_2$), 1.36 (d, 6H, *J* = 7 Hz, CH(C*H*$_3$)$_2$), 1.35–1.30 (m, 6H, -Cy), 1.09–1.05 (m, 6H, Cy), 1.01 (d, 12H, *J* = 7 Hz, CH(C*H*$_3$)$_2$), 0.78 (d, 6H, *J* = 7 Hz, CH(C*H*$_3$)$_2$) ppm. ^{13}C{^{1}H} NMR (125.7 MHz, C_6D_6, 20 ˚C): δ = 214.1 (*C*$_{imine}$), 149.5, 148.7, 147.6, 146.6, 140.1, 136.6, 134.8, 134.3, 132.5, 131.8, 130.2, 129.2, 129.0, 127.5, 126.6, 125.4, 125.3, 124.1, 122.7, 33.1, 32.9, 31.8, 31.5, 31.4, 31.2, 31.0, 31.0, 30.8, 30.2, 29.3, 27.3, 26.8, 25.8, 25.8, 25.3, 24.3, 22.6 ppm. *Note: The isocyanide C≡N resonance could not be conclusively identified.* ^{11}B NMR (160.5 MHz, C_6D_6, 20 ˚C): δ = 4.5 (br s) ppm. ^{31}P{^{1}H} NMR (202.5 MHz, C_6D_6, 20 ˚C): δ = 168.6 (s, $J_{Pt,P}$ = 2956 Hz) ppm. FTIR (C_6D_6, KBr windows, 20 ˚C): ν(C≡N) = 2187 (s) cm^{-1}; also 3062, 2962, 2925, 2867, 2844, 1594, 1577, 1463, 1446, 1410, 1384, 1361, 1252, 1180, 1055, 971, 934, 793, 757 cm^{-1}. Suitable combustion analysis has not been obtained.

Synthesis of Pt(SbF_2)(μ-F)(^{Cy2}BIM)(CNAr^{Dipp2}) (13). To solid SbF_3 (0.009 g, 0.051 mmol, 1.00 equiv) was added a DME solution of Pt(κ^2-*N,B*-^{Cy2}BIM)(CNAr^{Dipp2}) (0.062 g, 0.051 mmol, 3 mL). The solution was stirred vigorously for 7 min, at which time all volatiles were removed *in vacuo*. The resulting residue was washed 3 x 3 mL acetonitrile to afford Pt(SbF_2)(μ-F)(^{Cy2}BIM)(CNAr^{Dipp2}) as a pale pink solid which is

pure by ^{1}H, ^{13}C{^{1}H}, ^{11}B and ^{19}F NMR. Yield: 0.039 g, 0.028 mmol, 55%. Crystals of Pt(SbF_2)(μ-F)(^{Cy2}BIM)(CNAr^{Dipp2}) • MeCN suitable for X-ray diffraction were grown from a diethyl ether/acetonitrile solution stored at –35 ˚C. Analytically pure off-white crystals can be obtained via fractional crystallization from DME/acetonitrile. ^{1}H NMR (499.8 MHz, C_6D_6, 20 ˚C): δ = 8.56 (d, 1H, *J* = 20 Hz, C_{imine}-*H*), 7.48 (t, 2H, *J* = 8 Hz, *p*-Ar), 7.33–7.30 (m, 8H, *m*-Ar), 7.11–7.09 (m, 2H, *p*-Ar), 6.97 (d, 2H, *J* = 8 Hz, *m*-Ar), 6.90 (m, 3H, *m*- and *p*-Ar), 6.48 (t, 1H, *J* = 8 Hz, *p*-Ar), 2.86 (septet, 2H, *J* = 7 Hz, C*H*(CH_3)$_2$), 2.66 (septet, 4H, *J* = 7 Hz, C*H*(CH_3)$_2$), 2.15 (septet, 2H, *J* = 7 Hz, C*H*(CH_3)$_2$), 1.90 (br d, 2H, *J* = 11 Hz, –Cy), 1.84 (br d, 2H, *J* = 10 Hz, –Cy), 1.69 (br d, 2H, *J* = 11 Hz, –Cy), 1.59 (br d, 2H, *J* = 13 Hz, –Cy), 1.49 (d, 12H, *J* = 7 Hz, CH(C*H*$_3$)$_2$), 1.41–1.38 (m, 8H, –Cy and CH(C*H*$_3$)$_2$), 1.30 (d, 6H, *J* = 7 Hz, CH(C*H*$_3$)$_2$), 1.25–1.22 (m, 10H, –Cy and CH(C*H*$_3$)$_2$), 1.09 (d, 12H, *J* = 7 Hz, CH(C*H*$_3$)$_2$), 0.79 (m, 8H, –Cy and CH(C*H*$_3$)$_2$), 0.68–0.62 (m, 2H, –Cy), 0.56–0.48 (m, 2H, –Cy), 0.20–0.14 (m, 2H, –Cy) ppm. ^{13}C{^{1}H} NMR (125.7 MHz, C_6D_6, 20 ˚C): δ = 222.4 (*C*$_{imine}$), 152.2 (*C*$_{iso}$), 148.2, 146.5, 146.4, 140.4, 135.2, 134.0, 133.5, 133.1, 130.5, 129.8, 129.7, 129.1, 127.8, 127.6, 125.2, 123.8, 123.7, 123.7, 36.7, 31.7, 31.2, 30.9, 30.5, 30.3, 30.1, 29.7, 29.6, 29.5, 29.2, 28.1, 25.9, 25.8, 25.3, 24.8, 23.9, 23.2 ppm. ^{11}B NMR (160.5 MHz, C_6D_6, 20 ˚C): δ = 10.4 ppm. ^{19}F NMR (470.6 MHz, C_6D_6, 20 ˚C): δ = –133.8 (s, 2F, $J_{Pt,F}$ = 85 Hz, –SbF_2), –221.2 (s, 1F, $J_{Pt,F}$ = 1565 Hz, Pt-*F*-B) ppm. Anal. calcd. for $C_{74}H_{97}N_2BF_3PtSb$: C, 63.52; H, 6.99; N, 2.00. Found: C, 63.35; H, 6.99; N, 2.23.

Synthesis of Pt(μ-Me_2CO)(^{Cy2}BIM)(CNAr^{DIpp2}) (14). To a benzene solution of Pt(κ^2-*N,B*-^{Cy2}BIM)(CNAr^{Dipp2}) (0.050 g, 0.041 mmol, 2 mL) was added dry acetone

(0.015 mL, 0.204 mmol, 5.0 equiv). The reaction mixture was stirred for 12 h, during which time it became deep red in color. All volatiles were then removed under reduced pressure. The resulting red powder was dissolved in 1 mL of a 1:1 *n*-pentane/hexamethyldisiloxane mixture and stored at –40 ˚C for 6 h. The solution was then allowed to warm to room temperature and stand. After 24 h, bright-red crystals were produced and were collected and dried *in vacuo*. Yield: 0.036 g, 0.028 mmol, 68%. ^{1}H NMR (499.8 MHz, C_6D_6, 20 ˚C): δ = 7.35-7.28 (m, 5H), 7.20-7.16 (m, 6H), 6.98 (d, 2H, *J* = 8 Hz, *p*-Ar), 6.88-6.83 (m, 2H), 6.53 (t, 1H, *J* = 8 Hz, *p*-Ar), 6.40 (dd, 1H, *J* = 7, 2 Hz, *m*-Ar), 3.70 (septet, 1H, *J* = 7 Hz, C*H*$(CH_3)_2$), 3.54 (d, 1H, *J* = 9 Hz, B-C*H*-Cy), 3.14 (septet, 1H, *J* = 7 Hz, C*H*$(CH_3)_2$), 3.10 (septet, 1H, *J* = 7 Hz, C*H*$(CH_3)_2$), 2.90 (septet, 1H, *J* = 7 Hz, C*H*$(CH_3)_2$), 2.84 (septet, 2H, *J* = 7 Hz, C*H*$(CH_3)_2$), 2.61 (septet, 2H, *J* = 7 Hz, C*H*$(CH_3)_2$), 2.38 (m, 1H, Cy), 2.15 (m, 1H, Cy), 1.94 (m, 2H, Cy), 1.83-1.70 (m, 5H, Cy), 1.60 (d, 3H, *J* = 7 Hz, CH(C*H*$_3)_2$), 1.54 (d, 6H, *J* = 7 Hz, CH(C*H*$_3)_2$), 1.44 (s, 3H, C(O)-C*H*$_3$), 1.38 (d, 3H, *J* = 7 Hz, CH(C*H*$_3)_2$), 1.37 (d, 6H, *J* = 7 Hz, CH(C*H*$_3)_2$), 1.34 (d, 3H, *J* = 7 Hz, CH(C*H*$_3)_2$), 1.31-1.21 (m, 9H, Cy), 1.17 (d, 3H, *J* = 7 Hz, CH(C*H*$_3)_2$), 1.15 (d, 3H, *J* = 7 Hz, CH(C*H*$_3)_2$), 1.14 (s, 3H, C(O)-C*H*$_3$), 1.09-1.04 (m, 3H, Cy), 1.00 (d, 6H, *J* = 7 Hz, CH(C*H*$_3)_2$), 0.95 (d, 3H, *J* = 7 Hz, CH(C*H*$_3)_2$), 0.93 (d, 6H, *J* = 7 Hz, CH(C*H*$_3)_2$), 0.91 (d, 3H, *J* = 7 Hz, CH(C*H*$_3)_2$), 0.00 (m, 1H, Cy) ppm. ^{13}C{^{1}H} NMR (125.7 MHz, C_6D_6, 20 ˚C): δ = 166.1, 157.1, 147.8, 147.7, 147.6, 147.0, 146.7, 146.5, 146.3, 145.4, 144.5, 138.2, 136.2, 135.6, 133.5, 132.4, 130.1, 129.8, 129.3, 129.1, 126.5, 126.3, 125.8, 124.8, 124.7, 124.0, 123.9, 123.8, 123.1, 112.4, 69.4, 55.6, 53.6, 39.7, 39.4, 32.6, 32.6, 31.9, 31.7, 31.4, 31.3, 31.3, 31.2, 31.1, 31.1, 30.1, 29.7, 29.0, 28.5, 28.5, 28.2, 28.0, 28.0, 27.7, 26.9, 26.4, 26.2, 25.9, 25.7, 25.5, 25.4, 25.3, 25.3, 24.2, 23.1, 22.7 ppm.

Note: The isocyanide (C≡N) resonance for this compound could not be conclusively assigned. ^{11}B NMR (160.5 MHz, C_6D_6, 20 ˚C): δ = 49.4 (bs) ppm. FTIR (C_6D_6, KBr Windows, 20 ˚C): ν(C≡N) = 2096 cm^{-1}, also 2962, 2952, 2866, 2848, 1462, 1488, 1405, 1384, 1359, 1251, 1109, 761, 678 cm^{-1}. Anal. Calc'd for $C_{77}H_{103}N_2BOPt$: C, 72.33; H, 8.12; N, 2.19. Found: C, 71.87; H, 7.99; N, 2.12.

Synthesis of Pt(μ-PhCHO)(^{Cy2}BIM)(CNAr^{Dipp2}) (15). To a benzene solution of Pt(κ^2-*N,B*-^{Cy2}BIM)(CNAr^{Dipp2}) (0.085 g, 0.070 mmol, 2 mL) was added benzaldehyde (0.008 mL, 0.078 mmol, 1.1 equiv). The solution was stirred for 1 h, and then all volatiles were removed *in vacuo*. The resulting purple solid was twice slurried in 3 mL *n*-pentane and stirred for 5 min, whereupon the solution was decanted off from the remaining solid. Evaporation of all volatiles under reduced pressure yielded Pt(μ-PhCHO)(^{Cy2}BIM)(CNAr^{Dipp2}) as a purple powder. Yield: 0.060 g, 0.045 mmol, 65%. Allowing a saturated cyclohexane solution to stand at room temperature for several hours provided crystals of **15** • 4.5 *cyclo*-C_6H_{12} that were suitable for X-ray diffraction. ^{1}H NMR (499.8 MHz, C_6D_6, 20 ˚C): δ = 7.39-7.35 (m, 4H), 7.33 (d, 2H, *J* = 7 Hz, *m*-Ar), 7.31-7.28 (m, 1H), 7.22 (d, 2H, *J* = 8 Hz, *m*-Ar), 7.16 (d, 1H, *J* = 7 Hz, *m*-Ar), 7.12 (t, 2H, *J* = 8 Hz, *p*-Ar), 7.04 (d, 2H, *J* = 8 Hz, *m*-Ar), 7.00 (d, 2H, *J* = 8 Hz, *m*-Ar), 6.93-6.85 (m, 4H), 6.50 (t, 1H, *J* = 7 Hz, *p*-Ar), 6.34 (dd, 1H, *J* = 7, 2 Hz, *m*-Ar), 5.47 (t, 1H, *J* = 8 Hz, *p*-*Ph*C(H)-Pt), 5.29 (s, 1H, Pt-C(*H*)), 3.70 (septet, 1H, *J* = 7 Hz, C*H*$(CH_3)_2$), 3.66 (d, 1H, *J* = 8 Hz, BC*H*(Cy)), 3.20 (septet, 1H, *J* = 7 Hz, C*H*$(CH_3)_2$), 3.06 (septet, 1H, *J* = 7 Hz, C*H*$(CH_3)_2$), 2.83 (septet, 2H, *J* = 7 Hz, C*H*$(CH_3)_2$), 2.63 (septet, 1H, *J* = 7 Hz, C*H*$(CH_3)_2$), 2.60 (septet, 2H, *J* = 7 Hz, C*H*$(CH_3)_2$), 2.09 (m, 1H, Cy), 1.97-1.82 (m, 7H,

Cy), 1.72-1.58 (m, 2H, Cy), 1.69 (d, 3H, J = 7 Hz, CH(CH_3)$_2$), 1.58 (d, 3H, J = 7 Hz, CH(CH_3)$_2$), 1.52 (d, 3H, J = 7 Hz, CH(CH_3)$_2$), 1.52-1.48 (m, 3H, Cy), 1.48 (d, 6H, J = 7 Hz, CH(CH_3)$_2$), 1.37-1.22 (m, 8H, Cy), 1.35 (d, 3H, J = 7 Hz, CH(CH_3)$_2$), 1.13 (d, 6H, J = 7 Hz, CH(CH_3)$_2$), 1.04 (d, 3H, J = 7 Hz, CH(CH_3)$_2$), 1.03 (d, 6H, J = 7 Hz, CH(CH_3)$_2$), 0.98 (d, 6H, J = 7 Hz, CH(CH_3)$_2$), 0.92 (d, 3H, J = 7 Hz, CH(CH_3)$_2$), 0.80 (d, 3H, J = 7 Hz, CH(CH_3)$_2$), 0.64 (d, 3H, J = 7 Hz, CH(CH_3)$_2$), 0.57 (m, 1H, Cy) ppm. ^{13}C{1H} NMR (125.7 MHz, C_6D_6, 20 ˚C): δ = 166.2, 158.4, 153.8, 150.3, 148.7, 148.4, 147.4, 147.0, 146.4, 146.3, 144.5, 138.2, 136.4, 135.7, 132.5, 130.9, 130.2, 129.1, 128.9, 128.8, 128.5, 128.4, 127.9, 127.7, 127.5, 126.7, 126.7, 126.1, 125.6, 125.4, 125.3, 125.0, 124.5, 124.4, 124.1, 123.4, 122.8, 112.9, 61.5, 55.1, 51.4, 34.4, 32.2, 31.8, 31.6, 31.5, 31.3, 31.2, 31.0, 30.1, 29.0, 28.9, 28.4, 28.0, 28.0, 27.9, 27.8, 27.3, 27.0, 26.6, 26.2, 25.9, 25.8, 25.4, 25.0, 24.6, 24.1, 24.0, 23.8 ppm. *Note: The isocyanide (C≡N) resonance for this compound could not be conclusively assigned.* ^{11}B NMR (160.5 MHz, C_6D_6, 20 ˚C): δ = 51.7 ppm. FTIR (C_6D_6, KBr Windows, 25 ˚C): ν(C≡N) = 2091 cm^{-1}, also 2962, 2926, 2866, 2850, 1461, 1450, 1399, 1385, 1361, 1332, 1327, 1297, 1290, 1262, 1161, 1058, 870, 794, 758 cm^{-1}. Anal. Calc'd for $PtC_{81}H_{103}N_2BO$: C, 73.33; H, 7.82; N, 2.11. Found: C, 72.33; H, 7.83; N, 2.01.

Synthesis of boralactone 16 from Pt(κ^2-*N,B*-^{Cy2}BIM)(CNAr^{Dipp2}) (1). To a J-Young NMR tube was added a C_6D_6 solution of of Pt(κ^2-*N,B*-^{Cy2}BIM)(CNAr^{Dipp2}) (0.030 g, 0.025 mmol, 0.8 mL). After connecting the tube to a Schlenk line, the headspace was evacuated and subsequently backfilled with *ca.* 1 atm dry CO_2. The solution was warmed to room temperature, and shaken intermittently over the course of 24 h. At this time, ^{1}H

NMR analysis indicates an approximately 2:1 mixture of **16**/Pt(CNAr^{Dipp2}), the latter being formed due to ligand redistribution. Boralactone **16** was not isolated in bulk from these mixtures; however, drying the above mixture *in vacuo* and dissolving the resulting residue at –35 ˚C provides single crystals of **16** suitable for X-ray diffraction. For independent synthesis, characterization data, and discussion of boralactone **16** and the FLP behavior of free ^{Cy2}BIM in general, see ref. 55 and Chapter 3 of this dissertation.

Synthesis of imine isocyanide complex 17. To a benzene solution of Pt(κ^2-*N,B*-^{Cy2}BIM)(CNAr^{Dipp2}) (0.120 g, 0.098 mmol, 3 mL) was added dry acetonitrile (0.030 mL, 1.03 mmol, 10.5 equiv). After 2 h, all volatiles were removed from the reddish orange solution *in vacuo*. Dissolution of the resulting residue in 1 mL *n*-pentane and storage at –40 ˚C for 24 h provided yellow crystals which were washed with 2 mL *n*-pentane and dried *in vacuo*. Yield: 0.075 g, 0.059 mmol, 61%. ^{1}H NMR (499.8 MHz, C_6D_6, 20 ˚C): δ = 7.36 (t, 2H, *J* = 8 Hz, *p*-Ar), 7.30 (m, 4H), 7.21-7.16 (m, 3H), 7.09 (t, 1H, *J* = 8 Hz, *p*-Ar), 7.06 (d, 1H, *J* = 7 Hz, *m*-Ar), 7.03-7.00 (m, 3H), 6.99-6.96 (m, 2H), 6.93 (m, 1H), 6.84 (t, 1H, *J* = 8 Hz, *p*-Ar), 2.98 (septet, 1H, *J* = 7 Hz, C*H*$(CH_3)_2$), 2.97 (septet, 4H, *J* = 7 Hz, C*H*$(CH_3)_2$), 2.80 (qd, 1H, *J* = 12, 3 Hz, Cy), 2.56 (septet, 1H, *J* = 7 Hz, C*H*$(CH_3)_2$), 2.45 (s, 3H, C_{imine}-CH_3), 2.43 (septet, 1H, *J* = 7 Hz, C*H*$(CH_3)_2$), 2.06 (septet, 1H, *J* = 7 Hz, C*H*$(CH_3)_2$), 1.96 (m, 1H, Cy), 1.85-1.78 (m, 4H, Cy), 1.61 (d, 3H, *J* = 7 Hz, CH(C*H*$_3)_2$), 1.55 (m, 2H, Cy), 1.52 (dd, 12H, *J* = 7, 2 Hz, CH(C*H*$_3)_2$), 1.44-1.30 (m, 5H, Cy), 1.26-1.20 (m, 2H, Cy), 1.25 (d, 3H, *J* = 7 Hz, CH(C*H*$_3)_2$), 1.23 (d, 3H, *J* = 7 Hz, CH(C*H*$_3)_2$), 1.21 (d, 12H, *J* = 7 Hz, CH(C*H*$_3)_2$), 1.17 (d, 3H, *J* = 7 Hz, CH(C*H*$_3)_2$), 1.09 (3, 6H, *J* = 7 Hz, CH(C*H*$_3)_2$), 1.01-0.95 (m, 3H, Cy), 0.89 (d, 3H, *J* = 7 Hz, CH(C*H*$_3)_2$), 0.82 (m, 1H, Cy), 0.73 (d, 3H, *J* = 7 Hz, CH(C*H*$_3)_2$), 0.68 (m, 1H, Cy), 0.20 (m, 1H, Cy),

0.06 (m, 1H, Cy) ppm. $^{13}C\{^{1}H\}$ NMR (125.7 MHz, C_6D_6, 20 ˚C): δ = 189.5 (C_{imine}), 162.3 (C≡N), 149.0, 147.6, 147.0, 146.9, 146.6, 146.3, 141.6, 140.8, 138.8, 137.3, 137.2, 137.0, 134.4, 132.7, 132.4, 129.8 129.7, 129.5, 126.9, 124.4, 124.1, 123.4, 123.3, 123.0, 122.4, 69.7, 38.3, 31.5, 31.5, 31.3, 31.2, 31.1, 30.2, 29.6, 28.7, 28.4, 28.3, 27.7, 27.0, 26.5, 26.3, 26.0, 25.7, 24.8, 24.8, 24.5, 23.3, 23.1, 22.3, 22.2 ppm. ^{11}B NMR (160.5 MHz, C_6D_6, 20 ˚C): δ = 63.6 (bs) ppm. FTIR (C_6D_6, KBr Windows, 20 ˚C): ν(C≡N) = 2029 cm^{-1}, also 2961, 2924, 2863, 2140, 2074, 1987, 1578, 1479, 1460, 1409, 1401, 1385, 1362, 1242, 1188, 1054, 1045, 1028, 791, 785 cm^{-1}. HRMS (ESI-TOF): *m/z* calc'd for $C_{76}H_{101}N_3BPt$ $[M+H]^+$: 1261.7748. Found: 1261.7737. Complex **17** decomposes at room temperature in the solid state, thereby precluding a satisfactory combustion analysis.

Synthesis of Pt(μ-N_3Ad)(^{Cy2}BIM)(CNAr^{Dipp2}) (18). To solid Pt(κ^2-*N,B*-^{Cy2}BIM)(CNAr^{Dipp2}) (0.104 g, 0.085 mmol) was added an *n*-pentane solution of 1-azidoadamantane (0.017 g, 0.096 mmol, 1.13 equiv, 5 mL). The solution was stirred vigorously for 6 h, during which time the desired product precipitated from solution as a dark brown solid. This powder was isolated on a medium porosity fritted funnel topped with Celite and washed with an additional 5 mL *n*-pentane. The product was then carried through the fritted funnel using 10 mL benzene, which was subsequently lyophilized to afford an analytically pure mocha brown powder. The combined *n*-pentane filtrates above were stored at –35 ˚C for *ca*. 1 week to yield a crop of crystals, which were collected and dried. Yield: 0.098 g, 0.070 mmol, 82%. Crystals of Pt(μ-N_3Ad)(^{Cy2}BIM)(CNAr^{Dipp2}) • 1 C_6H_6 suitable for X-ray diffraction were grown from a diethyl ether/benzene solution stored at –35 ˚C. ^{1}H NMR (499.8 MHz, C_6D_6, 20 ˚C): δ = 7.36–7.30 (m, 4H, *m*- and *p*-

Ar), 7.27–7.22 (m, 5H, *m*- and *p*-Ar), 6.99 (br d, 1H, *J* = 6 Hz, *m*-Ar), 6.96 (dd, 1H, *J* = 8, 2 Hz, *m*-Ar), 6.92 (br d, 1H, *J* = 8 Hz, *m*-Ar), 6.86 (t, 1H, *J* = 8 Hz, *p*-Ar), 6.76 (t, 1H, *J* = 8 Hz, *p*-Ar), 6.47 (t, 1H, *J* = 8 Hz, *p*-Ar), 6.34 (d, 1H, *J* = 8 Hz, *m*-Ar), 6.31 (d, 1H, *J* = 8 Hz, *m*-Ar), 6.04 (dd, 1H, *J* = 8 Hz, *m*-Ar), 3.56 (d, 1H, *J* = 4 Hz, B-C*H*(Cy)-N), 3.50 (septet, 1H, *J* = 7 Hz, C*H*(CH_3)$_2$), 3.30 (septet, 1H, *J* = 7 Hz, C*H*(CH_3)$_2$), 3.29 (septet, 1H, *J* = 7 Hz, C*H*(CH_3)$_2$), 3.18 (br septet, 2H, *J* = 7 Hz, C*H*(CH_3)$_2$), 2.71 (septet, 1H, *J* = 7 Hz, C*H*(CH_3)$_2$), 2.66 (br d, 1H, -*J* = 13 Hz, -Cy), 2.25 (br septet, 1H, *J* = 7 Hz, C*H*(CH_3)$_2$), 2.19 (br septet, 1H, *J* = 7 Hz, C*H*(CH_3)$_2$), 2.10 (br d, 1H, *J* = 10 Hz, -Cy), 2.00–1.62 (m, 18H, –Cy), 1.50 (d, 6H, *J* = 7 Hz, CH(C*H*$_3$)$_2$), 1.45 (d, 6H, *J* = 7 Hz, CH(C*H*$_3$)$_2$), 1.42–1.34 (m, 21H, CH(C*H*$_3$)$_2$ and –Ad), 1.27–1.24 (m, 9H, CH(C*H*$_3$)$_2$), 1.20 (br d, 3H, *J* = 5 Hz, CH(C*H*$_3$)$_2$), 1.07 (d, 3H, *J* = 7 Hz, CH(C*H*$_3$)$_2$), 1.05 (d, 3H, *J* = 7 Hz, CH(C*H*$_3$)$_2$), 0.96 (d, 6H, *J* = 7 Hz, CH(C*H*$_3$)$_2$), 0.94 (d, 6H, *J* = 7 Hz, CH(C*H*$_3$)$_2$), 0.93–0.90 (m, 2H, –Cy) ppm. *Note: Peak assignments are tentative*. $^{13}C\{^1H\}$ NMR (125.7 MHz, C_6D_6, 20 ˚C): δ = 162.5, 157.8, 149.4, 148.2, 147.8, 147.7, 146.4, 142.4, 137.7, 136.6, 135.7, 134.9, 133.0, 132.0, 131.6, 131.5, 129.7, 129.7, 129.5, 128.5, 127.7, 127.5, 127.5, 125.6, 125.0, 124.8, 124.5, 124.4, 124.1, 124.0, 123.4, 123.1, 122.9, 122.6, 111.9, 110.6, 66.5, 61.8, 45.6, 41.6, 37.1, 33.1, 33.0, 32.4, 32.1, 31.7, 31.3, 31.2, 30.9, 30.8, 30.6, 30.5, 30.4, 29.6, 29.3, 29.0, 28.8, 28.1, 28.0, 27.9, 27.7, 27.7, 27.0, 26.9, 26.7, 26.2, 25.7, 25.6, 24.1, 23.8, 23.8, 23.7, 23.6, 22.4 ppm. *Note: The isocyanide C≡N resonance could not be conclusively identified.* ^{11}B NMR (160.5 MHz, C_6D_6, 20 ˚C): δ = 63.2 ppm. FTIR (C_6D_6, KBr windows, 20 ˚C): ν(C≡N)/ν(N_3) = 2109 (s), 2126 (m sh) cm^{-1}; also 3057, 2961, 2923, 2865, 2850, 1579, 1478, 1463, 1447, 1409, 1383, 1361, 1295, 1275,

1250, 1239, 1179, 1065, 1056, 1037, 995, 932, 901, 881, 787, 761, 749 cm^{-1}. Anal. calcd. for $C_{84}H_{112}N_5BPt$: C, 72.18; H, 8.08; N, 5.01. Found: C, 71.98; H, 8.09; N, 4.95.

Synthesis of Pt(μ-N_3Tol)(^{Cy2}BIM)(CNAr^{Dipp2}) (19). To a *n*-pentane solution of Pt(κ^2-*N,B*-^{Cy2}BIM)(CNAr^{Dipp2}) (0.095 g, 0.078 mmol, 5 mL) was added a 0.5 M solution of *para*-azidotoluene in *tert*-butyl methyl ether (0.175 mL, 0.088 mmol, 1.1 equiv). The solution was allowed to stir for 6 h, during which time it became dark brown in color. All volatiles were then removed *in vacuo*. The resulting dark greasy residue was subjected to two cycles of stirring in *n*-pentane (5 mL) for 5 min and drying *in vacuo*, affording a reddish brown powder. This powder was then dissolved in a minimal amount of *n*-pentane (*ca.* 3 mL), filtered through Celite, and slowly concentrated at room temperature over the course of 12 h. This provided large dark red crystals, which were collected and dried. Yield: 0.060 g, 0.044 mmol, 57%. ^{1}H NMR (499.8 MHz, C_6D_6, 20 ˚C): δ = 7.37–7.30 (m, 4H, *m*- and *p*-Ar), 7.25 (d, 2H, *J* = 8 Hz, *m*-Ar), 7.23–7.03 (m, XH, *m*- and *p*-Ar), 6.98 (d, 1H, *J* = 8 Hz, *m*-Ar), 6.94 (t, 1H, *J* = 8 Hz, *p*-Ar), 6.87 (d, 2H, *J* = 8 Hz, *m*-Ar), 6.59 (d, 1H, *J* = 8 Hz, *m*-Ar), 6.50 (t, 1H, *J* = 7 Hz, *p*-Ar), 6.40 (d, 2H, *J* = 8 Hz, *m*-Ar), 6.04 (d, 2H, *J* = 8 Hz, *m*-Ar), 3.68 (d, 1H, *J* = 2 Hz, B-C*H*(Cy)-N), 3.53 (septet, 1H, *J* = 7 Hz, C*H*$(CH_3)_2$), 3.31–3.15 (m, 3H, C*H*$(CH_3)_2$), 2.98 (br s, 1H, C*H*$(CH_3)_2$), 2.80–2.72 (m, 2H, C*H*$(CH_3)_2$ and –Cy), 2.49 (br s, 1H, C*H*$(CH_3)_2$), 2.41 (br s, 1H, C*H*$(CH_3)_2$), 2.12 (br d, 1H, *J* = 10 Hz, –Cy), 2.06 (s, 3H, *p*-CH_3), 1.98–1.93 (m, 3H, –Cy), 1.89–1.75 (m, 8H, –Cy), 1.57–1.30 (m, 10H, –Cy and C*H*$(CH_3)_2$), 1.48 (d, 3H, *J* = 7 Hz, CH(C*H*$_3)_2$), 1.43 (d, 3H, *J* = 7 Hz, CH(C*H*$_3)_2$), 1.24 (d, 3H, *J* = 7 Hz, CH(C*H*$_3)_2$), 1.16 (d, 3H, *J* = 7 Hz, CH(C*H*$_3)_2$), 1.05 (d, 3H, *J* = 7 Hz, CH(C*H*$_3)_2$), 1.05–0.88 (m, 17H, –Cy and C*H*$(CH_3)_2$), 1.01 (d, 3H, *J* = 7 Hz, CH(C*H*$_3)_2$), 0.96 (d, 3H, *J* = 7 Hz, CH(C*H*$_3)_2$), 0.94 (d,

3H, J = 7 Hz, CH(CH_3)$_2$), 0.84 (br s, 3H, CH(CH_3)$_2$), 0.60 (br s, 3H, CH(CH_3)$_2$) ppm. *Note: Peak assignments are tentative*. $^{13}C\{^1H\}$ NMR (125.7 MHz, C_6D_6, 20 ˚C): δ = 162.4, 159.1, 149.0, 148.3, 148.0, 147.2, 147.0, 146.4, 142.2, 138.5, 137.3, 136.0, 135.7, 135.5, 134.9, 133.1, 132.4, 132.0, 131.4, 130.0, 129.7, 129.6, 129.2, 128.6, 127.6, 126.0, 124.8, 124.6, 124.1, 124.0, 123.7, 123.6, 123.4, 122.6, 122.5, 112.3, 109.2, 66.8, 45.4, 33.7, 33.1, 32.4, 32.0, 31.0, 30.9, 30.8, 29.5, 29.5, 28.9, 28.7, 28.1, 27.9, 27.8, 27.8, 27.8, 27.3, 26.2, 26.1, 25.8, 25.6, 25.4, 24.0, 24.0, 23.6, 23.1, 23.0, 22.7, 22.4, 22.0, 20.9 ppm. *Note: The isocyanide C≡N resonance could not be conclusively identified.* ^{11}B NMR (160.5 MHz, C_6D_6, 20 ˚C): δ = 61.8 (br s) ppm. FTIR (C_6D_6, KBr windows, 20 ˚C): ν(C≡N)/ν(N_3) = 2112 (vs) cm^{-1}; also 3058, 3022, 2963, 2925, 2866, 2848, 1579, 1503, 1462, 1448, 1411, 1383, 1362, 1327, 1292, 1269, 1252, 1201, 1181, 1138, 1114, 1107, 1097, 1083, 1057, 1034, 996, 936, 888, 882, 787, 761, 754, 742 cm^{-1}. Anal. calcd. for $C_{81}H_{104}N_5BPt$: C, 71.87; H, 7.74; N, 5.17. Found: C, 71.91; H, 7.90; N, 5.15.

2.7. Details of DFT computational studies

General considerations. Density Functional Theory calculations on the model compounds Pt(κ^2-*N,B*-^{Me2}BIM)(CNMe) and ^{Me2}BIM were performed with the Amsterdam Density Functional (ADF) program suite,[82,83] version 2013.99.[84] The model complex Pt(κ^2-*N,B*-^{Me2}BIM)(CNMe) is a truncated version of the structurally characterized complex Pt(κ^2-*N,B*-^{Cy2}BIM)(CNAr^{Dipp2}) (**1**), while ^{Me2}BIM is a truncated version of the (boryl)iminomethane ^{Cy2}BIM (**2**). For all atoms, the triple-ξ Slater-type orbital TZ2P ADF basis set was utilized without frozen cores. Relativistic effects were

included by use of the zeroth-order regular approximation (ZORA).[85,86] The local density approximation (LDA) of Vosko, Wilk and Nusair (VWN)[87] was coupled with the generalized gradient approximation (GCA) corrections described by Becke[88] and Perdew[89,90] for electron exchange and correlation, respectively. Crystallographic atomic coordinates of complex **1** were used as the basis for generating the input file for Pt(κ^2-*N,B*-^{Me2}BIM)(CNMe). Optimized geometries and molecular orbitals were visualized with the ADFView graphical routine of the ADF-GUI.[91] Natural Bond Orbital (NBO) analyses were performed using the program NBO 6.0[92] via the standalone executable GenNBO.[93] Natural Localized Molecular Orbitals (NLMOs) were visualized using ChemCraft.[94]

Hardware Specifics. DFT calculations were performed on a home-built 72-CPU (1 x 8 master, 8 x 8 slave) Rocks 4.3 Linux cluster featuring Intel Xeon E5335 Quad-Core 2.00 GHz processors. Job control was implemented with the Sun Grid Engine v. 5.3.

Input for Geometry Optimization of Pt(κ^2-*N*-*B*-^{Me2}BIM)(CNMe)

```
$ADFBIN/adf -n8 \
 <<< "
TITLE PtBorane_CNMe

MAXMEMORYUSAGE 23000

RELATIVISTIC ZORA

UNRESTRICTED

CHARGE 0 0

SCF
DIIS
END

XC
```

```
 LDA VWN
 GGA Becke Perdew
END

SYMMETRY NOSYM
ATOMS
Pt       0.23126400       4.79642900       4.11596100
N        2.41867800       5.15665700       2.06197400
C       -1.16155900       6.08426500       5.90692800
B        0.04354800       6.83689300       5.17940800
C        1.33091600       7.04560400       6.15388400
C        3.41166100       5.07865400       1.08126800
N       -1.27396200       4.85581700       5.54583800
C       -2.28691100       4.00347200       6.11606200
C       -0.35028900       7.98797000       4.16043500
C        1.58665200       5.01330000       2.87670700
H       -1.72913400       6.38784600       6.54100500
H        2.25516218       6.58014511       5.84482571
H        1.17557858       6.87221276       7.20849567
H        1.61558681       8.08740894       6.15611945
H        4.34847904       5.53879892       1.35882630
H        3.10720702       5.43946362       0.10991626
H        3.66739880       4.04353654       0.90942498
H       -1.97857063       2.98229561       6.28495545
H       -3.23330101       4.01240478       5.59580614
H       -2.53989747       4.35678118       7.10478363
H        0.38486034       8.76381389       4.00544562
H       -1.32359823       8.43608903       4.29555895
H       -0.43963135       7.57417323       3.16686056
END

GEOMETRY
 GO
END

BASIS
 type TZ2P
 core none
END

END INPUT
```

Optimized Cartesian coordinates for Pt(κ^2-*N*-*B*-^{Me2}BIM)(CNMe)

Pt	0.211714	4.799357	4.111946
N	2.458789	5.039186	2.076886
C	-1.120526	6.099588	5.995677
B	0.052468	6.880599	5.236154
C	1.405094	7.111445	6.061564
C	3.500544	5.104594	1.127359
N	-1.250590	4.889575	5.554427
C	-2.239487	3.945972	6.056489
C	-0.403138	7.989500	4.173895
C	1.584942	4.947758	2.868885
H	-1.794698	6.448116	6.804631
H	2.238874	7.397126	5.401914
H	1.724564	6.244246	6.657033
H	1.260836	7.952547	6.767818
H	4.361295	5.648292	1.541592
H	3.160851	5.621491	0.218539
H	3.827946	4.091606	0.852178
H	-1.733761	3.051466	6.442542
H	-2.898078	3.632006	5.236117
H	-2.842136	4.402342	6.857256
H	0.424809	8.279207	3.508825
H	-0.708518	8.906980	4.714291
H	-1.254499	7.690399	3.545488

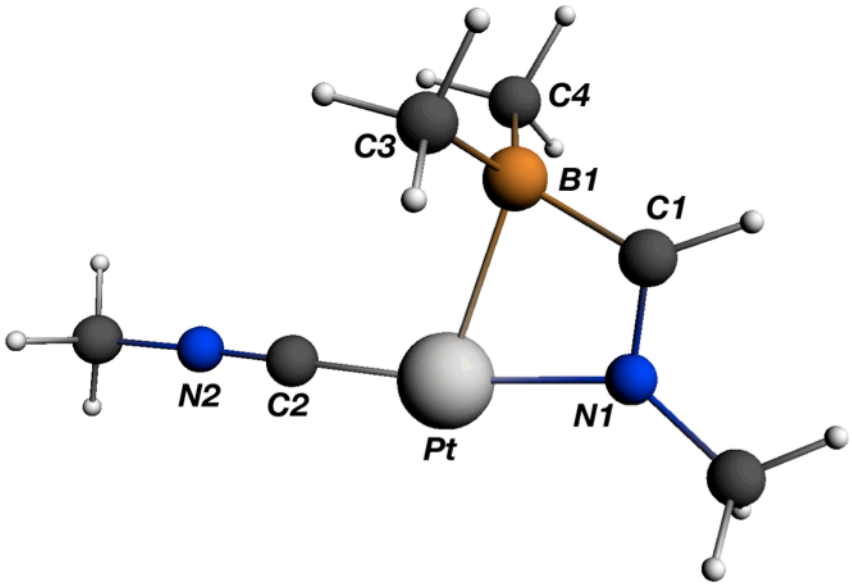

Figure 2.20. Optimized molecular structure of Pt(κ^2-*N*-*B*-^{Me2}BIM)(CNMe).

Table 2.1. Comparative metrical parameters between Pt(κ^2-*N*-*B*-^{Cy2}BIM)(CNAr^{Dipp2}) (Exp. X-ray) and Pt(κ^2-*N*-*B*-^{Me2}BIM)(CNMe) (calc'd).

Parameter	Exp. (X-ray)	Calculated	% Difference
Pt-B1	2.314(6) Å	2.371 Å	2.5
Pt-N1	2.077(2) Å	2.056 Å	1.0
Pt-C2	1.848(3) Å	1.858 Å	0.5
N1-C1	1.289(3) Å	1.295 Å	0.5
C1-B1	1.582(7) Å	1.601 Å	1.2
B1-Pt-N1	66.0(2)˚	65.2˚	1.2
C1-B1-C3	114.9(3)˚	116.4˚	1.3
C3-B1-C4	118.2(4)˚	118.8˚	0.5
C4-B1-C1	115.6(4)˚	116.4˚	0.7

Input for Geometry Optimization of ^{Me2}BIM

```
$ADFBIN/adf -n8 \
 <<< "
TITLE Me2BIM

MAXMEMORYUSAGE 23000

RELATIVISTIC ZORA

CHARGE 0 0
SCF

DIIS
END

XC
 LDA VWN
 GGA Becke Perdew
END

SYMMETRY NOSYM
ATOMS
H       0.57354806      -1.83507116       0.15772368
N       1.45154522       0.03984868       0.03746785
C       0.41896093      -0.73795292       0.07314483
B      -1.05088005      -0.15942747       0.00415899
C      -2.25012357      -1.17529618       0.06883841
H      -2.00690862      -2.20214064      -0.24031737
H      -2.25750913       1.73264617       0.21424849
```

```
H      -3.15334959      -0.83766738      -0.45990200
H      -0.47462728       1.98087047       0.34928037
H      -2.54315111      -1.24091287       1.13627480
H      -1.21094068       1.62910899      -1.20223496
C      -1.26940824       1.38737862      -0.12249117
C       2.75226091      -0.48907491       0.02005729
H       3.08571782      -0.65817098       1.03327642
H       3.49810318       0.17345015      -0.39368157
H       2.83345616      -1.45926413      -0.44742555
END

GEOMETRY
 Iterations 300
 GO
END

BASIS
 type TZ2P
 core none
END

END INPUT
```

Optimized Cartesian coordinates for ^{Me2}BIM

```
   H         0.595115   -1.813523   -0.157192
   N         1.444780    0.056724    0.082089
   C         0.425037   -0.715537   -0.047227
   B        -1.054770   -0.149130   -0.023889
   C        -2.234237   -1.182982    0.097857
   H        -2.016452   -2.172748   -0.330756
   H        -2.223334    1.735920    0.364794
   H        -3.198999   -0.821024   -0.285214
   H        -0.438926    1.990059    0.235654
   H        -2.387621   -1.357212    1.182098
   H        -1.407360    1.636188   -1.191459
   C        -1.293614    1.396558   -0.115227
   C         2.767648   -0.536037    0.083063
   H         3.266686   -0.287754    1.031850
   H         3.367818   -0.065239   -0.709752
   H         2.767395   -1.634291   -0.055339
```

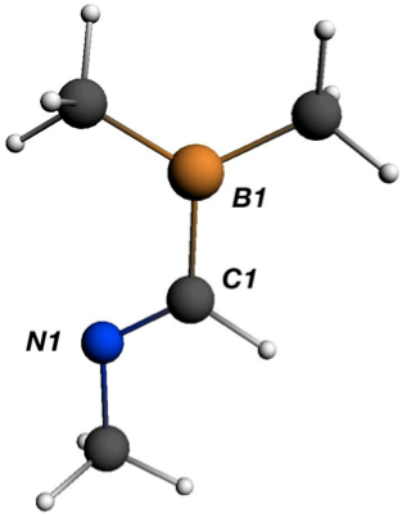

Figure 2.21. Optimized molecular structure of ^{Me2}BIM. Selected bond distances (Å) and angles (˚): N1-C1 = 1.289. C1-B1 = 1.590. N1-C1-B1 = 121.6.

Natural Bond Orbital (NBO) Analysis. NBO calculations were performed on the Pt-borane model complex Pt(κ^2-*N*-*B*-^{Me2}BIM)(CNMe) and the (boryl)iminomethane model compound ^{Me2}BIM. A Natural Localized Molecular Orbital describing the Pt-B dative interaction was found for Pt(κ^2-*N*-*B*-^{Me2}BIM)(CNMe) and is plotted in Figure 2.2. The atomic and fragment charges derived from the Natural Population Analysis (NPA) are shown in Table 2.2.

Table 2.2. Atomic and fragment charges (q) derived from the Natural Population Analysis calculations for Pt(κ^2-*N*-*B*-^{Me2}BIM)(CNMe) and ^{Me2}BIM.

Atom/Fragment	Pt(κ^2-*N*-*B*-^{Me2}BIM)(CNMe)	^{Me2}BIM
Pt	0.109	n/a
B	0.516	0.740
-BMe_2	0.002	0.237

2.8. CSD search results

The Cambridge Structural Database[42] was searched for structures containing a B-O single bond, with boron additionally coordinated to a total of four atoms. Structures

containing more than one boron atom were excluded, so as to eliminate data points stemming from polyboranes, borane clusters and carboranes, which typically involve non-classical/electron deficient bonding schemes. In addition, transition metal-containing structures were excluded. A total of 2879 data points were obtained and plotted in the histogram shown in Figure 2.22. The data set resulted in a mean B-O bond distance of 1.481 Å, with a standard deviation of 0.041 Å. In addition, the CSD was searched for structures containing a Pt-F bond, where the fluoride ligand is terminally bound. A total of 57 hits were obtained, indicating a mean Pt-F distance of 2.003 Å with a standard deviation of 0.009 Å. The resulting histogram is shown in Figure 2.23.

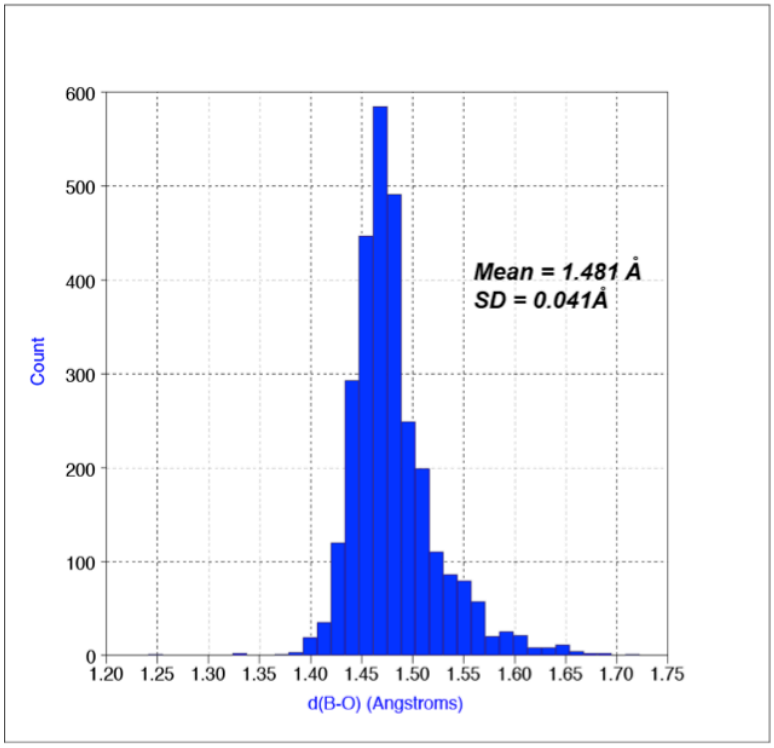

Figure 2.22. Histogram showing CSD search results for B-O bond distances in four-coordinate borates.

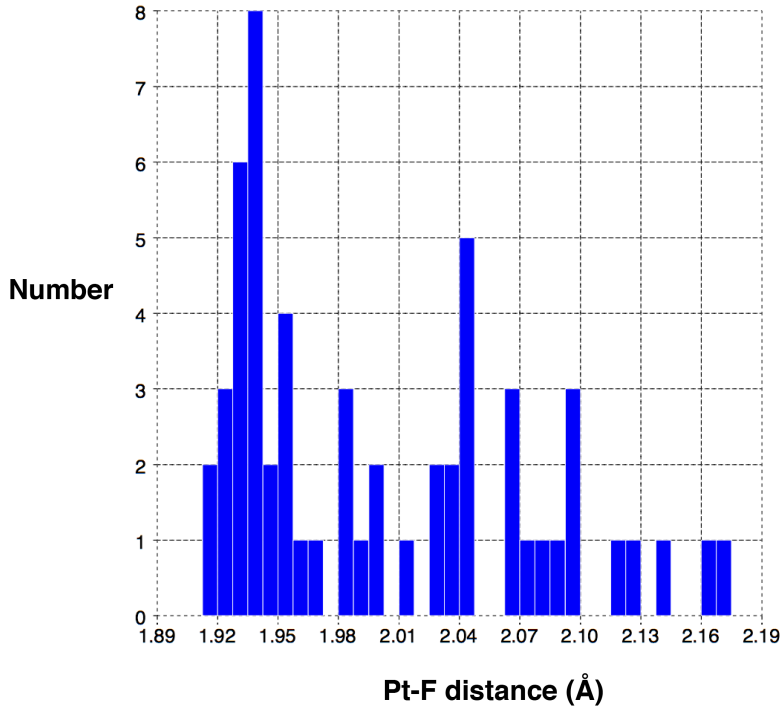

Figure 2.23. Histogram showing CSD search results for Pt-F bond distances in platinum fluorides.

2.9. Details of crystallographic structure determinations

General considerations. Single crystal X-ray structure determinations were carried out at low temperature on Bruker Kappa Diffractometers equipped with a Mo radiation source and a Bruker APEX, APEX-II or Photon 100 area detector. All structures were solved via direct methods with SIR 2004[95] or SHELXS[96] and refined by full-matrix least-squares procedures utilizing SHELXL[96] within the OLEX2 small molecule structure solution and refinement software package.[97] Crystallographic data collection and refinement information are listed in Tables 2.3-8. The platinum-borane

compound Pt(κ^2-*N,B*-^{Cy2}BIM)(CNAr^{Dipp2}) • 0.5 C_5H_{12} (**1** • 0.5 C_5H_{12}) contains two-site positional disorder of the boron atom and bound cyclohexyl groups, as well as positional disorder of a co-crystallized molecule of *n*-pentane. These disordered groups were modeled and refined anisotropically. The (boryl)iminomethane adduct of BCl_3 **3** • 2 C_5H_{12} contains two-site positional disorder of one boron-bound cyclohexyl group, as well as positional disorder of one molecule of co-crystallized *n*-pentane. These disordered groups were modeled and refined anisotropically. The diiodide PtI_2(κ^1-*N*-^{Cy2}BIM)(CNAr^{Dipp2}) • 1.5 C_6H_6 (**4** • 1.5 C_6H_6) contains positional disorder of one of the co-crystallized molecules of benzene, which was modeled and refined anisotropically. The water oxidative addition product PtH(μ-OH)(^{Cy2}BIM)(CNAr^{Dipp2}) • 0.5 Et_2O (**5** • 0.5 Et_2O) contains positional disorder of a co-crystallized molecule of diethyl ether, which was modeled and refined anisotropically. The borinic acid (Cy)(OH)BCH(Cy)NHAr^{Dipp2} (**6**) contains two-site positional disorder of both boron-bound cyclohexyl groups, which was modeled and refined anisotropically. The phenylacetylene activation product PtH(η^2-*C,C*-κ^1-*N*-PhCC-^{Cy2}BIM)(CNAr^{Dipp2}) • 1.5 Et_2O (**11** • 1.5 Et_2O) contains two-site positional disorder of one Et_2O molecule of co-crystallization, which was modeled and refined anisotropically. One of the two crystallographically independent molecules of PtBr(μ-PBr_2)(^{Cy2}BIM)(CNAr^{Dipp2}) • 1.5 C_5H_{12} (**12** • 1.5 C_5H_{12}) contains disorder in both cyclohexyl rings, which was modeled and refined anisotropically. The benzaldehyde insertion product **15** • 4.5 *cyclo*-C_6H_{12} contains two-site positional disorder of one *i*Pr group and positional disorder of two cyclohexane molecules of co-crystallization. These disordered components were modeled and refined anisotropically. The two-coordinate imine isocyanide complex **17** • 1.5 C_5H_{12} contains positional disorder of one co-

crystallized molecule of *n*-pentane, which was modeled and refined anisotropically. In addition, the following structures contained co-crystallized solvent molecules that were severely disordered and could not be properly modeled: **12** • 1.5 C_5H_{12}; **18** • C_6H_6; **19** • 2 C_5H_{12}. For these structures, the Platon routine SQUEEZE[98] was employed to account for the disordered components as a diffuse contribution to the overall scattering pattern without specific atom positions.

Table 2.3. Crystallographic data collection and refinement information.

Name	**1** • 0.5 C_5H_{12}	**3** • 2 C_5H_{12}	**4** • 1.5 C_6H_6
Formula	$PtC_{76.5}H_{103}N_2B$	$C_{53}H_{84}NB_2Cl_3$	$PtC_{83}H_{106}N_2BI_2$
Crystal System	Monoclinic	Monoclinic	Triclinic
Space Group	$P2_1/n$	$P2_1/c$	$P\text{-}1$
a, Å	14.221(2)	15.165(1)	12.721(2)
b, Å	21.092(3)	18.087(1)	12.798(2)
c, Å	22.585(3)	18.846(1)	24.396(4)
α, deg	90	90	75.829(5)
β, deg	99.809(5)	99.980(3)	78.633(5)
γ, deg	90	90	70.111(5)
V, Å^3	6675(2)	5091.2(6)	3593.0(9)
Z	4	4	2
Radiation (λ, Å)	Mo-Kα, 0.71073	Mo-Kα, 0.71073	Mo-Kα, 0.71073
ρ (calcd.), g/cm^3	1.250	1.126	1.471
μ, mm^{-1}	2.145	0.214	2.857
Temp, K	100	100	100
θ max, deg	26.470	25.434	25.614
data/parameters	13649 / 870	9393/560	13326 / 861
R_1	0.0254	0.0584	0.0296
wR_2	0.0501	0.1470	0.0670
GOF	1.010	1.063	1.004

Table 2.4. Crystallographic data collection and refinement information.

Name	**5** • $C_4H_{10}O$	**7** • 0.5 ($C_4H_{10}O$)	**8**
Formula	$PtC_{78}H_{108}N_2BO$	$PtC_{76}H_{104}N_2BO_{1.5}$	$C_{43}H_{62}NBO$
Crystal System	Monoclinic	Monoclinic	Monoclinic
Space Group	$P2_1/n$	$P2_1/c$	$P2_1/n$
a, Å	15.454(3)	11.742(2)	13.7552(3)
b, Å	18.996(4)	41.076(7)	12.2451(3)
c, Å	24.561(5)	15.151(2)	22.2006(5)
α, deg	90	90	90
β, deg	105.179(4)	110.606(3)	91.249(1)
γ, deg	90	90	90
V, Å^3	6959(2)	6840(2)	3738.4(2)
Z	4	4	4
Radiation (λ, Å)	Mo-Kα, 0.71073	Mo-Kα, 0.71073	Mo-Kα, 0.71073
ρ (calcd.), g/cm^3	1.237	1.239	1.101
μ, mm^{-1}	2.060	2.096	0.063
Temp, K	100	100	100
θ max, deg	26.431	26.428	26.403
data/parameters	14247 / 769	13625 / 787	7651 / 468
R_1	0.0323	0.0280	0.0457
wR_2	0.0608	0.0589	0.1058
GOF	1.020	1.042	1.107

Table 2.5. Crystallographic data collection and refinement information.

	9	**10**	**11** • 1.5($C_4H_{10}O$)
Formula	$PtC_{75}H_{101}N_2BO$	$PtC_{80}H_{102}N_4BO_2$	$C_{88}H_{117}N_2BO_{1.5}Pt$
Crystal System	Monoclinic	Monoclinic	Triclinic
Space Group	$P2_1/n$	$P2_1/n$	P-1
a, Å	16.5210(6)	17.3778(6)	12.1668(6)
b, Å	20.7264(6)	21.3169(7)	14.9438(8)
c, Å	20.3651(8)	19.5427(7)	22.741(1)
α, deg	90	90	100.915(2)
β, deg	104.659(1)	104.843(2)	100.665(2)
γ, deg	90	90	102.973(2)
V, Å^3	6776.2(4)	6997.8(4)	3842.7(3)
Z	4	4	2
Radiation (λ, Å)	Mo-Kα, 0.71073	Mo-Kα, 0.71073	Mo-Kα, 0.71073
ρ (calcd.), g/cm^3	1.228	1.289	1.238
μ, mm^{-1}	2.114	2.054	1.873
Temp, K	100	100	100
θ max, deg	25.372	26.408	26.428
data/parameters	12394 / 742	14332 / 813	14482 / 899
R_1	0.0346	0.0305	0.0476
wR_2	0.0682	0.0664	0.0867
GOF	1.066	1.043	1.060

Table 2.6. Crystallographic data collection and refinement information.

Name	**12** • 1.5 C_5H_{12}	**13** • MeCN	**14**
Formula	$C_{81.5}H_{115}N_2BBr_3PPt$	$C_{76}H_{100}N_3BF_3PtSb$	$PtC_{77}H_{103}N_2BO$
Crystal System	Triclinic	Monoclinic	Monoclinic
Space Group	*P*-1	$P2_1/c$	$P2_1/c$
a, Å	17.5743(16)	13.7463(6)	10.8582(6)
b, Å	20.599(2)	24.2768(11)	41.318(2)
c, Å	23.069(2)	21.6263(10)	15.8758(9)
α, deg	71.382(3)	90	90
β, deg	82.024(3)	104.379(2)	107.117(2)
γ, deg	72.954(3)	90	90
V, Å^3	7557.4(13)	6991.0(5)	6807.0(7)
Z	4	4	4
Radiation (λ, Å)	Mo-Kα, 0.71073	Mo-Kα, 0.71073	Mo-Kα, 0.71073
ρ (calcd.), g/cm^3	1.406	1.355	1.248
μ, mm^{-1}	3.507	2.435	2.105
Temp, K	100	100	100
θ max, deg	24.878	26.410	26.410
data/parameters	25956 / 1459	14281 / 777	13945 / 757
R_1	0.0597	0.352	0.0313
wR_2	0.1240	0.737	0.0582
GOF	1.005	1.019	1.221

Table 2.7. Crystallographic data collection and refinement information.

Name	**15** • 4.5 *cyclo*-C_6H_{12}	**17**	**18** • C_6H_6
Formula	$C_{108}H_{157}N_2BOPt$	$C_{76}H_{100}N_3BPt$	$C_{90}H_{118}N_5BPt$
Crystal System	Monoclinic	Triclinic	Triclinic
Space Group	$P2_1/n$	P-1	P-1
a, Å	15.773(1)	13.2573(8)	12.0006(7)
b, Å	25.858(2)	16.0292(9)	16.3235(10)
c, Å	24.212(2)	20.6749(13)	19.9669(11)
α, deg	90	73.037(3)	94.562(3)
β, deg	107.415(1)	81.441(3)	99.409(3)
γ, deg	90	66.363(2)	92.168(3)
V, Å^3	9422(1)	3847.2(4)	3841.4(4)
Z	4	2	2
Radiation (λ, Å)	Mo-Kα, 0.71073	Mo-Kα, 0.71073	Mo-Kα, 0.71073
ρ (calcd.), g/cm^3	1.202	1.089	1.276
μ, mm^{-1}	1.538	1.861	1.875
Temp, K	100	100	100
θ max, deg	26.403	23.31	26.421
data/parameters	19231 / 1104	10673 / 747	15364 / 836
R_1	0.0253	0.0519	0.0296
wR_2	0.0582	0.1261	0.0679
GOF	1.221	0.979	1.037

Table 2.8. Crystallographic data collection and refinement information.

Name	**19** • 2 C_5H_{12}
Formula	$C_{91}H_{128}N_5BPt$
Crystal System	Triclinic
Space Group	*P*-1
a, Å	12.1176(5)
b, Å	16.1485(6)
c, Å	23.0370(8)
α, deg	96.3950(10)
β, deg	98.6510(10)
γ, deg	111.1050(10)
V, Å^3	4090.2(3)
Z	2
Radiation (λ, Å)	Mo-Kα, 0.71073
ρ (calcd.), g/cm^3	1.216
μ, mm^{-1}	1.762
Temp, K	100
θ max, deg	26.061
data/parameters	16119 / 857
R_1	0.0275
wR_2	0.0574
GOF	1.019

2.10. Acknowledgements

Chapter 2 is adapted in part from Barnett, B. R.; Moore, C. E.; Rheingold, A. L.; Figueroa, J. S. *Journal of the American Chemical Society.* **2014**, *136*, 10262. Copyright 2014, American Chemical Society. Permission to include published material in this dissertation has been obtained from all coauthors. The dissertation author is the first author of this paper. Prof. Carlos A. Guerrero and Matthew Del Bel are thanked for a loan of dicyclohexylborane.

2.11. References

(1) Hill, A. F.; Owen, G. R.; White, A. J. P.; Williams, D. J. *Angew. Chem., Int. Ed.* **1999**, *38*, 2759.

(2) Braunschweig, H.; Kollann, C.; Rais, D. *Angew. Chem., Int. Ed.* **2006**, *45*, 5254.

(3) Kuzu, I.; Krummenacher, I.; Meyer, J.; Armbruster, F.; Breher, F. *Dalton Trans.* **2008**, 5836.

(4) Amgoune, A.; Bourissou, D. *Chem. Commun.* **2011**, *47*, 859.

(5) Braunschweig, H.; Dewhurst, R. D.; Schneider, A. *Chem. Rev.* **2010**, *110*, 3924.

(6) Braunschweig, H.; Dewhurst, R. D. *Dalton Trans.* **2011**, *40*, 549.

(7) Owen, G. R. *Chem. Soc. Rev.* **2012**, *41*, 3535.

(8) Landry, V. K.; Melnick, J. G.; Buccella, D.; Pang, K.; Ulichny, J. C.; Parkin, G. *Inorg. Chem.* **2006**, *45*, 2588.

(9) Parkin, G. *Organometallics* **2006**, *25*, 4744.

(10) Harman, W. H.; Peters, J. C. *J. Am. Chem. Soc.* **2012**, *134*, 5080.

(11) Fong, H.; Moret, M.-E.; Lee, Y.; Peters, J. C. *Organometallics* **2013**, *32*, 3053.

(12) Moret, M.-E.; Peters, J. C. *Angew. Chem., Int. Ed.* **2011**, *50*, 2063.

(13) Anderson, J. S.; Rittle, J.; Peters, J. C. *Nature* **2013**, *501*, 84.

(14) Suess, D. L. M.; Peters, J. C. *J. Am. Chem. Soc.* **2013**, *135*, 12580.

(15) Figueroa, J. S.; Melnick, J. G.; Parkin, G. *Inorg. Chem.* **2006**, *45*, 7056.

(16) For the spectroscopic characterization of a complex assigned as an unsupported platinum-borane adduct, see: Bauer, J.; Braunschweig, H.; Dewhurst, R. D.; Radacki, K. *Chem. Eur. J.* **2013**, *19*, 8797.

(17) Bontemps, S.; Bouhadir, G.; Miqueu, K.; Bourissou, D. *J. Am. Chem. Soc.* **2006**, *128*, 12056.

(18) A related "XZ-type" boryl-borane Pt(II) complex derived from the diborane Br(Mes)B–B(Mes)Br (Mes = 2,4,6-$Me_3C_6H_2$) has been shown to possess a reverse-dative, Pt-to-BR_3 interaction. See: Braunschweig, H.; Damme, A.; Kupfer, T. *Angew. Chem., Int. Ed.* **2011**, *50*, 7179.

(19) Hermanek, S. *Chem. Rev.* **1992**, *92*, 325.

(20) Bontemps, S.; Bouhadir, G.; Gu, W.; Mercy, M.; Chen, C.-H.; Foxman, B. M.; Maron, L.; Ozerov, O. V.; Bourissou, D. *Angew. Chem., Int. Ed.* **2008**, *47*, 1481.

(21) Ditri, T.; Fox, B.; Moore, C.; Rheingold, A.; Figueroa, J. *Inorg. Chem.* **2009**, *48*, 8362.

(22) Casanova, J., Jr; Schuster, R. E. *Tetrahedron Lett.* **1964**, *5*, 405.

(23) Casanova, J., Jr; Kiefer, H. R.; Kuwada, D.; Boulton, A. H. *Tetrahedron Lett.* **1965**, *6*, 703.

(24) Suginome, M.; Fukuda, T.; Nakamura, H.; Ito, Y. *Organometallics* **2000**, *19*, 719.

(25) Tamm, M.; Lügger, T.; Hahn, F. E. *Organometallics* **1996**, *15*, 1251.

(26) Qiu, G.; Ding, Q.; Wu, J. *Chem. Soc. Rev.* **2013**, *42*, 5257.

(27) Tsoureas, N.; Kuo, Y.-Y.; Haddow, M. F.; Owen, G. R. *Chem. Commun.* **2010**, *47*, 484.

(28) Harman, W. H.; Lin, T.-P.; Peters, J. C. *Angew. Chem., Int. Ed.* **2014**, *53*, 1081.

(29) Devillard, M.; Bouhadir, G.; Bourissou, D. *Angew. Chem., Int. Ed.* **2014**, *54*, 730.

(30) Welch, G. C.; San Juan, R. R.; Masuda, J. D.; Stephan, D. W. *Science* **2006**, *314*, 1124.

(31) Stephan, D. W.; Erker, G. *Angew. Chem., Int. Ed.* **2015**, *54*, 6400.

(32) Chase, P. A.; Welch, G. C.; Jurca, T.; Stephan, D. W. *Angew. Chem., Int. Ed.* **2007**, *46*, 8050.

(33) Chase, P. A.; Jurca, T.; Stephan, D. W. *Chem. Commun.* **2008**, 1701.

(34) Grotjahn, D. B.; Gong, Y.; DiPasquale, A. G.; Zakharov, L. N.; Rheingold, A. L. *Organometallics* **2006**, *25*, 5693.

(35) Ozerov, O. V. *Chem. Soc. Rev.* **2008**, *38*, 83.

(36) Millard, M. D.; Moore, C. E.; Rheingold, A. L.; Figueroa, J. S. *J. Am. Chem. Soc.* **2010**, *132*, 8921.

(37) Kläring, P.; Pahl, S.; Braun, T.; Penner, A. *Dalton Trans.* **2011**, *40*, 6785.

(38) Castellano, F. N.; Pomestchenko, I. E.; Shikhova, E.; Hua, F.; Muro, M. L.; Rajapakse, N. *Coord. Chem. Rev.* **2006**, *250*, 1819.

(39) Wang, W.; Yang, H.-B. *Chem. Commun.* **2014**, *50*, 5171.

(40) Rajagopalan, R. A.; Jayaraman, A.; Sterenberg, B. T. *J. Organomet. Chem.* **2014**, *761*, 84.

(41) Ebsworth, E. A. V.; Gould, R. O.; McManus, N. T.; Pilkington, N. J.; Rankin, D. W. H. *J. Chem. Soc., Dalton Trans.* **1984**, 2561.

(42) Cambridge Structural Database (CSD), version 5.37 (November **2015**).

(43) Carpenter, A. E. Ph.D. Dissertation, University of California, San Diego, **2015**.

(44) Sattler, W.; Ruccolo, S.; Parkin, G. *J. Am. Chem. Soc.* **2013**, *135*, 18714.

(45) Solé, S.; Gabbaï, F. P. *Chem. Commun.* **2004**, 1284.

(46) Yahav, A.; Goldberg, I.; Vigalok, A. *Inorg. Chem.* **2005**, *44*, 1547.

(47) Dubinsky-Davidchik, I. S.; Potash, S.; Goldberg, I.; Vigalok, A.; Vedernikov, A. N. *J. Am. Chem. Soc.* **2012**, *134*, 14027.

(48) Nova, A.; Erhardt, S.; Jasim, N. A.; Perutz, R. N.; Macgregor, S. A.; McGrady, J. E.; Whitwood, A. C. *J. Am. Chem. Soc.* **2008**, *130*, 15499.

(49) Nilsson, P.; Plamper, F.; Wendt, O. F. *Organometallics* **2003**, *22*, 5235.

(50) Ishiyama, T.; Matsuda, N.; Murata, M.; Ozawa, F.; Suzuki, A.; Miyaura, N. *Organometallics* **1996**, *15*, 713.

(51) Clark, G. R.; Irvine, G. J.; Roper, W. R.; Wright, L. J. *Organometallics* **1997**, *16*, 5499.

(52) Onozawa, S.-Y.; Tanaka, M. *Organometallics* **2001**, *20*, 2956.

(53) Laitar, D. S.; Tsui, E. Y.; Sadighi, J. P. *J. Am. Chem. Soc.* **2006**, *128*, 11036.

(54) Devillard, M.; Declercq, R.; Nicolas, E.; Ehlers, A. W.; Backs, J.; Saffon-Merceron, N.; Bouhadir, G.; Slootweg, J. C.; Uhl, W.; Bourissou, D. *J. Am. Chem. Soc.* **2016**, *138*, 4917.

(55) Barnett, B. R.; Moore, C. E.; Rheingold, A. L.; Figueroa, J. S. *Chem. Commun.* **2015**, *51*, 541.

(56) Cenini, S.; Gallo, E.; Caselli, A.; Ragaini, F.; Fantauzzi, S.; Piangiolino, C. *Coord. Chem. Rev.* **2006**, *250*, 1234.

(57) Proulx, G.; Bergman, R. G. *J. Am. Chem. Soc.* **1995**, *117*, 6382.

(58) Fickes, M. G.; Davis, W. M.; Cummins, C. C. *J. Am. Chem. Soc.* **1995**, *117*, 6384.

(59) Proulx, G.; Bergman, R. G. *Organometallics* **1996**, *15*, 684.

(60) Guillemot, G.; Solari, E.; Floriani, C.; Rizzoli, C. *Organometallics* **2001**, *20*, 607.

(61) Hanna, T. A.; Baranger, A. M.; Bergman, R. G. *Angew. Chem., Int. Ed.* **1996**, *35*, 653.

(62) Dias, H. V. R.; Polach, S. A.; Goh, S.-K.; Archibong, E. F.; Marynick, D. S. *Inorg. Chem.* **2000**, *39*, 3894.

(63) Barz, M.; Herdtweck, E.; Thiel, W. R. *Angew. Chem., Int. Ed.* **1998**, *37*, 2262.

(64) Albertin, G.; Antoniutti, S.; Baldan, D.; Castro, J.; García-Fontán, S. *Inorg. Chem.* **2008**, *47*, 742.

(65) Mankad, N. P.; Müller, P.; Peters, J. C. *J. Am. Chem. Soc.* **2010**, *132*, 4083.

(66) Waterman, R.; Hillhouse, G. L. *J. Am. Chem. Soc.* **2008**, *130*, 12628.

(67) Bouwstra, J. A.; Schouten, A.; Kroon, J. *Acta Crystallogr. C* **1983**, *39*, 1121.

(68) Hubig, S. M.; Lindeman, S. V.; Kochi, J. K. *Coord. Chem. Rev.* **2000**, *200*, 831.

(69) Winkler, J.; Gray, H. In *Structure and Bonding*; Mingos, D. M. P., Day, P., Dahl, J. P., Eds.; Springer, **2012**, 142, 17.

(70) Mindiola, D. J.; Hillhouse, G. L. *J. Am. Chem. Soc.* **2001**, *123*, 4623.

(71) Iluc, V. M.; Hillhouse, G. L. *J. Am. Chem. Soc.* **2010**, *132*, 15148.

(72) Brown, S. D.; Betley, T. A.; Peters, J. C. *J. Am. Chem. Soc.* **2003**, *125*, 322.

(73) Kogut, E.; Wiencko, H. L.; Zhang, L.; Cordeau, D. E.; Warren, T. H. *J. Am. Chem. Soc.* **2005**, *127*, 11248.

(74) Hay-Motherwell, R. S.; Wilkinson, G.; Hussain-Bates, B.; Hursthouse, M. B. *Polyhedron* **1993**, *12*, 2009.

(75) Poverenov, E.; Efremenko, I.; Frenkel, A. I.; Ben-David, Y.; Shimon, L. J. W.; Leitus, G.; Konstantinovski, L.; Martin, J. M. L.; Milstein, D. *Nature* **2008**, *455*, 1093.

(76) Laskowski, C. A.; Miller, A. J. M.; Hillhouse, G. L.; Cundari, T. R. *J. Am. Chem. Soc.* **2011**, *133*, 771.

(77) Iovan, D. A.; Betley, T. A. *J. Am. Chem. Soc.* **2016**, *138*, 1983.

(78) Armarego, W. L. F.; Chai, C. L. L. *Purification of Laboratory Chemicals*, 5th Ed.; Elsevier, 2003.

(79) Pangborn, A. B.; Giardello, M. A.; Grubbs, R. H.; Rosen, R. K.; Timmers, F. J. *Organometallics*, **1996**, *15*, 1518.

(80) Barnett, B. R.; Moore, C. E.; Rheingold, A. L.; Figueroa, J. S. *J. Am. Chem. Soc.* **2014**, *136*, 10262.

(81) Abiko, A. *Org. Synth.* **2002**, *79*, 103.

(82) te Velde, G.; Bickelhaupt, F. M.; Baerends, E. J.; Guerra, C. F.; Van Gisbergen,

S. J. A.; Snijders, J. G.; Ziegler, T. *J. Comput. Chem.* **2001**, *22*, 931.

(83) Guerra, C. F.; Snijders, J. G.; te Velde, G.; Baerends, E. J. *Theor. Chim. Acta* **1998**, *99*, 391.

(84) ADF 2013.99, SCM, Theoretical Chemistry, Vrije University, Amsterdam, Netherlands. www.scm.com.

(85) van Lenthe, E.; Baerends, E. J.; Snijders, J. G. *J. Chem. Phys.* **1993**, *99*, 4597.

(86) van Lenthe, E.; Snijders, J. G.; Baerends, E. J. *J. Chem. Phys.* **1996**, *105*, 6505.

(87) Vosko, S. H.; Wilk, L.; Nusair, M. *Can. J. Phys.* **1980**, *50*, 1200.

(88) Becke, A. D. *Phys. Rev. A.* **1988**, *38*, 3098.

(89) Perdew, J. P. *Phys. Rev. B.* **1986**, *34*, 7406.

(90) Perdew, J. P. *Phys. Rev. B.* **1986**, *33*, 8822.

(91) ADF-GUI 2007.01, SCM, Amsterdam, Netherlands. www.scm.com.

(92) Reed, A. E.; Curtiss, L. A.; Weinhold, F. *Chem. Rev.* **1988**, *88*, 899.

(93) NBO 6.0. Glendening, E. D.; Badenhoop, J. K.; Reed, A. E.; Carpenter, J. E.; Bohmann, J. A.; Morales, C. M.; Landis, C. R.; Weinhold, F. Theoretical Chemistry Institute, University of Wisconsin, Madison (**2013**). www.nbo6.chem.wisc.edu.

(94) ChemCraft. Zhurko, G. A.; Zhurko, D. A. (**2014**). www.chemcraftprog.com.

(95) Burla, M. C.; Caliandro, R.; Camalli, M.; Carrozzini, B.; Cascarano, G. L.; De Caro, L.; Giacovazzo, C.; Polidori, G.; Spagna, R. J. *J. Appl. Crystallogr.* **2005**, *38*, 381.

(96) Sheldrick, G. M.; *Acta Crystallogr. A.* **2008**, *64*, 112.

(97) Dolomanov, O. V.; Bourhis, L. J.; Gildea, R. J.; Howard, J. A. K.; Puschmann, H. *J. Appl. Cryst.* **2009**, *42*, 339.

(98) van der Sluis, P.; Spek, A. L. *Acta Crystallogr.* **1990**, *A46*, 194.

Chapter 3

Frustrated Lewis Pair Behavior of Monomeric (boryl)iminomethanes Accessed from Isocyanide 1,1-hydroboration

3.1. Introduction

With the advent of phosphine/borane Frustrated Lewis Pairs (FLPs) by Stephan,[1] there has been significant interest in the development of transition-metal-free small-molecule activation processes.[2-4] While a number of intra- and inter-molecular FLP platforms have been uncovered,[5,6] common traits among most of them include the usage of strongly Lewis basic and acidic groups to enhance activity. Computational investigations[7,8] have highlighted the potent activity that might be displayed by intramolecular FLP platforms that contain frontier orbitals mutually oriented in the direction of an incoming substrate.[9-15] Such "preorganized" FLPs show aptitude in decreasing reliance on strongly Lewis acidic groups (*e.g.* perfluorinated arylboranes and alanes), which can inhibit the imperative substrate release step in catalytic applications.[9] As such, new preorganized FLPs that can be readily synthesized promise to be of interest to a broad cross-section of the chemical community.

Recently, we reported the synthesis of the platinum-(boryl)iminomethane complex, Pt(κ^2-*N,B*-^{Cy2}BIM)(CNAr^{Dipp2}) (^{Cy2}BIM = $Cy_2BC(H)=NAr^{Dipp2}$; Ar^{Dipp2} = 2,6-(2,6-(*i*-Pr)$_2C_6H_3$)$_2C_6H_3$) and demonstrated that the rigid, bidentate ^{Cy2}BIM ligand promoted a significant reverse-dative σ-interaction between the Pt and boron centers.[16] We also showed that the free (boryl)iminomethane ^{Cy2}BIM could be easily prepared by

1,1-hydroboration of the *m*-terphenyl isocyanide[17] $CNAr^{Dipp2}$ and that it readily activated both H_2 and H_2O in a manner consistent with FLP behavior. To our knowledge, this constituted the first report of (boryl)iminomethane formation by 1,1-hydroboration of an isocyanide. While both the ease of synthesis and reactivity profile of ^{Cy2}BIM suggest that the (boryl)iminomethane (BIM) framework may be generally competent for small-molecule activation processes, it is critical to note that kinetically persistent (boryl)iminoalkane monomers are rare.[18-22] Indeed, when unencumbering substituents are present, (boryl)iminoalkanes rapidly dimerize to heterocyclic 1,3-diaza-2,4-diboretidines (Scheme 3.1).[23-36] Furthermore, of the few structurally-characterized (boryl)iminoalkane monomers that have been reported,[19] all possess an *anti* relationship between the borane center and the imino nitrogen lone pair, thus precluding exploitation of their ambiphilic properties toward exogenous substrates. In an effort to further detail the reaction profile available to monomeric (boryl)iminomethanes, we report here the reactivity of ^{Cy2}BIM toward unsaturated organic substrates and provide evidence for its "preorganized" intramolecular FLP-type behavior. Despite the presence of a dicyclohexylboryl group of mere moderate Lewis acidity, ^{Cy2}BIM readily activates carbon dioxide, organonitriles, and terminal acetylenes. In addition, we demonstrate that the formation of syn-*N,B* monomeric (boryl)iminomethanes is a general stereochemical outcome in the 1,1-hydroboration of *m*-terphenyl isocyanides.

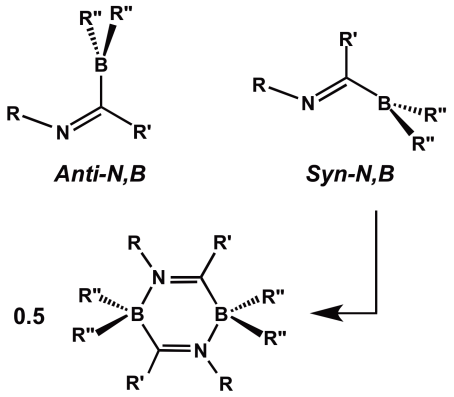

Scheme 3.1. Regioisomers of monomeric (boryl)iminomethanes and head-to-tail dimerization of sterically unencumbered *syn-N,B* (boryl)iminomethanes to 1,3-diaza-2,4-diboretidines.

3.2. Frustrated Lewis Pair reactivity of ^{Cy2}BIM

The ability of ^{Cy2}BIM (**1a**) to act as a competent Frustrated Lewis Pair allows it to effect the facile C=O bond reduction of carbon dioxide. Placing a frozen benzene solution of ^{Cy2}BIM (**1a**) under 1 atm of CO_2 causes an immediate color change from bright yellow to colorless upon thawing. Analysis of the solution by ^{1}H and ^{11}B NMR spectroscopy indicates complete conversion to a single new product. The absence of any ^{1}H NMR signals diagnostic for an aldimine functionality hints at reduction of the C=N double bond of ^{Cy2}BIM (**1a**), while the appearance of a strong infrared absorbance at 1772 cm^{-1} suggests the presence of an ester group. The solid-state structure as determined by X-ray diffraction reveals this product to be the boralactone (**2a**, racemic mixture, Figure 3.1) derived from nucleophilic attack of the imime nitrogen at the CO_2 carbon atom and coordination of one oxygen atom to boron. As opposed to the vast majority of FLP-activated CO_2 adducts which are zwitterionic,[4,27] the endocyclic C2-O1 distance in **2a** (1.391(9) Å) is consistent with that of a carbon-oxygen single bond, suggesting a larger degree of activation than is typically seen in such species. Formation of the five-

membered ring is accompanied by a 1,2-cyclohexyl shift, as observed previously for ^{Cy2}BIM (**1a**) in the heterolytic H-O bond cleavage of water.[16] This boron-to-carbon cyclohexyl migration,[28] reminiscent of a Wagner-Meerwein rearrangement,[29] has been observed with other (boryl)iminomethanes following their head-to-tail dimerization.[24,26] Relevantly, this 1,2-cyclohexyl shift may be at least partially responsible for the irreversibility of CO_2 reduction by ^{Cy2}BIM (**1a**), as heating solutions of **2a** to 80 ˚C under an N_2 atmosphere (or, alternatively, heating solid samples to 150 ˚C under vacuum) produces no evidence of reversion to ^{Cy2}BIM (**1a**) and free CO_2. This supposition is supported by Density Functional Theory calculations, which indicate that **2a** is stabilized by 18.2 kcal/mol with respect to its zwitterionic constitutional isomer **2a*** (Scheme 3.2). In the absence of cyclohexyl migration, the formation of **2a*** from ^{Cy2}BIM (**1a**) and CO_2 is computed to be enthalpically favored by 12.7 kcal/mol, indicating that the cyclohexyl migration event provides significant stabilization to the resulting adduct, and as such represents a substantial portion of the driving force toward irreversible CO_2 capture.

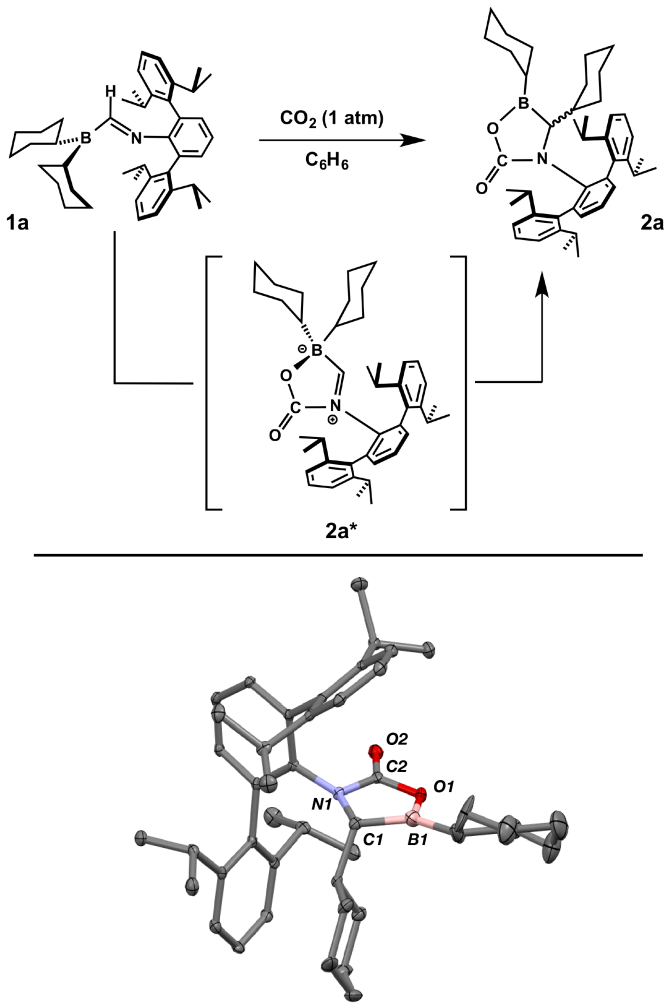

Figure 3.1. Synthesis (top) and molecular structure (bottom) of **2a**.

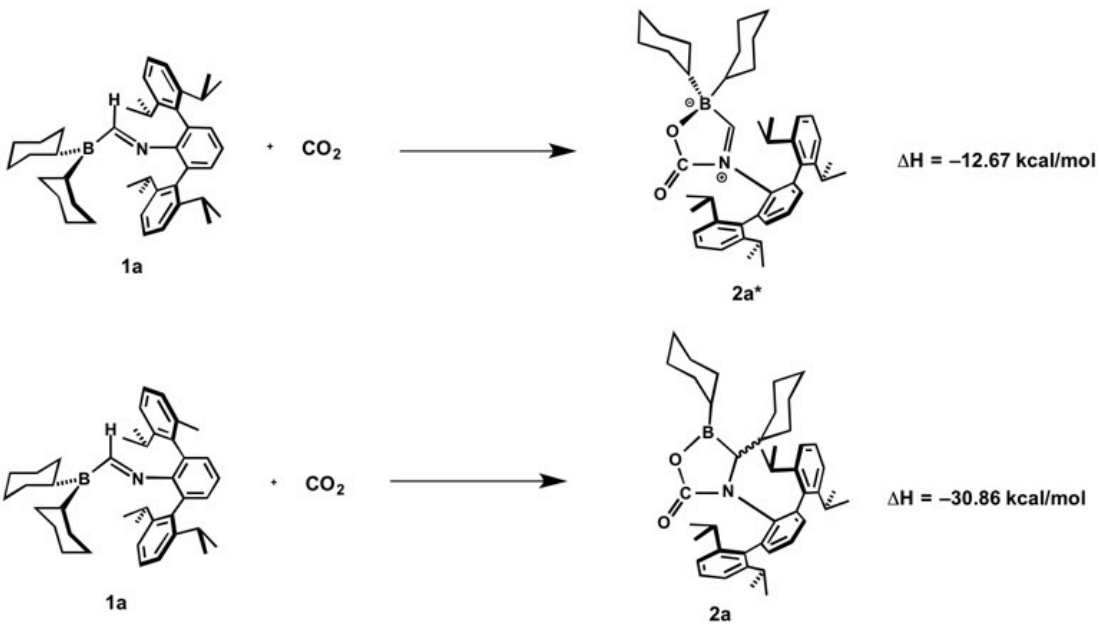

Scheme 3.2. Calculated enthalpies of reaction in the formation of **2a*** and **2a** from ^{Cy2}BIM (**1a**) and CO_2.

Despite the widespread progress that has been made in recent years toward the FLP-mediated activation of unsaturated organic molecules,[5,6] examples of nitrile C≡N bond reduction remain extremely limited.[30] As most FLP systems utilize strongly Lewis acidic fluorinated aryl-borane or alane moieties, there is likely a thermodynamic preference toward formation of a Lewis adduct with the nitrile *in lieu* of addition to its triple bond. It is therefore remarkable that treatment of ^{Cy2}BIM (**1a**) with acetonitrile results in formation of the eneamine **3** (racemic mixture, Scheme 3.3 and Figure 3.2), which undoubtedly is derived from 1,2-addition to the nitrile functionality accompanied by tautomerization of the resultant imine. Pursuant to this is the observation that benzonitrile, which lacks hydrogen atoms at the carbon *alpha* to the nitrile group, is similarly activated by ^{Cy2}BIM (**1a**) to give the 1,2-addition product imine (**4**, racemic mixture, Scheme 3.3 and Figure 3.3). Both transformations are essentially complete upon

mixing as evidenced by an immediate decoloration of the reaction solutions upon nitrile addition. We suggest that the observed activity of ^{Cy2}BIM (**1a**) toward nitriles is largely due the presence of a relatively weakly Lewis acidic –BCy_2 fragment that decreases the stabilization associated with formation of a nitrile-borane adduct. As is the case with CO_2 activation, the cyclohexyl migration event in the formation of **3** and **4** likely provides further driving force toward 1,2-addition to the nitrile.

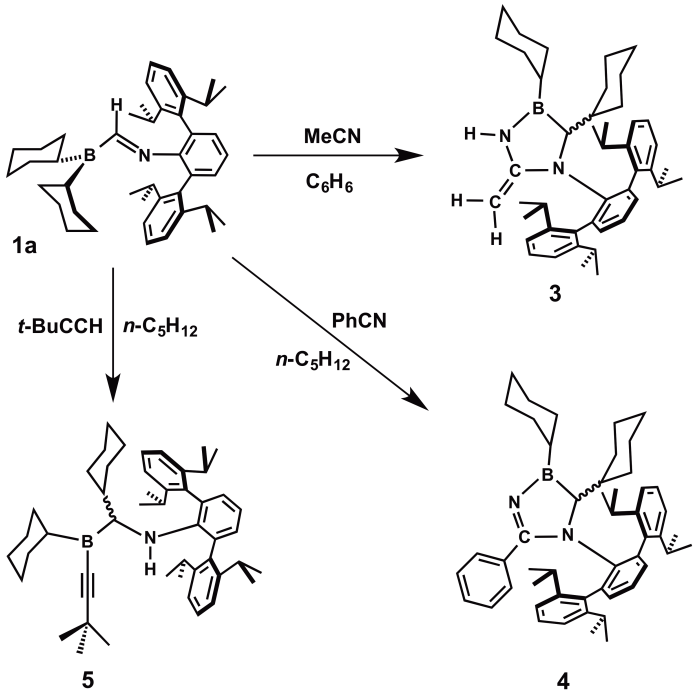

Scheme 3.3. Activation of MeCN, PhCN and *t*-BuCCH by ^{Cy2}BIM (**1a**).

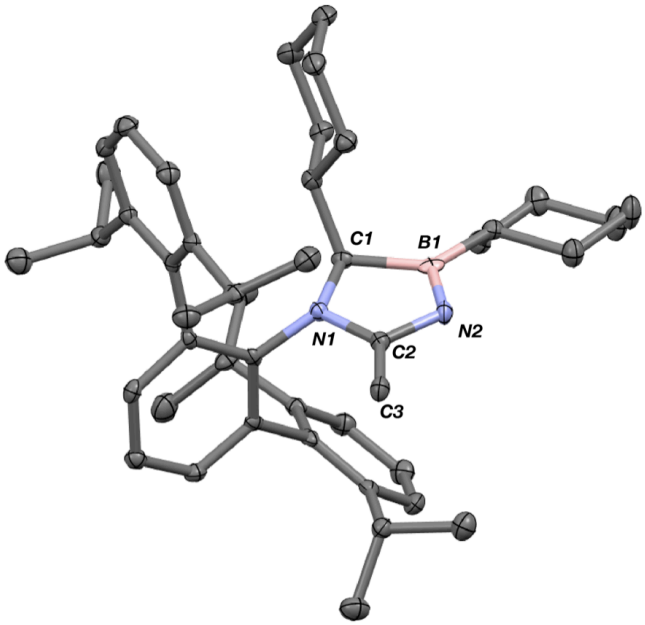

Figure 3.2. Molecular structure of **3** • 1.5 C_6H_6. Co-crystallized benzene molecules have been omitted for clarity. Selected bond distances (Å) and angles (º): C2-C3 = 1.332(3); C2-N2 = 1.399(3); N2-B1 = 1.396(3); B1-C1 = 1.592(3); C1-N1 = 1.487(3); N1-C2 = 1.402(3). N1-C2-C3 = 128.1(2); N1-C2-N2 = 107.7(2); C3-C2-N2 = 124.3(2).

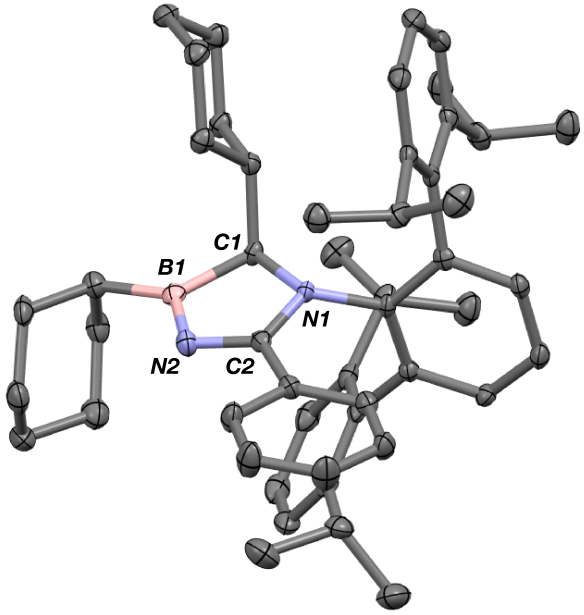

Figure 3.3. Molecular structure of **4**. Selected bond distances (Å) and angles (º): C2-N2 = 1.315(3); C2-N1 = 1.315(3); N2-B1 = 1.434(3); B1-C1 = 1.596(3); C1-N1 = 1.493(3). B1-N2-C2 = 107.6(2); N2-C2-N1 = 116.5(2).

^{Cy2}BIM (**1a**) is also reactive toward *t*-butylacetylene, effecting deprotonation of the acetylenic proton to give an alkynylborane as a racemic mixture (**5**, Scheme 3.3 and Figure 3.4). No evidence of products derived from 1,2-addition to the alkyne triple bond is seen. Both 1,2-addition and deprotonation reactions of terminal alkynes effected by FLPs have been reported,[31-36] although *t*-butylacetylene appears to typically undergo preferential deprotonation, likely due to the steric encumbrance that the *t*-butyl group imposes at the internal *sp* carbon atom.

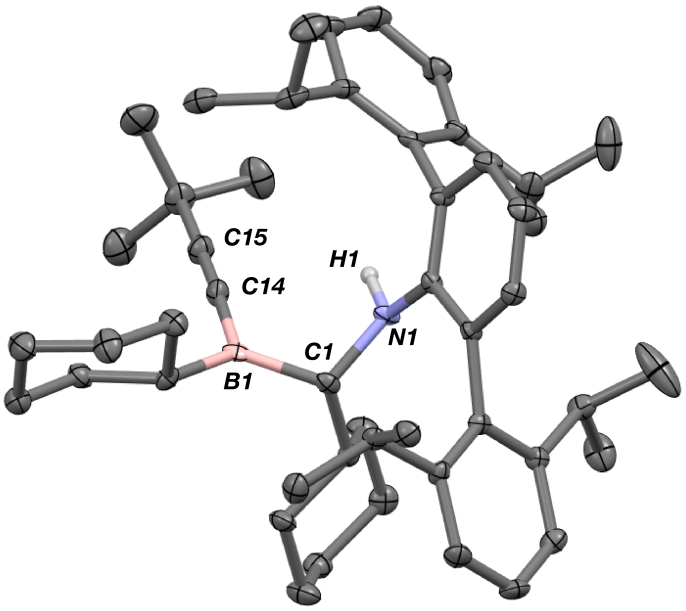

Figure 3.4. Molecular structure of (Cy)((CH$_3$)$_3$CC≡C)BCH(Cy)NHAr^{Dipp2} **(5)**. Selected bond distances (Å) and angles (º): N1-C1 = 1.485(4); C1-B1 = 1.579(5); B1-C14 = 1.522(5); C14-C15 = 1.211(4). B1-C1-N1 = 111.1(2).

3.3. Synthesis of a (boryl)iminomethane bearing a tethered organic backbone and examination of its FLP reactivity

In an effort to explore the generality of (boryl)iminomethane formation via isocyanide hydroboration, we targeted the synthesis of a BIM derived from 9-borabicyclo[3.3.1]nonane (9-BBN), due to both its commercial availability and the presence of a tethered carbon backbone. The latter trait was particularly attractive, as we envisioned that it might discourage 1,2-alkyl migration in the corresponding BIM.[37] Carrying out the reaction of $CNAr^{Dipp2}$ with 0.5 equivalents of 9-BBN dimer in the presence of THF allows for the hydroboration reaction to proceed smoothly to the THF-complexed (boryl)iminomethane $^{9\text{-BBN}}$BIM·THF (**1b**·THF, Scheme 3.4), which has been structurally characterized (Figure 3.5). The boron atom is oriented *syn* to the nitrogen lone pair across the imine double bond, as is seen with ^{Cy2}BIM (**1a**). The ^{11}B NMR spectrum of **1b**·THF features a singlet at 7.5 ppm, suggesting that the dative THF-borane interaction remains intact in solution. Indeed, successive *n*-pentane washes and exposure to high vacuum fail to liberate THF from **1b**·THF. Attempts to synthesize **1b** in the absence of THF resulted in the formation of several products. Although complete separation of these mixtures has proven unsuccessful, one of these species (**6**) was identified as the product of formal 1,1 and 1,2-double hydroboration of $CNAr^{Dipp2}$ by an independent synthesis (Scheme 3.4 and Figure 3.6). Presumably, this reaction proceeds via initial hydroboration of $CNAr^{Dipp2}$ to give the (boryl)iminomethane $^{9\text{-BBN}}$BIM (**1b**) which, in the presence of additional 9-BBN, undergoes hydroboration of its imine functionality to furnish **6**. Indeed, addition of 9-BBN dimer to **1b**·THF in benzene

solution results in conversion to **6** with release of THF (Scheme 3.4), lending credence to this proposed mechanistic pathway.

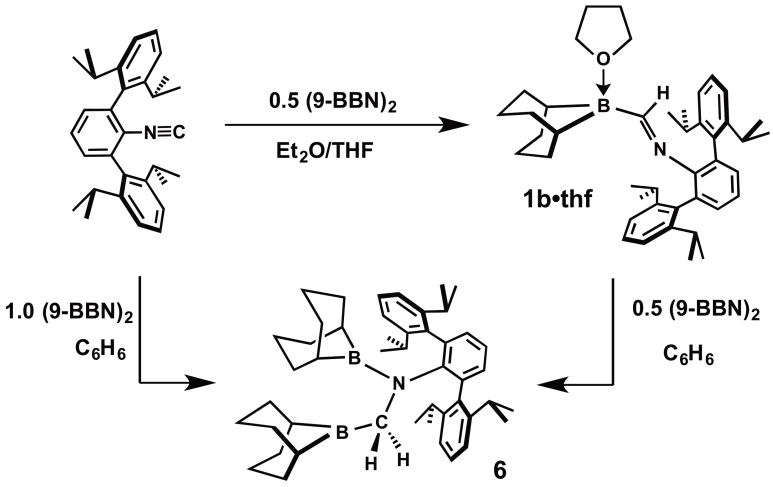

Scheme 3.4. Single- and double-hydroboration of $CNAr^{Dipp2}$ with 9-borabicyclo[3.3.1]nonane (9-BBN).

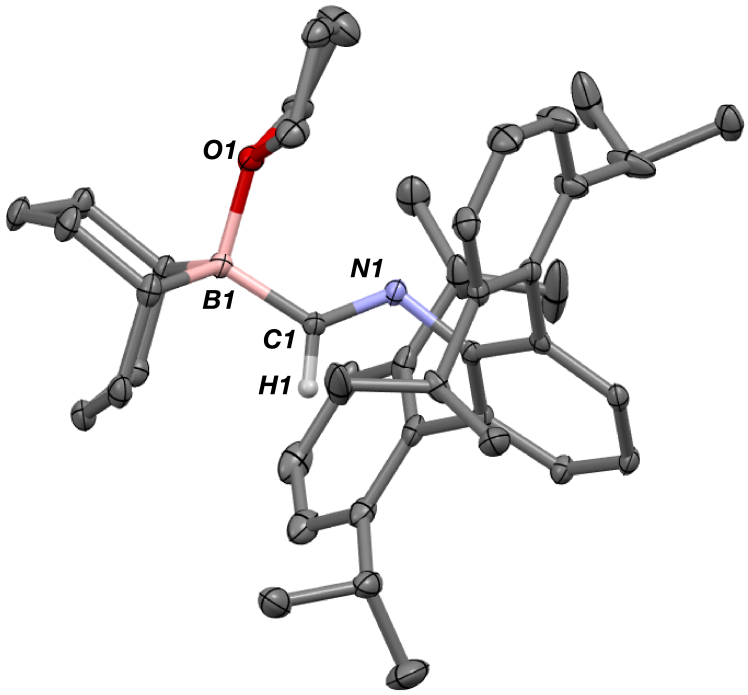

Figure 3.5. Molecular structure of $^{9\text{-BBN}}$BIM•THF • 1.5 (C_6H_6) (**1b•THF** • 1.5 (C_6H_6)). Co-crystallized benzene molecules have been omitted for clarity. Selected bond distances (Å) and angles (º): B1-O1 = 1.631(2); B1-C1 = 1.613(2); C1-N1 = 1.280(2); B1-C1-N1 = 125.8(1); C1-B1-O1 = 106.7(1).

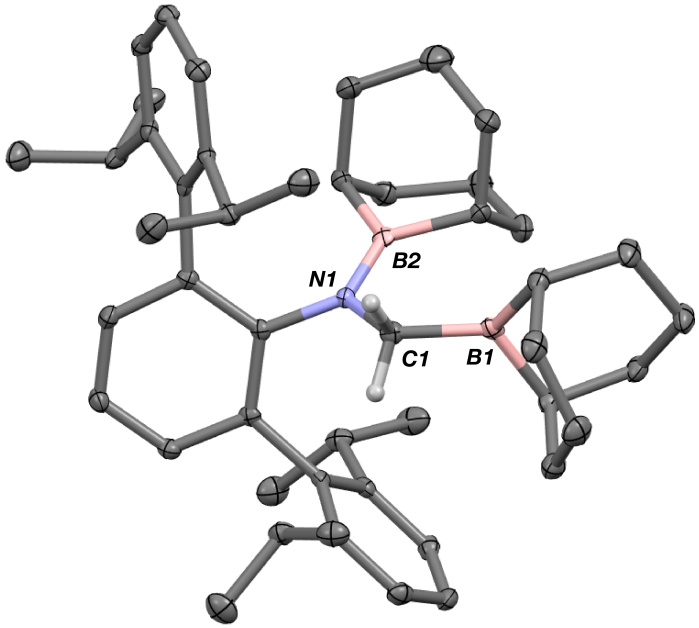

Figure 3.6. Molecular structure of (9-BBN)CH_2N(9-BBN)Ar^{Dipp2} • C_5H_{12} (**6** • C_5H_{12}). Co-crystallized molecules of *n*-pentane have been omitted for clarity. Selected bond distances (Å) and angles (º): B1-C1 = 1.600(3); C1-N1 = 1.490(2); N1-B2 = 1.406(3); B1-C1-N1 = 119.2(2); B2-N1-C1 = 120.1(2).

Despite the THF-complexed nature of the borane unit in $^{9\text{-BBN}}$BIM·THF (**1b**·THF), Frustrated Lewis pair reactivity is still accessible. Addition of CO_2 to a benzene solution of **1b**·THF results in immediate and irreversible conversion to a new product (**2b**, racemic mixture, Scheme 3.5) with liberation of one equivalent of THF as assayed by ^{1}H NMR. This product displays a ^{11}B NMR resonance at 55.7 ppm indicating the presence of a three-coordinate boron center.[38] Crystallographic characterization of **2b** (Figure 3.7) revealed the formation of a boralactone where the bicycloalkyl has undergone a ring expansion to produce a substituted 9-borabicyclo[3.3.2]decane structure. Concomitant with this process is the eradication of the imine C=N double bond. The ring expansion process of the bicycloalkyl group, which has been observed in other systems containing the 9-BBN framework,[39-43] amounts to a 1,2-alkyl shift that is

analogous to the cyclohexyl migration seen in reactions of ^{Cy2}BIM (**1a**). DFT calculations indicate that this ring expansion process is favored by 9.64 kcal/mol (Scheme 3.6). Importantly, this value is approximately half of that seen for ^{Cy2}BIM in the formation of **2a**, suggesting that the ring strain engendered by the formation of **2b** does indeed decrease the driving force associated with alkyl group migration. However, migration does appear to be general to the $^{9\text{-BBN}}$BIM framework, as ring expansion also occurs upon the heterolytic H-O bond cleavage of water by $^{9\text{-BBN}}$BIM·THF (**1b**·THF) to give the borinic acid **7** (racemic mixture, Scheme 3.5 and Figure 3.8). These results indicate that a more judicious choice of borane substituents will be required if alkyl migration is to be circumvented in the reaction chemistry of (boryl)iminomethanes.

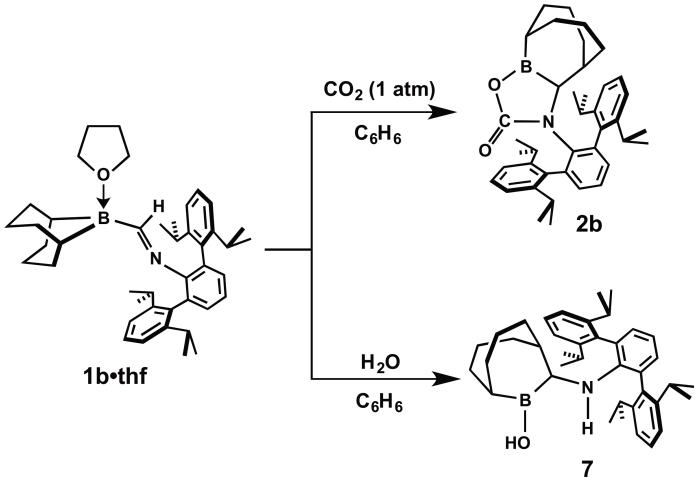

Scheme 3.5. CO_2 activation and heterolytic H-O cleavage of water by **1b**·THF.

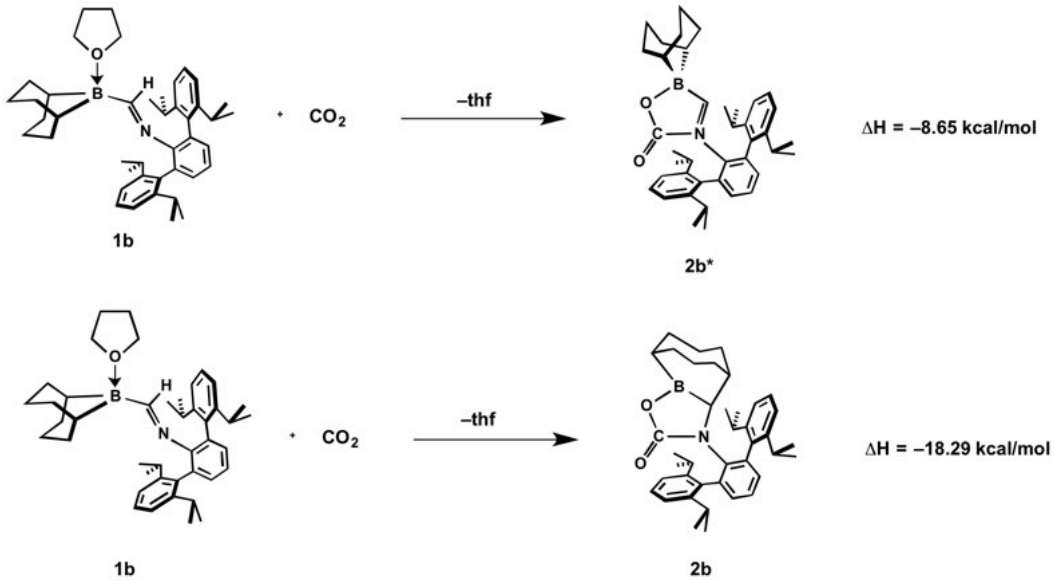

Scheme 3.6. Enthalpies of reaction in the formation of **2b*** and **2b** from $^{9\text{-BBN}}$BIM•THF (**1b•THF**) and CO_2.

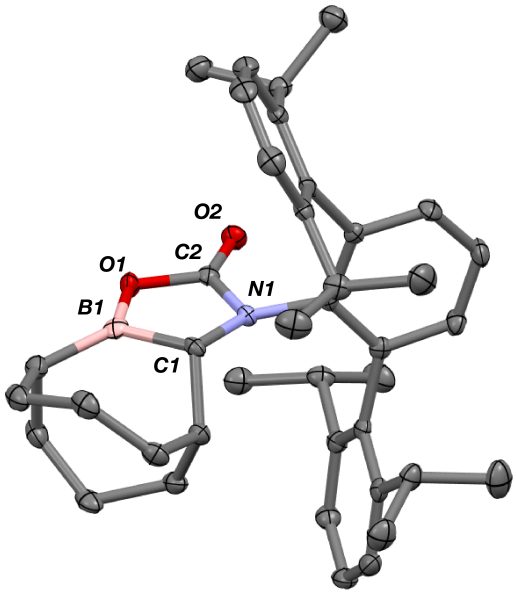

Figure 3.7. Molecular structure of **2b**. Selected bond distances (Å) and angles (º): C2-O1 = 1.389(2); C2-O2 = 1.202(2); C2-N1 = 1.365(2); O1-B1 = 1.381(2); N1-C1 = 1.480(2); C1-B1 = 1.576(2); N1-C2-O2 = 128.5(1); N1-C1-O1 = 110.1(1); O1-C2-O2 = 121.4(1).

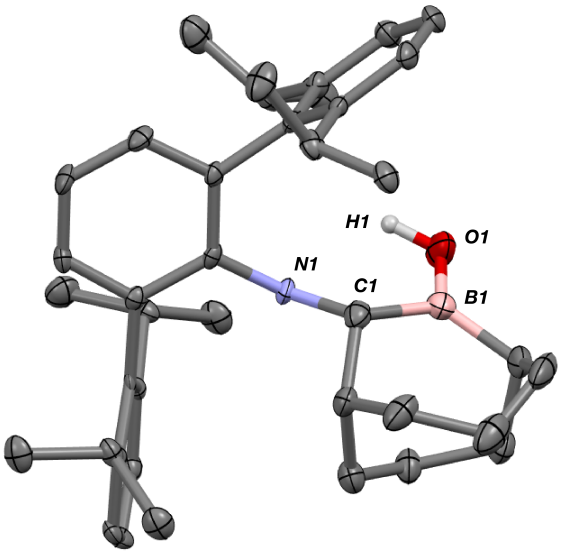

Figure 3.8. Molecular structure of **7**. Selected bond distances (Å) and angles (º): O1-B1 = 1.358(6); B1-C1 = 1.598(6); C1-N1 = 1.477(5). B1-C1-N1 = 109.1(3).

3.4. Synthesis of a (boryl)iminomethane bearing a borane unit of weak Lewis acidity

The dialkylboryl substituents in the (boryl)iminomethanes **1a** and **1b** are among the most weakly Lewis acidic components of a Frustrated Lewis Pair reported to date.[44,45] The competency of **1a** and **1b** to effect FLP-type reactivity is undoubtedly tied to the geminal relationship of the acidic and basic sites, as well as the rigid geometry enforced by the imine double bond, the same structural traits that allow (boryl)iminomethanes to foster reverse-dative σ-interactions between a Lewis-basic metal center and the borane unit.[16] In order to test the limits of this approach, we synthesized the pinacolboryl-substituted ^{Pin}BIM (**1c**; Figure 3.9), which contains a boron center of even further attenuated Lewis acidity. Unlike the syntheses of **1a** and **1b**, the use of excess borane and prolonged heating are required to drive the formation of **1c** to completion. Fractional

crystallization from *n*-pentane/hexamethyldisiloxane mixtures allows for isolation of analytically pure samples of ^{Pin}BIM (**1c**) in modest yields. Examination of the crystal structure of **1c** reveals a *syn* orientation of the imine lone pair and boron atom, as well as a nearly planar orientation of the C(H)N-BO_2 units (dihedral angle = 5.8(2)˚). Interestingly, the presence of the more weakly Lewis acidic pinacolboryl group inhibits the reactivity of the (boryl)iminomethane framework with CO_2, as ^{Pin}BIM (**1c**) and CO_2 fail to react under the conditions utilized in the syntheses of **2a** and **2b**. Furthermore, in the presence of CO_2 (1 atm), a broadening of signals suggestive of reversible formation of a CO_2 adduct is not observed by ^{1}H NMR spectroscopy. These observations seemingly suggest that more strongly Lewis acidic groups are necessary for stoichiometric FLP-type reactivity to occur between (boryl)iminomethanes and CO_2.[46]

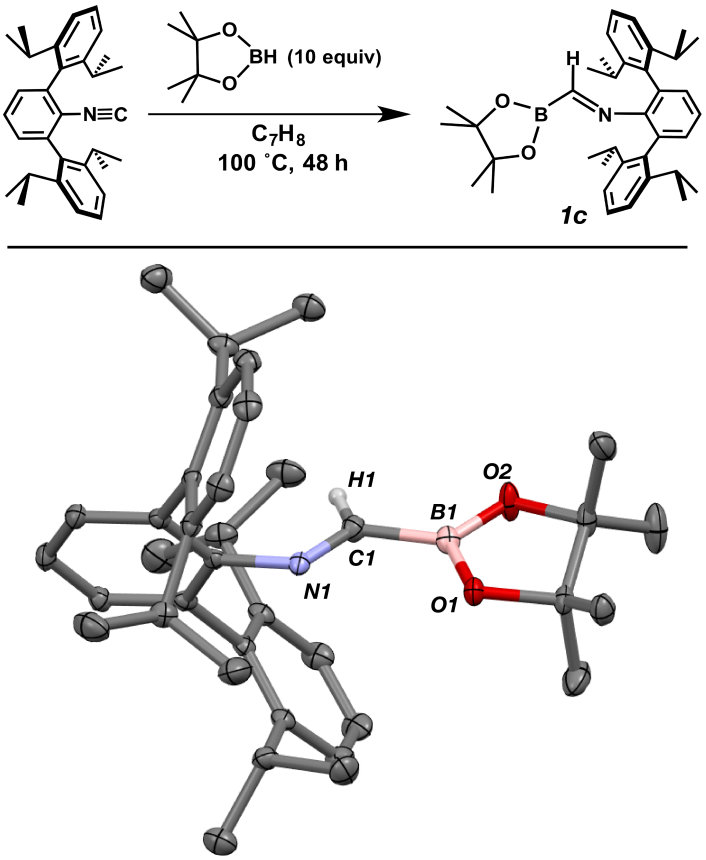

Figure 3.9. Synthesis (top) and molecular structure (bottom) of ^{Pin}BIM (**1c**). Selected bond distances (Å) and angles (º): N1-C1 = 1.275(2); C1-B1 = 1.570(2); B1-O1 = 1.356(2); 1.353(2); N1-C1-B1 = 119.2(1).

3.5. Concluding remarks

In conclusion, we have synthesized a series of ambiphilic and monomeric (boryl)iminomethanes (BIMs) via the 1,1-hydroboration of an *m*-terphenyl isocyanide. The same structural and electronic properties that allow (boryl)iminomethanes to behave as LZ-type chelating ligands toward electron-rich transition metal centers also promote the activation of unsaturated and protic substrates in an FLP manner. While this reactivity is accessible when a BIM bears a moderately Lewis acidic dialkylboryl group,

switching to the more weakly Lewis acidic pinacolboryl substituent inhibits reactivity with carbon dioxide. Further explorations of such weakly Lewis acidic (boryl)iminomethanes are currently being pursued, with an eye toward tailoring them to effect catalytic transformations of small molecules.

3.6. Synthetic procedures and characterization data

General considerations. All manipulations were carried out under an atmosphere of purified dinitrogen using standard Schlenk and glovebox techniques. Unless otherwise stated, reagent-grade starting materials were purchased from commercial sources and either used as received or purified by standard procedures.[47] Solvents were dried and deoxygenated according to standard procedures.[48] Benzene-d_6 (Cambridge Isotope Laboratories) was distilled from NaK alloy and stored over 4 Å molecular sieves under N_2 for at least 24 h prior to use. Celite 405 (Fisher Scientific) was dried under vacuum (24 h) at a temperature above 250 ˚C and stored in the glovebox prior to use. The (boryl)iminomethane[16] ^{Cy2}BIM and *m*-terphenyl isocyanide[17] CNAr^{Dipp2} were prepared as previously reported.

Solution ^{1}H, ^{13}C{^{1}H} and ^{11}B NMR spectra were recorded on a Bruker Avance 300, a Varian Mercury 400, a Jeol ECA 500, or a Varian X-SENS 500 spectrometer. ^{1}H and ^{13}C{^{1}H} chemical shifts are reported in ppm relative to $SiMe_4$ (^{1}H and ^{13}C δ = 0.0 ppm) with reference to residual solvent resonances of 7.16 ppm (^{1}H) and 128.06 ppm (^{13}C) for C_6D_6. ^{11}B NMR chemical shifts were referenced externally to a solution of phenylboronic acid in acetone-d_6 (δ = 29 ppm vs. $BF_3 \cdot Et_2O$ (δ = 0.0 ppm)). FTIR spectra were recorded on a Thermo-Nicolet iS10 FTIR spectrometer. Samples were prepared as

C_6D_6 solutions injected into a ThermoFisher solution cell equipped with KBr windows. For solution FTIR spectra, solvent peaks were digitally subtracted from all spectra by comparison with an authentic spectrum obtained immediately prior to that of the sample. The following abbreviations were used for the intensities and characteristics of important IR absorption bands: vs = very strong, s = strong, m = medium, w = weak, vw = very weak; b = broad, vb = very broad, sh = shoulder. High-resolution mass spectrometry (HRMS) was performed using an Agilent 6230 ESI-TOFMS instrument running in positive ion mode. Combustion analyses were performed by Robertson Microlit Laboratories of Madison, NJ (USA).

Synthesis of Boralactone 2a. A benzene solution of ^{Cy2}BIM (0.102 g, 0.170 mmol, 3 mL) was placed in an ampoule, degassed, and exposed to CO_2 gas (1 atm). Upon thawing the solution instantly changed in color from yellow to colorless. The ampoule was intermittently shaken over the course of 10 min, whereupon all volatiles were removed *in vacuo*. Dissolution of the resulting residue in 1 mL *n*-pentane and storage at –40 ˚C overnight provided colorless crystals, which were collected and dried *in vacuo*. Yield: 0.070 g, 0.108 mmol, 64%. ^{1}H NMR (499.8 MHz, C_6D_6, 20 ˚C): δ = 7.27 (t, 1H, *J* = 8 Hz, *p*-Ar), 7.25-7.18 (m, 5H), 7.11 (t, 1H, *J* = 8 Hz, *p*-Ar), 7.08 (dd, 1H, *J* = 8, 1 Hz, *m*-Ar), 7.02 (dd, 1H, *J* = 7, 3 Hz, *m*-Ar), 4.01 (septet, 1H, *J* = 7 Hz, C*H*$(CH_3)_2$), 3.32 (septet, 1H, *J* = 7 Hz, C*H*$(CH_3)_2$), 3.04 (d, 1H, *J* = 3 Hz, B-C*H*(Cy)-N), 2.59 (septet, 1H, *J* = 7 Hz, C*H*$(CH_3)_2$), 2.41 (septet, 1H, *J* = 7 Hz, C*H*$(CH_3)_2$), 1.69 (bd, 2H, *J* = 14 Hz, Cy), 1.58-1.49 (m, 6H, Cy), 1.55 (d, 3H, *J* = 7 Hz, CH(C*H*$_3)_2$), 1.48 (d, 3H, *J* = 7 Hz, CH(C*H*$_3)_2$), 1.39-1.32 (m, 2H, Cy), 1.30 (d, 3H, *J* = 7 Hz, CH(C*H*$_3)_2$), 1.28 (d, 3H, *J* = 7 Hz, CH(C*H*$_3)_2$), 1.18-1.13 (m, 8H, Cy), 1.08 (d, 3H, *J* = 7 Hz, CH(C*H*$_3)_2$), 1.07 (d, 3H, *J*

= 7 Hz, CH(CH_3)$_2$), 1.00 (d, 3H, *J* = 7 Hz, CH(CH_3)$_2$), 0.93 (d, 3H, *J* = 7 Hz, CH(CH_3)$_2$), 0.83-0.77 (m, 2H, Cy), 0.50 (qt, 1H, *J* = 13, 2 Hz, Cy), 0.23 (qd, 1H, *J* = 12, 4 Hz, Cy) ppm. ^{13}C{^{1}H} NMR (125.7 MHz, C_6D_6, 20 ˚C): δ = 158.3 (*C*(=O)OR), 149.2, 149.1, 147.8, 146.7, 142.6, 141.7, 138.0, 137.7, 136.1, 132.1, 131.8, 129.2, 129.1, 126.7, 124.1, 123.4, 122.9, 122.2, 61.4, 38.0, 31.4, 31.2, 31.0, 30.8, 30.5, 30.4, 29.0, 27.9, 27.8, 27.0, 26.9, 26.9, 26.8, 26.8, 26.7, 26.6, 26.2, 26.2, 26.1 ppm. ^{11}B NMR (125.7 MHz, C_6D_6, 20 ˚C): δ = 54.8 (bs) ppm. FTIR (C_6D_6, KBr windows, 25 ˚C): 2962 (s), 2923 (vs), 2864 (m), 2853 (m), 1772 (vs), 1575 (w), 1460 (m), 1447 (m), 1420 (m), 1383 (w), 1360 (m), 1319 (w), 1304 (m), 1263 (w), 1245 (m), 1172 (m), 1166 (m), 1103 (m), 1070 (m), 1054 (w), 951 (m), 793 (w), 782 (w), 760 (m) cm^{-1}. Anal. Calc'd. for $C_{44}H_{60}NBO_2$: C, 81.84; H, 9.36; N, 2.17. Found: C, 81.81; H, 9.19; N, 2.18.

Synthesis of Exocyclic Enamine 3. To a benzene solution of ^{Cy2}BIM (0.100 g, 0.166 mmol, 3 mL) was added 0.10 mL of a 3.1 M acetonitrile solution in C_6H_6 (0.31 mmol, 1.9 equiv). The solution immediately changed in color from bright yellow to colorless. After stirring for 20 min, all volatiles were removed under reduced pressure. The resulting colorless solid was dissolved in 1 mL *n*-pentane and stored at –40 ˚C for 24 h, affording colorless crystals, which were collected and dried *in vacuo*. Yield: 0.083 g, 0.129 mmol, 78%. ^{1}H NMR (500.2 MHz, C_6D_6, 20 ˚C): δ = 7.32 (t, 1H, *J* = 8 Hz, *p*-Ar), 7.26-7.22 (m, 3H), 7.20-7.14 (m, 3H), 7.07 (dd, 1H, *J* = 8, 2 Hz, *m*-Ar), 7.02 (t, 1H, *J* = 8 Hz, *p*-Ar), 5.32 (s, 1H, N-*H*), 3.77 (septet, 1H, *J* = 7 Hz, C*H*(CH$_3$)$_2$), 3.40 (septet, 1H, *J* = 7 Hz, C*H*(CH$_3$)$_2$), 3.21 (d, 1H, *J* = 2 Hz, C_{alkene}-*H*), 3.19 (d, 1H, *J* = 2 Hz, C_{alkene}-*H*), 2.87 (d, 1H, *J* = 2 Hz, B-C*H*(Cy)-N), 2.78 (septet, 1H, *J* = 7 Hz, C*H*(CH$_3$)$_2$), 2.41 (septet, 1H, *J* = 7 Hz, C*H*(CH$_3$)$_2$), 1.63-1.56 (m, 7H, Cy), 1.48 (d, 3H, *J* = 7 Hz, CH(CH_3)$_2$), 1.45-

1.39 (m, 4H, Cy), 1.37 (d, 3H, J = 7 Hz, CH(CH_3)$_2$), 1.33 (d, 3H, J = 7 Hz, CH(CH_3)$_2$), 1.30 (d, 3H, J = 7 Hz, CH(CH_3)$_2$), 1.23 (d, 3H, J = 7 Hz, CH(CH_3)$_2$), 1.18 (d, 3H, J = 7 Hz, CH(CH_3)$_2$), 1.15-1.10 (m, 4H, Cy), 1.09 (d, 3H, J = 7 Hz, CH(CH_3)$_2$), 1.00-0.90 (m, 3H, Cy), 0.89 (d, 3H, J = 7 Hz, CH(CH_3)$_2$), 0.75 (m, 1H, Cy), 0.63-0.49 (m, 2H, Cy), 0.42 (m, 1H, Cy) ppm. $^{13}C\{^1H\}$ NMR (125.7 MHz, C_6D_6, 20 ˚C): δ = 158.1, 149.0, 148.6, 147.6, 146.9, 144.2, 143.4, 142.8, 139.5, 137.6, 133.0, 131.8, 128.7, 128.6, 125.0, 123.4, 123.1, 122.9, 122.2, 64.7, 64.5, 40.9, 31.9, 31.4, 31.2, 31.0, 30.7, 29.9, 29.6, 28.7, 28.3, 27.6, 27.5, 27.3, 27.2, 26.8, 26.6, 26.2, 26.2, 26.0, 24.6, 23.5, 22.7, 22.0 ppm. ^{11}B NMR (125.7 MHz, C_6D_6, 20 ˚C): δ = 48.0 (bs) ppm. FTIR (C_6D_6, KBr windows, 20 ˚C): ν(N-H) = 3440 cm^{-1}, also 2965 (s), 2924 (s), 2856 (m), 2852 (m), 1650 (s), 1602 (w), 1594 (w), 1574 (w), 1468 (m), 1448 (m), 1413 (m), 1382, 1363 (m), 1322 (m), 1302 (m), 1257 (m), 1213 (w), 1189 (w), 1178 (w), 1160 (w), 1128 (w), 1091 (w), 1072 (w), 1056 (w), 1036 (w), 1027 (w), 986 (w), 848 (w), 793 (w), 774 (w), 760 (m), 720 (w), 700 (w), 677 (w), 656 (w) cm^{-1}. HRMS (ESI-TOF): *m/z* calc'd for $C_{43}H_{64}N_2B$ $[M+H]^+$: 642.5193 Found: 642.5193. Anal. Calc'd for $C_{45}H_{63}N_2B$: C, 84.08; H, 9.88; N, 4.36. Found: C, 83.51; H, 9.92; N, 4.19.

Synthesis of imine 4. To an *n*-pentane solution of ^{Cy2}BIM (0.100 g, 0.166 mmol, 2 mL) was added benzonitrile via microsyringe (0.019 mL, 0.184 mmol, 1.1 equiv). The solution was stirred for 30 min, during which time a colorless solid precipitated out of the solution. This solid was isolated via decantation of the solvent and washed with a single portion of *n*-pentane (2 mL) and dried *in vacuo* to afford **4** as an analytically pure colorless solid. Yield: 0.091 g, 0.129 mmol, 78%. Crystals suitable for X-ray diffraction were grown from a 2:1 Et_2O/C_6H_6 solution stored at –40 ˚C. ^1H NMR (499.8 MHz, C_6D_6,

20 ˚C): δ = 9.31 (bs, 1H, *Ph*C(NAr)=N), 7.26-7.21 (m, 2H), 7.15-6.99 (m, 8H), 6.82 (bs, 1H, *Ph*C(NAr)=N), 6.18 (bs, 1H, *Ph*C(NAr)=N), 3.37 (d, 1H, *J* = 4 Hz, B-C*H*(Cy)-N), 3.02 (septet, 1H, *J* = 7 Hz, C*H*(CH_3)$_2$), 2.90 (septet, 1H, *J* = 7 Hz, C*H*(CH_3)$_2$), 2.76 (septet, 1H, *J* = 7 Hz, C*H*(CH_3)$_2$), 2.30 (septet, 1H, *J* = 7 Hz, C*H*(CH_3)$_2$), 2.23 (bd, 1H, *J* = 15 Hz, Cy), 2.06-1.90 (m, 2H, Cy), 1.76-1.62 (m, 4H, Cy), 1.53-1.38 (m, 7H, Cy), 1.43 (d, 3H, *J* = 7 Hz, CH(C*H*$_3$)$_2$), 1.31 (d, 3H, *J* = 7 Hz, CH(C*H*$_3$)$_2$), 1.22 (d, 2H, *J* = 14 Hz, Cy), 1.13-1.10 (m, 2H, Cy), 1.05 (d, 3H, *J* = 7 Hz, CH(C*H*$_3$)$_2$), 0.96 (d, 3H, *J* = 7 Hz, CH(C*H*$_3$)$_2$), 0.88 (d, 3H, *J* = 7 Hz, CH(C*H*$_3$)$_2$), 0.87 (d, 3H, *J* = 7 Hz, CH(C*H*$_3$)$_2$), 0.73 (d, 3H, *J* = 7 Hz, CH(C*H*$_3$)$_2$), 0.63 (d, 3H, *J* = 7 Hz, CH(C*H*$_3$)$_2$), 0.63-0.52 (m, 2H, Cy), 0.25-0.13 (m, 2H, Cy). *Note: Two phenyl resonances cannot be conclusively assigned. We believe these resonances are coincident with multiplets between 7.26-7.21 ppm and 7.15-6.99 ppm, which arise from terphenyl unit aryl resonances.* $^{13}C\{^1H\}$ NMR (125.8 MHz, C_6D_6, 20 ˚C): δ = 182.1 (*C*=N), 149.6, 148.4, 147.3, 147.1, 143.0, 142.0, 141.1, 138.4, 136.0, 134.8, 133.2, 133.1, 130.9, 129.3, 129.2, 126.4, 124.0, 123.3, 123.2, 122.6, 70.6, 38.7, 31.9, 31.5, 31.3, 31.0, 30.6, 29.9, 29.2, 28.6, 27.8, 27.6, 26.8, 26.6, 26.4, 26.1, 25.8, 25.5, 23.1, 22.7, 22.4, 21.7 ppm. ^{11}B NMR (125.7 MHz, C_6D_6, 20 ˚C): δ = 64.4 (bs) ppm. FTIR (C_6D_6, KBr windows, 25 ˚C): 2963 (s), 2924 (vs), 2864 (m), 2850 (m), 1578 (w), 1469 (s), 1445 (m), 1427 (m), 1407 (m), 1383 (w), 1361 (m), 1302 (m), 1251 (m), 1242 (m), 1184 (w), 1077 (w), 1057 (w), 1031 (w), 999 (w), 794 (w), 760 (m), 720 (m), 704 (m) cm^{-1}. HRMS (ESI-TOF, NCMe): *m/z* calc'd for $C_{50}H_{65}N_2B$: 704.5241. Found: 705.5321 $[M+H]^+$. Anal Calc'd for $C_{50}H_{65}N_2B$: C, 85.20; H, 9.29; N, 3.97. Found: C, 85.43; H, 9.11; N, 3.95.

Synthesis of (Cy)((CH_3)$_3$CC≡C)BCH(Cy)NHAr^{Dipp2} (5). To an *n*-pentane solution of ^{Cy2}BIM (0.075 g, 0.125 mmol, 2 mL) was added *t*-BuCCH (0.017 mL, 0.139 mmol, 1.1 equiv) via microsyringe. The solution was stirred for 15 min, whereupon all volatiles were removed *in vacuo*. The resulting residue was dissolved in 0.5 mL of 3:1 hexamethyldisiloxane/*n*-pentane and stored at –40 ˚C overnight, resulting in the formation of colorless crystals, which were collected and dried *in vacuo*. Yield: 0.063 g, 0.092 mmol, 74%. ^{1}H NMR (499.8 MHz, C_6D_6, 20 ˚C): δ = 7.32 (t, 2H, *J* = 8 Hz, *p*-Ar), 7.23 (d, 2H, *J* = 8 Hz, *m*-Ar), 7.22 (d, 2H, *J* = 8 Hz, *m*-Ar), 7.03 (d, 2H, *J* = 8 Hz, *m*-Ar), 6.78 (t, 1H, *J* = 8 Hz, *p*-Ar), 3.88 (d, 1H, *J* = 10 Hz, N-*H*), 3.18 (dd, 1H, *J* = 10, 8 Hz, B-C*H*(Cy)-N), 3.10 (septet, 4H, *J* = 7 Hz, C*H*(CH_3)$_2$), 1.84-1.81 (m, 2H, Cy), 1.76-1.42 (m, 8H, Cy), 1.43 (d, 6H, *J* = 7 Hz, CH(C*H*$_3$)$_2$), 1.39 (d, 6H, *J* = 7 Hz, CH(C*H*$_3$)$_2$), 1.38-1.05 (m, 8H, Cy), 1.12 (d, 6H, *J* = 7 Hz, CH(C*H*$_3$)$_2$), 1.10 (d, 6H, *J* = 7 Hz, CH(C*H*$_3$)$_2$), 1.04 (s, 9H, *t*-Bu), 1.00-0.82 (m, 4H, Cy) ppm. ^{13}C{^{1}H} NMR (125.7 MHz, C_6D_6, 20 ˚C): δ = 148.0, 147.9, 146.4, 138.8, 134.3, 132.4, 128.6, 126.8, 123.6, 123.5, 116.8, 87.8, 56.4, 44.6, 37.2, 31.8, 31.1, 30.9, 30.6, 30.5, 28.9, 28.6, 28.5, 27.9, 27.8, 27.4, 27.3, 27.1, 26.1, 26.0, 23.9, 23.6 ppm. ^{11}B NMR (125.7 MHz, C_6D_6, 20 ˚C): δ = 68.1 (bs) ppm. FTIR (C_6D_6, KBr windows, 25 ˚C): ν(N-H) = 3352 (w), also 2961 (s), 2926 (s), 2866 (m), 2849 (m), 2174 (w, sh), 2155 (w), 1669 (w), 1578 (w), 1491 (w), 1461 (m), 1444 (m), 1412 (m), 1379 (w), 1360 (m), 1258 (m), 1055 (w), 761 (m) cm^{-1}. Anal. Calc'd for $C_{49}H_{70}NB$: C, 86.05; H, 10.31; N, 2.05. Found: C, 85.68; H, 10.74; N, 2.07.

Synthesis of $^{9\text{-BBN}}$BIM·THF (1b·THF). CNAr^{Dipp2} (0.250 g, 0.590 mmol) was slurried in 5 mL Et_2O. To this slurry was added a solution of 9-BBN dimer in 4:1 Et_2O/THF (0.072 g, 0.295 mmol, 0.5 equiv, 5 mL) dropwise over the course of 5 min.

The solution was stirred for 2 h, whereupon the solvent was removed *in vacuo*. Dissolution of the resulting residue in 7 mL 2:1 Et_2O/C_6H_6 and storage at –40 ˚C for 4 days resulted in the production of colorless crystals, which were collected and dried *in vacuo*. Yield: 0.272 g, 0.441 mmol, 75%. ^{1}H NMR (499.8 MHz, C_6D_6, 20 ˚C): δ = 8.52 (s, 1H, C_{imine}-*H*), 7.23 (t, 2H, *J* = 8 Hz, *p*-Dipp), 7.18 (d, 2H, *J* = 8 Hz, *m*-Ar), 7.12 (d, 4H, *J* = 8 Hz, *m*-Dipp), 7.04 (t, 1H, *J* = 8 Hz, *p*-Ar), 3.51 (m, 4H, THF), 3.03 (septet, 4H, *J* = 7 Hz, C*H*$(CH_3)_2$), 2.12 (m, 2H, 9-BBN), 1.80 (m, 4H, 9-BBN), 1.67 (m, 2H, 9-BBN), 1.48 (m, 4H, 9-BBN), 1.25 (d, 12H, *J* = 8 Hz, CH(C*H*$_3)_2$), 1.13 (d, 12H, *J* = 8 Hz, CH(C*H*$_3)_2$), 0.80 (bs, 2H, 9-BBN) ppm. ^{13}C{^{1}H} NMR (125.7 MHz, C_6D_6, 20 ˚C): δ = 193.5 (*C*$_{imine}$), 153.5, 146.8, 139.0, 131.7, 130.9, 127.9, 122.8, 122.5, 70.2, 31.8, 30.9, 25.5, 25.0, 24.5, 23.6, 22.8 ppm. ^{11}B NMR (125.7 MHz, C_6D_6, 20 ˚C): δ = 7.5 (s) ppm. FTIR (C_6D_6, KBr windows, 25 ˚C): 2961 (s), 2921 (m), 2867 (m), 2852 (m, sh), 2838 (m, sh), 1601 (m), 1577 (m), 1462 (m), 1450 (m, sh), 1415 (m), 1382 (w), 1361 (m), 1353 (w, sh), 1252 (w), 1205 (w), 1188 (w), 1178 (w), 1120 (w), 1071 (w), 1056 (w), 1043 (w), 1017 (w), 914 (w), 868 (m), 846 (w), 759 (m), 679 (w) cm^{-1}. Anal. Calc'd for $C_{43}H_{60}NBO$: C, 83.60; H, 9.79; N, 2.27. Found: C, 82.98; H, 9.70; N, 2.48.

Synthesis of (9-BBN)CH$_2$N(9-BBN)Ar^{Dipp2} (6). Benzene (5 mL) was added to solid CNAr^{Dipp2} (0.068 g, 0.160 mmol) and 9-BBN dimer (0.040 g, 0.164 mmol, 1.0 equiv). The solution was stirred over the course of 3 h and gradually changed in color from colorless to light yellow. All volatile materials were then removed *in vacuo*. The resulting solid was then extracted three times with *n*-pentane (2 mL), leaving behind **6** as an off-white solid, which was dried *in vacuo*. Yield: 0.066 g, 0.099 mmol, 62%. Crystals of **6** • C_5H_{12} suitable for X-ray diffraction were grown by storing an *n*-pentane solution at

–40 ºC overnight. ^{1}H NMR (499.8 MHz, C_6D_6, 20 ˚C): δ = 7.28 (t, 2H, *J* = 8 Hz, *p*-Ar), 7.23-7.21 (m, 4H), 7.17 (d, 2H, *J* = 8 Hz, *m*-Ar), 7.07 (t, 1H, *J* = 8 Hz, *p*-Ar), 3.45 (s, 2H, B-C*H*$_2$-N), 3.10 (septet, 2H, *J* = 7 Hz, C*H*(CH$_3$)$_2$), 3.07 (septet, 2H, *J* = 7 Hz, C*H*(CH$_3$)$_2$), 1.90-1.87 (m, 6H, BBN), 1.85-1.67 (m, 10H, BBN), 1.50-1.45 (m, 4H, BBN), 1.35-1.29 (m, 3H, BBN), 1.34 (d, 6H, *J* = 7 Hz, CH(C*H*$_3$)$_2$), 1.26 (d, 6H, *J* = 7 Hz, CH(C*H*$_3$)$_2$), 1.10 (d, 6H, *J* = 7 Hz, CH(C*H*$_3$)$_2$), 1.06 (d, 6H, *J* = 7 Hz, CH(C*H*$_3$)$_2$), 0.98-0.91 (m, 4H, Cy), –1.30 (s, 1H, BBN) ppm. ^{13}C{^{1}H} NMR (125.7 MHz, C_6D_6, 20 ˚C): δ = 147.1, 146.9, 146.8, 140.8, 137.8, 134.9, 128.4, 127.8, 127.7, 124.2, 123.6, 123.2, 49.0, 38.2, 34.1, 33.6, 33.1, 31.3, 31.0, 30.5, 30.2, 26.9, 26.1, 23.8, 23.5, 22.9, 22.7 ppm. ^{11}B NMR (125.7 MHz, C_6D_6, 20 ˚C): δ = 63.6 (bs), 46.8 (bs) ppm. FTIR (C_6D_6, KBr windows, 20 ˚C): 2961 (s), 2925 (s), 2899 (m, sh), 2886 (m, sh), 2870 (m, sh), 2844 (m), 2739 (b, m), 1616 (m), 1572 (w), 1551 (w), 1486 (w, sh), 1467 (m), 1450 (s), 1413 (m), 1398 (w, sh), 1383 (m), 1361 (w), 1275 (m), 1249 (m), 1184 (w), 1067 (w), 1053 (w), 1037 (w), 971 (w), 859 (w), 794 (w), 763 (m), 729 (w), 687 (w), 663 (w), 642 (w) cm^{-1}. Anal. Calc'd for $C_{47}H_{67}NB_2$: C, 84.55; H, 10.11; N, 2.10. Found: C, 85.02; H, 10.56; N, 2.00.

Synthesis of Boralactone 2b. A benzene solution of $^{9\text{-BBN}}$BIM·THF (0.114 g, 0.185 mmol, 5 mL) was placed in an ampoule, degassed, and exposed to 1 atm CO_2 gas. The ampoule was intermittently shaken over the course of 15 min, whereupon all volatiles were removed *in vacuo*. The resulting residue was washed with 3 mL *n*-pentane and dried *in vacuo*, affording **2b** as a colorless solid. Yield: 0.102 g, 0.173 mmol, 93%. Crystals suitable for X-ray diffraction were grown by storing an *n*-pentane solution at –40 ˚C overnight. ^{1}H NMR (499.8 MHz, C_6D_6, 20 ˚C): δ = 7.27-7.18 (m, 6H), 7.14-7.11 (m, 2H), 7.04 (dd, 1H, *J* = 7, 1 Hz), 3.83 (septet, 1H, *J* = 7 Hz, CH(CH$_3$)$_2$), 3.53 (septet, 1H, *J*

= 7 Hz, $CH(CH_3)_2$), 3.38 (d, 1H, *J* = 3 Hz, B-C*H*-N), 2.65 (septet, 1H, *J* = 7 Hz, $CH(CH_3)_2$), 2.43 (septet, 1H, *J* = 7 Hz, $CH(CH_3)_2$), 1.94 (m, 1H, bicycloalkyl), 1.67 (m, 2H, bicycloalkyl), 1.57 (d, 3H, *J* = 7 Hz, $CH(CH_3)_2$), 1.47 (d, 3H, *J* = 7 Hz, $CH(CH_3)_2$), 1.36-1.15 (m, 7H, bicycloalkyl), 1.33 (d, 3H, *J* = 7 Hz, $CH(CH_3)_2$), 1.19 (d, 3H, *J* = 7 Hz, $CH(CH_3)_2$), 1.08 (d, 3H, *J* = 7 Hz, $CH(CH_3)_2$), 1.05 (d, 3H, *J* = 7 Hz, $CH(CH_3)_2$), 1.04 (d, 3H, *J* = 7 Hz, $CH(CH_3)_2$), 0.96 (d, 3H, *J* = 7 Hz, $CH(CH_3)_2$), 0.92 (m, 2H, bicycloalkyl), 0.45 (m, 1H, bicycloalkyl), 0.11 (t, 1H, *J* = 14 Hz, bicycloalkyl) ppm. *Note: Peak assignments of bicycloalkyl backbone protons are tentative*. $^{13}C\{^1H\}$ NMR (125.7 MHz, C_6D_6, 20 ˚C): δ = 158.2 (B-*C*(O)-OR), 149.4, 149.3, 147.5, 147.0, 142.7, 141.7, 137.6, 136.9, 136.3, 132.3, 132.1, 129.4, 128.9, 126.6, 124.5, 123.7, 122.7, 121.8, 59.7, 31.8, 31.4, 31.4, 30.8, 28.4, 27.4, 27.2, 26.9, 26.4, 26.2, 25.3, 24.0, 23.7, 23.6, 23.3, 22.3, 22.1, 19.9 ppm. ^{11}B NMR (125.7 MHz, C_6D_6, 20 ˚C): δ = 55.7 (s) ppm. FTIR (C_6D_6, KBr windows, 20 ˚C): ν(C=O) = 1772 (vs) cm^{-1}, also 2960 (s), 2925 (s), 2865 (m), 1575 (w), 1466 (m), 1421 (m), 1384 (m), 1360 (m), 1326 (w), 1302 (m), 1293 (w, sh), 1263 (m), 1248 (w), 1239 (w), 1215 (w), 1171 (w), 1148 (w), 1112 (m), 1081 (w), 1067 (w), 1055 (w), 957 (w), 950 (w), 940 (w), 907 (w), 848 (w), 794 (w), 781 (w), 768 (w), 760 (m) cm^{-1}. Anal. Calc'd for $C_{40}H_{52}NBO_2$: C, 81.48; H, 8.89; N, 2.38. Found: C, 81.62; H, 9.40; N, 2.49.

Synthesis of borninic acid 7. To a benzene solution of $^{9\text{-BBN}}$BIM·THF (0.082 g, 0.133 mmol, 3 mL) was added deionized H_2O via microsyringe (0.010 mL, 0.556 mmol, 4.2 equiv). The solution was shaken intermittently over the course of 1 h, whereupon all volatiles were removed *in vacuo*. Dissolution of the resulting residue in 2 mL Et_2O and storage at –40 ˚C for 1 week produced colorless crystals, which were collected and dried

in vacuo. Yield: 0.012 g, 0.021 mmol, 16%. ^{1}H NMR (499.8 MHz, C_6D_6, 20 ˚C): δ = 7.29 (t, 2H, *J* = 8 Hz, *m*-Ar), 7.23 (dd, 2H, *J* = 8, 2 Hz, *m*-Ar), 7.19-7.17 (m, 4H), 6.95 (t, 1H, *J* = 8 Hz, *p*-Ar), 6.11 (bs, 1H, O-*H*), 3.38 (d, 1H, *J* = 11 Hz, N-*H*), 3.01 (septet, 2H, *J* = 7 Hz, C*H*$(CH_3)_2$), 2.99 (septet, 2H, *J* = 7 Hz, C*H*$(CH_3)_2$), 2.60 (dd, 1H, *J* = 11, 3 Hz, R_2B-C*H*R-NHAr), 2.07 (m, 1H, bicycloalkyl), 1.52-1.42 (m, 4H, bicycloalkyl), 1.39-1.30 (m, 6H, bicycloalkyl), 1.34 (d, 6H, *J* = 7 Hz, CH(C*H*$_3)_2$), 1.31 (d, 6H, *J* = 7 Hz, CH(C*H*$_3)_2$), 1.26-1.18 (m, 4H, bicycloalkyl), 1.07 (d, 6H, *J* = 7 Hz, CH(C*H*$_3)_2$), 1.06 (d, 6H, *J* = 7 Hz, CH(C*H*$_3)_2$) ppm. *Note: Peak assignments of bicycloalkyl backbone protons are tentative.* ^{13}C{^{1}H} NMR (125.7 MHz, C_6D_6, 20 ˚C): δ = 147.6, 147.4, 146.0, 137.6, 131.8, 129.1, 128.4, 127.6, 124.0, 123.6, 120.0, 38.6, 36.4, 34.0, 31.7, 31.2, 31.1, 30.3, 28.6, 27.0, 26.7, 26.4, 26.2, 25.0, 24.2, 23.4, 22.8, 21.4 ppm. ^{11}B NMR (125.7 MHz, C_6D_6, 20 ˚C): δ = 53.4 (s) ppm. FTIR (C_6D_6, KBr windows, 20 ˚C): ν(O-H) = 3485 (b, w) cm^{-1}, ν(N-H) = 3345 (w), also 2962 (s), 2925 (s), 2866 (m), 1578 (w), 1466 (m), 1417 (m), 1383 (m), 1361 (m), 1250 (w), 1229 (m), 1179 (w), 1117 (m), 1081 (w), 1055 (w), 1043 (w), 989 (w), 944 (w), 934 (w), 867 (w), 795 (w), 778 (w), 759 (m), 698 (w) cm^{-1}. Anal. Calc'd for $C_{39}H_{54}NBO$: C, 83.10; H, 9.66; N, 2.48. Found: C: 81.91; H, 9.99; N, 2.38.

Synthesis of ^{Pin}BIM (1c). A toluene (5 mL) solution of $CNAr^{Dipp2}$ (0.102 g, 0.240 mmol) and pinacolborane (0.34 mL, 2.33 mmol, 10.0 equiv) was placed in a sealed ampoule and heated to 100 ºC for 60 h. After cooling to room temperature, all volatiles were removed *in vacuo*. Fractional crystallization from 2:1 hexamethyldisiloxane/*n*-pentane solution provided light yellow crystals of ^{Pin}BIM, which were collected and dried *in vacuo*. Yield: 0.037 g, 0.067 mmol, 28%. ^{1}H NMR (499.8 MHz, C_6D_6, 20 ˚C): δ =

7.85 (s, 1H, C_{imine}-*H*), 7.24 (t, 2H, *J* = 8 Hz, *p*-Ar), 7.16 (d, 2H, *J* = 8 Hz, *m*-Ar), 7.15 (d, 4H, *J* = 8 Hz, *m*-Ar), 7.03 (t, 1H, *J* = 8 Hz, *p*-Ar), 3.05 (septet, 4H, *J* = 7 Hz, C*H*$(CH_3)_2$), 1.36 (d, 12H, *J* = 7 Hz, CH(C*H*$_3)_2$), 1.15 (d, 12H, *J* = 7 Hz, CH(C*H*$_3)_2$), 0.72 (s, 12H, Pin –CH_3) ppm. $^{13}C\{^1H\}$ NMR (125.7 MHz, C_6D_6, 20 ˚C): δ = 168.2 (C_{imine}), 153.4, 147.1, 136.8, 130.4, 130.0, 128.4, 124.0, 122.9, 83.8, 31.3, 25.3, 24.4, 23.5 ppm. ^{11}B NMR (125.7 MHz, C_6D_6, 20 ˚C): δ = 26.0 (bs) ppm. FTIR (C_6D_6, KBr windows, 20 ˚C): 2961 (s), 2926 (m), 2905 (m, sh), 2867 (m), 1577 (w), 1463 (m), 1420 (m), 1382 (s), 1372 (s), 1362 (s), 1278 (w, sh), 1262 (m), 1143 (m), 1055 (w), 968 (m), 896 (w), 850 (m), 835 (w), 791 (w), 769 (m), 758 (m), 733 (w) cm^{-1}. Anal. Calc'd for $C_{37}H_{50}NBO_2$: C, 80.56; H, 9.14; N, 2.54. Found: C, 80.21; H, 9.02; N, 2.55.

3.7. Details of DFT computational studies

General considerations. Density Functional Theory calculations on the (boryl)iminomethanes ^{Cy2}BIM (**1a**) and $^{9\text{-BBN}}$BIM•thf (**1b·thf**), their adducts with carbon dioxide **2a** and **2b**, and the putative zwitterionic intermediates in CO_2 capture **2a*** and **2b*** were performed with the Amsterdam Density Functional (ADF) program suite,[49,50] version 2013.99.[51] For all atoms, the triple-ζ Slater-type orbital TZ2P ADF basis set was utilized without frozen cores. The local density approximation (LDA) of Vosko, Wilk, and Nusair (VWN)[52] was coupled with the generalized gradient approximation (GCA) corrections described by Becke[53] and Perdew[54,55] for electron exchange and correlation, respectively. Crystallographic atomic coordinates were used as input where appropriate. Optimized geometries and molecular orbitals were visualized with the ADFView graphical routine of the ADF-GUI.[56]

Hardware Specifics. DFT calculations were performed on a home-built 72-CPU (1 x 8 master, 8 x 8 slave) Rocks 4.3 Linux cluster featuring Intel Xeon E5335 Quad-Core 2.00 GHz processors. Job control was implemented with the Sun Grid Engine v. 5.3.

Representative input file for geometry optimization

```
$ADFBIN/adf -n8 \
 <<< "
TITLE Cy2BIM

MAXMEMORYUSAGE 23000

RELATIVISTIC ZORA

CHARGE 0 0
SCF

DIIS
END

XC
 LDA VWN
 GGA Becke Perdew
END

SYMMETRY NOSYM
ATOMS
H      -1.15892094      -3.25104810      -4.63730701
C      -0.52407905      -1.69060415      -3.26787853
H      -0.41847060      -0.97243931      -4.10645783
N       0.88155178       0.00000000       0.88528208
C       0.00000000       0.00000000       0.00000000
H      -1.04854095       0.05622577       0.25650887
C       0.56444189       0.09400638       2.27792745
C       0.75511378      -1.02409897       3.10637211
C       0.52710315      -0.92040129       4.48490082
H       0.66963154      -1.77992666       5.12825826
C       0.10991052       0.29216261       5.03760380
H      -0.06259636       0.36871791       6.10316179
C      -0.10225978       1.40178466       4.21653546
H      -0.44118122       2.33150176       4.65622269
C       0.10874295       1.30914923       2.83248243
C       1.15506355      -2.32249853       2.52153558
C       2.53327358      -2.64565412       2.38166279
C       2.88610549      -3.89970013       1.84915900
H       3.92433520      -4.18481876       1.74627704
C       1.90872067      -4.80626085       1.45222364
H       2.19975227      -5.76730381       1.04873064
C       0.56078321      -4.48561035       1.57150012
```

H	-0.17145814	-5.21843429	1.25861398
C	0.15556621	-3.24310328	2.09347522
C	3.63809415	-1.67773440	2.80144882
H	3.21598878	-0.71192675	3.14940191
C	4.43459535	-2.24464902	3.97808068
H	3.75159600	-2.45770270	4.82585171
H	5.18684686	-1.50301045	4.32000989
H	4.96086390	-3.18085826	3.69532637
C	4.55590320	-1.32945322	1.62270874
H	5.13422528	-2.21638902	1.28455385
H	5.27444966	-0.53712551	1.92247621
H	3.95464725	-0.94430127	0.77238697
C	-1.33806829	-2.93155576	2.19940506
H	-1.50466883	-1.88627345	2.52774582
C	-2.00015597	-3.82535028	3.24971614
H	-3.06579137	-3.53974089	3.37319939
H	-1.49054594	-3.70094261	4.23090646
H	-1.95182871	-4.89389100	2.95279702
C	-2.04883486	-3.05818847	0.84212219
H	-2.08334846	-4.11321059	0.49840286
H	-1.52746924	-2.45198675	0.07368892
H	-3.09167930	-2.68245095	0.92338730
C	-0.19581332	2.47399767	1.96541389
C	-1.55150211	2.78726054	1.64767806
C	-1.81806609	3.90673722	0.83955178
H	-2.83482606	4.19100931	0.60445495
C	-0.78480050	4.67576627	0.32069477
H	-1.01167088	5.52632482	-0.30849467
C	0.53756298	4.36102904	0.60714427
H	1.31421770	4.98495909	0.18634634
C	0.85993497	3.27321101	1.43844868
C	-2.72862195	1.96677026	2.18211990
H	-2.37298558	1.03542257	2.66800320
C	-3.49498208	2.75885405	3.24724917
H	-2.80770598	3.06496654	4.06407832
H	-4.29706138	2.12829223	3.68737414
H	-3.95835984	3.66900600	2.80993689
C	-3.67947191	1.51097894	1.06358450
H	-4.24475762	2.36500441	0.63455269
H	-4.41357632	0.78118156	1.46840950
H	-3.11788379	1.01265515	0.24831831
C	2.32927041	3.01090216	1.76977849
H	2.43610017	2.14541076	2.45318476
C	2.95083373	4.20542112	2.50488065
H	3.00394619	5.09950393	1.85009987
H	3.98050322	3.95369621	2.83718455
H	2.34852528	4.45397115	3.40389539
C	3.13300506	2.66769444	0.50847661
H	2.69623625	1.78202616	0.00519797
H	4.18186908	2.42242876	0.78078141
H	3.14476063	3.51429742	-0.20920803
C	0.28809629	1.41671350	-2.24714587
H	0.59888948	2.17758096	-1.49613351
C	-1.17008165	1.72852310	-2.63642910
H	-1.81930137	1.68694754	-1.73517463

```
H      -1.54898308       0.98362524      -3.36757766
C      -1.28311752       3.13054472      -3.24854469
H      -2.33055865       3.30474180      -3.57711391
H      -1.03549208       3.89491420      -2.48008456
C      -0.34073736       3.28767909      -4.44865400
H      -0.40402043       4.32962705      -4.82928999
H      -0.66005000       2.60357138      -5.26616591
C       1.11051263       2.98021018      -4.05446682
H       1.75742797       3.05069193      -4.95592722
H       1.46710177       3.73367214      -3.31689293
C       1.22983814       1.57342238      -3.45489980
H       2.28274940       1.41194452      -3.13464149
H       0.98075955       0.83593081      -4.24569259
C       1.96492937      -1.70479532      -2.75039677
H       2.71492629      -1.58721402      -1.93803572
H       2.21731071      -0.98903351      -3.55683849
H      -1.53497027      -1.56043958      -2.82211754
B       0.41541297      -0.00000000      -1.49098107
C       0.55218677      -1.44267889      -2.19587006
H       0.38717551      -2.19247924      -1.39020926
C       2.06822679      -3.12851950      -3.31574882
H       3.07303430      -3.27327175      -3.76715152
H       1.95442817      -3.86734244      -2.49264840
C       0.99448142      -3.37746348      -4.38351246
H       1.06008651      -4.43098295      -4.73121379
H       1.17767652      -2.71617254      -5.25843852
C      -0.41092799      -3.11479983      -3.82677392
H      -0.63854277      -3.85084186      -3.02461192
END

GEOMETRY
 Iterations 300
 GO
END

BASIS
 type TZ2P
 core none
END

END INPUT
```

Optimized Cartesian coordinates of ^{Cy2}BIM (1a)

```
H       1.19986532      -3.88509636      -3.81435461
C       0.75129802      -1.96951364      -2.88968103
H       0.33970483      -1.55800104      -3.82836396
N       0.73124256      -0.17222877       0.80637146
C      -0.06232169       0.23260109      -0.12457379
H      -1.04635895       0.65489301       0.16055704
C       0.44233879      -0.00006303       2.16929775
C       0.52895396      -1.14858342       2.99674912
C       0.35862640      -1.01034366       4.37600140
```

H	0.41143779	-1.90134113	5.00107921
C	0.14866294	0.24245709	4.95232287
H	0.04562059	0.34110731	6.03163617
C	0.07568296	1.36782385	4.13570192
H	-0.08261665	2.35077537	4.57772726
C	0.19418814	1.27766254	2.74059870
C	0.78095663	-2.50982833	2.41498987
C	2.10450906	-3.00046050	2.33081219
C	2.31583720	-4.29577145	1.83928764
H	3.33322561	-4.68328449	1.76934004
C	1.25054912	-5.09759434	1.44067734
H	1.43260117	-6.10417031	1.06496355
C	-0.04981452	-4.60726631	1.52593782
H	-0.88132645	-5.24132796	1.21639318
C	-0.30787785	-3.31642369	2.00607910
C	3.30680953	-2.16195101	2.75199353
H	2.92725565	-1.20249196	3.12762082
C	4.09502764	-2.82437129	3.89692422
H	3.45446719	-3.01147300	4.76966481
H	4.92619108	-2.17765098	4.21476452
H	4.52274578	-3.78789948	3.58305445
C	4.22756092	-1.85320888	1.55711200
H	4.66133760	-2.77453261	1.14096968
H	5.05843377	-1.20425281	1.87113234
H	3.67201586	-1.34457961	0.75882347
C	-1.75199068	-2.83431814	2.11124036
H	-1.72636261	-1.74976941	2.28593151
C	-2.46687808	-3.47451724	3.31778516
H	-3.49593039	-3.09483492	3.40385796
H	-1.94245201	-3.25470477	4.25736960
H	-2.51577106	-4.56814037	3.20714857
C	-2.55711088	-3.07271767	0.82180075
H	-2.70074658	-4.14466199	0.62439962
H	-2.05566901	-2.63353613	-0.05100782
H	-3.55526222	-2.61974194	0.90941666
C	0.08121303	2.54530398	1.93827990
C	-1.19090021	3.13837452	1.74586295
C	-1.27498419	4.35800879	1.05855728
H	-2.25019536	4.82182533	0.90663530
C	-0.13698151	4.98649402	0.56530094
H	-0.22039370	5.93366483	0.03271202
C	1.11136014	4.39998093	0.75942892
H	1.99969322	4.90102040	0.37590139
C	1.24672519	3.18613554	1.44540900
C	-2.47710162	2.50543658	2.27453820
H	-2.22498440	1.50640712	2.65421210
C	-3.05646066	3.31420436	3.45190271
H	-2.33349626	3.40461456	4.27337517
H	-3.96161544	2.82866175	3.84542553
H	-3.32911583	4.33111036	3.13299072
C	-3.54433611	2.32551982	1.17992026
H	-3.89354406	3.29307170	0.79211386
H	-4.41897655	1.79696623	1.58570525
H	-3.15941178	1.74449378	0.33100047
C	2.63881112	2.61543441	1.70006203

H	2.53183860	1.53257907	1.84780401
C	3.24036559	3.20301993	2.99362150
H	3.36781865	4.29218681	2.90101069
H	4.22653262	2.75894661	3.19500408
H	2.59639316	3.00854947	3.86155565
C	3.60991222	2.81527625	0.52565483
H	3.18531547	2.44562907	-0.41724437
H	4.54331899	2.26783715	0.71640148
H	3.87719849	3.87297352	0.38809039
C	-0.38109073	1.31507595	-2.51674074
H	-0.48898978	2.21670251	-1.87669251
C	-1.84097291	0.79054313	-2.72114310
H	-2.28818773	0.49062397	-1.76146057
H	-1.81517376	-0.11549137	-3.35117518
C	-2.73323167	1.84626804	-3.39618560
H	-3.74197190	1.43364152	-3.55673442
H	-2.84536699	2.70502836	-2.71287025
C	-2.13675305	2.32981691	-4.72588408
H	-2.76965576	3.11817503	-5.16207328
H	-2.13670536	1.49345954	-5.44676427
C	-0.69870226	2.83590829	-4.54227010
H	-0.27236019	3.13210555	-5.51327630
H	-0.71172273	3.74375997	-3.91462596
C	0.19360766	1.77948451	-3.87007592
H	1.20638625	2.18495153	-3.73342666
H	0.29297208	0.91245998	-4.54497183
C	2.68957285	-0.33066645	-2.89740455
H	3.21725289	0.45654502	-2.33622755
H	2.35819645	0.12664953	-3.84269292
H	-0.10072010	-2.36753798	-2.31609935
B	0.39448800	0.24061630	-1.64423369
C	1.46453376	-0.83213434	-2.09241115
H	1.85086371	-1.30011063	-1.16873224
C	3.66161411	-1.47885784	-3.21457563
H	4.51748501	-1.10045359	-3.79567884
H	4.07140818	-1.87535003	-2.27018166
C	2.96121533	-2.61356413	-3.97765813
H	3.66079847	-3.44504621	-4.15577206
H	2.65486764	-2.24322659	-4.97209060
C	1.72126142	-3.11560984	-3.22283707
H	2.03543190	-3.59740152	-2.28209692

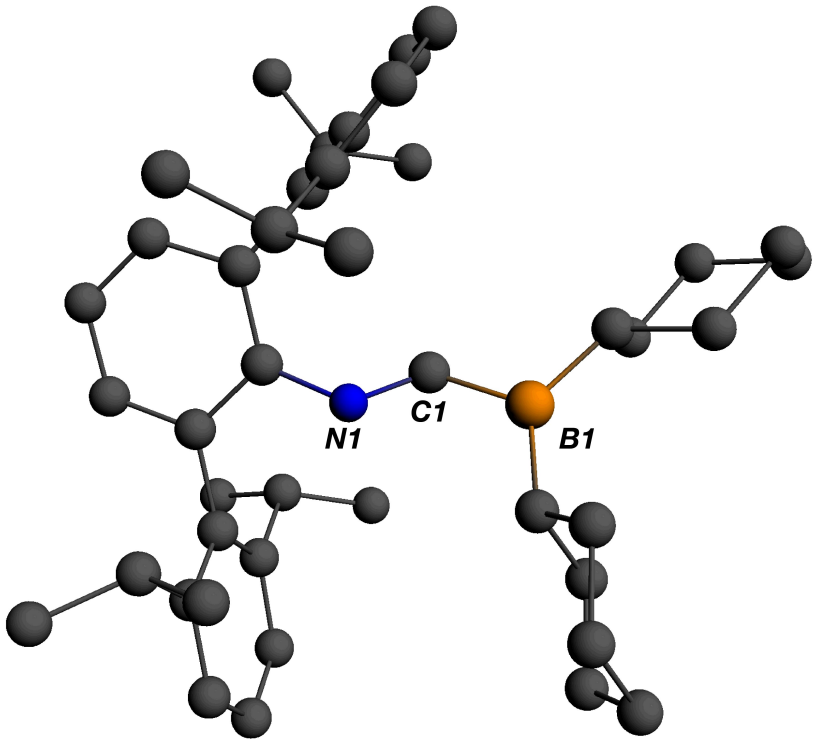

Figure 3.10. Optimized molecular structure of ^{Cy2}BIM (**1a**).

Optimized Cartesian coordinates of boralactone 2a

O	2.17797669	7.92519584	7.75093539
O	0.17421755	7.50062554	6.74431373
N	0.27864406	7.39559922	9.00940963
C	1.18605839	4.62214987	9.55793258
C	1.55410150	5.81429621	10.40584909
C	1.35309757	8.15967506	11.12393465
C	0.06617366	3.82866817	9.92726094
C	2.01215972	4.22594291	8.47671643
C	1.03406182	7.12107759	10.21261991
C	2.45526943	5.59420035	11.45588996
H	2.86286790	4.59337464	11.58967995
C	2.28833621	7.88913714	12.13527215
H	2.57151059	8.69985233	12.80415981
C	0.72157268	9.52954155	11.14897274
C	1.25734868	10.60191663	10.39561048
C	2.85056810	6.62893259	12.29640789
H	3.58181203	6.45002913	13.08334057
C	-0.34595668	9.76412421	12.05933564
C	-1.11645476	6.97426129	8.70784743
H	-1.25394278	5.93807021	9.05720446
C	-0.75937442	4.12539467	11.18000670
H	-0.69643488	5.20602480	11.37414331
C	-2.21798016	7.85776345	9.35291441
H	-1.95631150	7.98604839	10.41645268

C	1.00626160	7.64411065	7.86550988
C	3.31699780	4.94266738	8.13766620
H	3.28795153	5.93724898	8.59932192
C	-0.91317852	11.04426780	12.11894418
H	-1.73842510	11.23294860	12.80490751
C	-0.24521889	2.69901372	9.15905344
H	-1.10866508	2.08997141	9.42352235
C	0.65289721	11.86418065	10.49154744
H	1.05435890	12.69087409	9.90608544
C	-0.43384483	12.08542345	11.32962980
H	-0.89246671	13.07251667	11.38635841
C	-0.83518923	8.70079979	13.04626835
H	-0.55045219	7.71570141	12.65032904
C	2.53068395	10.45651654	9.57059087
H	2.69766160	9.38957791	9.38626444
C	1.65610206	3.08566123	7.73967976
H	2.27845110	2.78023134	6.89911417
C	0.53304270	2.33400108	8.06418020
H	0.27065521	1.45540243	7.47490284
C	-0.14494815	8.86881084	14.41766742
H	0.94696194	8.80700346	14.34067602
H	-0.48153770	8.08632863	15.11410953
H	-0.39789299	9.84632625	14.85476722
C	-2.35818488	8.69440089	13.25945536
H	-2.69789409	9.59512602	13.78997501
H	-2.64466891	7.83060644	13.87582299
H	-2.90731266	8.63493152	12.31225338
C	-2.30708688	9.25959065	8.71685918
H	-1.35216397	9.78926709	8.85101134
H	-2.46483140	9.15120849	7.62665165
C	-0.17415610	3.40315199	12.41219968
H	-0.19699386	2.31339379	12.26280898
H	-0.76519848	3.63796081	13.31006615
H	0.86445604	3.69928462	12.60318522
C	2.45138065	11.13999754	8.19570000
H	1.57534358	10.80306918	7.62748296
H	3.34434656	10.89123516	7.60656169
H	2.40642713	12.23580078	8.28280982
C	4.51859885	4.17795859	8.73205206
H	4.43707344	4.07119198	9.82209010
H	5.45470747	4.71213987	8.51275535
H	4.59336275	3.16861846	8.29960694
C	-3.58046801	7.13760872	9.29063551
H	-3.51780939	6.17963481	9.82833268
H	-3.81561538	6.89178137	8.24176229
C	3.52420069	5.15440289	6.62819546
H	3.67188883	4.20262916	6.09677174
H	4.42217700	5.76525150	6.46200194
H	2.67629018	5.68161504	6.17488650
C	-2.24668983	3.76001169	11.04232836
H	-2.68877801	4.16366494	10.12235487
H	-2.81141369	4.15672916	11.89725620
H	-2.39589667	2.67107344	11.03515177
C	3.74262165	10.99279514	10.36162893
H	3.63181628	12.06742762	10.57266517

H	4.66653746	10.85297529	9.78130294
H	3.86375053	10.47176030	11.32128139
C	-3.45958473	10.09773243	9.29186884
H	-3.24630307	10.32623813	10.34916992
H	-3.50916206	11.06551258	8.77021614
C	-4.72747809	7.98496429	9.86236405
H	-5.67999887	7.44512119	9.74694231
H	-4.57749705	8.12064808	10.94649395
C	-4.80370592	9.36318797	9.19029213
H	-5.60641817	9.96432503	9.64470781
H	-5.07151117	9.23356954	8.12691810
B	-1.07087935	7.02866005	7.10978177
C	-2.11276702	6.63721040	5.99598320
C	-3.57124807	4.75918670	5.04332220
C	-2.54670813	5.14914829	6.11975342
C	-1.61544342	6.93936953	4.56397129
C	-2.64292696	6.54001855	3.49537606
C	-3.05511220	5.06668608	3.62964658
H	-3.02592785	7.24234239	6.16851610
H	-4.50702564	5.31910997	5.21685915
H	-3.82187097	3.69080102	5.13500310
H	-1.65669320	4.50358142	6.02128499
H	-2.95983610	4.95437375	7.12054486
H	-0.67570361	6.39067378	4.38936990
H	-1.36316959	8.00537433	4.47081165
H	-2.23646953	6.73216146	2.49048549
H	-3.53927499	7.17671287	3.59758658
H	-2.18090150	4.42636095	3.41837487
H	-3.81992022	4.81145821	2.88010900

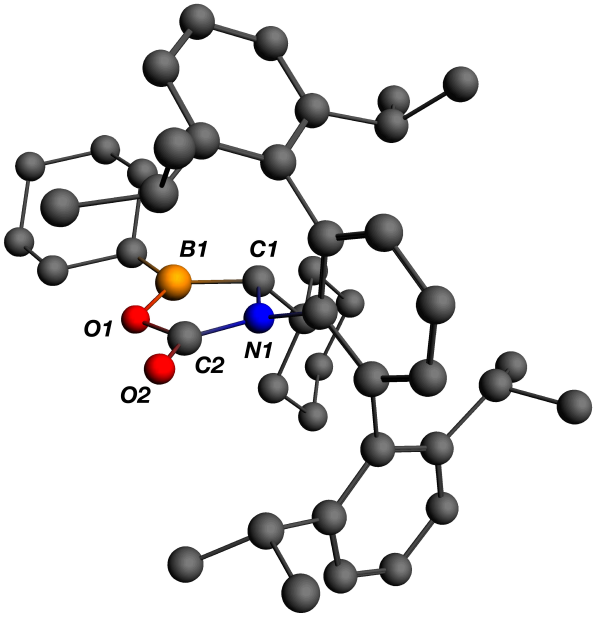

Figure 3.11. Optimized molecular structure of **2a**.

Table 3.1. Comparative metrical parameters between experimental (X-ray crystal structure) and calculated versions of **2a**.

Parameter	Exp. (X-ray)	Calculated	% Difference
C2-O1	1.391(3) Å	1.404 Å	0.9 %
C2-O2	1.198(3) Å	1.210 Å	1.0 %
C2-N1	1.367(3) Å	1.378 Å	0.8 %
O1-B1	1.378(4) Å	1.381 Å	0.2 %

Optimized Cartesian coordinates of putative zwitterionic boralactone 2a*

O	2.40394074	7.47023544	7.50703968
O	0.31976209	7.41350035	6.57665543
N	0.45665370	7.07765607	8.81779151
C	1.63115784	4.47790951	9.52572299
C	1.78205793	5.70953548	10.37412290
C	1.22420861	8.04689425	10.94323377
C	0.47315647	3.67430782	9.68735377
C	2.66475345	4.08159323	8.64237566
C	1.16229425	6.94030733	10.07156349
C	2.50933045	5.62481297	11.56879964
H	2.98393644	4.67791210	11.82000767
C	1.97262345	7.90661176	12.12059673
H	2.03525612	8.75642823	12.79841736
C	0.50121663	9.34314197	10.70438741
C	1.13269091	10.39064715	9.99099181
C	2.61908390	6.71369179	12.42872836
H	3.19542390	6.62712745	13.34850654
C	-0.78023330	9.53296339	11.28054710
C	-0.83193536	7.04422065	8.59963171
H	-4.28341599	11.71287188	5.71172818
C	-0.59275652	3.99178851	10.73488751
H	-0.52503239	5.06370915	10.97015404
C	-1.72299979	5.81041887	6.43426268
C	-1.84152835	4.23997885	4.43110725
C	1.20163214	7.34440774	7.52316122
C	3.97558204	4.85363165	8.51936922
H	3.80740378	5.86239688	8.91683547
C	-1.41667484	10.76995165	11.11129284
H	-2.40283182	10.93081836	11.54629146
C	0.34899950	2.51080965	8.91772496
H	-0.53852769	1.88826024	9.02403928
C	0.45312699	11.60846021	9.84948683
H	0.92595713	12.42182319	9.29972728
C	-0.80992344	11.80032614	10.39991805
H	-1.32126462	12.75471684	10.27793358
C	-1.46146665	8.45963146	12.12924925
H	-0.95730428	7.50296014	11.93039419
C	2.54590918	10.25330064	9.43289961

H	2.78047228	9.18329063	9.36151763
C	2.49245791	2.90559041	7.89819955
H	3.27549472	2.59282827	7.20800203
C	1.34476280	2.13072380	8.02288688
H	1.22854495	1.22463027	7.42870180
C	-1.29157023	8.75615581	13.63348957
H	-0.23272135	8.81941882	13.91598902
H	-1.75981758	7.96566714	14.23830756
H	-1.76768872	9.71275668	13.89437360
C	-2.95292167	8.27476222	11.79886482
H	-3.54317675	9.15798529	12.07986835
H	-3.36047960	7.42061099	12.35762877
H	-3.11999012	8.09660167	10.72824352
C	-1.45013632	5.64611078	4.92006821
C	-3.20605430	5.50268989	6.72998507
C	-3.60845122	4.09710420	6.24858053
C	-0.31191177	3.22700617	12.04563157
H	-0.35328726	2.14139517	11.87290273
H	-1.06216459	3.48090969	12.80930908
H	0.68039398	3.46726936	12.44942221
C	2.69810971	10.83829433	8.01871285
H	1.95723499	10.41988576	7.32607209
H	3.69522171	10.59978690	7.62477475
H	2.59515933	11.93320477	8.01506399
C	5.08242212	4.18269952	9.35953147
H	4.80657937	4.10727331	10.41989857
H	6.01521284	4.76149191	9.29215768
H	5.28715660	3.16524838	8.99387774
C	-3.30747283	3.91071528	4.75353645
H	-1.13202957	5.00699696	6.92091056
H	-1.18744827	3.49677918	4.91915026
C	4.44819129	5.01909815	7.06505123
H	4.73328223	4.05685037	6.61547562
H	5.33482849	5.66782412	7.03685763
H	3.67311246	5.48427250	6.44543332
C	-2.02803065	3.71179134	10.26140296
H	-2.24143455	4.18849780	9.29581641
H	-2.74915429	4.08810903	11.00071349
H	-2.21511406	2.63468284	10.15066898
C	3.57193155	10.89482747	10.38991342
H	3.38381217	11.97368932	10.49778459
H	4.59143427	10.76388867	9.99894608
H	3.53205498	10.44439565	11.39106477
H	-1.66234646	4.15298692	3.34743582
H	-2.02682261	6.39491809	4.35309351
H	-0.38986340	5.83727413	4.70453784
H	-3.84266148	6.24292333	6.21690481
H	-3.42880153	5.60452300	7.80539194
H	-4.67700824	3.91640397	6.44867239
H	-3.04652153	3.34340534	6.82733747
H	-3.96438862	4.57964601	4.16990976
H	-3.54984848	2.88303757	4.43933684
B	-1.15490858	7.24205683	7.06299538
C	-1.92134701	8.68483527	6.79400853
C	-3.83657634	10.29771206	7.30744302

C	-3.28255894	8.87457909	7.49989697
C	-2.05449627	9.04783075	5.29814663
C	-2.59141834	10.47677460	5.10394936
C	-3.93595723	10.67321562	5.82110510
H	-1.24289002	9.44522594	7.23256101
H	-3.16669249	11.01118762	7.81748380
H	-4.82308543	10.39027066	7.79041343
H	-4.01640852	8.15306531	7.10514541
H	-3.19351319	8.66621154	8.57847144
H	-2.74860797	8.34291904	4.80961123
H	-1.08423941	8.93636593	4.79229153
H	-2.69541128	10.70165949	4.03034634
H	-1.85657732	11.19547107	5.50675017
H	-4.69773107	10.03603540	5.33766236
H	-1.47745821	6.86663952	9.46230859

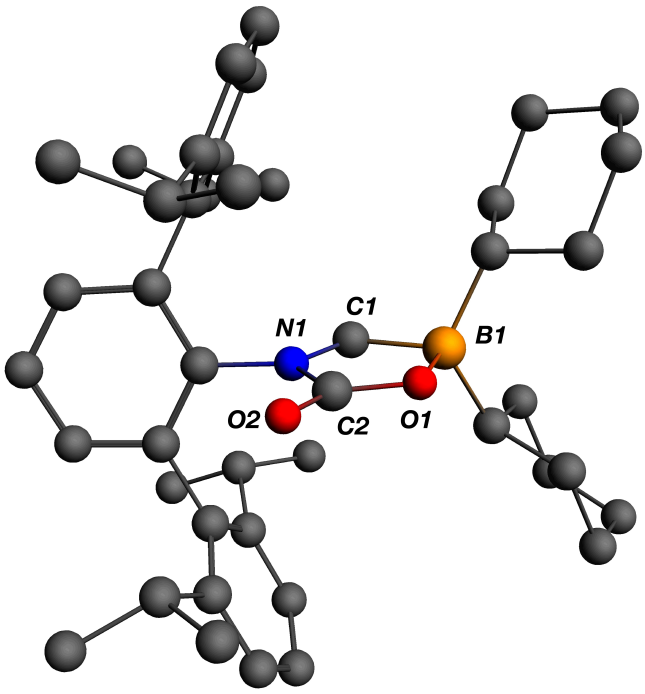

Figure 3.12. Optimized molecular structure of **2a***.

Table 3.2. Listing of total bonding energies for reactants and products (including putative intermediate **2a***) in the formation of **2a** (BP86/TZ2P).

Compound	Total Bonding Energy (kcal/mol)
^{Cy2}BIM (1a)	–14183.97
CO_2	–529.21
2a*	–14725.85
2a	–14744.04

Optimized Cartesian coordinates of $^{9\text{-BBN}}$BIM•thf (1b•thf)

N	-0.02480405	0.04823565	0.05774898
O	-1.46703620	2.54444891	-0.33462914
C	0.69844131	1.11860097	0.05429563
H	1.79915208	0.98580128	0.11187323
C	-2.67419614	-2.70824351	-0.99940831
H	-2.00545103	-2.71430779	-0.12854459
C	-1.92326285	-2.03902268	-2.14713635
C	-0.53510422	-1.77463506	-2.07429016
C	0.23540507	-2.17515528	-0.84876901
B	0.17025899	2.62181049	-0.07817449
C	0.81323274	3.44805007	-1.33601825
H	0.68962971	2.90695233	-2.29234614
C	0.11913813	4.82359935	-1.50564755
H	0.61161523	5.39476143	-2.31342368
H	-0.91423037	4.65323087	-1.85304919
C	0.06605699	5.70157788	-0.23548093
H	-0.66484456	6.51224642	-0.39049575
H	1.03329612	6.20443407	-0.09986201
C	2.76712246	4.16547816	0.25478768
H	2.71805225	5.26136113	0.18949668
H	3.83002017	3.93406282	0.43495093
C	1.93889884	3.68234336	1.46836811
H	2.13353225	4.35767833	2.32058786
H	2.30675797	2.69329410	1.78429688
C	0.40746517	3.56663190	1.23305711
H	-0.00036608	3.10457213	2.15068086
C	-2.00926413	1.98447757	-1.58518080
H	-1.70997346	0.92947622	-1.63721475
H	-1.55864197	2.55136603	-2.40428192
C	-3.51921072	2.17230847	-1.43302415
H	-3.84370555	3.11519148	-1.88987811
H	-4.05777416	1.35390213	-1.92588932
C	-3.76398416	2.20148935	0.10438597
H	-4.40826588	1.37807131	0.43696868
H	-4.24346944	3.14231168	0.40103817
C	-2.36939891	2.07669808	0.72618186
H	-2.19590550	2.72141231	1.59245582
H	-2.09242617	1.03967189	0.95544646
C	-2.61780409	-1.70720786	-3.31967654
H	-3.68654566	-1.91359922	-3.38811397
C	-1.96458360	-1.12441864	-4.40178714
H	-2.51803090	-0.87448464	-5.30677720
C	-0.59682452	-0.87164062	-4.32609413
H	-0.08981757	-0.42266434	-5.17991839
C	0.13804081	-1.19107200	-3.17619474
C	1.64723989	-0.96431510	-3.15747093
H	1.95626537	-0.90888175	-2.10430583
C	2.08332007	0.34407390	-3.83577746
H	3.15806332	0.50844511	-3.67529984
H	1.54433768	1.21049396	-3.43103973
H	1.92021246	0.31585153	-4.92276990
C	2.38920190	-2.15924504	-3.79091587
H	2.11041557	-2.26965055	-4.84974114

H	2.15219016	-3.09960732	-3.27659333
H	3.47757618	-2.00697785	-3.73857173
C	0.67906838	-3.49463148	-0.72934782
H	0.45678475	-4.19614769	-1.53289837
C	1.38268420	-3.91891748	0.39742718
H	1.70546263	-4.95468400	0.48974632
C	1.66729552	-3.00058992	1.40292620
H	2.21547953	-3.31862268	2.28941523
C	1.27458695	-1.65530360	1.31286442
C	1.67045100	-0.74645211	2.44449612
C	3.02123177	-0.33718421	2.56828423
C	4.08840828	-0.70901510	1.53986587
H	3.57942156	-1.17671714	0.68690722
C	5.08142313	-1.74179748	2.10885085
H	5.82221053	-2.02509567	1.34657772
H	4.56962634	-2.65442500	2.44170315
H	5.62527483	-1.32932670	2.97168845
C	4.84958896	0.51775163	1.00571085
H	5.43578989	1.00703778	1.79671079
H	4.16589065	1.26683692	0.58487002
H	5.55131615	0.21368862	0.21555330
C	3.40156436	0.42522157	3.68254294
H	4.43908752	0.74490943	3.78405297
C	2.47928981	0.78407094	4.65850640
H	2.79136405	1.37752120	5.51735298
C	1.15204494	0.38034337	4.53178070
H	0.43583611	0.66350881	5.30226053
C	0.72667346	-0.38726090	3.44049471
C	-0.71924622	-0.87145413	3.37297516
H	-0.97442002	-0.98720815	2.31010958
C	-0.87449643	-2.25258969	4.04269952
H	-0.21935190	-3.00135041	3.57929846
H	-1.91236168	-2.60828664	3.95566334
H	-0.62271044	-2.19196622	5.11236192
C	-1.72656055	0.11729678	3.98160342
H	-1.64069925	0.16575504	5.07660767
H	-2.75260628	-0.20530139	3.75478673
H	-1.58765159	1.13257071	3.58782511
C	2.34548566	3.55521739	-1.10227229
H	2.77601404	2.54443750	-1.18852846
H	2.80655310	4.14356278	-1.91584618
C	-0.29519122	4.93654587	1.05676787
H	-1.38741445	4.77827718	1.07351928
H	-0.07653120	5.58323694	1.92572648
C	0.53071893	-1.23758757	0.17652046
C	-3.01157798	-4.17406087	-1.33631689
H	-3.67601725	-4.23190771	-2.21149651
H	-3.52122453	-4.65800213	-0.49003942
H	-2.10621661	-4.75183601	-1.56444324
C	-3.94799269	-1.94756809	-0.59483253
H	-3.72200600	-0.90279951	-0.34330456
H	-4.40914522	-2.41887136	0.28503208
H	-4.69753439	-1.95026913	-1.39941818

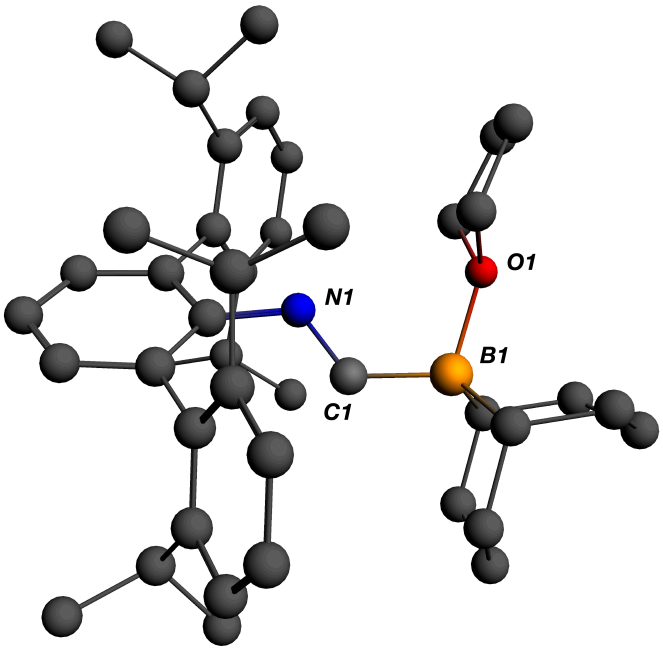

Figure 3.13. Optimized molecular structure of **1b•thf**.

Table 3.3. Comparative metrical parameters between the experimental (X-ray crystal structure) and calculated versions of **1b•thf**.

Parameter	Exp. (X-ray)	Calculated	% Difference
N1-C1	1.280(2) Å	1.292 Å	0.9 %
C1-B1	1.613(2) Å	1.599 Å	0.9 %
B1-O1	1.631(2) Å	1.659 Å	1.7%
N1-C1-B1	125.8(1)º	127.0º	1.0 %
C1-B1-O1	106.7(1)º	107.2º	0.9 %

Optimized Cartesian coordinates of boralactone 2b

O	-1.23567943	-0.18567339	0.11118469
O	-3.15177472	1.06115730	0.14671161
N	-1.05454009	2.07590881	-0.06300347
C	2.64372414	4.25539553	2.31226354
H	3.11964307	4.33762859	3.29966013
H	3.14661241	4.97633934	1.65263076
H	2.83834909	3.24586659	1.92938439
C	1.13987450	4.56925739	2.38036446
H	0.76698043	4.64079192	1.34821824
C	0.31758653	3.49787730	3.09845973
C	-1.01000093	3.17652184	2.70573768
C	-1.61088124	3.89025694	1.52098976
C	-1.54392988	3.41377951	0.18530920
C	-2.02961486	4.21044227	-0.88207480
C	-1.89213528	3.87697301	-2.34637844

C	-0.80258100	4.42205312	-3.07817832
C	0.21303179	5.37889966	-2.44945643
H	0.23663631	5.18130183	-1.36777193
C	1.64533379	5.21766512	-2.98940716
H	1.98653348	4.17518388	-2.96492895
H	2.34063894	5.82028956	-2.38824252
H	1.72671847	5.57331308	-4.02622471
C	1.49470966	-0.21718003	-2.68929512
H	1.26695931	-0.49876701	-3.73000141
H	2.59546519	-0.19593486	-2.63135033
C	0.96301684	-1.33395844	-1.77473125
H	1.48530017	-2.27141539	-2.02946546
H	-0.10486192	-1.50734607	-1.98139703
C	1.15423392	-1.08249857	-0.23631966
H	0.82739624	-2.01000509	0.26019200
C	2.64503230	-0.81410456	0.11775054
H	2.89897514	-1.38100098	1.02652346
H	3.28113798	-1.23728472	-0.67814770
C	3.06173368	0.64943072	0.38241964
H	4.14721606	0.65956708	0.57410218
H	2.60233921	0.96663845	1.33207574
C	2.77839334	1.72767769	-0.69143288
H	3.39208790	1.52975479	-1.58429797
H	3.15293882	2.67908459	-0.28373021
C	1.30146966	1.94364303	-1.14107597
H	1.18399948	3.01497718	-1.35499903
C	0.35181268	1.61681201	0.03985656
H	0.78064344	2.01748449	0.97117847
C	-1.94453972	1.02947007	0.07153014
C	0.94316233	5.95128671	3.03917758
H	-0.10932336	6.25916647	3.03733719
H	1.52251952	6.71728459	2.50238153
H	1.28995763	5.92967359	4.08312035
C	0.86411630	2.85974832	4.21965306
H	1.88450964	3.08944533	4.52401309
C	0.12382800	1.94126468	4.95863832
H	0.56800847	1.45021019	5.82430157
C	-1.19081171	1.66978215	4.59789353
H	-1.77570620	0.97193345	5.19608502
C	-1.78550284	2.28251703	3.48401287
C	-3.26507761	2.03102444	3.20651041
H	-3.47283262	2.33136121	2.17214383
C	-4.13945759	2.89928159	4.13595942
H	-3.96671805	2.63936690	5.19144218
H	-5.20473996	2.73697031	3.91554300
H	-3.92747234	3.97009366	4.01387044
C	-3.66855310	0.55247135	3.33549734
H	-3.04620075	-0.09289044	2.70393304
H	-4.71110853	0.42534238	3.01350741
H	-3.59958780	0.19796167	4.37450188
C	-2.24124625	5.11668366	1.76921328
H	-2.31189617	5.46466853	2.79856721
C	-2.78559107	5.87273181	0.73690938
H	-3.29395653	6.81163526	0.95149656
C	-2.66023917	5.42601366	-0.57286472

H	-3.06428289	6.01959797	-1.39107418
C	-0.69981422	4.13873263	-4.44691496
H	0.13878692	4.53900954	-5.01565244
C	-1.65388265	3.36334435	-5.09828481
H	-1.55298092	3.14861105	-6.16197973
C	-2.75117091	2.88853231	-4.38883400
H	-3.51659834	2.31389459	-4.90950303
C	-2.90209517	3.14513598	-3.01826065
C	-4.19159053	2.71747121	-2.32460325
H	-4.00753246	2.70464262	-1.24435177
C	-5.31383225	3.73963153	-2.60482908
H	-5.03901428	4.74921574	-2.27058642
H	-6.23385106	3.44736816	-2.07718939
H	-5.53946307	3.79005924	-3.68100649
C	-4.65904879	1.30543214	-2.71268675
H	-4.98869957	1.25489190	-3.76096931
H	-5.51227212	1.01364827	-2.08535960
H	-3.86619701	0.56325750	-2.55976604
C	-0.22370258	6.84783093	-2.64120320
H	-0.27668338	7.09284368	-3.71245699
H	0.50207136	7.52804065	-2.17079329
H	-1.20777110	7.04491023	-2.19989609
C	0.94551662	1.20834490	-2.46556770
H	-0.15131728	1.21213534	-2.58779764
H	1.32517808	1.82966190	-3.29264252
B	0.12557505	0.05579541	0.08310027

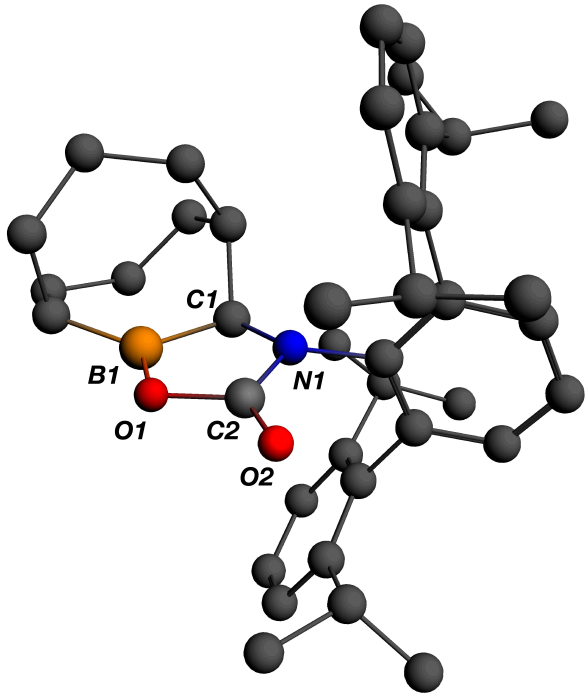

Figure 3.14. Optimized molecular structure of **2b**.

Table 3.4. Comparative metrical parameters between the experimental (X-ray crystal structure) and calculated versions of **2b**.

Parameter	Exp. (X-ray)	Calculated	% Difference
C2-O1	1.389(2)	1.407 Å	1.3 %
C2-O2	1.202(2)	1.210 Å	0.7 %
C2-N1	1.365(2)	1.380 Å	1.1 %
O1-B1	1.381(2)	1.383 Å	0.1 %

Optimized Cartesian coordinates of putative zwitterionic boralactone 2b*

O	0.01645051	-2.19967965	0.07697900
O	2.04029197	-1.15744083	-0.10195510
N	-0.00048037	0.04865527	-0.14810857
C	-3.45451591	1.95915196	-2.48092250
H	-3.96167314	1.88594515	-3.45306129
H	-4.02115050	2.67985970	-1.87470582
H	-3.52129428	0.97485510	-1.99894389
C	-1.99731139	2.42817827	-2.63513518
H	-1.59744914	2.60656838	-1.62645802
C	-1.09813097	1.39955957	-3.31917263
C	0.21615164	1.12346033	-2.86512051
C	0.73861576	1.84295691	-1.65193786
C	0.59711689	1.34892592	-0.33869975
C	1.02387075	2.07733419	0.79044621
C	0.80289865	1.61567023	2.20401440
C	-0.43594919	1.89441283	2.83537020
C	-1.54671934	2.67759749	2.13770674
H	-1.35828765	2.63705476	1.05536238
C	-2.95076322	2.10073497	2.38561406
H	-3.00064476	1.02944906	2.15000582
H	-3.69048556	2.62636985	1.76537055
H	-3.26161914	2.22515422	3.43224559
C	-2.51163269	-4.62804248	0.31807826
H	-2.22278556	-5.68793008	0.39160121
H	-3.61419089	-4.61721193	0.34474035
C	-2.03067817	-4.05142455	-1.02378570
H	-2.53825490	-4.58016666	-1.85050219
H	-0.95371212	-4.24587201	-1.14150850
C	-2.28444347	-2.53208550	-1.16695698
H	-1.85991749	-2.21341740	-2.13122349
C	-3.80332411	-2.18129257	-1.13679442
H	-4.06226141	-1.58098704	-2.02350485
H	-4.38940263	-3.11195076	-1.22773365
C	-4.27581076	-1.41855495	0.11834840
H	-5.37704420	-1.39291699	0.14220112
H	-3.96583002	-0.36427758	0.03482380
C	-3.74145299	-1.99049924	1.44755189
H	-4.31639083	-2.89784901	1.70023919
H	-3.96507017	-1.26809398	2.24881626
C	-2.22018262	-2.33230562	1.45463625
H	-1.74974763	-1.87284807	2.33753313

C	-1.27856967	-0.25041153	-0.07691084
B	-1.47708183	-1.79400975	0.07914495
C	0.83131921	-1.19426796	-0.05071631
C	-1.95688193	3.77822564	-3.38138830
H	-0.93589265	4.17704481	-3.44131507
H	-2.58427712	4.52212925	-2.86837046
H	-2.33452256	3.66259229	-4.40806138
C	-1.56337685	0.74993795	-4.47032692
H	-2.57336959	0.94881666	-4.82844554
C	-0.75630051	-0.14288149	-5.16835618
H	-1.13703753	-0.64266216	-6.05882928
C	0.54027550	-0.38883548	-4.72908528
H	1.17091400	-1.07987596	-5.28716517
C	1.05327130	0.23477540	-3.58274450
C	2.50511552	-0.01227372	-3.18340005
H	2.61851723	0.27405403	-2.12982655
C	3.45417641	0.87109758	-4.01983198
H	3.37660089	0.62347817	-5.08929353
H	4.49681386	0.71149773	-3.70830022
H	3.22566884	1.93937382	-3.90482200
C	2.92213436	-1.48850375	-3.29039271
H	2.24799134	-2.13947448	-2.72091586
H	3.93340467	-1.61696006	-2.88102710
H	2.94372353	-1.83380220	-4.33424094
C	1.35947746	3.08895808	-1.81405622
H	1.47840283	3.48301744	-2.82199448
C	1.81147327	3.81863713	-0.71797804
H	2.29174942	4.78450293	-0.86723087
C	1.63292960	3.32026604	0.56951953
H	1.96026242	3.89840036	1.43203804
C	-0.61668041	1.50022767	4.16744128
H	-1.56446223	1.70556676	4.66451781
C	0.39727856	0.85786389	4.87169659
H	0.23771764	0.55681542	5.90684813
C	1.61700183	0.60985774	4.25157575
H	2.41039260	0.11645697	4.81184082
C	1.84811191	0.98206142	2.91934278
C	3.22598633	0.74176036	2.30900748
H	3.12737210	0.81738026	1.21866009
C	4.22403460	1.82130594	2.77724056
H	3.88722342	2.83333796	2.51458975
H	5.20754785	1.65909140	2.31241265
H	4.35453233	1.78421199	3.86927404
C	3.78332039	-0.65992682	2.60944638
H	4.00094520	-0.79341157	3.67905823
H	4.72491907	-0.80786241	2.06255609
H	3.08542746	-1.44244612	2.28994128
C	-1.50607751	4.16569673	2.54277905
H	-1.67855328	4.27612066	3.62354526
H	-2.28607703	4.73203456	2.01239605
H	-0.53473570	4.62082494	2.30804466
C	-1.96627160	-3.85684004	1.53177476
H	-0.88389785	-4.03397425	1.62231909
H	-2.42883475	-4.25390508	2.45298851
H	-1.98307385	0.57978779	-0.14586616

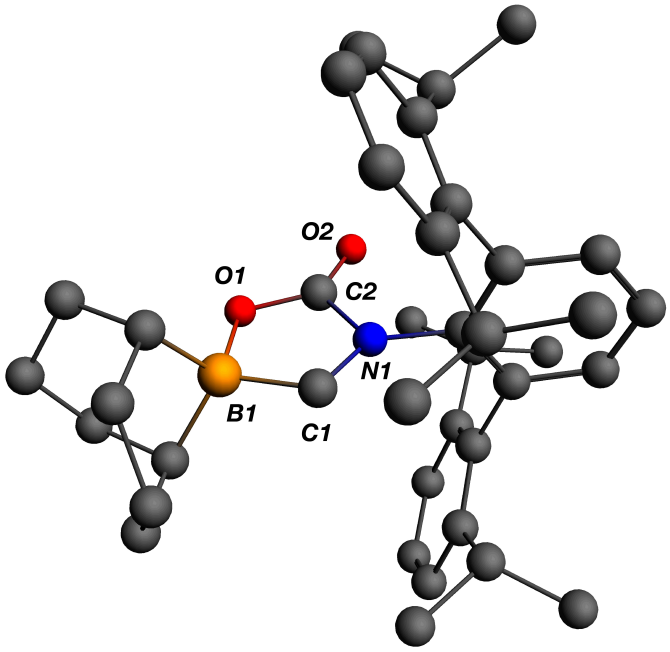

Figure 3.15. Optimized molecular structure of **2b***.

Table 3.5. Listing of total bonding energies for reactants and products (including putative intermediate **2b***) in the formation of **2b** (BP86/TZ2P).

Compound	Total Bonding Energy (kcal/mol)
$^{9\text{-BBN}}$BIM•thf (1b)	–14323.85
CO_2	–529.21
2b*	–13223.83
2b	–13233.47
THF	–1637.88

3.8. Details of crystallographic structure determinations

General. Single crystal X-ray structure determinations were carried out at low temperature on Bruker Kappa Diffractometers equipped with a Mo or Cu radiation source and a Bruker APEX or APEX-II area detector. All structures were solved via direct methods with SIR 2004[57] and refined by full-matrix least-squares procedures using SHELXL-2013[58] within the Olex2 small-molecule solution, refinement and analysis software.[59] Crystallographic data collection and refinement information are listed in

Tables 3.6-8. The boralactone **2a** contains rotational disorder of the boron-bound cyclohexyl group, which was modeled and refined anisotropically. The exocyclic eneamine **3**•1.5(C_5H_{12}) contains positional disorder of one co-crystallized molecule of *n*-pentane, which was modeled and refined anisotropically. The (boryl)iminomethane $^{9\text{-BBN}}$BIM•thf (**1b•thf**•1.5 (C_6H_6)) contains positional disoder of the boron-bound THF, as well as positional disorder of one *i*-Pr group. These disordered groups were modeled and refined anisotropically. This structure also contains co-crystallized molecules of benzene (two per unit cell) that were highly disordered and could not be properly modeled. The Platon routine SQUEEZE[60] was utilized to account for these electrons as a diffuse contribution to the overall scattering without specific atom positions. The double-hydroboration product **6** contains positional disorder of a co-crystallized molecule of *n*-pentane, which was modeled and refined anisotropically.

Table 3.6. Crystallographic data collection and refinement information.

Name	Boralactone **2a**	Enamine **3**•1.5(C_6H_6)	Heterocycle **4**
Formula	$C_{44}H_{60}NBO_2$	$C_{52.5}H_{81}N_2B$	$C_{50}H_{65}N_2B$
Crystal System	Monoclinic	Triclinic	Monoclinic
Space Group	$P2_1/c$	P-1	$P2_1/c$
a, Å	18.442(2)	10.3180(8)	12.3306(9)
b, Å	11.960(1)	12.816(1)	13.054(1)
c, Å	19.592(2)	17.806(1)	25.512(2)
α, deg	90	83.969(4)	90
β, deg	116.965(3)	86.164(4)	90.626(4)
γ, deg	90	85.117(4)	90
V, Å^3	3851.7(7)	2329.1(3)	4106.4(6)
Z	4	2	4
Radiation (λ, Å)	Mo-Kα, 0.71073	Cu-Kα, 1.54178	Mo-Kα, 0.71073
ρ (calcd.), g/cm^3	1.114	1.071	1.140
μ, mm^{-1}	0.066	0.443	0.064
Temp, K	100	100	100
θ max, deg	26.410	44.878	25.371
data/parameters	7152/492	3308/539	7524/486
R_1	0.0626	0.0329	0.0574
wR_2	0.1157	0.0866	0.1163
GOF	1.007	1.046	1.025

Table 3.7. Crystallographic data collection and refinement information.

Name	(Cy)(*t*-BuC≡C) BCH(Cy)NHAr^{Dipp2} (**5**)	$^{9\text{-BBN}}$BIM•thf (**1b•thf**•1.5 (C_6H_6))	(9-BBN)CH_2N(9-BBN) Ar^{Dipp2} (**6**•C_5H_{12})
Formula	$C_{49}H_{70}NB$	$C_{52}H_{69}NBO$	$C_{52}H_{79}NB_2$
Crystal System	Triclinic	Monoclinic	Monoclinic
Space Group	*P*-1	$P2_1/n$	$P2_1/c$
a, Å	10.9523(6)	10.6296(3)	20.9432(9)
b, Å	12.2836(6)	23.2451(8)	12.5599(6)
c, Å	18.200(1)	18.4090(6)	17.1099(8)
α, deg	77.103(2)	90	90
β, deg	81.075(3)	104.193(1)	91.099(2)
γ, deg	65.736(2)	90	90
V, Å^3	2170.4(2)	4409.8(2)	4499.8(4)
Z	2	4	4
Radiation (λ, Å)	Mo-Kα, 0.71073	Mo-Kα, 0.71073	Mo-Kα, 0.71073
ρ (calcd.), g/cm^3	1.046	1.107	1.092
μ, mm^{-1}	0.058	0.063	0.060
Temp, K	100	100	100
θ max, deg	25.371	26.398	25.448
data/parameters	7662/475	9019/496	8280/516
R_1	0.0698	0.0532	0.0557
wR_2	0.1396	0.1316	0.1364
GOF	1.010	1.045	1.033

Table 3.8. Crystallographic data collection and refinement information.

Name	Boralactone **2b**	Borinic acid **7**	^{Pin}BIM (**1c**)
Formula	$C_{40}H_{52}NBO_2$	$C_{39}H_{54}NBO$	$C_{37}H_{50}NBO_2$
Crystal System	Monoclinic	Monoclinic	Monoclinic
Space Group	$P2_1/n$	$P2_1/c$	$P2_1/n$
a, Å	10.1073(3)	17.347(2)	13.437(1)
b, Å	16.6024(4)	10.634(1)	14.329(1)
c, Å	20.2451(5)	19.7137(2)	18.587(1)
α, deg	90	90	90
β, deg	94.273(1)	112.174(4)	105.742(3)
γ, deg	90	90	90
V, Å^3	3387.8(2)	3367.6(6)	3444.6(5)
Z	4	4	4
Radiation (λ, Å)	Mo-Kα, 0.71073	Mo-Kα, 0.71073	Mo-Kα, 0.71073
ρ (calcd.), g/cm^3	1.156	1.112	1.064
μ, mm^{-1}	0.069	0.064	0.064
Temp, K	100	100	100
θ max, deg	26.399	25.388	25.465
data/parameters	6949/405	6129/395	6102/382
R_1	0.0433	0.0872	0.0382
wR_2	0.0909	0.1893	0.0944
GOF	1.020	1.082	1.019

3.9. Acknowledgements

Chapter 3 is adapted from Barnett, B. R.; Moore, C. E.; Rheingold, A. L.; Figueroa, J. S. "Frustrated Lewis Pair Behavior of Monomeric (boryl)iminomethanes Accessed from Isocyanide 1,1-hydroboration", *Chemical Communications*, **2015**, *51*, 541. Copyright 2015, Royal Society of Chemistry. Permission to include published material in this dissertation has been obtained from all coauthors. The dissertation author is the first author of this paper. Prof. Didier Bourissou is thanked for helpful comments.

3.10. References

(1) Welch, G. C.; San Juan, R. R.; Masuda, J. D.; Stephan, D. W. *Science* **2006**, *314*, 1124.

(2) Chase, P. A.; Welch, G. C.; Jurca, T.; Stephan, D. W. *Angew. Chem., Int. Ed.* **2007**, *46*, 8050.

(3) Stephan, D. W.; Erker, G. *Angew. Chem., Int. Ed.* **2010**, *49*, 46.

(4) Stephan, D. W.; Erker, G. *Chem. Sci.* **2014**, *5*, 2625.

(5) Stephan, D. W. *Top. Curr. Chem.,* **2013**, *332*, 1.

(6) Kehr, G.; Schwendemann, S.; Erker, G. *Top. Curr. Chem.* **2013**, *332*, 45.

(7) Grimme, S.; Kruse, H.; Goerigk, L.; Erker, G. *Angew. Chem., Int. Ed.* **2010**, *49*, 1402.

(8) Stirling, A.; Hamza, A.; Rokob, T. A.; Pápai, I. *Chem. Commun.* **2008**, 3148.

(9) Bertini, F.; Lyaskovskyy, V.; Timmer, B. J. J.; de Kanter, F. J. J.; Lutz, M.; Ehlers, A. W.; Slootweg, J. C.; Lammertsma, K. *J. Am. Chem. Soc.* **2012**, *134*, 201.

(10) Lu, G.; Li, H.; Zhao, L.; Huang, F.; Wang, Z.-X. *Inorg. Chem.* **2010**, *49*, 295.

(11) Stute, A.; Kehr, G.; Fröhlich, R.; Erker, G. *Chem. Commun.* **2011**, *47*, 4288.

(12) Stute, A.; Kehr, G.; Daniliuc, C. G.; Fröhlich, R.; Erker, G. *Dalton Trans.* **2013**, *42*, 4487.

(13) Rosorius, C.; Kehr, G.; Fröhlich, R.; Grimme, S.; Erker, G. *Organometallics* **2011**, *30*, 4211.

(14) Theuergarten, E.; Schlösser, J.; Schlüns, D.; Freytag, M.; Daniliuc, C. G.; Jones, P. G.; Tamm, M. *Dalton Trans.* **2012**, *41*, 9101.

(15) Appelt, C.; Westenberg, H.; Bertini, F.; Ehlers, A. W.; Slootweg, J. C.; Lammertsma, K.; Uhl, W. *Angew. Chem., Int. Ed.* **2011**, *50*, 3925.

(16) Barnett, B. R.; Moore, C. E.; Rheingold, A. L.; Figueroa, J. S. *J. Am. Chem. Soc.* **2014**, *136*, 10262.

(17) Ditri, T. B.; Fox, B. J.; Moore, C. E.; Rheingold, A. L.; Figueroa, J. S. *Inorg. Chem.* **2009**, *48*, 8362.

(18) Hesse, G.; Witte, H.; Gulden, W. *Tetrahedron Lett.* 1966, *7*, 2707.

(19) Suginome, M.; Fukuda, T.; Nakamura, H.; Ito, Y. *Organometallics* **2000**, *19*, 719.

(20) Suginome, M.; Fukuda, T.; Ito, Y. *J. Organomet. Chem.* **2002**, *643-644*, 508.

(21) Sicker, U.; Meller, A.; Maringgele, W. *J. Organomet. Chem. 231*, 191.

(22) Yamamoto, Y.; Kondo, K.; Moritani, I. *Bull. Chem. Soc. Jpn.* **1975**, *48*, 3682.

(23) Casanova Jr., J.; Schuster, R. E. *Tetrahedron Lett.* **1964**, *5*, 405.

(24) Casanova Jr., J.; Kiefer, H. R.; Kuwada, D.; Boulton, A. H. *Tetrahedron Lett.* **1965**, *6*, 703.

(25) Tamm, M.; Lügger, T.; Hahn, F. E. *Organometallics* **1996**, *15*, 1251.

(26) Casanova Jr., J.; Kiefer, H. R. *J. Org. Chem* **1969**, *34*, 2579.

(27) Mömming, C. M.; Otten, E.; Kehr, G.; Fröhlich, R.; Grimme, S.; Stephan, D. W.; Erker, G. *Angew. Chem., Int. Ed.* **2009**, *48*, 6643.

(28) For a generalized discussion of alkyl migrations in four-coordinate borates, see: Aggarwal, V. K.; Fang, G. Y.; Ginesta, X.; Howells, D. M.; Zaja, M. *Pure Appl. Chem.*, **2006**, *78*, 215.

(29) Olah, G. A. *Acc. Chem. Res.* **1976**, *9*, 41.

(30) Dureen, M. A.; Stephan, D. W. *J. Am. Chem. Soc.* **2010**, *132*, 13559.

(31) Dureen, M. A.; Stephan, D. W. *J. Am. Chem. Soc.* **2009**, *131*, 8396.

(32) Dureen, M. A.; Brown, C. C.; Stephan, D. W. *Organometallics* **2010**, *29*, 6594.

(33) Jiang, C.; Blacque, O.; Berke, H. *Organometallics* **2010**, *29*, 125.

(34) Chernichenko, K.; Madarász, Á.; Pápai, I.; Nieger, M.; Leskelä, M.; Repo, T. *Nature Chem* **2013**, *5*, 718.

(35) Freitag, S.; Krebs, K. M.; Henning, J.; Hirdler, J.; Schubert, H.; Wesemann, L. *Organometallics* **2013**, *32*, 6785.

(36) Uhl, W.; Tannert, J.; Layh, M.; Hepp, A.; Grimme, S.; Risthaus, T. *Organometallics* **2013**, *32*, 6770.

(37) (*a*) Knights, E. F.; Brown, H. C. *J. Am. Chem. Soc.* **1968**, *90*, 5280; (*b*) Knights, E. F.; Brown, H. C. *J. Am. Chem. Soc.* **1968**, *90*, 5283.

(38) Hermanek, S. *Chem. Rev.* **1992**, *92*, 325.

(39) Wrackmeyer, B.; Klaus, U.; Milius, W.; Klaus, E.; Schaller, T. *J. Organomet. Chem.* **1996**, *517*, 235.

(40) Burgos, C. H.; Canales, E.; Matos, K.; Soderquist, J. A. *J. Am. Chem. Soc.,* **2005**, *127*, 8044.

(41) Canales, E.; Prasad, K. G.; Soderquist, J. A. *J. Am. Chem. Soc.* **2005**, *127*, 11572.

(42) Khan, E.; Kempe, R.; Wrackmeyer, B. *Appl. Organometal. Chem.* **2009**, *23*, 204.

(43) Wang, T.; Stephan, D. W. *Chem. Eur. J.* **2014**, *20*, 3036.

(44) Miller, A. J. M.; Labinger, J. A.; Bercaw, J. E. *J. Am. Chem. Soc.* **2010**, *132*, 3301.

(45) Li, H.; Aquino, A. J. A.; Cordes, D. B.; Hung-Low, F.; Hase, W. L.; Krempner, C. *J. Am. Chem. Soc.* **2013**, *135*, 16066.

(46) For the catalytic reduction of CO_2 to methanol by a related FLP-type system featuring a weakly Lewis acidic catecholboryl group, see: (*a*) Courtemanche, M.-A.; Légaré, M.-A.; Maron, L.; Fontaine, F.-G. *J. Am. Chem. Soc.* **2013**, *135*, 9326; (*b*) Courtemanche, M.-A.; Légaré, M.-A.; Maron, L.; Fontaine, F.-G. *J. Am. Chem. Soc.* **2014**, *136*, 10708.

(47) Armarego, W. L. F.; Chai, C. L. L. *Purification of Laboratory Chemicals*, 5th Ed.; Elsevier, 2003.

(48) Pangborn, A. B.; Giardello, M. A.; Grubbs, R. H.; Rosen, R. K.; Timmers, F. J. *Organometallics*, **1996**, *15*, 1518.

(49) te Velde, G.; Bickelhaupt, F. M.; Baerends, E. J.; Guerra, C. F.; Van Gisbergen, S. J. A.; Snijders, J. G.; Ziegler, T. *J. Comput. Chem.* **2001**, *22*, 931.

(50) Guerra, C. F.; Snijders, J. G.; te Velde, G.; Baerends, E. J. *Theor. Chim. Acta* **1998**, *99*, 391.

(51) ADF 2013.99, SCM, Theoretical Chemistry, Vrije University, Amsterdam, Netherlands. www.scm.com.

(52) Vosko, S. H.; Wilk, L.; Nusair, M. *Can. J. Phys.* **1980**, *50*, 1200.

(53) Becke, A. D. *Phys. Rev. A.* **1988**, *38*, 3098.

(54) Perdew, J. P. *Phys. Rev. B.* **1986**, *34*, 7406.

(55) Perdew, J. P. *Phys. Rev. B.* **1986**, *33*, 8822.

(56) ADF-GUI 2007.01, SCM, Amsterdam, Netherlands. www.scm.com

(57) Burla, M. C.; Caliandro, R.; Camalli, M.; Carrozzini, B.; Cascarano, G. L.; De Caro, L.; Giacovazzo, C.; Polidori, G.; Spagna, R. J. *J. Appl. Crystallogr.* **2005**, *38*, 381.

(58) Sheldrick, G. M.; *Acta Crystallogr. A.* **2008**, *64*, 112.

(59) Dolomanov, O. V.; Bourhis, L. J.; Gildea, R. J.; Howard, J. A. K.; Puschmann, H. *J. Appl. Cryst.* **2009**, *42*, 339.

(60) van der Sluis, P.; Spek. A. L. *Acta Crystallogr.* **1990**, *A46*, 194.

Chapter 4

Metal-only Lewis Pairs Between Group 10 Metals and Tl(I) or Ag(I): Insights into the Electronic Consequences of Z-type Ligand Binding

4.1. Introduction

On account of their relatively electropositive nature and ability to act as formal acceptors toward Lewis bases, the transition metals in coordination complexes are traditionally viewed as Lewis acids. Classical "Werner-type" complexes utilize their empty n*d*, as well as (n+1)*s* and (n+1)*p*, orbitals to form dative bonds with electron-donor ligands. In the case of highly reduced and electron-rich complexes, the transition metal center may also be capable of exhibiting Lewis basic behavior.[1] Although this phenomenon was initially invoked for the case of carbonyl metalates acting as Brønstead bases,[2-4] it is now recognized as a central tenet of transition-metal bonding to π-acidic ligands[5-7] as well as an essential component of many oxidative addition mechanisms.[8-12] More recently, the extension of this concept to the binding of various main-group acceptor fragments (Z-type ligands)[13] in a σ-fashion by electron-rich transition metals has been realized, and the study of such complexes continues to be of intense interest.[14-27]

In addition to these examples, a related topic concerning transition metal Lewis basicity is the ability to form dative interactions to another metal center. Judicious ligand design strategies that constrain an electron-rich metal center in close proximity to a coordinatively unsaturated metal fragment has proven to be a reliable approach for engendering metal-metal dative bonding.[28-34] Furthermore, in certain instances,

unsupported Metal-only Lewis Pairs (MOLPs), which do not rely on a ligand buttress, can be generated.[2,35-39] The formation of such unsupported metal-metal interactions, while sometimes labile in solution, offers an interesting approach toward tuning the reactivity profiles of low-valent complexes, as the addition of metallic Lewis acids has been shown to enhance the rates of certain catalytic processes.[40-43]

While synthetic methods leading to MOLPs and their structural chemistry have advanced, a detailed understanding of how the presence of a metal-metal dative bond affects the electronic properties of the constituent fragments remains of significant interest. It is generally accepted that protonation of a transition metal complex is best viewed as involving a two-electron oxidation of the metal center to give a hydride ligand.[44] As the electrons involved in the M-H bond have necessarily come from the metal, an increase of its valence by two units is required.[45] In the case of other main group Lewis acids (*e.g.* boranes), the degree of charge transfer is often not as clear. As such, the adoption and assignment of formalisms to adequately describe the electronic structure of such adducts has been a point of debate in the community.[46,47] Similar ambiguities in the electronic structures of MOLPs exist, although considerably less effort has been put toward uncovering satisfactory electronic descriptors for such compounds.[39] Despite the fact that X-ray Absorption Near-Edge Spectroscopy (XANES) holds promise in this regard,[30,34] its thus-far limited use in this capacity has not yet led to the development of general principles for properly describing the electronic structures of complexes containing metal-metal dative interactions.

Work from our research group has demonstrated the utility of encumbering *m*-terphenyl isocyanides in stabilizing low-valent and coordinatively unsaturated complexes

of late transition metals.[27,48-55] Such electron-rich metal centers are prime candidates for acting as Lewis bases toward appropriate Lewis acidic substrates, a concept that has been demonstrated by the heterobimetallics [TlNi(η^4-COD)($CNAr^{Mes2}$)$_2$]X (X = OTf, BAr^F_4),[49] [TlNi($CNAr^{Mes2}$)$_3$]OTf,[49] and [TlPd($CNAr^{Dipp2}$)$_2$]OTf (**2**),[50] as well as by the platinum (boryl)iminomethane complex Pt(κ^2-*N,B*-^{Cy2}BIM)($CNAr^{Dipp2}$).[27] In addition, the response of the isocyanide υ(C≡N) IR bands to the electron density on the Lewis-basic metal center renders them a convenient spectroscopic reporter on the degree of formal charge transfer upon binding a σ-acceptor fragment.[25] In this work, we demonstrate the ability of the two-coordinate complexes M($CNAr^{Dipp2}$)$_2$ (M = Pt, Pd)[27,50] to form unsupported metal-metal linkages with Tl(I). Two Tl-containing MOLPs have also been examined by X-ray Absorption Near-Edge Spectroscopy (XANES), illustrating that the spectroscopic oxidation state of the group 10 metal is not affected by its interaction with Tl(I). We also show that the zero-valent platforms M($CNAr^{Dipp2}$)$_2$ (M = Pt, Pd) can form Metal-only Lewis Pairs with Ag(I), yielding the heterobimetallic salts [AgM($CNAr^{Dipp2}$)$_2$(solv)]OTf (**5**, M = Pt; **6**, M = Pd; solv = solvent). Spectroscopic and structural investigations provide insight into the nature of the M-Ag interactions in these compounds, and give strong evidence that formation of the M→Ag linkage results in only a marginal degree of metal-to-metal charge transfer. In the case of the Pt variant **5**, further aggregation with additional AgOTf leads to dimeric {[Ag_2Pt($CNAr^{Dipp2}$)$_2$(η^1-C_6H_6)]$_2$(μ-OTf)$_2$}(OTf)$_2$ (**7**) containing *triangulo*-$PtAg_2$ cores. It is shown that binding of one (Compounds **5**-**6**) and two (Compound **7**) equivalents of Ag(I) results in a sequential increase in the Lewis

acidity of the group 10 metal center, thus illustrating how σ-acceptor fragments can be used to rationally tune the properties of electron-rich transition metal complexes.

4.2. Synthesis and spectroscopic features of Metal-only Lewis Pairs containing a Tl(I) Lewis acidic center

Similar to the zero-valent Pd congener, $Pd(CNAr^{Dipp2})_2$,[50] the addition of TlOTf to a solution of $Pt(CNAr^{Dipp2})_2$ in Et_2O yields the unsupported heterobimetallic compound $[TlPt(CNAr^{Dipp2})_2]OTf$ (**1**) as a yellow microcrystalline solid. Structural characterization of **1** (Scheme 4.1 and Figure 4.1) reveals a T-shaped coordination geometry about Pt, while the Tl center makes long but non-negligible contacts with the $[OTf]^-$ anion (d(Tl-O3) = 2.799(5) Å) and the C_{aryl} atoms of the Dipp rings (shortest d(Tl-C_{aryl}) = 3.355 Å). The presence of a Pt-Tl bonding interaction is apparent given their interatomic separation of 2.8617(3) Å. Importantly, this value is comparable to the most reasonable range for the sum of the covalent radii between Pt and Tl (2.67–2.84 Å),[56] thereby suggesting that the solid-state structure of **1** does not simply arise from the co-crystallization of $Pt(CNAr^{Dipp2})_2$ with TlOTf. While the role of closed-shell metallophilic interactions[57] cannot be completely discounted, spectroscopic evidence indicates that this interaction is formed by a reverse-dative σ-bond, whereby Pt donates two electrons to an empty 6*p* orbital on Tl. Analysis of these solutions by FTIR spectroscopy shows a strong υ(C≡N) band at 2112 cm^{-1}, which is shifted to higher energy relative to those of $Pt(CNAr^{Dipp2})_2$ (2065, 2020 cm^{-1}),[27] consistent with a decrease in π-backbonding interactions to the isocyanides as a result of the formation of a Pt→Tl retrodative σ-bonding interaction. A similar blue-shift of this band for the palladium analogue $[TlPd(CNAr^{Dipp2})_2]OTf$ (**2**) with

respect to $Pd(CNAr^{Dipp2})_2$ was observed previously.[50] Surprisingly, bonds between electron-rich, late transition metals (especially third-row metals) and Tl(I) have often been rationalized largely based on metallophilic interactions.[58-61] However, the FTIR spectra of **1** and **2** compared with those of $M(CNAr^{Dipp2})_2$ (M = Pt, Pd) provide strong experimental evidence that late-metal-Tl(I) bonds likely contain a substantial dative-bonding component in a manner analogous to that seen for complexes bearing main-group Z-type ligands.[23-25]

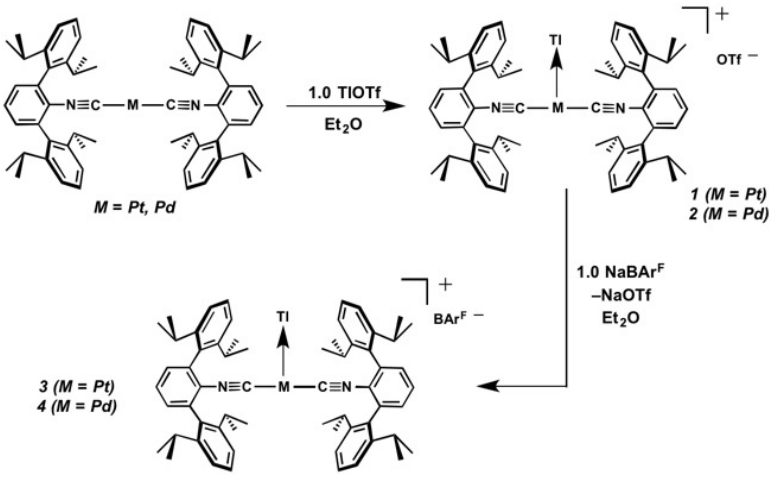

Scheme 4.1. Synthesis of Tl(I)-containing MOLPs based off of the $M(CNAr^{Dipp2})_2$ (M = Pt, Pd) platform.

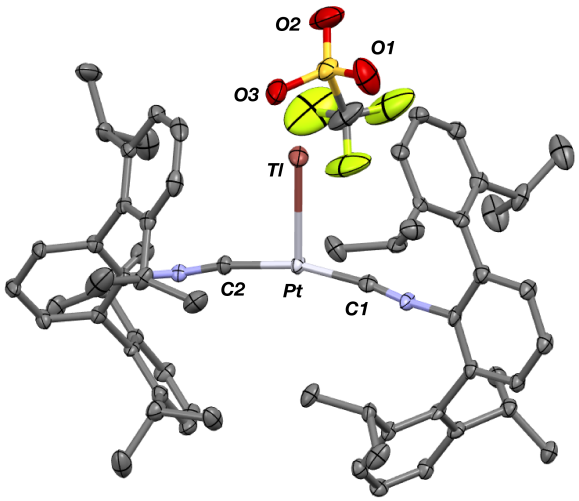

Figure 4.1. Molecular structure of [TlPt(CNAr^{Dipp2})$_2$]OTf • 1.5 Et_2O (**1** • 1.5 Et_2O). Co-crystallized molecules of diethyl ether have been omitted for clarity. Selected bond distances (Å) and angles (º): Pt-Tl = 2.8617(3); Tl-O3 = 2.799(5); Pt-C1 = 1.919(5); Pt-C2 = 1.916(5); C1-Pt-Tl = 95.9(1); C2-Pt-Tl = 95.9(1); C1-Pt-C2 = 165.3(2).

Although [TlPt(CNAr^{Dipp2})$_2$]OTf (**1**) gives rise to a sharp set of ^{1}H and ^{13}C{^{1}H} NMR resonances in benzene-d_6, other spectroscopic data suggest that the metal-metal interaction is labile in solution. While the IR absorption bands of Pt(CNAr^{Dipp2})$_2$ are not apparent in the IR spectrum of **1**, it is important to note that υ(C≡N) bands corresponding to Pd(CNAr^{Dipp2})$_2$ are readily observable as a minor component in the IR spectrum of [TlPd(CNAr^{Dipp2})$_2$]OTf (**2**) in C_6D_6 solution, thereby suggesting the presence of an equilibrium between bound and unbound Tl(I) (Figure 4.2). In addition, extended scanning failed to locate the ^{195}Pt NMR[62] resonance for the platinum analogue [TlPt(CNAr^{Dipp2})$_2$]OTf (**1**). We suggest that this observation is indicative of lability in the Pt-Tl interaction on the NMR timescale, resulting in a broadening of this resonance that obviates its detection at room temperature.

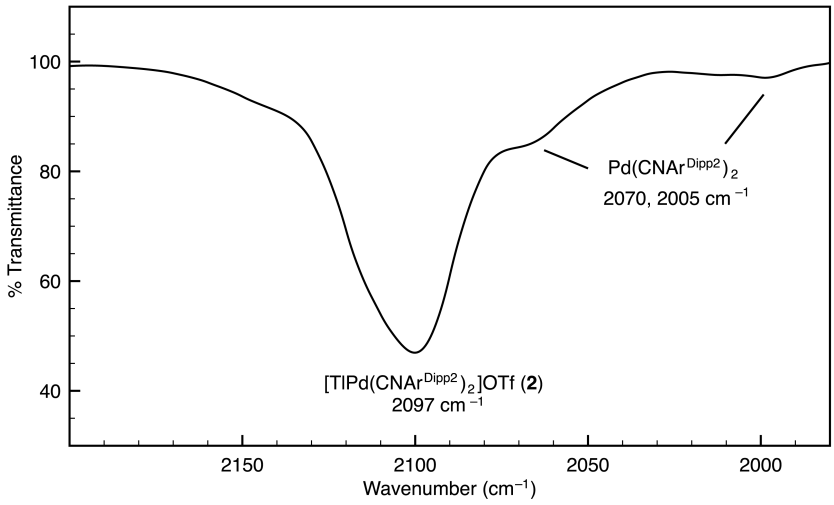

Figure 4.2. FTIR spectrum (υ(C≡N) region) of $[TlPd(CNAr^{Dipp2})_2]OTf$ (**2**) showing the presence of $Pd(CNAr^{Dipp2})_2$. Conditions: C_6D_6, 20 ˚C, KBr windows.

As the lability of unsupported M-Tl linkages have been observed to display a dependence on counteranion identity,[58] we sought to explore the behavior of $[TlM(CNAr^{Dipp2})_2]^+$ (M = Pt, Pd) when accompanied by a traditionally non-coordinating anion. Addition of an Et_2O solution of $NaBAr^F_4$ (BAr^F_4 = $[B(3,5\text{-}(CF_3)_2C_6H_3)_4]^-$) to **1** or **2** results in precipitation of NaOTf and smooth formation of $[(Et_2O)TlM(CNAr^{Dipp2})_2]BAr^F_4$ (M = Pt (**3**(Et_2O)), Pd (**4**(Et_2O))) following crystallization from Et_2O (Figure 4.3). Structural determinations of **3**(Et_2O) and **4**(Et_2O) reveal discreet cation-anion pairs (two independent pairs per asymmetric unit). While no contact between the Tl center and the $[BAr^F_4]^-$ anion is evident in the solid state, the Tl center is bound to a molecule of Et_2O in both complexes (average d(Tl-O) = 2.760(3) Å (**3**) and 2.729(3) Å (**4**)). Furthermore, as noted for **1**, long-range contacts (ca. 3.4 Å) between Tl and several C_{aryl} atoms of the flanking Dipp rings are apparent. The Tl-bound ether molecules are easily liberated from crystalline samples upon prolonged exposure to vacuum (~100 mTorr) as assayed by ^1H NMR spectroscopy. Subsequent crystallization

of **3** from toluene produces solvent-free $[TlPt(CNAr^{Dipp2})_2]BAr^F_4$ (**3**, Figure 4.4), which contains Tl-(η^2-arene) interactions with the flanking Dipp rings (d(Tl-C) = 3.188–3.616 Å).[63] In the case of **4**, cooling a saturated toluene solution to –35 ˚C yields $[(\eta^6\text{-}Tol)_2TlPd(CNAr^{Dipp2})_2]BAr^F_4$ (**4**$(Tol)_2$, Figure 4.5), which displays two toluene molecules bound in an η^6-fashion to Tl (d(Tl-C) = 3.192–3.589 Å). Although the Tl-C_{arene} distances in **3** and **4**$(Tol)_2$ are seemingly long, they are well in line with other structurally characterized examples of Tl-arene π-complexes.[60,64-67]

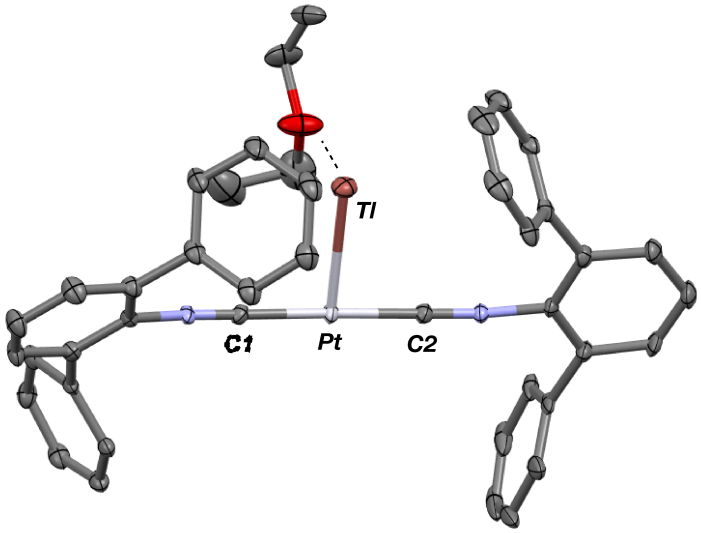

Figure 4.3. Molecular structure of $[(Et_2O)TlPt(CNAr^{Dipp2})_2]BAr^F_4$ (**3**(Et_2O)). Isopropyl groups and BAr^F_4 counteranion have been omitted for clarity. Only one of two crystallographically independent molecules is shown, with metrical parameters reported as averages between these molecules. Selected bond distances (Å) and angles (º): Pt-Tl = 2.7710(4); Pt-C1 = 1.932(4); Pt-C2 = 1.914(4); Tl-O = 2.760(3); C1-Pt-Tl = 94.5(1); C2-Pt-Tl = 86.2(1); C1-Pt-C2 = 173.4(1). The Pd analogue **4**(Et_2O) is isostructural and isomorphous.

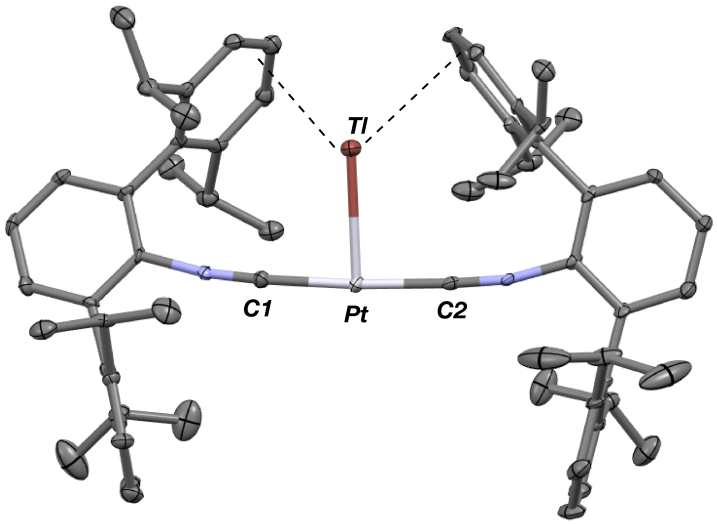

Figure 4.4. Molecular structure of $[TlPt(CNAr^{Dipp2})_2]BAr^F_4$ (**3**). BAr^F_4 counterion has been omitted for clarity. Only one of two crystallographically independent molecules is shown, with metrical parameters reported as averages between these molecules. Selected bond distances (Å) and angles (º): Pt-Tl = 2.7659(5); Pt-C1 = 1.933(8); Pt-C2 = 1.934(8); C1-Pt-Tl = 93.2(2); C2-Pt-Tl = 86.6(2); C1-Pt-C2 = 173.8(3).

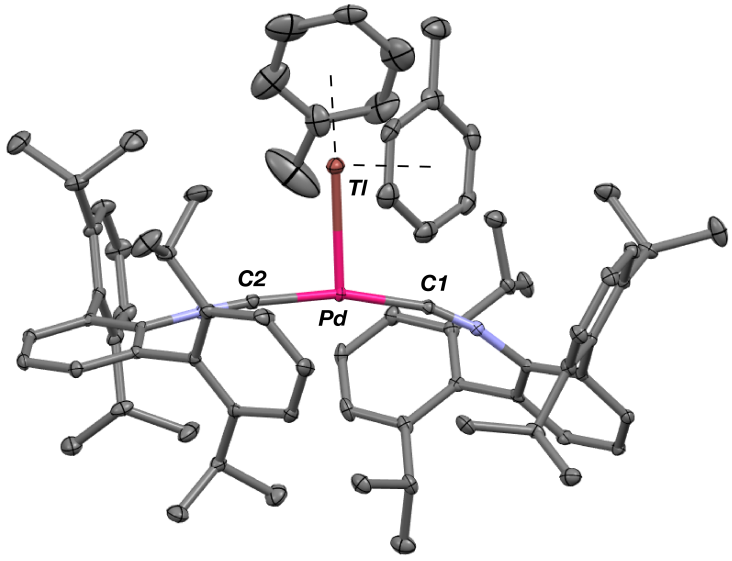

Figure 4.5. Molecular structure of $[(\eta^6\text{-}C_7H_8)_2TlPd(CNAr^{Dipp2})_2]BAr^F_4$ (**4**$(Tol)_2$). BAr^F_4 counterion has been omitted for clarity. Selected bond distances (Å) and angles (º): Pd-Tl = 2.7770(2); Pd-C1 = 1.960(3); Pd-C2 = 1.969(3); C1-Pd-Tl = 88.34(7); C2-Pd-Tl = 104.32(7); C1-Pd-C2 = 166.5(1).

Examination of the solid-state and solution-phase behavior of **1-4** reveals that replacement of the triflate anion with $[BAr^{F}_{4}]^{-}$ has important ramifications for the lability of the M→Tl linkage. In both solvates of **3** and **4**, the M-Tl distance is significantly contracted relative to **1** and **2** (Table 4.1), consistent with an increase in the degree of M→Tl donation. As the triflate anion likely stabilizes the Tl center through contact ion pairing, replacement of $[OTf]^{-}$ with neutral Et_2O or arene donors appears to only partially compensate for the loss of this ionic association. Accordingly, in an attempt to recoup some of this stabilization, we contend that the degree of M→Tl σ-donation is increased. This notion is supported by the progression of the υ(C≡N) bands in **3** (2121 cm^{-1}) and **4** (2116 cm^{-1}) to higher energies relative to **1-2**, as the increased withdrawal of electron density from the group 10 metal by Tl serves to attenuate backbonding interactions with the isocyanide ligands. Importantly, and in contrast to the triflate salt $[TlPd(CNAr^{Dipp2})_2]OTf$ (**2**), the solution FTIR spectra of **3** and **4** in benzene-d_6 are devoid of υ(C≡N) features corresponding to $M(CNAr^{Dipp2})_2$, signalling that Tl(I) dissociation in benzene can be significantly inhibited by the use of the weakly coordinating $[BAr^{F}_{4}]^{-}$ anion. Interestingly, this replacement also allows for detection of the ^{195}Pt NMR resonance of $[TlPt(CNAr^{Dipp2})_2]BAr^{F}_{4}$ (**3**), which appears as a doublet with well-resolved coupling to ^{205}Tl (δ = –3802 ppm, $^{1}J_{Pt,Tl}$ = 11.2 kHz).[68] This resonance is shifted significantly downfield respective to that of $Pt(CNAr^{Dipp2})_2$ (δ = –5993 ppm (s), C_6D_6), further suggestive of decreased electron density at the Pt center upon coordination of Tl(I).[69,70] However, it is also important to note that dissolution of **1-4** in THF results in complete dissociation of the Tl(I) center and formation of $M(CNAr^{Dipp2})_2$ according to

FTIR spectroscopy. This result, which was similarly observed in the case of [TlNi(CNAr^{Dipp2})$_3$]OTf,[54] serves as a reminder of the weak dissociation energies inherent in most unsupported metal-metal dative bonds, as dissolution in solvents of moderate coordinating strength is sufficient to completely disrupt this interaction.

Table 4.1. Selected bond distances (X-ray structure) of Pt(CNAr^{Dipp2})$_2$, Pd(CNAr^{Dipp2})$_2$, and their Tl-containing MOLPs.

Complex	d(M-C$_{iso}$)	d(M-Tl)
Pt(CNAr^{Dipp2})$_2$[a]	1.906(3) Å	–
Pd(CNAr^{Dipp2})$_2$[b]	1.930(4) Å	–
1	1.918(5) Å	2.8617(3) Å
2[b]	1.951(7) Å	2.855(1) Å
3(Et$_2$O)[c]	1.922(4) Å	2.7710(4) Å
4(Et$_2$O)[c]	1.958(4) Å	2.7481(5) Å
3	1.933(8) Å	2.7659(5) Å
4(Tol)$_2$	1.965(3) Å	2.7770(2) Å

[a]Data from Ref. 27. [b]Data from Ref. 50. [c]One of the two crystallographically independent molecules in the Xray structures of **3**(Et$_2$O) and **4**(Et$_2$O) contain two-site disorder of the Tl atom. We have used the major component of this disorder to calculate the average d(M-Tl).

Although limited experimental techniques are capable of probing metal-metal dative interactions, X-ray Absorption Near-Edge Spectroscopy (XANES)[71] has begun to find an important use in this regard.[30,34] Importantly, its utility lies in its ability to decipher the spectroscopic oxidation states of the metals involved in a given bonding interaction. In order to assess the degree of charge transfer inherent in the formation of a reverse-dative σ-interaction to Tl(I), Pd K-edge XANES was carried out on the palladium-thallium adduct [TlPd(CNAr^{Dipp2})$_2$]OTf (**2**, Figure 4.6). While neither the Pd K-edge spectra of **2** nor that of Pd(CNAr^{Dipp2})$_2$ display a discernable pre-edge feature, both exhibit nearly identical energies for the rising edge of the XANES region. In comparison, the rising edge energy of the Pd(II) peroxo complex[50,72] Pd(η^2-O$_2$)(CNAr^{Dipp2})$_2$ is shifted to higher energy by *ca*. 4.0 eV relative to that of

$Pd(CNAr^{Dipp2})_2$ and **2**. Despite their differing geometries, the rising edge transition for each of these three Pd complexes should involve the promotion of a core 1s electron to a 5*p* orbital that is relatively unperturbed by ligand field effects. Accordingly, the marked shift of the rising edge to higher energy for $Pd(\eta^2\text{-}O_2)(CNAr^{Dipp2})_2$ can be reasonably attributed to the presence of an oxidized Pd center relative to that found in $Pd(CNAr^{Dipp2})_2$ or **2**. However, the near-identical rising edge energies observed for $Pd(CNAr^{Dipp2})_2$ and **2** strongly reflect that Tl(I) binding to an electron rich Pd center does not result in a formal oxidative event.

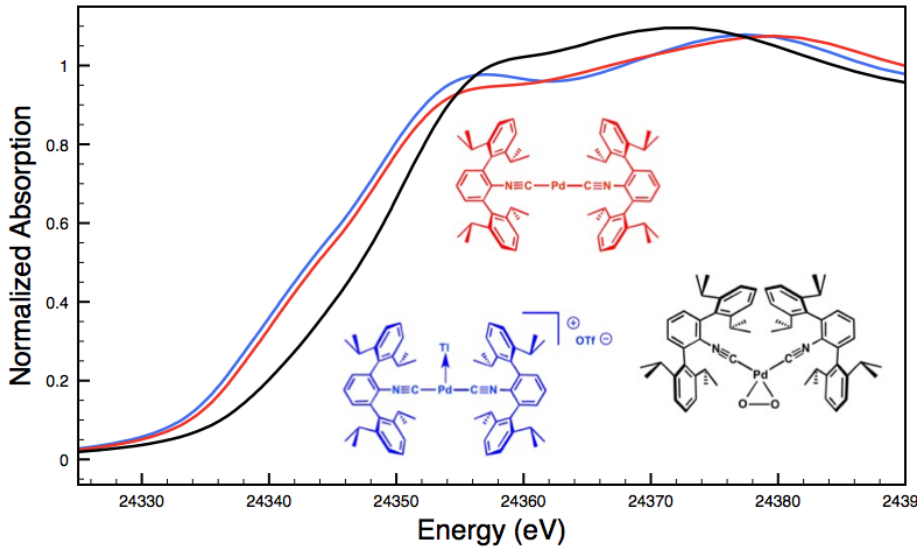

Figure 4.6. Comparative Pd K-edge XANES spectra of $Pd(CNAr^{Dipp2})_2$ (red), $[TlPd(CNAr^{Dipp2})_2]OTf$ (**2**, blue), and $Pd(\eta^2\text{-}O_2)(CNAr^{Dipp2})_2$ (black).

For an additional comparison, XANES measurements were carried out on the binary nickel tris-isocyanide complex $Ni(CNAr^{Mes2})_3$ and its adduct with Tl(I), $[TlNi(CNAr^{Mes2})_3]OTf$.[49] Despite the unambiguous d^{10} configuration of $Ni(CNAr^{Mes2})_3$, its Ni K-edge absorption spectrum (Figure 4.7) displays a prominent pre-edge feature,

which is likely the result of a 1s to isocyanide π* transition. The analogous absorption band for [TlNi(CNAr^{Mes2})$_3$]OTf occurs at an identical energy, again signalling that the formation of a reverse-dative M→Tl σ-interaction does not result in significant formal charge transfer from the Group 10 metal.

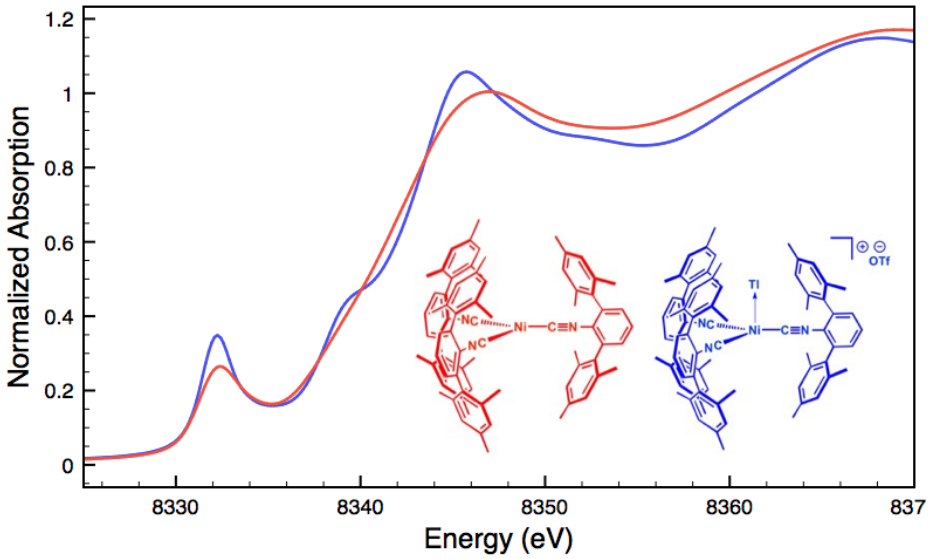

Figure 4.7. Comparative Ni K-edge XANES spectra of Ni(CNAr^{Mes2})$_3$ (red) and [TlNi(CNAr^{Mes2})$_3$]OTf (blue).

The fact that neither Pd(CNAr^{Dipp2})$_2$ nor Ni(CNAr^{Mes2})$_3$ undergo significant charge transfer via the formation of a reverse-dative σ-interaction to Tl(I) suggests some important guidelines regarding the proper formalisms that should be used to describe such MOLPs. Although Tl(I) can exhibit Lewis basic properties under extraordinary conditions,[73] the stabilization of its 6*s*^{2} "inert pair" due to relativistic effects[74] should render it a very weak 2e$^-$ donor. As such, the electrons involved in a covalent interaction between an electron-rich transition metal and Tl(I) center will most plausibly be supplied by the former, meaning that the valence count of the transition metal must necessarily increase by two units. However, this interaction should *not* be described as effecting a

two-unit increase in the formal oxidation state of the transition metal, as such an event would be readily apparent in the comparative XANES spectra of $M(CNR)_n$ and $[TlM(CNR)_n]^+$ complexes. This conclusion is further supported by the modest changes in the FTIR υ(C≡N) energies between the neutral parent compounds and their Tl(I) adducts (*ca.* 50 cm^{-1}). For comparison, the Pd(II) and Ni(II) complexes *trans*-$PdCl_2(CNAr^{Dipp2})_2$ and *trans*-$NiCl_2(CNAr^{Mes2})_2$ display IR υ(C≡N) bands that are blue-shifted by *ca*. 200 cm^{-1} relative to $Pd(CNAr^{Dipp2})_2$ and $Ni(CNAr^{Mes2})_3$.[49,75]

4.3. Synthesis and spectroscopic features of Metal-only Lewis Pairs containing a Ag(I) Lewis acidic center

The abilities of $M(CNAr^{Dipp2})_2$ (M = Pt, Pd) to act as the basic components of Metal-Only Lewis Pairs can also be extended to Lewis acidic Ag(I) centers.[76] Treatment of $Pt(CNAr^{Dipp2})_2$ with AgOTf in Et_2O results in precipitation of the heterobimetallic salt $[AgPt(CNAr^{Dipp2})_2]OTf$ (**5**) as a yellow powder (Scheme 4.2). Attempts to synthesize the palladium analogue $[AgPd(CNAr^{Dipp2})_2]OTf$ (**6**) in the same fashion results in the formation of metallic mirrors and free $CNAr^{Dipp2}$. However, performing the synthesis at reduced temperatures (*ca*. –100 ˚C) allows for **6** to be precipitated from solution as a pale yellow powder in modest yields. Crystallization of **5** or **6** from THF/$(TMS)_2O$ at –35 ˚C yields *trans*-$[AgM(CNAr^{Dipp2})_2(THF)]OTf$ (**5**(THF), M = Pt; **6**(THF), M = Pd), where a molecule of THF is bound to the Group 10 metal *trans* to the coordinated Ag center (Figure 4.8). The $M\text{-}O_{THF}$ distances in **5**(THF) (2.366(5) Å) and **6**(THF) (2.326(7) Å) are long relative to Pd and Pt etherate complexes reported in the Cambridge Structural Database (see Figures 4.13-14),[77] thereby suggesting an attenuated interaction of THF

with the Group 10 metal center. Indeed, the ^{1}H NMR spectra obtained from crystalline **5**(THF) and **6**(THF) in C_6D_6 show sharp peaks occurring at the expected chemical shift values for free THF.[78] Further, prolonged exposure of crystalline samples to vacuum (~100 mTorr) successfully liberates all THF as analyzed by ^{1}H NMR spectroscopy. Subsequent recrystallization of these samples from Et_2O/C_6H_6 (**5**) or *n*-hexane/toluene (**6**) yields **5**(C_6H_6) and **6**(C_7H_8) (Figures 4.9 and 4.10), which display η^1-C_{arene} interactions between the Group 10 metal and arene solvent in the position *trans* to Ag (for **5**, d(Pt-C63 = 2.885(7) Å); for **6**, d(Pd-C64) = 2.496(3)). These interactions are notable given the likely intermediacy of transient π-complexes[79] in the C-H activation of arenes by electrophilic group 10 complexes.[80,81]

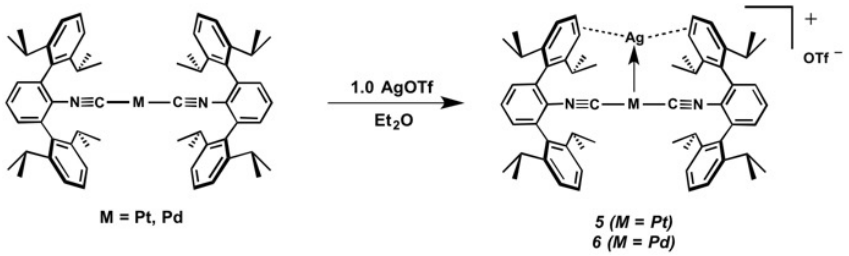

Scheme 4.2. Synthesis of Ag-containing MOLPs based off of the $M(CNAr^{Dipp2})_2$ (M = Pt, Pd) platform.

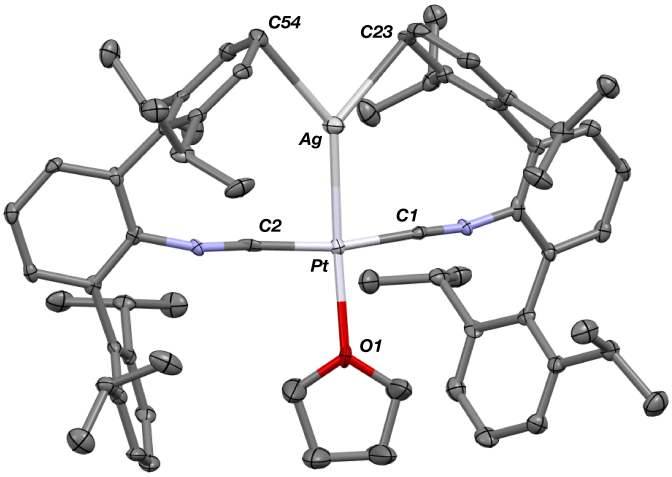

Figure 4.8. Molecular structure of [AgPt(CNAr^{Dipp2})$_2$(THF)]OTf • 3 THF (**5**(THF) • 3 THF). Triflate counteranion has been omitted for clarity. Non-coordinating THF molecules were accounted for using SQUEEZE. Selected bond distances (Å) and angles (º): Pt-Ag = 2.6299(6); Pt-C1 = 1.932(8); Pt-C2 = 1.920(9); Pt-O1 = 2.366(5); Ag-C23 = 2.661(8); Ag-C54 = 2.660(8); C1-Pt-Ag = 83.9(2); C2-Pt-Ag = 86.4(2); O1-Pt-Ag = 173.0(1). The palladium analogue **6**(THF) • 6.5 (THF) is isostructural and isomorphous.

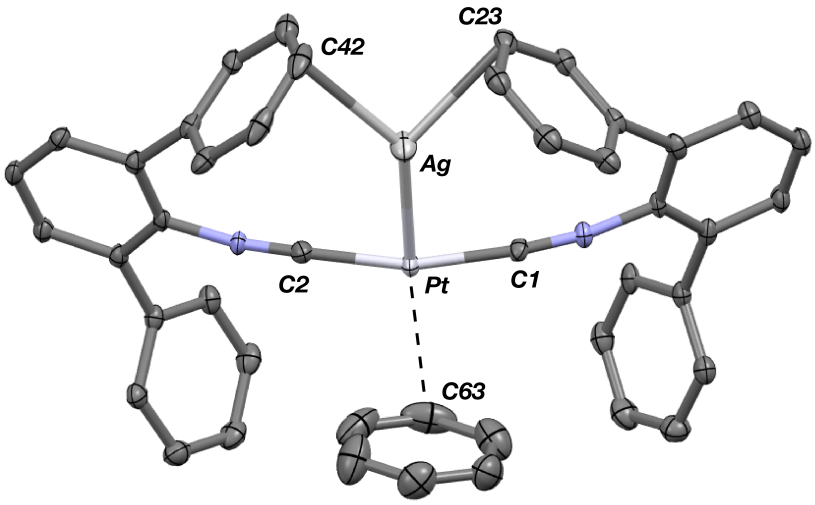

Figure 4.9. Molecular structure of [AgPt(CNAr^{Dipp2})$_2$(η^1-C_6H_6)]OTf • 3 C_6H_6 (**5**(C_6H_6) • 3 C_6H_6). Isopropyl groups, co-crystallized benzene molecules and triflate counteranion have been omitted for clarity. Selected bond distances (Å) and angles (º): Pt-Ag = 2.6463(5); Pt-C1 = 1.923(5); Pt-C2 = 1.909(4); Pt-C63 = 2.885(7); Ag-C23 = 2.587(5); Ag-C42 = 2.633(5); C1-Pt-Ag = 86.7(2); C2-Pt-Ag = 84.9(1).

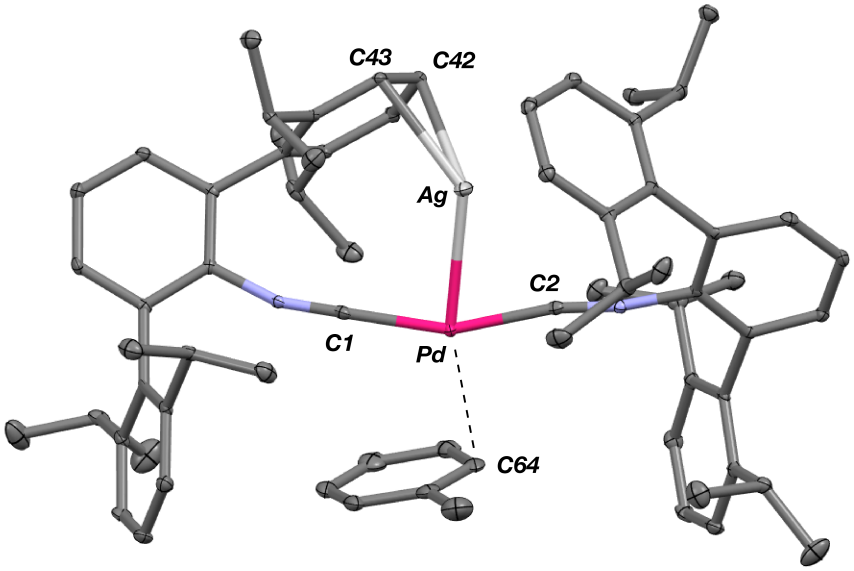

Figure 4.10. Molecular structure of [AgPd(CNAr^{Dipp2})$_2$(η^1-C_7H_8)]OTf • C_7H_8 (**6**(C_7H_8) • C_7H_8). Triflate counteranion and co-crystallized toluene molecule have been omitted for clarity. Selected bond distances (Å) and angles (º): Pd-Ag = 2.6112(4); Pd-C1 = 1.962(3); Pd-C2 = 1.939(3); Pd-C64 = 2.496(3); Ag-C42 = 2.632(2); Ag-C43 = 2.506(2); C1-Pd-Ag = 86.88(7); C2-Pd-Ag = 72.49(7).

The M-Ag bond lengths in both solvates of **5** and **6** are among the shortest reported in the Cambridge Structural Database (see Table 4.2 and Figures 4.15-16). As was seen for the M-Tl adducts above, the metal-metal interactions in **5**-**6** can be rationalized via M→Ag σ-donation, a notion that is supported by the increase in isocyanide υ(C≡N) stretching frequencies relative to M(CNAr^{Dipp2})$_2$ (M = Pt, Pd) upon coordination of Ag(I) (υ(C≡N) = 2094 cm^{-1} (**5**); 2082 cm^{-1} (**6**)). An examination of the solid state structures of **5** and **6** also implicates a role of the flanking Dipp aryl rings in buttressing the M-Ag linkage through π-type interactions. Interestingly, these contacts are reflected in the room temperature ^{1}H NMR spectra of **5** and **6** (measured in C_6D_6)**,** for which the resonances corresponding to the Dipp aryl protons are broadened and shifted downfield by *ca.* 0.2 ppm relative to those typically observed for diamagnetic

mononuclear complexes containing the $CNAr^{Dipp2}$ ligand. It is also notable that the different solvates of both **5** and **6** both display a square-planar coordination environment around the Group 10 metal. While these geometries are certainly reminiscent of Pt(II) and Pd(II), it is critical to note that the progression of the IR υ(C≡N) stretching frequencies to higher energies upon binding of Ag(I) is quite modest and actually less than that seen for Tl(I). This observation serves to suggest that similar bonding descriptions laid out above for Tl-containing **1**-**4** can be extended to **5** and **6**. While the use of electrons from the Group 10 metal to form a covalent interaction with Ag requires an increase of two valence units, minimal charge transfer to Ag occurs. As such, we do not believe that these M/Ag MOLPs should not be described as containing formal M(II) centers (M = Pt, Pd).

Table 4.2. Selected bond distances (X-ray structure) in Ag-containing Metal-only Lewis pairs.

Complex	d(M-C_{iso})	d(M-Ag)
5(THF)	1.926(8) Å	2.6299(6) Å
6(THF)	1.941(9) Å	2.6303(9) Å
5(C_6H_6)	1.916(4) Å	2.6463(5) Å
6(C_7H_8)	1.950(3) Å	2.6112(4) Å

4.4. Rationalization of observed solvent binding *trans* to Ag

Despite the fact that formation of a M-Ag bonding interaction does not result in a formal oxidative event at Pt/Pd, it is remarkable that the Ag-containing heterobimetallics **5**-**6** will bind THF and arene molecules at the group 10 metal center in the solid state, whereas the zero-valent precursors $M(CNAr^{Dipp2})_2$ (M = Pt, Pd) do not. Furthermore, $Pt(CNAr^{Dipp2})_2$ and $Pd(CNAr^{Dipp2})_2$ do not participate in addition reactions with stronger σ-donors (*e.g.* phosphines) to form species of the type $ML(CNAr^{Dipp2})_2$, as the attempted syntheses of such compounds has led invariably to isocyanide dissociation and/or

decomposition. While the ability of **5** and **6** to bind an additional Lewis base may be partly attributable to increased positive charge on the complexes, molecular orbital considerations provide a basis for enhanced Lewis acidity at the Group 10 metal center of these MOLPs specifically. It has been suggested previously that coordination of a Z-type acceptor ligand to a square-planar d^8 complex should result in enhanced affinity for Lewis bases at the open coordination site *trans* to the acceptor.[82] Similarly, formation of a reverse-dative σ-interaction by $M(CNAr^{Dipp2})_2$ (nominally from the nd_Z^2 orbital) to an acceptor may have a stabilizing effect on the coaxial empty $(n+1)p_z$ orbital of the Group 10 metal (Figure 4.11). While such stabilization may not be drastic, it is plausible that such effects could promote the binding of Lewis bases at a coordination site *trans* to the acceptor, resulting in square-planar $[AgML_2L']^+$-type species. Similar behavior was observed by Peters in the trigonal-pyramidal Pt salt $[(SiP^{Ph}_3)Pt]BAr^F_4$,[83] (SiP^{Ph}_3 = (2-$Ph_2PC_6H_4)_3Si$) for which the crystal structure shows a molecule of toluene bound in the apical position *trans* to the silyl group. As silyl ligands can be viewed in certain systems as silylium Lewis acids,[84] the binding of an arene molecule may be a result of Pt-to-Si σ-donation, thereby in effect enhancing the Lewis acidic nature of the Pt complex. In addition, similar phenomena have been observed by Gabbaï for a Hg(II) complex[85] and by Berry for a bimetallic Mo_2 system.[86] In these examples, association of a Z-type fragment was shown to increase Lewis acidity at the coordination site *trans* to the acceptor ligand. However, to our knowledge, the MOLPs derived from $M(CNAr^{Dipp2})_2$ (M = Pt, Pd) represent unique cases where Z-ligand-promoted Lewis acidity has been unambiguously observed for mononuclear transition metal complexes. Importantly, these observations highlight the ability of σ-acceptor ligands to open up a previously

unavailable coordination site on a transition metal center without effecting a formal oxidative event. Furthermore, the observation that the Ag-containing complexes **5** and **6** bind solvent molecules at the Group-10 metal center, while the Tl-containing complexes **1** and **2** exhibit binding at the Tl center, is likely attributable to the greater electronegativity of Ag relative to Tl.[87] As stabilization of the empty p_z orbital on the Group 10 metal by a bound Lewis acid is expected to be marginal at best, Lewis acids possessing greater group electronegativity may be expected to more effectively stabilize this orbital and render it accessible to an exogenous Lewis base.

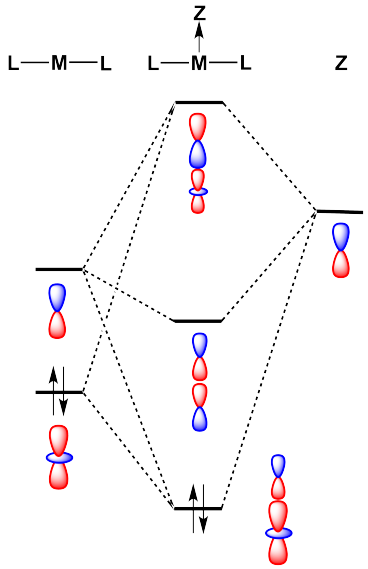

Figure 4.11. Molecular orbital diagram for a transition metal (**M**) bound to a σ-acceptor fragment (**Z**), showing how the LUMO of the resulting adduct can be stabilized with respect to the acceptor-free complex.

Although [AgPt(CNAr^{Dipp2})$_2$]OTf (**5**) contains one acceptor fragment bound to platinum, its Pt-Ag unit can accommodate another equivalent of Ag(I). Stirring [AgPt(CNAr^{Dipp2})$_2$]OTf (**5**) and equimolar AgOTf in THF followed by crystallization from benzene/THF (20:1) yields {[Ag$_2$Pt(CNAr^{Dipp2})$_2$(η^1-C$_6$H$_6$)]$_2$(μ-OTf)$_2$}(OTf)$_2$ (**7**) as determined by X-ray diffraction. Attempts to synthesize a palladium analogue from

[AgPd(CNAr^{Dipp2})$_2$]OTf (**6**) resulted only in decomposition. The solid-state structure of **7** (Figure 4.12) reveals a centro-symmetric dimer composed of *triangulo*-PtAg$_2$ cores (average d(Pt-Ag) = 2.6843(6) Å; d(Ag-Ag) = 2.7684(8) Å) bridged by two triflate groups. Consistent with the coordination of an additional Lewis acid to the Pt-Ag unit in **5**, the isocyanide stretching frequencies of **7** are shifted to higher energies (2132, 2169 cm^{-1}, KBr pellet) compared to **5**. In the solid state, the platinum centers in **7** also feature η^1-*C*-bound benzene molecules *trans* to one of the silver atoms as seen in **5**(C_6H_6). Interestingly however, the Pt-$C_{benzene}$ distance in **7** (d(Pt-C1) = 2.529(7) Å) is significantly contracted relative to that in **5**(C_6H_6), a further indication of an increase in the Lewis acidity in the Pt center in **7** promoted by the presence of a second Ag center. It is also important to note that relative to complex **5,** the second Ag atom in **7** (i.e. Ag(2), Figure 12) can best be described as occupying the axial position of a nominally square-planar Pt center. As the binding of Lewis acids to the axial position square planar Pt(II) centers is known,[88-92] complex **7** provides additional evidence that the presence of one Z-type ligand effectively results in the formation of a divalent Pt center capable of binding a second Z-type ligand. However, this electronic modulation occurs without formal oxidation of the Pt center.

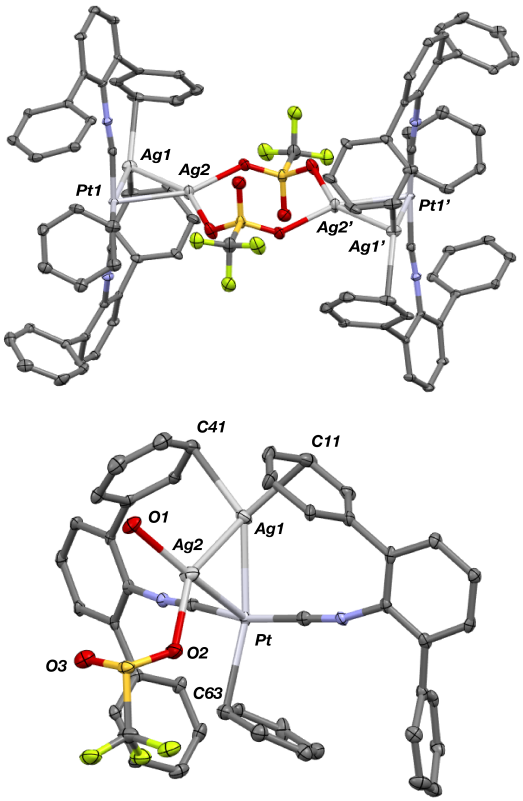

Figure 4.12. Top: Molecular structure $\{[Ag_2Pt(CNAr^{Dipp2})_2(\eta^1\text{-}C_6H_6)]_2(\mu\text{-}OTf)_2\}(OTf)_2 \bullet 2\ C_6H_6$ (**7** • 2 C_6H_6), with isopropyl groups, co-crystallized benzene molecules and two non-coordinating triflate counteranions omitted for clarity. Bottom: Zoom-in on one half of the dimeric structure (other half of dimer is related by a crystallographic inversion center), clearly showing the Pt-η^1-C_6H_6 interaction. Selected bond distances (Å) and angles (º): Pt-Ag1 = 2.6799(7); Pt-Ag2 = 2.6888(7); Ag1-Ag2 = 2.7684(8); Pt-C63 = 2.529(7); Ag1-C11 = 2.490(7); Ag1-C41 = 2.608(7); Pt-Ag1-Ag2 = 59.12(2); Ag1-Ag2-Pt = 58.80(2); Ag2-Pt-Ag1 = 62.08(2).

4.5. Concluding Remarks

Zero-valent binary *m*-terphenyl isocyanide complexes of Pt and Pd are excellent candidates for acting as the Lewis basic component of Metal-only Lewis Pairs (MOLPs). In addition to stabilizing low oxidation states, the steric encumbrance of the *m*-terphenyl isocyanide ligand promotes coordinative unsaturation, yielding electron-rich metal centers that can accommodate an exogenous Lewis acid in the primary coordination sphere. Furthermore, the IR υ(C≡N) resonances provide a convenient handle to assess the

degree of Group 10 metal σ-donation in these complexes. In this work, it has been demonstrated that $Pt(CNAr^{Dipp2})_2$ and $Pd(CNAr^{Dipp2})_2$ can form discreet and unsupported adducts with Tl(I). Although these bonding interactions are not particularly robust, use of the weakly coordinating anion $BAr^{F}_{4}^{-}$ diminishes the lability of the M-Tl bond in non-coordinating solvents. Analysis of two M→Tl adducts by XANES spectroscopy provides compelling evidence that any degree of formal charge transfer inherent in these metal-metal interactions is minimal, and that therefore no formal oxidative event takes place upon binding of Tl(I). The ability of $Pt(CNAr^{Dipp2})_2$ and $Pd(CNAr^{Dipp2})_2$ to form Lewis Pairs with Ag(I) has also been demonstrated, with FTIR spectroscopy and X-ray crystallography suggesting, again, that no significant charge transfer to Ag occurs in the adducts. Despite this fact, the binding of Ag(I) activates the Group 10 metal toward the ligation of Lewis bases *trans* to the Ag acceptor, thus highlighting how σ-acceptor ligands can be utilized to tune the reactivity profiles of electron-rich transition metal complexes. The Pt/Ag MOLP $[AgPt(CNAr^{Dipp2})_2]OTf$ (**5**) can also accommodate an additional equivalent of AgOTf to form dimeric **7**, which further increases the Lewis acidity of the Pt center. These results indicate that the presence of a reverse-dative σ-interaction can activate the coordination site *trans* to it for binding of Lewis bases despite the high *trans* influence exhibited by Z-type ligands.[24,25] Such modulation can be thought of as a novel type of cooperative effect between a Lewis acid and Lewis base, whereby the former alters the reactivity profile of the electron rich metal without directly participating in the reaction with an incoming substrate. A more detailed understanding of the possibilities afforded by such cooperative effects is currently being pursued in our laboratory.

4.6. Synthetic procedures and characterization data

General considerations. All manipulations were carried out under an atmosphere of purified dinitrogen using standard Schlenk and glovebox techniques. Unless otherwise stated, reagent-grade starting materials were purchased from commercial sources and either used as received or purified by standard procedures.[93] Solvents were dried and deoxygenated according to standard procedures.[94] Benzene-d_6 (Cambridge Isotope Laboratories) was distilled from NaK alloy/benzophenone and stored over activated 4 Å molecular sieves for 2 d prior to use. Celite 405 (Fisher Scientific) was dried under vacuum (24 h) at a temperature above 250 °C and stored in the glovebox prior to use. KBr (FTIR grade from Aldrich) was stirred overnight in anhydrous THF, filtered and dried under vacuum (24 h) at a temperature above 250 °C and stored in the glovebox prior to use. $Pt(CNAr^{Dipp2})_2$, $[TlNi(CNAr^{Mes2})_3]OTf$ and $[TlPd(CNAr^{Dipp2})_2]OTf$ were prepared as previously described.[27,49,50] $NaBAr^F_4$ was prepared according to a literature procedure.[95]

Solution ^1H, $^{13}C\{^1H\}$, ^{19}F, and ^{195}Pt NMR spectra were recorded on a Jeol ECA 500, a Varian X-SENS 500, or a Bruker Avance 300 spectrometer. ^1H and $^{13}C\{^1H\}$ chemical shifts are reported in ppm relative to $SiMe_4$ (^1H and ^{13}C δ = 0.0 ppm) with reference to residual solvent resonances of 7.16 ppm (^1H) and 128.06 ppm (^{13}C) for C_6D_6. ^{19}F NMR spectra were referenced externally to neat trifluoroacetic acid, $F_3CC(O)OH$ (δ = −78.5 ppm vs. $CFCl_3$ = 0.0 ppm). ^{195}Pt spectra (direct detection) were referenced externally to 1.2 M $Na_2[PtCl_6]$ in D_2O (δ = 0 ppm). FTIR spectra were recorded on a Thermo-Nicolet iS10 FTIR spectrometer. Samples were prepared as either KBr pellets or as C_6D_6 solutions injected into a ThermoFisher solution cell equipped with KBr

windows. For solution FTIR spectra, solvent peaks were digitally subtracted from all spectra by comparison with an authentic spectrum obtained immediately prior to that of the sample. The following abbreviations were used for the intensities and characteristics of important IR absorption bands: vs = very strong, s = strong, m = medium, w = weak, vw = very weak; b = broad, vb = very broad, sh = shoulder. Combustion analyses were performed by Midwest Microlabs of Indianapolis, IN (USA) or Robertson Microlit Laboratories of Madison, NJ (USA) or Midwest Microlabs of Indianapolis, IN (USA).

Synthesis of [TlPt(CNAr^{Dipp2})$_2$]OTf (1). To a solid mixture of Pt(CNAr^{Dipp2})$_2$ (0.100 g, 0.096 mmol) and TlOTf (0.036 g, 0.102 mmol, 1.06 equiv) was added 10 mL Et_2O. This solution was stirred vigorously for 3 h, during which time a yellow precipitate formed. Benzene (1.5 mL) was added to the reaction mixture, which was stirred until no precipitate was visible. Filtration of this solution and storage at –35 ˚C overnight yielded a crop of crystals, which were collected and dried. Yield: 0.088 g, 0.063 mmol, 66%. ^{1}H NMR (C_6D_6, 499.8 MHz, 20 ºC): δ = 7.42 (t, 4H, *J* = 8 Hz, *p*-Dipp), 7.27 (d, 8H, *J* = 8 Hz, *m*-Dipp), 6.87 (t, 2H, *J* = 8 Hz, *p*-*Ar*^{Dipp2}), 6.80 (d, 4H, *J* = 8 Hz, *m*-*Ar*^{Dipp2}), 2.50 (septet, 8H, *J* = 7 Hz, C*H*(CH$_3$)$_2$), 1.24 (d, 24H, *J* = 7 Hz, CH(C*H*$_3$)$_2$), 1.06 (d, 24H, *J* = 7 Hz, CH(C*H*$_3$)$_2$) ppm. ^{13}C{^{1}H} NMR (C_6D_6, 125.7 MHz, 20 ºC): δ = 159.8 (*C*≡N), 147.1, 139.6, 134.4, 130.4, 129.9, 129.4, 126.9, 123.9, 31.5, 24.4, 24.4 ppm. ^{19}F NMR (C_6D_6, 282.3 MHz, 20 ºC): δ = –78.2 (s, OTf) ppm. FTIR (C_6D_6, 20 ºC): υ(C≡N) = 2112 cm^{-1} (vs), also 3063, 2963, 2927, 2868, 1461, 1413, 1385, 1362, 1294, 1232, 1220, 1163, 1056, 1023, 805, 793, 758, 636 cm^{-1}. Anal. calcd for $C_{63}H_{74}N_2F_3O_3SPtTl$: C, 54.21; H, 5.34; N, 2.01. Found: C, 54.30; H, 5.07; N, 2.01.

Synthesis of [TlPt(CNAr^{Dipp2})$_2$]BAr$^F_4$ (3). To an Et_2O solution of [TlPt(CNAr^{Dipp2})$_2$]OTf (0.096 g, 0.069 mmol, 5 mL) was added an Et_2O solution of NaBAr$^F_4$ (0.062 g, 0.070 mmol, 1.01 equiv, 3 mL). The solution was allowed to stir for 3 h, during which time NaOTf precipitated from solution. After filtration of this solution through Celite, all volatiles were removed *in vacuo*. Storage of a 2:1 Et_2O/$(TMS)_2O$ solution (1.5 mL) at –35 ºC overnight provided yellow crystals, which were collected and dried *in vacuo*. Yield: 0.100 g, 0.047 mmol, 68%. Crystals grown by this method correspond to **3**(Et_2O). Crystals of solvent-free **3** suitable for X-ray diffraction were grown from a toluene solution stored at –35 ˚C. ^{1}H NMR (C_6D_6, 499.8 MHz, 20 ºC): δ = 8.39 (br s, 8H, *o*-BAr$^F_4$), 7.74 (br s, 4H, *p*-BAr$^F_4$), 7.14 (t, 4H, *J* = 8 Hz, *p*-Dipp), 7.07 (d, 8H, *J* = 8 Hz, *m*-Dipp), 6.98 (t, 2H, *J* = 8 Hz, *p*-*Ar*^{Dipp2}), 6.84 (d, 4H, *J* = 8 Hz, *m*-*Ar*^{Dipp2}), 2.42 (septet, 8H, *J* = 7 Hz, C*H*$(CH_3)_2$), 1.09 (d, 24H, *J* = 7 Hz, CH(C*H*$_3)_2$), 1.02 (d, 24H, *J* = 7 Hz, CH(C*H*$_3)_2$) ppm. ^{13}C{^{1}H} NMR (C_6D_6, 125.7 MHz, 20 ºC): δ = 162.8 (q, $^1J_{C,B}$ = 50 Hz, *ipso*-BAr$^F_4$), 156.7 (*C*≡N), 147.6, 139.4, 135.6 (br s, *o*-BAr$^F_4$), 134.5, 130.7, 130.5, 130.2, 130.0 (qq, $^2J_{C,F}$ = 32 Hz, $^4J_{C,F}$ = 2 Hz, *m*-BAr$^F_4$), 125.8, 125.4 (q, $^1J_{C,F}$ = 272 Hz, -CF_3), 123.7, 118.1 (br s, *p*-BAr$^F_4$), 31.4, 24.4, 24.0 ppm. ^{19}F NMR (C_6D_6, 282.3 MHz, 20 ºC): δ = –62.9 (s, -CF_3) ppm. ^{195}Pt NMR (107.5 MHz, C_6D_6, 20 ºC): –3802 (d, $J_{Pt,Tl}$ = 11.2 kHz) ppm. Anal. calcd. for $C_{94}H_{86}N_2BF_{24}PtTl$: C, 53.51; H, 4.11; N, 1.33. Found: C, 52.82; H, 4.27; N, 1.26.

Synthesis of [TlPd(CNAr^{Dipp2})$_2$]BAr$^F_4$ (4). To an Et_2O solution of [TlPd(CNAr^{Dipp2})$_2$]OTf (0.069 g, 0.053 mmol, 5 mL) was added an Et_2O solution of NaBAr$^F_4$ (0.047 g, 0.053 mmol, 1.00 equiv, 3 mL). This solution was allowed to stir for 24 h, during which time NaOTf precipitated from solution. After filtration of this solution

through Celite, all volatiles were removed *in vacuo*. Storage of a 2:1 $Et_2O/(TMS)_2O$ solution (1 mL) at –35 ºC for 3 days yielded orange crystals, which were collected and dried *in vacuo*. Yield: 0.081 g, 0.040 mmol, 58%. Crystals grown by this method correspond to **4**(Et_2O). Crystals of **4**$(Tol)_2$ suitable for X-ray diffraction were grown from a toluene solution stored at –35 ˚C. ^{1}H NMR (C_6D_6, 499.8 MHz, 20 ºC): δ = 8.43 (br s, 8H, *o*-$BAr^F{}_4$), 7.73 (br s, 4H, *p*-$BAr^F{}_4$), 7.15 (t, 4H, *J* = 8 Hz, *p*-Dipp), 7.08 (d, 8H, *J* = 8 Hz, *m*-Dipp), 6.92 (t, 2H, *J* = 8 Hz, *p*-Ar^{Dipp2}), 6.79 (d, 4H, *J* = 8 Hz, *m*-Ar^{Dipp2}), 2.43 (septet, 8H, *J* = 7 Hz, C*H*$(CH_3)_2$), 1.11 (d, 24H, *J* = 7 Hz, CH(C*H*$_3)_2$), 1.04 (d, 24H, *J* = 7 Hz, CH(C*H*$_3)_2$) ppm. ^{13}C{^{1}H} NMR (C_6D_6, 125.7 MHz, 20 ºC): δ = 167.9 (*C*≡N), 162.8 (q, $^1J_{C,B}$ = 50 Hz, *ipso*-$BAr^F{}_4$), 147.5, 139.0, 135.5 (br s, *o*-$BAr^F{}_4$), 134.7, 130.6, 130.3, 130.1, 129.9 (qq, $^2J_{C,F}$ = 32 Hz, $^4J_{C,F}$ = 2 Hz, *m*-$BAr^F{}_4$), 126.5, 125.3 (q, $^1J_{C,F}$ = 272 Hz, -CF_3), 123.5, 118.1 (septet, $^3J_{C,F}$ = 4 Hz, *p*-$BAr^F{}_4$), 31.4, 24.5, 23.9 ppm. ^{19}F NMR (C_6D_6, 282.3 MHz, 20 ºC): δ = –62.8 (s, -CF_3) ppm. FTIR (C_6D_6, 20 ºC): υ(C≡N) = 2116 cm^{-1} (vs), also 3063, 2964, 2927, 2869, 1464, 1353, 1278, 1178, 1163, 1128, 1106, 1097, 1055, 935, 886, 840, 794, 761, 744, 714, 682, 670 cm^{-1}. Anal. calc'd for $C_{94}H_{86}N_2BF_{24}PdTl$: C, 55.86; H, 4.29; N, 1.39. Found: C, 55.84; H, 4.36; N, 1.33.

Synthesis of [AgPt(CNAr^{Dipp2})$_2$]OTf (5). To a solid mixture of Pt(CNAr^{Dipp2})$_2$ (0.100 g, 0.096 mmol) and AgOTf (0.026 g, 0.102 mmol, 1.06 equiv) was added 5 mL Et_2O. The solution was stirred vigorously for 2 h in the dark, during which time a yellow precipitate formed. The mother liquor was decanted off from the solid, which was washed once with Et_2O (3 mL) and dried. The mother liquor was dried *in vacuo*, and the resulting residue was taken up in 1.5 mL of 2:1 Et_2O/C_6H_6. Storage of this solution at –35 ºC overnight yielded a crop of crystals, which were also collected and dried. Yield: 0.105

g, 0.081 mmol, 84%. Crystals grown by this method correspond to **5**(C_6H_6) • 3 C_6H_6. Crystals of **5**(THF) • 3 THF were grown from a 1:1 solution of THF/$(TMS)_2O$ stored at –35 ˚C. ^{1}H NMR (C_6D_6, 499.8 MHz, 20 ºC): δ = 7.61 (br t, 4H, *J* = 7 Hz, *p*-Dipp), 7.45 (br d, 8H, *J* = 8 Hz, *m*-Dipp), 6.89 (t, 2H, *J* = 7 Hz, *p*-*Ar*^{Dipp2}), 6.82 (d, 4H, *J* = 8 Hz, *m*-*Ar*^{Dipp2}), 2.52 (septet, 8H, J = 7 Hz, $CH(CH_3)_2$), 1.23 (d, 24H, *J* = 7 Hz, $CH(CH_3)_2$), 1.10 (d, 24H, *J* = 7 Hz, $CH(CH_3)_2$) ppm. $^{13}C\{^1H\}$ NMR (C_6D_6, 125.7 MHz, 20 ºC): δ = 162.4 (*C*≡N), 147.3, 139.4, 134.7, 129.9, 129.5, 129.0, 127.6, 123.831.5, 24.5, 24.3 ppm. ^{19}F NMR (C_6D_6, 282.3 MHz, 20 ºC): δ = –77.7 (s, OTf) ppm. FTIR (C_6D_6, 20 ºC): υ(C≡N) = 2094 cm^{-1} (vs), also 3091, 3071, 3036, 2963, 2926, 2869, 1577, 1463, 1412, 1385, 1363, 1304, 1250, 1234, 1217, 1163, 1056, 1025, 812, 793, 760, 680, 637 cm^{-1}. Anal. calcd. for $C_{63}H_{74}N_2F_3O_3SAgPt$: C, 58.24; H, 5.74; N, 2.16. Found: C, 58.50; H, 5.85; N, 2.19.

Synthesis of [AgPd(CNAr^{Dipp2})$_2$]OTf (6). To a thawing Et_2O solution of Pd(CNAr^{Dipp2})$_2$ (0.100 g, 0.105 mmol, 4 mL) was added an equally cold 1:1 Et_2O/THF solution of AgOTf (0.028 g, 0.109 mmol, 1.04 equiv, 2 mL). The solution was stirred vigorously while keeping the temperature near the freezing point of the solvent, during which time a pale yellow precipitate formed. After 30 min, this precipitate was isolated via filtration over a fritted funnel and dried, affording [AgPd(CNAr^{Dipp2})$_2$]OTf as an analytically pure pale yellow powder. Yield: 0.044 g, 0.036 mmol, 35%. Crystals of **6**(THF) • 6.5 THF were grown from a 1:1 THF/$(TMS)_2O$ solution stored at –35 ˚C overnight. Crystals of **6**(C_7H_8) • C_7H_8 were grown from a toluene solution layered with *n*-hexane stored at –35 ˚C. ^{1}H NMR (C_6D_6, 499.8 MHz, 20 ºC): δ = 7.53 (br t, 4H, *J* = 7 Hz, *p*-Dipp), 7.41 (br d, 8H, *J* = 8 Hz, *m*-Dipp), 6.89 (t, 2H, *J* = 7 Hz, *p*-*Ar*^{Dipp2}), 6.84 (d, 4H, *J* = 8 Hz, *m*-*Ar*^{Dipp2}), 2.55 (septet, 8H, J = 7 Hz, $CH(CH_3)_2$), 1.27 (d, 24H, *J* = 7 Hz,

$CH(CH_3)_2$), 1.11 (d, 24H, J = 7 Hz, $CH(CH_3)_2$) ppm. $^{13}C\{^1H\}$ NMR (C_6D_6, 125.7 MHz, 20 ºC): δ = 158.9 (C≡N), 147.3, 139.3, 135.1, 130.0, 129.3, 128.4, 123.8, 31.5, 24.6, 24.3 ppm. *Note: One C_{aryl} resonance is believed to be overlapped by the resonances of the C_6D_6 solvent*. ^{19}F NMR (C_6D_6, 282.3 MHz, 20 ºC): δ = –77.6 (s, OTf) ppm. FTIR (C_6D_6, 20 ºC): υ(C≡N) = 2082 cm^{-1} (vs), also 3063, 3025, 2963, 2926, 2868, 2850, 1595, 1578, 1460, 1413, 1384, 1363, 1301, 1235, 1218, 1205, 1162, 1035, 1026, 792, 759, 731, 696, 636 cm^{-1}. Anal. calcd. for $C_{63}H_{74}N_2F_3O_3SAgPd$: C, 62.50; H, 6.16; N, 2.31. Found: C, 61.92; H, 6.05; N, 2.27.

Synthesis of {[$Ag_2Pt(CNAr^{Dipp2})_2(\eta^1\text{-}C_6H_6)]_2(\mu\text{-}OTf)_2$}$(OTf)_2$ (7). To a THF solution of [$AgPt(CNAr^{Dipp2})_2$]OTf (0.081 g, 0.062 mmol, 2 mL) was added a THF solution of AgOTf (0.024 mmol, 0.094 mmol, 1.50 equiv, 2 mL). This solution was stired in the dark for 30 min, whereupon all volatiles were removed in vacuo. Addition of 3 mL C_6H_6 to this residue resulted in precipiation of a yellow solid after a few minutes of stiring. This precipitate was isolated via decantation, washed with additional C_6H_6 (3 mL), and dried *in vacuo*. Yield: 0.060 g, 0.019 mmol, 62%. Crystals of **7** • 2 C_6H_6 suitable for X-ray diffraction were grown from a 20:1 C_6H_6/THF solution at room temperature. As **7** is only soluble in coordinating solvents, which outcompete Pt for ligation of Ag, NMR data was not obtained. FTIR (KBr pellet, 20 ºC): υ(C≡N) = 2132 cm^{-1} (vs) and 2169 (m sh), also 3089, 3065, 3034, 2962, 2928, 2870, 1617, 1593, 1576, 1466, 1412, 1385, 1364, 1289, 1276, 1262, 1240, 1220, 1170, 1152, 1056, 1043, 1029, 1020, 832, 825, 807, 796, 772, 762, 714, 688, 636, 625 cm^{-1}. Anal. calcd. for $C_{128}H_{148}N_4F_{12}O_{12}S_4Pt_2Ag_4$: C, 49.39; H, 4.79; N, 1.80. Found: C, 47.67; H, 5.06; N, 1.40.

Repeated attempts to obtain a more satisfactory combustion analysis were unsuccessful, a result that we attribute to the light sensitivity exhibited by complex **7**.

X-ray Absorption Near-Edge Spectroscopy (XANES). X-ray absorption measurements were conducted at the Stanford Synchrotron Radiation Lightsource (SSRL) at beamlines 7-3 and 9-3. At both beam lines, a Si(220) double-crystal monochromator was used energy for energy selection, in combination with a harmonic rejection mirror. Incident and transmitted X-ray intensities were monitored using Ar- (at the Pd K-edge) or N_2- (at the Ni K-edge) filled ionization chambers. X-ray absorption was measured in transmittance mode. During data collection, samples were maintained at a temperature of approximately 10 K using an Oxford Instruments liquid helium flow cryostat. Internal energy calibrations were performed by simultaneous measurement of Pd and Ni reference foils placed between the second and third ionization chamber, with the inflection point assigned at 24350 eV and 8333.0 eV for the first inflection point of the Pd and Ni foils, respectively. Data represent 2–5 scan averages and were processed by fitting a second-order polynomial to the pre-edge region and subtracting this background from the entire spectrum. A spline was used to model the smooth background above the edge. The data were normalized by subtracting the spline and normalizing the postedge to 1.0.

4.7. CSD search results

The Cambridge Structural Database was queried using the CSD Conquest software. The desired metrical parameters were plotted using the CSD Legacy Vista program. All results that were returned for a given set of search constraints are represented in the histograms below (Figures 4.13-16).

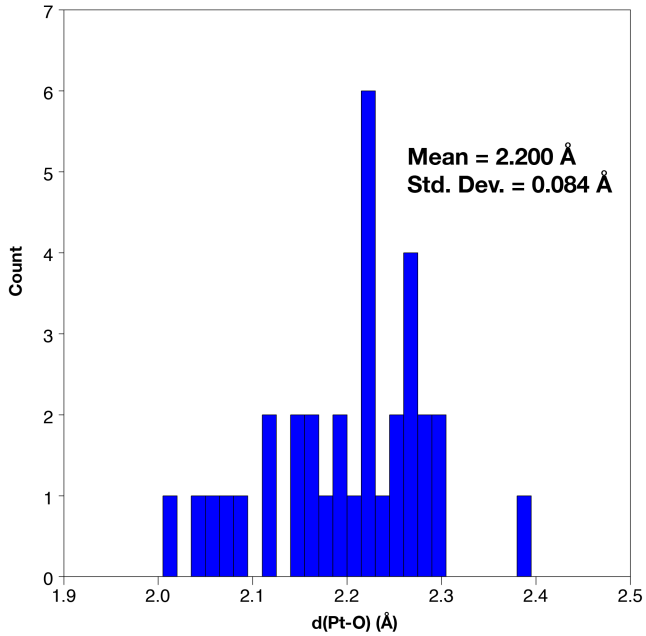

Figure 4.13. CSD search results for complexes containing Pt-O_{Ether} bonds. The search was constrained to compounds containing single bonds between Pt and O, with the oxygen atom additionally containing single bonds to exactly two carbon atoms and no additional atoms. A total of 33 data points were obtained.

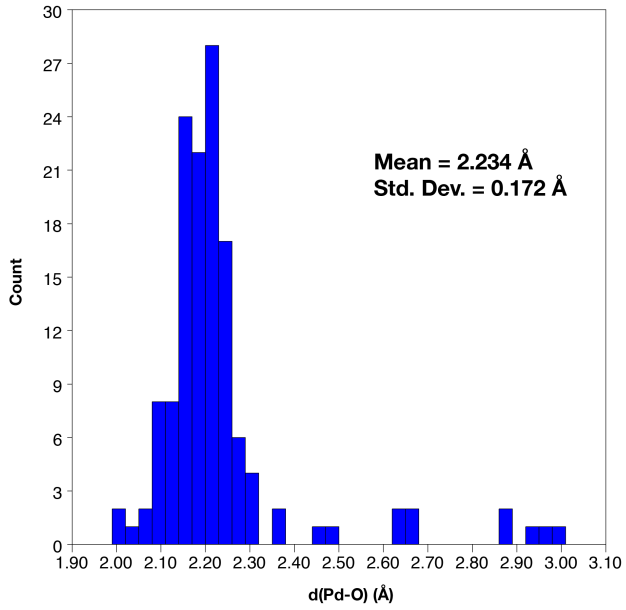

Figure 4.14. CSD search results for complexes containing Pd-O_{Ether} bonds. The search was constrained to compounds containing single bonds between Pd and O, with the oxygen atom additionally containing single bonds to exactly two carbon atoms and no additional atoms. A total of 135 data points were obtained.

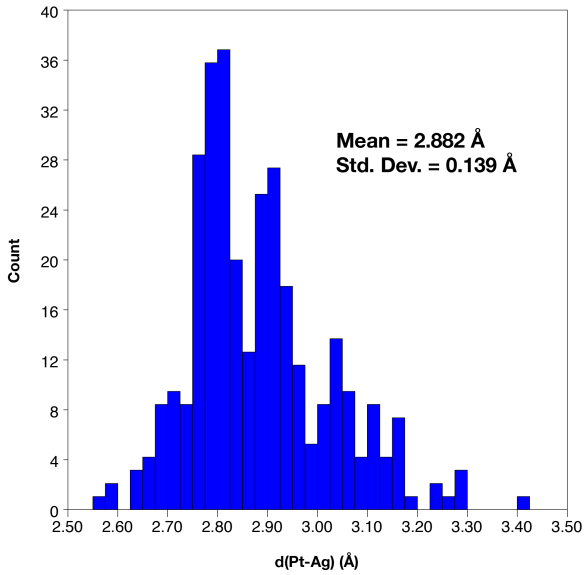

Figure 4.15. CSD search results for complexes containing Pt-Ag bonding interactions. The search was constrained to compounds that were defined as containing a bonding interaction between Pt and Ag. A total of 306 data points were obtained.

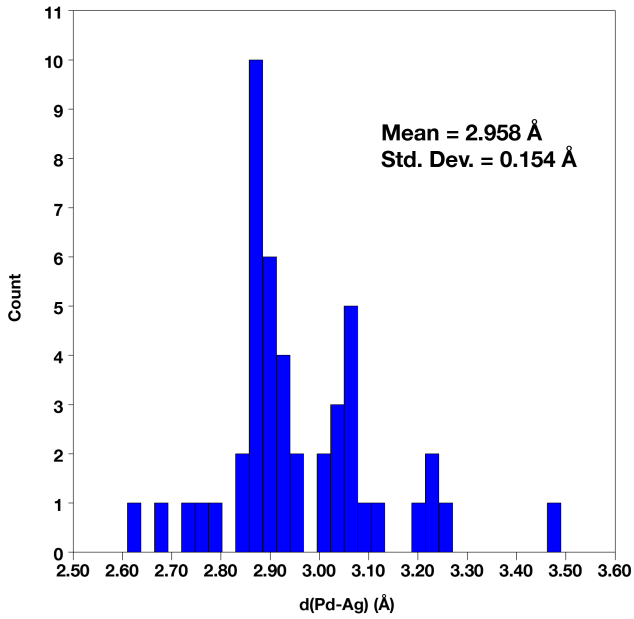

Figure 4.16. CSD search results for complexes containing Pd-Ag bonding interactions. The search was constrained to compounds that were defined as containing a bonding interaction between Pd and Ag. A total of 46 data points were obtained.

4.8. Details of crystallographic structure determinations

Single crystal X-ray structure determinations were carried out at low temperature on Bruker Kappa diffractometers equipped with a Mo radiation source and a Bruker APEX or APEX-II detector. All structures were solved via direct methods with SHELXS[96] and refined by full-matrix least-squares procedures using SHELXL[96] within the Olex2 small-molecule solution, refinement and analysis software.[97] Crystallographic data collection and refinement information are listed in Tables 4.3-6.

Information on Crystallographic Disorder. The following molecules contained positionally disordered components that were modeled and refined anisotropically. They are listed along with their respective disordered components:

$[(Et_2O)TlPt(CNAr^{Dipp2})_2]BAr^F_4$ (**3**(Et_2O)): Two-site positional disorder of one Tl atom and its coordinated diethyl ether; two-site positional disorder of the other Tl-bound diethyl ether; two-site disorder of one Dipp ring; two-site disorder of several isopropyl groups; rotational disorder of several $–CF_3$ groups.

$[TlPt(CNAr^{Dipp2})_2]BAr^F_4$ (**3**): Two-site disorder of one isopropyl group; rotational disorder of several $–CF_3$ groups.

$[(Et_2O)TlPd(CNAr^{Dipp2})_2]BAr^F_4$ (**4**(Et_2O)): Two-site positional disorder of one Tl atom and its coordinated diethyl ether; rotational disorder of several $–CF_3$ groups.

$[(\eta^6\text{-}C_7H_8)_2TlPd(CNAr^{Dipp2})_2]BAr^F_4$ (**4**$(Tol)_2$): Two-site disorder of one Tl-bound toluene; rotational disorder of several $–CF_3$ groups.

$[AgPt(CNAr^{Dipp2})_2(\eta^1\text{-}C_6H_6)]OTf \bullet 3\ C_6H_6$ (**5**$(C_6H_6 \bullet 3\ C_6H_6)$): Two-site disorder of triflate anion; two-site disorder of one isopropyl group.

$[AgPt(CNAr^{Dipp2})_2(THF)]OTf \bullet 3$ THF (**5**(THF • 3 THF)): Two-site disorder of the Pt-

bound molecule of THF.

$\{[Ag_2Pt(CNAr^{Dipp2})_2(\eta^1\text{-}C_6H_6)]_2(\mu\text{-}OTf)_2\}(OTf)_2 \bullet 2\ C_6H_6$ (**7** • 2 C_6H_6): Two-site disorder of one bridging triflate anion; two-site disorder of one co-crystallized molecule of benzene.

In addition, the following molecules contained co-crystallized solvent molecules that were severely disordered and could not be properly modeled. The Platon routine SQUEEZE[98] was used to account for these disordered molecules as a diffuse contribution to the overall scattering pattern without specific atom positions:

$[TlPt(CNAr^{Dipp2})_2]OTf \bullet 1.5\ Et_2O$ (**1** • 1.5 Et_2O): Three molecules of diethyl ether per unit cell.

$[AgPt(CNAr^{Dipp2})_2(THF)]OTf \bullet 3$ THF (**5**(THF • 3 THF)): Twelve molecules of THF per unit cell.

$[AgPd(CNAr^{Dipp2})_2(THF)]OTf \bullet 6.5$ THF (**6**(THF) • 6.5 THF): Twenty-six molecules of THF per unit cell.

Table 4.3. Crystallographic data collection and refinement information.

Name	[TlPt($CNAr^{Dipp2}$)$_2$]OTf • 1.5 Et_2O (**1**• 1.5(Et_2O))	[(Et_2O)TlPt($CNAr^{Dipp2}$)$_2$]BAr^F_4 (**3**(Et_2O))	[(Et_2O)TlPd($CNAr^{Dipp2}$)$_2$]BAr^F_4 (**4**(Et_2O))
Formula	$C_{71}H_{94}N_2F_3SO_5PtTl$	$C_{98}H_{96}N_2BOF_{24}PtTl$	$C_{98}H_{96}N_2BOF_{24}PdTl$
Crystal System	Triclinic	Triclinic	Triclinic
Space Group	*P*-1	*P*-1	*P*-1
a, Å	13.9500(8)	12.732(1)	12.7422(9)
b, Å	16.277(1)	26.642(3)	26.679(2)
c, Å	17.621(1)	28.428(3)	28.503(2)
α, deg	68.887(3)	99.200(4)	99.098(1)
β, deg	70.018(3)	90.224(4)	90.144(1)
γ, deg	71.465(3)	90.514(4)	90.509(1)
V, $Å^3$	3379.6(4)	9519(2)	9567(1)
Z	2	4	4
Radiation (λ, Å)	Mo-Kα, 0.71073	Mo-Kα, 0.71073	Mo-Kα, 0.71073
ρ (calcd.), g/cm^3	1.517	1.524	1.455
μ (Mo Kα), mm^{-1}	4.537	3.253	1.963
Temp, K	100	100	100
θ max, deg	25.408	25.474	24.713
data/parameters	12410/683	35166/2838	32575/2560
R_1	0.0344	0.0305	0.0454
wR_2	0.0737	0.0671	0.0803
GOF	1.057	1.010	1.029

Table 4.4. Crystallographic data collection and refinement information.

Name	$[TlPt(CNAr^{Dipp2})_2]BAr^F_4$ (**3**)	$[(\eta^6\text{-}C_7H_8)_2 TlPd(CNAr^{Dipp2})_2]BAr^F_4$ (**4**$(Tol)_2$)	$[AgPt(CNAr^{Dipp2})_2(THF)]OTf \cdot 3\ THF$ (**5**$(THF) \cdot 3\ THF$)
Formula	$C_{94}H_{86}N_2BF_{24}PtTl$	$C_{108}H_{102}N_2BF_{24}PdTl$	$C_{79}H_{106}N_2F_3O_7SPtAg$
Crystal System	Triclinic	Triclinic	Orthorhombic
Space Group	*P*-1	*P*-1	$P2_12_12_1$
a, Å	14.6265(7)	12.5519(5)	15.648(2)
b, Å	20.654(1)	20.2591(8)	21.250(2)
c, Å	31.199(2)	21.6470(8)	24.077(2)
α, deg	76.597(2)	105.597(1)	90
β, deg	79.378(3)	102.325(1)	90
γ, deg	89.566(3)	97.308(1)	90
V, $Å^3$	9005.2(8)	5079.1(3)	8006(1)
Z	4	2	4
Radiation (λ, Å)	Mo-Kα, 0.71073	Mo-Kα, 0.71073	Mo-Kα, 0.71073
ρ (calcd.), g/cm^3	1.556	1.442	1.312
μ (Mo Kα), mm^{-1}	3.434	1.853	2.071
Temp, K	100	100	100
θ max, deg	25.408	25.549	25.404
data/parameters	32879/2461	18800/1339	13450/741
R_1	0.0601	0.0294	0.0359
wR_2	0.1030	0.0653	0.0851
GOF	1.013	1.029	1.033

Table 4.5. Crystallographic data collection and refinement information.

Name	[AgPd(CNAr^{Dipp2})$_2$(THF)]OTf • 6.5 THF (**6**(THF) • 6.5 THF)	[AgPt(CNAr^{Dipp2})$_2$(η^1-C_6H_6)]OTf •3 C_6H_6 (**5**(C_6H_6) • 3(C_6H_6))	[AgPd(CNAr^{Dipp2})$_2$(η^1-C_7H_8)]OTf • C_7H_8 (**6**(C_7H_8) • C_7H_8)
Formula	$C_{93}H_{134}N_2O_{10.5}F_3SPdAg$	$C_{81}H_{92}N_2O_3F_3SPtAg$	$C_{84}H_{98}N_2O_3F_3SPdAg$
Crystal System	Orthorhombic	Monoclinic	Triclinic
Space Group	$P2_12_12_1$	$P2_1/n$	P-1
a, Å	15.594(2)	18.606(1)	14.529(2)
b, Å	21.315(2)	19.772(1)	15.663(2)
c, Å	24.141(3)	20.951(1)	17.673(2)
α, deg	90	90	96.662(4)
β, deg	90	106.515(2)	109.412(4)
γ, deg	90	90	94.019(4)
V, Å^3	8024(1)	7389.4(8)	3742.0(8)
Z	4	4	2
Radiation (λ, Å)	Mo-Kα, 0.71073	Mo-Kα, 0.71073	Mo-Kα, 0.71073
ρ (calcd.), g/cm^3	1.450	1.378	1.320
μ (Mo Kα), mm^{-1}	0.565	2.240	0.586
Temp, K	100	150	100
θ max, deg	25.436	25.448	25.422
data/parameters	14709/728	13613/891	13526/884
R_1	0.0618	0.0419	0.0350
wR_2	0.1691	0.0885	0.0696
GOF	1.069	1.078	1.028

Table 4.6. Crystallographic data collection and refinement information.

Name	{[$Ag_2Pt(CNAr^{Dipp2})_2(\eta^1$-$C_6H_6)]_2(\mu$-$OTf)_2$}$(OTf)_2$ • 2 C_6H_6 (**7** • 2 C_6H_6)
Formula	$C_{152}H_{172}N_4O_{12}F_{12}S_4Pt_2Ag_4$
Crystal System	Monoclinic
Space Group	$P2_1/n$
a, Å	11.780(1)
b, Å	29.620(2)
c, Å	20.936(2)
α, deg	90
β, deg	90.390(4)
γ, deg	90
V, $Å^3$	7305(1)
Z	2
Radiation (λ, Å)	Mo-Kα, 0.71073
ρ (calcd.), g/cm^3	1.557
μ (Mo Kα), mm^{-1}	2.566
Temp, K	100
θ max, deg	25.460
data/parameters	13466/953
R_1	0.0503
wR_2	0.0810
GOF	1.003

4.9. Acknowledgements

Chapter 4 is adapted from Barnett, B. R.; Moore, C. E.; Chandrasekaran, P; Sproules, S.; Rheingold, A. L.; DeBeer, S.; Figueroa, J. S. "Metal-only Lewis Pairs Between Group 10 Metals and Tl(I) or Ag(I): Insights into the Electronic Consequences of Z-type Ligand Binding", *Chemical Science,* **2015**, *6*, 7169. Copyright 2015, Royal Society of Chemistry. Permission to include published material in this dissertation has been obtained from all coauthors. The dissertation author is the first author of this paper.

4.10. References

(1) Shriver, D. F. *Acc. Chem. Res.,* **1970**, *3*, 231.

(2) Hieber, W., in *Advances in Organometallic Chemistry*, **1970**, *8*, 1. Eds. Stone, F. G. A. and West, R., Academic Press, San Diego.

(3) Hieber, W.; Leutert, F. *Naturwissenschaften*, **1931**, *19*, 360.

(4) Hieber, W. *Angew. Chem.* **1936**, *49*, 463.

(5) Mingos, D. M. P. *J. Organomet. Chem.* **2001**, *635*, 1.

(6) Chatt, J.; Duncanson, L. A. *J. Chem. Soc.* **1953**, 2939.

(7) Mingos, D. M. P., in *Advances in Organometallic Chemistry*, **1977**, *15*, 1. Eds. Stone, F. G. A. and West, R., Academic Press, San Diego.

(8) Vaska, L. *Acc. Chem. Res.*, **1968**, *1*, 335.

(9) Rendina, L. M.; Puddephatt, R. J. *Chem. Rev.*, **1997**, *97*, 1735.

(10) Stille, J. K.; Lau, K. S. Y. *Acc. Chem. Res.*, **1977**, *10*, 434.

(11) Johnson, C. E.; Eisenberg, R. *J. Am. Chem. Soc.*, **1985**, *107*, 3148.

(12) Collman, J. P.; Roper, W. R., in *Advances in Organometallic Chemistry*, **1969**, *7*, 53. Eds. Stone, F. G. A. and West, R., Academic Press, San Diego.

(13) Green, M. L. H. *J. Organomet. Chem.* **1995**, *500*, 127.

(14) Burlitch, J. M.; Leonowicz, M. E.; Petersen, R. B.; Hughes, R. E. *Inorg. Chem.* **1979**, *18*, 1097.

(15) La Placa, S. J.; Ibers, J. A. *Inorg. Chem.*, **1966**, *5*, 405.

(16) Muir, K. W.; Ibers, J. A. *Inorg. Chem.* **1969**, *8*, 1921.

(17) Fischer, R. A.; Weiss, J. *Angew. Chem., Int. Ed.* **1999**, *38*, 2830.

(18) Hill, A. F.; Owen, G. R.; White, A. J. P.; Williams, D. J. *Angew. Chem., Int. Ed.* **1999**, *38*, 2759.

(19) Figueroa, J. S.; Melnick, J. G.; Parkin, G. *Inorg. Chem.* **2006**, *45*, 7056.

(20) Pang, K.; Tanski, J. M.; Parkin, G. *Chem. Commun.* **2008**, 1008.

(21) Moret, M.-E.; Peters, J. C. *J. Am. Chem. Soc.* **2011**, *133*, 18118.

(22) Harman, W. H.; Peters, J. C. *J. Am. Chem. Soc.* **2012**, *134*, 5080.

(23) Braunschweig, H.; Dewhurst, R. D.; Schneider, A. *Chem. Rev.*, **2010**, *110*, 3924.

(24) Braunschweig, H.; Dewhurst, R. D. *Dalton Trans.* **2010**, *40*, 549.

(25) Amgoune, A.; Bourissou, D. *Chem. Commun.*, **2010**, *47*, 859.

(26) Devillard, M.; Bouhadir, G.; Bourissou, D. *Angew. Chem., Int. Ed.*, **2014**, *54*, 730.

(27) Barnett, B. R.; Moore, C. E.; Rheingold, A. L.; Figueroa, J. S. *J. Am. Chem. Soc.* **2014**, *136*, 10262.

(28) Gualco, P.; Lin, T.-P.; Siroglou, M.; Mercy, M.; Ladeira, S.; Bouhadir, G.; Pérez, L. M.; Gabbaï, F. P.; Bourissou, D. *Angew. Chem., Int. Ed.* **2009**, *48*, 9892.

(29) Lin, T.-P.; Wade, C. R.; Pérez, L. M.; Gabbaï, F. P. *Angew. Chem., Int. Ed.* **2010**, *49*, 6357.

(30) Wade, C. R.; Lin, T.-P.; Nelson, R. C.; Mader, E. A.; Miller, J. T.; Gabbaï, F. P. *J. Am. Chem. Soc.*, **2011**, *133*, 8948.

(31) Wade, C. R.; Gabbaï, F. P. *Angew. Chem., Int. Ed.*, **2011**, *50*, 7369.

(32) Lin, T.-P.; Ke, I.-S.; Gabbaï, F. P. *Angew. Chem., Int. Ed.* **2012**, *51*, 4985.

(33) Jones, J. S.; Wade, C. R.; Gabbaï, F. P. *Angew. Chem., Int. Ed.* **2014**, *53*, 8876.

(34) Krogman, J. P.; Gallagher, J. R.; Zhang, G.; Hock, A. S.; Miller, J. T.; Thomas, C. M. *Dalton Trans.*, **2014**, *43*, 13852.

(35) Scheldrick, G. M.; Simpson, R. N. F. *J. Chem. Soc. A*. **1968**, 1005.

(36) Clegg, W.; Wheatley, P. J. *J. Chem. Soc. A.* **1971**, 3572.

(37) Sosinsky. B. A.; Shong, R. G.; Fitzgerald, B. J.; Norem, N.; O'Rourke, C. *Inorg. Chem.* **1983**, *22*, 3124.

(38) Tanase, T.; Yamamoto, Y.; Puddephatt, R. J. *Organometallics*, **1996**, *15*, 1502.

(39) Bauer, J.; Braunschweig, H.; Dewhurst, R. D. *Chem. Rev.* **2012**, *112*, 4329.

(40) Grigg, R.; Loganthan, V.; Santhakumar, V.; Teasdale, A. *Tetrahedron Lett.* **1991**, *32*, 687.

(41) Grigg, R.; Kennewell, P.; Teasdale, A. J. *Tetrahedron Lett.* **1992**, *33*, 7789.

(42) Grigg, R.; Sridharan, V. *Tetrahedron Lett.* **1993**, *34*, 7471.

(43) Roberts, C. C.; Matias, D. M.; Goldfogel, M. J.; Meek, S. J. *J. Am. Chem. Soc.* **2015**, *137*, 6488.

(44) Pearson, R. G. *Chem. Rev.* **1985**, *85,* 41.

(45) Parkin, G. *J. Chem. Educ.* **2006**, *83,* 791.

(46) Parkin, G. *Organometallics*, **2006**, *25*, 4744.

(47) Hill, A. F. *Organometallics*, **2006**, *25*, 4741.

(48) Fox, B. J.; Sun, Q. Y.; DiPasquale, A. G.; Rheingold, A. L.; Figueroa, J. S. *Inorg. Chem.* **2008**, *47*, 9010.

(49) Fox, B. J.; Millard, M. D.; DiPasquale, A. G.; Rheingold, A. L.; Figueroa, J. S. *Angew. Chem., Int. Ed.* **2009**, *48*, 3473.

(50) Labios, L. A.; Millard, M. D.; Rheingold, A. L.; Figueroa, J. S. *J. Am. Chem. Soc.* **2009**, *131*, 11318.

(51) Margulieux, G. W.; Weidemann, N.; Lacy, D. C.; Moore, C. E.; Rheingold, A. L.; Figueroa, J. S. *J. Am. Chem. Soc.* **2010**, *132*, 5033.

(52) Carpenter, A. E.; Margulieux, G. W.; Millard, M. D.; Moore, C. E.; Weidemann, N.; Rheingold, A. L.; Figueroa, J. S. *Angew. Chem., Int. Ed.* **2012**, *51*, 9412.

(53) Carpenter, A. E.; Wen, I.; Moore, C. E.; Rheingold, A. L.; Figueroa, J. S. *Chem. Eur. J.* **2013**, 10452.

(54) Emerich, B. M.; Moore, C. E.; Fox, B. J.; Rheingold, A. L.; Figueroa, J. S. *Organometallics*, **2011**, *30*, 2598.

(55) Mokhtarzadeh, C. C.; Margulieux, G. W.; Carpenter, A. E.; Weidemann, N.; Moore, C. E.; Rheingold, A. L.; Figueroa, J. S. *Inorg. Chem.* **2015**, *54*, 5579.

(56) Given the uncertainty in values for the covalent radii of transition metals and heavy main-group elements, we present a range for the sum of the covalent radii of Pt and Tl based on several commonly used tabulations (in Å): r_{cov}(Pt) 1.36 + r_{cov}(Tl) 1.45 = 2.81, a): Cordero, B.; Gómez, V.; Platero-Prats, A. E.; Revés, M.; Echeverría, J.; Cremades, E.; Barragán, F.; Alvarez, S. *Dalton Trans.* **2008**, 2832. r_{cov}(Pt) 1.30 + r_{cov}(Tl) 1.44 = 2.74, b): Pauling, L. *The Nature of the Chemical Bond,* 3rd Ed.; Cornell University Press: Cornell, NY, 1960; Chapter 11, p 403. r_{cov}(Pt) 1.23 + r_{cov}(Tl) 1.44 = 2.67, c): Pyykkö, P; Atsumi, M. *Chem. Eur. J.* **2009**, *15*, 186.

(57) Pyykkö, P. *Chem. Rev.* **1997**, *97*, 597.

(58) Catalano, V. J.; Bennett, B. L.; Muratidis, S.; Noll, B. C. *J. Am. Chem. Soc.* **2001**, *123*, 173.

(59) Wang, S.; Fackler, J. P.; King, C.; Wang, J. C. *J. Am. Chem. Soc.* **1988**, *110*, 3308.

(60) Fernández, E. J.; Laguna, A.; Lopez-de-Luzuriaga, M. A.; Olmos, M. E.; Perez, J. *Chem. Commun.* **2003**, 1760.

(61) Jamali, S.; Ashtiani, M. M.; Jamshidi, Z.; Lalinde, E.; Moreno, M. T.; Samouei, H.; Escudero-Adán, E.; Benet-Buchholz, J. *Inorg. Chem.* **2013**, *52*, 10729.

(62) Still, B. M.; Kumar, P. G. A.; Aldrich-Wright, J. R.; Price, W. S. *Chem. Soc. Rev.* **2007**, *36*, 665.

(63) For each arene ring seen to be interacting with Tl in **3** (two per molecule, two independent molecules per asymmetric unit), there are two Tl-C bond lengths that are appreciably shorter than the others for that given arene ring. As such, we believe this interaction is best characterized as having η^2 hapticity.

(64) Fernández, E. J.; Laguna, A.; López-de-Luzuriaga, J. M.; Monge, M.; Montiel, M.; Olmos, M. E. *Inorg. Chem.* **2007**, *46*, 2953.

(65) Strauss, S. H.; Noirot, M. D.; Anderson, O. P. *Inorg. Chem.* **1986**, *25*, 3850.

(66) Noirot, M. D.; Anderson, O. P; Strauss, S. H. *Inorg. Chem.* **1987**, *26*, 2216.

(67) Sarazin, Y.; Kaltsoyannis, N.; Wright, J. A.; Bochmann, M. *Organometallics*, **2007**, *26*, 1811.

(68) While naturally-occuring thallium also consists of 29.5% ^{203}Tl (I = 1/2), complexes containing Pt-Tl bonds typically only resolve coupling to ^{205}Tl in their ^{195}Pt NMR spectra. For example, see Ref. 58.

(69) Fuertes, S.; Woodall, C. H.; Raithby, P. R.; Sicilia, V. *Organometallics*, **2012**, *31*, 4228.

(70) Belío, U.; Fuertes, S.; Martín, A. *Dalton Trans.* **2014**, *43*, 10828.

(71) de Groot, F. *Chem. Rev.* **2001**, *101*, 1779.

(72) Tomson, N. C.; Labios, L. A.; Weyhermüller, T.; Figueroa, J. S.; Wieghardt, K. *Inorg. Chem.* **2011**, *50*, 5763.

(73) Wright, R. J.; Phillips, A. D.; Hino, S.; Power, P. P. *J. Am. Chem. Soc.* **2005**, *127*, 4974.

(74) Pyykkö, P. *Chem. Rev.* **1988**, *88*, 563.

(75) Carpenter, A. E.; McNeece, A. J.; Barnett, B. R.; Estrada, A. L.; Mokhtarzadeh, C. C.; Moore, C. E.; Rheingold, A. L.; Perrin, C. L.; Figueroa, J. S. *J. Am. Chem. Soc.* **2014**, *136*, 15481.

(76) For other examples of Metal-only Lewis Pairs with Ag as the Lewis acidic component, see Ref. 39 and references cited therein.

(77) Cambridge Structural Database (CSD), version 5.36 (May 2015 update).

(78) Fulmer, G. R.; Miller, A. J. M.; Sherden, N. H.; Gottlieb, H. E.; Nudelman, A.; Stoltz, B. M.; Bercaw, J. E.; Goldberg, K. I. *Organometallics,* **2010**, *29*, 2176.

(79) Hubig, S. M. Lindeman, S. V.; Kochi, J. K. *Coord. Chem. Rev.* **2000**, *200-202*, 831.

(80) Stahl, S. S.; Labinger, J. A.; Bercaw, J. E. *J. Am. Chem. Soc.*, **1996**, *118*, 5961.

(81) Wick, D. D.; Goldberg, K. I. *J. Am. Chem. Soc.*, **1997**, *119*, 10235.

(82) Aullón, G.; Alvarez, S. *Inorg. Chem.* **1996**, *35*, 3137.

(83) Tsay, C.; Mankad, N. P.; Peters, J. C. *J. Am. Chem. Soc.* **2010**, *132*, 13975.

(84) Dioumaev, V. K.; Harrod, J. F. *Organometallics*, **1996**, *15*, 3859.

(85) Lin, T.-P.; Nelson, R. C.; Wu, T.; Miller, J. T.; Gabbaï, F. P. *Chem. Sci.*, **2012**, *3*, 1128.

(86) Dolinar, B. S.; Berry, J. F. *Inorg. Chem.* **2013**, *52*, 4658.

(87) Suresh, C. H.; Koga, N. *J. Am. Chem. Soc.*, **2002**, *124*, 1790.

(88) Moret, M.-E.; Chan, P. *J. Am. Chem. Soc.,* **2009**, *131*, 5675.

(89) Yamaguchi, T.; Yamazaki, F.; Ito, T. *J. Am. Chem. Soc.*, **2001**, *123*, 743.

(90) Usón, R.; Forniés, J.; Tomás, M. Ara, I.; Casas, M.; Martín, A. *J. Chem. Soc., Dalton Trans.* **1991**, 2253.

(91) Yamaguchi, T.; Yamazaki, F.; Ito, T. *J. Am. Chem. Soc.* **1999**, *121*, 7405.

(92) Falvello, L. R.; Forniés, J.; Martín, A. Navarro, R.; Sicilia, V.; Villarroya, P. *Inorg. Chem.* **1997**, *36*, 6166.

(93) Armarego, W. L. F.; Chai, C. L. L. *Purification of Laboratory Chemicals*, 5th Ed.; Elsevier, 2003.

(94) Pangborn, A. B.; Giardello, M. A.; Grubbs, R. H.; Rosen, R. K.; Timmers, F. J. *Organometallics*, **1996**, *15*, 1518.

(95) Reger, D. L.; Wright, T. D.; Little, C. A.; Lambda, J. J. S.; Smith, M. D. *Inorg. Chem.* **2001**, *40*, 3810.

(96) Sheldrick, G. M.; *Acta Crystallogr. A.* **2008**, *64*, 112.

(97) Dolomanov, O. V.; Bourhis, L. J.; Gildea, R. J.; Howard, J. A. K.; Puschmann, H. *J. Appl. Cryst.* **2009**, *42*, 339.

(98) van der Sluis, P.; Spek. A. L. *Acta Crystallogr.* **1990**, *A46*, 194.

Chapter 5

Monomeric Chini-Type Triplatinum Clusters Featuring Dianionic and Radical Anionic π*-Systems

5.1. Introduction

Highly-reduced carbonyl metalates have long interested organometallic chemists due to their abilities to place a relatively electropositive transition metal center in a formal negative oxidation state.[1,2] This phenomenon is made possible in large part due to the strong π-acidic properties of the carbonyl ligand, and has allowed for the isolation of many mono- and multi-nuclear binary carbonyl metalates from most members of the transition series.[3-6] With regard to topology and electronic structure, one of the most intriguing classes of such complexes are the so-called "Chini clusters," $[Pt_3(CO)_6]_n^{2-}$.[6-8] In these clusters, *triangulo*-Pt_3 units bearing both terminal and bridging carbonyl ligands stack one on top of the other along a common C_3 axis to form columnar structures bearing an overall doubly anionic charge. Recent work has demonstrated the ability of the higher nuclearity oligomers (n = 5-8) to self-assemble into continuous chains, with the dimentionality of long-range ordering being highly dependent upon the identity of the charge-balancing cations.[9-11] Many of the higher-ordered structures display remarkable conductive properties, leading to interest in their use as tunable conductive materials based off of a molecular platform.[12,13] As such, a furthered understanding of the electronic structure and reactivity profiles available to these clusters continues to be of much interest.[14]

While the oligomeric members of $[Pt_3(CO)_6]_n^{2-}$ with n = 2-8 have all been isolated and structurally characterized,[7-11,15] the parent species $[Pt_3(CO)_6]^{2-}$ (n = 1) has eluded complete characterization. Although reportedly synthesized *in situ* via reduction of $[Pt_3(CO)_6]_2^{2-}$ with Na/K alloy,[8] it could not be crystallized or precipitated from solution, with characterization relying solely upon IR and atomic absorption spectroscopies. Interestingly, although several mixed carbonyl/phosphine clusters of the type $Pt_3(\mu\text{-}CO)_3(PR_3)_3$ have been long-known,[16-20] their reduction to the corresponding platinates has not been reported, potentially implying that the weak π-accepting properties of triorganophosphines are insufficient to stabilize the presence of two negative charge equivalents.[21] Building off of our success in isolating isocyano analogues to classical carbonyl metalates using sterically encumbering *m*-terphenyl isocyanides,[22-25] we report herein the synthesis and structural characterization of $K_2[Pt_3(\mu\text{-}CO)_3(CNAr^{Dipp2})_3]$ (Ar^{Dipp2} = 2,6-(2,6-(*i*-Pr)$_2$C$_6$H$_3$)$_2$C$_6$H$_3$), as well as the open-shell monoanion $K(THF)_4[Pt_3(\mu\text{-}CO)_3(CNAr^{Dipp2})_3]$. These anionic clusters serve as isolobal mimics to $[Pt_3(CO)_6]^{2-}$ as well as putative $[Pt_3(CO)_6]^{\bullet-}$, with the highest occupied orbital shown to be primarily located on the ligand π* framework. Occupation of this highly delocalized π-symmetric orbital results in the aggregate set of isocyanide and carbonyl ligands functioning in a redox non-innocent fashion akin to canonical multidentate redox active ligands.[26-28]

5.2. Syntheses and characterization data of the clusters $[Pt_3(\mu\text{-}CO)_3(CNAr^{Dipp2})_3]^{n-}$ (n = 0, 1, 2)

Exposure of a diethyl ether solution of two-coordinate $Pt(CNAr^{Dipp2})_2$[29,30] to 1 atm CO gas results in displacement of one isocyanide ligand and aggregation to afford the trinuclear cluster $Pt_3(\mu\text{-}CO)_3(CNAr^{Dipp2})_3$ (**1**, Scheme 5.1). Despite the presence of excess CO, further CO-for-isocyanide substitution is not observed even upon stirring for several days. Crystallographic characterization of **1** (Figure 5.1) reveals an equilateral *triangulo*-Pt_3 core with Pt-Pt distances (mean = 2.6496(2) Å) similar to those seen for $Pt_3(\mu\text{-}CO)_3(PR_3)_3$.[16-20] Trinuclear **1** adopts nearly rigorous D_{3h} site symmetry, with the Pt-CO and Pt-CNR bond vectors all essentially coincident with the Pt_3 plane (maximum torsion angle = 8.56˚). In accordance with its high symmetry in the solid state, the solution FTIR spectrum of **1** displays only a single υ(C≡N) and υ(C=O) mode (2118 and 1834 cm^{-1}, respectively; *E*' symmetric in the D_{3h} point group).

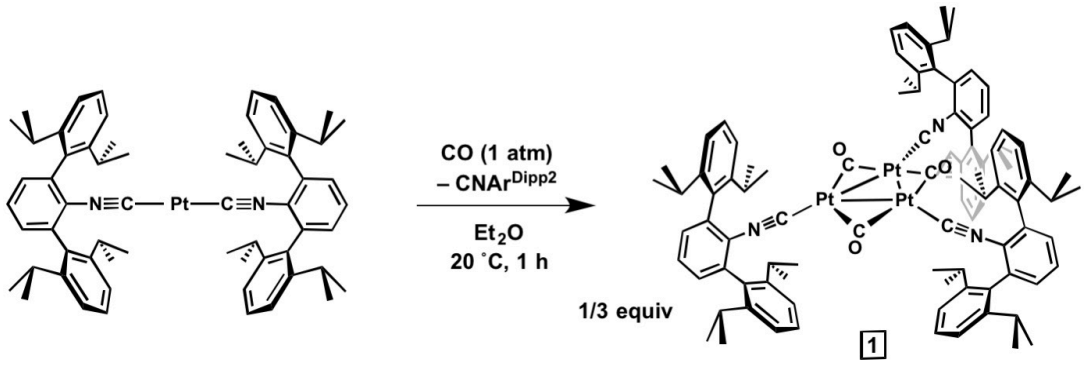

Scheme 5.1. Synthesis of $Pt_3(\mu\text{-}CO)_3(CNAr^{Dipp2})_3$ (**1**).

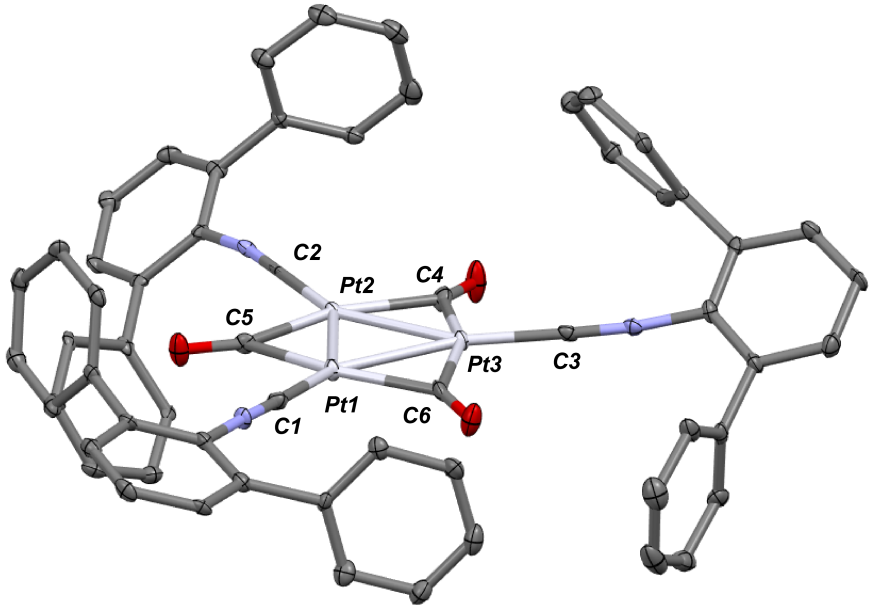

Figure 5.1. Molecular structure of $Pt_3(\mu\text{-}CO)_3(CNAr^{Dipp2})_3 \cdot C_5H_{12}$ (**1**$\cdot C_5H_{12}$). Flanking isopropyl groups omitted for clarity. Co-crystallized *n*-pentane was accounted for using SQUEEZE. Selected bond distances (Å): Pt1-Pt2 = 2.6485(4); Pt2-Pt3 = 2.6465(4); Pt3-Pt1= 2.6539(4); Pt1-C1 = 1.911(6); Pt2-C2 = 1.917(5); Pt3-C3 = 1.924(6); Pt1-C5 = 2.078(6); Pt1-C6 = 2.048(7); Pt2-C4 = 2.057(6); Pt2-C5 = 2.061(7); Pt3-C4 = 2.058(6); Pt3-C6 = 2.071(6).

Remarkably, cyclic voltammetry of **1** in THF (Figure 5.2) shows the presence of two reversible reduction events centered at –1.95 V (ΔE_p = 86 mV) and –2.60 V (ΔE_p = 81 mV) vs. Fc, suggesting the accessibility of the anionic clusters $[Pt_3(\mu\text{-}CO)_3(CNAr^{Dipp2})_3]^{n-}$ (n = 1, 2). Chemical reduction of **1** in benzene solution using an excess of KC_8 results in smooth formation of a deep purple diamagnetic product as assayed by ^1H and $^{13}C\{^1H\}$ NMR (Scheme 5.2). Retention of the *triangulo*-$Pt_3(\mu\text{-}CO)_3(CNR)_3$ motif is suggested by peaks at δ = 242.2 and δ = 194.5 ppm in the $^{13}C\{^1H\}$ NMR spectrum corresponding to bridging carbonyl and terminal isocyanide ligands, respectively. This new species gives rise to a ^{195}Pt NMR signal at δ = –4271 ppm, which is strikingly similar to that of **1** (δ = –4319 ppm) given the wide chemical shift range

inherent in ^{195}Pt NMR.[31] FTIR spectra in C_6D_6 show a single υ(C=O) band at 1722 cm^{-1}, as well as broad υ(C≡N) stretching modes centered at 2043 and 1985 cm^{-1}. These bands are shifted to significantly lower energies relative to **1** and can be compared with the terminal and bridging υ(CO) modes reported for *in situ* generated $[Pt_3(CO)_6]^{2-}$ (1945, 1740 cm^{-1}, THF).[8]

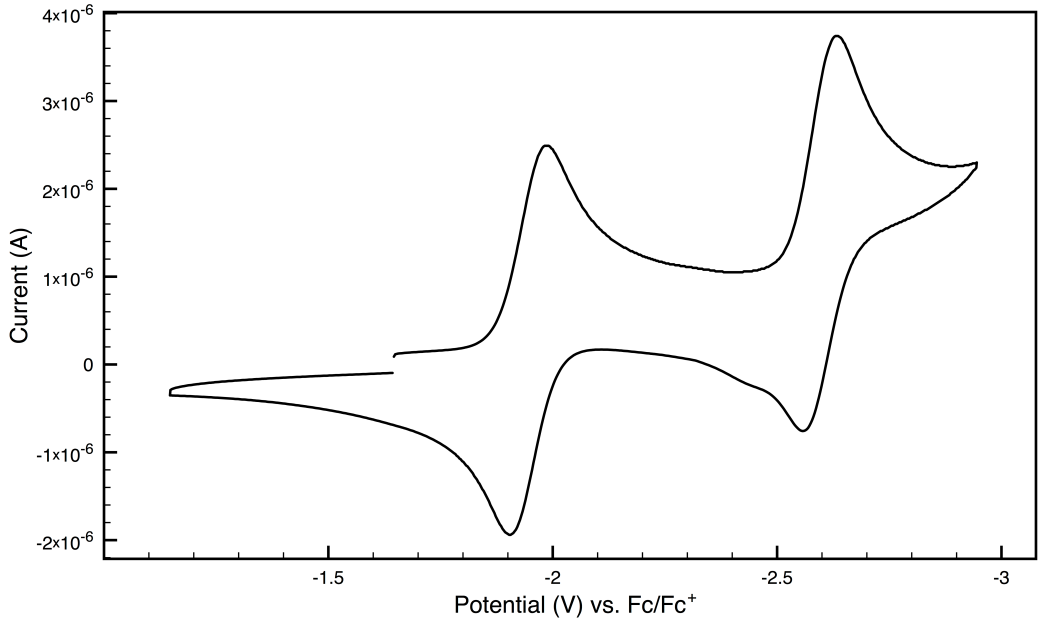

Figure 5.2. Cyclic voltammogram of **1** showing two reversible redox events.

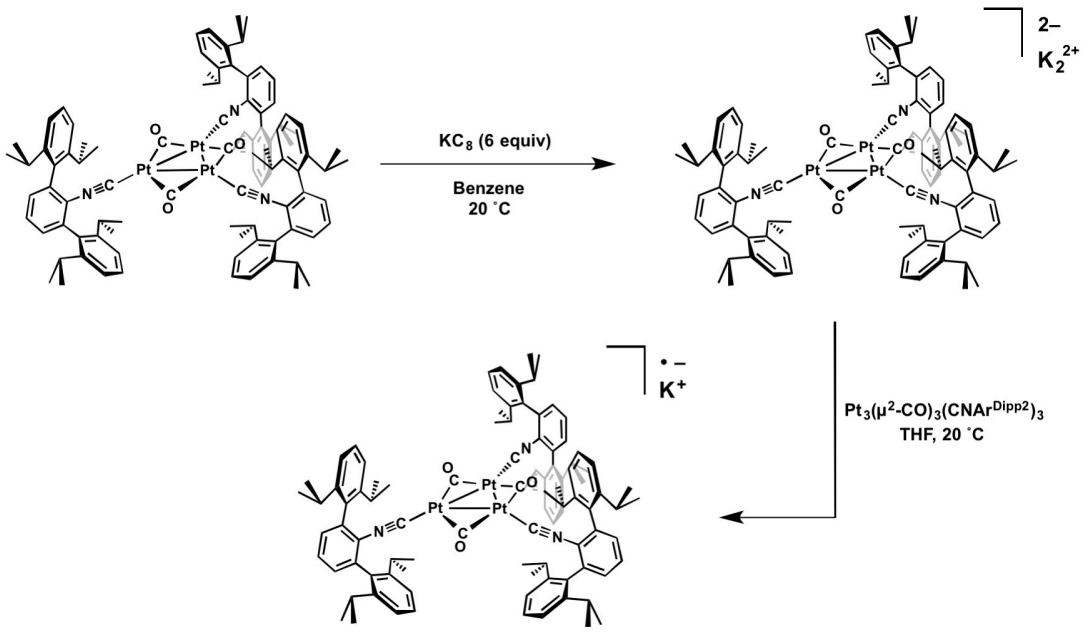

Scheme 5.2. Synthesis of the anionic cluster $K_2[Pt_3(\mu\text{-}CO)_3(CNAr^{Dipp2})_3]^{n-}$ (K_2[**1**]) via reduction of **1** and comproportionation to give the monoanionic radical $K[Pt_3(\mu\text{-}CO)_3(CNAr^{Dipp2})_3]^{n-}$ (K[**1**]).

Structure determination on single crystals grown from DME/*n*-hexane at –35 ˚C confirmed the identity of this species to be the dianion $K_2(DME)_3[Pt_3(\mu\text{-}CO)_3(CNAr^{Dipp2})_3]$ ($K_2(DME)_3$[**1**], Figure 5.3). Each Pt_3 unit exists as a discreet entity and no oligimerization to higher nuclearity, stacked structures is observed. Most notably, despite the introduction of two negative charge equivalents, the structural features of the $[Pt_3(\mu\text{-}CO)_3(CNAr^{Dipp2})_3]$ core in $K_2(DME)_3$[**1**] are essentially unchanged relative to **1**. The Pt-C bond vectors remain nearly coincident with the Pt_3 plane, with only very minor perturbations of the Pt-Pt, Pt-C_{CNR}, and Pt-C_{CO} distances apparent (Table 5.1). The two potassium counterions sit directly over the centroid on either face of the Pt_3 triangle and are chelated by one or two molecules of DME. In contrast to Chini's $[Pt_3(CO)_6]^{2-}$,[8] K_2[**1**] exhibits remarkable kinetic stability. As a solid, it can be stored for weeks in a glovebox freezer at –35 ˚C without change, while benzene-d_6 solutions of K_2[**1**] at 25 ˚C undergo

decomposition over the course of several weeks to give free $CNAr^{Dipp2}$ as the sole isocyanide-containing species according to ^{1}H NMR spectroscopy. This kinetic stability results in an exceedingly simple synthetic protocol whereby analytical quality K_2[**1**] can be obtained in excellent yields (99%) via simple lyophilization of the benzene solvent after filtration of the reaction mixture.

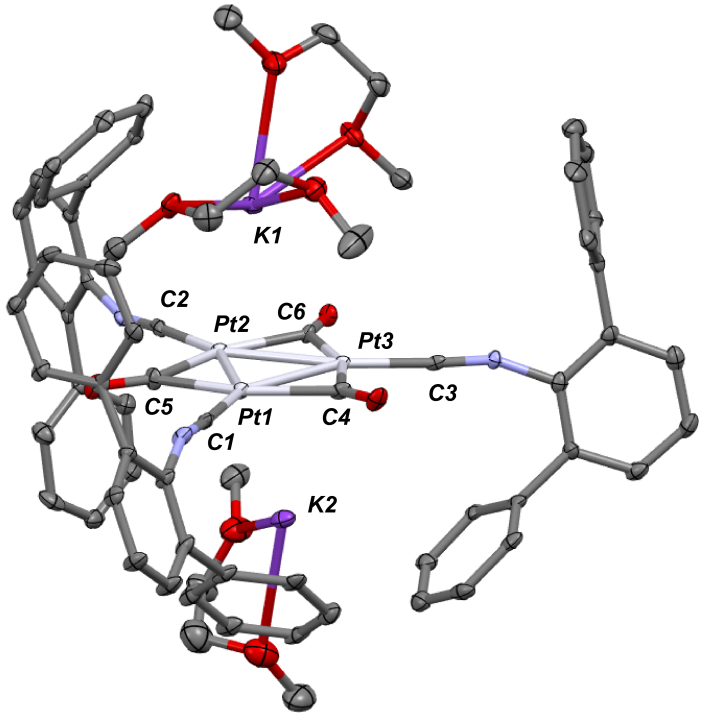

Figure 5.3. Molecular structure of $K_2(DME)_3[Pt_3(\mu\text{-}CO)_3(CNAr^{Dipp2})_3]\cdot 2DME$ ($K_2(DME)_3$[**1**]·2 DME). Flanking isopropyl groups omitted for clarity. Co-crystallized DME molecules were accounted for using SQUEEZE. Selected bond distances (Å): Pt1-Pt2 = 2.6367(4); Pt2-Pt3 = 2.6386(5); Pt3-Pt1 = 2.6325(4); Pt1-C1 = 1.897(7); Pt2-C2 = 1.897(7); Pt3-C3 = 1.894(8); Pt1-C4 = 2.039(8); Pt1-C5 = 2.040(8); Pt2-C5 = 2.052(7); Pt2-C6 = 2.048(6); Pt3-C4 = 2.035(7); Pt3-C6 = 2.048(6).

Table 5.1. Selected bond distances from the solid-state structures of complexes **1**, $K(THF)_4$[**1**], and $K_2(DME)_3$[**1**].

Complex	Mean d(Pt-Pt)	Mean d(Pt-C_{CNR})	Mean d(Pt-C_{CO})
1	2.6496(2) Å	1.917(3) Å	2.062(2) Å
$K(THF)_4$[**1**]	2.6448(3) Å	1.924(6) Å	2.047(4) Å
$K_2(DME)_3$[**1**]	2.6359(2) Å	1.896(4) Å	2.044(3) Å

While Chini clusters of many nuclearities have been isolated, a common feature among all of them is an overall charge of 2–. Their reactions with oxidizing agents have been proposed to proceed via single-electron transfer to transiently form $[Pt_3(CO)_6]_n^{\bullet-}$, followed by dimerization and further aggregation to yield $[Pt_3(CO)_6]_{2n}^{2-}$ stacked clusters.[32] However, such monoradical species have not been observed to date during the course of these oxidations. The apparent resistance of $K_2[Pt_3(\mu\text{-}CO)_3(CNAr^{Dipp2})_3]$ (K_2[**1**]) toward aggregation, as well as the clean electrochemical data for **1**, suggested the potential accessibility of the open-shell monoanion $[Pt_3(\mu\text{-}CO)_3(CNAr^{Dipp2})_3]^{\bullet-}$. Accordingly, simple comproportionation of **1** and K_2[**1**] in THF-d_8 (Scheme 5.2) produces a dark green solution, which gives rise to only broad ^{1}H NMR signals indicative of the presence of a paramagnetic species (μ_{eff} = 1.7(2) μ_B, Evans method). Analysis by FTIR spectroscopy shows υ(C=O) (1775 cm^{-1}) and υ(C≡N) (2061, 2022 cm^{-1}) bands intermediate in energy with respect to those of **1** and K_2[**1**]. Storage of this solution at –35 ˚C yields black crystals of $K(THF)_4[Pt_3(\mu\text{-}CO)_3(CNAr^{Dipp2})_3]$ ($K(THF)_4$[**1**]) as determined by X-ray diffraction (Figure 5.4). As noted for $K_2(DME)_3$[**1**], the anionic fragment in $K(THF)_4$[**1**] is essentially isostructural to that of neutral **1** (Table 5.1). The coordination geometry about each platinum center remains almost perfectly planar, while the Pt-Pt, Pt-C_{CNR} and Pt-C_{CO} bond lengths are basically unchanged from those in **1** and $K_2(DME)_3$[**1**] (Table 5.1). The room temperature solid-state EPR spectrum of $K(THF)_4$[**1**] displays axial symmetry, with $g_\perp$ = 2.020 and $g_\parallel$ = 1.974 (Figure 5.5). The small degree of *g* anisotropy and the minimal deviation of these values from 2.002 (*g* of a free electron) differ from EPR spectra typically seen for Pt-based *S* = 1/2 metalloradicals.[33-35] However, they are very much in accord with spectra exhibited by

systems containing closed-shell platinum centers bound to radical ligands.[36,37] Noticeably, no coupling to the ^{195}Pt nucleus (I = 1/2, 33.8% abundant) is resolved, suggesting that minimal spin density resides at the Pt_3 core.

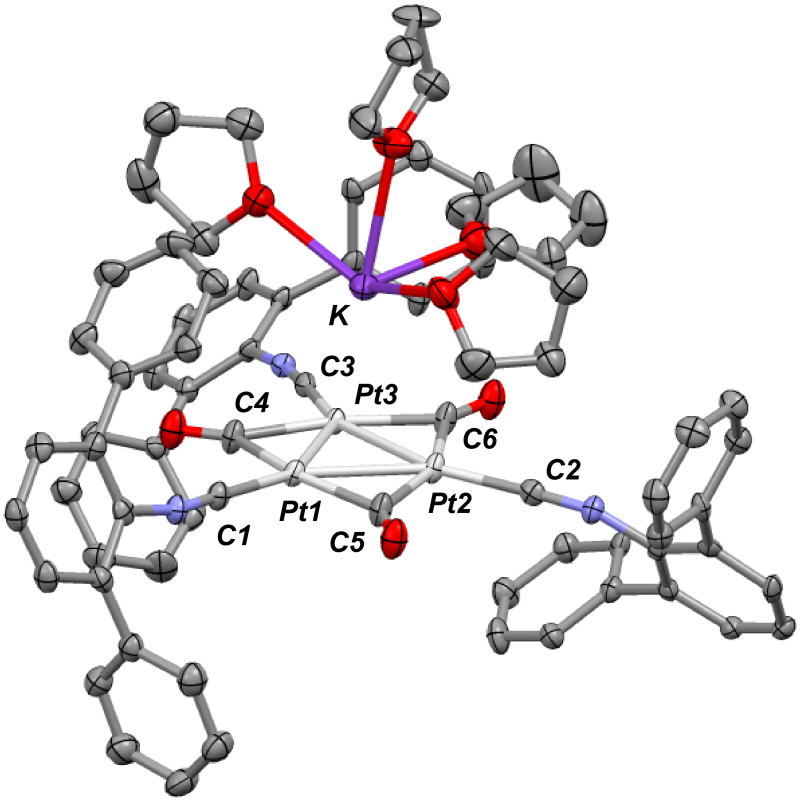

Figure 5.4. Molecular structure of $K(THF)_4[Pt_3(\mu\text{-}CO)_3(CNAr^{Dipp2})_3]\cdot 2THF$ ($K(THF)_4$[**1**]·2(THF)). Flanking isopropyl groups omitted for clarity. Co-crystallized THF molecules were accounted for using SQUEEZE. Selected bond distances (Å): Pt1-Pt2 = 2.6367(5); Pt2-Pt3 = 2.6351(5); Pt3-Pt1 = 2.6547(5); Pt1-C1 = 1.902(12); Pt2-C2 = 1.924(10); Pt3-C3 = 1.947(10); Pt1-C4 = 2.066(10); Pt1-C5 = 2.074(10); Pt2-C5 = 2.030(10); Pt2-C6 = 2.056(10); Pt3-C4 = 2.012(10); Pt3-C6 = 2.042(10).

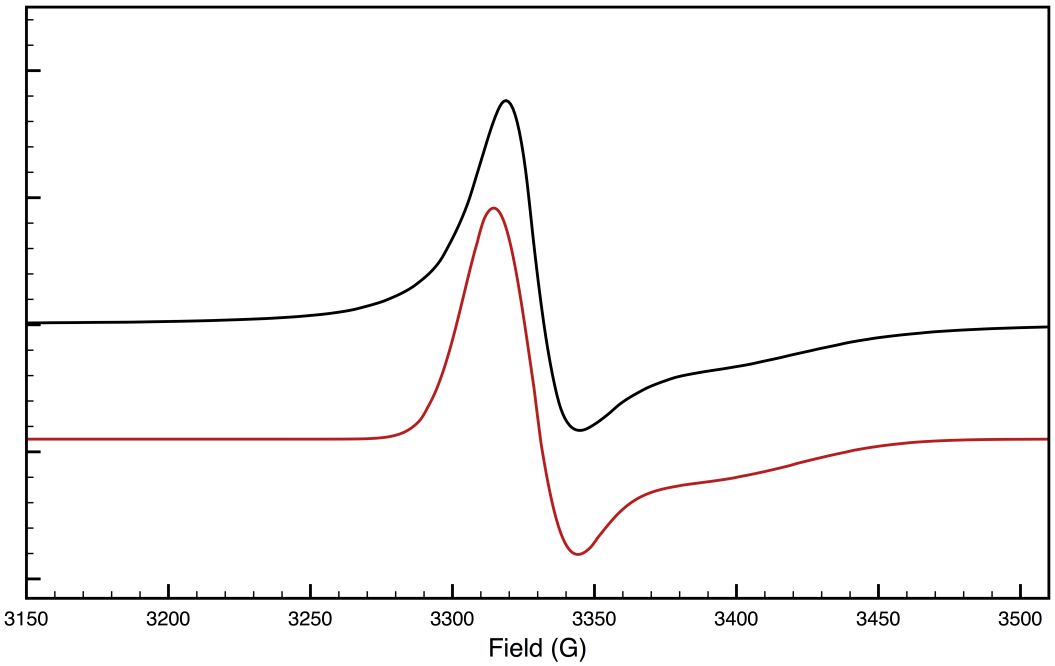

Figure 5.5. Experimental (black) and simulated (red) solid-state X-band EPR spectrum of $K(THF)_4[Pt_3(\mu\text{-}CO)_3(CNAr^{Dipp2})_3]$ recorded at 294 K.

5.3. Electronic structure insights via Density Functional Theory (DFT) calculations revealing ligand-based redox-noninnocence

Density Functional Theory (DFT) studies were undertaken in order to interrogate the electronic structure of the clusters $[Pt_3(\mu\text{-}CO)_3(CNAr^{Dipp2})_3]^{n-}$ (n = 0, 1, 2). The optimized geometries of the truncated models $[Pt_3(\mu\text{-}CO)_3(CNAr^{Ph2})_3]^{n-}$ ($[\mathbf{1}^*]^{n-}$, n = 0, 1, 2) satisfactorily reproduce the important metrical parameters of the corresponding structurally characterized triplatinum clusters **1**, $K(THF)_4[\mathbf{1}]$ and $K_2(DME)_3[\mathbf{1}]$. Remarkably, the calculated HOMO of $[\mathbf{1}^*]^{2-}$ (Figure 5.6A) and SOMO of $[\mathbf{1}^*]^{-}$ consist of the in-phase combination of the out-of-plane π* orbitals of the carbonyl and isocyanide ligands (a_2'' in D_{3h} symmetry) with only a modest contribution from Pt-based orbitals (20.5% for $[\mathbf{1}^*]^{2-}$ HOMO; 25.7% for $[\mathbf{1}^*]^{-}$ SOMO).[38] The primarily ligand-based

parentage of this orbital is in accord with the minimal shortening of the Pt-C bond distances upon reduction of **1** (Table 5.1), despite the sizeable shift of the IR υ(C=O) and υ(C≡N) bands to lower energies, which are usually attributable to increased metal-to-ligand π-backdonation. It is also consistent with semi-empirical extended Hückel calculations on $[Pt_3(CO)_6]^{2-}$, which predict a HOMO that is primarily CO π* in character.[39-41] Indeed, DFT calculations on $[Pt_3(CO)_6]^{2-}$ yield a HOMO that is entirely analogous to that of $[\mathbf{1}^*]^{2-}$, namely the a_2'' combination of bridging and terminal CO out-of-plane π* orbitals (Figure 5.6B). This confirms that $K_2[\mathbf{1}]$ indeed functions as an isolobal analogue of $[Pt_3(CO)_6]^{2-}$, while $K(THF)_4[\mathbf{1}]$ is isolobal with the monoanion $[Pt_3(CO)_6]^{\bullet-}$, a putative fleeting intermediate in the oxidation of $[Pt_3(CO)_6]^{2-}$ to $[Pt_3(CO)_6]_2^{2-}$. The all-π-acid ligand sets employed in $K_2[\mathbf{1}]$ and $[Pt_3(CO)_6]^{2-}$ can be contrasted with the hypothetical dianions of the phosphine-substituted triplatinum clusters $Pt_3(\mu\text{-}CO)_3(PR_3)_3$.[16-20] DFT calculations for $[Pt_3(\mu\text{-}CO)_3(PMe_3)_3]^{2-}$ illustrate that the primarily σ-donating nature of the trimethylphosphine ligands precludes delocalization of electron density onto the terminal ligands in the cluster. For this complex, the HOMO is again a_2''-symmetric, but consists primarily of the out-of-plane π* orbitals of the bridging carbonyl ligands (Figure 5.6C). The relative localization of electron density onto the bridging ligands in $[Pt_3(\mu\text{-}CO)_3(PMe_3)_3]^{2-}$, along with the strongly σ-donating nature of the phosphine ligands, likely renders the reduction of $Pt_3(\mu\text{-}CO)_3(PR_3)_3$ to the corresponding dianion more difficult than the reduction of **1** to $K_2[\mathbf{1}]$, and serves to highlight the central role played by the all-π-acid ligand sets of $K_2[\mathbf{1}]$ and $[Pt_3(CO)_6]^{2-}$ in stabilizing the negative charge equivalents.

Interestingly, the modest contribution of platinum-based atomic orbitals to the a_2''-symmetric HOMO of $[\mathbf{1}^*]^{2-}$ is mostly $6p_z$ in parentage, while the molecular orbital contains only 0.8% 5*d* character. Similarly small 5*d* contributions are apparent in the SOMO of $[\mathbf{1}^*]^-$ (1.3% 5*d*) and the HOMO of $[Pt_3(CO)_6]^{2-}$ (1.4% 5*d*), an effect we believe can be traced to the intratriangular Pt-Pt bonding interactions.[42] The only symmetry-adapted linear combination of Pt 5*d* orbitals for the $[Pt(\mu\text{-}CO)_3L_3]$ (L = CO, CNR) fragment with a_2'' symmetry (Figure 5.7) has significant Pt-Pt bonding character, which serves to stabilize it in energy. Importantly, the resulting energy gap between this orbital and the a_2''-symmetric HOMO is rather large (*ca.* 4.4 eV), which is thought to preclude significant mixing of 5*d* character into the latter. Remarkably, due to the primarily ligand-based nature of the a_2'' HOMO/SOMO found for $[\mathbf{1}^*]^{2-}$ and $[\mathbf{1}^*]^-$, it can be noted that population of this orbital in $K_2[\mathbf{1}]$ and $K(THF)_4[\mathbf{1}]$ results in the CO/CNAr^{Dipp2} ligand set acting in a formally redox non-innocent fashion. Distinct from these ligands merely functioning as π-acids, the successive reduction on going from **1** to $K(THF)_4[\mathbf{1}]$ and $K_2[\mathbf{1}]$ yields clusters best described as containing a $(Pt_3)^0$ core supported by a ligand set that, as an aggregate, bears a singly- or doubly-reduced π*-manifold. In essence, combining the out-of-plane π* orbitals of all six ligands in-phase renders them accessible in energy, allowing the a_2'' orbital to function as an electron reservoir reminiscent of multidentate redox non-innocent ligand systems bearing extended π-systems.[26]

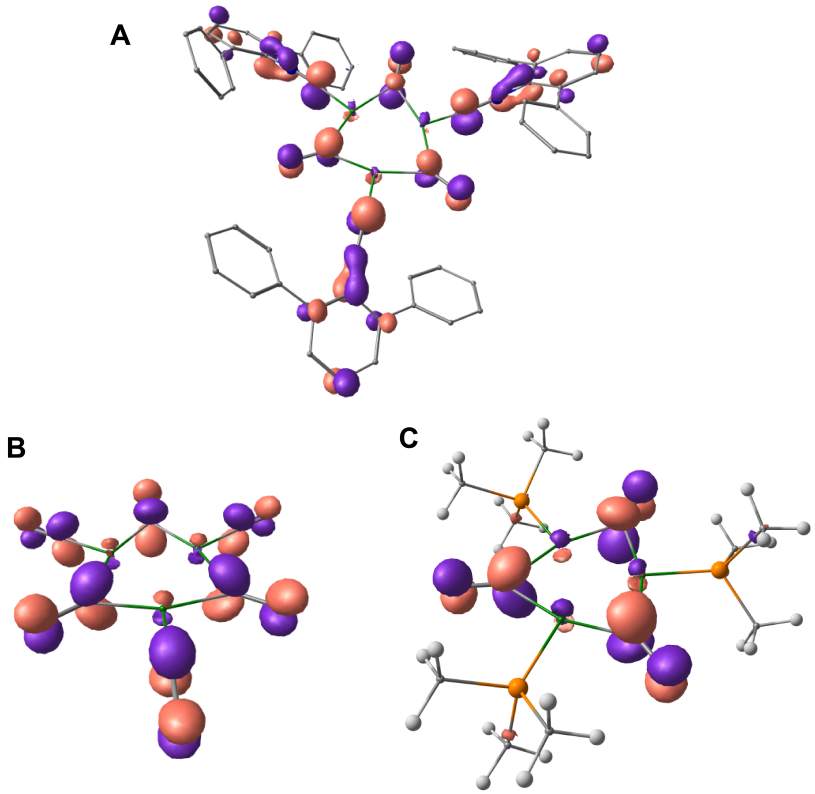

Figure 5.6. DFT Calculated HOMOs of $[\mathbf{1}^*]^{2-}$ (A), $[Pt_3(CO)_6)]^{2-}$ (B), and $[Pt_3(\mu\text{-}CO)_3(PMe_3)_3]^{2-}$ (C). BP86/def2-TZVP/ZORA.

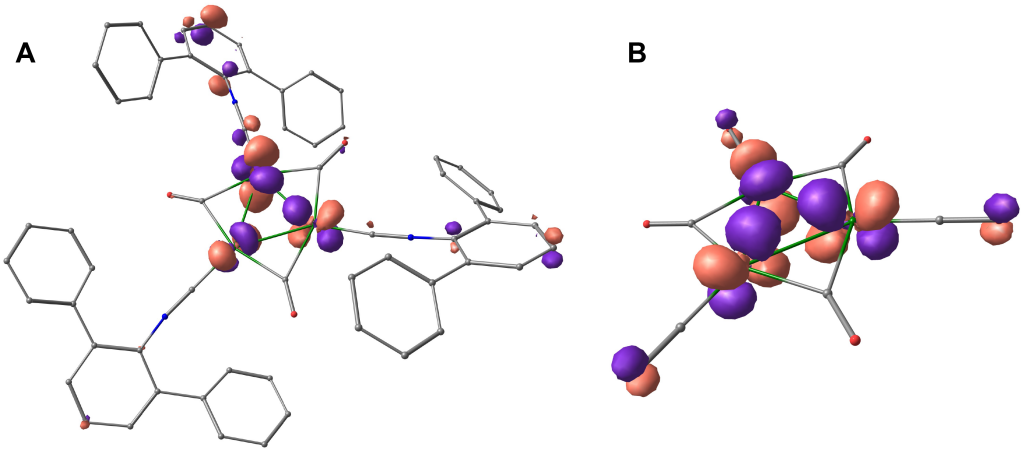

Figure 5.7. (A) DFT calculated metal-based a_2''-symmetric valence orbitals of $[\mathbf{1}^*]^{2-}$, which is HOMO–19 and is calculated to lie 4.40 eV below the HOMO. (B) DFT calculated metal-based a_2''-symmetric valence orbitals of $[Pt_3(CO)_6]^{2-}$, which is HOMO–10 and is calculated to lie 4.40 eV below the HOMO.

5.4. Metal-based reactivity of $K_2[Pt_3(\mu\text{-}CO)_3(CNAr^{Dipp2})_3]$ with electrophiles

The robust and highly-reduced nature of $K_2[Pt_3(\mu\text{-}CO)_3(CNAr^{Dipp2})_3]$ (K_2[**1**]) allows it to undergo well-defined reactivity with main-group and transition-metal electrophiles (Scheme 5.3). Addition of a benzene solution of Ph_3SnCl or Et_3SiCl to K_2[**1**] proceeds with elimination of KCl and formation of the diamagnetic triplatinum clusters $K[Pt_3(\mu^3\text{-}SnPh_3)(\mu\text{-}CO)_3(CNAr^{Dipp2})_3]$ (**2**, Figure 5.8) or $K[Pt_3(SiEt_3)(\mu\text{-}CO)_3(CNAr^{Dipp2})_3]$ (**3**, Figure 5.9) as determined by X-ray diffraction. In **2**, the triphenylstannyl ligand is bound in a μ^3 fashion, a binding mode that is unprecedented for triorganostannyl ligands.[43] Contrastingly, the triethylsilyl ligand in **3** is terminally bound to a single Pt center, with the Pt-Si bond vector being nearly orthogonal to the Pt_3 plane. The isocyanide bound to the silyl-ligated platinum center bends significantly out of the plane toward the opposite face of the cluster. However, despite the asymmetry evident in the solid-state structure of **3**, only a single sharp set of $-Ar^{Dipp2}$ resonances are seen by ^{1}H NMR at 20 ˚C, indicating that exchange of the silyl ligand between the three Pt centers is fast on the NMR timescale. Dianionic K_2[**1**] also reacts with one or two equivalents of $AuCl(PPh_3)$, providing dark blue $K(Et_2O)_2[Pt_3(\mu^3\text{-}AuPPh_3)(\mu\text{-}CO)_3(CNAr^{Dipp2})_3]$ (**4**, Figure 5.10) or forest green $Pt_3(\mu^3\text{-}AuPPh_3)_2(\mu\text{-}CO)_3(CNAr^{Dipp2})_3$ (**5**, Figure 5.11). In both clusters, the $-AuPPh_3$ fragments symmetrically bridge the three Pt centers affording a Pt_3Au tetrahedron (**4**) or a Pt_3Au_2 trigonal bipyramid (**5**). While reminiscent of the formation of $[Pt_3(\mu^3\text{-}AuPCy_3)(\mu\text{-}CO)_3(PCy_3)_3]^+$, which is produced by capping the corresponding neutral Pt_3 cluster with a $[AuPCy_3]^+$ fragment,[44] it should be noted that the two additional valence electrons possessed by K_2[**1**] compared to $Pt_3(\mu\text{-}CO)_3(PCy_3)_3$ allows for the isolation of a anionic Pt/Au cluster, of which only one other structurally

characterized example is known.[45] These extra electrons also allow for the formation of **5** via addition a second equivalent of $[AuPCy_3]^+$, a transformation which is not accessible for $[Pt_3(\mu^3\text{-}AuPCy_3)(\mu\text{-}CO)_3(PCy_3)_3]^{+}$[46] and has not been reported for any phosphine-substituted $Pt_3(\mu\text{-}CO)_3(PR_3)_3$ cluster. Thus, although formation of K_2[**1**] is effected by reduction of the combined ligand π^* manifold, the reducing equivalents thereby introduced can be leveraged to mediate reactivity at the platinum centers and allow for systematic electrophilic functionalization of the Pt_3 core.

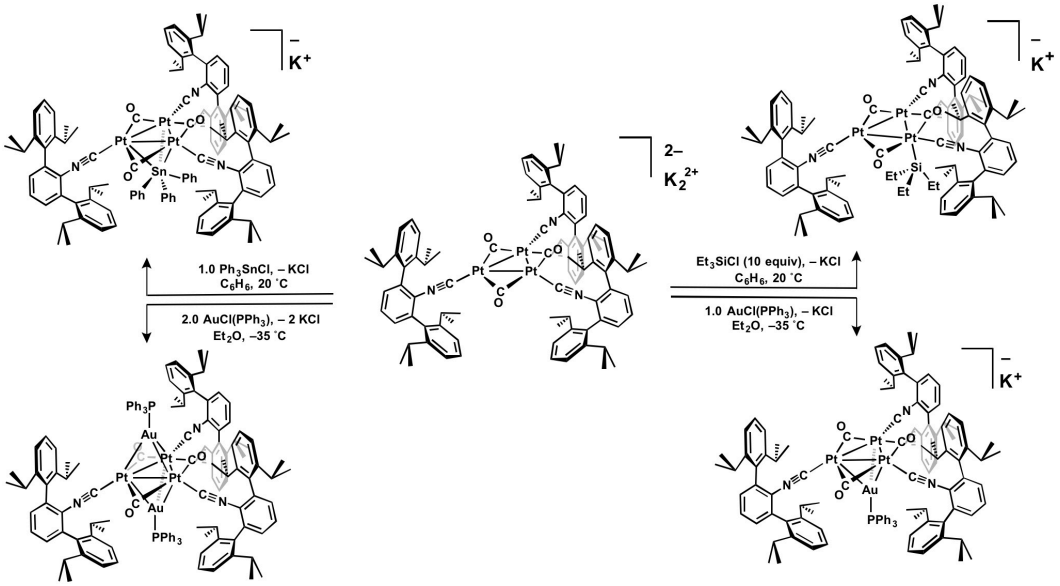

Scheme 5.3. Reactivity pinwheel for K_2[**1**].

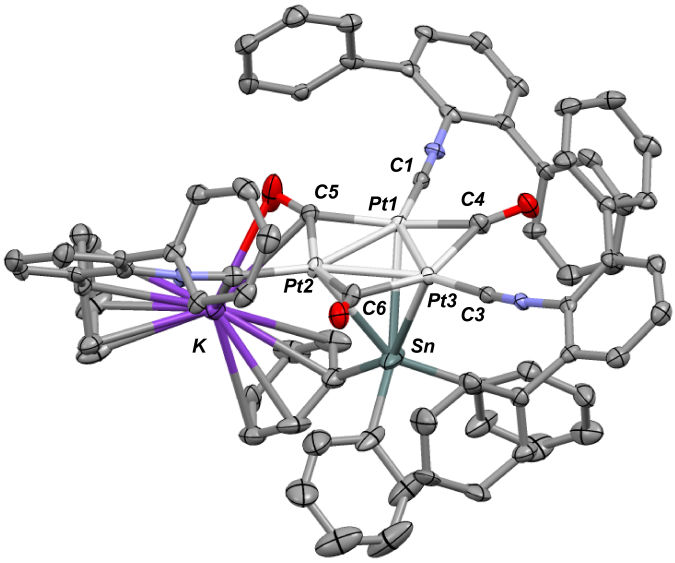

Figure 5.8. Molecular structure of $K[Pt_3(\mu^3\text{-}SnPh_3)(\mu\text{-}CO)_3(CNAr^{Dipp2})_3]\cdot 4(C_5H_{12})$ (**2**$\cdot 4(C_5H_{12})$). Flanking isopropyl groups omitted for clarity. Co-crystallized *n*-pentane molecules were accounted for using SQUEEZE. Selected bond distances (Å): Pt1-Pt2 = 2.6353; Pt2-Pt3 = 2.6322(5); Pt3-Pt1 = 2.6353(5); Pt1-Sn = 3.0372(8); Pt2-Sn = 2.9479(8); Pt3-Sn = 3.0024(9); Pt1-C1 = 1.903(9); Pt2-C2 = 1.902(9); Pt3-C3 = 1.916(9); Pt1-C4 = 2.073(10); Pt1-C5 = 2.073(9); Pt2-C5 = 2.079(9); Pt2-C6 = 2.102(9); Pt3-C4 = 2.020(10); Pt3-C6 = 2.062(9).

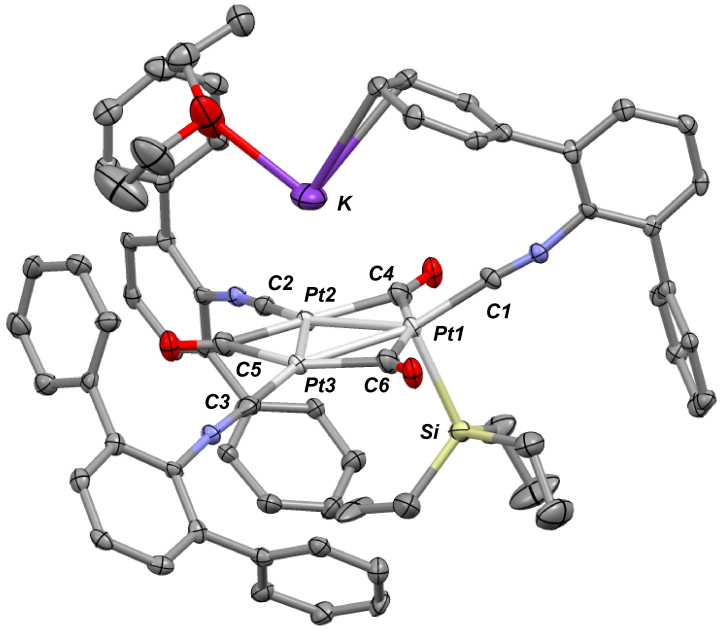

Figure 5.9. Molecular structure of $K(Et_2O)[Pt_3(SiEt_3)(\mu\text{-}CO)_3(CNAr^{Dipp2})_3]$ (**3**). Flanking isopropyl groups omitted for clarity. Selected bond distances (Å) and angles (˚): Pt1-Pt2 = 2.6435(5); Pt2-Pt3 = 2.6315(5); Pt3-Pt1 = 2.6440(5); Pt1-Si1= 2.417(3); Pt1-C1 = 1.953(9); Pt2-C2 = 1.918(9); Pt3-C3 = 1.872(11); Pt1-C4 = 2.069(10); Pt1-C6 = 2.073(11); Pt2-C4 = 2.039(11); Pt2-C5 = 2.062(11); Pt3-C5 = 2.075(10); Pt3-C6 = 2.076(10); C1-Pt1-Si = 99.4(3).

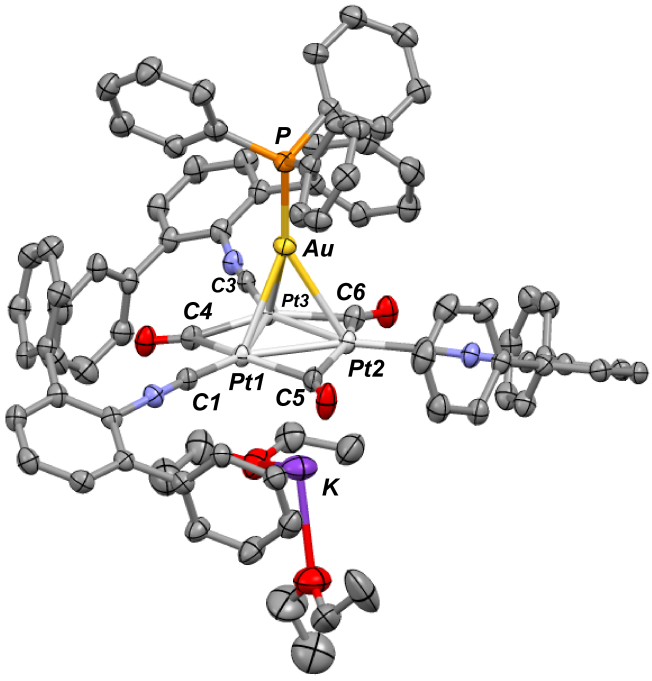

Figure 5.10. Molecular structure of $K(Et_2O)_2[Pt_3(\mu^3\text{-}AuPPh_3)(\mu\text{-}CO)_3(CNAr^{Dipp2})_3]\cdot 2(Et_2O)$ (**4**·2(Et_2O)). Flanking isopropyl groups and co-crystallized diethyl ether molecules omitted for clarity. Selected bond distances (Å): Pt1-Pt2 = 2.6465(3); Pt2-Pt3 = 2.6443(3); Pt3-Pt1 = 2.6446(3); Pt1-Au = 2.8410(4); Pt2-Au = 2.8421(4); Pt3-Au = 2.8284(4); Pt1-C1 = 1.912(6); Pt2-C2 = 1.898(6); Pt3-C3 = 1.900(6); Pt1-C4 = 2.078(6); Pt1-C5 = 2.066(6); Pt2-C5 = 2.069(5); Pt2-C6 = 2.071(6); Pt3-C4 = 2.070(6); Pt3-C6 = 2.079(6).

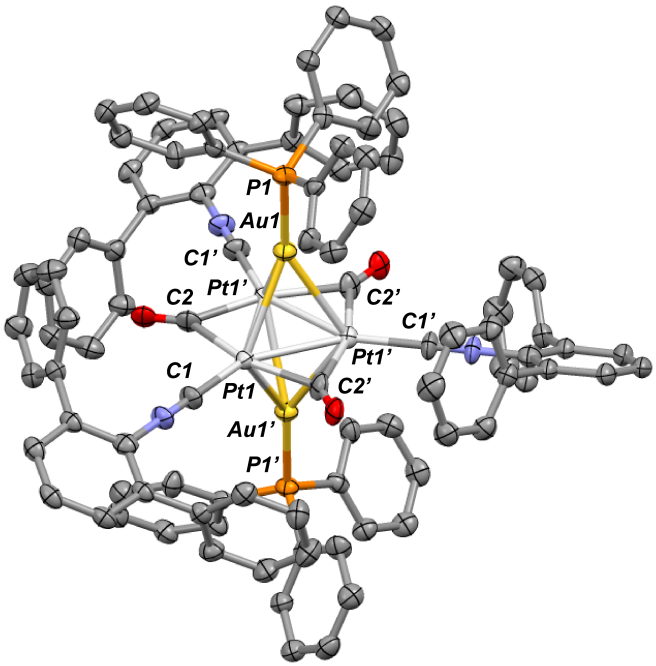

Figure 5.11. Molecular structure of $Pt_3(\mu^3\text{-}AuPPh_3)_2(\mu\text{-}CO)_3(CNAr^{Dipp2})_3 \cdot 3Et_2O$ (**5**·3 Et_2O). Flanking isopropyl groups omitted for clarity. Co-crystallized diethyl ether molecules were accounted for using SQUEEZE. Selected bond distances (Å): Pt1-Pt1' = 2.6388(7); Pt1-Au1 = 2.8292(5); Pt1-C1 = 1.985(10); Pt1-C2 = 2.085(1).

5.5. Synthesis of the neutral tripalladium cluster $Pd_3(\mu\text{-}CO)_3(CNAr^{Dipp2})_3$, its electrochemical behavior, and attempted chemical reductions

Given the central role played by the all π-acidic ligand set in housing the negative charge equivalents in the clusters $K(THF)_4$[**1**] and K_2[**1**], we wished to explore whether analogous metalates based off of the lighter Group 10 congeners could be accessed. Initial efforts have focused on palladium, a metal for which there are no known binary carbonyl clusters.[21] Utilizing the bis-*m*-terphenyl isocyanide complex $Pd(CNAr^{Dipp2})_2$,[47] the corresponding neutral tripalladium cluster $Pd_3(\mu\text{-}CO)_3(CNAr^{Dipp2})_3$ (**6**) was synthesized via substitution of one isocyanide ligand with CO (Scheme 5.4). Unlike in the synthesis of $Pt_3(\mu\text{-}CO)_3(CNAr^{Dipp2})_3$ (**1**), attempted syntheses using excess (*ca*. 1 atm) CO resulted in a mixture of **6**, $Pd(CNAr^{Dipp2})_2$, free $CNAr^{Dipp2}$, and other unidentified

species. However, addition of 1.05 equivalents of CO to a frozen diethyl ether solution of $Pd(CNAr^{Dipp2})_2$ allowed for smooth formation of **6** with liberation of one equivalent of $CNAr^{Dipp2}$ (Scheme 5.4). Following extraction with *n*-pentane and crystallization from toluene/*n*-pentane, **6** could be isolated as a golden yellow solid in moderate (52%) yields. Structural characterization via X-ray diffraction shows that **6** is isostructural to its platinum analogue **1**, with the coordination geometry around each Pd center being nearly rigorously planar (Figure 5.12). As was observed for **1**, a single set of υ(C=O) and υ(C≡N) bands (1871 and 2107 cm^{-1}, respectively) is observed for **6**, consistent with the D_{3h} site symmetry displayed in the solid state.

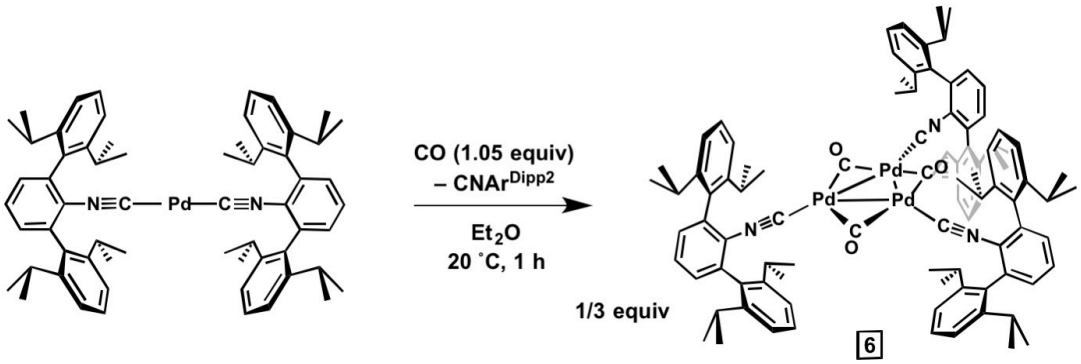

Scheme 5.4. Synthesis of $Pd_3(\mu\text{-}CO)_3(CNAr^{Dipp2})_3$ (**6**).

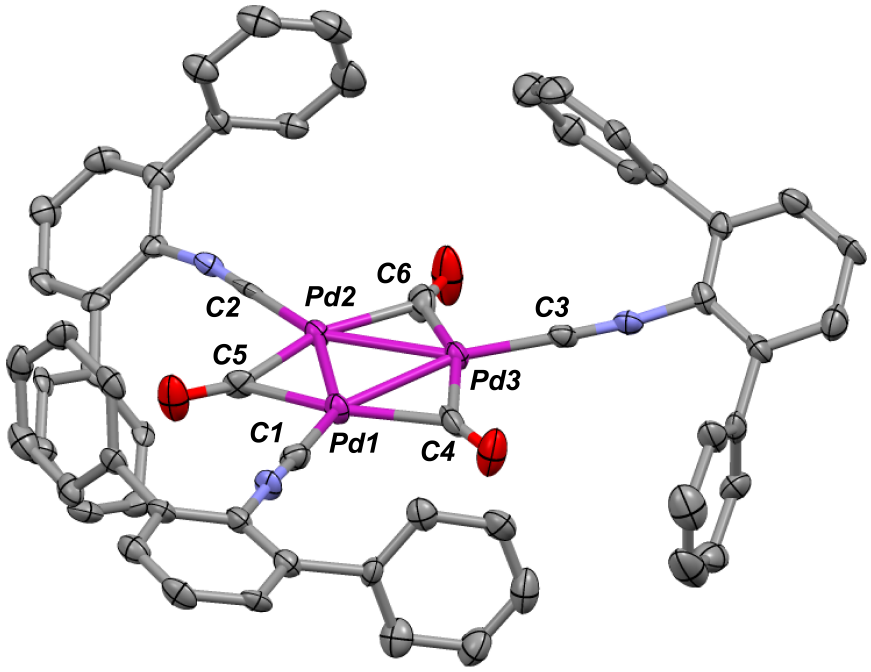

Figure 5.12. Molecular structure of $Pd_3(\mu\text{-}CO)_3(CNAr^{Dipp2})_3 \bullet Et_2O$ (**6** • Et_2O). Isopropyl groups and co-crystallized diethyl ether molecule omitted for clarity. Selected bond distances (Å): Pd1-Pd2 = 2.6750(11); Pd2-Pd3 = 2.6851(11); Pd1-Pd3 = 2.6726(13); Pd1-C1 = 1.985(6); Pd2-C2 = 1.956(6); Pd3-C3 = 1.977(6); Pd1-C4 = 2.036(6); Pd1-C5 = 2.063(6); Pd2-C5 = 2.080(6); Pd2-C6 = 2.039(6); Pd3-C6 = 2.056(7); Pd3-C4 = 2.064(7).

Cyclic voltammetry studies of **6** show the presence of a reversible redox wave centered at –2.46 V vs. Fc (ΔE_p = 92 mV), suggesting the potential accessibility of the corresponding radical monoanion (Figure 5.13). Scanning to more negative potentials evidences several superimposed redox events. Despite the reversibility of the first wave, attempted chemical reductions of **6** with a variety reducing agents (KC_8, Na metal, $Na[C_{10}H_8]$) have thus far led exclusively to ejection of free $CNAr^{Dipp2}$ and the formation of palladium metal as assessed by IR spectroscopy. The apparent resistance of **6** toward reduction is in line with the relative dearth of homometallic carbonyl palladate clusters

compared to those based off of platinum.[48] Computational investigations are underway in our laboratory with the aim of understanding why **6** is more difficult to reduce than **1**.

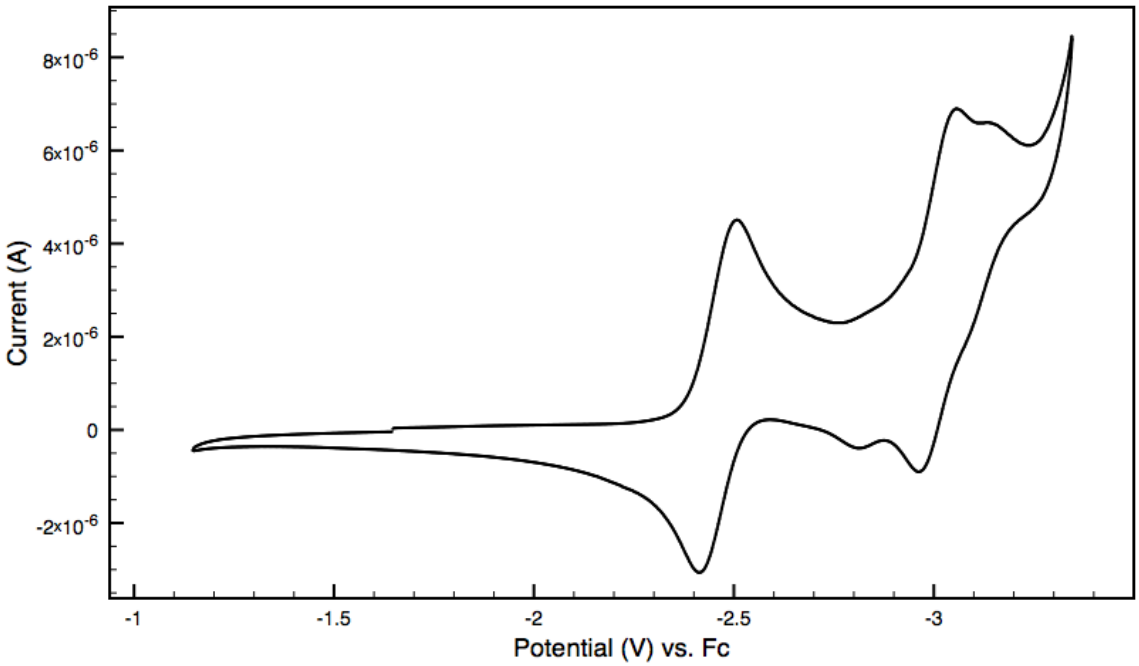

Figure 5.13. Cyclic voltammogram of complex **6**.

5.6. Concluding remarks

The kinetic stabilization afforded by encumbering *m*-terphenyl isocyanides, in concert with their isolobal relationship to CO, allows for the isolation of a robust analogue to Chini's delicate $[Pt_3(CO)_6]^{2-}$. Remarkably, the corresponding monoanion also proved isolable and was shown to contain one unpaired electron located primarily on the aggregate ligand π* system. Importantly, this study provides precedent for a set of isocyanide and carbonyl ligands to act in a redox non-innocent fashion. We are currently probing for other highly-reduced organometallic systems in which such an unusual situation may be fostered.

5.7. Synthetic procedures and characterization data

All manipulations were carried out under an atmosphere of purified dinitrogen using standard Schlenk and glovebox techniques. Unless otherwise stated, reagent-grade starting materials were purchased from commercial sources and either used as received or purified by standard procedures.[49] Solvents were dried and deoxygenated according to standard procedures.[50] Benzene-d_6 and THF-d_8 (Cambridge Isotope Laboratories) were distilled from NaK alloy/benzophenone and stored over activated 3 Å molecular sieves for 2 d prior to use. Celite 405 (Fisher Scientific) was dried under vacuum (24 h) at a temperature above 250 ˚C and stored in the glovebox prior to use. Other than for the synthesis of **1** and **6**, all reactions that were mechanically mixed by stirring utilized borosilicate-coated magnetic stirbars due to the propensity of the metalates reported herein to be oxidized by Teflon. $AuCl(PPh_3)$ was prepared by mixing $AuCl(SMe_2)$ with PPh_3 (1.00 equiv) in THF, stirring for 5 min, filtering through Celite, and drying *in vacuo*. $Pt(CNAr^{Dipp2})_2$ and $Pd(CNAr^{Dipp2})_2$ were prepared as previously reported.[29,47]

Solution ^1H, $^{13}C\{^1H\}$, $^{31}P\{^1H\}$ and ^{195}Pt NMR spectra were recorded on a Jeol ECA 500, a Varian X-SENS 500, or a Bruker Avance 300 spectrometer. ^1H and $^{13}C\{^1H\}$ chemical shifts are reported in ppm relative to $SiMe_4$ (^1H and ^{13}C δ = 0.0 ppm) with reference to residual solvent resonances of 7.16 ppm (^1H) and 128.06 ppm (^{13}C) for C_6D_6, 3.58 ppm (^1H) for THF-d_8. $^{31}P\{^1H\}$ NMR spectra were referenced externally to 85% H_3PO_4 (δ = 0 ppm). ^{195}Pt NMR spectra (direct detection) were referenced externally to 1.2 M $Na_2[PtCl_6]$ in D_2O (δ = 0 ppm). FTIR spectra were recorded on a Thermo-Nicolet iS10 FTIR spectrometer. Samples were prepared as C_6D_6 or THF solutions injected into a ThermoFisher solution cell equipped with KBr windows. Solvent peaks were digitally

subtracted from all spectra by comparison with an authentic spectrum obtained immediately prior to that of the sample. The following abbreviations were used for the intensities and characteristics of important IR absorption bands: vs = very strong, s = strong, m = medium, w = weak, vw = very weak; b = broad, vb = very broad, sh = shoulder. Combustion analyses were performed by Midwest Microlabs of Indianapolis, IN (USA).

Cyclic voltammetry measurements on $Pt_3(\mu\text{-}CO)_3(CNAr^{Dipp2})_3$ (**1**) and $Pd_3(\mu\text{-}CO)_3(CNAr^{Dipp2})_3$ (**6**) were carried out using a EG&G potentiostat (PAR-model 263A) and an electrochemical cell with a Pt disk working electrode, Pt wire counter-electrode, and Ag as a (pseudo) reference electrode. Measurements were performed in an argon-filled glovebox using a THF solution of **1** or **6** containing $[(n\text{-}Bu)_4N]PF_6$ (0.1 M) and decamethylferrocene as an internal standard ($Cp^*_2Fe/Cp^*_2Fe^+$ = –0.43 V vs. Cp_2Fe/Cp_2Fe^+ in THF)[51] at a scan rate of 0.1 V/s. For **1** (Figure 5.2), it is noted that the return (oxidative) peak of the latter wave contains a shoulder at *ca.* –2.45 V. With successive scanning, this shoulder was seen to increase in intensity. We tentatively ascribe its origin to oxidation of a species formed via reaction between *in situ*-produced $Pt_3(\mu\text{-}CO)_3(CNAr^{Dipp2})_3]^{\bullet-}$ or $[Pt_3(\mu\text{-}CO)_3(CNAr^{Dipp2})_3]^{2-}$ and the $[(n\text{-}Bu)_4N]PF_6$ electrolyte.

Synthesis of $Pt_3(\mu\text{-}CO)_3(CNAr^{Dipp2})_3$ (1). A resealable ampoule was charged with a diethyl ether solution of $Pt(CNAr^{Dipp2})_2$ (0.500 g, 0.480 mmol, 50 mL). The ampoule was connected to a Schlenk line and the solution was frozen in a liquid nitrogen bath. After evacuating the headspace of the ampoule, it was placed under 1.0 atm of CO gas, thawed, and allowed to stir vigorously for 1 hour at room temperature. All volatiles

were then removed *in vacuo*. The resulting orange residue was extracted 4 x 10 mL *n*-pentane to remove liberated $CNAr^{Dipp2}$. The remaining solid was taken up in 5 mL toluene, layered with 3 mL *n*-pentane, and stored at –35 ˚C for 3 days, whereupon red/orange crystals were obtained. The mother liquor was dried *in vacuo*, and the remaining residue taken up in 2 mL toluene, layered with 1 mL *n*-pentane, and stored at –35 ˚C for 1 week to provide a second crop of crystals, which were subsequently collected and dried. Yield: 0.272 g, 0.140 mmol, 88%. Crystals suitable for X-ray diffraction were grown from a dilute *n*-pentane solution stored at –35 ˚C. ^{1}H NMR (499.8 MHz, C_6D_6, 20 ˚C): δ = 7.34 (t, 6H, *J* = 8 Hz, *p*-Dipp), 7.25 (d, 12H, *J* = 8 Hz, *m*-Dipp), 7.02 (apparent s, 9H, *m*- and *p*-Ar), 2.81 (septet, 12H, *J* = 7 Hz, C*H*$(CH_3)_2$), 1.41 (d, 36H, *J* = 7 Hz, CH(C*H*$_3)_2$), 1.18 (d, 36H, *J* = 7 Hz, CH(C*H*$_3)_2$) ppm. ^{1}H NMR (300.0 MHz, THF-d_8, 20 ˚C): δ = 7.60 (t, 3H, *J* = 8 Hz, *p*-Ar), 7.32 (d, 6H, *J* = 8 Hz, *m*-Ar), 7.28–7.15 (m, 18H, *m*- and *p*-Dipp), 2.61 (septet, 12H, *J* = 7 Hz, C*H*$(CH_3)_2$), 1.14 (d, 36H, *J* = 7 Hz, CH(C*H*$_3)_2$), 1.12 (d, 36H, *J* = 7 Hz, CH(C*H*$_3)_2$) ppm. ^{13}C{^{1}H} NMR (125.7, C_6D_6, 20 ˚C): δ = 242.0 (μ-*C*O), 168.1 (*C*NR), 146.7, 139.2, 134.8, 129.9, 129.7, 129.1, 127.6, 123.5, 31.6, 24.8, 24.2 ppm. ^{195}Pt NMR (107.5 MHz, C_6D_6, 20 ˚C): δ = –4319 (s) ppm. FTIR (KBr windows, C_6D_6, 20 ˚C): υ(C=O) = 1834 (vs) cm^{-1}; υ(C≡N) = 2118 (vs) cm^{-1}; also 3064, 3026, 2962, 2926, 2906, 2887, 2868, 1579, 1471, 1462, 1385, 1418, 1363, 1103, 1056, 937, 793, 756 cm^{-1}. Anal. calcd. for $C_{96}H_{111}N_3O_3Pt_3$: C, 59.49; H, 5.77; N, 2.16. Found: C, 59.79; H, 5.86; N, 2.19.

Synthesis of $K_2[Pt_3(\mu\text{-}CO)_3(CNAr^{Dipp2})_3]$ (K_2[1]). Three filter pipettes were each loaded with 0.019 g KC_8 (total = 0.057 g, 0.425 mmol, 5.3 equiv). A benzene solution of $Pt_3(\mu^2\text{-}CO)_3(CNAr^{Dipp2})_3$ (0.156 g, 0.080 mmol, 6 mL) was prepared.

Subsequently, each of the KC_8-filled filter pipettes was charged with 2 mL of the above solution. The solution was mechanically agitated with the KC_8 for 10 s using a pipette, and then eluted through the filter at a rate of three drops per second. The eluents from each filter pipette were combined and lyophilized, affording a deep purple solid. Yield: 0.160 g, 0.079 mmol, 99%. Crystals of $K_2(DME)_3[Pt_3(\mu\text{-}CO)_3(CNAr^{Dipp2})_3]\cdot 2DME$ suitable for X-ray diffraction were grown from a 1:1 DME/*n*-hexane solution at –35 ˚C. ^{1}H NMR (499.8 MHz, C_6D_6, 20 ˚C): δ = 7.18–7.15 (m, 9H, *m*- and *p*-Ar), 7.07–6.97 (m, 18H, *m*- and *p*-Dipp), 3.05 (septet, 12H, *J* = 7 Hz, C*H*$(CH_3)_2$), 1.61 (d, 36H, *J* = 7 Hz, CH(C*H*$_3)_2$), 1.24 (d, 36H, *J* = 7 Hz, CH(C*H*$_3)_2$) ppm. ^{1}H NMR (300.0 MHz, THF-d_8, 20 ˚C): δ = 7.25–7.05 (m, 27 H, *m*- and *p*-Dipp, *m*- and *p*-Ar), 2.78 (septet, 12H, *J* = 7 Hz, C*H*$(CH_3)_2$), 1.23 (d, 36H, *J* = 7 Hz, CH(C*H*$_3)_2$), 1.09 (d, 36H, *J* = 7 Hz, CH(C*H*$_3)_2$) ppm. ^{13}C{^{1}H} NMR (125.7, C_6D_6, 20 ˚C): δ = 242.2 (μ-*C*O), 194.5 (*C*NR), 148.3, 138.1, 137.5, 132.1, 130.0, 125.4, 122.7, 31.6, 24.8, 24.8 ppm. *Note:* One aryl carbon resonance likely overlaps with the C_6D_6 solvent resonance. ^{195}Pt NMR (107.5 MHz, C_6D_6, 20 ˚C): δ = –4271 (s) ppm. FTIR (KBr windows, C_6D_6, 20 ˚C): υ(C=O) = 1722 (vs) cm^{-1}; υ(C≡N) = 2044 (s), 1983 (vs) cm^{-1}; also 2962, 2927, 2903, 2886, 2867, 1576, 1420, 1384, 1248, 1208, 1058, 756 cm^{-1}. Anal. calcd. for $C_{96}H_{111}N_3O_3Pt_3K_2$: C, 57.13; H, 5.54; N, 2.08. Found: C, 56.68; H, 5.33; N, 1.91.

Synthesis of $K(THF)_4[Pt_3(\mu\text{-}CO)_3(CNAr^{Dipp2})_3]$ ($K(THF)_4$[1]). To a THF solution of $K_2[Pt_3(\mu\text{-}CO)_3(CNAr^{Dipp2})_3]$ (0.044 g, 0.022 mmol, 0.5 mL) was added a THF solution of $Pt_3(\mu\text{-}CO)_3(CNAr^{Dipp2})_3$ (0.042 g, 0.022 mmol, 1.00 equiv, 0.5 mL). The solution rapidly turned dark forest green in color and contained solely $K[Pt_3(\mu^2\text{-}CO)_3(CNAr^{Dipp2})_3]$ as assayed by ^{1}H NMR (THF-d_8) and IR spectroscopy. Storing this

solution at –35 ˚C for one week yields black single crystals of $K(THF)_4[Pt_3(\mu^2\text{-}CO)_3(CNAr^{Dipp2})_3]$, although these are obtained in consistently poor yields. Yield: 0.010 g, 0.005 mmol, 10%. ^{1}H NMR (500.0 MHz, THF-d_8, 20 ˚C): δ = 8.08 (br s, 9H), 7.15 (br s, 9H), 2.87 (br s, 12H), 1.31 (br s, 36H), 0.57 (br s, 36H) ppm. μ_{eff} = 1.7(2) μ_B (Evans method, THF-d_8/$(TMS)_2O$, 20 ˚C, average of 3 independent trials). FTIR (KBr windows, THF, 20 ˚C): υ(C=O) = 1775 (vs) cm^{-1}; υ(C≡N) = 2061 (s), 2022 (vs) cm^{-1}; also 1578, 1414, 757 cm^{-1}. *Note*: Peaks between 1400-800 cm^{-1} and above 2700 cm^{-1} are obscured by the THF solvent. Anal. calcd. for $C_{96}H_{111}N_3O_3Pt_3K$: C, 58.25; H, 5.65; N, 2.12. Found: C, 57.92; H, 5.66; N, 2.26.

Synthesis of $K[Pt_3(\mu^3\text{-}SnPh_3)(\mu\text{-}CO)_3(CNAr^{Dipp2})_3]$ (2). To a benzene solution of $K_2[Pt_3(\mu\text{-}CO)_3(CNAr^{Dipp2})_3]$ (0.076 g, 0.038 mmol, 2 mL) was added drop-wise a benzene solution of Ph_3SnCl (0.015 g, 0.039 mmol, 1.03 equiv, 1 mL). The solution was gently shaken over the course of 10 min, whereupon it was frozen in a glovebox freezer and subsequently lyophilized. The resulting magenta solid was slurried in *n*-pentane (2 mL), filtered through Celite, and stored at –35 ˚C. After 1 day, magenta crystals were collected and dried *in vacuo*. Yield: 0.063 g, 0.027 mmol, 71%. ^{1}H NMR (499.8 MHz, C_6D_6, 20 ˚C): δ = 7.38 (t, 6H, *J* = 8 Hz, *p*-Dipp), 7.23 (d, 12H, *J* = 8 Hz, *m*-Dipp), 7.10 (apparent s, 15H, Sn-*Ph*), 7.02 (m, 9H, *m*- and *p*-Ar), 2.82 (septet, 12H, *J* = 7 Hz, C*H*$(CH_3)_2$), 1.27 (d, 36H, *J* = 7 Hz, CH(C*H*$_3)_2$), 1.19 (d, 36H, *J* = 7 Hz, CH(C*H*$_3)_2$) ppm. ^{13}C{^{1}H} NMR (125.7 MHz, C_6D_6, 20 ˚C): δ = 223.8 (μ-*C*O, $J_{Pt,C}$ = 754 Hz), 174.9 (*C*NR, $J_{Pt,C}$ = 138 Hz), 151.4, 146.7, 138.4, 137.7, 135.4, 129.9, 129.8, 129.4, 127.4, 127.1, 125.6, 123.7, 123.5, 31.5, 24.7, 24.2 ppm. FTIR (KBr windows, C_6D_6, 20 ˚C): υ(C=O) =

1865 (s), 1832 (vs), 1736 (s) cm^{-1}; υ(C≡N) = 2114 (sh), 2094 (vs), 2041 (s), 2002 (s) cm^{-1}; also 3055, 3040, 2962, 2926, 2867, 1580, 1470, 1461, 1449, 1417, 1384, 1363, 1254, 1180, 1058, 804, 792, 770, 756, 739, 728, 708, 701 cm^{-1}. Anal. calcd. for $C_{114}H_{126}N_3O_3Pt_3SnK$: C, 58.78; H, 5.45; N, 1.80. Found: C, 58.68; H, 5.43; N, 1.61.

Synthesis of $K[Pt_3(SiEt_3)(\mu\text{-}CO)_3(CNAr^{Dipp2})_3]$ (3). To a benzene solution of $K_2[Pt_3(\mu\text{-}CO)_3(CNAr^{Dipp2})_3]$ (0.051 g, 0.025 mmol, 2 mL) was added a benzene solution of Et_3SiCl (0.038 g, 0.252 mmol, 10.1 equiv, 1 mL). The solution was gently shaken over the course of 30 min, at which time it was frozen in a glovebox freezer and lyophilized. The resulting dark residue was taken up in 2 mL of 4:1 *n*-pentane/diethyl ether, filtered through Celite, and stored at –35 ˚C overnight to give brown crystals of $K(Et_2O)[Pt_3(SiEt_3)(\mu\text{-}CO)_3(CNAr^{Dipp2})_3]$, which were collected and dried *in vacuo*. Yield: 0.025 g, 0.012 mmol, 48%. ^{1}H NMR (499.8 MHz, C_6D_6, 20 ˚C): δ = 7.20 (apparent s, 18H, *m*- and *p*-Dipp), 7.02–6.98 (m, 9H, *m*- and *p*-Ar), 2.89 (septet, 12H, *J* = 7 Hz, C*H*$(CH_3)_2$), 1.48 (d, 36H, *J* = 7 Hz, CH(C*H*$_3)_2$), 1.18 (d, 36H, *J* = 7 Hz, CH(C*H*$_3)_2$), 0.71 (t, 9H, *J* = 8 Hz, –$SiCH_2CH_3$), 0.16 (q, 6H, *J* = 8 Hz, –$SiCH_2CH_3$) ppm. $^{13}C\{^1H\}$ NMR (125.7 MHz, C_6D_6, 20 ˚C): δ = 233.8 (μ-*C*O), 177.4 (*C*NR), 147.4, 138.6, 136.3, 130.4, 130.1, 128.7, 126.8, 123.1, 31.5, 24.8, 24.3 14.2, 10.4 ppm. FTIR (KBr windows, C_6D_6, 20 ˚C): υ(C=O) = 1833 (m), 1821 (m), 1782 (vs) cm^{-1}; υ(C≡N) = 2112 (s), 2084 (vs), 2053 (s), 2014 (s) cm^{-1}; also 3063, 2961, 2928, 2905, 2867, 1579, 1469, 1461, 1418, 1384, 1363, 1252, 1178, 1056, 1001, 792, 756, 720, 689 cm^{-1}. Anal. calcd. for $C_{102}H_{126}N_3O_3SiPt_3K$: C, 58.49; H, 6.06; N, 2.01. Found: C, 58.14; H, 6.17; N, 2.04.

Synthesis of $K[Pt_3(\mu^3\text{-}AuPPh_3)(\mu\text{-}CO)_3(CNAr^{Dipp2})_3]$ (4). A diethyl ether solution of $K_2[Pt_3(\mu\text{-}CO)_3(CNAr^{Dipp2})_3]$ (0.072 g, 0.036 mmol, 3 mL) and a diethyl ether

slurry of $AuCl(PPh_3)$ (0.020 g, 0.040 mmol, 1.11 equiv, 3 mL) were both cooled to –35 ˚C in a glovebox freezer. Both vials were removed from the freezer, the $AuCl(PPh_3)$ solution was added dropwise to the $K_2[Pt_3(\mu^2\text{-}CO)_3(CNAr^{Dipp2})_3]$ solution, and the reaction mixture placed back into the freezer. The reaction was briefly removed and shaken for 10 s at every 5 min interval. After 20 min, the dark blue solution was filtered through Celite and all volatiles removed *in vacuo*. The resulting solid was twice slurried in 1 mL *n*-pentane, shaken for a few seconds, and dried. To this solid was then added 3.5 mL Et_2O. The solution was filtered through Celite and stored overnight at –35 ˚C. The microcrystalline material thereby produced was disposed of. The mother liquor was again filtered through Celite and stored at –35 ˚C for one week, yielding dark blue crystals of $K(Et_2O)_2[Pt_3(\mu^3\text{-}AuPPh_3)(\mu\text{-}CO)_3(CNAr^{Dipp2})_3]\cdot 2Et_2O$, which were collected and dried *in vacuo*. Yield: 0.033 g, 0.013 mmol, 35%. ^{1}H NMR (499.8 MHz, C_6D_6, 20 ˚C): δ = 7.37–7.13 (m, 18H, *m*- and *p*-Dipp), 7.17 (apparent s, 15H, P-*Ph*), 7.11 (d, 6H, *J* = 7 Hz, *m*-Ar), 7.01 (t, 3H, *J* = 7 Hz, *p*-Ar), 2.98 (septet, 12H, *J* = 7 Hz, C*H*$(CH_3)_2$), 1.42 (d, 36 H, *J* = 7 Hz, CH(C*H*$_3)_2$), 1.24 (d, 36 H, *J* = 7 Hz, CH(C*H*$_3)_2$) ppm. ^{13}C{^{1}H} NMR (125.7 MHz, C_6D_6, 20 ˚C): δ = 230.5 (μ-*C*O), 182.1 (*C*NR), 147.1, 138.1, 136.3, 135.0, 134.3, 130.9, 129.7, 128.6, 127.7, 127.6, 125.7, 123.2, 31.5, 25.0, 24.3 ppm. ^{31}P{^{1}H} NMR (202.5 MHz, C_6D_6, 20 ˚C): ∂ = 34.1 ($J_{Pt,P}$ = 290 Hz) ppm. FTIR (KBr windows, C_6D_6, 20 ˚C): υ(C=O) = 1777 (s), 1818 (m) cm^{-1}; υ(C≡N) = 2057 (vs), 2027 (vs) cm^{-1}; also 3058, 2960, 2926, 2903, 2867, 1579, 1416, 1363, 1118, 1096, 1056, 1028, 936, 756, 694 cm^{-1}. Anal. calcd. for $C_{114}H_{126}N_3O_3KPAuPt_3$: C, 56.15; H, 5.21; N, 1.72. Found: C, 55.79; H, 5.14; N, 1.40.

Synthesis of $Pt_3(\mu^3\text{-}AuPPh_3)_2(\mu\text{-}CO)_3(CNAr^{Dipp2})_3$ (5). A diethyl ether solution of $K_2[Pt_3(\mu\text{-}CO)_3(CNAr^{Dipp2})_3]$ (0.078 g, 0.039 mmol, 3 mL) was frozen in a glovebox cold well. A room temperature $AuCl(PPh_3)$ slurry in *n*-pentane (0.039 g, 0.079 mmol, 2.0 equiv, 4 mL) was layered on top of the frozen solution. The combined reaction mixture was shaken as it warmed to room temperature over the course of 30 min, during which time it slowly changed in color from purple to blue to deep emerald green. At this time, the reaction mixture was frozen in a glovebox cold well. As the solution thawed, it was filtered through a medium porosity fritted funnel, and the filter cake subsequently washed with 2 x 5 mL thawing *n*-pentane and the mother liquor disposed. The product was then isolated via subsequent washes with benzene (4 mL) and diethyl ether (4 mL), and the filtrate dried *in vacuo*. The resulting residue was washed with 4 x 5 mL acetonitrile and dried, affording a deep green powder. Yield: 0.020 g, 0.007 mmol, 18%. Analytically pure single crystals of $Pt_3(\mu^3\text{-}AuPPh_3)_2(\mu\text{-}CO)_3(CNAr^{Dipp2})_3 \cdot 3Et_2O$ (**5**$\cdot 3Et_2O$) suitable for X-ray diffraction were grown from a diethyl ether solution stored at –35 ˚C. ^{1}H NMR (499.8 MHz, C_6D_6, 20 ˚C): δ = 7.62 (t, 6H, *J* = 8 Hz, *p*-Ph), 7.33–7.16 (m, 42H, *o, m*-Ph and *m*-, *p*-Dipp), 7.13 (d, 6H, *J* = 8 Hz, *m*-Ar), 7.02 (t, 3H, *J* = 8 Hz, *p*-Ar), 2.88 (septet, 12H, *J* = 7 Hz, C*H*$(CH_3)_2$), 1.24 (d, 36 H, *J* = 7 Hz, CH(C*H*$_3)_2$), 1.13 (d, 36 H, *J* = 7 Hz, CH(C*H*$_3)_2$) ppm. $^{13}C\{^1H\}$ NMR (125.7 MHz, C_6D_6, 20 ˚C): δ = 226.6 (μ-CO), 174.3 (CNR), 146.6, 138.7, 125.3, 134.8, 134.8, 133.2, 130.0, 129.3, 129.1, 128.8, 126.3, 123.6, 31.5, 24.9, 24.1 ppm. $^{31}P\{^1H\}$ NMR (121.4 MHz, C_6D_6, 20 ˚C): δ = 37.2 ($J_{Pt,P}$ = 234 Hz) ppm. FTIR (KBr windows, C_6D_6, 20 ˚C): υ(C=O) = 1824 (vs) cm^{-1}; υ(C≡N) = 2086 (vs), 2036 (m) cm^{-1}; also 3070, 3057, 2959, 2925, 2902, 2866, 1579, 1478, 1435, 1417, 1383,

1362, 1119, 1097, 1056, 1027, 936, 789, 755, 722, 708, 695 cm^{-1}. Anal. calcd. for $C_{132}H_{141}N_3O_3P_2Au_2Pt_3$: C, 55.46; H, 4.97; N, 1.47. Found: C, 55.01; H, 5.01; N, 1.52.

Synthesis of $Pd_3(\mu\text{-}CO)_3(CNAr^{Dipp2})_3$ (6). A resealable ampoule was charged with a diethyl ether solution of $Pd(CNAr^{Dipp2})_2$ (0.303 g, 0.318 mmol, 25 mL). The ampoule was connected to a Schlenk line and the solution was frozen in a liquid nitrogen bath. After evacuating all volatiles from the ampoule, 8.0 mL CO gas (0.333 mmol, 1.05 equiv) was added through the evacuated ampoule sidearm. The solution was allowed to thaw and warmed to room temperature with stirring over 1 h, during which time it changed in color from orange to yellow. All volatiles were then removed *in vacuo*. The resulting yellow residue was extracted 3 x 10 mL *n*-pentane to remove liberated $CNAr^{Dipp2}$. The remaining solid was taken up in 3 mL toluene, layered with 1 mL *n*-pentane, and stored at –35 ˚C for 3 days, whereupon yellow crystals were obtained. Yield: 0.093 g, 0.056 mmol, 52%. Single crystals suitable for X-ray diffraction were grown by storing an Et_2O solution at –35 ˚C. ^1H NMR (499.8 MHz, C_6D_6, 20 ˚C): ∂ = 7.35 (t, 6H, J = 8 Hz, *p*-Dipp), 7.26 (d, 12H, J = 8 Hz, *m*-Dipp), 6.98 (m, 9H, *m*- and *p*-Ar), 2.77 (septet, 12H, J = 7 Hz, C*H*$(CH_3)_2$), 1.42 (d, 36H, J = 7 Hz, CH(C*H*$_3)_2$), 1.17 (d, 36H, J = 7 Hz, CH(C*H*$_3)_2$) ppm. $^{13}C\{^1H\}$ NMR (125.7, C_6D_6, 20 ˚C): ∂ = 231.8 (μ-*C*O), 161.0 (*C*NR), 146.7, 139.4, 134.9, 129.8, 129.7, 128.7, 128.3, 123.4, 31.5, 24.8, 24.2 ppm. FTIR (KBr windows, C_6D_6, 20 ˚C): υ(CO) = 1871 (vs) cm^{-1}; υ(CN) = 2107 (vs) cm^{-1}; also 3062, 3025, 2962, 2926, 2869, 1460, 1417, 1384, 1363, 1055, 805, 793, 758, 731, 695 cm^{-1}. Anal. calcd. for $C_{96}H_{111}N_3O_3Pd_3$: C, 68.87; H, 6.68; N, 2.51. Found: C, 68.70; H, 6.68; N, 2.62.

5.8. X-band EPR procedures and measurements

The X-band continuous wave (CW) EPR spectrum of $K(THF)_4$[**1**] was measured on a Bruker E500 spectrometer equipped with a Bruker ER 041 X Microwave Bridge. In a dinitrogen-filled glovebox, crystals of $K(THF)_4$[**1**] were ground to a powder and placed into a 4 mm quartz tube outfitted with a J-Young-style resealable cap. The spectrum was recorded at 294 K with the spectrometer operating at 9.3977 MHz and a modulation amplitude of 0.5 G. Decreasing the modulation amplitude to 0.1 G did not result in resolution of any hyperfine coupling.

Spectral simulation details. Simulation of the X-band EPR spectrum of $K(THF)_4$[**1**] was performed using the program *Easyspin*.[52] The "pepper" function for simulation of solid-state spectra was utilized. The HStrain parameter was employed to account for spectral broadening due to unresolved hyperfine coupling.

Input file for *Easyspin* EPR simulation

```
Sys.g=[2.0200,1.9740]
Sys.HStrain=[80,200]
Exp.mwFreq=9.3977
Exp.CenterSweep=[330, 50]
pepper(Sys,Exp);
```

5.9. Details of DFT computational studies

Density Functional Theory (DFT) calculations were carried out on $[Pt_3(\mu\text{-}CO)_3(CNAr^{Ph2})_3]^{n-}$ ($[\mathbf{1}^*]^{n-}$, n = 0, 1, 2), which are truncated models of the structurally characterized complexes $[Pt_3(\mu\text{-}CO)_3(CNAr^{Dipp2})_3]^{n-}$ ($[\mathbf{1}]^{n-}$, n = 0, 1, 2). Calculations were carried out using the ORCA program package.[53] Geometry optimizations and single-point calculations were performed using the BP86 pure density functional.[54–56] The

all-electron Ahlrichs triple-zeta basis sets def2-TZVP (standard)[57] and def2-TZVP/J (auxiliary)[58] were used in all calculations. The resolution of identity (RI) approximation was employed.[59] Relativistic effects were included by use of the zeroth-order regular approximation (ZORA).[60–62] Crystallographic atomic coordinates were used as input for geometry optimizations where appropriate. Viewing of optimized structures and rendering of molecular orbitals was performed using the program *Chemcraft*.[63] After each geometry optimization, the optimized coordinates were reoriented so as to make the Pt_3 triangle coplanar with the Cartesian *xy* plane. These coordinates were then used to run a single point calculation using a larger integration grid (*Grid4*) than in the geometry optimization.

Example input file for geometry optimization

```
%pal nprocs 8 end
!  RKS  Opt  BP86  ZORA  def2-TZVP  def2-TZVP/J  KeepDens  VerySlowConv
TightSCF
%SCF
 MaxIter 3000
end
%geom
 MaxIter 1000
end

* xyz -2 1
Pt       5.02597300       8.13131200       3.89742500
Pt       6.25088800       5.99213700       4.86503400
Pt       4.01053700       6.84537100       5.98425400
O       7.47010400       7.16300900       2.33369200
N       8.65331000       4.08073600       4.91543900
O       2.36845400       9.19692000       4.92536100
O       5.18741400       4.27440900       7.14197100
C       2.68277900       6.68735500       7.37415000
N       1.87542900       6.59216500       8.19173600
N       5.01807600      10.56663800       2.01816800
C       5.17650800       5.21896500       6.43749800
C       0.89627500       6.23611400       9.12243500
C       0.29117500       7.23635900       9.87255000
C      -0.68885500       6.83715600      10.78935800
H      -1.11597900       7.47823900      11.30927900
C      -1.03311600       5.50935000      10.93620600
H      -1.68808500       5.26372100      11.54741100
```

C	-0.40142100	4.53973500	10.16624600
H	-0.64467900	3.64930500	10.27142100
C	0.57720900	4.86076200	9.25539200
C	1.28500700	3.84749700	8.43979000
C	0.93735800	3.62748900	7.07847000
C	5.15335300	14.11605200	-0.07937700
H	5.20458700	14.92215000	-0.54175000
C	5.55871500	12.94179700	-0.69455100
H	5.87317100	12.96367400	-1.56968600
C	5.49730400	11.72468200	-0.00992200
C	5.89593100	10.39877600	-0.61120500
C	7.23898700	9.94992000	-0.39688600
C	7.56750900	8.70820600	-0.88902600
H	8.41986600	8.36405200	-0.74614700
C	6.61959500	7.95714900	-1.60937500
C	1.59364800	2.61480200	6.35216700
H	1.36949200	2.45877800	5.46314200
C	2.56648500	1.86031800	6.95940400
H	2.97283100	1.16945200	6.48710900
C	2.94622700	2.11485200	8.26912900
H	3.63034400	1.61258700	8.65014000
C	2.33045700	3.09929100	9.02122900
C	5.35513000	8.41089700	-1.79194200
H	6.86420700	7.13346100	-1.96458800
H	4.73553700	7.88768000	-2.25034600
C	4.98064900	9.64821700	-1.29980300
C	10.49234500	6.15673200	1.42085300
H	10.77366400	7.04188100	1.40497800
C	2.82047900	12.69223300	3.70295000
C	2.49170200	12.53519200	5.01267600
H	1.60095100	12.40545800	5.24485400
C	3.44627500	12.56504200	6.00489200
C	0.77680500	8.64996900	9.72173300
C	1.79079600	9.08317200	10.57503900
C	2.32980400	10.36457700	10.36468900
H	3.00195700	10.68075800	10.92429900
C	1.87419000	11.14596600	9.34270700
H	2.24897400	11.98640500	9.20776500
C	0.86109200	10.70727400	8.50130700
H	0.57623600	11.24819100	7.80080300
C	0.26231500	9.44893400	8.69975100
C	10.68478800	5.39576500	2.56587100
C	4.17452300	12.86867800	3.35567500
C	3.29152200	8.49052600	4.95115800
H	3.19854900	12.43368400	6.89193300
C	4.78132200	12.79117400	5.68539800
H	5.41767000	12.86553500	6.35812100
C	5.15475600	12.90615800	4.34987500
H	9.78113600	6.13118400	-0.44649700
H	9.01962000	3.95803600	-0.42466800
C	5.00579100	9.63288200	2.71668800
C	5.03415600	11.77354900	1.29583400
C	4.60642800	12.92596200	1.93085300
C	6.72459800	7.14320800	3.21279600
C	7.75608900	4.79640100	4.87376500

```
C       9.77094300       3.22444700       4.90948500
C      10.55582700       3.18137000       3.77439000
C      11.62483900       2.27991700       3.76049900
H      12.17619400       2.22207200       3.01435200
C      11.85850700       1.47469000       4.85590600
H      12.55978200       0.86379100       4.83606100
C      11.08082800       1.56737300       5.96123400
H      11.27785800       1.03342500       6.69745900
C      10.00087800       2.43228800       6.03267400
C       9.15898800       2.57980600       7.23722400
C       8.04889700       1.74110400       7.45948100
C       7.32616500       1.86499500       8.63426400
H       6.60081200       1.30328000       8.79103500
C       7.67880200       2.82404800       9.58282300
H       7.18520800       2.89826100      10.36865800
C       8.74210500       3.65579600       9.37247300
H       8.96628100       4.28800700      10.01542900
C       9.50481600       3.56375800       8.18578300
C       9.89214600       5.61176900       0.31750900
C       4.68179800      14.10058700       1.19859700
H       4.40183500      14.89725000       1.58754600
C      10.29146100       4.06785000       2.55991800
C       9.64810100       3.51440400       1.45855800
C       9.44853200       4.30881700       0.32147800
H       0.17813152       4.22695060       6.59823991
H       7.98503464      10.53295599       0.12261563
H       2.65706502       3.27885624      10.03487762
H       3.98032103      10.02574422      -1.45217474
H       2.03313800      12.67733194       2.96384777
H       2.14679130       8.44745256      11.37223919
H      -0.56177699       9.10888327       8.09012989
H      11.13332859       5.82989305       3.44720191
H       6.19578880      13.02340990       4.08738176
H       7.75188544       1.00302576       6.72912174
H      10.33472562       4.23149094       8.00750582
H       9.31044841       2.48890308       1.48573510
*
```

Example input file for single point calculation

```
%pal nprocs 8 end
! RKS BP86 ZORA def2-TZVP def2-TZVP/J KeepDens NormalPrint SlowConv
TightSCF Grid4 PrintMOs
%SCF
 MaxIter 3000
end
%output
Print[ P_Basis ] 2
Print[ P_MOs ] 1
end

* xyz -2 1
Pt      -2.31519615      -1.37567136      -0.00000000
```

Pt	0.03032381	-2.69589054	-0.00000000
Pt	0.00000000	0.00000000	0.00000000
O	-2.49004547	-4.43976009	-0.02257458
N	1.56974452	-5.35864081	-0.32459537
O	-2.56467817	1.68389997	0.05061682
O	2.77485335	-1.30983330	0.15253898
C	0.88581308	1.66726225	0.08371257
N	1.37732177	2.75792814	0.22220806
N	-5.40000376	-1.57228832	-0.04418369
C	1.59189515	-1.32694305	0.07718995
C	1.94360598	3.92963455	0.60427939
C	1.46374361	5.17349513	0.06359709
C	2.12983340	6.35516334	0.41274835
H	1.73942800	7.29893830	0.02687387
C	3.23857648	6.35914635	1.26278180
H	3.71766800	7.29933033	1.54233169
C	3.69675985	5.14890032	1.78786310
H	4.53236145	5.14373265	2.49127635
C	3.07612172	3.92842050	1.49270628
C	3.60219612	2.69471750	2.12197640
C	2.76053133	1.71924901	2.69351372
C	-9.52797803	-1.93163893	-0.63183702
H	-10.60251518	-2.03334836	-0.79432957
C	-8.86400336	-2.77478909	0.26406364
H	-9.42416628	-3.54030465	0.80470364
C	-7.48128135	-2.69974657	0.47033506
C	-6.86634381	-3.60208257	1.47321363
C	-5.63419572	-4.25145042	1.26220042
C	-5.10222408	-5.11159520	2.22375498
H	-4.13370133	-5.57569352	2.03305666
C	-5.78542725	-5.35308810	3.41892416
C	3.29206652	0.59266339	3.32059019
H	2.61359568	-0.15749733	3.72856461
C	4.67485330	0.40775265	3.39790366
H	5.08492993	-0.48746944	3.86883072
C	5.52517268	1.36420402	2.83495628
H	6.60805633	1.21975707	2.86296298
C	4.99530150	2.48867271	2.20305942
C	-7.00980753	-4.71648867	3.64695076
H	-5.35920245	-6.01828037	4.17284392
H	-7.54835645	-4.87866250	4.58353080
C	-7.53758616	-3.84967304	2.69009402
C	-1.78644429	-7.73992391	0.67732746
H	-2.69264034	-7.20116460	0.40020032
C	-7.26693640	1.41553493	-2.23739138
C	-6.66134418	2.36062465	-3.06448199
H	-7.12052975	3.34497831	-3.18704316
C	-5.45634506	2.06295386	-3.70879653
C	0.31486338	5.26013126	-0.86902219
C	0.37747562	6.13951828	-1.97186373
C	-0.69830012	6.28223986	-2.84792394
H	-0.61423857	6.96177510	-3.69993544
C	-1.86774445	5.54004654	-2.65143087
H	-2.70685344	5.63760902	-3.34320282
C	-1.94329625	4.65530283	-1.57166591

```
H      -2.83320646       4.04659750      -1.40906411
C      -0.86821682       4.51593185      -0.69271551
C      -0.58768309      -7.39865227       0.05099051
C      -6.69473520       0.14070993      -2.03539995
C      -1.96353484       0.65902642      -0.02258985
H      -4.96797609       2.80661434      -4.34143032
C      -4.86778446       0.81074333      -3.50897875
H      -3.91460572       0.56988869      -3.98178879
C      -5.47483947      -0.13776513      -2.68608718
H      -2.75876978      -8.99356362       2.15135762
H      -0.63450188     -10.15109752       2.79020729
C      -4.20321590      -1.44781012      -0.00767471
C      -6.72723792      -1.72410602      -0.27255603
C      -7.40329059      -0.86047667      -1.20560907
C      -1.90175169      -3.40202624       0.03279359
C       0.99895159      -4.31516578      -0.13613369
C       2.31309842      -6.43451527      -0.67864883
C       1.89684224      -7.76261679      -0.30589701
C       2.74847551      -8.83533516      -0.60222030
H       2.41224515      -9.84316516      -0.35098712
C       3.97530435      -8.65664446      -1.24495061
H       4.60191445      -9.51653203      -1.48913680
C       4.36313408      -7.36797160      -1.62268510
H       5.29354020      -7.22194048      -2.17539658
C       3.56163685      -6.24823436      -1.37362667
C       4.02240738      -4.92649933      -1.85736518
C       5.37503070      -4.55455079      -1.70844267
C       5.85107133      -3.34183892      -2.20547356
H       6.89831422      -3.06934785      -2.05426993
C       4.98479620      -2.46222692      -2.86159187
H       5.34628609      -1.49909615      -3.22561718
C       3.64033866      -2.81174117      -3.01142966
H       2.94463290      -2.12224365      -3.49150822
C       3.16320296      -4.02503790      -2.51734283
C      -1.81992471      -8.73814537       1.65588155
C      -8.79152666      -0.98651918      -1.34835648
H      -9.29227266      -0.35341550      -2.08390910
C       0.61745497      -8.05053945       0.38171418
C       0.56732230      -9.04315058       1.38587168
C      -0.63151311      -9.38598542       2.00983849
H       1.67841932       1.83390796       2.64287641
H      -5.07257763      -4.09019694       0.34383414
H       5.66569816       3.21169472       1.73375616
H      -8.47436790      -3.32659187       2.89328403
H      -8.18719037       1.67283342      -1.70882531
H       1.29928691       6.69569790      -2.15428443
H      -0.96365547       3.81544840       0.13526791
H      -0.59638020      -6.61406139      -0.70320171
H      -4.98952280      -1.10316203      -2.54814294
H       6.05002861      -5.21787449      -1.16322394
H       2.10824239      -4.26813539      -2.63864961
H       1.49350143      -9.53130446       1.69587479
*
```

Optimized Cartesian coordinates of $Pt_3(\mu\text{-}CO)_3(CNAr^{Ph2})_3$ (1*).

Pt	5.18756996913550	8.16353835442854	4.14988170952617
Pt	6.58973139643705	6.12860201224229	5.23584288637362
Pt	3.99086619695868	6.46647911043212	5.87422335553920
O	8.13074925280117	7.94080771040692	3.30116079712257
N	9.29008580763042	4.65019460679864	5.58046111365251
O	2.21619006993536	8.69614991456750	4.73770029825483
O	5.37742710834544	4.02835570335644	7.13419143738787
C	2.42795764296157	5.95830782111786	6.85693854742756
N	1.43857732882539	5.67963194407480	7.44296359965216
N	5.08501006296723	10.62865374123840	2.27820760158995
C	5.34326304695079	4.99839755603165	6.47333577005034
C	0.29519457184351	5.37880874084852	8.14808822866733
C	-0.03736532566347	6.15449491532887	9.28989655162795
C	-1.15176722433933	5.76054370977092	10.04438369661883
H	-1.42837498280393	6.35834545109798	10.91412537867546
C	-1.91423159747219	4.65032142087163	9.68779580074145
H	-2.78339295520853	4.37154037297386	10.28499050714923
C	-1.58153953565757	3.91172565504419	8.55401550375924
H	-2.19462857814484	3.06014733386875	8.25549132521827
C	-0.48045938427181	4.25619833626502	7.75747308607477
C	-0.15854623713112	3.44276193492433	6.55746563700197
C	0.00971027216507	4.03325287469235	5.29303887292752
C	4.77467263267203	13.98835567122809	-0.16451166131186
H	4.67855096857605	14.87216515135023	-0.79667657294517
C	4.29570623814290	12.75762655730220	-0.60948864800373
H	3.83382993888798	12.67289171665679	-1.59384067857246
C	4.41710181419145	11.60081831221121	0.17403956073504
C	3.88459924274798	10.31189139370853	-0.33636085211584
C	4.67179137031125	9.14734916035884	-0.35960959103006
C	4.16663521414287	7.95828117717458	-0.88619305077822
H	4.79368706696333	7.06544788966332	-0.89839731528708
C	2.86621201835915	7.90857770775137	-1.39506399161806
C	0.26385229414936	3.24657853215795	4.16934977547582
H	0.38755523491410	3.72350516759176	3.19589789559032
C	0.36187516279916	1.85784181166987	4.28812778053294
H	0.56913897989729	1.24557298609614	3.40933701123374
C	0.19887596083880	1.25897805739549	5.53967538687962
H	0.28409309726702	0.17591464001064	5.64497869056300
C	-0.06338096064038	2.04404153367840	6.66335992279624
C	2.07341156312958	9.05877385765504	-1.37764272428443
H	2.47203579815819	6.97613930622926	-1.80158484224596
H	1.05410448931674	9.02810652994934	-1.76519315268273
C	2.57893195066260	10.25022143215254	-0.85533320171529
C	9.71804464265869	4.77763507417103	1.36343421209306
H	9.43638408372275	5.73958629024688	0.93379147491513
C	5.81515792825147	14.14622930692170	4.09427477261232
C	6.45826284112274	14.34205045609826	5.31713964276250
H	6.12282573690785	15.13875405348358	5.98332571495772
C	7.52248775599196	13.51754408516629	5.68949662358735
C	0.75414859902439	7.33656446708157	9.71539103064026
C	1.17173783971625	7.45172358903342	11.05352478995072
C	1.88227077391602	8.57256105236623	11.48642283890362
H	2.20852822245855	8.63757364139722	12.52563172216556

C	2.18265955187925	9.60153470131898	10.59041765127045
H	2.73995627639063	10.47714985025822	10.92685749787095
C	1.76866359521562	9.50114952080588	9.25954241726452
H	1.99698612953650	10.29949745731356	8.55205284144439
C	1.06295906206615	8.37894995203771	8.82394087513225
C	10.20002799977866	4.72814425104949	2.67187363560831
C	6.21938832829053	13.11773887678932	3.22430198406884
C	3.23111229228717	8.11156941564197	4.85515380108579
H	8.02720361105360	13.66970960200635	6.64452599426307
C	7.93505666018273	12.49393599123206	4.83267998004319
H	8.76680417803803	11.84571839256268	5.11210261148491
C	7.28803128035019	12.29187545103738	3.61324260003795
H	9.21082104310138	3.64663555378632	-0.40846199056595
H	9.85973690749393	1.45984609079701	0.60212903412165
C	5.11358871141554	9.69147964871878	3.00035195643055
C	5.04173158407671	11.72269855708110	1.44387223187494
C	5.55353325713782	12.96388381974240	1.90569013109161
C	7.17196819674149	7.60058329276860	3.89765346845665
C	8.24595755287196	5.19125899736084	5.44872790661070
C	10.50309508276448	4.02139548470343	5.74803404623037
C	11.13469829409496	3.42495396625641	4.62448931233742
C	12.32489255599659	2.71579339250241	4.84395789447316
H	12.82870054135147	2.26934040291315	3.98594417855056
C	12.87697929715841	2.60062488091343	6.11816832075981
H	13.81171135117928	2.05702557065341	6.26013681861341
C	12.24759600537408	3.20073738829400	7.20697919363872
H	12.69062253289112	3.13587270608035	8.20168330611232
C	11.05536666787628	3.92289255806793	7.05281170014908
C	10.41338679937280	4.53620574287894	8.24332140103444
C	10.19878998622094	3.76125032322007	9.39691768989024
C	9.63158226581846	4.32487350838389	10.54077107356886
H	9.45899197170541	3.70356452787811	11.42114558030918
C	9.27479077018174	5.67525659043645	10.55390568724603
H	8.82735602400423	6.11603170030357	11.44597069953945
C	9.48850717342885	6.45722682171547	9.41572723864660
H	9.21406629755946	7.51302504101920	9.41757065165256
C	10.04987206923000	5.89361313166544	8.26954865778000
C	9.59424763014379	3.60615856555900	0.61195594901507
C	5.40010808312487	14.08465863783583	1.07698070309021
H	5.80268068199324	15.03985264785813	1.41593823307921
C	10.57389536816579	3.50322383145905	3.25152116450773
C	10.44877022226258	2.33154507673205	2.48314056921262
C	9.96047971566053	2.38191486250271	1.17694645509868
H	-0.07731322281003	5.11506404999155	5.18451498115114
H	5.69220866078190	9.17657982120470	0.02258040176893
H	-0.17359747974537	1.57263583302230	7.64190063760121
H	1.94979635914875	11.14168543406674	-0.82653370355110
H	4.97429801241147	14.78402395970143	3.81462081139390
H	0.95388563010115	6.64228035443411	11.75263044735653
H	0.73567804139780	8.32168837307834	7.78576148825880
H	10.29763401258576	5.65333077517781	3.24022838757574
H	7.62918137296406	11.49629921932670	2.94967555403554
H	10.45993330493395	2.70176604723893	9.38426943032242
H	10.22215502580105	6.51697569297344	7.39160416969526
H	10.71701465143824	1.37077937928359	2.92620957343133

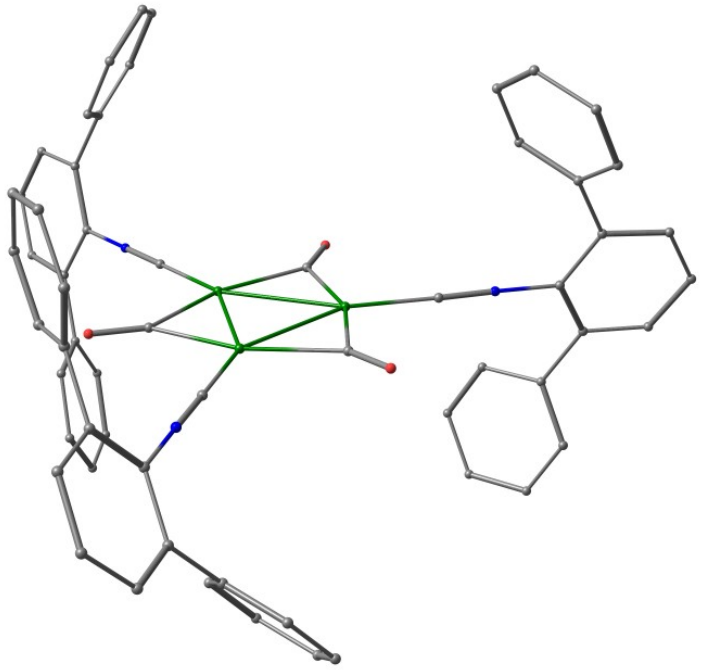

Figure 5.14. Optimized molecular structure of $Pt_3(\mu\text{-}CO)_3(CNAr^{Ph2})_3$ (**1***).

Table 5.2. Comparison of selected metrical parameters between crystallographically characterized $Pt_3(\mu\text{-}CO)_3(CNAr^{Dipp2})_3$ (**1**, "Crystal") and optimized coordinates of $Pt_3(\mu\text{-}CO)_3(CNAr^{Ph2})_3$ (**1***, "DFT").

Parameter	Mean d(Pt-Pt) (Å)	Mean d(Pt-C_{CNR}) (Å)	Mean d(Pt-C_{CO}) (Å)
Crystal	2.6496(2)	1.917(3)	2.062(2)
DFT	2.6986	1.915	2.080
% Difference	1.8%	0.1%	0.9%

Optimized Cartesian coordinates of $[Pt_3(\mu\text{-}CO)_3(CNAr^{Ph2})_3]^{\bullet-}$ ($[\mathbf{1}^*]^-$).

Pt	5.03562911796546	8.22012499063970	4.21919667698528
Pt	6.36805450334329	6.00559979188301	4.97731839670971
Pt	4.06876191155313	6.68719753296040	6.21203648013078
O	7.63154656947639	7.61705673919336	2.69525006906699
N	8.88386886081023	4.21994594599248	4.79127799653279
O	2.37553083615755	9.13256356116279	5.44998389736310
O	5.39750462318658	4.09525444088157	7.19060061772895
C	2.68416789036503	6.33872934024342	7.45965874442477
N	1.74695580571844	6.14775416013319	8.17612782882386
N	5.04226911431279	10.66237045623663	2.33366737854832
C	5.32374861560065	5.06040527593932	6.51289337524856
C	0.60660527634860	5.83661589138031	8.86074926966422
C	-0.07336967878534	6.85167211018447	9.59908633121658

C	-1.20644448679025	6.48648324226485	10.33954957915658
H	-1.74298369571051	7.26674451522144	10.88182445901488
C	-1.67017362757321	5.17177051905925	10.36888590187675
H	-2.56805897694362	4.91854425110642	10.93461042798530
C	-0.99530828714721	4.18834580514978	9.64708799554620
H	-1.36841966042798	3.16264839484721	9.64005319879024
C	0.14162716324108	4.48635424046536	8.88263354619187
C	0.81448010489051	3.39101824500441	8.14058340824810
C	1.17711552116544	3.51277220480862	6.78711542723157
C	5.54225930342314	14.03247120064100	-0.07928557768478
H	5.68045543581275	14.91220071996284	-0.70958866956013
C	5.49400623008057	12.76072624756234	-0.64988401481368
H	5.59791071247657	12.64200482351062	-1.72988511204678
C	5.34082969828128	11.60849575966679	0.13405175137811
C	5.24238277128300	10.28686376619247	-0.53645977430069
C	5.95983559097391	9.16016602612183	-0.09537296006017
C	5.85077133164340	7.94028321376326	-0.76519355792636
H	6.40537746168732	7.07866677471240	-0.39193872941723
C	5.03013790669961	7.81871681522582	-1.88921646522664
C	1.77031069053316	2.44811758978406	6.10841513842459
H	2.05542358091081	2.57354953927955	5.06313196050052
C	2.01533794037090	1.23938965239019	6.76428529291101
H	2.49456915826804	0.41436376428171	6.23474339047675
C	1.65949900586788	1.10233074297595	8.10822293321427
H	1.86184635456301	0.16848720491663	8.63670576828330
C	1.06608380833132	2.16622820571814	8.78782871496932
C	4.31524347423832	8.93065285571103	-2.34228932263096
H	4.94049945474640	6.85975620866542	-2.40268911016682
H	3.66199783024871	8.84643083639331	-3.21312586244150
C	4.42007422222461	10.14992733450195	-1.67178456997489
C	9.59058117273954	5.38999161649499	0.78676088463855
H	9.27986815990920	6.42281317076924	0.62776080517085
C	4.34412480587391	14.28922397221502	4.10447089741262
C	4.26554398648426	14.55736220014708	5.47130485937504
H	3.59403023106718	15.33972037074158	5.83131095090883
C	5.02930658639399	13.81638750584473	6.37669559287073
C	0.38497017816355	8.26335677358661	9.64057012164365
C	0.42721676470742	8.94059696181511	10.87519597661744
C	0.81301115125602	10.27918876297818	10.94944111205686
H	0.85002892996309	10.77809407402101	11.92025377800456
C	1.16692138610737	10.97193845469810	9.78816485386946
H	1.47800469819246	12.01653431726706	9.84363400558689
C	1.13313513171962	10.31279598835960	8.55673177749851
H	1.41940997529679	10.83019806999038	7.64089189993607
C	0.74809311061552	8.97340855082179	8.48209493823261
C	9.93792774869339	4.97984522622192	2.07431391240455
C	5.18858374741603	13.27640480210863	3.61010991125364
C	3.32881843267730	8.43122440481661	5.36871018040698
H	4.96291089280127	14.01723083093161	7.44753516621291
C	5.86754528018558	12.80457180076484	5.90148208888202
H	6.46015554870116	12.20953600062487	6.59769288023385
C	5.94723017288015	12.53569737652709	4.53460808745082
H	9.34518658721978	4.80810564895521	-1.28195070803546
H	10.02243723248913	2.44099462085883	-0.86315446902557
C	4.97675885757823	9.73400127954778	3.08329210745870

C	5.24255923589015	11.76269975595416	1.54942379721577
C	5.29141610400766	13.05836342837474	2.14533198521858
C	6.79052893511346	7.37520437370423	3.50157059611946
C	7.88382585683045	4.87123796161894	4.85610399270538
C	10.04756601277188	3.50984665646945	4.86522806336015
C	10.76461522672827	3.19627371797460	3.67021207086532
C	11.91524775497955	2.40197436120385	3.77623213276653
H	12.48042420125756	2.18637341711166	2.86809739771804
C	12.36285117601783	1.91978827947268	5.00557716447358
H	13.27249557922133	1.31999624770095	5.06229909588117
C	11.65779396157411	2.23731042385357	6.16610553962676
H	12.02046541137772	1.89376272543554	7.13628794726647
C	10.50455165049620	3.03311294931298	6.13269380151153
C	9.81030728787316	3.34375327889467	7.40677785064551
C	9.55885922664420	2.31445003963731	8.33394182429880
C	8.95031628907589	2.58402744955021	9.55987425193773
H	8.74690525688887	1.76630693247621	10.25412383335309
C	8.58029055383511	3.89084176586543	9.88691475555306
H	8.08789371464332	4.10229360351106	10.83721405597442
C	8.82364713116843	4.92234956932751	8.97699765000083
H	8.52394864398458	5.94410012495418	9.21379815031602
C	9.43030529664819	4.65379541552153	7.75011920207666
C	9.62557854642356	4.48565294262230	-0.27764661927257
C	5.43721785943518	14.17060089775978	1.30352250259851
H	5.50297163454422	15.15948850084375	1.76033243357866
C	10.33363761558192	3.65408500968106	2.32595539308840
C	10.35683166645239	2.75200958117591	1.24384978244015
C	10.00777460187247	3.16189273794033	-0.04298947437496
H	0.99256379028402	4.44587040052824	6.25544251644765
H	6.61117262332822	9.22528883417997	0.77542493640187
H	0.81488469739037	2.06192111969853	9.84511406374762
H	3.83517662204647	11.00700066106167	-2.01098078214401
H	3.72465992281686	14.85388105952048	3.40508383106129
H	0.17665706636674	8.39799370386908	11.78885048526015
H	0.73093295230267	8.48735292377819	7.50732172898474
H	9.90272056449789	5.70415720694221	2.88690899348985
H	6.61235328583908	11.74606467907651	4.18592670220281
H	9.82011630447610	1.28712611913986	8.07223398236611
H	9.61151397420855	5.47223049298901	7.05380579229497
H	10.63006491255170	1.71056248342149	1.42479233148827

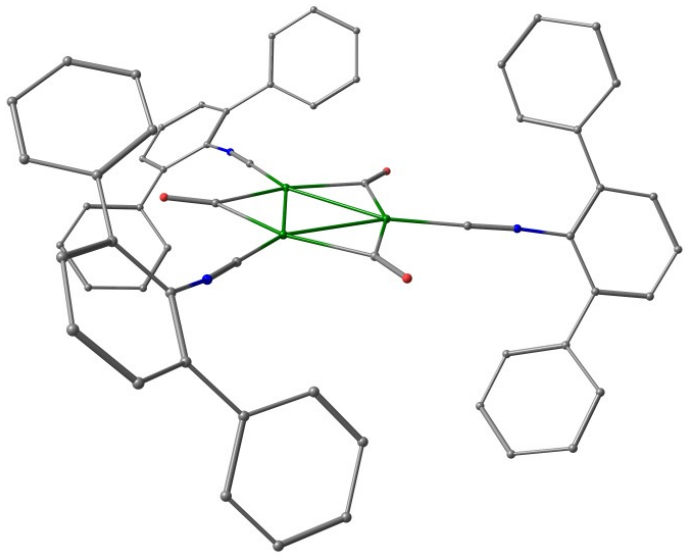

Figure 5.15. Optimized molecular structure of $[Pt_3(\mu\text{-}CO)_3(CNAr^{Ph2})_3]^{\bullet-}$ ($[\mathbf{1}^*]^-$).

Table 5.3. Comparison of selected metrical parameters between crystallographically characterized $K(THF)_4[Pt_3(\mu\text{-}CO)_3(CNAr^{Dipp2})_3]$ ($K(THF)_4[\mathbf{1}]$, "Crystal") and optimized coordinates of $[Pt_3(\mu\text{-}CO)_3(CNAr^{Ph2})_3]^-$ ($[\mathbf{1}^*]^-$, "DFT").

Parameter	Mean d(Pt-Pt) (Å)	Mean d(Pt-C_{CNR}) (Å)	Mean d(Pt-C_{CO}) (Å)
Crystal	2.6448(3)	1.924(6)	2.047(4)
DFT	2.6948	1.896	2.073
% Difference	1.9%	1.4%	1.3%

Optimized Cartesian coordinates of $[Pt_3(\mu\text{-}CO)_3(CNAr^{Ph2})_3]^{2-}$ ($[\mathbf{1}^*]^{2-}$).

Pt	5.05147131750973	8.16498431495529	4.16652699961745
Pt	6.31198943142978	5.89358735358336	4.87100728439583
Pt	4.15112782637489	6.72172049467050	6.25434308833882
O	7.50267398373779	7.40305048162663	2.48403361677169
N	8.76977735343837	4.03593293499878	4.59931647491469
O	2.55042451822865	9.25069872712039	5.57782752903255
O	5.35015439919965	4.03042279968579	7.12497187765608
C	2.84363616488207	6.46620007512021	7.59472022622552
N	1.93103657146859	6.32594031639200	8.36789748502659
N	4.96730047416276	10.59890577368075	2.26242876704766
C	5.30584323908836	5.01151942633156	6.46100935138839
C	0.81562665986013	6.02337264721843	9.07773248629309
C	0.09877050361561	7.05947024580984	9.77229235998969
C	-0.99643171478744	6.69708409247175	10.56672948923055
H	-1.55707531773514	7.49161801136971	11.06313784623929
C	-1.40738657114394	5.36880860679287	10.70341993690823
H	-2.28422902439631	5.12029942915054	11.30426372877478
C	-0.71007251542223	4.36819889250214	10.02307359709253
H	-1.05047606851160	3.33207448231207	10.08322813258700

C	0.38813134473445	4.65455920350164	9.20220438193063
C	1.04834083080844	3.53844707390433	8.48584175493372
C	1.41732395152349	3.62430526004935	7.12824346922867
C	5.24509611589270	14.10191769601346	-0.01053800288364
H	5.32959356044253	15.01628759946036	-0.60059442291455
C	5.44652091743147	12.85326853813174	-0.60610988967856
H	5.69017888695527	12.79243064498519	-1.66866235421578
C	5.38416586376055	11.66146970180081	0.12589204056105
C	5.56528576016391	10.37882309487968	-0.59531328741988
C	6.31721628629540	9.30846768161277	-0.07249985986269
C	6.48185989837672	8.12630110318010	-0.79555220433422
H	7.05054160147044	7.31167810591423	-0.34524129504916
C	5.90723537015850	7.97999475307859	-2.06122034738438
C	1.99355395658001	2.53690180360740	6.47214713139525
H	2.29331108706600	2.64431447873160	5.42901957245120
C	2.21577627689961	1.33457055616083	7.14837595425320
H	2.68882768331019	0.49455593771393	6.63656004231873
C	1.85767557838708	1.23164829745715	8.49593780059114
H	2.05070678789301	0.30710324618763	9.04570293881341
C	1.28614289118647	2.31959401314234	9.15488503092315
C	5.15611330353979	9.03148076998591	-2.59652853839456
H	6.02974069622897	7.04854375579135	-2.61793824842013
H	4.68387034825098	8.92743472270600	-3.57616034094450
C	4.98370775088480	10.20983777672008	-1.87041179856475
C	9.79074519611686	5.49192826684063	0.75535183335261
H	9.44509003607064	6.52209138737903	0.66852567696332
C	3.71371977289768	14.12443017095872	4.05739349084011
C	3.50008967028311	14.35134039487823	5.41639654867964
H	2.74486386533132	15.07616740706579	5.73117353121419
C	4.22502483097394	13.63281670099980	6.37241157020149
C	0.48266252558827	8.48982658512292	9.70969872553632
C	0.43799949402451	9.27516966477372	10.88219296658428
C	0.74980184760184	10.63432553856017	10.85731330832500
H	0.71827024985952	11.21252487666052	11.78437823192762
C	1.12595560435653	11.24709633524618	9.65727964543734
H	1.38518439763386	12.30752768012313	9.63591241949228
C	1.18746655962834	10.48251006785870	8.48852127601810
H	1.50111452898396	10.92891612465960	7.54446180308286
C	0.87120773038343	9.12340840887626	8.51295218519741
C	9.99296598893011	4.95957272735904	2.02873200372113
C	4.66419979518899	13.18122710764562	3.60978959738853
C	3.46648786159756	8.50190298976545	5.44655992833967
H	4.04717699485622	13.79243152565465	7.43761293040026
C	5.16010941692433	12.68438991938397	5.94759941004615
H	5.71601079288967	12.09525807601431	6.67835746346002
C	5.37883920832960	12.45981400621866	4.58853444489647
H	9.83596605176623	5.13033079638605	-1.37936047476521
H	10.56824657695549	2.75249715431589	-1.11440736653975
C	4.94988630941691	9.65894154282235	3.01428841273828
C	5.10903969177209	11.73487836670046	1.53701212880008
C	4.91220032455422	13.01861487969831	2.15891701553441
C	6.69013969363134	7.21273431907571	3.33820838539878
C	7.77311887856530	4.70606864770789	4.68736482511532
C	9.90553667154564	3.30406464701433	4.69858522042396
C	10.71161734820044	3.04753702913495	3.53218292936753

C	11.82001919806655	2.19991741139110	3.66178907601333
H	12.44870087126571	2.03798725894650	2.78404866005741
C	12.16455268702394	1.60513501802766	4.87738448608313
H	13.05212370880749	0.97402146351758	4.95213149792417
C	11.39052397485046	1.87525298048961	6.00950145271800
H	11.68209815463924	1.46124565916845	6.97699979580599
C	10.27685726729551	2.72132370725005	5.96313139045697
C	9.54554457993671	2.99800698801140	7.22087700882837
C	9.27688878020222	1.94864486313650	8.12463398436157
C	8.64206289320422	2.18750443544381	9.34293883040672
H	8.42516832176625	1.35177668089767	10.01252635726518
C	8.25171382481404	3.48434180437307	9.69004334670153
H	7.72788700461335	3.67135077512400	10.62889549747538
C	8.50366108104012	4.53433189439553	8.80335227712340
H	8.17593761228704	5.54642478818166	9.04450380532198
C	9.14060574839480	4.29770491696011	7.58590478760755
C	10.00676499357352	4.71243367476130	-0.38520012543017
C	4.97724021624334	14.16660136201323	1.35806761956033
H	4.86306468610681	15.13859593580667	1.84262409018457
C	10.42335745721840	3.62849615485220	2.20104315038433
C	10.61825935952474	2.85069704550427	1.03778728093785
C	10.41868889486160	3.38387787880226	-0.23499175261231
H	1.26162523194668	4.55111374536852	6.57737036442264
H	6.78139906284542	9.38430352081146	0.90913014016475
H	1.04377478007205	2.24243159810180	10.21683686471148
H	4.36315512263073	11.01014438042743	-2.27892605187247
H	3.11445272088538	14.66312506593783	3.32041399576348
H	0.18092198509160	8.79786455093744	11.83005377891457
H	0.93276905912528	8.56056055605886	7.58303033914763
H	9.81127909271530	5.59251037724682	2.89524466395862
H	6.11203613449039	11.71172383156978	4.28964416073531
H	9.54323747903389	0.92707472802319	7.84474689752546
H	9.31557229081152	5.13283539049040	6.90863281625287
H	10.90564321051657	1.80253684255879	1.14254724105960

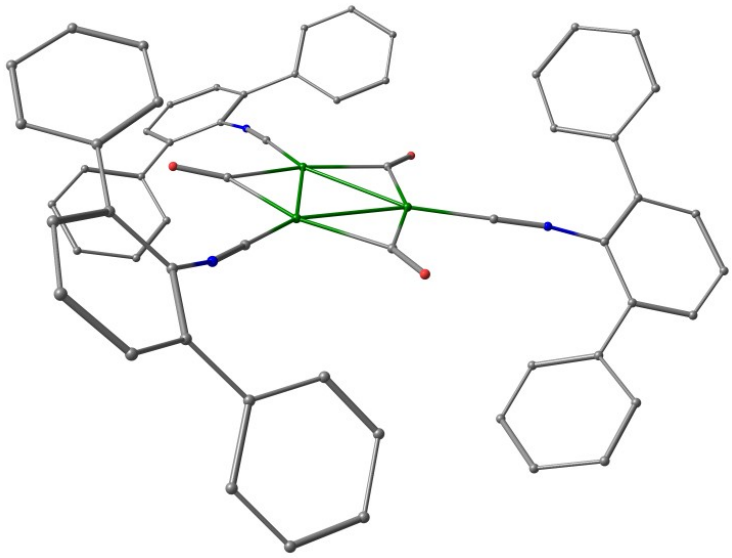

Figure 5.16. Optimized molecular structure of $[Pt_3(\mu\text{-}CO)_3(CNAr^{Ph2})_3]^{2-}$ ($[\mathbf{1}^*]^{2-}$).

Table 5.4. Comparison of selected metrical parameters between crystallographically characterized $K_2(DME)_3[Pt_3(\mu\text{-}CO)_3(CNAr^{Dipp2})_3]$ ($K_2(DME)_3[\mathbf{1}]$, "Crystal") and optimized coordinates of $[Pt_3(\mu\text{-}CO)_3(CNAr^{Ph2})_3]^{2-}$ ($[\mathbf{1}^*]^{2-}$, "DFT").

Parameter	Mean d(Pt-Pt) (Å)	Mean d(Pt-C_{CNR}) (Å)	Mean d(Pt-C_{CO}) (Å)
Crystal	2.6359(2)	1.896(4)	2.044(3)
DFT	2.6936	1.890	2.069
% Difference	2.2%	0.3%	1.2%

Optimized Cartesian coordinates of $[Pt_3(CO)_6]^{2-}$

```
Pt   0.00836434070195      0.01884565150495      0.01242890307375
Pt   0.92842990648968     -2.51915158390694      0.01572217189017
Pt  -1.72917430195351     -2.04708671407873     -0.01059794182979
O    3.06488831753978     -0.30847444490107      0.04138143099052
O    3.25653024492891     -4.46530407756790      0.03831168535588
O   -2.97419776724681      0.76376594065184     -0.02038444378051
O   -0.88283706890572     -5.00261070870413     -0.01260162919278
C   -3.47392428346705     -2.67958192662077     -0.02804730617864
O   -4.58201971173344     -3.08063959948465     -0.03788477390360
O    0.53640209354547      3.00705890773608      0.01983956586913
C   -0.67349769690077     -3.82306655326818     -0.00595828256531
C    0.33150470041490      1.84644612971574      0.01891243829002
C    2.35097771494177     -3.71097707182639      0.02867269829136
C   -2.05760472930209     -0.00758121222990     -0.01099394889115
C    1.93857127094692     -0.71649825701996      0.02966901258096
```

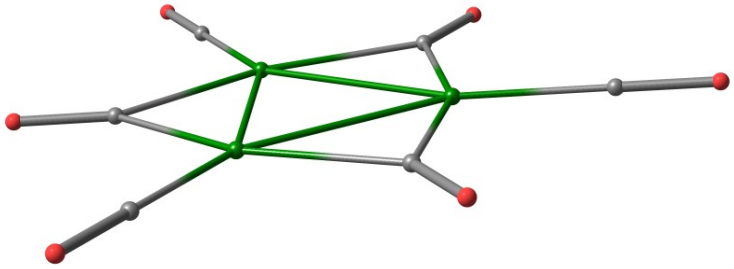

Figure 5.17. Optimized molecular structure of $[Pt_3(CO)_6]^{2-}$.

Optimized Cartesian coordinates of $[Pt_3(\mu\text{-}CO)_3(PMe_3)_3]^{2-}$.

Pt	2.66556844618658	0.11868000950116	-0.17299597618862
Pt	0.01645966820162	-0.01505486405272	0.06247598013535
Pt	1.21993047343027	2.35455949008961	-0.10279159954745
C	3.26184675692368	2.09371904267997	-0.25933335985883
C	-0.78252448449465	1.88864033149561	0.08589860766214
C	1.42467231234024	-1.52346840457546	-0.02008966377698
O	4.27935327975531	2.75380972633296	-0.34723230755384
O	-1.86176752431487	2.44257825925033	0.16889199408902
C	5.98570847419653	-0.03544132779944	-1.23299981445667
O	1.48888547130944	-2.73734767882603	0.00949137537760
P	1.11014121226758	4.55339706103863	-0.12051267709524
C	5.54547350483872	-1.20386215015637	1.30844416071183
C	2.41588246775918	5.49094294981409	-1.05117411476045
C	-0.42790494245963	5.35146117951227	-0.78907313327889
C	1.21748399778694	5.45940399392055	1.51424399276941
P	4.62502635080088	-0.87747524274850	-0.28882096478491
C	4.70722970003606	-2.58340739883229	-1.01923151270009
P	-1.82184684503551	-1.21379976440723	0.23727545680664
C	-2.69723604692506	-1.73832306895931	-1.33249717072730
C	-1.71078784946616	-2.87024196339455	1.06986576401758
C	-3.27073689814302	-0.47504719594722	1.13477429538338
H	6.96856747788204	-0.52129424229121	-1.10003686198253
H	6.02549695037014	1.01158112802214	-0.89793114820101
H	5.71657790825898	-0.03245251374314	-2.29874017810431
H	6.52237964687104	-1.70221144121402	1.15904489362257
H	4.90676936264900	-1.82746135439179	1.94944979609560
H	5.69562772705542	-0.24201489704575	1.81831660887754
H	3.39381138991361	5.08628496224092	-0.75110913884499
H	2.37672784039597	6.58007359254027	-0.87262938150530
H	2.28911106242891	5.28801306927109	-2.12401092043974
H	-0.46420075697364	6.44022856729669	-0.60789414285014
H	-1.29130833432690	4.85386414258228	-0.32322019098262
H	-0.47749886160662	5.15503022712220	-1.86947196946519
H	2.16760779928786	5.18616460250510	1.99414681524147
H	0.40141292732678	5.10168840979543	2.15745300542603
H	1.15557710378430	6.55975366248260	1.41198974608470
H	5.69181442677417	-3.06421193146339	-0.88161499576526
H	4.47767281711667	-2.51273944766059	-2.09184869849754
H	3.91498930824225	-3.18573671054219	-0.55069638994402
H	-2.95702254189214	-0.83189724581252	-1.89693352877933

H	-3.61044729513060	-2.33572973263729	-1.14745716241955
H	-1.99139170932232	-2.32162312702537	-1.94016453308085
H	-0.85714912961782	-3.40772445025497	0.63111922934450
H	-2.63505528409192	-3.46687593566441	0.97293186668283
H	-1.48645809583852	-2.70713135064048	2.13353917146406
H	-3.00757415917955	-0.37947620280474	2.19771045681083
H	-4.19257078067238	-1.07451543574688	1.03312974271658
H	-3.42491381469889	0.54028194114398	0.74054664627198

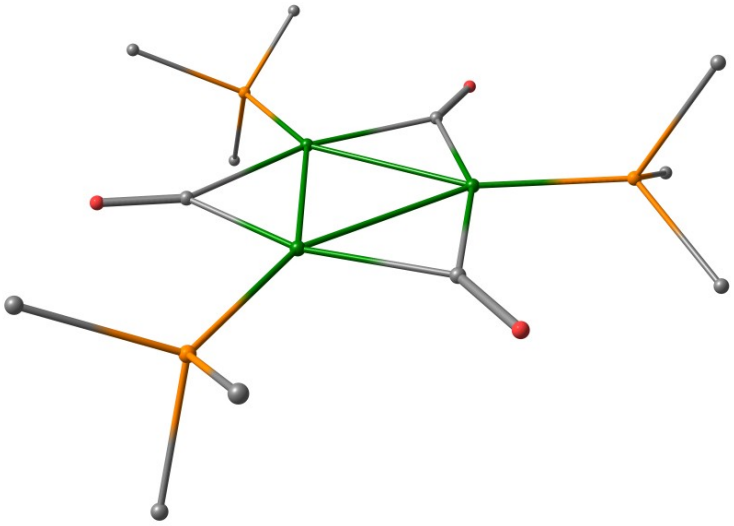

Figure 5.18. Optimized molecular structure of $[Pt_3(\mu\text{-}CO)_3(PMe_3)_3]^{2-}$.

5.10. Details of crystallographic structure determinations

Single crystal X-ray structure determinations were carried out at low temperature on Bruker Kappa diffractometers equipped with a Mo or Cu radiation source and a Bruker APEX-II or Proteum Pt135 detector. All structures were solved via direct methods with SHELXS[64] and refined by full-matrix least-squares procedures using SHELXL[64] within the Olex2 small-molecule solution, refinement and analysis software package.[65] Crystallographic data collection and refinement information are listed in Tables 5.5-7.

The following molecules contained positionally disordered components that were modeled and refined anisotropically. They are listed along with their respective

disordered components:

$Pt_3(\mu\text{-}CO)_3(CNAr^{Dipp2})_3 \cdot C_5H_{12}$ (**1**$\cdot C_5H_{12}$): Two-site positional disorder of one *i*Pr methyl group.

$K[Pt_3(\mu^3\text{-}SnPh_3)(\mu\text{-}CO)_3(CNAr^{Dipp2})_3] \cdot 4\ C_5H_{12}$ (**2**$\cdot$ 4 C_5H_{12}): Two-site rotational disorder of one Sn-*Ph* ring; two-site positional disorder of one Dipp ring; two-site positional disorder of the K counterion.

$K(Et_2O)[Pt_3(SiEt_3)(\mu\text{-}CO)_3(CNAr^{Dipp2})_3]$ (**3**): Two-site positional disorder of one Si-Et methyl group.

$K(Et_2O)_2[Pt_3(\mu^3\text{-}AuPPh_3)(\mu\text{-}CO)_3(CNAr^{Dipp2})_3] \cdot$ 2 Et_2O (**4**$\cdot$2 Et_2O): Two-site positional disorder of one potassium-bound Et_2O methyl group.

In addition, the following molecules contained co-crystallized solvent molecules that were severely disordered and could not be properly modeled. The Platon routine SQUEEZE[66] was used to account for these disordered molecules as a diffuse contribution to the overall scattering pattern without specific atom positions:

$Pt_3(\mu\text{-}CO)_3(CNAr^{Dipp2})_3 \cdot C_5H_{12}$ (**1**$\cdot C_5H_{12}$): Two molecules of *n*-pentane per unit cell.

$K(THF)_4[Pt_3(\mu\text{-}CO)_3(CNAr^{Dipp2})_3] \cdot 2$ THF ($K(THF)_4$[**1**]$\cdot 2$ THF): Four molecules of THF per unit cell.

$K_2(DME)_3[Pt_3(\mu\text{-}CO)_3(CNAr^{Dipp2})_3] \cdot 2DME$ ($K_2(DME)_3$[**1**]$\cdot 2$ DME): Eight molecules of 1,2-dimethoxyethane (DME) per unit cell.

$K[Pt_3(\mu^3\text{-}SnPh_3)(\mu\text{-}CO)_3(CNAr^{Dipp2})_3] \cdot 4(C_5H_{12})$ (**2**$\cdot$4 C_5H_{12}): Sixteen molecules of *n*-

pentane per unit cell.

$Pt_3(\mu^3\text{-}AuPPh_3)_2(\mu\text{-}CO)_3(CNAr^{Dipp2})_3 \cdot 3\ Et_2O$ (**5**·3 Et_2O): Eighteen molecules of diethyl ether per unit cell.

Table 5.5. Crystallographic data collection and refinement information.

Name	$Pt_3(\mu\text{-}CO)_3(CNAr^{Dipp2})_3 \cdot C_5H_{12}$	$K(THF)_4[Pt_3(\mu\text{-}CO)_3(CNAr^{Dipp2})_3] \cdot 2THF$	$K_2(DME)_3[Pt_3(\mu\text{-}CO)_3(CNAr^{Dipp2})_3] \cdot 2\ DME$
Formula	$C_{101}H_{123}N_3O_3Pt_3$	$C_{120}H_{159}N_3O_9KPt_3$	$C_{116}H_{161}N_3O_{13}K_2Pt_3$
Crystal System	Triclinic	Triclinic	Monoclinic
Space Group	*P*-1	*P*-1	*P*2(1)/n
a, Å	15.6588(10)	12.3546(3)	15.0706(16)
b, Å	16.2542(11)	16.6783(4)	34.881(4)
c, Å	20.1925(15)	27.5023(7)	22.793(2)
α, deg	79.487(4)	86.066(2)	90
β, deg	83.909(4)	87.103(2)	105.635(5)
γ, deg	64.304(3)	77.605(2)	90
V, $Å^3$	4551.3(6)	5518.1(2)	11539(2)
Z	2	2	4
Radiation (λ, Å)	Mo-Kα, 0.71073	Cu-Kα, 1.54178	Mo-Kα, 0.71073
ρ (calcd.), g/cm^3	1.468	1.452	1.421
μ, mm^{-1}	4.649	7.747	3.758
Temp, K	100	100	100
θ max, deg	25.409	68.416	25.369
data/parameters	16526/963	19363/1123	21121/1156
R_1	0.0394	0.0640	0.0495
wR_2	0.0644	0.1580	0.0867
GOF	0.957	1.038	1.098

Table 5.6. Crystallographic data collection and refinement information.

Name	$K[Pt_3(\mu^3\text{-}SnPh_3)(\mu\text{-}CO)_3(CNAr^{Dipp2})_3]\cdot 4(C_5H_{12})$	$K(Et_2O)[Pt_3(SiEt_3)(\mu\text{-}CO)_3(CNAr^{Dipp2})_3]$	$K(Et_2O)_2[Pt_3(\mu^3\text{-}AuPPh_3)(\mu\text{-}CO)_3(CNAr^{Dipp2})_3\cdot 2(Et_2O)$
Formula	$C_{134}H_{174}N_3O_3KSnPt_3$	$C_{106}H_{136}N_3O_4KSiPt_3$	$C_{130}H_{166}N_3O_7AuKPPt_3$
Crystal System	Orthorhombic	Monoclinic	Triclinic
Space Group	*P*2(1)2(1)2(1)	*P*2(1)/n	*P*-1
a, Å	12.3866(6)	15.316(3)	15.6337(8)
b, Å	24.4811(11)	24.691(5)	18.8546(10)
c, Å	35.8919(16)	26.343(5)	21.8314(11)
α, deg	90	90	86.645(2)
β, deg	90	97.1089(11)	83.258(3)
γ, deg	90	90	73.304(2)
V, $Å^3$	10883.8(9)	9884.4(3)	6119.2(6)
Z	4	4	2
Radiation (λ, Å)	Mo-Kα, 0.71073	Cu-Kα, 1.54178	Cu-Kα, 1.54178
ρ (calcd.), g/cm^3	1.598	1.457	1.484
μ, mm^{-1}	4.159	8.657	9.309
Temp, K	100	100	100
θ max, deg	25.375	65.270	68.391
data/parameters	19879/1167	16871/1019	22009/1340
R_1	0.0350	0.0606	0.0417
wR_2	0.0886	0.1510	0.1056
GOF	1.009	1.018	1.062

Table 5.7. Crystallographic data collection and refinement information.

Name	$Pt_3(\mu^3\text{-}AuPPh_3)_2(\mu\text{-}CO)_3(CNAr^{Dipp2})_3 \cdot 3(Et_2O)$	$Pd_3(\mu\text{-}CO)_3(CNAr^{Dipp2})_3 \bullet Et_2O$ (**6** • Et_2O)
Formula	$C_{144}H_{171}N_3O_6Au_2P_2Pt_3$	$C_{100}H_{121}N_3O_4Pd$
Crystal System	Trigonal	Triclinic
Space Group	*R*-3c	*P*-1
a, Å	20.3338(3)	15.618(8)
b, Å	20.3338(3)	16.161(8)
c, Å	58.1220(11)	20.549(10)
α, deg	90	80.016(7)
β, deg	90	84.921(7)
γ, deg	120	65.649(6)
V, $Å^3$	20811.7(7)	4653(4)
Z	6	2
Radiation (λ, Å)	Cu-Kα, 1.54178	Mo-Kα, 0.71073
ρ (calcd.), g/cm^3	1.475	1.248
μ, mm^{-1}	10.009	0.623
Temp, K	100	100
θ max, deg	66.598	48.814
data/parameters	4088/218	15041/993
R_1	0.0427	0.0496
wR_2	0.0984	0.0700
GOF	1.060	0.754

5.11. Acknowledgements

Chapter 5 is adapted from Barnett, B.R.; Rheingold, A.L.; Figueroa, J.S. "Monomeric Chini-Type Triplatinum Clusters Featuring Dianionic and Radical Anionic π*-Systems", *Angewandte Chemie, International Edition*, **2016**, *In Press*. DOI: 10.1002/anie.201604903. Copyright 2016 Wiley-VCH, Weinheim. Permission to include published material in this dissertation has been obtained from all coauthors. The dissertation author is the first author of this paper. Dr. Mohand Melaimi is thanked for assistance with cyclic voltammetry measurements. Douglas W. Agnew and Prof. Michael J. Tauber are also acknowledged for assistance with EPR. Dr. Milan Gembicky is thanked for helpful discussions regarding X-ray diffraction collection strategies and data refinement. Computational work utilized resources at the W. M. Keck Laboratory for Integrated Biology II, which is funded by the W. M. Keck Foundation.

5.12. References

(1) Abel, E. W.; Stone, F. G. A. *Q. Rev., Chem. Soc.* **1970**, *24*, 498.

(2) Collman, J. P. *Acc. Chem. Res.* **1975**, *8*, 342.

(3) Ellis, J. E., in *Advances in Organometallic Chemistry*, ed. F.G.A. Stone and R. West, Academic Press, **1990**, *31*, 1.

(4) Ellis, J. E. *Organometallics* **2003**, *22*, 3322.

(5) Behrens, H., in *Advances in Organometallic Chemistry*, ed. F.G.A. Stone and R. West, Academic Press, **1980**, *18*, 1.

(6) Chini, P. *J. Orgaonomet. Chem.* **1980**, *200*, 37.

(7) Calabrese, J. C.; Dahl, L. F.; Chini, P.; Longoni, G.; Martinengo, S. *J. Am. Chem. Soc.* **1974**, *96*, 2614.

(8) Longoni, G.; Chini, P. *J. Am. Chem. Soc.* **1976**, *98*, 7225.

(9) Femoni, C.; Kaswalder, F.; Iapalucci, M. C.; Longoni, G.; Mehlstäubl, M.; Zacchini, S.; Ceriotti, A. *Angew. Chem., Int. Ed.* **2006**, *45*, 2060.

(10) Femoni, C.; Kaswalder, F.; Iapalucci, M. C.; Longoni, G.; Zacchini, S. *Eur. J. Inorg. Chem.* **2007**, 1483.

(11) Femoni, C.; Iapalucci, M. C.; Longoni, G.; Lovato, T.; Stagni, S.; Zacchini, S. *Inorg. Chem.* **2010**, *49*, 5992.

(12) Greco, P.; Cavallini, M.; Stoliar, P.; Quiroga, S. D.; Dutta, S.; Zacchini, S.; Iapalucci, M. C.; Morandi, V.; Milita, S.; Merli, P. G.; Biscarini, F. *J. Am. Chem. Soc.* **2008**, *130*, 1177.

(13) Serban, D. A.; Greco, P.; Melinte, S.; Vlad, A.; Dutu, C. A.; Zacchini, S.; Iapalucci, M. C.; Biscarini, F.; Cavallini, M. *Small* **2009**, *5*, 1117.

(14) Zacchini, S. *Eur. J. Inorg. Chem.* **2011**, 4125.

(15) Femoni, C.; Kaswalder, F.; Iapalucci, M. C.; Longoni, G.; Mehlstäubl, M.; Zacchini, S. *Chem. Commun.* **2005**, 5769.

(16) Albinati, A. *Inorg. Chim Acta,* **1977**, *22*, L31.

(17) Yoshida, T.; Otsuka, S. *J. Am. Chem. Soc.* **1977**, *99*, 2134.

(18) Burrow, R. A.; Farrar, D. H.; Irwin, J. J. *Inorg. Chim Acta,* **1991***, 181*, 65.

(19) Ortega-Moreno, L.; Peloso, R.; Maya, C.; Suárez, A.; Carmona, E. *Chem. Commun.* **2015**, *51*, 17008.

(20) Poverenov, E.; Gandelman, M.; Shimon, L. J. W.; Rozenberg, H.; Ben-David, Y.; Milstein, D. *Organometallics* **2005**, *24*, 1082.

(21) For ligand substitution studies of $[Pt_3(CO)_6]_n^{2-}$ (n=2-6) with PPh_3 to give mixed carbonyl/phosphine anionic oligomers, see: Ciabatti, I.; Femoni, C.; Iapalucci, M. C.; Longoni, G.; Lovato, T.; Zacchini, S. *Inorg. Chem.* **2013**, *52*, 4384.

(22) Margulieux, G. W.; Weidemann, N.; Lacy, D. C.; Moore, C. E.; Rheingold, A. L.; Figueroa, J. S. *J. Am. Chem. Soc.* **2010**, *132*, 5033.

(23) Stewart, M. A.; Moore, C. E.; Ditri, T. B.; Labios, L. A.; Rheingold, A. L.; Figueroa, J. S. *Chem. Commun.* **2011**, *47*, 406.

(24) Carpenter, A. E.; Margulieux, G. W.; Millard, M. D.; Moore, C. E.; Weidemann, N.; Rheingold, A. L.; Figueroa, J. S. *Angew. Chem., Int. Ed.* **2012**, *51*, 9412.

(25) Mokhtarzadeh, C. C.; Margulieux, G. W.; Carpenter, A. E.; Weidemann, N.; Moore, C. E.; Rheingold, A. L.; Figueroa, J. S. *Inorg. Chem.* **2015**, *54*, 5579.

(26) Kaim, W. *Inorg. Chem.* **2011**, *50*, 9752.

(27) Pierpont, C. *Coord. Chem. Rev.* **2001**, *216–217*, 99.

(28) Eisenberg, R.; Gray, H. B. *Inorg. Chem.* **2011**, *50*, 9741.

(29) Barnett, B. R.; Moore, C. E.; Rheingold, A. L.; Figueroa, J. S. *J. Am. Chem. Soc.* **2014**, *136*, 10262.

(30) Barnett, B. R.; Moore, C. E.; Chandrasekaran, P.; Sproules, S.; Rheingold, A. L.; DeBeer, S.; Figueroa, J. S. *Chem. Sci.* **2015**, *6*, 7169.

(31) Still, B. M.; Kumar, P. G. A.; Aldrich-Wright, J. R.; Price, W. S. *Chem. Soc. Rev.* **2007**, *36*, 665.

(32) Archirel, P. *J. Phys. Chem. C,* **2016**, *120*, 8343.

(33) Arrizabalaga, P.; Castan, P.; Geoffroy, M.; Laurent, J. P. *Inorg. Chem.* **1985**, *24*, 3656.

(34) Matsunami, J.; Urata, H.; Matsumoto, K. *Inorg. Chem.* **1995**, *34*, 202.

(35) Schmauke, T.; Möller, E.; Roduner, E. *Chem. Commun.* **1998**, 2589.

(36) Braterman, P. S.; Song, J.-I.; Vogler, C.; Kaim, W. *Inorg. Chem.* **1992**, *31*, 222.

(37) Hirani, B.; Li, J.; Djurovich, P. I.; Yousufuddin, M.; Oxgaard, J.; Persson, P.; Wilson, S. R.; Bau, R.; Goddard, W. A.; Thompson, M. E. *Inorg. Chem.* **2007**, *46*, 3865.

(38) Percent orbital contributions are reported as the Löwdin reduced orbital populations.

(39) Lauher, J. W. *J. Am. Chem. Soc.* **1978**, *100*, 5305.

(40) Underwood, D. J.; Hoffmann, R.; Tatsumi, K.; Nakamura, A.; Yamamoto, Y. *J. Am. Chem. Soc.* **1985**, *107*, 5968.

(41) Mealli, C. *J. Am. Chem. Soc.* **1985**, *107*, 2245.

(42) While a detailed analysis of the Pt-Pt bonding situation in *triangulo*-Pt_3 clusters is outside the scope of this text, it has been examined with EHMO calculations and discussed at length elsewhere. See Refs. 39–41, also: Gilmour, D. I.; Michael P Mingos, D. *J. Organomet. Chem.* **1986**, *302*, 127.

(43) Cambridge Structural Database (CSD), version 5.37 (November **2015**).

(44) Briant, C. E.; Wardle, R. W. M.; Mingos, D. M. P. *J. Organomet. Chem.* **1984**, *267*, C49.

(45) Ceriotti, A.; Macchi, P.; Sironi, A.; Afefey, El, S.; Daghetta, M.; Fedi, S.; de Biani, F. F.; Pergola, Della, R. *Inorg. Chem.* **2013**, *52*, 1960.

(46) Mingos, D. M. P.; Oster, P.; Sherman, D. J. *J. Organomet. Chem.* **1987**, *320*, 257.

(47) Labios, L. A.; Millard, M. D.; Rheingold, A. L.; Figueroa, J. S. *J. Am. Chem. Soc.* **2009**, *131*, 11318.

(48) Willocq, C.; Tinant, B.; Aubriet, F.; Carré, V.; Devillers, M.; Hermans, S. *Inorg. Chim. Acta*, **2011**, *373*, 233.

(49) Armarego, W. L. F.; Chai, C. L. L. *Purification of Laboratory Chemicals*, 5th Ed.; Elsevier, **2003.**

(50) Pangborn, A. B.; Giardello, M. A.; Grubbs, R. H.; Rosen, R. K.; Timmers, F. J. *Organometallics*, **1996**, *15*, 1518.

(51) Noviandri, I.; Brown, K. N.; Fleming, D. S.; Gulyas, P. T.; Lay, P. A.; Masters, A. F.; Phillips, L. *J. Phys. Chem. B,* **1999***, 103*, 6713.

(52) Stoll, S.; Schweiger, A. *Mag. Res.* **2006**, *178*, 42.

(53) Neese, F. *Wiley Interdiscip. Rev.: Comput. Mol. Sci.* **2012**, *2*, 73.

(54) Becke, A. D. *Phys. Rev. A,* **1988**, *38*, 3098.

(55) Perdew, J. P. *Phys. Rev. B,* **1986**, *33*, 8822.

(56) Perdew, J. P. *Phys. Rev. B,* **1986**, *34*, 7406 (*Erratum*).

(57) Schaefer, A.; Horn, H.; Ahlrichs, R. *J. Chem. Phys.* **1992**, *97*, 2571.

(58) Weigent, F.; Ahlrichs, R. *Phys. Chem. Chem. Phys.* **2005**, *7*, 3297.

(59) Werner, H.-J.; Manby, F. R.; Knowles, P. J. *J. Chem. Phys.* **2003**, *118*, 8149.

(60) van Lenthe, E.; Baerents, E. J.; Snijders, J. G. *J. Chem. Phys.* **1993**, *99*, 4597.

(61) van Lenthe, A.; Snijders, J. G.; Baerents, E. J. *J. Chem. Phys.* **1996**, *105*, 6505.

(62) Pantazis, D. A.; Chen, X. Y.; Landis, C. R.; Neese, F. *J. Chem. Theory Comput.* **2008**, *4*, 908.

(63) *Chemcraft*. Zhurko, G. A.; Zhurko, D. A. **2014**, www.chemcraftprog.com

(64) Sheldrick, G. M. *Acta Crystallogr. A.,* **2008**, *64*, 112.

(65) Dolomanov, O. V.; Bourhis, L. J.; Gildea, R. J.; Howard, J. A. K.; Puschmann, H. *J. Appl. Cryst.* **2009**, *42*, 339.

(66) van der Sluis, P.; Spek, A. L. *Acta Crystallogr.*, **1990**, *A46*, 194.

Chapter 6

Solution Dynamics of Redox-Noninnocent Nitrosoarene Ligands: Mapping the Electronic Criteria for the Formation of Persistent Metal-Coordinated Nitroxide Radicals

6.1. Introduction

Redox non-innocent ligands offer unique opportunities to modulate the electronic structure and reactivity of transition metal complexes.[1] As opposed to traditional "innocent" ligands, which act as formal spectators in redox transformations, non-innocent ligands can directly participate in the redox activity of coordination complexes due to the presence of ligand frontier orbitals and metal valence *d* orbitals of similar energies. Classical bidentate non-innocent ligand frameworks such as 1,2-dioxolenes[2,3] and 1,2-dithiolenes[4-6] have received extensive study, while the more recent development of larger, poly-dentate non-innocent systems has led to the discovery of new paradigms in metal-based reactivity and catalysis.[7-15]

Despite the current prevalence of non-innocent ligand systems containing extended π-systems,[16-19] ligand redox participation can be readily observed in simple diatomics such as O_2[20,21] and NO.[22-25] The electronic structures of coordination complexes containing these ligands, along with the related nitroxyl (HNO),[26] have been extensively investigated, in part due to their relevance and implication in biological systems.[21,25,27-32] Contrastingly, the non-innocent properties of the closely related class of *C*-organonitroso compounds (*i.e.* O=N-R)[33-35] have been relatively understudied. *C*-Organonitroso compounds are known isoelectronic analogues of singlet dioxygen, and

coordination compounds of nitrosoarenes often display structural properties and reactivity reminiscent of those bearing peroxide or superoxide ligands.[36-39] Transition metal compounds bearing nitrosoarenes have also been observed as intermediates in the allylic amination of olefins[40,41] and the metal-mediated deoxygenation of nitroaromatics.[42-44] Most importantly, *C*-organonitroso compounds have been frequently utilized as spin traps for organic- and transition metal-based radicals,[45,46] with EPR spectroscopy suggesting that many such spin adducts are best described as nitroxide radicals.[47,48] However, it is critical to note that despite the prevalence EPR data in spin-trapping experiments, structurally characterized coordination complexes described as containing singly-reduced nitroso radical anions (i.e. $[ONR]^{-\cdot}$; isoelectronic to the superoxide anion) are quite few.[38,49-51] This observation is likely tied to the inherent instabilities of many such transition metal-nitroxide radical species, their ill-defined reactivity and the difficulties associated with assigning formal oxidation states in nitroso-containing complexes.[52]

In our studies of transition metal centers supported by *m*-terphenyl isocyanides,[53-60] we reported that the zero-valent bis-isocyanide $Pd(CNAr^{Dipp2})_2$ (Ar^{Dipp2} = 2,6-(2,6-(*i*-Pr)$_2$C$_6$H$_3$)$_2$C$_6$H$_3$) reacts with two equivalents of nitrosobenzene (PhNO) to form the four-coordinate complex *trans*-$Pd(\kappa^1$-*N*-PhNO$)_2(CNAr^{Dipp2})_2$ (**1a**).[49] X-ray crystallography, X-ray absorption spectroscopy (XAS) and computational studies indicated that, in the solid state, complex **1a** possessed a divalent palladium center and two monoanionic nitroxide radicals.[52] In addition, magnetic susceptibility measurements on crystalline samples of **1a** showed that the nitroxide radicals exhibit weak antiferromagnetic coupling mediated by superexchange across the Pd center resulting in a

ground-state, open shell singlet (*i.e.* singlet diradical) at low temperature and a triplet excited state that is thermally accessible at *ca.* 290 K (singlet-triplet gap = 0.4 kcal/mol). Accordingly, **1a** represented a rare example of a well-characterized nitroxide-radical complex formally related to traditional spin-trapping experiments. In addition, treatment of $Pd(CNAr^{Dipp2})_2$ with *ortho*-nitrosotoluene (*o*-TolNO; *o*-MeC_6H_4NO) sterically precluded the formation of a bis-nitroxide radical complex and led to the selective formation of $Pd(\eta^2$-*N,O*-TolNO$)(CNAr^{Dipp2})_2$.[52] The latter features a side-on-bound and doubly reduced nitrosoarene ligand (metalloxaziridine), which is best thought of as a doubly-deptrotonated *N*-arylhydroxylamine.[61] Importantly, however, *trans*-$Pd(\kappa^1$-*N*-PhNO$)_2(CNAr^{Dipp2})_2$ (**1a**) and $Pd(\eta^2$-*N,O*-TolNO$)(CNAr^{Dipp2})_2$ represented the first set of *C*-organonitroso analogues to metal-bound κ^1-superoxide and η^2-peroxide on the same coordination platform.

While computational and magnetic studies conclusively elucidated the singly-reduced nature of the nitrosobenzene ligands in $Pd(\kappa^1$-*N*-PhNO$)_2(CNAr^{Dipp2})_2$ (**1a**), our preliminary studies of this molecule had reported that it produced well-defined solution NMR spectra characteristic of a diamagnetic molecule.[49] This observation was quickly realized to conflict with the solid-state properties of **1a** and indicated more complex behavior for this bis-nitroxide radical species in solution. Furthermore, this discrepancy highlighted the lack of information available for the solution phase properties and reactivity of coordinated nitroxide ligands in general. Accordingly, here we provide a more complete description of the solution phase properties and dynamics of the bis-nitroxide radical complex $Pd(\kappa^1$-*N*-PhNO$)_2(CNAr^{Dipp2})_2$ (**1a**) and other nitrosoarene

derivatives. Our results demonstrate that, for this system, there is a facile interconversion between κ^1-*N* nitroxide and η^2-*N*,*O* metalloxaziridine forms of coordinated nitrosoarenes. In addition, the relative kinetic stability of κ^1-*N* arylnitroxide radical ligands is sensitive to both the substituent identity and pattern of the aryl group. Most notably, this finding has led to the identification of aryl substituents that promote the formation of kinetically persistent nitroxide radical complexes in solution and has important ramifications for the formation and isolation of metal-coordinated nitroxide radicals generally.

6.2. Solution dynamics of Pd(κ^1-*N*-PhNO)$_2$(CNAr^{Dipp2})$_2$ (1a): Identification of an equilibrium between a bis-nitroxide and an η^2-metalloxaziridine complex

While the solid-state structure of Pd(κ^1-*N*-PhNO)$_2$(CNAr^{Dipp2})$_2$ (**1a**) is established by X-ray crystallography and combustion analysis, as noted above, preliminary observations of its spectroscopic signatures in solution were inconsistent with its established magnetic properties.[52] Dissolution of forest green crystals of Pd(κ^1-*N*-PhNO)$_2$(CNAr^{Dipp2})$_2$ (**1a**) in benzene-d_6 or THF-d_8 produces a deep red solution. Analysis by ^{1}H and ^{13}C{^{1}H} NMR spectroscopy reveals the prominence of diamagnetic species in solution, with only one Ar^{Dipp2} environment apparent. This observation is inconsistent with the presence of Pd(κ^1-*N*-PhNO)$_2$(CNAr^{Dipp2})$_2$ (**1a**) in solution, as its thermally accessible triplet state would be reasonably expected to produce paramagnetically shifted and broadened NMR spectra.[62,63] Evans' method measurements (C_6D_6, 20 ˚C) failed to detect any significant magnetic moment in these solutions, suggesting that very little of the diradical Pd(κ^1-*N*-PhNO)$_2$(CNAr^{Dipp2})$_2$ (**1a**) is present in solution under these

conditions. The FTIR spectra of these solutions show two strong υ(C≡N) absorbances at 2146 and 2115 cm^{-1} (Figure 6.1), as well as the υ(N=O) stretch of free nitrosobenzene (1506 cm^{-1}). The υ(C≡N) bands are of similar energy and relative intensity to those displayed by Pd(η^2-*N,O*-*o*-Me-C_6H_4NO)($CNAr^{Dipp2}$)$_2$,[52] thereby suggesting that the predominant complex in solution is the η^2-*N,O* mono-nitrosobenzene metalloxaziridine complex Pd(η^2-*N,O*-PhNO)($CNAr^{Dipp2}$)$_2$ (**2a**). An independent synthesis of the metalloxaziridine Pd(η^2-*N,O*-PhNO)($CNAr^{Dipp2}$)$_2$ (**2a**, Scheme 6.1 and Figure 6.2) was achieved upon the addition of an equimolar amount of nitrosobenzene to Pd($CNAr^{Dipp2}$)$_2$ followed by crystallization from an *n*-pentane/hexamethyldisiloxane ($(Me_3Si)_2O$) mixture. As expected, pure samples of Pd(η^2-*N,O*-PhNO)($CNAr^{Dipp2}$)$_2$ (**2a**) produce identical NMR and FTIR spectroscopic features as do solutions prepared from solid samples of Pd(κ^1-*N*-PhNO)$_2$($CNAr^{Dipp2}$)$_2$ (**1a**), thus confirming that the latter undergoes nitrosobenzene dissociation to produce **2a** in solution. Accordingly, as suspected, the NMR spectroscopic data reported for **1a**,[49] which was indicative of a diamagnetic compound, corresponds in fact to that of the metalloxaziridine **2a**.

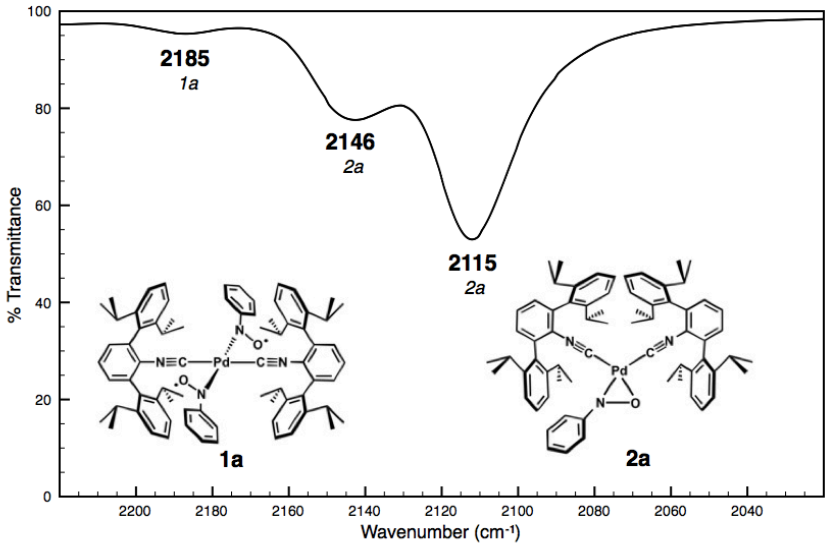

Figure 6.1. Solution FTIR spectrum (C_6D_6, 25 ºC, υ(C≡N) region) of a solution prepared from a crystalline sample of *trans*-Pd(κ^1-*N*-PhNO)$_2$(CNAr^{Dipp2})$_2$ (**1a**).

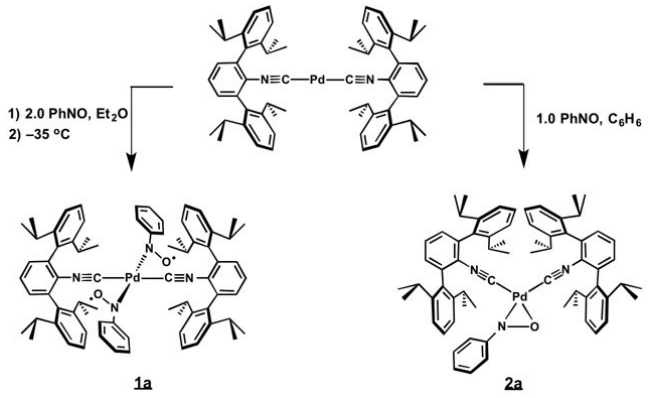

Scheme 6.1. Reactivity of Pd(CNAr^{Dipp2})$_2$ with one and two equivalents of nitrosobenzene.

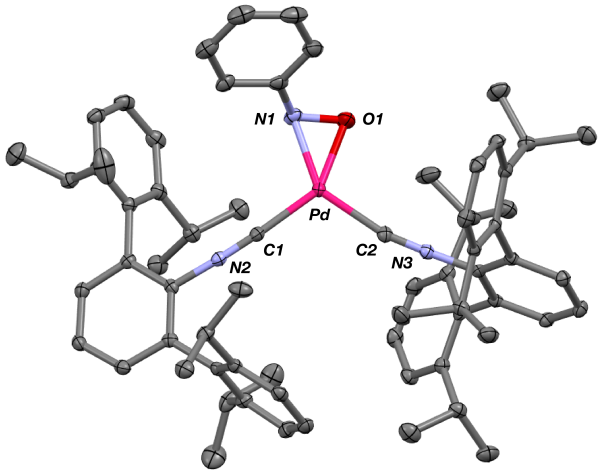

Figure 6.2. Molecular structure of Pd(η^2-*N,O*-PhNO)($CNAr^{Dipp2}$)$_2$ (**2a**). Selected bond distances (Å) and angles (º): N1-O1 = 1.349(3); Pd-N1 = 2.072(2); Pd-O1 = 2.037(2); Pd-C1 = 1.985(2); Pd-C2 = 2.033(2); C1-Pd-N1 = 109.21(8); C2-Pd-O1 = 103.56(8); C1-Pd-C2 = 108.61(9).

In the solid state, complex **2a** features an N-O bond distance of 1.349(3) Å, which is elongated relative to those in Pd(κ^1-*N*-PhNO)$_2$($CNAr^{Dipp2}$)$_2$ (**1a**; d(N-O) = 1.291(2) Å).[49] However, the N-O bond distance in **2a** is comparable to that in Pd(η^2-*N,O*-*o*-TolNO)($CNAr^{Dipp2}$)$_2$ (d(N-O) = 1.364(4) Å),[52] lending credence to a description of **2a** as bearing a doubly-reduced nitrosobenzene ligand supported by a divalent Pd center. Notably, the values of d(N-O) for Pd(η^2-*N,O*-PhNO)($CNAr^{Dipp2}$)$_2$ (**2a)** and Pd(η^2-*N,O*-*o*-TolNO)($CNAr^{Dipp2}$)$_2$ are the shortest reported among structurally characterized mononuclear metalloxaziridines,[64-68] and are somewhat shorter than expected for a N-O single bond.[33] However, we have shown that this discrepancy can be ascribed to a high degree of covalency in the η^2-*N,O* interaction between Pd center and the nitroso unit as computed for Pd(η^2-*N,O*-*o*-TolNO)($CNAr^{Dipp2}$)$_2$.[52] Corroborating this notion for **2a** is the presence of isocyanide υ(C≡N) stretching frequencies (2146, 2115 cm^{-1}) that, while

higher in energy than those seen for $Pd(CNAr^{Dipp2})_2$, are considerably red-shifted relative to those of the isovalent η^2-peroxo complex $Pd(\eta^2\text{-}O_2)(CNAr^{Dipp2})_2$ (2175, 2149 cm^{-1}).[49]

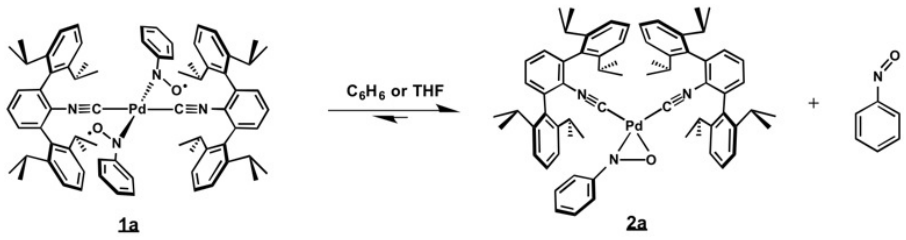

Scheme 6.2. Equilibrium between bis-nitroxide diradical **1a** and metalloxaziridine **2a**.

The formation of metalloxaziridine **2a** and free PhNO upon dissolution of crystalline bis-nitroxide **1a** suggested the presence of an equilibrium between these species, with **2a** being overwhelmingly favored at higher temperatures (Scheme 6.2). Notably, attempts to observe $Pd(\kappa^1\text{-}N\text{-}PhNO)_2(CNAr^{Dipp2})_2$ (**1a**) at lower temperatures in this mixture by variable-temperature ^1H NMR spectroscopy proved unsuccessful, as the combined effects of the compound's paramagnetism, low abundance in solution and the presence of free PhNO precluded an unambiguous assignment of its resonances. However, room-temperature FTIR spectra of C_6D_6 solutions originating from crystalline **1a** revealed a very weak absorbance at 2185 cm^{-1}. This band closely matches the $\upsilon(C{\equiv}N)$ band observed in the solid state FTIR spectra obtained from crystalline **1a** (2188 cm^{-1}, KBr pellet), thereby indicating that detectable quantities of $Pd(\kappa^1\text{-}N\text{-}PhNO)_2(CNAr^{Dipp2})_2$ (**1a**) are present in solution at room temperature. In addition, variable-temperature FTIR studies in toluene revealed that this band becomes more pronounced with decreasing temperature (Figure 3), which provides strong support for an equilibrium between **1a**, **2a**

and PhNO in solution. However, it is critical to note that even at –80 ˚C in toluene solution, metalloxaziridine **2a** remains the predominant isocyanide-containing component of the mixture (Figure 6.3). Therefore we contend that the ability to isolate crystalline Pd(κ^1-*N*-PhNO)$_2$(CNAr^{Dipp2})$_2$ (**1a**) in good yields (60-70%) when a 2:1 PhNO/Pd(CNAr^{Dipp2})$_2$ ratio is employed stems from its high crystallinity, which results in selective precipitation from ethereal solutions. Importantly, the ability of *trans*-spanning *m*-terphenyl isocyanides to induce the selective crystallization of minor components of an equilibrium mixture has been reported previously for cobalt-carbonyl complexes.[69]

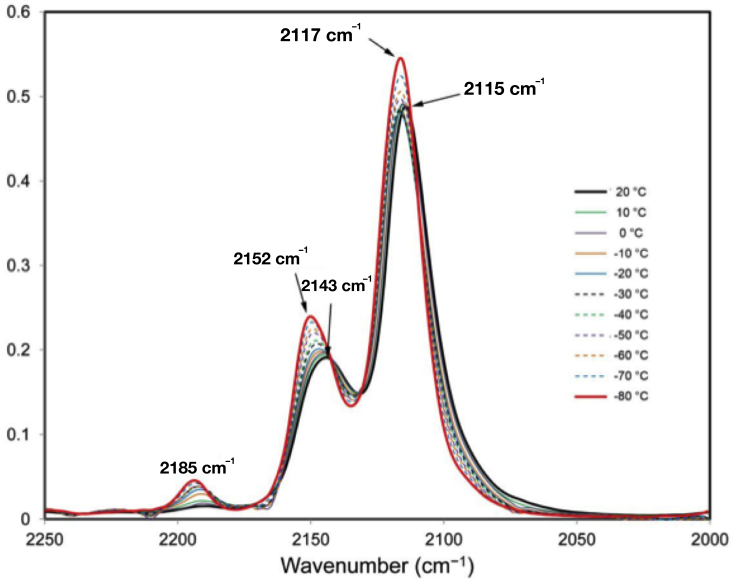

Figure 6.3. Variable temperature FTIR spectra (υ(C≡N) region; CaF_2 windows) of toluene solutions prepared from crystalline samples of Pd(κ^1-*N*-PhNO)$_2$(CNAr^{Dipp2})$_2$ (**1a**). The peaks ranging from 2143-2152 cm^{-1} and 2115-2117 cm^{-1} correspond to Pd(η^2-*N,O*-PhNO)(CNAr^{Dipp2})$_2$ (**2a**), while that seen to grow in at decreasing temperatures and centered at 2185 cm^{-1} is ascribed to Pd(κ^1-*N*-PhNO)$_2$(CNAr^{Dipp2})$_2$ (**1a**).

In an attempt to chemically drive equilibrium between **1a** and **2a** toward the bis-nitroxide complex, 5.0 additional equivalents of nitrosobenzene were added to an equilibrated mixture in benzene solution at room temperature. Analysis by FTIR

spectroscopy immediately after the addition of excess PhNO indicated the equilibrium between **1a** and **2a** was not significantly altered, further signifying that simple binding of PhNO to **2a** is strongly disfavored at room temperature. However, after *ca.* 6 hours, the presence of excess equivalents of PhNO results in the formation of three new products, with the complete consumption of both **1a** and **2a**. Analysis by ^{1}H NMR, FTIR, GC-MS and X-ray crystallography indicated that the organic isocyanate, OCNAr^{Dipp2} (**3**), and azoxybenzene (*i.e.* PhN=N(O)Ph) are produced from this mixture, while the Pd-containing product formed is the cyclic metalloxaziridine trimer [Pd(μ^2:η^2-*N,O*-η^1-*N*-PhNO)(CNAr^{Dipp2})]$_3$ (**4**, Figure 6.4).[70] This process is reminiscent of the production of *tert*-butylisocyanate mediated by the reaction of nitrosobenzene with Ni(*t*-BuNC)$_4$, a transformation in which the isolable mononuclear metalloxaziridine Ni(η^2-*N,O*-PhNO)(*t*-BuNC)$_2$ has been proposed as an intermediate.[71] Likewise, we believe that production of OCNAr^{Dipp2} (**3**), azoxybenzene and trimer **4** may proceed by the mechanism outlined in Scheme 6.3, where an additional equivalent of PhNO inserts into metalloxaziridine functionality of **2a** followed by oxygen-atom transfer and elimination of the weakly coordinating isocyanate and azoxybenzene fragments from the palladium center. Similar insertion reactions of unsaturated substrates into late metal metalloxaziridines have been observed previously, with those involving Pt(η^2-*N,O*-PhNO)(PPh$_3$)$_2$ being the most well-studied.[64,72-74] In addition, the formation of the trinuclear metalloxaziridine complex **4** can be rationalized by trapping of a resultant monoligated [Pd(CNAr^{Dipp2})] species by free PhNO and subsequent trimerization.[75] Most importantly however, the formation of OCNAr^{Dipp2} (**3**), azoxybenzene and trimer **4** highlights that an additional process

significantly competes with the simple formation of bis-nitroxide complex **1a** from free nitrosobenzene and metalloxaziridine **2a**.

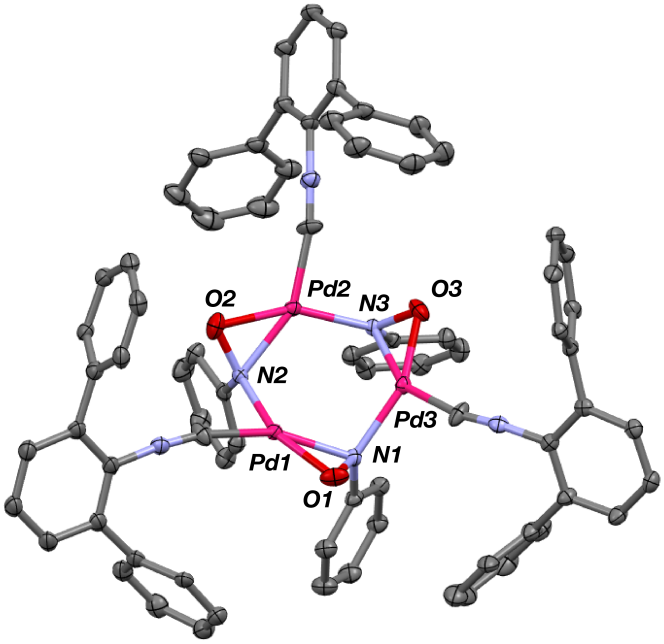

Figure 6.4. Molecular structure of [Pd(μ^2:η^{2-}*N,O*-η^1-*N*-PhNO)(CNAr^{Dipp2})]$_3$ (**4**), showing the major component of the modeled positional disorder. Flanking *i*-Pr groups have been omitted for clarity.

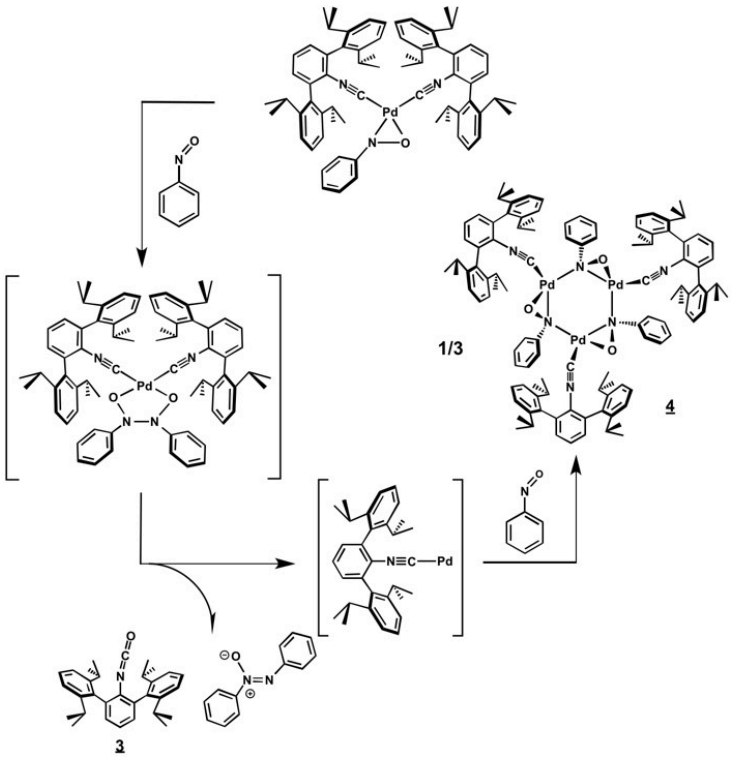

Scheme 6.3. Proposed mechanism leading to the formation of azoxybenzene, $OCNAr^{Dipp2}$ (**3**), and $[Pd(\mu^2{:}\eta^{2\text{-}}N,O\text{-}\eta^1\text{-}N\text{-PhNO})(CNAr^{Dipp2})]_3$ (**4**).

6.3. Formation and solution-phase behavior of Pd bis-nitroxide diradicals featuring mono-substituted aryl groups

To address the dissociation of PhNO from the Pd center in **1a** and access a kinetically persistent bis-nitroxide diradical complex, we sought to modify the electronic profile of the nitrosoarene framework. While the introduction of electron-releasing substituents on the aryl ring may be expected to result in more effective σ-donation of the nitrosoarene ligand to a palladium center, it is important to note that such substituents also decrease the reduction potential of the ArNO unit.[76,77] Correspondingly, electron-withdrawing substituents, which may be expected to promote N=O bond reduction, will also diminish the σ-donor abilities of the ArNO ligand. Therefore, we surveyed a range of electronically-varied nitrosoarenes to determine if a balance between σ-donation and

N=O bond reduction could be found and promote the generation of a solution-phase persistent bis-nitroxide diradical complex.

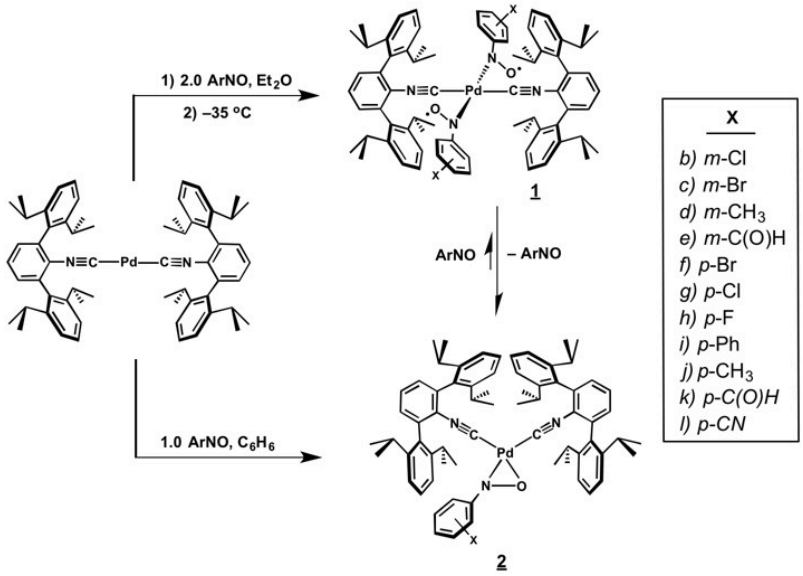

Scheme 6.4. Formation of **1b-l** and **2b-l** from $Pd(CNAr^{Dipp2})_2$ and monosubstituted nitrosoarenes.

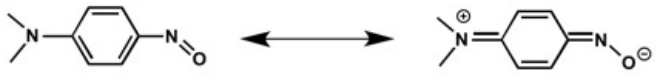

Scheme 6.5. Quinonoid resonance structure of nitrosoarenes bearing *para*-oriented electron releasing groups as exemplified by 4-(dimethylamino)nitrosobenzene.

As shown in Scheme 6.4, the synthesis of palladium bis-nitroxide diradical complexes is indeed general and is not exclusively limited to nitrosobenzene. Accordingly, treatment of 0.5 equivalents of $Pd(CNAr^{Dipp2})_2$ in Et_2O with nitrosoarenes bearing *m/p*-chloro, *m/p*-bromo, *p*-fluoro, *m*/*p*-methyl, *p*-phenyl or *m*-formyl substitution patterns readily provides the bis-nitroxide diradical complexes *trans*-$Pd(\kappa^1$-*N*-$ArNO)_2(CNAr^{Dipp2})_2$ (**1b–j**, Figure 6.5) following crystallization at –35 ˚C. However, it is notable that the strongly-donating nitrosoarenes *p*-$Me_2NC_6H_4NO$ or *p*-$MeOC_6H_4NO$, for

which a dipolar quinonoid form is a major resonance contributor (Scheme 6.5), do not react with $Pd(CNAr^{Dipp2})_2$ over the course of days at room temperature. This lack of reactivity of nitrosoarenes featuring strongly electron-releasing substituents indicates that N=O bond reduction is a critical kinetic component to the formation of bis-nitroxide species, as the quinonoid form of such strongly-donating nitrosoarenes is also expected to inhibit their ability to form η^2-*N,O* metalloxaziridine complexes.[33] Crystallographic characterization of complexes **1b–j** revealed a *trans, anti*-disposition of the nitroxide groups about a square planar Pd center, resulting in approximate C_{2h} site symmetry in a manner identical to the parent bis-nitroxide complex **1a**. The N-O bond lengths in complexes **1b–j** range from 1.256(3)-1.288(3) Å[78] (Table 6.1) and are consistent with a singly-reduced nitroxide radical description.[52] Correspondingly, the Pd-C_{iso} distances are significantly elongated relative to those seen in $Pd(CNAr^{Dipp2})_2$ (1.930(4) Å),[49] indicative of decreased backbonding to the isocyanide ligands as a result of an increase in formal oxidation state of the Pd center. The solid state FTIR spectra (KBr pellet) of **1b-j** corroborate this description and feature high energy υ(C≡N) stretches (2180–2196 cm^{-1}; Table 6.1).

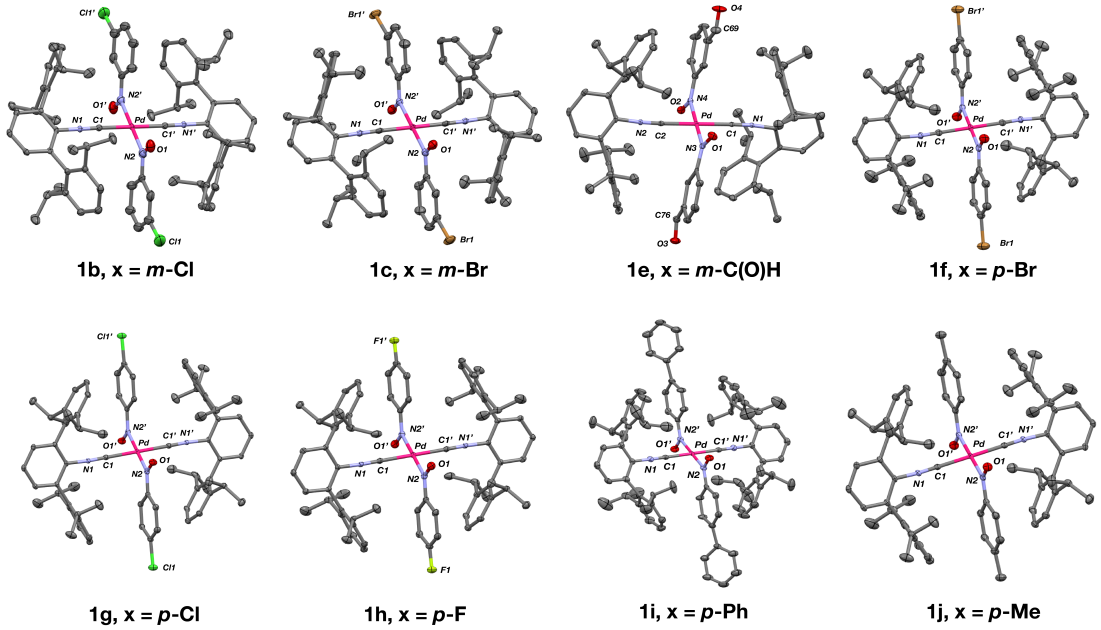

Figure 6.5. Molecular structures of $Pd(\kappa^1\text{-}N\text{-}ArNO)_2(CNAr^{Dipp2})_2$ (**1b-c, e-j**). Co-crystallized solvent molecules have been omitted for clarity.

Table 6.1. Nitrosoarene N-O bond lengths and isocyanide stretching frequencies for complexes **1a-l** in the solid state.

Complex (substituent)	Nitrosoarene d(N-O) (Å)	Isocyanide υ(C≡N) (cm^{-1})[a]
1a (H)[b]	1.291(2)	2185
1b (*m*-Cl)	1.267(6)	2185
1c (*m*-Br)	1.280(5)	2187
1d (*m*-CH_3)	–[c]	2180
1e (*m*-COH)	1.270(4)[d]	2196
1f (*p*-Br)	1.256(3)	2188
1g (*p*-Cl)	1.279(2)	2188
1h (*p*-F)	1.287(3)	2188
1i (*p*-Ph)	1.288(3)	2186
1j (*p*-CH_3)	1.267(3)	2180
1k (*p*-COH)	1.275(4)	2189
1l (*p*-CN)	1.275(3)	2186

[a] KBr pellet. [b] Data from reference 49. [c] Crystallographic positional disorder prevented a precise determination of the N-O bond length in complex **1d**. [d] Average of two crystallographically independent Pd-bound nitrosoarenes. Error is reported as the standard error of the average.

Whereas bis-nitroxide complexes **1b-j** can be readily isolated and characterized in the solid state, they all display solution phase behavior similar to that of the parent diradical **1a**. Accordingly, dissolution of crystalline samples of **1b-j** in arene or ethereal solvents results in the rapid dissociation of one nitrosoarene ligand to produce the η^2-*N,O* metalloxaziridine complexes **2b-j** and free nitrosoarene as assayed by solution FTIR, ^{1}H NMR and $^{13}C\{^1H\}$ NMR spectroscopies. The metalloxaziridines **2b-j** could be independently generated by treatment of $Pd(CNAr^{Dipp2})_2$ with one equivalent of the corresponding nitrosoarene (Scheme 6.4). As with Pd(η^2-*N,O*-PhNO)$(CNAr^{Dipp2})_2$ (**2a**), the solution FTIR spectra of **2b-j** display two diagnostic υ(C≡N) bands in the 2100-2160 cm^{-1} region (Table 6.2). In addition, crystallographic characterization of complexes **2b-j** (Figure 6.6) revealed N-O bond lengths (1.334(3)-1.354(7) Å; Table 6.2) similar to that found in Pd(η^2-*N,O*-PhNO)$(CNAr^{Dipp2})_2$ (**2a**) and consistent with a η^2-*N,O* metalloxaziridine formulation.[79] Most importantly however, for the arene substitution patterns represented by complexes **1b-j**, there is no apparent inhibition of nitrosoarene dissociation that leads to reasonable solution phase persistence.

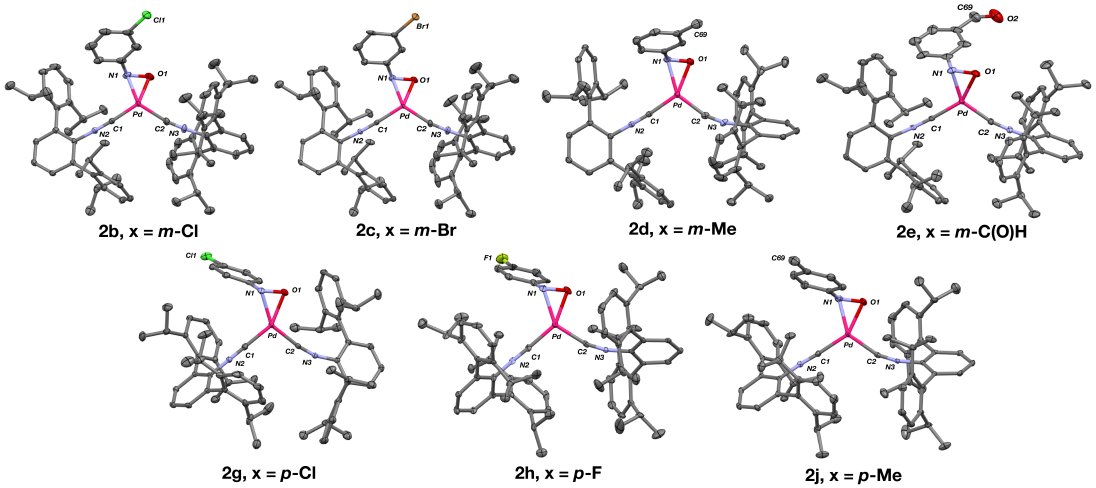

Figure 6.6. Molecular structures of Pd(η^2-*N,O*-ArNO)($CNAr^{Dipp2}$)$_2$ (**2b-e, g-h, j**). Co-crystallized solvent molecules have been omitted for clarity.

Table 6.2. Nitrosoarene N-O bond lengths and isocyanide stretching frequencies for complexes **2a-l** in the solid state.

Complex (substituent)	Nitrosoarene d(N-O) (Å)	Isocyanide υ(C≡N) (cm^{-1})[a]
2a (H)	1.349(3)	2149, 2105
2b (*m*-Cl)	1.334(3)	2153, 2111
2c (*m*-Br)	1.341(4)	2155, 2112
2d (*m*-CH_3)	1.349(2)	2148, 2108
2e (*m*-COH)	1.349(3)	2151, 2121
2g (*p*-Cl)	1.354(3)	2150, 2121
2h (*p*-F)	1.35(1)	2145, 2117
2i (*p*-Ph)	– [b]	2143, 2114
2j (*p*-CH_3)	1.354(7)	2137, 2117

[a] KBr pellet. [b] Complex **2i** was not crystallographically characterized.

In contrast, the specific use of either *para*-formyl (*p*-CHO) or *para*-cyano (*p*-CN) nitrosobenzene leads to bis-nitroxide Pd complexes that show marked persistence in solution. Accordingly, treatment of 0.5 equivalents of Pd($CNAr^{Dipp2}$)$_2$ with (*p*-CHO)C_6H_4NO or (*p*-CN)C_6H_4NO in Et_2O at room temperature generates the bis-nitroxide diradicals Pd(κ^1-*N*-*p*-C(O)H-C_6H_4NO)$_2$($CNAr^{Dipp2}$)$_2$ (**1k**) and Pd(κ^1-*N*-*p*-CN-

$C_6H_4NO)_2(CNAr^{Dipp2})_2$ (**1l**), respectively. Unlike complexes **1a-j**, both **1k** and **1l** readily precipitate from the reaction mixture upon formation and can be isolated as dark purple (**1k**) or green (**1l**) microcrystalline solids, respectively, in good yields (*ca*. 70%). Crystallographic characterization of **1k** and **1l** (Figures 6.7 and 6.8) on single crystals obtained from cooling dilute Et_2O/THF solutions to –35 ˚C reveals square planar Pd centers and N-O bond lengths indicative of nitroxide radical ligands (d(N-O) = 1.267(3) Å (**1k**) and 1.274(3) Å (**1l**); Table 6.1). Most importantly, the solution phase properties of **1k** and **1l** are consistent with a significant retention of their bis-nitroxide radical formulation. For example, solution IR spectra **1k** and **1l** in THF or C_6D_6 revealed intense ν(C≡N) bands centered around 2190 cm^{-1} consistent with the presence of Pd(κ^1-*N*-$ArNO)_2(CNAr^{Dipp2})_2$ bis-nitroxide complexes (Figure 6.9). While ν(C≡N) bands attributable to the corresponding metalloxaziridines **2k** and **2l** are also present in these spectra, the fact that these are not the dominant species stands in stark contrast to the solution phase behavior of the bis-nitroxide complexes **1a-j** (*vida supra*). In addition, the ^{1}H NMR spectra of *para*-formyl **1k** and *para*-cyano **1l** in C_6D_6 feature broad and shifted resonances indicative of the presence of paramagnetic species. These solutions give rise to measureable solution-phase magnetic moments of *ca*. 1.9 μ_B (Evans Method, 20 ˚C),[80] which, when compared to the negligible magnetic moment observed for C_6D_6 solutions originating from complexes **1a-j,** provide further indication for the existence of paramagnetic species in solution.

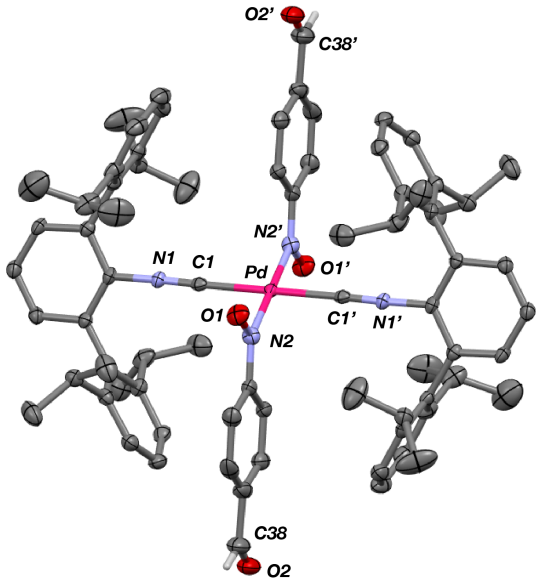

Figure 6.7. Molecular structure of Pd(κ^1-*N*-*p*-C(O)H-$C_6H_4NO)_2$($CNAr^{Dipp2}$)$_2$ (**1k**). Selected bond distances (Å) and angles (º): N2-O1 = 1.275(4); Pd-N2 = 2.023(3); Pd-C1 = 2.007(4); C1-Pd-N2 = 88.8(1); N2-Pd-C1': 91.2(1).

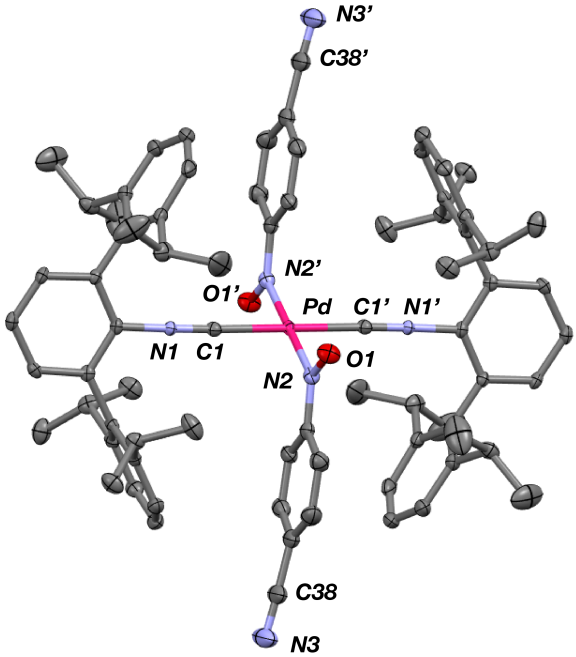

Figure 6.8. Molecular structure of Pd(κ^1-*N*-*p*-CN-$C_6H_4NO)_2$($CNAr^{Dipp2}$)$_2$ • 3 Et_2O (**1l** • 3 Et_2O). Co-crystallized molecules of diethyl ether were accounted for using SQUEEZE. Selected bond distances (Å) and angles (º): N2-O1 = 1.275(3); Pd-N2 = 2.014(3); Pd-C1 = 2.001(3); C1-Pd-N2 = 91.8(1); N2-Pd-C1': 88.2(1).

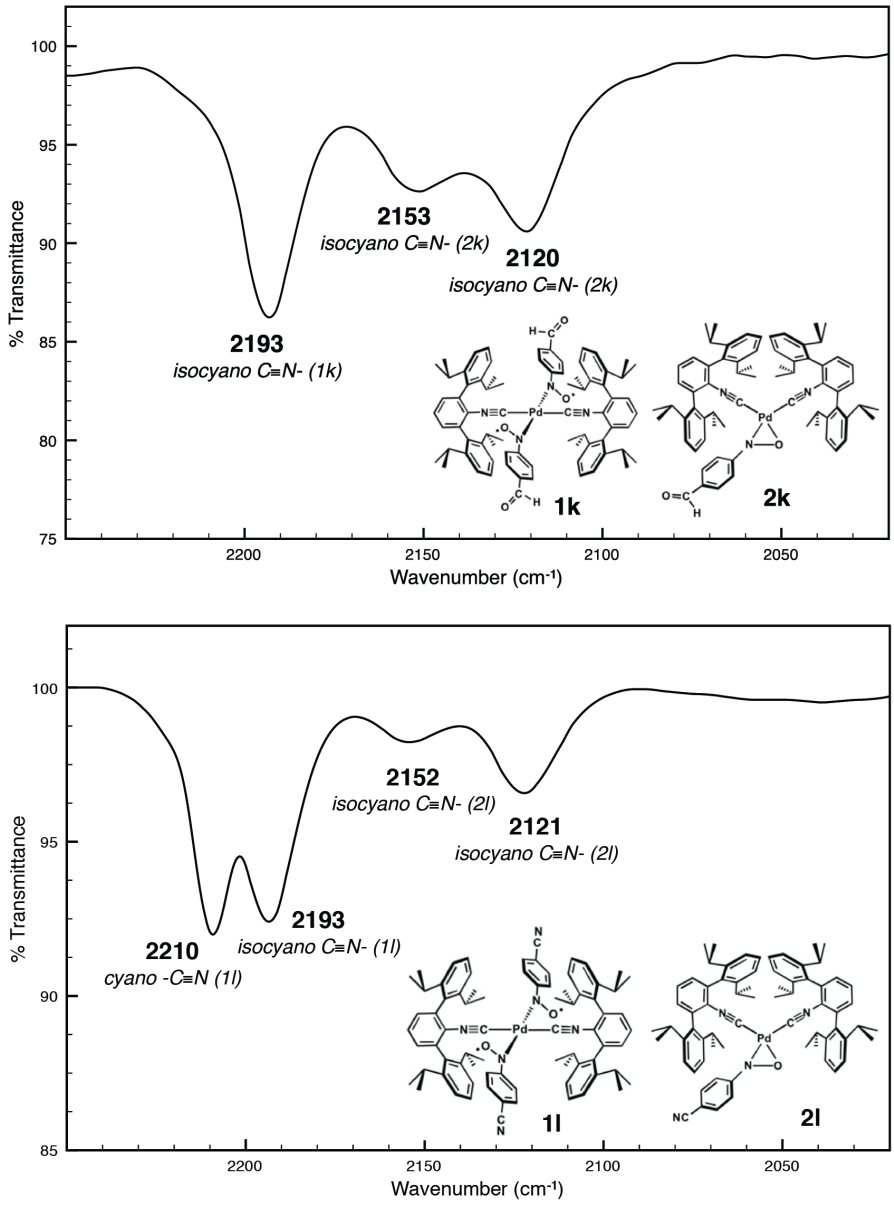

Figure 6.9. FTIR spectra (υ(C≡N) region) of THF solutions freshly prepared from crystalline samples of $Pd(\kappa^1\text{-}N\text{-}p\text{-}C(O)H\text{-}C_6H_4NO)_2(CNAr^{Dipp2})_2$ (**1k**, Top) and $Pd(\kappa^1\text{-}N\text{-}p\text{-}CN\text{-}C_6H_4NO)_2(CNAr^{Dipp2})_2$ (**1l**, bottom). Conditions: 25 ºC, KBr windows.

It is important to note that while spectroscopically observable by both ^{1}H NMR and IR spectroscopy, the metalloxaziridines **2k** and **2l** are not readily isolated in pure form. Indeed, treatment of $Pd(CNAr^{Dipp2})_2$ with 1.0 equiv of either *para*-formyl or *para*-cyano nitrosobenzene leads to the formation of a mixture of metalloxaziridine and bis-

nitroxide complexes, as well as unreacted $Pd(CNAr^{Dipp2})_2$. Furthermore, the metalloxaziridines **2k** and **2l** do not selectively deposit from these mixtures by crystallization. Accordingly, we believe the production of these mixtures suggests that the bis-nitroxide complexes are formed rapidly in solution and that a kinetic barrier to ArNO dissociation arises when either *para*-formyl and *para*-cyano substituents are present on the aryl ring. It is also critical to note that room temperature solutions of **1k** and **1l** are observed to slowly become enriched in the metalloxaziridines **2k** and **2l**, with the presence of $OCNAr^{Dipp2}$ (**3**) and azoxyarenes also becoming evident (Figure 6.10), thus demonstrating the abidance of analogous equilibration and insertion chemistry as that seen for the parent diradical **1a**. This observation further serves to highlight a diminution in the lability of a nitroxide ligand in **1k-l** as a result of the installation of *para*-formyl and cyano substituents.

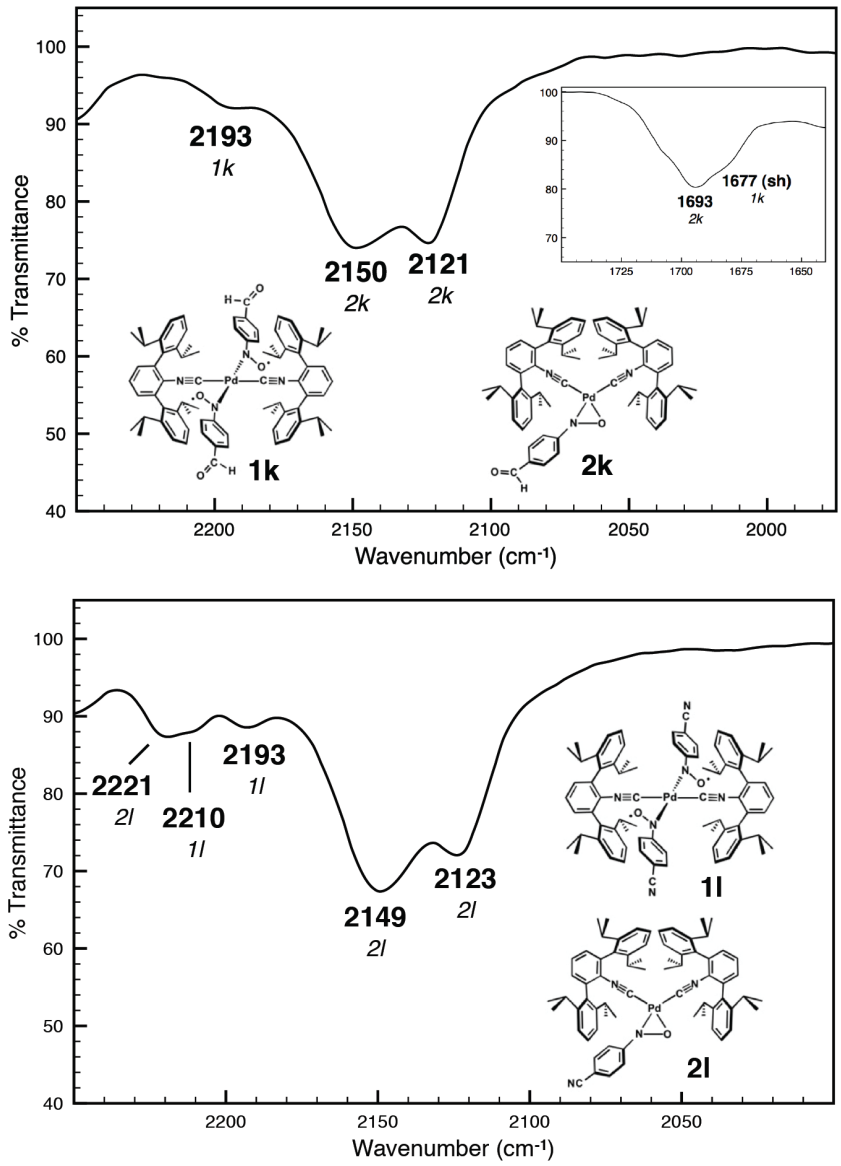

Figure 6.10. FTIR spectra (υ(C≡N) region) of C_6D_6 solutions prepared as 0.013 M Pd(κ^1-*N*-*p*-C(O)H-$C_6H_4NO)_2$(CNAr^{Dipp2})$_2$ (**1k**, Top (includes inset of υ(C=O) region) or Pd(κ^1-*N*-*p*-CN-$C_6H_4NO)_2$(CNAr^{Dipp2})$_2$ (**1l**, bottom) and allowed to stir at 20 ºC for three days. Conditions: 20 ºC, KBr windows. The peaks at 2150 cm^{-1} (top) and 2149 cm^{-1} (bottom) are overlapped by another band that grows in over time and is believed to be attributable to the trinuclear compounds [Pd(μ^2:η^2-*N,O*-η^1-*N*-ArNO)(CNAr^{Dipp2})]$_3$ (Ar = *p*-C(O)H-C_6H_4, *p*-CN-C_6H_4)

.

6.4. Origin of the solution-phase persistence of *para*-cyano and *para*-formyl bis-arylnitroxide radical complexes

It is evident from the results above that the solution-phase kinetic persistence of $Pd(\kappa^1\text{-}N\text{-}ArNO)_2(CNAr^{Dipp2})_2$ bis-nitroxide complexes is sensitive to very specific electronic modulations of the nitrosoarene framework. This suggestion is highlighted by the marked differences in the solution-phase properties between complexes **1a-j** and **1k-l**, but also more directly between complexes **1e** and **1k**, which feature *meta*-formyl and *para*-formyl substituents, respectively. To account for this dichotomy, it is important to note that *para*-oriented electron releasing groups, such as $–NMe_2$ (Hammett $\sigma = –0.88$), are known to increase the Lewis basicity, and therefore σ-donor abilities, of nitrosoarenes.[35] By analogy, the presence of *para*-formyl ($\sigma = 0.42$) and *para*-cyano ($\sigma = 0.66$)[81] substituents are expected to attenuate σ-donor abilities of nitrosoarenes. Such ligands should therefore display a decreased *trans* effect and, given the *trans* disposition of the nitroxide ligands in **1k** and **1l**, might be expected to diminish the prevalence of nitrosoarene dissociation from these species.

However, as a critical point, other bis-nitroxide diradicals in this series bearing substituents with large and positive Hammett σ-values (*e.g.* *m*-Br $\sigma = +0.39$, *m*-Cl $\sigma = +0.37$)[81] do not exhibit the prolonged kinetic persistence exhibited by **1k** and **1l**. This indicates that an additional electronic effect governs the relative solution-phase stability of complexes **1k** and **1l**. In this regard, it is noteworthy that the presence of electronically-unsaturated electron-withdrawing substituents in the *para* position has been found to significantly increase the reduction potentials of uncoordinated

nitrosoarenes.[76,77] Furthermore, inductive-type electron-withdrawing substituents (*e.g.* F, Cl, Br) have been reported to induce relatively smaller changes in the reducton potentials of the corresponding nitrosoarenes, with *para*-oriented halogens resulting in decreased potentials relative to that of nitrosobenzene.[76] This finding suggests that electronically-unsaturated substituents are capable efficiently of delocalizing spin density to positions exo of the aryl ring, thereby increasing the stability of the arylnitroxide radical. Indeed, for transition metal-bound arylnitroxide radicals, such behavior has been recently observed in a series of ruthenium(II) complexes supported by chelating 2-(2-nitrosoaryl)pyridine ligands. In this case, introduction of a nitro (NO_2) group on the nitrosoaryl ring has been found to decrease the spin density on the nitroso –N=O moiety relative to an unsubstituted nitrosoaryl derivative in singly-reduced nitroxide complexes.[51] Furthermore, the effect was most pronounced when the nitro group was oriented *para* to the NO functionality. Spin-density plots[82] derived from broken-symmetry DFT calculations on the model complexes Pd(κ^1-*N*-*p*-C(O)H-$C_6H_4NO)_2(CNPh)_2$ (**1k***) and Pd(κ^1-*N*-*p*-CN-$C_6H_4NO)_2(CNPh)_2$ (**1l***) are consistent with this notion. As shown in Figure 6.11, model complexes **1k*** and **1l*** both show a moderate degree of spin delocalization onto the *para*-formyl and *para*-cyano substitutents, respectively. These spin-density plots can also be compared to that previously reported for the model complex Pd(κ^1-*N*-$PhNO)_2(CNPh)_2$, which does not possess substituted arylnitroxide ligands and accordingly does not show spin delocalization onto positions exo to the phenyl ring.[52]

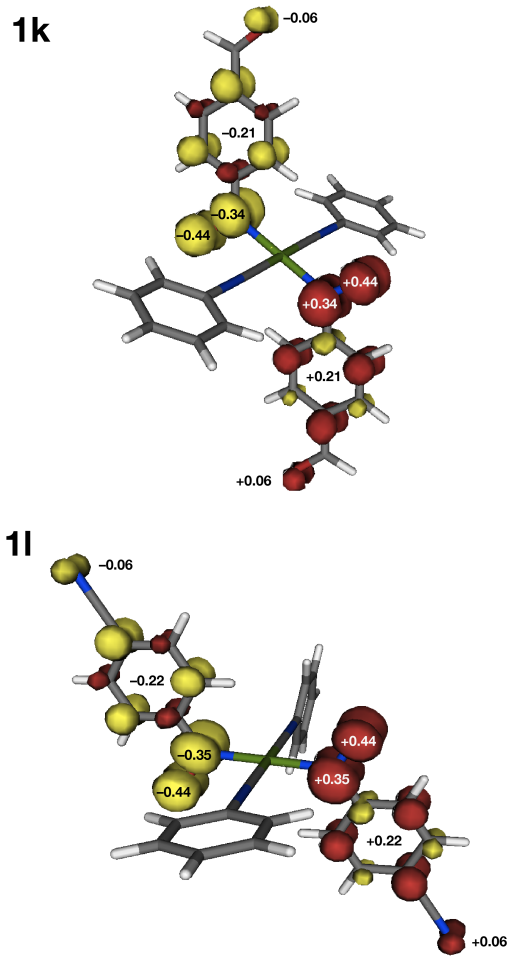

Figure 6.11. Spin density plots overlaid with Mulliken spin populations of the BS(1,1) solutions for the model complexes Pd(k^1-*N*-*p*-C(O)H-$C_6H_4NO)_2(CNPh)_2$ (top) and Pd(k^1-*N*-*p*-CN-$C_6H_4NO)_2(CNPh)_2$ (bottom). B3LYP, ZORA-def2-TZVP, α-spin in red, β-spin in yellow.

Most importantly however, experimental evidence for spin delocalization onto the *para*-formyl and *para*-cyano substituents in complexes **1k** and **1l** is apparent in their solution-phase IR spectra and solid-state magnetic susceptibility. For example, in C_6D_6 at room temperature, the formyl ν(C=O) stretch of **1k** is found at 1677 cm^{-1}, which is 16 cm^{-1} lower than that observed for the metalloxaziridine **2k** (1693 cm^{-1}). As the Pd→(NO π∗) π-backbonding interactions attendant in the η^2-N,O metalloxaziridine complexes are

also expected to marginally affect the degree of electron density on the nitrosoaryl unit,[52] we interpret the fact that the *para*-formyl ν(C=O) stretch in **1k** is of lower energy than that in **2k** as an indication that greater charge/spin delocalization onto the formyl unit is present in the nitroxide radical form of the coordinated nitrosoarene. Similarly, the *para*-cyano υ(C≡N) stretch for bis-nitroxide **1l** (2210 cm^{-1}) is red-shifted relative to that of the metalloxaziridine **2l** (2221 cm^{-1}), again indicating a greater degree of spin delocalization in the nitroxide radical. In addition, solid-state magnetic susceptibility measurements also provide evidence for spin delocalization onto the *para* substituents in bis-nitroxides **1k** and **1l**. Both **1k** and **1l** display magnetic behavior in the solid state similar to the parent bis-nitroxide **1a** and the susceptibility curves can be readily fitted to a singlet diradical model ($\hat{H} = -2J \cdot S_1 \cdot S_2$, where $S_1 = S_2 = 1/2$) possessing a thermally-accessible triplet ($S = 1$) excited state (Figure 6.12). However, the antiferromagnetic coupling constants (J) derived for complexes **1k** ($J = -89.4$ cm^{-1}) and **1l** ($J = -88.9$ cm^{-1}) are non-negligibly more positive than that of **1a** ($J = -115$ cm^{-1}). This finding indicates that *para*-formyl and *para*-cyano substituents contract the energy difference of the $S = 0$ ground and $S = 1$ excited states of complexes **1k** and **1l** relative to **1a**. In effect, these data indicate that *para*-formyl and *para*-cyano groups perturb the electronic structure of these complexes toward a more magnetically-uncoupled, spin-isolated nitroxide radical continuum and is consistent with increased spin delocalization over the aryl fragment. For further comparison, it is notable that solid-state magnetic susceptibility measurements on the *para*-chloro derivative **1g** (Figure 6.13) give rise to an antiferromagnetic coupling constant (J) of -102.5 cm^{-1}. This J value, which is roughly intermediate between that of **1a** and **1k-l**, signifies that inductive-type electron withdrawing groups can increase spin

delocalization over the aryl substituent, but not to the extent of electronically-unsaturated groups such as formyl and cyano.

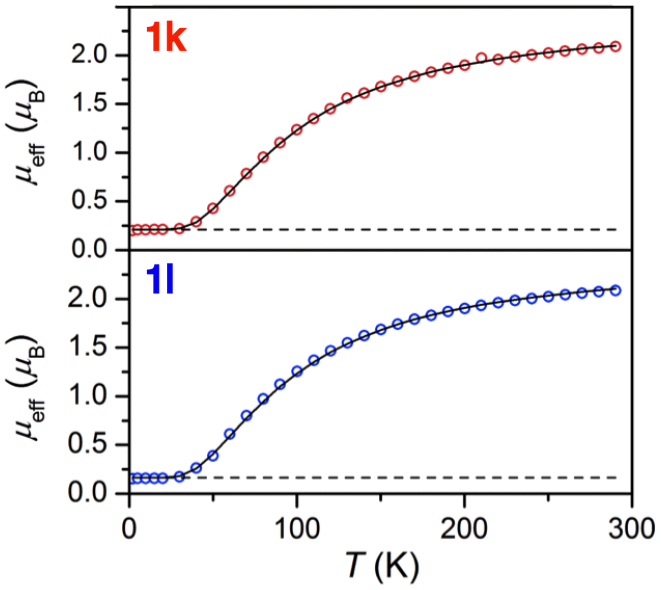

Figure 6.12. Variable temperature SQUID data (circles) and simulation (line) for Pd(κ^1-*N*-*p*-C(O)H-$C_6H_4NO)_2$($CNAr^{Dipp2}$)$_2$ (**1k**) and Pd(κ^1-*N*-*p*-CN-$C_6H_4NO)_2$($CNAr^{Dipp2}$)$_2$ (**1l**). Data for both samples were simulated as an antiferromagnetically coupled singlet diradical. Simulation parameters for **1k**: J = –89.4 cm^{-1}; Paramagnetic impurity = 1.5 %; Mol. weight = 1300 g/mol; χ_{dia} = –675 x 10^{-6} emu. Simulation parameters for **1l:** J = –88.9 cm^{-1}; Paramagnetic impurity = 0.9 %; Mol. weight = 1320 g/mol; χ_{dia} = –800 x 10^{-6} emu.

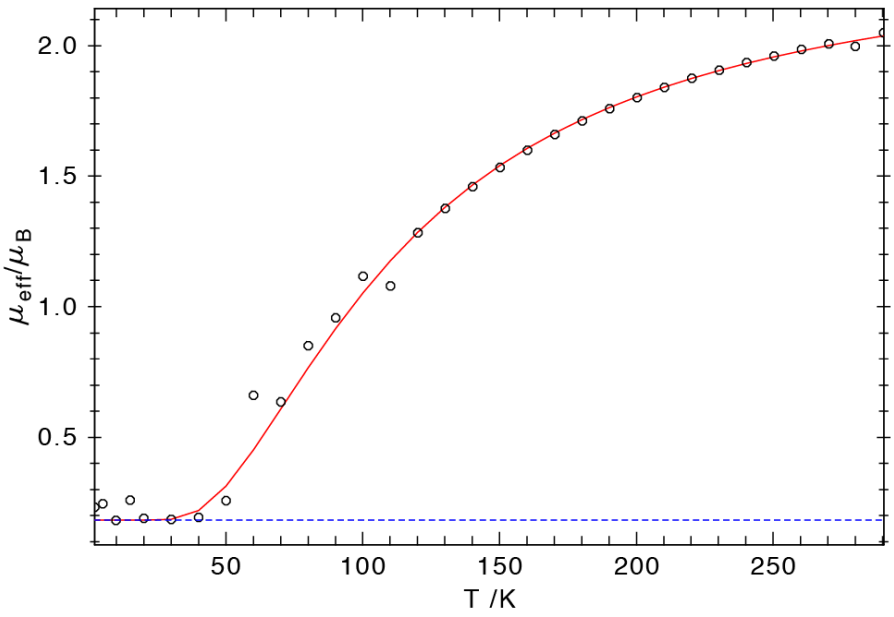

Figure 6.13. SQUID variable temperature magnetic data (circles) and simulation (line) for Pd(κ^1-*N*-*p*-$ClC_6H_4NO)_2(CNAr^{Dipp2})_2$ (**1g**). Data were recorded between 4-300 K. The data was modeled as a singlet diradical ($g_1 = g_2 = 2.000$). Simulation parameters: $J = -102.5$ cm^{-1}; Paramagnetic impurity (S = ½) = 1.1%; Molecular weight = 1237 g/mol; $\chi_{dia} = -640 \times 10^{-6}$ emu.

Based on the experimental observations above, we believe that the increased solution-phase persistence of *para*-formyl and *para*-cyano bis-nitroxide complexes **1k** and **1l** originates from the unequal combination of two phenomena. First, attenuation of the *trans* influence of the nitrosoarene ligand by introduction of electron withdrawing groups likely diminishes the extent of dissociation from a metal center. However, this effect is likely minor and specific to these Pd(κ^1-*N*-ArNO)$_2$(CNAr^{Dipp2})$_2$ complexes, where two nitroxide radical ligands are *trans* oriented. More generally, the ability to increasingly delocalize spin of an aryl nitroxide radical away from the NO unit significantly promotes the kinetic stabilization of such species. Implicit within this suggestion is that an inherent instability of aryl nitroxide radicals exists, which is reasonably supported by the fact that there are limited reports on the isolation of either

free *C*-organonitroxide radical anions (*i.e.* $[RNO]^{\bullet-}$) or monodentate *C*-organonitroxide radical complexes despite decades of study. Accordingly, as shown here for arylnitroxide ligands, incorporation of electronically-unsaturated functional groups *para* to the NO unit serves as an effective strategy for stabilizing monodentate, metal-coordinated nitroxide radicals and allows for more systematic studies of their chemical and physical properties in both solution and the solid-state.

6.5. Concluding remarks

In conclusion, we have demonstrated the inherent kinetic lability of a nitrosobenzene ligand in $Pd(\kappa^1\text{-}N\text{-}PhNO)_2(CNAr^{Dipp2})_2$ (**1a**), and have reconciled this lability with the diradical character of **1a**. We have also shown that judicious nitrosoarene substitution schemes can readily attenuate the lability of the corresponding bis-nitrosoarene diradical complexes. This effect is likely mediated by a combination of inductive effects of these substituents, as well as their ability to effect further delocalization of spin density across the nitrosoarene ring. We envision that the kinetic persistence imparted by the substituents in $Pd(\kappa^1\text{-}N\text{-}p\text{-}C(O)H\text{-}C_6H_4NO)_2(CNAr^{Dipp2})_2$ (**1k**) and $Pd(\kappa^1\text{-}N\text{-}p\text{-}CN\text{-}C_6H_4NO)_2(CNAr^{Dipp2})_2$ (**1l**) may be generalized to other systems upon utilization of similar substitution patterns, including nitrosoarene spin adducts of metalloradicals. Importantly, the chemical principles delineated herein represent additional tools for studies aimed at trapping transition metal or other unstable $S = ½$ radicals in solution.

6.6. Synthetic procedures and characterization data

General considerations. All manipulations were carried out under an atmosphere of purified dinitrogen using standard Schlenk and glovebox techniques. Unless otherwise stated, reagent-grade starting materials were purchased from commercial sources and either used as received or purified by standard procedures.[83] Solvents were dried and deoxygenated according to standard procedures.[84] Benzene-d_6 and toluene-d_8 (Cambridge Isotope Laboratories) were distilled from NaK alloy/benzophenone and stored over activated 4 Å molecular sieves for 2 d prior to use. Celite 405 (Fisher Scientific) was dried under vacuum (24 h) at a temperature above 250 °C and stored in the glovebox prior to use. KBr (FTIR grade from Aldrich) was stirred overnight in anhydrous THF, filtered and dried under vacuum (24 h) at a temperature above 250 °C and stored in the glovebox prior to use. $Pd(CNAr^{Dipp2})_2$ and $CNAr^{Dipp2}$ were prepared as previously reported.[49,55] All methyl-, chloro-, and bromo-substituted nitrosoarenes were prepared via oxidation of the corresponding anilines.[85] The following nitrosoarenes were prepared through nitrosation of the corresponding aryltrifluoroborate salts[86]: *para*-fluoro, *para*-phenyl, *para*-cyano, *para*-formyl, *meta*-formyl. The synthesis of *para*-fluoronitrosobenzene via direct nitrosation has not been reported previously and accordingly is described herein.

Solution ^1H, $^{13}C\{^1H\}$ and ^{19}F NMR spectra were recorded on a Varian Mercury 300 or 400, a Jeol ECA 500, or a Varian X-SENS 500 spectrometer. ^1H and $^{13}C\{^1H\}$ chemical shifts are reported in ppm relative to $SiMe_4$ (^1H and ^{13}C δ = 0.0 ppm) with reference to residual solvent resonances of 7.16 ppm (^1H) and 128.06 ppm (^{13}C) for C_6D_6. ^{19}F NMR spectra were referenced externally to neat trifluoroacetic acid, $F_3CC(O)OH$ (δ =

−78.5 ppm vs. $CFCl_3$ = 0.0 ppm). FTIR spectra were recorded on a Thermo-Nicolet iS10 FTIR spectrometer. Samples were prepared as either KBr pellets or as C_6D_6 solutions injected into a ThermoFisher solution cell equipped with KBr or CaF_2 windows. For solution FTIR spectra, solvent peaks were digitally subtracted from all spectra by comparison with an authentic spectrum obtained immediately prior to that of the sample. The following abbreviations were used for the intensities and characteristics of important IR absorption bands: vs = very strong, s = strong, m = medium, w = weak, vw = very weak; b = broad, vb = very broad, sh = shoulder. Combustion analyses were performed by Robertson Microlit Laboratories of Madison, NJ (USA). High-resolution mass spectrometry (HRMS) was performed using an Agilent 6230 ESI-TOFMS instrument running in positive ion mode. Variable temperature magnetization data were recorded in a 1 T magnetic field on a SQUID magnetometer (MPMS Quantum Design).

Synthesis of Pd(κ^1-*N*-*m*-Cl-$C_6H_4NO)_2$(CNAr^{Dipp2})$_2$ (1b). A mixture of Pd(CNAr^{Dipp2})$_2$ (0.100 g, 0.105 mmol) and *meta*-chloronitrosobenzene (0.030 g, 0.210 mmol, 2.0 equiv) was stirred in 2 mL Et_2O for 15 min. The resulting red solution was filtered and stored at –35 ºC overnight to produce dark green crystals, which were collected and dried *in vacuo*. Yield: 0.084 g, 0.068 mmol, 65%. FTIR (KBr pellet): υ(C≡N) = 2185 (s) cm^{-1}, υ(N=O) = 1318 (m) cm^{-1}, also 3061, 2961, 2926, 2868, 1564, 1455, 1412, 1382, 1363, 1310, 1254, 1057, 980, 953, 909, 858, 825, 804, 799, 754, 714, 666 cm^{-1}. Anal. Calcd. for $C_{74}H_{82}Cl_2N_4O_2Pd$: C, 71.86; H, 6.68; N, 4.53. Found: C, 70.71; H, 6.99; N, 4.47.

Synthesis of Pd(κ^1-*N*-*m*-Br-$C_6H_4NO)_2$(CNAr^{Dipp2})$_2$ (1c). A mixture of Pd(CNAr^{Dipp2})$_2$ (0.100 g, 0.105 mmol) and *meta*-bromonitrosobenzene (0.039 g, 0.210

mmol, 2.0 equiv) was stirred in 2 mL Et_2O for 15 min. The resulting brown solution was filtered and stored at –35 ºC overnight to produce dark green crystals, which were collected and dried *in vacuo*. Yield: 0.072 g, 0.054 mmol, 51%. FTIR (KBr pellet): υ(C≡N) = 2187 (s) cm^{-1}, υ(N=O) = 1316 (m) cm^{-1}, also 3062, 2961, 2926, 2867, 1561, 1455, 1413, 1384, 1362, 1252, 1179, 1114, 1046, 915, 805, 795, 755, 726, 694, 666 cm^{-1}. Anal. Calcd. for $C_{74}H_{82}Br_2N_4O_2Pd$: C, 67.04; H, 6.23; N, 4.23. Found: C, 65.06; H, 6.36; N, 3.87.

Synthesis of Pd(κ^1-*N*-*m*-Me-$C_6H_4NO)_2(CNAr^{Dipp2})_2$ (1d). To a mixture of solid $Pd(CNAr^{Dipp2})_2$ (0.092 g, 0.096 mmol) and *meta*-nitrosotoluene (0.024 g, 0.198 mmol, 2.0 equiv) was added 5 mL Et_2O. After stirring for 15 min, the red solution was concentrated *in vacuo* to a volume of 2 mL, filtered, and stored at –35 ºC for 1 week to yield dark green crystals, which were collected and dried *in vacuo*. Yield: 0.049 g, 0.041 mmol, 43%. FTIR (KBr pellet): υ(C≡N) = 2180 (s) cm^{-1}, υ(N=O) = 1316 (m) cm^{-1}, also 3061, 3020, 2961, 2926, 2866, 1580, 1471, 1461, 1412, 1382, 1362, 1328, 1316, 1305, 1251, 1230, 1179, 1066, 1056, 827, 820, 753, 673 cm^{-1}. Anal. Calcd. for $C_{76}H_{88}N_4O_2Pd$: C, 76.32; H, 7.42; N, 4.68. Found: C, 76.07; H, 7.38; N, 4.51.

Synthesis of Pd(κ^1-*N*-*m*-C(O)H-$C_6H_4NO)_2(CNAr^{Dipp2})_2$ (1e). A mixture of $Pd(CNAr^{Dipp2})_2$ (0.045 g, 0.047 mmol) and *meta*-formylnitrosobenzene (0.013 g, 0.096 mmol, 2.0 equiv) was stirred in 4 mL of a 3:1 Et_2O/THF solution for 30 min. The resulting brown solution was dried *in vacuo* to yield a royal blue residue, which was dissolved in 1 mL of THF. Filtration of this solution and storage at –35 ºC for 5 d produced bright blue crystals, which were collected and dried *in vacuo*. Yield: 0.025 g, 0.020 mmol, 43%. FTIR (KBr pellet): υ(C≡N) = 2196 (s) cm^{-1}, υ(C=O) = 1695 (vs) cm^{-}

[1], υ(N=O) = 1317 (m) cm^{-1}, also 3066, 2960, 2926, 2867, 1579, 1553, 1461, 1438, 1414, 1385, 1364, 1235, 856, 826, 809, 799, 780, 761, 719, 670 cm^{-1}. Anal. Calcd. for $C_{76}H_{84}N_4O_4Pd$: C, 74.58; H, 6.92; N, 4.58. Found: C, 73.96; H, 6.94; N, 4.55.

Synthesis of Pd(κ[1]-*N*-*p*-Br-$C_6H_4NO)_2(CNAr^{Dipp2})_2$ (1f). A mixture of $Pd(CNAr^{Dipp2})_2$ (0.100 g, 0.105 mmol) and *para*-bromonitrosobenzene (0.039 g, 0.210 mmol, 2.0 equiv) was stirred in 2 mL Et_2O for 15 min. The resulting brown solution was filtered and stored at –35 ºC overnight to produce dark green crystals, which were collected and dried *in vacuo*. Yield: 0.080 g, 0.060 mmol, 57%. FTIR (KBr pellet): υ(C≡N) = 2188 (s) cm^{-1}, υ(N=O) = 1318 (m) cm^{-1}, also 3062, 3024, 2923, 2866, 1462, 1403, 1362, 1058, 823, 805, 794, 758, 727 cm^{-1}. Anal. calcd. for $C_{74}H_{82}Br_2N_4O_2Pd$: C, 67.04; H, 6.23; N, 4.23. Found: C, 67.04; H, 6.23; N, 4.23.

Synthesis of Pd(κ[1]-*N*-*p*-Cl-$C_6H_4NO)_2(CNAr^{Dipp2})_2$ (1g). A mixture of $Pd(CNAr^{Dipp2})_2$ (0.100 g, 0.105 mmol) and *para*-chloronitrosobenzene (0.030 g, 0.210 mmol, 2.0 equiv) was stirred in 2 mL Et_2O for 15 min. The resulting red solution was filtered and stored at –35 ºC overnight to produce dark brown crystals, which were collected and dried *in vacuo*. Yield: 0.091 g, 0.074 mmol, 70%. FTIR (KBr pellet): υ(C≡N) = 2188 (s) cm^{-1}, υ(N=O) = 1320 (m) cm^{-1}, also 3062, 3025, 2961, 2927, 2867, 1493, 1464, 1408, 1383, 1363, 1252, 1212, 1174, 1078, 1056, 1046, 825, 806, 794, 756, 727, 694 cm^{-1}. Anal. Calcd. for $C_{74}H_{82}Cl_2N_4O_2Pd$: C, 71.86; H, 6.68; N, 4.53. Found: C, 71.59; H, 6.96; N, 4.34.

Synthesis of Pd(κ[1]-*N*-*p*-F-$C_6H_4NO)_2(CNAr^{Dipp2})_2$ (1h). A mixture of $Pd(CNAr^{Dipp2})_2$ (0.100 g, 0.105 mmol) and *para*-fluoronitrosobenzene (0.026 g, 0.210

mmol, 2.0 equiv) was stirred in 2 mL Et_2O for 15 min. The resulting red solution was filtered and stored at –35 ºC overnight to produce dark green crystals, which were collected and dried *in vacuo*. Yield: 0.064 g, 0.053 mmol, 50%. FTIR (KBr pellet): υ(C≡N) = 2188 (s) cm^{-1}, υ(N=O) = 1315 (m) cm^{-1}, also 3062, 2960, 2926, 2867, 1507, 1486, 1476, 1462, 1412, 1385, 1363, 1214, 1056, 820, 807, 793, 757 cm^{-1}. Anal. Calcd. for $C_{74}H_{82}F_2N_4O_2Pd$: C, 73.83; H, 6.87; N, 4.65. Found: C, 74.31; H, 7.03; N, 4.78.

Synthesis of Pd(κ^1-*N*-*p*-Ph-$C_6H_4NO)_2(CNAr^{Dipp2})_2$ (1i). A mixture of $Pd(CNAr^{Dipp2})_2$ (0.066 g, 0.069 mmol) and *para*-phenylnitrosobenzene (0.026 g, 0.142 mmol, 2.1 equiv) was stirred in 4 mL of a 3:1 Et_2O/THF solution for 20 min. The solution changed in color from orange to dark red. The solution was then filtered and stored at –35 ºC for 2 days to yield black crystals, which were collected and dried *in vacuo*. Yield: 0.052 g, 0.039 mmol, 57%. FTIR (KBr pellet): υ(C≡N) = 2186 cm^{-1}, υ(N=O) = 1317 (m) cm^{-1}, also 3060, 3027, 2960, 2925, 2867, 1596, 1580, 1490, 1470, 1460, 1445, 1411, 1383, 1362, 1317, 1251, 1179, 1115, 1044, 844, 824, 804, 794, 757, 697 cm^{-1}. Anal. Calc'd for $C_{86}H_{92}N_4O_2Pd$: C, 78.25; H, 7.02; N, 4.24. Found: C, 77.21; H, 6.81; N, 4.04

Synthesis of Pd(κ^1-*N*-*p*-Me-$C_6H_4NO)_2(CNAr^{Dipp2})_2$ (1j). A mixture of $Pd(CNAr^{Dipp2})_2$ (0.100 g, 0.105 mmol) and *para*-nitrosotoluene (0.025 g, 0.210 mmol, 2.0 equiv) was stirred in 2 mL Et_2O for 15 min. The resulting red solution was filtered and stored at –35 ºC overnight to produce dark green crystals, which were collected and dried *in vacuo*. Yield: 0.087 g, 0.073 mmol, 70%. FTIR (KBr pellet): υ(C≡N) = 2180 (s) cm^{-1}, υ(N=O) = 1314 (m) cm^{-1}, also 3063, 3022, 2960, 2924, 2870, 1479, 1460, 1411, 1385,

1362, 1328, 1295, 1252, 1178, 1118, 1103, 1056, 824, 800, 756 cm^{-1}. Anal. Calcd. for $C_{76}H_{88}N_4O_2Pd$: C, 76.32; H, 7.42; N, 4.68. Found: C, 76.18; H, 7.37; N, 4.56.

Synthesis of Pd(κ^1-*N*-*p*-C(O)H-$C_6H_4NO)_2(CNAr^{Dipp2})_2$ (1k). A mixture of $Pd(CNAr^{Dipp2})_2$ (0.050 g, 0.052 mmol) and *para*-formylnitrosobenzene (0.014 g, 0.105 mmol, 2.02 equiv) was stirred in 3 mL of a 2:1 Et_2O/THF solution for 20 min. The solution became dark purple, and the product began to precipitate from solution as a purple microcrystalline solid. This solid was isolated via decantation of the mother liquor and dried *in vacuo*. The mother liquor was stored at –35 ºC for 2 days to provide a crop of crystals, which were collected and dried *in vacuo*. Yield: 0.041 g, 0.034 mmol, 65%. FTIR (KBr pellet): υ(C≡N) = 2189 cm^{-1}, υ(C=O) = 1672 cm^{-1}, υ(N=O) = 1323 (m) cm^{-1}, also 3063, 3026, 2961, 2925, 2868, 1573, 1550, 1459, 1426, 1384, 1363, 1332, 1292, 1213, 1176, 1130, 1101, 820, 806, 758 cm^{-1}. Anal. Calcd. for $C_{76}H_{84}N_4O_4Pd$: C, 74.58; H, 6.92; N, 4.58. Found: C, 75.21; H, 7.16; N, 4.44.

Synthesis of Pd(κ^1-*N*-*p*-CN-$C_6H_4NO)_2(CNAr^{Dipp2})_2$ (1l). A mixture of $Pd(CNAr^{Dipp2})_2$ (0.097 g, 0.102 mmol) and *para*-cyanonitrosobenzene (0.027 g, 0.204 mmol, 2.0 equiv) was stirred in 5 mL of a 1:1 Et_2O/THF solution for 30 min. The solution became forest green, and the product began to precipitate from solution as a dark green microcrystalline solid. This solid was isolated via decantation of the mother liquor and dried *in vacuo*. The volume of the mother liquor was reduced to 1 mL under reduced pressure and stored at –35 ºC for 2 days to provide a crop of crystals, which were collected and dried *in vacuo*. Yield: 0.094 g, 0.077 mmol, 75%. FTIR (KBr pellet): cyano υ(C≡N) = 2247 (m) cm^{-1}, isocyano υ(C≡N) = 2186 (s) cm^{-1}, υ(N=O) = 1318 (m) cm^{-1}, also 3059, 3026, 2961, 2925, 2906, 2867, 1597, 1578, 1469, 1460, 1445, 1412, 1384,

1362, 1344, 1327, 1259, 1253, 1180, 1116, 842, 822, 803, 794, 758, 697 cm^{-1}. Anal. Calcd. for $C_{76}H_{82}N_6O_2Pd$: C, 74.95; H, 6.79; N, 6.90. Found: C, 73.89; N, 6.70; N, 6.68.

Synthesis of Pd(η^2-*N,O*-C_6H_5NO)($CNAr^{Dipp2}$)$_2$ (2a). To a solution of Pd($CNAr^{Dipp2}$)$_2$ (0.050 g, 0.052 mmol) in 2 mL C_6H_6 was added a solution of nitrosobenzene (0.006 g, 0.052 mmol, 1.0 equiv) in 2 mL C_6H_6. Upon addition, the reaction mixture turned red in color. After stirring for 1 h, the solvent was removed under reduced pressure. To the resulting residue was added a 3:1 *n*-pentane/hexamethyldisiloxane solution (0.6 mL total). Filtration and slow evaporation of this solution overnight at room temperature produced dark red crystals, which were collected and dried *in vacuo.* Yield: 0.054 g, 0.050 mmol, 48%. ^{1}H NMR (500.1 MHz, C_6D_6, 20 ^{o}C): δ = 7.30 (m, 6H, *p*-Dipp and *o*-PhNO), 7.18 (d, 8H, *J* = 8 Hz, *m*-Dipp), 7.12 (t, 2H, *J* = 8 Hz, *m*-PhNO), 7.05 (t, 1H, *J* = 8 Hz, *p*-PhNO), 6.89 (m, 6H, *m*-Ph and *p*-Ph), 2.61 (septet, 8H, *J* = 7 Hz, C*H*(CH_3)$_2$), 1.22 (d, 24H, *J* = 7 Hz, CH(C*H*$_3$)$_2$), 1.10 (d, 24H, *J* = 7 Hz, CH(C*H*$_3$)$_2$) ppm. ^{13}C{^{1}H} NMR (125.7 MHz, C_6D_6, 20 ^{o}C): δ = 162.6 (ON-C_{ipso}), 159.1 (*C*≡N), 146.4, 139.3, 134.3, 130.1, 129.8, 128.6, 128.5, 128.4, 128.2, 127.9, 123.6, 123.3, 120.6, 31.4 (*C*H(CH_3)$_2$), 24.6 (CH(*C*H$_3$)$_2$) , 24.4 (CH(*C*H$_3$)$_2$) ppm. FTIR (KBr pellet): υ(C≡N) = 2149 (s) and 2105 (vs) cm^{-1}, also 3062, 2962, 2927, 2868, 1458, 1450, 1384, 1363, 1253, 1132, 1046, 914, 807, 793, 759 cm^{-1}. Anal. Calcd. for $C_{68}H_{79}N_3OPd$: C, 76.99; H, 7.51; N, 3.96. Found: C, 75.61; H, 7.55; N, 3.94.

Synthesis of Pd(η^2-*N,O*-*m*-Cl-C_6H_4NO)($CNAr^{Dipp2}$)$_2$ (2b). To a solution of Pd($CNAr^{Dipp2}$)$_2$ (0.050 g, 0.052 mmol) in 2 mL C_6H_6 was added a solution of *meta*-chloronitrosobenzene (0.007 g, 0.052 mmol, 1.0 equiv) in 2 mL C_6H_6. Upon addition, the reaction mixture turned red in color. After stirring for 1 h, the solvent was removed

under reduced pressure. To the resulting residue was added a 3:1 *n*-pentane/hexamethyldisiloxane solution (0.6 mL total). Filtration and slow evaporation of this solution overnight at room temperature produced red crystals, which were collected and dried *in vacuo*. Yield: 0.037 g, 0.034 mmol, 65%. ^{1}H NMR (500.1 MHz, C_6D_6, 20 °C): δ = 7.55 (q, 1H, *J* = 2 Hz, *o*-ArNO), 7.34 (t, 4H, *J* = 7 Hz, *p*-Dipp), 7.20 (d, 8H, *J* = 7 Hz, *m*-Dipp), 7.01 (dt, 2H, *J* = 8, 2 Hz, *m*-ArNO and *p*-ArNO), 6.89 (m, 6H, *m*-Ph and *p*-Ph), 6.80 (td, 1H, *J* = 8, 2 Hz, *o*-ArNO), 2.59 (septet, 8H, *J* = 6 Hz, C*H*$(CH_3)_2$), 1.20 (s br, 24H, CH(C*H*$_3)_2$), 1.09 (dd, 24H, *J* = 7, 2 Hz, CH(C*H*$_3)_2$) ppm. ^{13}C{^{1}H} NMR (125.7 MHz, C_6D_6, 20 °C): δ = 164.0 (ON-C_{ipso}), 158.2 (*C*≡N), 146.4, 139.5, 134.9, 134.2, 130.1, 129.9, 129.5, 128.8, 123.6, 122.8, 119.8, 119.2, 119.1, 31.4 (*C*H$(CH_3)_2$), 24.6 (CH(*C*H$_3)_2$), 24.4 (CH(*C*H$_3)_2$) ppm. FTIR (KBr pellet): υ(C≡N) = 2153 (s) and 2111 (vs) cm^{-1}, also 3059, 2960, 2924, 2865, 1581, 1458, 1416, 1383, 1362, 1253, 1057, 909, 877, 822, 807, 792, 774, 759, 683 cm^{-1}. Anal. calcd. for $C_{68}H_{78}ClN_3OPd$: C, 74.57; H, 7.18; N, 3.84. Found: C, 74.47; H, 7.05; N, 3.74.

Synthesis of Pd(η^2-*N,O*-*m*-Br-C_6H_4NO)(CNAr^{Dipp2})$_2$ (2c). To a solution of Pd(CNAr^{Dipp2})$_2$ (0.050 g, 0.052 mmol) in 2 mL C_6H_6 was added a solution of *meta*-bromonitrosobenzene (0.010 g, 0.052 mmol, 1.0 equiv) in 2 mL C_6H_6. Upon addition, the reaction mixture turned red in color. After stirring for 1 h, the solvent was removed under reduced pressure. To the resulting residue was added a 3:1 *n*-pentane/hexamethyldisiloxane solution (0.6 mL total). Filtration and slow evaporation of this solution overnight at room temperature produced red crystals, which were collected and dried *in vacuo*. Yield: 0.037 g, 0.032 mmol, 71 %. ^{1}H NMR (500.1 MHz, C_6D_6, 20 °C): δ = 7.69 (s, 1H, *o*-ArNO), 7.34 (t br, 4H, *J* = 7 Hz, *p*-Dipp), 7.20 (s br, 8H, *m*-Dipp),

7.15 (s, 1H, *o*-ArNO), 7.02 (d, 1H, *J* = 8 Hz, *p*-ArNO), 6.89 (m, 6H, *m*-Ph and *p*-Ph), 6.72 (t, 1H, *J* = 8 Hz, *m*-ArNO), 2.59 (septet, 8H, *J* = 7 Hz, C*H*(CH_3)$_2$), 1.19 (br, 24H, CH(C*H*$_3$)$_2$), 1.09 (d, 24H, *J* = 7 Hz, CH(C*H*$_3$)$_2$) ppm. $^{13}C\{^1H\}$ NMR (125.7 MHz, C_6D_6, 20 °C): δ = 164.1 (ON-C_{ipso}), 146.4, 139.5, 134.2, 130.1, 129.9, 128.8, 125.7, 123.6, 123.4, 121.9, 120.3, 31.4 (*C*H(CH_3)$_2$), 24.6 (CH(*C*H$_3$)$_2$), 24.4 (CH(*C*H$_3$)$_2$) ppm (extended scanning (12 h) failed to locate the C_{iso} ^{13}C resonance for this complex). FTIR (KBr pellet): υ(C≡N) = 2155 (s) and 2112 (vs) cm^{-1}, also 3060, 2961, 2925, 2866, 1579, 1563, 1455, 1416, 1388, 1363, 1261, 1253, 1090, 1053, 806, 792, 758 cm^{-1}. Anal. calcd. for $C_{68}H_{78}BrN_3OPd$: C, 71.66; H, 6.90; N, 3.69. Found: C, 71.80; H, 6.92; N, 3.70.

Synthesis of Pd(η^2-*N,O*-*m*-Me-C_6H_4NO)($CNAr^{Dipp2}$)$_2$ (2d). To a solution of Pd($CNAr^{Dipp2}$)$_2$ (0.050 g, 0.052 mmol) in 2 mL C_6H_6 was added a solution of *meta*-nitrosotoluene (0.006 g, 0.052 mmol, 1.0 equiv) in 2 mL C_6H_6. Upon addition, the reaction mixture turned red in color. After stirring for 1 h, the solvent was removed under reduced pressure. To the resulting residue was added a 3:1 *n*-pentane/hexamethyldisiloxane solution (0.6 mL total). Filtration and slow evaporation of this solution overnight at room temperature produced red crystals, which were collected and dried *in vacuo*. Yield: 0.035 g, 0.033 mmol, 63 %. ^1H NMR (500.1 MHz, C_6D_6, 20 °C): δ = 7.34 (s, 1H, *o*-ArNO), 7.30 (t, 4H, *J* = 8 Hz, *p*-Dipp), 7.18 (d, 8H, *J* = 8 Hz, *m*-Dipp), 7.09 (d, 1H, *J* = 8 Hz, *o*-ArNO), 7.03 (t, 1H, *J* = 8 Hz, *m*-ArNO), 6.92−6.88 (m, 7H, *p*-ArNO, *m*-Ph and *p*-Ph), 2.61 (septet, 8H, *J* = 7 Hz, C*H*(CH_3)$_2$), 2.33 (s, 3H, ON-Tol-C*H*$_3$), 1.22 (d, 24H, *J* = 7 Hz, CH(C*H*$_3$)$_2$), 1.10 (d, 24H, *J* = 7 Hz, CH(C*H*$_3$)$_2$) ppm. $^{13}C\{^1H\}$ NMR (125.7 MHz, C_6D_6, 20 °C): δ = 162.8 (ON-C_{ipso}), 159.3 (*C*≡N), 146.4,

139.4, 137.5, 134.4, 130.0, 129.8, 128.5, 128.3, 124.5, 123.6, 120.2, 118.9, 100.3, 31.4 (CH(CH$_3$)$_2$), 24.6 (CH(CH$_3$)$_2$), 24.4 (CH(CH$_3$)$_2$), 21.7 (ON-Tol-CH$_3$) ppm. FTIR (KBr pellet): υ(C≡N) = 2148 (s) and 2108 (vs) cm^{-1}, also 3062, 2962, 2928, 2868, 1636, 1460, 1416, 1384, 1363, 1253, 1058, 1047, 806, 794, 758 cm^{-1}. Anal. calcd. for $C_{69}H_{81}N_3OPd$: C, 77.10; H, 7.60; N, 3.91. Found: C, 76.97; H, 7.37; N, 3.69.

Synthesis of Pd(η^2-*N,O*-*m*-C(O)H-C$_6$H$_4$NO)(CNAr^{Dipp2})$_2$ (2e). To a solution of Pd(CNAr^{Dipp2})$_2$ (0.050 g, 0.052 mmol) in 1 mL C_6H_6 was added a solution of *meta*-formylnitrosobenzene (0.006 g, 0.052 mmol, 1.0 equiv) in 2 mL C_6H_6. Upon addition, the reaction mixture turned red in color. After stirring for 1 h, the solvent was removed under reduced pressure. To the resulting residue was added a 9:3:1 *n*-pentane/hexamethyldisiloxane/toluene solution (0.6 mL total). Filtration and slow evaporation of this solution for 1 h at room temperature produced red crystals, which were collected and dried *in vacuo.* Yield: 0.020 g, 0.018 mmol, 35 %. ^{1}H NMR (499.8 MHz, C_6D_6, 20 °C): δ = 10.02 (s, 1H, *H*C(O)Ar), 7.97 (s, 1H, *o*-ArNO), 7.55 (d, 1H, *J* = 8 Hz, *p*-ArNO), 7.34-7.28 (m, 5H, *p*-Dipp and *o*-ArNO), 7.17 (d, 8H, *J* = 8 Hz, *m*-Dipp), 7.02 (d, 1H, *J* = 8 Hz, *m*-ArNO), 6.87 (m, 6H, *m*-Ph and *p*-Ph), 2.59 (septet, 8H, *J* = 7 Hz, C*H*(CH$_3$)$_2$), 1.20 (br, 24H, CH(C*H*$_3$)$_2$), 1.09 (d, 24H, *J* = 7 Hz, CH(C*H*$_3$)$_2$) ppm. ^{13}C{^{1}H} NMR (125.7 MHz, C_6D_6, 20 °C): δ = 192.0 (H*C*(O)ArNO), 163.1 (ON-C_{ipso}), 157.8 (*C*≡N), 146.4, 139.4, 138.0, 134.2, 130.1, 129.9, 129.0, 128.8, 127.8, 127.7, 126.8, 123.6, 120.9, 31.4 (CH(CH$_3$)$_2$), 24.5 (CH(CH$_3$)$_2$), 24.4 (CH(CH$_3$)$_2$) ppm. FTIR (KBr pellet): υ(C≡N) = 2151 (s) and 2121 (vs) cm^{-1}, υ(C=O) = 1696 (vs) cm^{-1}, also 3060, 2961, 2925, 2866, 1594, 1577, 1459, 1414, 1383, 1363, 1328, 1218, 1064, 1056, 824,

805, 793, 757 cm^{-1}. Anal. calcd. for $C_{69}H_{79}N_3O_2Pd$: C, 76.13; H, 7.32; N, 3.86. Found: C, 75.12; H, 7.22; N, 3.69.

Synthesis of Pd(η^2-*N,O-p*-Cl-C_6H_4NO)($CNAr^{Dipp2}$)$_2$ (2g). To a solution of $Pd(CNAr^{Dipp2})_2$ (0.050 g, 0.052 mmol) in 2 mL C_6H_6 was added a solution of *para*-chloronitrosobenzene (0.007 g, 0.052 mmol, 1.0 equiv) in 2 mL C_6H_6. Upon addition, the reaction mixture turned red in color. After stirring for 1 h, the solvent was removed under reduced pressure. To the resulting residue was added a 3:1 *n*-pentane/hexamethyldisiloxane solution (0.6 mL total). Filtration and slow evaporation of this solution overnight at room temperature produced red crystals, which were collected and dried *in vacuo*. Yield: 0.036 g, 0.033 mmol, 63 %. ^{1}H NMR (500.1 MHz, C_6D_6, 20 °C): δ = 7.30 (t, 4H, *J* = 8 Hz, *p*-Dipp), 7.15–7.12 (m, 10H, *m*-Dipp and *o*-ArNO), 7.01 (d, 2H, *J* = 8 Hz, *m*-ArNO), 6.87 (m, 6H, *m*-Ph and *p*-Ph), 2.58 (septet, 8H, *J* = 7 Hz, C*H*$(CH_3)_2$), 1.18 (d, 24H, *J* = 7 Hz, CH(C*H*$_3)_2$), 1.08 (d, 24H, *J* = 7 Hz, CH(C*H*$_3)_2$) ppm. $^{13}C\{^1H\}$ NMR (125.7 MHz, C_6D_6, 20 °C): δ = 161.1 (ON-C_{ipso}), 158.2 (*C*≡N), 146.4, 139.5, 134.3, 130.1, 129.9, 129.3, 128.7, 128.6, 128.5, 128.4, 125.7, 123.6, 121.6, 31.4 (*C*H$(CH_3)_2$), 24.5 (CH(*C*H$_3)_2$), 24.4 (CH(*C*H$_3)_2$) ppm. FTIR (KBr pellet): υ(C≡N) = 2150 (s) and 2121 (vs) cm^{-1}, also 3062, 3024, 2961, 2927, 2867, 1460, 1413, 1383, 1348, 1177, 1066, 1056, 805, 791, 757 cm^{-1}. Anal. calcd. for $C_{68}H_{78}ClN_3OPd$: C, 74.57; H, 7.18; N, 3.84. Found: C, 74.68; H, 7.28; N, 3.74.

Synthesis of Pd(η^2-*N,O-p*-F-C_6H_4NO)($CNAr^{Dipp2}$)$_2$ (2h). To a solution of $Pd(CNAr^{Dipp2})_2$ (0.050 g, 0.052 mmol) in 2 mL C_6H_6 was added a solution of *para*-fluoronitrosobenzene (0.007 g, 0.052 mmol, 1.0 equiv) in 2 mL C_6H_6. Upon addition, the

reaction mixture turned red in color. After stirring for 1 h, the solvent was removed under reduced pressure. To the resulting residue was added a 3:1 *n*-pentane/hexamethyldisiloxane solution (0.6 mL total). Filtration and slow evaporation of this solution overnight at room temperature produced red crystals, which were collected and dried *in vacuo*. Yield: 0.017 g, 0.016 mmol, 31 %. ^{1}H NMR (500.1 MHz, C_6D_6, 20 °C): δ = 7.29 (t, 4H, *J* = 8 Hz, *p*-Dipp), 7.17−7.14 (m, 10H, *m*-Dipp and *o*-ArNO), 6.88 (m, 6H, *m*-Ph and *p*-Ph), 6.81 (t, 2H, *J* = 9 Hz, *m*-ArNO), 2.59 (septet, 8H, *J* = 7 Hz, C*H*(CH$_3$)$_2$), 1.19 (d, 24H, *J* = 7 Hz, CH(C*H*$_3$)$_2$), 1.09 (d, 24H, *J* = 7 Hz, CH(C*H*$_3$)$_2$) ppm. ^{13}C{^{1}H} NMR (125.7 MHz, C_6D_6, 20 °C): δ = 159.7 (d, $^{1}J_{CF}$ = 240 Hz, *C*-F), 159.0 (ON-C_{ipso}), 158.6 (*C*≡N), 146.4, 139.4, 134.3, 130.1, 129.8, 128.7, 123.6, 121.6 (d, J_{CF} = 8 Hz), 115.1 (d, J_{CF} = 22 Hz), 31.4 (*C*H(CH$_3$)$_2$), 24.5 (CH(*C*H$_3$)$_2$), 24.4 (CH(*C*H$_3$)$_2$) ppm. ^{19}F{^{1}H} NMR (282.3 MHz, C_6D_6, 20 °C) δ = −120.7 (m) ppm. FTIR (KBr pellet): υ(C≡N) = 2145 (s) and 2117 (vs) cm^{-1}, also 3062, 2961, 2927, 2867, 1595, 1579, 1486, 1475, 1462, 1412, 1384, 1363, 1227, 1177, 1093, 1056, 820, 804, 792, 756 cm^{-1}. Anal. calcd. for $C_{68}H_{78}FN_3OPd$: C, 75.71; H, 7.29; N, 3.90. Found: C, 73.32; H, 7.48; N, 3.72. Repeated attempts failed to give a more satisfactory combustion analysis.

Synthesis of Pd(η^2-*N,O*-*p*-Ph-C$_6$H$_4$NO)(CNAr^{Dipp2})$_2$ (2i). To a benzene solution of Pd(CNAr^{Dipp2})$_2$ (0.051 g, 0.053 mmol, 1 mL) was added a benzene solution of *para*-phenylnitrosobenzene (0.010 g, 0.055 mmol, 1.0 equiv, 2 mL). The solution was stirred for 10 min, whereupon all volatiles were removed under reduced pressure. The resulting deep red residue was extracted with *n*-pentane and filtered through Celite. This solution was dried *in vacuo*, yielding Pd(η^2-*N,O*-*p*-Ph-C$_6$H$_4$NO)(CNAr^{Dipp2})$_2$ as a red powder.

Yield: 0.052 g, 0.046 mmol, 86%. ^{1}H NMR (499.8 MHz, C_6D_6, 20 °C): δ = 7.70 (d, 2H, *J* = 8 Hz, *o*-*Ph*ArNO), 7.44 (d, 2H, *J* = 8 Hz, Ph*Ar*NO), 7.40 (d, 2H, *J* = 8 Hz, Ph*Ar*NO), 7.33-7.27 (m, 7H, *m*- and *p*-*Ph*ArNO, *p*-Dipp), 7.18 (d, 8H, *J* = 8 Hz, *m*-Dipp), 6.91-6.87 (m, 6H, *m*- and *p*-*Ar*^{Dipp2}), 2.62 (septet, 8H, *J* = 7 Hz, C*H*$(CH_3)_2$), 1.24 (bd, 24H, *J* = 7 Hz, CH(C*H*$_3)_2$, 1.10 1.24 (bd, 24H, *J* = 7 Hz, CH(C*H*$_3)_2$ ppm. ^{13}C{^{1}H} NMR (125.7 MHz, C_6D_6, 20 °C): δ = 162.2 (ON-*C*$_{ipso}$), 158.9 (*C*≡N), 146.4, 139.4, 134.3, 130.0, 129.8, 129.1, 128.5, 127.6, 127.5, 127.1, 126.8, 123.6, 123.0, 121.0, 31.4, 24.6, 24.4 ppm. FTIR (C_6D_6, 20 ºC): υ(C≡N) = 2143 (s) and 2114 (vs) cm^{-1}, also 3052, 2962, 2927, 2868, 1597, 1478, 1461, 1445, 1415, 1386, 1363, 1252, 1179, 1161, 1056, 1040, 792, 758 cm^{-1}. Anal. Calc'd for $C_{74}H_{83}N_3OPd$: C, 78.18; H, 7.36; N, 3.70. Found: C, 77.65; H, 7.32; N, 3.43.

Synthesis of Pd(η^2-*N,O*-*p*-Me-C_6H_4NO)(CNAr^{Dipp2})$_2$ (2j). To a solution of Pd(CNAr^{Dipp2})$_2$ (0.050 g, 0.052 mmol) in 2 mL C_6H_6 was added a solution of *para*-nitrosotoluene (0.006 g, 0.052 mmol, 1.0 equiv) in 2 mL C_6H_6. Upon addition, the reaction mixture turned red in color. After stirring for 1 h, the solvent was removed under reduced pressure. To the resulting residue was added a 3:1 *n*-pentane/hexamethyldisiloxane solution (0.6 mL total). Filtration and slow evaporation of this solution overnight at room temperature produced red crystals, which were collected and dried *in vacuo*. Yield: 0.029 g, 0.027 mmol, 52 %. ^{1}H NMR (500.1 MHz, C_6D_6, 20 °C): δ = 7.30 (t, 4H, *J* = 8 Hz, *p*-Dipp), 7.24 (d, 2H, *J* = 8 Hz, *o*-ArNO), 7.18 (d, 8H, *J* = 8 Hz, *m*-Dipp), 6.92 (d, 2H, *J* = 8 Hz, *m*-ArNO), 6.90 (m, 6H, *m*-Ph and *p*-Ph), 2.61 (septet, 8H, *J* = 7 Hz, C*H*$(CH_3)_2$), 2.16 (s, 3H, ON-Tol-C*H*$_3$), 1.22 (d, 24H, *J* = 7 Hz, CH(C*H*$_3)_2$), 1.09 (d, 24H, *J* = 7 Hz, CH(C*H*$_3)_2$) ppm. ^{13}C{^{1}H} NMR (125.7 MHz, C_6D_6,

20 °C): δ = 160.7 (ON-C_{ipso}), 159.6 (C≡N), 146.4, 139.4, 134.5, 132.1, 130.0, 129.7, 129.1, 128.4, 128.4, 123.5, 120.4, 31.4 (CH(CH_3)$_2$), 24.6 (CH(CH_3)$_2$), 24.4 (CH(CH_3)$_2$), 21.6 (ON-Tol-CH_3) ppm. FTIR (KBr pellet): υ(C≡N) = 2137 (s) and 2117 (vs) cm^{-1}, also 3061, 2961, 2926, 2867, 1579, 1458, 1415, 1384, 1363, 1252, 1056, 804, 792, 756 cm^{-1}. Anal. calcd. for $C_{69}H_{81}N_3OPd$: C, 77.10; H, 7.60; N, 3.91. Found: C, 77.63; H, 7.72; N, 4.03.

Isolation of OCNAr^{Dipp2} from solutions of Pd(η^2-*N,O*-PhNO)(CNAr^{Dipp2})$_2$ (2a) and excess PhNO. To a solution of Pd(CNAr^{Dipp2})$_2$ (0.100 g, 0.105 mmol) in C_6H_6 was added a solution of PhNO (0.056 g, 0.524 mmol, 5.0 equiv) in C_6H_6. The reaction mixture was stirred for 24 h and then concentrated under reduced pressure. The resulting residue was extracted with acetonitrile (3 x 2 mL) and then concentrated under reduced pressure. The product was then purified by passing through a plug of silica, eluting with hexanes. All volatiles were then removed *in vacuo*. Dissolution in CH_2Cl_2 and storage at 4 ºC yielded colorless crystals, which were collected and dried *in vacuo*. Yield: 0.016 g, 0.036 mmol, 34%. ^{1}H NMR (400.1 MHz, C_6D_6, 20 ^{o}C): δ = 7.32 (t, 2H, J = 8 Hz, *p*-Dipp), 7.19 (d, 4H, J = 8 Hz, *m*-Dipp), 7.02-6.93 (m, 3H, *m*-Ph and *p*-Ph), 2.78 (septet, 2H, J = 7 Hz, CH(CH_3)$_2$), 1.23 (d, 12H, J = 7 Hz, CH(CH_3)$_2$), 1.10 (d, 12H, J = 7 Hz, CH(CH_3)$_2$) ppm. ^{13}C{^{1}H} NMR (125.7 MHz, C_6D_6, 20 ^{o}C): δ = 147.2, 137.0, 135.6, 133.6, 129.8, 129.6, 126.8 (O=C=N), 125.5, 123.4, 31.2, 24.5, 24.0 ppm. FTIR (KBr pellet): υ(O=C=N) = 2280 (s) and 2249 (vs) cm^{-1}, also 2962, 2926, 2868, 1579, 1494, 1463, 1383, 1362, 1251, 1178, 1056, 936, 807, 791, 756 cm^{-1}. Anal. Calcd. for $C_{31}H_{37}NO$: C, 84.69; H, 8.48; N, 3.19. Found: C, 85.11; H, 8.29; N, 3.16.

Independent synthesis of OCNAr^{Dipp2} (3). The isocyanate was prepared according to a modified literature procedure.[87] While open to air, a resealable ampoule was charged with CNAr^{Dipp2}, (0.074 g, 0.174 mmol) anhydrous dimethylsulfoxide, (0.038 mL, 0.042 g, 0.538 mmol, 3.1 equiv), Br_2 (0.5 mL, 0.009 mmol, 5 mol%), and anhydrous $CHCl_3$ (5 mL). The ampoule was sealed and stirred while heating to 60 ºC for 24 h. All volatiles were removed *in vacuo*, and the light orange residue was passed through a plug of silica, eluting with a 2.3:1 mixture of hexanes/ethyl acetate. The resulting colorless eluent was dried *in vacuo* to yield analytically pure OCNAr^{Dipp2} as a colorless solid. Yield: 0.064 g, 0.146 mmol, 83%.

Isolation of [Pd(μ^2:η^2-*N,O*-η^1-*N*-PhNO)(CNAr^{Dipp2})]$_3$ (4) from solutions of Pd(η^2-*N,O*-PhNO)(CNAr^{Dipp2})$_2$ (2a) and excess PhNO. To a solution of Pd(CNAr^{Dipp2})$_2$ (0.100 g, 0.105 mmol) in C_6H_6 was added a solution of PhNO (0.056 g, 0.524 mmol, 5.0 equiv) in C_6H_6. The reaction mixture was stirred for 24 h and then concentrated under reduced pressure. The resulting residue was isolated and placed on a fritted funnel, washed with acetonitrile (3 x 10 mL), and dried *in vacuo*. Dissolution of the resulting residue in *n*-pentane (2 mL) followed by filtration and slow evaporation over the course of 24 h at room temperature yielded orange crystals, which were collected and dried *in vacuo*. Yield: 0.015 g, 0.008 mmol, 22 %. ^{1}H NMR (500.1 MHz, C_6D_6, 20 ºC): δ = 7.36-7.32 (m, 12 H, *p*-Dipp, *p*-CN*Ar*^{Dipp2}, and PhNO), 7.19-7.14 (m, 6H, *m*-CN*Ar*^{Dipp2}), 7.00-6.91 (m, 12H, *m*-Dipp), 6.83 (t br, 6H, *J* = 7 Hz, PhNO), 6.75 (s br, 6H, PhNO), 2.69 (septet, 6H, *J* = 7 Hz, C*H*(CH$_3$)$_2$), 2.63 (septet, 6H, *J* = 7 Hz, C*H*(CH$_3$)$_2$), 1.49 (d, 18H, *J* = 7 Hz, CH(C*H*$_3$)$_2$, 1.22 (d, 18H, *J* = 7 Hz, CH(C*H*$_3$)$_2$, 1.18 (d, 18H, *J* = 7 Hz, CH(C*H*$_3$)$_2$, 1.13 (d, 18H, *J* = 7 Hz, CH(C*H*$_3$)$_2$ ppm. ^{13}C{^{1}H} NMR

(125.7 MHz, C_6D_6, 20 ºC): δ = 162.4 (ON-C_{ipso}), 159.1 (C≡N), 146.4, 146.3, 139.6, 134.3, 129.9, 129.7, 128.5, 128.4, 128.3, 128.2, 123.7, 123.5, 122.7, 120.1, 31.5, 31.4, 25.0, 24.7, 24.2, 24.0 ppm. FTIR (KBr pellet): υ(C≡N) = 2135 (vs) cm^{-1}, also 3062, 2960, 2926, 2867, 1580, 1474, 1459, 1450, 1416, 1384, 1363, 1081, 1054, 803, 792, 755 cm^{-1}. Anal. calc'd for $C_{111}H_{126}N_6O_3Pd$: C, 69.75; H, 6.64; N, 4.40. Found: C, 69.82; H, 6.67; N, 4.70.

Synthesis of *para*-fluoronitrosobenzene. To a stirred solution of potassium (4-fluorophenyl)trifluoroborate (0.202 g, 1.00 mmol) in MeCN (3 mL) open to the air was added solid $NOBF_4$ (0.120 g, 1.03 mmol, 1.03 equiv). The reaction mixture immediately turned green, then quickly became dark gray and warm to the touch. The reaction mixture was stirred for 1 min, whereupon addition of H_2O (20 mL) restored the dark green color. The resulting residue was then extracted with CH_2Cl_2 (3 x 10 mL). The combined organic layers were dried over anhydrous $MgSO_4$ and filtered. All solvents were removed via distillation under a static vacuum (0.2 Torr) at 20 ºC, leaving behind *para*-fluoronitrosobenzene as a pale yellow powder. Yield: 0.039 g, 0.312 mmol, 31 %. *Note: This compound is a volatile solid that will be carried over with the distillate if lower pressures or increased temperatures are employed during the distillation, resulting in significantly reduced yields*. ^{1}H NMR (500.1 MHz, C_6D_6, 20 ^{o}C): δ = 7.43 (m, 2H), 6.54 (m, 2H) ppm. $^{13}C\{^1H\}$ NMR (125.7 MHz, C_6D_6, 20 ^{o}C): δ = 166.4 (d, $^1J_{CF}$ = 259 Hz, C-F), 163.5 (s), 123.4 (d, J_{CF} = 9 Hz), 115.9 (m) ppm. ^{19}F NMR (282.3 MHz, C_6D_6, 20 ^{o}C): δ = –101.9 (m) ppm. HRMS (ESI, NCMe): *m/z* calcd. for C_6H_4NOF: 125.0271; Found 125.0273 $[M]^+$.

6.7. Details of DFT computational studies

Computational Details. Density Functional Theory calculations on the model compounds Pd(κ^1-*N*-*p*-COH-$C_6H_4NO)_2(CNPh)_2$ (**1k***) and Pd(κ^1-*N*-*p*-CN-$C_6H_4NO)_2(CNPh)_2$ (**1l***), which are truncated versions of the structurally characterized complexes Pd(κ^1-*N*-*p*-COH-$C_6H_4NO)_2(CNAr^{Dipp2})_2$ (**1k**) and Pd(κ^1-*N*-*p*-CN-$C_6H_4NO)_2(CNAr^{Dipp2})_2$ (**1l**), were carried out using the ORCA program package.[88] Geometry optimizations and single-point calculations were performed using the B3LYP hybrid functional.[89-91] The all-electron Ahlrichs triple-zeta basis sets def2-TZVP (standard)[92-94] and def2-TZVP/J (auxiliary)[95-97] were used in all calculations. Relativistic effects were included by use of the zeroth-order regular approximation (ZORA).[98-100] Crystallographic atomic coordinates were used as input for geometry optimizations. For both model complexes surveyed, a broken symmetry[101,102] BS(1,1) singlet diradical solution was located and found to be lower in energy than the corresponding triplet state solution.

Hardware Specifics. DFT calculations were performed on a home-built 72-CPU (1 x 8 master, 8 x 8 slave) Rocks 4.3 Linux cluster featuring Intel Xeon E5335 Quad-Core 2.00 GHz processors. Job control was implemented with the Sun Grid Engine v. 5.3.

Input for geometry optimization of Pd(κ^1-*N*-*p*-COH-$C_6H_4NO)_2(CNPh)_2$

```
%pal nprocs 16 end

! UKS B3LYP/G ZORA def2-TZVP def2-TZVP/J Opt SlowConv XYZFile
%SCF
 MaxIter 300
 BrokenSym 1,1
end
```

```
* xyz 0 3
Pd       0.00000000       0.00000000       0.00000000
N        3.13966968       0.03347102       0.01473776
N       -3.13966889      -0.03347181      -0.01473690
H       -0.01854232       2.46301366      -4.38013660
O        0.20438427      -4.60788422       5.85570870
C        4.54336419       0.10795589       0.09013786
C        5.20022843      -0.59555617       1.10441219
O        0.00413280       2.57121089       1.14418238
C       -1.99910332      -0.00000039       0.00000043
C       -0.01472485       2.79362293      -1.15673546
C       -0.08526951       4.29685942      -3.50391094
C       -0.07633259       4.94441429      -2.24092825
H       -0.08473929       5.87368730      -2.19639561
O       -0.00413279      -2.57121088      -1.14418239
C        1.99910411      -0.00000039       0.00000043
C        5.21823518       0.89956824      -0.84934168
C        6.60437198       0.99175873      -0.72800336
H        7.08578215       1.51549629      -1.32854952
C        7.27517939       0.31150825       0.27919862
H        8.19827047       0.38570721       0.35018173
C        6.58227540      -0.47666979       1.17564260
H        7.04681864      -0.93515628       1.83755547
C       -5.21823438      -0.89956902       0.84934254
C       -0.05716020       4.20738904      -1.08851620
C       -6.60437128      -0.99175853       0.72800404
N        0.00465306       2.02840995       0.00000025
H       -7.08578145      -1.51549610       1.32855020
C       -7.27517860      -0.31150903      -0.27919776
H       -8.19826977      -0.38570702      -0.35018105
C       -6.58227469       0.47666999      -1.17564192
H       -7.04681784       0.93515550      -1.83755462
H       -0.07006463       4.63488856      -0.26276764
C       -0.16334897       5.09977549      -4.72851059
C       -0.03014371       2.89560558      -3.55709789
N       -0.00465235      -2.02840976       0.00000043
C        0.01472555      -2.79362274       1.15673614
C       -0.00750727      -2.16226995       2.39761700
H       -0.04743178      -1.23486931       2.44112713
C        0.03014441      -2.89560539       3.55709857
H        0.01854311      -2.46301445       4.38013746
C       -5.20022842       0.59555617      -1.10441220
C        0.08527032      -4.29686021       3.50391180
C        0.07633330      -4.94441410       2.24092893
H        0.08473929      -5.87368730       2.19639560
C        0.05716090      -4.20738884       1.08851688
H        0.07006534      -4.63488837       0.26276832
C        0.16334976      -5.09977628       4.72851144
H        0.18173906      -6.02703744       4.65089819
C        0.00750798       2.16227014      -2.39761632
H       -0.18173835       6.02703763      -4.65089751
O       -0.20438357       4.60788441      -5.85570802
H        0.04743256       1.23486852      -2.44112627
C       -4.54336340      -0.10795668      -0.09013701
H        4.65868171      -1.20970094       1.80865175
```

```
H      -4.69070806      -1.41831169       1.63612206
H      -4.65868303       1.20970114      -1.80865262
H       4.69070869       1.41831040      -1.63612143
*
```

Optimized Cartesian coordinates for Pd(κ^1-*N*-*p*-COH-$C_6H_4NO)_2(CNPh)_2$

```
Pd  -0.00121226986427     -0.00141701325287      0.00177429145951
N    3.14924165943389      0.18043539923216      0.02285157779000
N   -3.15120404353966     -0.18356335556189     -0.02471504771706
H    0.40548636307557      2.21323626292579     -4.71459133716757
O   -0.41760425673691     -4.39112270948377      6.16822946947894
C    4.53255872428073      0.23434856421863      0.02522796031783
C    5.25921761907545     -0.95274952907645     -0.05327160272922
O   -0.37336362488633      2.67354093904464      0.88676102741152
C   -1.99537663272035     -0.12878278329352     -0.01303611061127
C   -0.06445221535144      2.75081584151234     -1.38569781467574
C    0.14248491044376      4.13948649699596     -3.81026108252986
C   -0.06752002774440      4.82689574157195     -2.60682097245045
H   -0.14938578648664      5.90882373318210     -2.62486470624418
O    0.36493728374179     -2.67637461315300     -0.88392242959852
C    1.99338774289106      0.12537070899695      0.01330095397711
C    5.16701561224315      1.47290829854062      0.10460873513314
C    6.55286651449005      1.51526030659664      0.10532944557948
H    7.05674446830406      2.47074910110915      0.16631973753270
C    7.29129886824372      0.33887006147217      0.02758989727842
H    8.37288390170705      0.38013621773352      0.02817133086534
C    6.64433398631461     -0.89011267261404     -0.05152018643445
H    7.21884485296359     -1.80480016002946     -0.11277205845895
C   -5.17180341336966     -1.47099446039081     -0.11030177166469
C   -0.17123037135613      4.15623184945708     -1.40669465480981
C   -6.55780364162207     -1.51017355184128     -0.11277767932974
N   -0.16408101854325      2.05054535796854     -0.19480134769625
H   -7.06375528967273     -2.46446175817759     -0.17540169342256
C   -7.29357551496117     -0.33218711974102     -0.03476685904712
H   -8.37525501738028     -0.37099473989465     -0.03675635288489
C   -6.64388444201243      0.89526977179746      0.04640626549461
H   -7.21638613463210      1.81119845609092      0.10785768613667
H   -0.33266037362581      4.67594524786933     -0.47406252740229
C    0.24805808821023      4.88170723712459     -5.06860828950611
C    0.24615915504333      2.73922668582245     -3.78228006526174
N    0.16001098901254     -2.05330489038654      0.19833239030252
C    0.06298570043295     -2.75343070819118      1.38958413780104
C   -0.14247595712514     -2.05606773836083      2.59822501895560
H   -0.21698062230639     -0.97518988777650      2.58125293072243
C   -0.24097175663624     -2.74151978289838      3.78691017272024
H   -0.39746216304457     -2.21542709841383      4.71965177218194
C   -5.25866013003916      0.95473314764797      0.04992498373335
C   -0.13814156204141     -4.14183096984791      3.81463672937471
C    0.06796037203584     -4.82948302698701      2.61068518738899
H    0.14907862404937     -5.91147738648268      2.62853178724223
C    0.16874500325868     -4.15891444241052      1.41022844170689
H    0.32719269621893     -4.67874446766416      0.47715151339226
C   -0.24070883718185     -4.88383696045471      5.07342573773052
H   -0.14025040917803     -5.98512952531093      4.96614529647520
```

```
C    0.14478268726791      2.05371899361566     -2.59389299953940
H    0.14848151076160      5.98307059153922     -4.96118749577881
O    0.43076049709295      4.38952371603624     -6.16271353051855
H    0.21946705946718      0.97284426954587     -2.57684935419475
C   -4.53469178518496     -0.23395657973917      -0.02886203566117
H    4.73737017293240     -1.89756982431335     -0.11635043526371
H   -4.58292512435723     -2.37567581415279      -0.16990302573814
H   -4.73451585959360      1.89817529316708       0.11463328174316
H    4.57599963820184      2.37621883908580       0.16395284641063
```

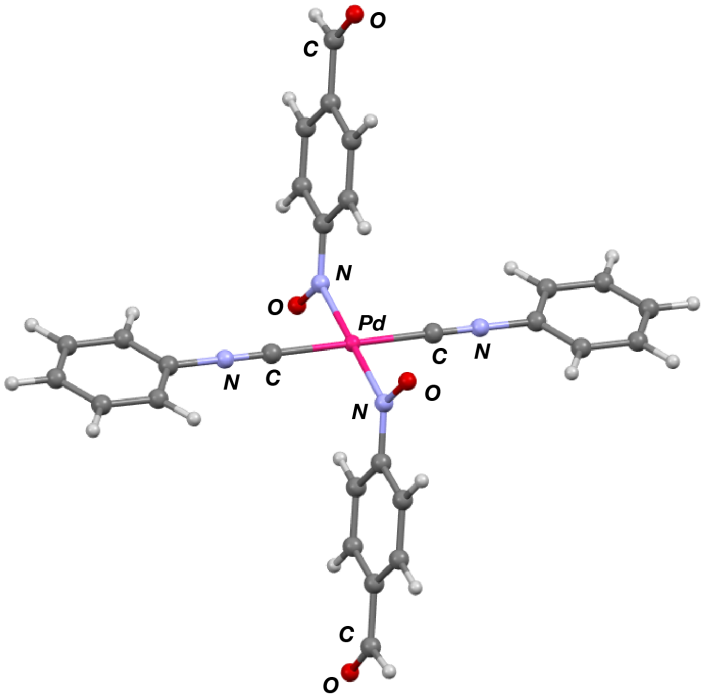

Figure 6.14. Optimized molecular structure of Pd(κ^1-*N*-*p*-COH-$C_6H_4NO)_2(CNPh)_2$.

Input for geometry optimization of Pd(κ^1-*N*-*p*-CN-$C_6H_4NO)_2(CNPh)_2$

```
#UKS OPT of Pd(CNPh)2(pCNArNO)2

%pal nprocs 16 end
! UKS B3LYP/G ZORA def2-TZVP def2-TZVP/J Opt SlowConv XYZFile PrintMOs

%SCF
 MaxIter 300
 BrokenSym 1,1
end

* xyz 0 3
C      -2.03367419       0.00000000       0.00000000
C      -4.61834572      -0.00167493      -0.00699722
C      -5.30453554       0.00175087      -1.26145867
```

C	-6.71961619	-0.00428290	-1.23383179
H	-7.26420115	-0.00602223	-2.19143272
C	-7.42584544	0.00051616	-0.01371349
H	-8.52786715	0.00108580	-0.01634509
C	-6.72546315	0.00444066	1.20976691
H	-7.27450867	0.00673899	2.16474178
C	-5.31053034	-0.00393385	1.24416285
C	2.03370623	0.00015146	0.00016854
C	4.61834651	0.00207899	0.00569980
C	5.30499460	-0.00020214	1.25991159
C	6.72005684	0.00600305	1.23181280
H	7.26498037	0.00807711	2.18921917
C	7.42583102	0.00047570	0.01142328
H	8.52785346	-0.00044468	0.01363077
C	6.72498074	-0.00437565	-1.21178514
H	7.27368744	-0.00772477	-2.16695104
C	5.31002091	0.00351284	-1.24571405
N	-0.05619613	-5.88837364	5.72517505
C	0.01343170	2.24449847	-2.44111941
H	0.01210128	1.14334632	-2.50218915
O	0.00287435	-2.65884032	-1.18283824
C	0.02163366	3.01754724	-3.60681302
N	0.06019937	5.88674043	-5.72669641
H	0.02680495	2.52460449	-4.59120502
C	0.02431985	4.44534082	-3.53387629
Pd	0.00000000	0.00000000	0.00000000
C	0.01707212	5.07096639	-2.24739359
N	-0.00099309	-2.09191497	0.00000000
O	-0.00294796	2.65923343	1.18219738
H	0.01864028	6.17100543	-2.18381317
C	0.00926464	4.30306540	-1.07879157
C	0.00763412	2.87461774	-1.16102099
H	0.00373252	4.76692961	-0.08187469
C	0.03658495	5.23427813	-4.72987269
N	3.22425411	0.00330804	0.00323667
N	0.00113977	2.09193742	-0.00046075
C	-0.01273666	-2.24519425	2.44060125
C	-0.00710733	-2.87494674	1.16031889
H	-0.01170131	-1.14405416	2.50195063
C	-0.02024218	-3.01857311	3.60607589
C	-0.03377096	-5.23563753	4.72850444
H	-0.02526160	-2.52593259	4.59062306
C	-0.02264909	-4.44635047	3.53272720
C	-0.01567975	-5.07160664	2.24606063
H	-0.01671872	-6.17162770	2.18216837
C	-0.00822772	-4.30336726	1.07767657
N	-3.22423044	-0.00325309	-0.00370172
H	-0.00314770	-4.76694639	0.08062398
H	-4.77077746	0.00867799	-2.20031665
H	-4.78127174	-0.01172057	2.18555793
H	4.77156817	-0.00641675	2.19896305
H	4.78039352	0.01033915	-2.18690917

*

Optimized Cartesian coordinates of Pd(κ^1-*N*-*p*-CN-$C_6H_4NO)_2(CNPh)_2$

C	-1.97354945470683	0.03274486081696	-0.00963575882897
C	-4.51619762690419	0.04606712168696	-0.03079939800227
C	-5.18550330053605	-0.01879876032020	-1.25150907825591
C	-6.57205663428156	-0.01576938166422	-1.25483957207122
H	-7.10269514474393	-0.06606392002014	-2.19627012198659
C	-7.27697975822111	0.05043748863918	-0.05750174780270
H	-8.35917908292801	0.05272946993034	-0.06816773760053
C	-6.59525684937480	0.11397539379795	1.15327586096162
H	-7.14370546167280	0.16530204064573	2.08436312341980
C	-5.20881802191158	0.11284307346920	1.17672679156962
C	2.02522982221475	-0.02549108953170	0.01010650916731
C	4.56670882486089	-0.03556071243284	0.04964397144738
C	5.24214870080842	1.15836185991822	0.29890695256658
C	6.62843883144308	1.14949890743363	0.32109070523436
H	7.16405003375651	2.06931060252119	0.51437099606692
C	7.32662325729252	-0.03294080800434	0.09730393556150
H	8.40871643899642	-0.03200855847849	0.11607182298955
C	6.63874980564843	-1.21666650995495	-0.15026558686822
H	7.18252100931359	-2.13557587315115	-0.32414305853272
C	5.25247646864833	-1.22812282008385	-0.17586576506521
N	0.04674734484377	-6.14223602866715	5.32261262507942
C	-0.07117716861061	2.35206630940931	-2.33859165697345
H	-0.07641850853288	1.27571605802176	-2.46220495392245
O	-0.06823008888169	-2.55089129710834	-1.24129780438620
C	-0.13759464863212	3.17260354317782	-3.44423606834844
N	-0.25302549465264	6.10186163309175	-5.36400068795817
H	-0.19834382624910	2.74346912754993	-4.43541730297335
C	-0.12496248126781	4.56845272562342	-3.29476122858589
Pd	0.02724971647645	0.00279848879959	-0.00272794426533
C	-0.04187870428274	5.11767299333535	-2.00418065051792
N	-0.01465993023966	-2.06244899448997	-0.07441422481829
O	0.17136425743100	2.56775244105494	1.21817290252773
H	-0.03255717120955	6.19357815300272	-1.88661472349919
C	0.02618109154900	4.30333072250383	-0.89531293893315
C	0.01110328542730	2.90192290097820	-1.04666160514679
H	0.08937117470129	4.71409414929560	0.10131954863225
C	-0.19529661732015	5.41593371895987	-4.43751486153546
N	3.18215861329032	-0.03573822726385	0.02659485797135
N	0.07703686878049	2.06841660699724	0.05847658511038
C	0.06458798356344	-2.36729379783523	2.32301048456302
C	-0.00332297481077	-2.90527348036300	1.02525264676449
H	0.10683177403282	-1.29270053280621	2.45457035130057
C	0.07794949300354	-3.19717672169621	3.42352367962084
C	0.03633888322013	-5.44812592086943	4.40048836018270
H	0.13166146182098	-2.77732659019915	4.41906953050204
C	0.02301186321975	-4.59085409968766	3.26299672699678
C	-0.04565189237829	-5.12815008464352	1.96651046697771
H	-0.08959995283215	-6.20224243504575	1.84061477864122
C	-0.05845907223613	-4.30447463411258	0.86258196514500
N	-3.13049984791861	0.04429951534136	-0.01789270219646
H	-0.11234325090880	-4.70585036266869	-0.13840714715810
H	-4.62041022299576	-0.07201055313750	-2.17154919629636
H	-4.66149556387632	0.16384001993193	2.10762449655967

```
H    4.68077482234338      2.06598952306377      0.47199361620043
H    4.69969702643009     -2.13742645476159     -0.36661402923092
```

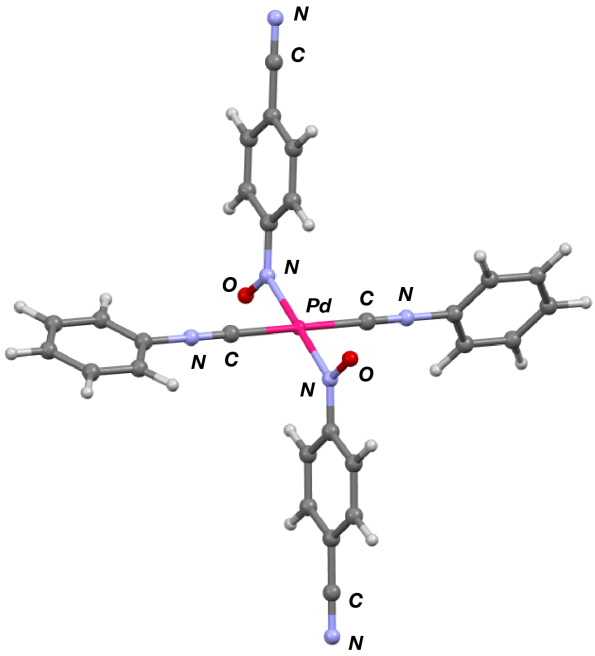

Figure 6.15. Optimized molecular structure of Pd(κ^1-*N*-*p*-CN-$C_6H_4NO)_2(CNPh)_2$.

6.8. Details of crystallographic structure determinations

Single crystal X-ray structure determinations were carried out at low temperature on Bruker Kappa, Platform, or P4 diffractometers equipped with a Mo or Cu radiation source and a Bruker APEX or APEX-II detector. All structures were solved via direct methods with SHELXS[103] and refined by full-matrix least-squares procedures using SHELXL[103] within the Olex2 small-molecule solution, refinement and analysis software.[104] Crystallographic data collection and refinement information are listed in Table 6.3-9.

The *p*-Ph-substituted diradical **1i** contains two-site positional disorder of one diisopropylphenyl (Dipp) flanking aryl ring, as well as three-fold rotational disorder of

the *para*-phenyl nitrosoarene substituent. These disordered groups were modeled and refined anisotropically. The *p*-COH substituted diradical **1k** contains two-site positional disorder of the formyl groups. This disorder was modeled and refined anisotropically. The *m*-Cl- and *m*-Br substituted metalloxaziridines **2b** and **2c** contain two-site 180º rotational disorder of the nitrosoaryl rings about the $N_{nitroso}$-C_{ipso} bond. As one of these orientations is only a minor component, only the halogen atom was modeled and refined over both positions. In addition, **2b** and **2c** contain two-site positional disorder of one isopropyl group. These disordered groups were modeled and refined anisotropically. The *m*-COH substituted metalloxaziridine **2e** contains two-site 180º rotational disorder of the nitrosoaryl ring about the $N_{nitroso}$-C_{ipso} bond. This disorder was modeled and refined anisotropically. The *p*-Cl and *p*-Me substituted metalloxaziridines **2g** and **2j** contain two-site positional disorder of one isopropyl group, which was modeled and refined anisotropically. The *m*-Me substituted metalloxaziridine **2d** contains two-site positional disorder of a central terphenyl aryl ring, as well as two-site positional disorder of two isopropyl groups. These disordered groups were modeled and refined anisotropically. The crystal of *p*-F substituted metalloxaziridine **2h** used for X-ray diffraction was twinned. The twin law was determined using Olex2 and the structure refined using SHELXL as a two-component twin. The trimer $[Pd(\mu^2{:}\eta^2\text{-}N,O\text{-}\eta^1\text{-}N\text{-}PhNO)(CNAr^{Dipp2})]_3$ (**4**) contains two-site positional disorder of the Pd and $N_{nitroso}$ atoms and the nitrosobenzene phenyl rings. These disordered groups were modeled and refined anisotropically. In addition, the following molecules contain co-crystallized solvent molecules that were highly disordered and could not be properly modeled: **1i** (16 molecules of diethyl ether per unit cell), **1l** (6 molecules of diethyl ether per unit cell). The Platon routine SQUEEZE[105] was

utilized to account for these electrons as a diffuse contribution to the overall scattering without specific atom positions.

Table 6.3. Crystallographic data collection and refinement information.

Name	Pd(κ^1-*N*-*m*-$ClC_6H_4NO)_2$ $(CNAr^{Dipp2})_2$ • 2 Et_2O (**1b** • 2 Et_2O)	Pd(κ^1-*N*-*m*-$BrC_6H_4NO)_2$ $(CNAr^{Dipp2})_2$ • 2 Et_2O (**1c** • 2 Et_2O)	Pd(κ^1-*N*-*m*-COH-$C_6H_4NO)_2(CNAr^{Dipp2})_2$ (**1e**)
Formula	$C_{82}H_{102}N_4O_4Cl_2Pd$	$C_{82}H_{102}N_4O_4Br_2Pd$	$C_{76}H_{84}N_4O_4Pd$
Crystal System	Monoclinic	Monoclinic	Monoclinic
Space Group	*C*2/c	*P*2(1)/n	*P*2(1)/c
a, Å	21.312(5)	12.130(2)	17.7788(9)
b, Å	14.111(4)	24.738(4)	16.2474(6)
c, Å	25.056(6)	12.783(2)	24.684(1)
α, deg	90	90	90
β, deg	97.197(3)	99.112(3)	107.670(2)
γ, deg	90	90	90
V, $Å^3$	7476(3)	3787(1)	6794.0(5)
Z	4	2	4
Radiation (λ, Å)	Mo-Kα, 0.71073	Mo-Kα, 0.71073	Mo-Kα, 0.71073
ρ (calcd.), g/cm^3	1.231	1.292	1.197
μ (Mo Kα), mm^{-1}	0.371	1.351	0.324
Temp, K	100	100	100
θ max, deg	28.332	26.075	25.477
data/parameters	8788/419	7450/431	12596/782
R_1	0.0742	0.0554	0.0440
wR_2	0.1961	0.1253	0.0928
GOF	1.055	1.022	0.983

Table 6.4. Crystallographic data collection and refinement information.

Name Formula	$Pd(\kappa^1\text{-}N\text{-}p\text{-}BrC_6H_4NO)_2(CNAr^{Dipp2})_2 \cdot 2\ Et_2O$ (**1f** • 2 Et_2O) $C_{82}H_{102}N_4O_4Br_2Pd$	$Pd(\kappa^1\text{-}N\text{-}p\text{-}ClC_6H_4NO)_2(CNAr^{Dipp2})_2 \cdot 2\ Et_2O$ (**1g** • 2 Et_2O) $C_{82}H_{102}N_4O_4Cl_2Pd$	$Pd(\kappa^1\text{-}N\text{-}p\text{-}FC_6H_4NO)_2(CNAr^{Dipp2})_2 \cdot 2\ Et_2O$ (**1h** • 2 Et_2O) $C_{82}H_{102}N_4O_4F_2Pd$
Crystal System	Monoclinic	Monoclinic	Monoclinic
Space Group	*P*2(1)/c	P2(1)/c	P2(1)/n
a, Å	14.146(1)	13.967(3)	13.887(1)
b, Å	17.591(2)	17.490(4)	17.149(1)
c, Å	17.014(2)	16.936(5)	16.718(1)
α, deg	90	90	90
β, deg	114.090(1)	114.091(3)	113.685(3)
γ, deg	90	90	90
V, Å^3	3865.2(7)	3777(2)	3646.0(5)
Z	2	2	2
Radiation (λ, Å)	Mo-Kα, 0.71073	Mo-Kα, 0.71073	Mo-Kα, 0.71073
ρ (calcd.), g/cm^3	1.266	1.218	1.232
μ (Mo Kα), mm^{-1}	1.323	0.367	0.311
Temp, K	100	100	90
θ max, deg	25.691	28.278	25.426
data/parameters	7289/431	8716/425	6598/437
R_1	0.0422	0.0367	0.0425
wR_2	0.1069	0.0853	0.0844
GOF	1.039	1.021	1.005

Table 6.5. Crystallographic data collection and refinement information.

Name	$Pd(\kappa^1\text{-}N\text{-}p\text{-}PhC_6H_4NO)_2(CNAr^{Dipp2})_2 \cdot 4\ Et_2O$ (**1i** • 4 Et_2O)	$Pd(\kappa^1\text{-}N\text{-}p\text{-}MeC_6H_4NO)_2(CNAr^{Dipp2})_2 \cdot 2\ Et_2O$ (**1j** • 2 Et_2O)	$Pd(\kappa^1\text{-}N\text{-}p\text{-}COH\text{-}C_6H_4NO)_2(CNAr^{Dipp2})_2$ (**1k**)
Formula	$C_{102}H_{132}N_4O_6Pd$	$C_{84}H_{108}N_4O_4Pd$	$C_{76}H_{84}N_4O_4Pd$
Crystal System	Monoclinic	Monoclinic	Monoclinic
Space Group	*C*2/c	*P*2(1)/c	*P*2(1)/n
a, Å	31.302(3)	13.973(2)	14.3005(9)
b, Å	16.798(1)	17.461(3)	17.108(1)
c, Å	16.962(1)	16.912(3)	16.624(1)
α, deg	90	90	90
β, deg	101.541(4)	113.135(2)	113.702(2)
γ, deg	90	90	90
V, $Å^3$	8739(1)	3794(1)	3724.0(4)
Z	4	2	2
Radiation (λ, Å)	Mo-Kα, 0.71073	Mo-Kα, 0.71073	Mo-Kα, 0.71073
ρ (calcd.), g/cm^3	1.229	1.176	1.091
μ (Mo Kα), mm^{-1}	0.271	0.295	0.295
Temp, K	100	100	100
θ max, deg	25.390	28.276	25.375
data/parameters	7983/447	8777/433	6685/393
R_1	0.0440	0.0518	0.0559
wR_2	0.1182	0.1170	0.1523
GOF	1.037	1.027	1.051

Table 6.6. Crystallographic data collection and refinement information.

Name	Pd(κ^1-*N*-*p*-CN-$C_6H_4NO)_2$($CNAr^{Dipp2}$)$_2$ • 3 Et_2O (**1l** • 3 Et_2O)	Pd(η^2-*N,O*-C_6H_5NO)($CNAr^{Dipp2}$)$_2$ (**2a**)	Pd(η^2-*N,O*-*m*-ClC_6H_4NO)($CNAr^{Dipp2}$)$_2$ (**2b**)
Formula	$C_{88}H_{112}N_6O_5Pd$	$C_{68}H_{79}N_3OPd$	$C_{68}H_{78}N_3OClPd$
Crystal System	Monoclinic	Monoclinic	Monoclinic
Space Group	*P*2(1)/n	*P*2(1)/c	P2(1)/c
a, Å	14.702(1)	25.388(1)	25.5580(7)
b, Å	16.958(1)	11.7589(5)	11.7890(3)
c, Å	16.284(2)	19.8229(9)	20.0170(5)
α, deg	90	90	90
β, deg	112.810(5)	98.724(1)	100.393(1)
γ, deg	90	90	90
V, $Å^3$	3742.5(6)	5849.5(4)	5932.2(3)
Z	2	4	4
Radiation (λ, Å)	Mo-Kα, 0.71073	Mo-Kα, 0.71073	Mo-Kα, 0.71073
ρ (calcd.), g/cm^3	1.278	1.204	1.226
μ (Mo Kα), mm^{-1}	0.296	0.361	0.402
Temp, K	90	100	100
θ max, deg	25.532	25.399	25.389
data/parameters	6947/393	10732/658	10836/699
R_1	0.0394	0.0345	0.0419
wR_2	0.1205	0.0848	0.1002
GOF	1.152	1.019	1.024

Table 6.7. Crystallographic data collection and refinement information.

Name	Pd(η^2-*N,O*-*m*-BrC_6H_4NO)($CNAr^{Dipp2}$)$_2$ (**2c**)	Pd(η^2-*N,O*-*m*-Me-C_6H_4NO)($CNAr^{Dipp2}$)$_2$ (**2d**)	Pd(η^2-*N,O*-*m*-COH-C_6H_4NO)($CNAr^{Dipp2}$)$_2$ (**2e**)
Formula	$C_{68}H_{78}N_3OBrPd$	$C_{69}H_{81}N_3OPd$	$C_{69}H_{79}N_3O_2Pd$
Crystal System	Monoclinic	Triclinic	Monoclinic
Space Group	P2(1)/c	P-1	P2(1)/c
a, Å	25.8348(8)	11.7787(7)	25.661(1)
b, Å	11.8191(3)	13.4861(8)	11.7309(4)
c, Å	20.1027(5)	20.815(1)	20.0171(8)
α, deg	90	72.022(2)	90
β, deg	102.268(1)	77.910(2)	99.014(1)
γ, deg	90	76.771(2)	90
V, Å^3	5998.1(3)	3027.0(3)	5951.3(4)
Z	4	2	4
Radiation (λ, Å)	Mo-Kα, 0.71073	Mo-Kα, 0.71073	Mo-Kα, 0.71073
ρ (calcd.), g/cm^3	1.262	1.179	1.217
μ (Mo Kα), mm^{-1}	1.019	0.350	0.358
Temp, K	100	100	100
θ max, deg	25.395	26.423	26.406
data/parameters	10989/699	12315/787	12219/735
R_1	0.0398	0.0282	0.0419
wR_2	0.0989	0.0808	0.1002
GOF	1.061	1.208	1.024

Table 6.8. Crystallographic data collection and refinement information.

Name	Pd(η^2-*N,O-p*-Cl-C_6H_4NO)($CNAr^{Dipp2}$)$_2$ • 0.5 C_6H_6 (**2g** • 0.5 C_6H_6)	Pd(η^2-*N,O-p*-F-C_6H_4NO)($CNAr^{Dipp2}$)$_2$ • C_6H_6 (**2h** • C_6H_6)	Pd(η^2-*N,O-p*-Me-C_6H_4NO)($CNAr^{Dipp2}$)$_2$ • C_6H_6 (**2j** • C_6H_6)
Formula	$C_{71}H_{81}N_3OClPd$	$C_{74}H_{84}N_3OFPd$	$C_{75}H_{87}N_3OPd$
Crystal System	Monoclinic	Monoclinic	Monoclinic
Space Group	*P*2(1)/n	*Cc*	*Cc*
a, Å	16.727(1)	14.0835(8)	14.2644(8)
b, Å	17.151(1)	20.4568(8)	20.3118(8)
c, Å	21.902(2)	21.970(1)	22.273(1)
α, deg	90	90	90
β, deg	93.309(4)	95.090(3)	96.404(3)
γ, deg	90	90	90
V, Å^3	6272.9(8)	6304.7(5)	6413.0(5)
Z	4	4	4
Radiation (λ, Å)	Mo-Kα, 0.71073	Mo-Kα, 0.71073	Mo-Kα, 0.71073
ρ (calcd.), g/cm^3	1.201	1.219	1.194
μ (Mo Kα), mm^{-1}	0.382	0.343	0.335
Temp, K	100	100	90
θ max, deg	25.418	25.403	25.468
data/parameters	11525/710	10909/728	10692/747
R_1	0.0373	0.0697	0.0367
wR_2	0.0843	0.1650	0.0995
GOF	1.080	1.304	1.208

Table 6.9. Crystallographic data collection and refinement information.

Name	$OCNAr^{Dipp2} \cdot CH_2Cl_2$ (**3** $\cdot CH_2Cl_2$)	$[Pd(\mu^2{:}\eta^2\text{-}N\text{-}O\text{-}\kappa^1\text{-}N\text{-}C_6H_5NO)(CNAr^{Dipp2})]_3$ (**4**)
Formula	$C_{32}H_{39}NOCl_2$	$C_{111}H_{126}N_6O_3Pd_3$
Crystal System	Monoclinic	Monoclinic
Space Group	*P*2(1)/n	*P*2(1)/c
a, Å	18.3452(3)	17.368(3)
b, Å	8.2117(1)	18.616(3)
c, Å	20.3727(3)	30.754(6)
α, deg	90	90
β, deg	104.632(1)	97.594(9)
γ, deg	90	90
V, $Å^3$	2929.52(8)	9856(3)
Z	4	4
Radiation (λ, Å)	Cu-Kα, 1.54178	Cu-Kα, 1.54178
ρ (calcd.), g/cm^3	1.173	1.288
μ (Cu Kα), mm^{-1}	2.136	4.773
Temp, K	100	100
θ max, deg	67.961	70.808
data/parameters	5357/333	17729/1312
R_1	0.0352	0.0850
wR_2	0.0903	0.2057
GOF	1.036	1.137

6.9. Acknowledgements

Chapter 6 is adapted from Barnett, B. R.; Labios, L. A.; Moore, C. E.; England, J.; Rheingold, A. L.; Wieghardt, K.; Figueroa, J.S. "Solution Dynamics or Redox Noninnocent Nitrosoarene Ligands: Mapping the Electronic Criteria for the Formation of Persistent Metal-Coordinated Nitroxide Radicals", *Inorganic Chemistry*, **2015**, 54, 7110. Copyright 2015, American Chemical Society. Permission to include published material in this dissertation has been obtained from all coauthors. The dissertation author is the first author of this paper. Dr. Liezel A. Labios is thanked for her integral experimental contributions to this work. SQUID magnetometry measurements were performed by Dr. Jason England and supervised by Prof. Karl Wieghardt, who is also thanked for insightful conversations. In addition, we thank Prof. Clifford P. Kubiak for access to VT-IR instrumentation, as well as Profs. William C. Trogler and Jeffrey D. Rinehart for helpful discussions.

6.10. References

(1) Kaim, W. *Inorg. Chem.* **2011**, *50*, 9752.

(2) Pierpont, C. G. *Coord. Chem. Rev.* **2001**, *216–217*, 99.

(3) Griffith, W. P. *Transition Met. Chem.* **1993**, *18*, 250.

(4) Beswick, C. L.; Schulman, J. M.; Stiefel, E. I. *Prog. Inorg. Chem.* **2003**, *52*, 55.

(5) Hine, F. J.; Taylor, A. J.; Garner, C. D. *Coord. Chem. Rev.* **2010**, *254*, 1570.

(6) Eisenberg, R.; Gray, H. B. *Inorg. Chem.* **2011**, *50*, 9741.

(7) Chirik, P. J.; Wieghardt, K. *Science* **2010**, *327*, 794.

(8) Bart, S. C.; Lobkovsky, E. L.; Chirik, P. J. *J. Am. Chem. Soc.* **2004**, *126*, 13794.

(9) Tondreau, A. M.; Atienza, C. C. H.; Weller, K. J.; Nye, S. A.; Lewis, K. M.; Delis, J. G. P.; Chirik, P. J. *Science* **2012**, *335*, 567.

(10) Luca, O. R.; Crabtree, R. H. *Chem. Soc. Rev.* **2013**, *42*, 1440.

(11) Zhu, D.; Thapa, I.; Korobkov, I.; Gambarotta, S.; Budzelaar, P. H. M. *Inorg. Chem.* **2011**, *50*, 9879.

(12) Knijnenburg, Q.; Gambarotta, S.; Budzelaar, P. H. M. *Dalton Trans.* **2006**, 5442.

(13) Blackmore, K. J.; Ziller, J. W.; Heyduk, A. F. *Inorg. Chem.* **2005**, *44*, 5559.

(14) Lu, C. C.; Bill, E.; Weyhermüller, T.; Bothe, E.; Wieghardt, K. *Inorg. Chem.* **2007**, *46*, 7880.

(15) Dunn, T. J.; Webb, M. I.; Hazin, K.; Verma, P.; Wasinger, E. C.; Shimazaki, Y.; Storr, T. *Dalton Trans.* **2013**, *42*, 3950.

(16) Kaim, W. *Eur. J. Inorg. Chem.* **2012**, 343.

(17) Heyduk, A. F.; Zarkesh, R. A.; Nguyen, A. I. *Inorg. Chem.* **2011**, *50*, 9849.

(18) Praneeth, V. K. K.; Ringenberg, M. R.; Ward, T. R. *Angew. Chem., Int. Ed.* **2012**, *51*, 10228.

(19) Lyaskovskyy, V.; de Bruin, B. *ACS Catal.* **2012**, *2*, 270.

(20) Valentine, J. S. *Chem. Rev.* **1973**, *73*, 235.

(21) Cramer, C. J.; Tolman, W. B. *Acc. Chem. Res.* **2007**, *40*, 601.

(22) Jørgensen, C. *Coord. Chem. Rev.* **1966**, *1*, 164.

(23) Hayton, T. W.; Legzdins, P.; Sharp, W. B. *Chem. Rev.* **2002**, *102*, 935.

(24) Ford, P. C.; Lorkovic, I. M. *Chem. Rev.* **2002**, *102*, 993.

(25) McCleverty, J. A. *Chem. Rev.* **2004**, *104*, 403.

(26) Farmer, P. J.; Sulc, F. *J. Inorg. Biochem.* **2005**, *99*, 166.

(27) Fukuto, J. M.; Bartberger, M. D.; Dutton, A. S.; Paolocci, N.; Wink, D. A.; Houk, K. N. *Chem. Res. Toxicol.* **2005**, *18*, 790.

(28) Weiss, J. J. *Nature* **1964**, *202*, 83.

(29) Pauling, L. *Nature* **1964**, *203*, 182.

(30) Chen, H.; Ikeda-Saito, M.; Shaik, S. *J. Am. Chem. Soc.* **2008**, *130*, 14778.

(31) Wanat, A.; Schneppensieper, T.; Stochel, G.; van Eldik, R.; Bill, E.; Wieghardt, K. *Inorg. Chem.* **2002**, *41*, 4.

(32) Kaim, W.; Schwederski, B. *Coord. Chem. Rev.* **2010**, *254*, 1580.

(33) Lee, J.; Chen, L.; West, A. H.; Richter-Addo, G. B. *Chem. Rev.* **2002**, *102*, 1019.

(34) Gowenlock, B. G.; Richter-Addo, G. B. *Chem. Rev.* **2004**, *104*, 3315.

(35) Cameron, M.; Gowenlock, B. G.; Vasapollo, G. *Chem. Soc. Rev.* **1990**, *19*, 355.

(36) Mansuy, D.; Battioni, P.; Chottard, J.-C.; Riche, C.; Chiaroni, A. *J. Am. Chem. Soc.* **1983**, *105*, 455.

(37) Muccigrosso, D. A.; Jacobson, S. E.; Apgar, P. A.; Mares, F. *J. Am. Chem. Soc.* **1978**, *100*, 7063.

(38) Askari, M. S.; Girard, B.; Murugesu, M.; Ottenwaelder, X. *Chem. Commun.* **2011**, *47*, 8055.

(39) Hoard, D. W.; Sharp, P. R. *Inorg. Chem.* **1993**, *32*, 612.

(40) Srivastava, R. S.; Khan, M. A.; Nicholas, K. M. *J. Am. Chem. Soc.* **2005**, *127*, 7278.

(41) Liebeskind, L. S.; Sharpless, K. B.; Wilson, R. D.; Ibers, J. A. *J. Am. Chem. Soc.* **1978**, *100*, 7061.

(42) Packett, D. L.; Trogler, W. C.; Rheingold, A. L. *Inorg. Chem.* **1987**, *26*, 4308.

(43) Skoog, S. J.; Campbell, J. P.; Gladfelter, W. L. *Organometallics* **1994**, *13*, 4137.

(44) Berman, R. S.; Kochi, J. K. *Inorg. Chem.* **1980**, *19*, 248.

(45) Rehorek, D. *Chem. Soc. Rev.* **1991**, *20*, 341.

(46) *Electron Paramagnetic Resonance: A Practitioner's Toolkit*; Brustolon, M.; Giamello, E., Eds.; John Wiley and Sons, Inc.: Hoboken, NJ, 2009.

(47) Swanwick, M. G.; Waters, W. A. *J. Chem. Soc. B.* **1971**, 1059.

(48) Hudson, A.; Lappert, M. F.; Lednor, P. W.; Nicholson, B. K. *J. Chem. Soc., Chem. Commun.* **1974**, 966.

(49) Labios, L. A.; Millard, M. D.; Rheingold, A. L.; Figueroa, J. S. *J. Am. Chem. Soc.* **2009**, *131*, 11318.

(50) Iwasa, T.; Shimada, H.; Takami, A.; Matsuzaka, H.; Ishii, Y.; Hidai, M. *Inorg. Chem.* **1999**, *38*, 2851.

(51) Chan, S.-C.; England, J.; Lee, W.-C.; Wieghardt, K.; Wong, C.-Y. *ChemPlusChem* **2013**, *78*, 214.

(52) Tomson, N. C.; Labios, L. A.; Weyhermüller, T.; Figueroa, J. S.; Wieghardt, K. *Inorg. Chem.* **2011**, *50*, 5763.

(53) Fox, B. J.; Sun, Q. Y.; DiPasquale, A. G.; Fox, A. R.; Rheingold, A. L.; Figueroa, J. S. *Inorg. Chem.* **2008**, *47*, 9010.

(54) Fox, B. J.; Millard, M. D.; DiPasquale, A. G.; Rheingold, A. L.; Figueroa, J. S. *Angew. Chem., Int. Ed.* **2009**, *48*, 3473.

(55) Ditri, T. B.; Fox, B. J.; Moore, C. E.; Rheingold, A. L.; Figueroa, J. S. *Inorg. Chem.* **2009**, *48*, 8362.

(56) Stewart, M. A.; Moore, C. E.; Ditri, T. B.; Labios, L. A.; Rheingold, A. L.; Figueroa, J. S. *Chem. Commun.* **2011**, *47*, 406.

(57) Margulieux, G. W.; Weidemann, N.; Lacy, D. C.; Moore, C. E.; Rheingold, A. L.; Figueroa, J. S. *J. Am. Chem. Soc.* **2010**, *132*, 5033.

(58) Carpenter, A. E.; Margulieux, G. W.; Millard, M. D.; Moore, C. E.; Weidemann, N.; Rheingold, A. L.; Figueroa, J. S. *Angew. Chem., Int. Ed.* **2012**, *51*, 9412.

(59) Barnett, B. R.; Moore, C. E.; Rheingold, A. L.; Figueroa, J. S. *J. Am. Chem. Soc.* **2014**, *136*, 10262.

(60) Carpenter, A. E.; Mokhtarzadeh, C. C.; Ripatti, D. S.; Havrylyuk, I.; Kamezawa, R.; Moore, C. E.; Rheingold, A. L.; Figueroa, J. S. *Inorg. Chem.* **2015**, *54*, 2936.

(61) Wieghardt, K. *Adv. Inorg. Bioinorg. Mech.* **1984**, *3*, 213.

(62) *NMR of Paramagnetic Molecules*; La Mar, G. N.; Horrocks, W. D.; Holm, R. H., Eds.; Academic Press: New York, NY, 1973.

(63) Bowman, A. C.; Milsmann, C.; Atienza, C. C. H.; Lobkovsky, E.; Wieghardt, K.; Chirik, P. J. *J. Am. Chem. Soc.* **2010**, *132*, 1676.

(64) Pizzotti, M.; Porta, F.; Cenini, S.; Demartin, F.; Masciocchi, N. *J. Organomet. Chem.* **1987**, *330*, 265.

(65) Brouwer, E. B.; Legzdins, P.; Rettig, S. J.; Ross, K. J. *Organometallics* **1994**, *13*, 2088.

(66) Ridouane, F.; Sanchez, J.; Arzoumanian, H.; Pierrot, M. *Acta Cryst. C* **1990**, *46*, 1407.

(67) Dutta, S. K.; McConville, D. B.; Youngs, W. J.; Chaudhury, M. *Inorg. Chem.* **1997**, *36*, 2517.

(68) Graham, P. M.; Buschhaus, M. S. A.; Baillie, R. A.; Semproni, S. P.; Legzdins, P. *Organometallics* **2010**, *29*, 5068.

(69) Carpenter, A. E.; Wen, I.; Moore, C. E.; Rheingold, A. L.; Figueroa, J. S. *Chem. Eur. J.* **2013**, *19*, 10452.

(70) In the absence of added equivalents of nitrosobenzene, the isocyanate $OCNAr^{Dipp2}$ (**3**) and azoxybenzene are slowly produced from equilibrated mixtures of $Pd(\kappa^1\text{-}N\text{-PhNO})_2(CNAr^{Dipp2})_2$ (**1a**) and $Pd(\eta^2\text{-}N,O\text{-PhNO})(CNAr^{Dipp2})_2$ (**2a**), presumably via reaction between **2a** and liberated PhNO. However, formation of **3** and azoxybenzene is greatly accelerated upon addition of excess PhNO.

(71) Otsuka, S.; Aotani, Y.; Tatsuno, Y.; Yoshida, T. *Inorg. Chem.* **1976**, *15*, 656.

(72) Cenini, S.; Porta, F.; Pizzotti, M.; La Girolamo, M. *J. Chem. Soc., Dalton Trans.* **1984**, 355.

(73) Jones, C. J.; McCleverty, J. A.; Rothin, A. S. *J. Chem. Soc., Dalton Trans.* **1985**, 401.

(74) Wiese, S.; Kapoor, P.; Williams, K. D.; Warren, T. H. *J. Am. Chem. Soc.* **2009**, *131*, 18105.

(75) For an example of the trapping of a mono-coordinated Pd(0)-L fragment, see: Fantasia, S.; Nolan, S. P. *Chem. Eur. J.* **2008**, *14*, 6987.

(76) Lutz, R. E.; Lytton, M. R. *J. Org. Chem* **1937**, *2*, 68.

(77) Colón, D.; Weber, E. J.; Anderson, J. L.; Winget, P.; Suárez, L. A. *Environ. Sci. Technol.* **2006**, *40*, 4449.

(78) Single crystals of $Pd(\kappa^1\text{-}N\text{-}m\text{-}CH_3\text{-}C_6H_4NO)_2(CNAr^{Dipp2})_2$ (**1d**) were analyzed by X-ray diffraction, but the data possessed severe whole molecule positional disorder that could not be satisfactorily modeled. Solid-state IR and combustion analysis data are included in the supporting information.

(79) Repeated attempts to grow single crystals suitable for X-ray diffraction of the *p*-Br or *p*-Ph substituted metalloxaziridines **2f** or **2i** were unsuccessful.

(80) As freshly prepared solutions of the bis-nitroxide diradicals **1k** or **1l** do contain small amounts of the corresponding metalloxaziridines **2k** or **2l**, precise magnetic moment determinations by Evans method are not possible. However, we do note that the values observed (*ca*. 1.9 μ_B) are close to those observed in the solid state at *ca.* 290 K for **1k-l** by SQUID magnetometry (see Figure 6.12).

(81) Hansch, C.; Leo, A.; Taft, R. W. *Chem. Rev.* **1991**, *91*, 165.

(82) The concept of spin density in an open shell singlet molecule, while a non-physical artifact, is a helpful way to visualize the multireference character of the ground state. These plots are therefore included here for comparison with the physically meaningful spin density representations of paramagnetic molecules. See: Noodleman, L.; Peng, C. Y.; Case, D. A.; Mouesca, J.-M. *Coord. Chem. Rev.* **1995**, 144, 199.

(83) Armarego, W. L. F.; Chai, C. L. L. *Purification of Laboratory Chemicals*, 5th Ed.; Elsevier, 2003.

(84) Pangborn, A. B.; Giardello, M. A.; Grubbs, R. H.; Rosen, R. K.; Timmers, F. J. *Organometallics*, **1996**, *15*, 1518.

(85) Zhao, D.; Johansson, M.; Backvall, J.-E. *Eur. J. Org. Chem.* **2012**, 77, 4402.

(86) Molander, G. A.; Cavalcanti, L. N. *J. Org. Chem.* **2012**, 77, 4402.

(87) Johnson Jr., H. W.; Daughhetee Jr., P. H. *J. Org. Chem.* **1964**, 29, 246.

(88) Neese, F. *Wiley Interdiscip. Rev.: Comput. Mol. Sci.* **2012**, 2, 73.

(89) Becke, A. D. *J. Chem. Phys.* **1986**, 84, 4524.

(90) Becke, A. D. *J. Chem. Phys.* **1993**, 98, 5648.

(91) Lee, C. T.; Yang, W. T.; Parr, R. G. *Phys. Rev. B* **1988**, 37, 785.

(92) Schafer, A.; Horn, H.; Ahlrichs, R. *J. Chem. Phys.* **1992**, 97, 2571.

(93) Weigend, F.; Ahlrichs, R. *Phys. Chem. Chem. Phys.* **2005**, 7, 3297.

(94) Pantazis, D. A.; Chen, X.-Y.; Landis, C. R.; Neese, F. *Chem. Theor. Comput.* **2008**, 4, 908.

(95) Eichkorn, K.; Treutler, O.; Ohm, H.; Haser, M.; Ahlrichs, R. *Chem. Phys. Lett.* **1995**, 240, 283.

(96) Eichkorn, K.; Treutler, O.; Ohm, H.; Haser, M.; Ahlrichs, R. *Chem. Phys. Lett.* **1995**, 242, 652.

(97) Eichkorn, K.; Treutler, O.; Ohm, H.; Haser, M.; Ahlrichs, R. *Theor. Chem. Acta* **1997**, 97, 119.

(98) van Wuellen, C. *J. Chem. Phys.* **1998**, 109, 392.

(99) van Lenthe, E.; Baerends, E. J.; Snijders, J. G. *J. Chem. Phys.* **1993**, 99, 4597.

(100) van Lenthe, E.; Baerends, E. J.; Snijders, J. G. *J. Chem. Phys.* **1994**, 101, 9783.

(101) Ginsberg, A. P. *J. Am. Chem. Soc.* **1980,** 102, 111.

(102) Noodleman, L.; Peng, C. Y.; Case, D. A.; Mouesca, J. M. *Coord. Chem. Rev.* **1995**, 144, 199.

(103) Sheldrick. G. M. *Acta Crystallogr. A.* **2008**, 64, 112.

(104) Dolomanov, O. V.; Bourhis, L. J.; Gildea, R. J.; Howard, J. A. K.; Puschmann, H. *J. Appl. Cryst.* **2009**, 42, 339.

(105) van der Sluis, P.; Spek. A. L. *Acta Crystallogr.* **1990**, A46, 194.